

VICK POST

Environmental Assessment of the Alaskan Continental Shelf

**Annual Reports of Principal Investigators
for the year ending March 1977**

Volume XVI. Hazards



**U.S. DEPARTMENT OF COMMERCE
National Oceanic and Atmospheric Administration**



**U.S. DEPARTMENT OF INTERIOR
Bureau of Land Management**

VOLUME I	RECEPTORS -- MAMMALS
VOLUME II	RECEPTORS -- BIRDS
VOLUME III	RECEPTORS -- BIRDS
VOLUME IV	RECEPTORS -- BIRDS
VOLUME V	RECEPTORS -- BIRDS
VOLUME VI	RECEPTORS -- FISH
VOLUME VII	RECEPTORS -- FISH
VOLUME VIII	RECEPTORS -- FISH
VOLUME IX	RECEPTORS -- FISH
VOLUME X	RECEPTORS -- FISH
VOLUME XI	RECEPTORS -- MICROBIOLOGY
VOLUME XII	EFFECTS
VOLUME XIII	CONTAMINANT BASELINES
VOLUME XIV	TRANSPORT
VOLUME XV	TRANSPORT
VOLUME XVI	HAZARDS
VOLUME XVII	HAZARDS
VOLUME XVIII	HAZARDS DATA MANAGEMENT

Environmental Assessment of the Alaskan Continental Shelf

**Annual Reports of Principal Investigators
for the year ending March 1977**

Volume XVI. Hazards

Outer Continental Shelf Environmental Assessment Program

Boulder, Colorado

March 1977

U.S. DEPARTMENT OF COMMERCE
National Oceanic and Atmospheric Administration
Environmental Research Laboratory

U.S. DEPARTMENT OF INTERIOR
Bureau of Land Management

GC
57
US
NGES
197
V.16

MF

DISCLAIMER

The Environmental Research Laboratories do not approve, recommend, or endorse any proprietary product or proprietary material mentioned in this publication. No reference shall be made to the Environmental Research Laboratories or to this publication furnished by the Environmental Research Laboratories in any advertising or sales promotion which would indicate or imply that the Environmental Research Laboratories approve, recommend, or endorse any proprietary product or proprietary material mentioned herein, or which has as its purpose an intent to cause directly or indirectly the advertised product to be used or purchased because of this Environmental Research Laboratories publication.

VOLUME XVI

HAZARDS

CONTENTS

<u>RU #</u>	<u>PI - Agency</u>	<u>Title</u>	<u>Page</u>
59	Hayes, M. - Coastal Research Div. Ruby, C. Univ. of South Carolina, Columbia, SC	Coastal Morphology, Sedimentation and Oil Spill Vulnerability	1 ✓
87	Martin, S. - Dept. of Oceanography, Univ. of Washington, Seattle, WA	The Interaction of Oil with Sea Ice in the Arctic Ocean	87
88	Kovacs, A. - Cold Regions Research & Weeks, W. Engineering Lab (CRREL) Hanover, NH	Dynamics of Near - Shore Ice	151
98	Untersteiner, N. - AIDJEX, Coon, M. Univ. of Washington, Seattle, WA	Dynamics of Near Shore Ice	164
99	Cannon, P. - Dept. of Solid Earth Science, Univ. of Alaska, Fairbanks, AK	The Environmental Geology and Geomorphology of the Gulf of Alaska Coastal Plain and the Coastal Zone of Kotzebue Sound	333 ✓
*99		Final Report	346 ✓
105	Sellman, P. - CRREL Hanover, NH	Delineation and Engineering Characteristics of Perma- frost beneath the Beaufort Sea	385
204	Hopkins, D. - U.S. Geological Survey, Menlo Park, CA	Offshore Permafrost Studies, Beaufort Sea	396

* indicates final report

ANNUAL REPORT

April 1, 1977
Research Unit - 59

Coastal Morphology, Sedimentation
and Oil Spill Vulnerability

Miles O. Hayes - Principal Investigator
Christopher H. Ruby - Co-investigator
Coastal Research Division
University of South Carolina
Columbia, S. C. 29208

Contract No. 03-5-022-82

- Project 1. Shoreline of the Northern Gulf of Alaska (Hinchinbrook Island to Dry Bay)
- Project 2. Shoreline of Kotzebue Sound (Cape Prince of Wales to Point Hope)

Task Objectives

The major emphasis of this project falls under Task D-Y, which is to: evaluate present rates of change in coastal morphology, with particular emphasis on rates and patterns of man-induced changes and locate areas where coastal morphology is likely to be changed by man's activities; and evaluate the effect of these changes, if any. The relative susceptibility of different coastal areas will be evaluated.

I. Summary of objectives, conclusions and implications with respect to OCS oil and gas development

Conclusions regarding the vulnerability of the various environments of the Gulf of Alaska are presented in detail in the first paper, "Potential Oil Spill Impacts" by Miles O. Hayes and Christopher H. Ruby, of this report. Very briefly, they indicate that slightly more than 50% of the 1773.4 kms of shoreline classified are considered high risk environments. Oil would remain in these areas for periods of time ranging from a few years to as much as 10 years.

In the second section of this report, "Sedimentology" by Christopher H. Ruby, detailed sedimentological analysis of the 400+ sediment samples collected is presented. This section is followed by an appendix which contains the grain size data as well as compositional data. Briefly, the grain size and compositional trends agree with the transport trends detailed in Nummedal and Stephen's progress report "Coastal Dynamics and Sediment Transportation, Northeast Gulf of Alaska".

II. Introduction

This report is broken into two subdivisions. The first, Project 1, dealing with the Gulf of Alaska, contains the two sections mentioned above. The second, Project 2, deals with ongoing research in the Kotzebue Sound area.

III. Current state of knowledge

This is discussed in each of the individual sections.

IV. Study area

Located in Figure 8 of "Potential Oil Spill Impacts" section.

V. Sources, methods and rational of data collection

This is discussed in detail in each of the individual sections.

VI. Results

The results are discussed in detail in each section. Topographic maps of the study area with an oil vulnerability risk classification overlay are provided in a folder following this report. In addition, magnetic tapes containing grain size data and beach profile data are being submitted under separate cover.

VII. Discussion and VIII Conclusions

Included in individual reports.

IX. Needs for further study

Two requests for extensions in funding have been submitted: One for Bristol Bay consisting of 1) Geomorphic classification, 2) Sedimentological study, 3) Oil spill vulnerability, and 4) Hydrography associated with tidal sand bodies. The second pertains to an ice study of the Kotzebue Sound area and its interaction on potential oil spills in the area.

X. Summary of 4th quarter operation

Detailed under each project section.

Project 1. Shoreline of the Northern Gulf of Alaska (Hinchinbrook Island to Dry Bay).

a) Field and Laboratory Activities

No field work has been carried out on this project since the 1975 field session. All laboratory analyses of sediment samples have been completed for both textural and compositional parameters. Our main emphasis, at this time, is placed on completion of our analysis of the coastal morphology of the study area.

b) Results

The results are presented in the two sections below. They are:

1. Potential Oil Spill Impacts by Miles O. Hayes and Christopher H. Ruby.

2. Sedimentology by Christopher H. Ruby.

The first section utilizes an oil vulnerability scale devised by our Oil Spill Assessment Team (OSAT) to delineate the relative impact of potential oil spills on the various coastal environments in the Northern Gulf of Alaska. The second section presents a detailed analysis of sedimentological trends on the beaches of the study area. Both textural and compositional parameters have been used to delineate these trends. The raw compositional and textural data are given in an appendix included at the end of the Sedimentology section. Additionally, magnetic tapes are being submitted under separate cover. These tapes contain the grain size data and the beach profile data in the formats developed by NODC.

POTENTIAL OIL SPILL IMPACTS

Miles O. Hayes
Christopher H. Ruby

Introduction

As oil exploration and development continue to escalate in Alaska, the potential for oil spills in the coastal environment increases. The Trans-Alaska Pipeline, soon to be operative, will open a new era with regard to petroleum transport via tankers in Alaskan coastal waters. These tankers will operate on a route between the west coast of the lower 48 states and Valdez. This route will take them into the coastal waters on the western edge of the study area where it borders Prince William Sound. In addition, exploration is rapidly advancing in the Gulf of Alaska itself. Any production facilities and their support facilities located in the Gulf would subject the adjacent shorelines to potential oil spills. Large spills or chronic small spillages could result in serious environmental damage. Estuarine and open marine assemblages could be seriously affected by oil spills and clean-up efforts, thus reducing or eliminating their productivity, and, therefore, affecting the food chain. It is unclear, at this time, what effect oil spills would have on economic species harvested by the numerous fishing villages within the area. Trends in sedimentation can also be altered by oil spills. Some of the more sensitive geomorphic environments can retain spilled oil for periods of time ranging to 10 years. Thus, development of this area will require careful evaluation of the possible impacts of potential oil spills.

Case Studies

Introduction. - The Coastal Research Division has developed an interdisciplinary Oil Spill Assessment Team (OSAT). During the past two years, they have had the opportunity to study two major oil spills in considerable detail and three moderate spills in slightly less detail (Table 1). The authors are members of

TABLE 1: MAJOR OIL SPILLS STUDIED BY OSAT*

<u>Oil Spill</u>	<u>Date</u>	<u>Type & Amount of Oil</u>	<u>Affected Coastline</u>	<u>Control/Treatment Methods</u>	<u>OSAT Field Studies</u>
<u>Metula</u> Strait of Magellan, Chile	August 1974	Type: Saudi Arabian Crude 3% Bunker C 53,000 tons total 40,000 tons on coastline	150 km Sand & Gravel Beaches Estuaries Marshes/Tidal Flats	No clean-up or control activities	12-20 August 1975 4 Feb.-13 March 1976 12-23 August 1976
<u>Urquiola</u> La Coruna, Spain	May 1976	Type: Persian Gulf Crude 2% Bunker C 110,000 tons total 25-30,000 ashore	215 km Sandy Beaches Rocky Shores Estuaries Marshes/Tidal Flats	Dispersants Booms and Pumps Heavy Machinery Manual Labor	17 May-10 June 1976
<u>Jakob Maersk</u> Porto, Portugal	Jan. 1975	Type: Iranian Crude 2% Bunker C 80,000 tons total 15-20,000 tons ashore	Sandy Beaches Rocky Shores Shore Facilities	Dispersants Booms Heavy Machinery Manual Labor	4-6 June 1976
<u>Argo Merchant</u> 17 miles off Nantucket Island, U.S.	Dec. 1976	Type: No. 6 fuel oil 27,000 tons	None	Rough Sea Conditions prevented effective use of control equipment	Overflight 23 Dec. 1976
<u>Bouchard #65</u> Wings Neck Area Buzzards Bay, Mass., U.S.	Jan. 1977	Type: No. 2 fuel oil 275 tons	Approx. 1-2 kms, Fast ice protected beaches	Suction pumps Sorbents Oiled ice removal Burning	30 Jan.-3 Feb. 1977
<u>Ethel II</u> Lower Hudson R., New York, U.S.	Feb. 1977	Type: No. 6 fuel oil 1500 tons lost	10 km of shoreline Little apparent damage due to fast ice along shoreline	Booms Ice Skimmer (Suction truck on LCM)	7-8 Feb. 1977

*Oil Spill Assessment Team, Coastal Research Division, University of South Carolina

that team; however, many of the concepts summarized in this sub-section are the results of interaction by the entire group.¹

The Metula spill. - The VLCC Metula ran aground on 9 August 1974, while navigating through the eastern passage of the Strait of Magellan (Fig. 1). Over the next month, 53,000 tons of oil leaked from the ship, and 40,000 tons washed onto the nearby shores (Hann, 1974). Because of the remoteness of the area and questionable legal responsibility for the accident, no attempt was made to control or clean up any of the spreading oil. We were able to visit the spill site during August 1975 and found that oil coverage was still extensive in many of the coastal environments that were originally affected (Fig. 2), including beach face and low-tide terrace portions of gravel and sand beaches, tidal flats, marsh areas, and tidal channels (Hayes and Gundlach, 1975; Hayes et al., 1976). Because of the great similarity of the area to the coasts of New England and Alaska, a full study was sponsored by NSF-RANN during January - March, 1976. A total of 66 zonal stations was set up in a manner similar to those in the Gulf of Alaska study area. A geomorphic breakdown was made of the affected area, and the distribution and perseverance of the oil was analyzed within the framework of that breakdown. Sixteen stations were selected as representative areas and studied in much greater detail. Trenches were analyzed to determine oil distribution beneath the present beach surface, and plan-view oil distribution maps were superimposed on our physiographic maps for each locality. A full report of this spill is now in preparation and will be published sometime this year.

The oil distribution on the affected environments assumed many forms primarily as a result of process variables (tide, wave and wind energy) in the particular en-

¹ Anne E. Blount
Ian A. Fischer
Erich R. Gundlach
Miles O. Hayes

Jacqueline Michel
Christopher H. Ruby
Robert J. Stein
Larry G. Ward

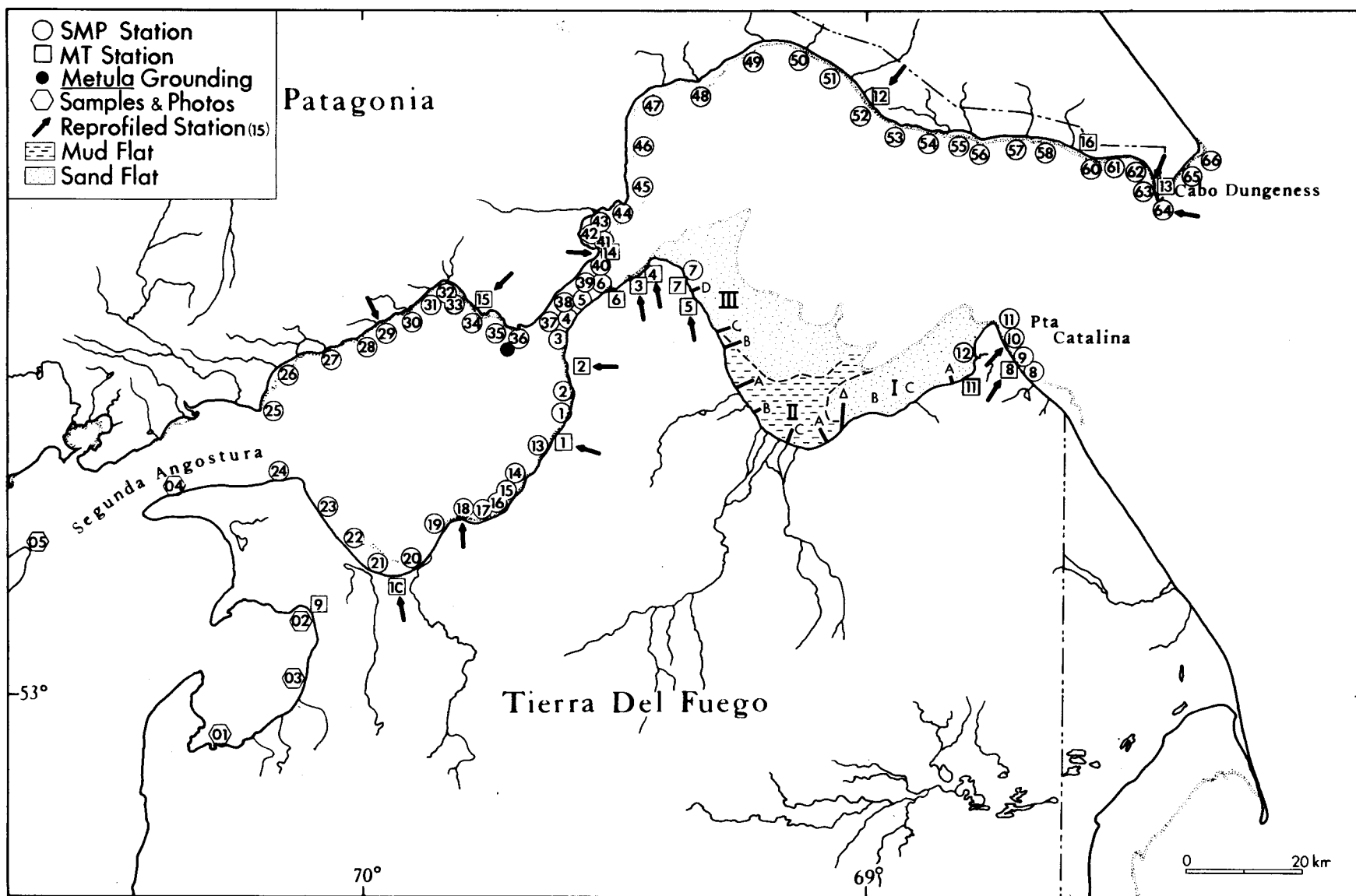


Figure 1. METULA oil spill site in the Strait of Magellan. Numbers within circles indicate SMP stations which consist of beach profiles, trenches, sediment samples and photo and tape descriptions. Numbers within squares are MT stations which consist of more detailed SMP information plus an oil concentrations map superimposed on a geomorphic base map. Photo and sample sites are indicated by open hexagons. Short heavy lines on the sand and mud flats just west of Pta. Catalina represent profiles. This represents part of the data base developed by the METULA oil spill field teams.

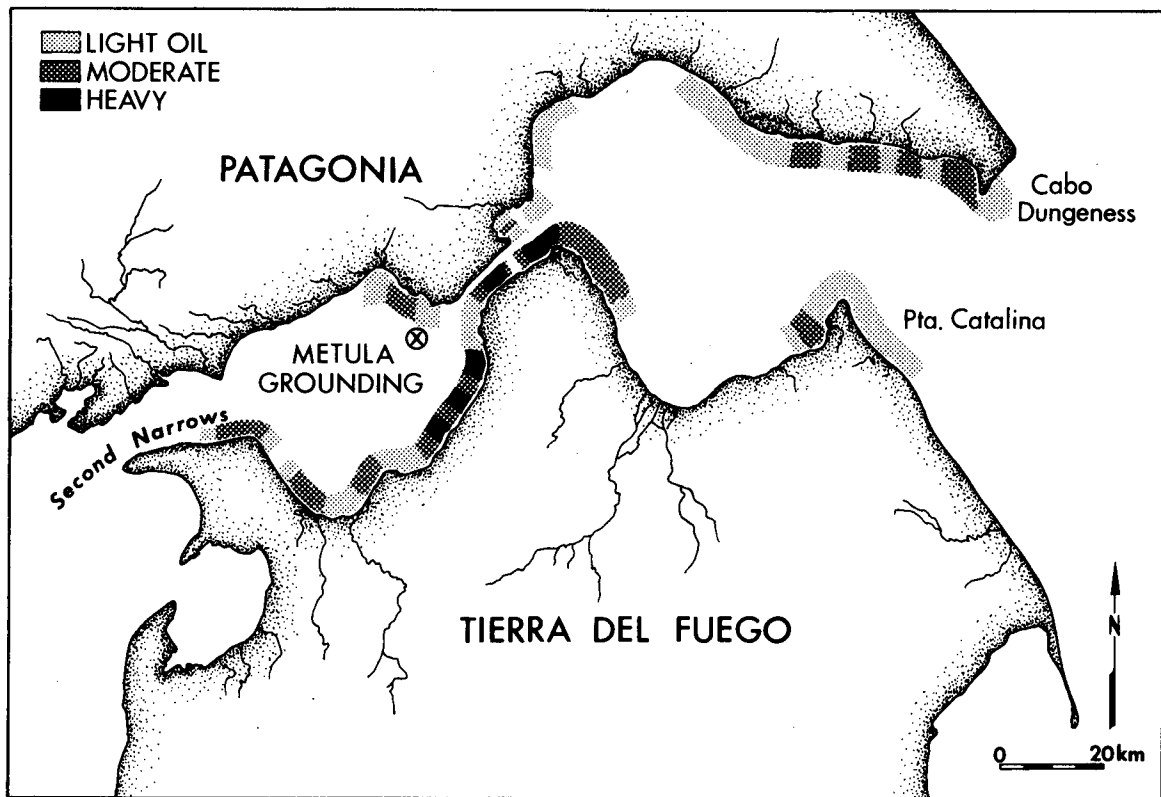


Figure 2. Oil concentration map of the Metula oil spill site in the Strait of Magellan. This represents the relative concentration of oil within the beach zone 18 months after the spill. Oil was moved primarily by the strong westerly winds and tidal currents.

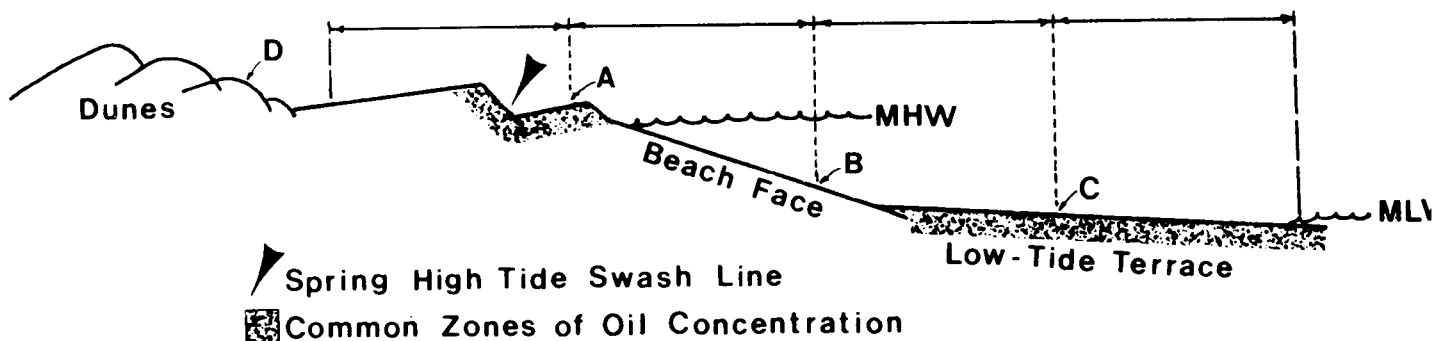


Figure 3. Typical beach profile for the Metula impact site. Letters indicate sampling localities, which are located between the upper limit of normal high waves and the low water line. B is in the center of the sampling zone, and stations A and C are located at the midpoint of the upper and lower halves of the sampling zone. D is usually a dune sample. A core sample 15 cm in length is taken at each station.

vironments and the topographic setting. On open beaches, the oil was generally deposited on the surface of berm top overwashes or at the high tide swash lines, and often at the base of the beach face if a low-tide terrace was present (Fig. 3). In the mid-beach face, the oil was either never deposited, deposited and later eroded, or buried beneath more recent beach deposits usually in the form of berms. Sheltered tidal flats and salt marshes, where the oil was still present in much the same form as when it was deposited, were by far the most severely impacted areas (Fig. 4). Large pools of oil covered most of the meandering tidal channels, killing much of the vegetation and covering a large percentage of the marsh surface with a thick (a few centimeters) layer of oil. Gravel accumulations, due to their very high permeability, were also highly affected. In some areas, the gravels and sand had been mixed with the oil to form a "blacktop" which was extremely resistant to erosion.

The Metula spill site presents an exceptional analogue for many of the areas in the Gulf of Alaska study area. Similar tidal range, recent geologic history, and sediment types make the oil behavior documented at the Metula site an ideal comparative tool for predictive purposes in this Alaskan study.

Figure 4. A. Aerial view of the meandering tidal channels in the East Estuary on the first Narrows, Strait of Magellan. Oil spilled by the Metula can be seen as glossy areas fringing the channels, (arrows). Oil thickness ranged to 10 cm. Deposition of this oil took place during spring high tides, washing the oil over the levee bordering the channels, and into the marsh. Much of the vegetation was devastated by the oil.

Figure 4. B. Ground view of a tidal channel in the East Estuary marsh. Arrows indicate heavy oil accumulations washed out of the channels. Man on the left stands at the edge of this heavy accumulation. Note that the vegetation around the oil has been killed. This photo was taken 18 months after the oil spill. We estimate a 10 year life span for this oil.

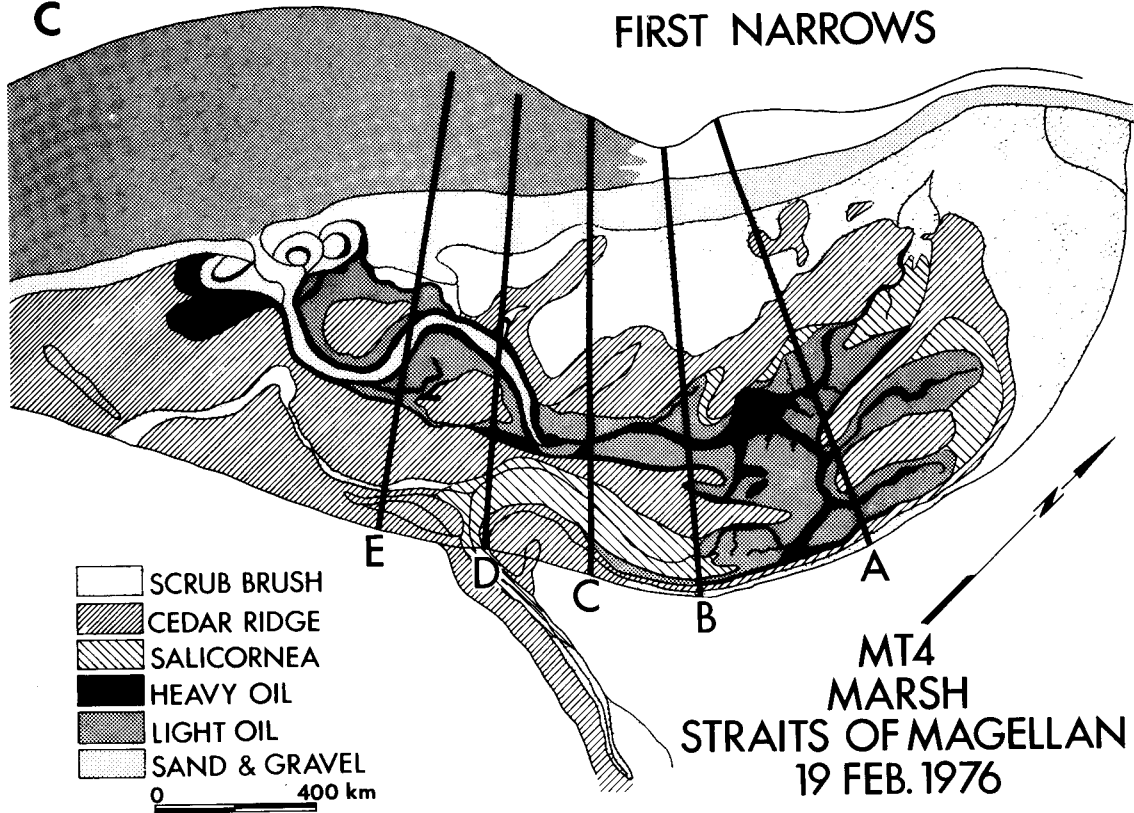
Figure 4. C. Map of East Estuary showing zones of oil accumulation. Heavy lines indicate transit profiles across the marsh system. Note the oil accumulations fringing the marsh channels and on the low tide terrace on the upper left of the map.



B



C



The Urquiola spill. - at 8:00 a.m., 12 May, 1976, the supertanker Urquiola ran aground at the entrance to La Coruna harbor in northwestern Spain. The ship exploded in the early afternoon. Part of its cargo of 100,000 tons of crude oil burned, but approximately 25-30,000 tons washed into the coastal environments of this classic "Ria" system. After 9 days, the oil had dispersed over 60 km of coastline. One month after the grounding, a total of 215 km of coastline had been impacted by the oil.

A preliminary study of the Urquiola spill was carried out by the authors and 5 associates immediately after the spill, from 17 May through 10 June 1976. Many different coastal environments were affected by the spilled oil. The area classified as a Ria system (flooded river valleys) has numerous rock headlands protecting quieter embayments. Bay mouth bars are common in the inner reaches of the rias, protecting tidal flat and marsh complexes behind them.

It was found that floating oil masses did not contaminate the rock headlands due to their exposed character. Waves reflecting from the rock cliffs kept the oil mass a few meters from the rocks. Even where oil splashed onto the cliffs, the intense wave attack soon cleaned them. However, on rock scarps within the rias, the lower wave energies permitted the oil to coat the rocks, where it will remain for a variable period of time dependent on the intensity of wave and tidal action. On the fine sand beaches within the rias, heavy deposition of oil took place, devastating infauna. However, the fine compact nature of the sediment did not permit penetration of the oil to more than a few centimeters, thus repeated wave attack should clear the beaches within a few months. This type of beach also lends itself to mechanized clean-up. For a complete discussion of mechanized clean-up methods for beaches, the reader is referred to Sartor and Foget (1971). Within the tidal flats and marshes, oil pollution was considerably worse. Oil entered these areas primarily via tidal currents and once into the marsh, it tended to adhere to the marsh vegetation. It sank into burrows of the abundant infauna often with devastating biological impact. The extremely fine grain size of the marsh and tidal flat sediments prevents direct penetration of the oil to a depth of more than a centimeter or two; thus most of

the oil remains on the surface where it is reactivated by each tide and moved from one area to another. This results in repeated contamination of areas within the marsh-tidal flat system. Two primary factors make these areas extremely sensitive to oil spill damage:

- 1) The biomass of these areas is high. They are breeding grounds for many economic species as well as habitats for juvenile forms of economically important fin and shellfish. In addition, large populations of infauna exist within these areas.
- 2) The relatively low energies (tides, winds, waves, etc.) in these areas result in very long residence times for the oil. Degradation of the oil is often orders of magnitude slower than on exposed sections of coast.

Finally, there were a small number of exposed sand beaches, both north and south of the Ria system, which were contaminated by oil. Although they received a heavy dose of the oil, the high wave energies present tended to re-work the sediments, resulting in a natural cleansing of the beach. These areas should clean themselves within a few months. Figures 5 through 7 show some of the environments contaminated by the Urquiola oil spill.

These two oil spills, plus the analysis of numerous other spills in the literature, all point the obvious fact that the physical degradation of the oil is directly related to the energy in the environment where the oil is deposited. Table 2, from Rashid (1974), gives supportive quantitative data in this regard.

Cold water spills. - There is abundant literature dealing with case studies of the numerous major and minor oil spills that have taken place in coastal waters of the lower 48 states. Predictive models for oil spill dispersal, spreading, biodegradation and physical degradation have been developed from these studies. The Arctic and sub-Arctic areas, however, have been to a large extent omitted due to the difficulties inherent in any study of these environments and a general lack of actual oil spills in these environments from which to base detailed case studies. The Arrow oil spill in Chedabucto Bay, Nova Scotia, probably comes closest to a comparative model for the sub-Arctic. However, the clean-up effort and later studies (Owens



Figure 5 A. Fine sand beach near La Coruna, Spain, oiled by the Urquiola oil spill. Oil covers the beach from the present swash zone to the high tide swash. Note the erosion of the oil at the present swash line (arrow). The fine grained nature of this beach has prevented the penetration of the oil. Most of the oil should be cleaned by natural processes within six months.

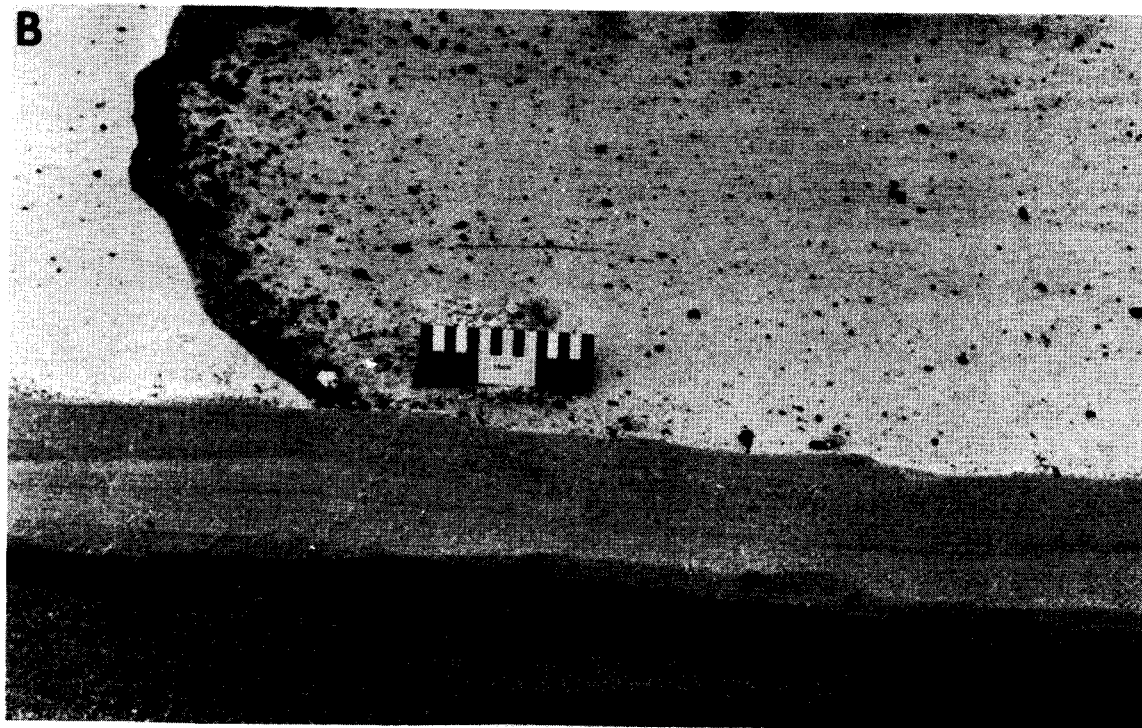


Figure 5 B. Photo of a trench in a mixed sand beach. The lower unit in the trench is composed of coarse sand deposited during spring tides. The spilled oil then polluted the beach forming a layer of mixed sand and oil. Later, a neap berm of finer sand was deposited on top of the oiled layer, resulting in some erosion of the oil. Small oil droplets can be seen as a swash line on the present beach face. Scale is 15 cm.



Figure 6. A. This photo of a coarse sand beach in the La Coruna area displays two prominent oil concentrations (arrows). This high energy beach has two berms and two berm top overwash areas. These overwash areas act as traps for the oil, resulting in heavy accumulations. The high wave energy at this location should result in rapid natural cleaning (about 6 months).

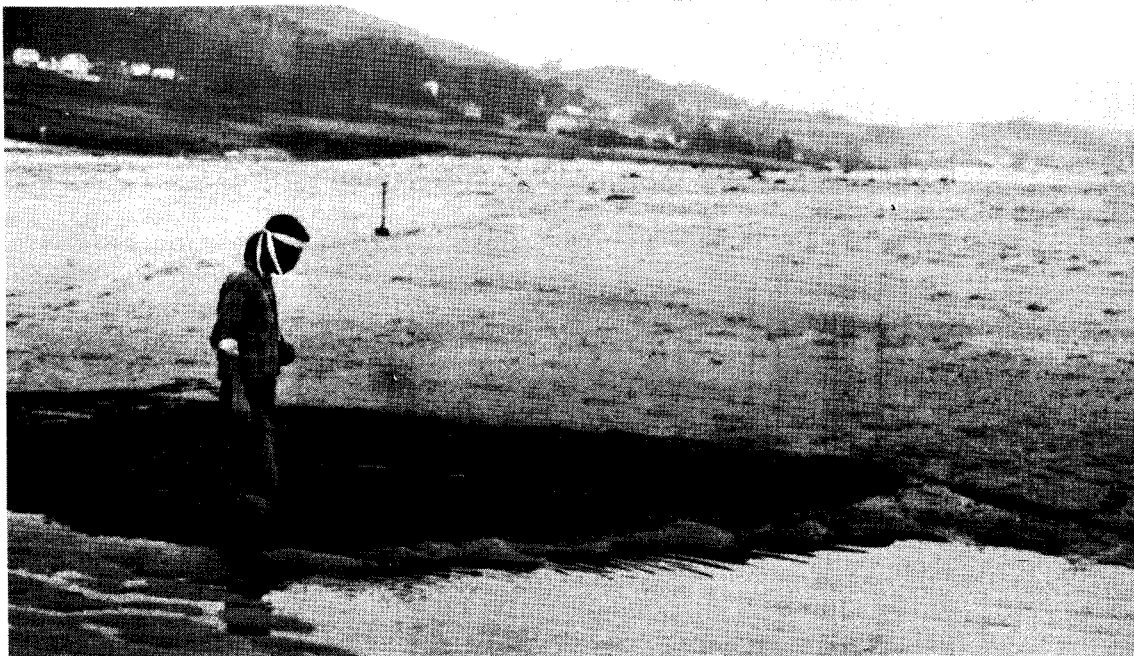


Figure 6. B. Photo shows a thick deposit of mixed sand and oil on a low-tide terrace at the toe of the beach face. This is a common zone of oil accumulation. The high wave energies at this location have eroded most of the oil. In addition, the fine grained nature of the sediments prevented penetration of the oil.



Figure 7. This small pocket beach in the La Coruna area shows the variable impact of oil pollution on sediments of different grain size. The high tide swash line on the gravels is evident to the left (arrow). The oil left a heavy coating on the gravels, but not the sand in the middle of the beach. In addition, the low energy of this pocket beach permitted the oil to leave a coating on the large bedrock outcrops. The relationship of grain size to oil penetration is an extremely important factor to be considered when designing a vulnerability scale.

Table 2. Chemical and physical characteristics of original and residual Bunker C oils extracted from sediments collected in Chedabucto Bay 3½ years after the Arrow spill (from Rashid, 1974).

Characteristics	Bunker C oil		Low energy coast	Moderate energy coast	High energy coast
	Original ^a	Stored sample			
Hydrocarbons (%)					
Saturated	--	26	25	23	18
Aromatic	--	25	24	24	16
Total hydrocarbons	73.1	51	49	47	34
Ratio of saturate to aromatic	--	1.04	1.04	0.96	1.12
Non-hydrocarbons (%)					
Asphaltenes	16.3	20	22	23	22
Resins and NSOs	10.6	29	29	30	44
Total of non-hydrocarbons	26.9	49	51	53	66
Hydrocarbons/non-hydrocarbons	2.72	1.04	0.96	0.88	0.52
Physical properties					
Specific gravity	0.950	0.963	0.9953	0.9765	0.9823
Viscosity (cP)		19.584	28.600	1210.000	3640.000

^a Task Force Operation Oil Report, 1970

and Drapeau, 1973; Owens, 1973; Drapeau, 1973; Owens, 1971; Owens and Rashid, 1976), made very little reference to the special problems encountered as a result of the colder environment (i.e. oil on ice and snow; ice-oil interaction with the beach sediments; oil dispersal in heavily iced waters, etc.). Our investigations of the Buzzards Bay Oil Spill (Ruby *et al.*, in prep.) and the Ethyl H. Oil Spill in the frozen Hudson River (Ruby and Gundlach, in prep.), have given new insight into the extremely limiting effects of oil spills in ice-choked waters.

Further, evaporation losses and biodegradation are slower in colder environments. Biodegradation can be reduced as much as 90% in water of 0°C when compared to water of 25°C, (Robertson, 1972). Isakson *et al.*, (1975) states that burning may be the only feasible method of cleaning oil spills in iced areas; however, this simply represents a trade of one type of pollution for another. It did not prove to be an effective clean-up method at the Buzzards Bay oil spill.

Finally, intense tidal currents and winds in the study area can disperse

the spilled oil in an unpredictable manner, making it nearly impossible to recover before it impacts on the shorelines. Drapeau et al., (1970) concluded that it is not feasible to recover or disperse oil slicks in regions of strong tidal currents.

Conclusion. - In summary, the potential for oil spills in the Gulf of Alaska is increasing as exploration and development continue to escalate in the Gulf and other areas of Alaska. There is a very complex interaction of marine processes during an oil spill which can make it extremely difficult to predict the track and dispersal pattern the oil spill will follow. However, numerous case studies permit the construction of an oil spill vulnerability scale which is based on the biologic sensitivity and natural cleaning ability of particular environments. This scale has been applied to lower Cook Inlet (Michel et al., 1977) and is here modified for the Gulf of Alaska.

Environmental Vulnerability to Oil Spills

This scale has been devised on the basis of the case studies summarized above and a careful study of the literature. It is based primarily on the longevity of oil in each sub-environment which is generally a function of the intensity of the marine processes, sediment size and transport trends. The biologic sensitivity has also been utilized to modify the ratings of the various environments.

Coastal environments are listed and discussed below in order of increasing vulnerability to oil spills:

1. Straight, rocky headlands:

Most areas of this type are exposed to maximum wave energy. Waves reflect off the rocky scarps with great force, readily dispersing the oil. In fact, waves reflecting off the scarps at high tide tend to generate a surficial return flow that keeps the oil off the rocks (observed at the Urquiola spill site in Spain). Parts of Kayak Island and Hinchinbrook Island fall into this category. Even if oiled, natural cleaning will only require a few days or weeks. No human intervention is necessary.

2. Eroding wave-cut platforms:

These areas are also swept clean by wave erosion. All of the areas of this type at the Metula spill site had been cleaned of oil after one year. The rate of removal of the oil is a function of wave climate. In general, no clean-up procedures are needed for this type of coast. Kayak Island, Hinchinbrook Island, and Point Riou have wave-cut platforms.

3. Flat, fine-grained sandy beaches:

Beaches of this type are generally flat and hard-packed. Oil that is emplaced on such beaches will not penetrate more than a few centimeters at most. Usually, the oil will be deposited on the surface of the sand where it can be easily removed by elevated scrapers or other road grading machinery. Furthermore, these types of beaches change slowly, so sand deposition and resultant burial of oil will take place at a slow rate. If left to natural processes, these beaches will be cleaned within several months. Much of the Yakutat Foreland and all of the Copper River delta barriers fall into this category.

4. Steeper, medium- to coarse-grained sandy beaches:

On these beaches, the depth of penetration would be greater than for the fine-grained beaches (though still only a few centimeters), but rates of burial of the oil would be greatly increased. Based on earlier studies by our group in numerous localities, it is possible for oil to be buried as much as 50-100 cm within a period of a few days on beaches of this class. In this type of situation, removal of the oil becomes a serious problem, since removal of the oiled sediments will often result in large scale erosion, as the beach changes into a new equilibrium state. This was a common problem encountered during the clean-up of the Arrow spill in Chedabucto Bay, Nova Scotia (Owens and Rashid, 1976). Another problem is that burial of the oil preserves it for release at a later date when the beach erodes as part of the natural beach cycle, thus causing longer term pollution of the environment. Many of the spits

between Cape Suckling and Icy Bay fall into this category.

5. Impermeable muddy tidal flats (exposed to winds and currents):

One of the major surprises of the study of the Metula site was the discovery that oil had not remained on the mud flats. At the Urquiola site, oil was observed as it became refloated with rising tides on the mud flats. Penetration of the oil is prevented by the extremely fine sediment size, saturated with water. Therefore, if an oiled tidal flat is subject to winds and some currents, the oil will tend to be removed, although not at the rapid rate encountered on exposed beaches. Mechanized clean-up is considered impossible. These are often areas of high biologic importance. There are large areas of mud and fine sand tidal flats behind the barriers on the Copper River Delta.

6. Mixed sand and gravel beaches:

On beaches of this type, the oil may penetrate several centimeters, and rates of burial are quite high (a few days in Spain). Again, any attempt to remove the oiled sediment will result in considerable erosion. Most of the beaches between Cape Suckling and Icy Cape are of this type. There are also many beaches within Icy Bay and all along the Malaspina Foreland which are mixes of sand and gravel. The longevity of the oil at the Metula site, particularly on the low-tide terraces and berm top areas, attests to the high susceptibility of this type of beach to long-term oil spill damage. Natural cleaning may require a few years.

7. Gravel beaches:

Pure gravel beaches allow the oil to penetrate to considerable depth (up to 45 cm in Spain). Furthermore, rapid burial is also possible. A heavily-oiled gravel beach will be impossible to clean up without completely removing the gravel. Natural cleaning will be quite slow for this type of beach; the exact time required will depend on the intensity of the marine processes. There are pure gravel beaches within both Icy Bay and Yakutat Bay (both under consideration as harbor sites). The bays are quite sheltered, and, thus, spilled oil will remain for periods of at least

a few years in these bays. The beaches just east of Sitkagi Bluffs are also composed of pure gravel; however, their exposed nature will result in considerably more rapid natural cleaning.

8. Sheltered rocky headlands:

Our experience in Spain indicates that oil tends to stick to rough rocky surfaces. In the absence of abrasion by wave action, oil could remain on such areas for years, with only chemical and biological processes left to degrade it. There are a number of sheltered rock headlands and cliffs within Icy Bay and Yakutat Bay. However, the Elias Mountains, just inland, develop nearly continuous orographic winds blowing from the north across the bays. These winds increase in intensity as the bay heads are approached. Given this wind and its domination over tidal processes, it is considered unlikely that an oil slick could penetrate deeply enough into the bays to damage the rock headlands.

9. Protected estuarine tidal flats:

If oil reaches a quiet, protected estuarine tidal flat, it will remain there for long periods because natural cleaning progresses at an extremely slow rate. Because of the low intensity of marine process parameters, removal of the oil will have to be accomplished by natural chemical and biogenic processes. This will take many years, dependent on the amount of oil deposited. Because of their high populations, these environments are very sensitive to the toxic effects of oil. A number of areas of this type exist on the Copper River Delta and in Controller Bay.

10. Protected estuarine salt marshes:

In sheltered estuaries, oil from a spill may have long-term deleterious effects. We observed oil from the Metula on the salt marshes of East Estuary, in the south shore of the Strait of Magellan, that had shown essentially no change in 1½ years. We predict a life span of at least 10 years for that oil. These areas are extremely important biologically, supporting large communities of organisms. The inner parts of the Copper River Delta contain massive salt marshes.

Applications to the Northern Gulf of Alaska

Oil spill vulnerability. - Utilizing a combination of the vulnerability classification just described and a classification of coastal morphology, it is possible to delineate the coastal environments of the Gulf of Alaska with respect to oil spill vulnerability. Generally, the Gulf is a high risk area especially in the Copper River delta section. Many of the environments have a high risk rating as explained below. In addition, the entire study area is remote and almost inaccessible to standard clean-up operations. Of all the environments, the erosional shorelines in rock scarps on Hinchinbrook Island and Kayak Island as well as scarps into glacial sediments, are most apt to be rapidly cleaned by natural processes. The marsh and tidal flat areas on the Copper River delta and other smaller river mouths are extremely high risk areas. The rest of the beaches of the study area are variable, depending essentially upon the wave energy and beach grain size. Oil burial can be a problem with these sand and gravel beaches.

Using the ten morphological subdivisions discussed earlier, a risk classification has been devised and applied to the northern Gulf of Alaska study area (Fig. 8). Table 3 shows the results of this application.

Oil longevity within these risk classifications is estimated as follows:

<u>Risk Class</u>	<u>Longevity</u>
1-2	A few days to a few weeks
3-4	A month to six months
5-6	Less than 12 months
7-8	A year or two
9-10	Up to ten years

Table 3

<u>Km of shoreline</u>	<u>% of shoreline</u>	<u>Discussion</u>	<u>Risk Classification</u>
130.4	7	Oil easily removed by wave erosion; some problems in areas of gravel accumulation and pocket beaches. This includes most of the Type 1 and 2 shorelines	1-2
298.5	17	Generally low risk areas. Fine sands prevent penetration of oil. Possibility of oil burial. Most Type 3 and 4 beaches fall into this risk class	3-4
421	24	Mud tidal flats do not permit deep penetration of the oil, but the relatively low energies require as much as a year to remove the oil. Sand and gravel beaches are highly prone to oil burial and thus fall into this risk class. Most beaches of Type 5 and 6 fall into this risk class.	5-6
513.5	29	These areas include mud tidal flats which are highly sheltered as well as sand and/or gravel beaches within bays and sheltered areas. Oil will remain for periods of a few years in these areas. Includes coastal types 7 and 8.	7-8
410	23	These highly sensitive marsh and tidal flat areas can retain oil for up to 10 years. In addition, these areas are of extreme biological importance. Coastal Types 9 and 10 fall into this category.	9-10






Table 3 shows that over half of the 1773.4 kms of shoreline classified fall into the high risk categories of 7-10. Oil longevity in these areas is estimated to be a few years to as much as 10 years. However, some of these high risk areas located on the Copper River delta and other river mouths are unlikely to receive oil spills because of fluvial flushing.

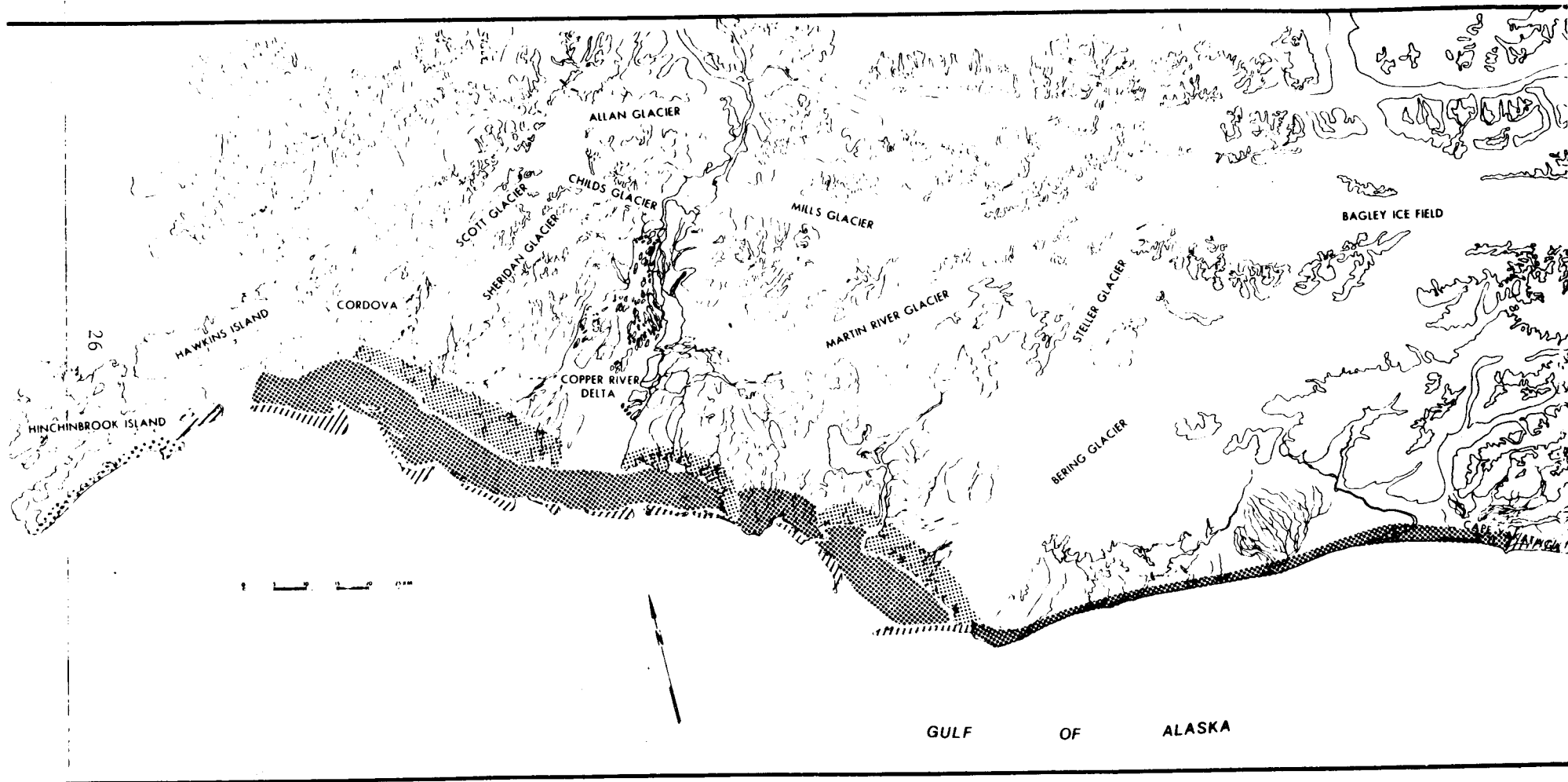
Included with this annual report is a set of topographic maps which have a color coded key to oil spill vulnerability. These maps are enclosed in a folder at the end of this report.

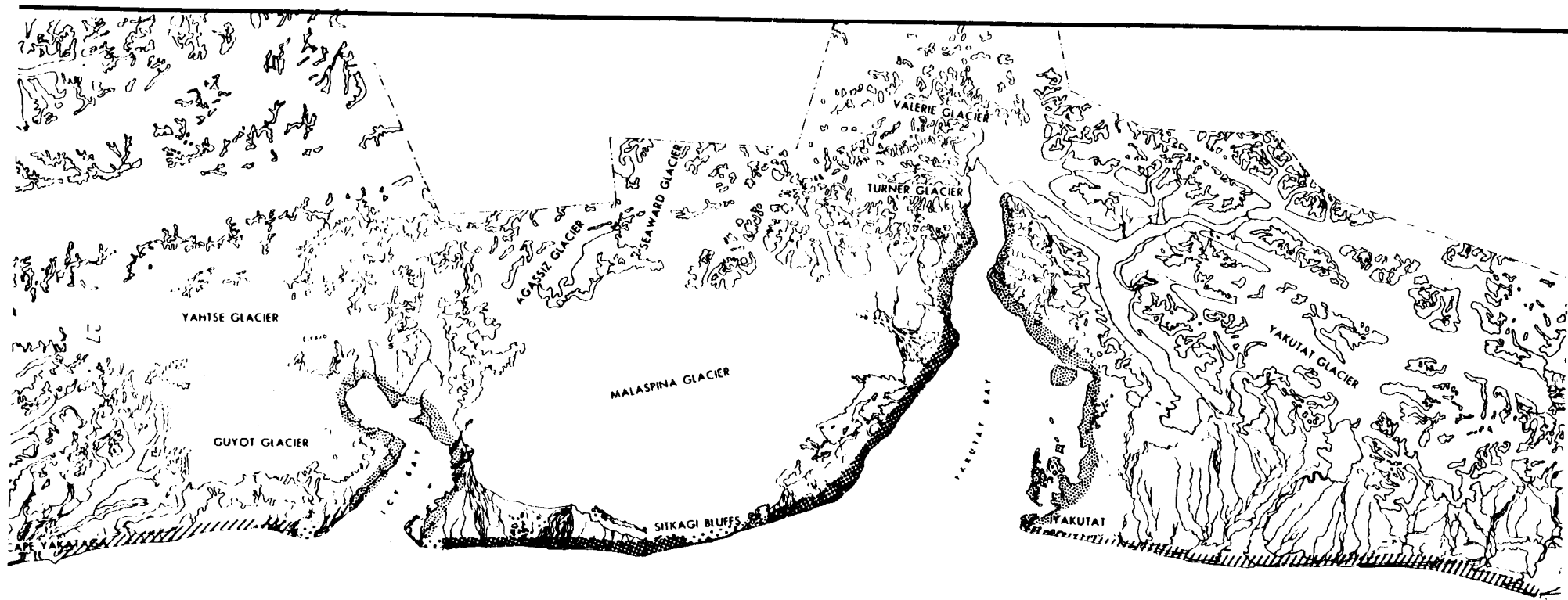
Figure 8. The following two pages display the Northern Gulf study area with the oil spill vulnerability risk classification. A set of topographic maps has been included with this report. The topographic maps utilize a color-coded key with considerably more detail than these black and white prints.

KEY TO FIGURE 8

OIL VULNERABILITY RISK CLASS

<u>RISK CLASS</u>	<u>OIL LONGEVITY</u>
 1-2	A few days to a few weeks.
 3-4	A month to six months.
 5-6	Less than 12 months.
 7-8	A year or two.
 9-10	Up to 10 years.





GULF
OF
ALASKA

1 2 3 4 5 6 7 8 9 10

REFERENCES CITED

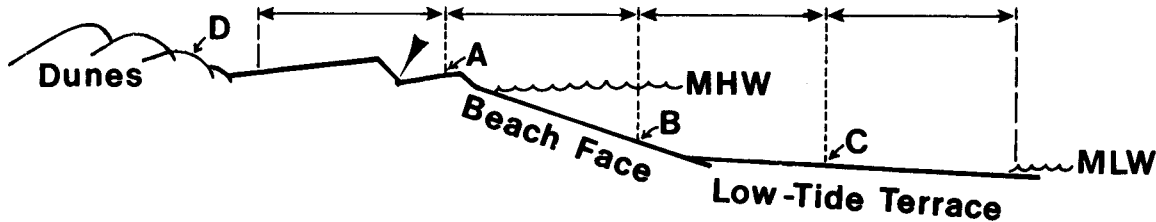
- Drapeau, G., Harrison, W., Bien, W., and Leinonen, P., 1974, Oil Slick fate in a region of strong tidal currents: Proc. 14th Coastal Eng. Conf., p. 2245-2259.
- Drapeau, G., 1973, Natural cleaning of oil polluted seashores, Proc. 13th Coastal Eng. Conf., Vancouver, B. C., p. 2557-2575.
- Hann, R. W., 1974, Oil pollution from the tanker Metula: Report to the U. S. Coast Guard, Texas A&M, Civil Eng. Dept., 61 p.
- Hayes, M. O. and Gundlach, E. R., 1975, Coastal morphology and sedimentation of the Metula oil spill site in the Strait of Magellan: Final Rept., Dept. Geology, U.S.C., 103 p.
- Hayes, M. O., Gundlach, E. R., and Perhac, R. M., 1976, The great Patagonian oil spill: Abstract, AAPG-SEPM Annual Meeting.
- Isakson, J. S., et al., 1975, Comparison of ecological impacts of postulated oil spills at selected Alaskan locations: USCG Rept. No. CG-D-155-75, V.I, 633 p., V.II, 865 p.
- Michel, J., Hayes, M. O., Brown, P. J., 1977, Application of an oil spill vulnerability index to the shoreline of lower Cook Inlet, Alaska, (in prep.).
- Owens, E. H., 1971, The restoration of beaches contaminated by oil in Chedabucto Bay, Nova Scotia, Marine Sci. Branch, Ottawa, Can., Manus. Rep. Serv., No. 19, 75 p.
- Owens, E. H., 1973, The cleaning of gravel beaches polluted by oil, Proc. 13th Coastal Eng. Conf., Vancouver, B. C., p. 2543-2556.
- Owens, E. H., and Drapeau, G., 1973, Changes in beach profiles at Chedabucto Bay, Nova Scotia, following large scale removal of sediments, Can. Jour. Earth Sci., 10, p. 1226-1232.
- Owens, E. H., and Rashid, M. A., 1976, Coastal environments and oil spill residues in Chedabucto Bay, Nova Scotia, Can. Jour. Earth Sci., 13, p. 908-928.
- Rashid, M. A., 1974, Degradation of bunker C oil under different coastal environments of Chedabucto Bay, Nova Scotia: Estuarine and Coastal Marine Sci., 2, p. 137-144.
- Robertson, B., Arhelger, S., Kinney, P. J., and Button, D. K., 1973, Hydrocarbon biodegradation in Alaskan waters: Center for Wetlands Resources, Louisiana State Univ., LSU-SG-73-01.
- Ruby, C. H., Fischer, F. A., Ward, L. G., Brown, P. J., 1977, Buzzards Bay oil spill - an Arctic analogue, Abstract, 4th Intern. Conf., Port and Ocean Eng. under Arctic conditions, Newfoundland, (in prep).
- Ruby, C. H., and Gundlach, E. R., 1977, Ethyl H. oil spill in ice bound Hudson River, in prep.
- Sartor, J. D. and Foget, C. R., 1971, Evaluation of selected earthmoving equipment for the restoration of oil contaminated beaches, Proc. Joint Conf. on Prevention and Control of Oil Spills, Wash., D. C., p. 505-522.

SEDIMENTOLOGY

Christopher H. Ruby

Sampling Technique and Method of Analysis

Sediment samples were collected at each of the DBC profile sites (Fig. 1) and at each of the permanent profile sites (Fig. 2). The sampling plan illustrated in Figure 3 was used. In all cases, at least 3 samples were taken, using a 15 cm coring tube. Where dunes were present behind the beach, a "D" sample was taken. In addition, sediments with unusual composition or texture were also sampled and are labeled with an X, Y, or Z (see Appendix, Table 1). Finally, where the grain size of the sediments present was too large to collect a representative sample, photographs were taken and later analyzed using a projector.



▲ SPRING HIGH TIDE SWASH LINE

Fig. 3. Beach zone sampling plan. Samples A, B, and C are taken from the upper, mid, and lower beach face, respectively. Sample D is taken from any dunes present behind the beach face. All samples are 15 cm cores.

All sediment samples were analyzed for grain size parameters using a Ro-Tap machine and sieves at $\frac{1}{4} \phi$ intervals. Grain size parameters were then computed

¹ The symbol ϕ designates units (ϕ units) used in grain size conversions (from mm) for ease of statistical computation. The ϕ scale, devised by Krumbein (1934), is a logarithmic transformation of the Wentworth size scale that is based on a constant ratio of 2 between classes. Hence, the following relationships exist:

ϕ	mm	sediment type
-4.0	16	pebble
-1.0	2.0	boundary between sand and gravel
+1.5	0.35	medium sand
+4.0	0.0625	boundary between sand and silt
+6.0	0.0156	medium silt

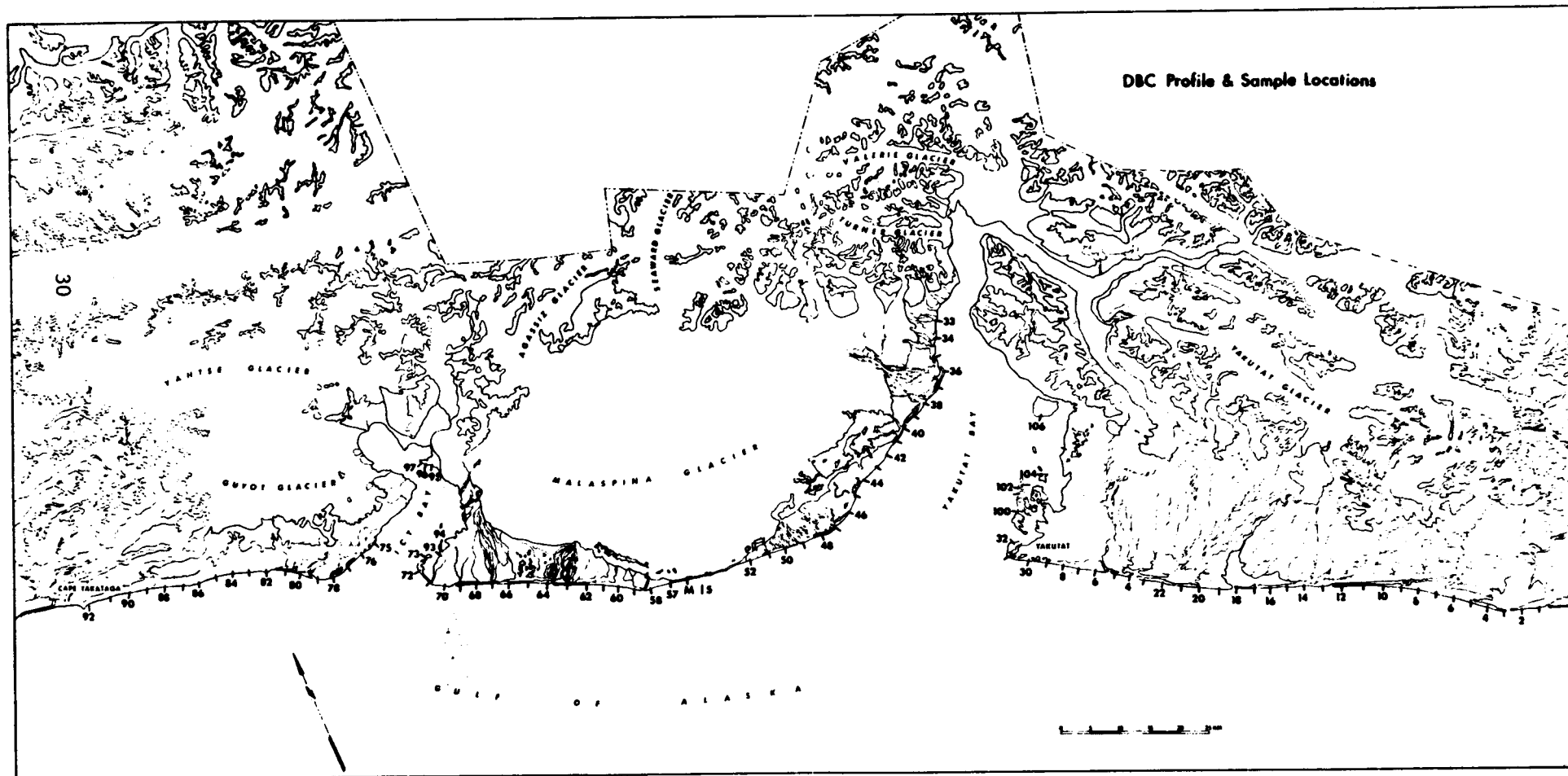


Figure 1. DBC sample sites in the Northern Gulf of Alaska

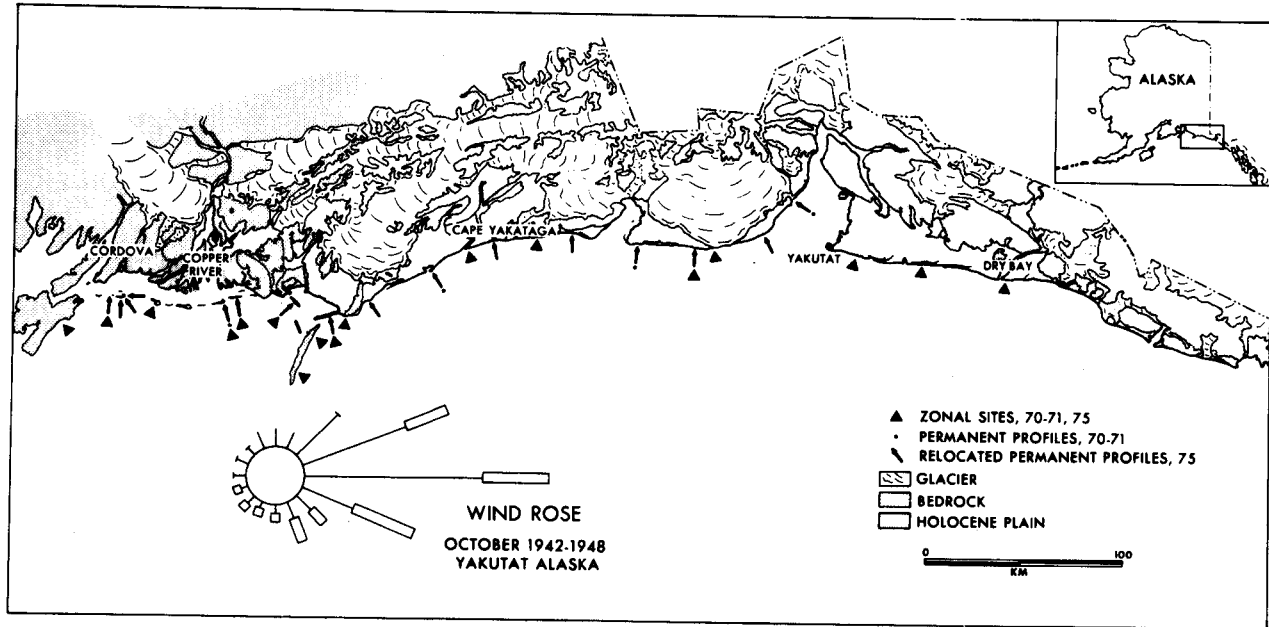


Figure 2. Permanent profile sampling sites in the Northern Gulf of Alaska.

by the method described by Folk (1968). They are as follows:

Graphic mean (Mz)	$\frac{\phi 16 + \phi 50 + \phi 84}{3}$
Inclusive graphic standard deviation	$(\sigma_I) \frac{\phi 84 - \phi 16}{4} + \frac{\phi 95 - \phi 5}{6.6}$
Inclusive graphic skewness (a measure of symmetry of of the grain size distribu- tion)	$\frac{\phi 16 + \phi 84 - 2(\phi 50)}{2(\phi 84 - \phi 16)} + \frac{\phi 5 + \phi 95 - 2(\phi 50)}{2(\phi 95 - \phi 5)}$

The results were synthesized by computer. Mean grain size, standard deviation and skewness for each of the samples is given in Table 1 in the Appendix. Complete sediment data are available on magnetic tapes from NODC (see reference list).

TEXTURE

Introduction

The sediments of the study area vary over an extremely wide grain size range, from large glacial erratics 10's of m in diameter, left behind by retreating glaciers, to silts and clays on tidal flats and marshes. Most of the beaches, however, are composed of mixes of sand and gravel. Sorting, therefore, is usually poor.

1969-1970 Data. - Using the samples collected during the 1969-1970 field seasons, a comparison of the beach sediments of the Copper River delta vs. beaches bordering outwash plains has been made. Figure 4 shows the result of this comparison. Note that the Copper River delta beach sediments are finer and better sorted than those of the beaches bordering outwash streams. Compositional analysis (Fig. 5) indicates a higher percentage of quartz in the Copper River delta beach sediments, although they still plot as litharenites in Folk's (1974) classification (Fig.6). Thus, the Copper River delta beach sediments are considerably more mature, both texturally and compositionally, than the sediments of the beaches bordering outwash streams. The poorest sorting occurs in sediments with a mean grain size between the 0 ϕ and -2 ϕ (Fig. 4). That size is at the midpoint between the two pri-

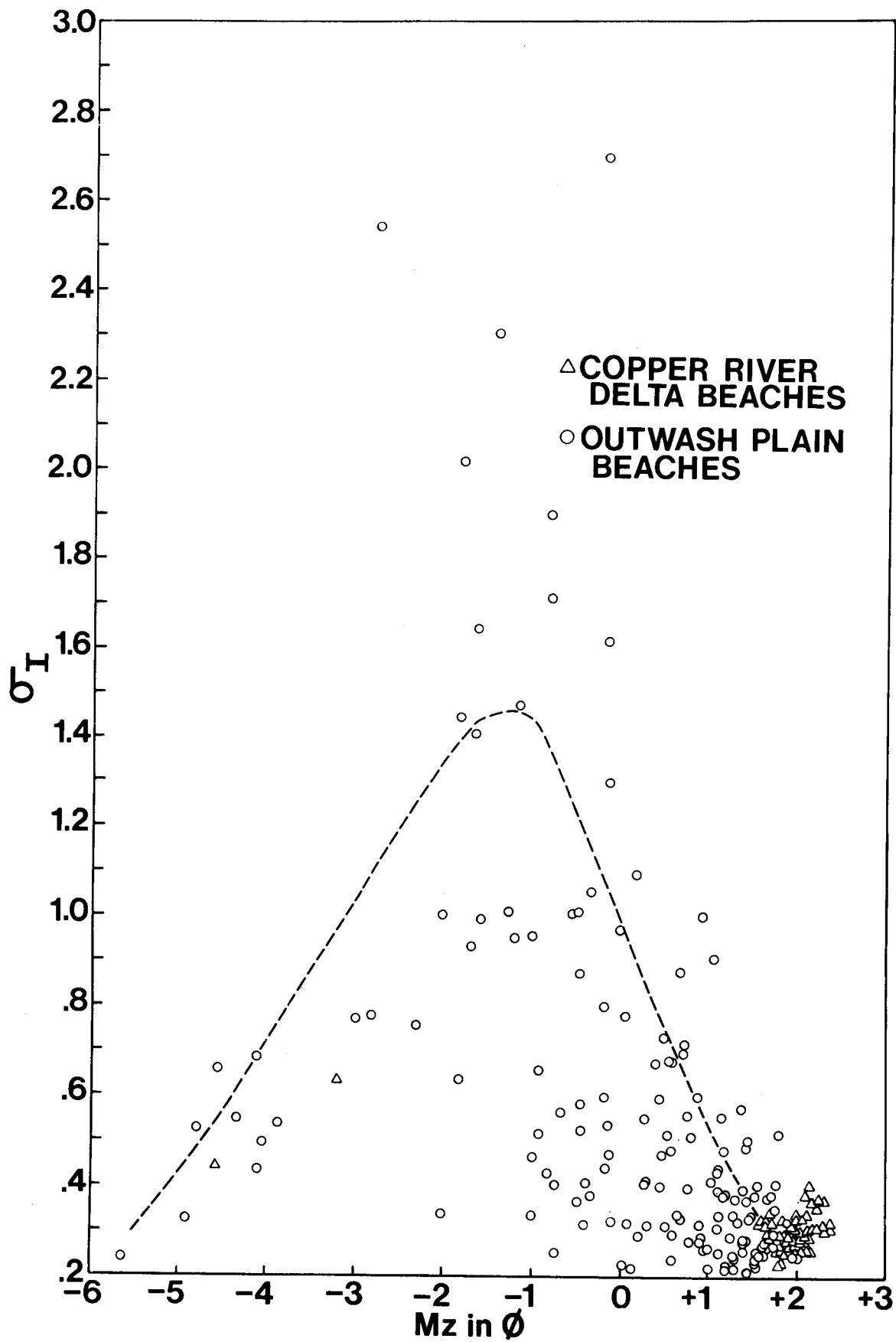


Figure 4. Graph of grain size vs. standard deviation (sorting) for sediment samples collected during 1969-1970 field seasons. Note inverted "v" distribution explained in the text. Also note the finer better sorted nature of the sediments from the Copper River delta beaches.

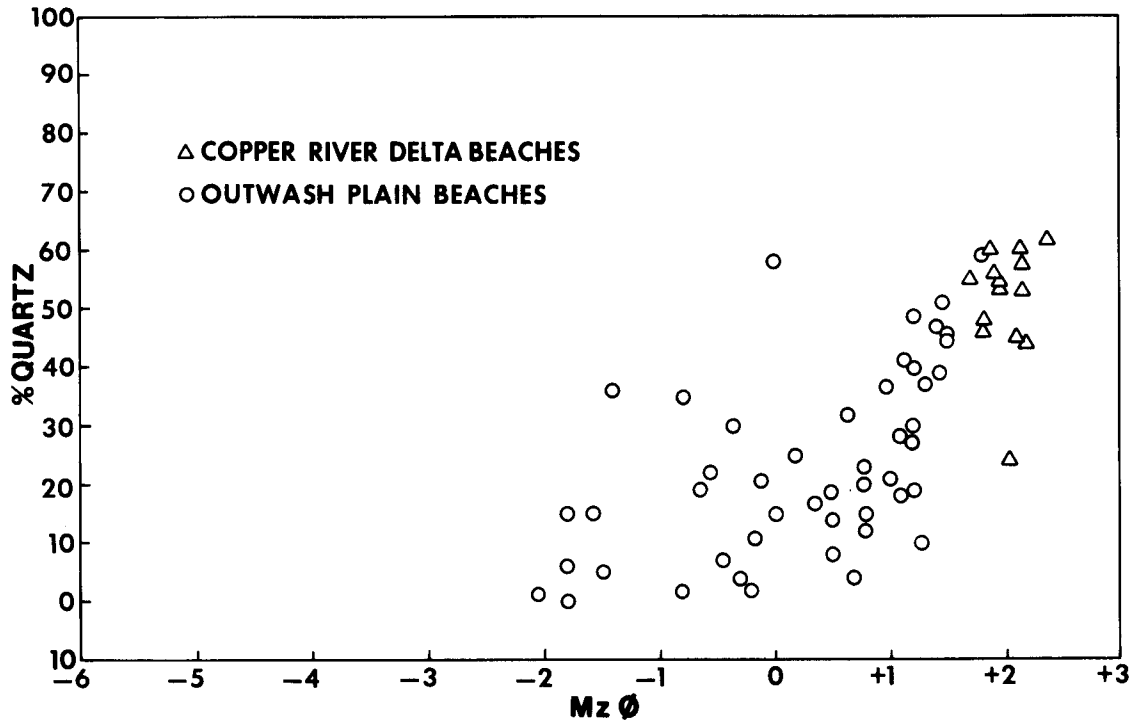


Figure 5. Graph of % quartz vs. grain size for 1969-1970 sediment samples. Note the high quartz % and fine texture of the Copper River delta sediments.

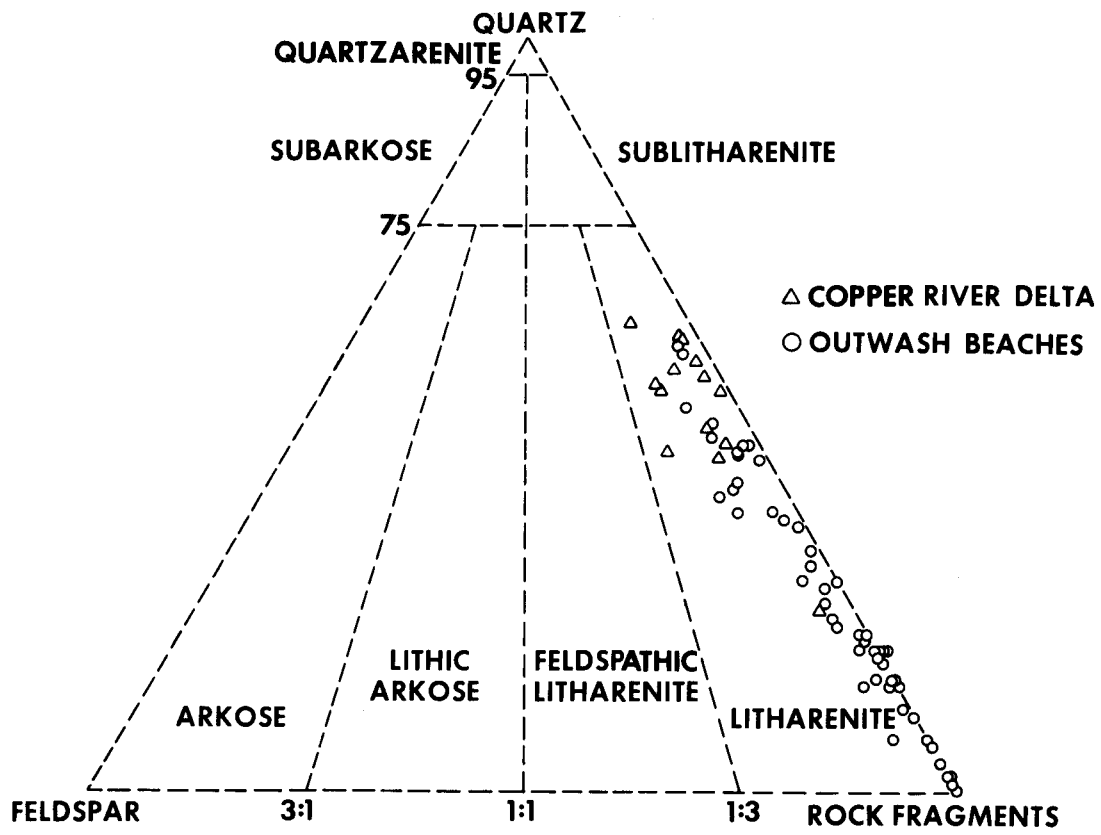


Figure 6. Compositional diagram of the 1969-1970 sediments of the Copper River delta as more quartz rich but still plot as litharenites.

mary grain size modes (sand and gravel) of the sediments of the area. Decreasing the grain size (moving to the right on the diagram) (Fig.4) results in a loss of the coarse mode and thus better sorting. Increasing the grain size (moving to the left on the diagram), results in a loss of the fine mode and thus better sorting. This natural mixing at two modal sizes is a common occurrence and has been well documented in the literature (Folk and Ward, 1957; Folk, 1968). Thus, the inverted "V" distribution shown in Figure 4 conforms with these concepts and should not be considered unusual.

1975 Data (Yakutat Foreland). - During the 1975 field season, over 400 sediment samples were collected at the DBC sites and at the permanent profile sites. The 3 km spacing of the DBC sites permits a more detailed analysis of grain-size parameter changes along the beaches of the study area. Numerous trends are evident.

The 90 km stretch of coast from Dry Bay (DBC-3) to Yakutat Bay (DBC-32) demonstrates some of these trends. A 25-km wide outwash plain, called the Yakutat Foreland, was formed by outwash streams that drained numerous glaciers in the St. Elias Mountains in early to middle Holocene times. The present outwash streams must flow across 25 km of relatively flat topography before reaching the Gulf of Alaska. Much of the coarse sediment transported by these streams is deposited close to their glacial sources. The sediment that does reach the coast, is considerably more mature than it would otherwise have been if the stream sources were close to the coast, as they are on the Malaspina Foreland. Additionally, many of these streams emanate from glacial margin lakes which act as sediment traps. This geomorphic setting results in the supply of relatively fine sediments to the coast. The sediments carried by these rivers at their mouths are primarily sands.

The grain size parameters of the beach sediments of the Yakutat Foreland are graphically represented in Figure 7. Part A shows the relationship between mean grain size and sorting (standard deviation σ_1). The sediments cluster between $+1\phi$ and $+2\phi$ (medium to fine sand) and generally are relatively well sorted. Part B

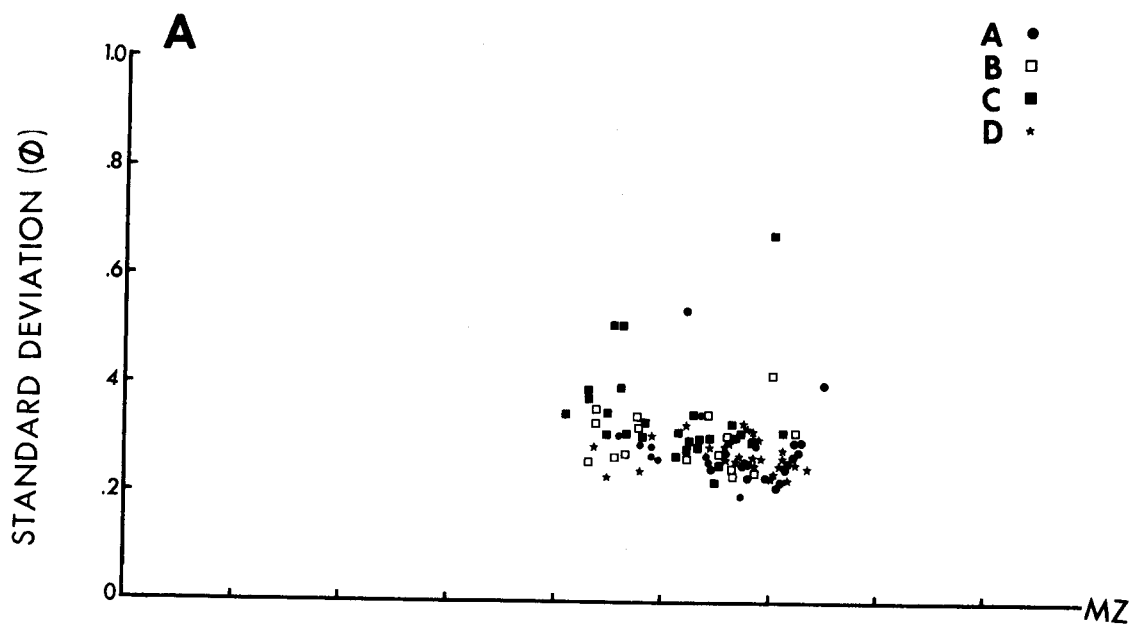


Figure 7 A. Graph of grain size vs. standard deviation (sorting) of sediment samples from the Uakutat Foreland. Note the highly clustered nature of the sediments between the 1.0 and 2.0 ϕ size interval.

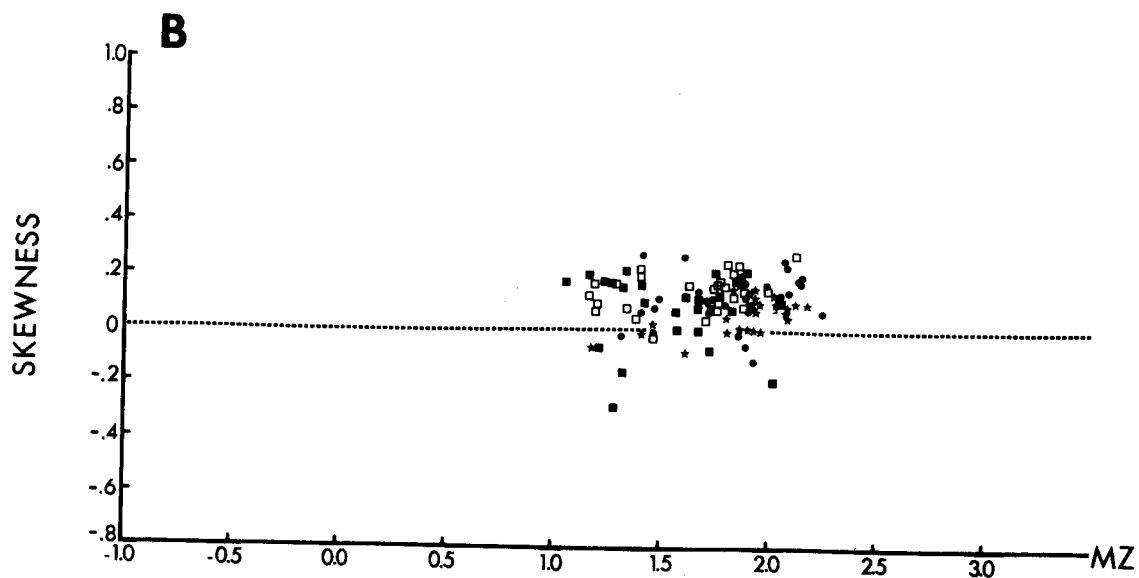


Figure 7 B. Graph of grain size vs. skewness for the sediments from the Yakutat Foreland. The samples are generally positively skewed.

shows the relationship between mean grain size and skewness. The samples are generally positively skewed, indicating the presence of a finer minor size mode. Thus, the sediments in this stretch of coast are relatively mature with regard to grain size parameters. This tends to support the statements made above regarding the outwash stream length.

In order to test a hypothesis that most of the sediment supplied to this area is derived from the Alsek River, which empties into Dry Bay, grain size parameters were graphed against increasing distance downdrift (west) of Dry Bay. Since drift is to the west, we would expect a maturing of sediments in that direction. Figure 8 shows the relationship between the mean grain size of each A, B, C, and D sample with increasing distance from Dry Bay. There is a general reduction in grain size along this 90 km shoreline. Sample A is consistently finer than either B or C samples. The A sample is taken from high on the beach face at about the location of the storm berm. As can be seen in Figure 8, the A and D samples are similar in size, both being finer than the B and C samples taken from the mid and lower beach face respectively.

The considerable scatter evident in Fig. 8 made it difficult to determine what was taking place at the numerous river inlets on this shoreline. In order to get a clearer picture of grain size variation across these inlets, the cumulative frequency graphs (plotted by computer) were analyzed for grain size modes. Major modes were defined as those containing 10% or more of the distribution. Minor modes were picked out visually from the curves. The results of this modal analysis are given in Table 2 in the Appendix. Figure 9 shows the relationship of the grain size of the major modes versus distance from Dry Bay. Since the modes were defined at $\frac{1}{2}\phi$ intervals, there is less scatter in the distribution. Note that A and D samples are again finer than B and C samples. Also, there is considerable stability in the modal grain size of the B sample over distance. By following the B sample, one can see that most of the variation occurs at the inlets. There is a prominent fining across the Akwe River inlet, indicating that it is acting as a supplier of

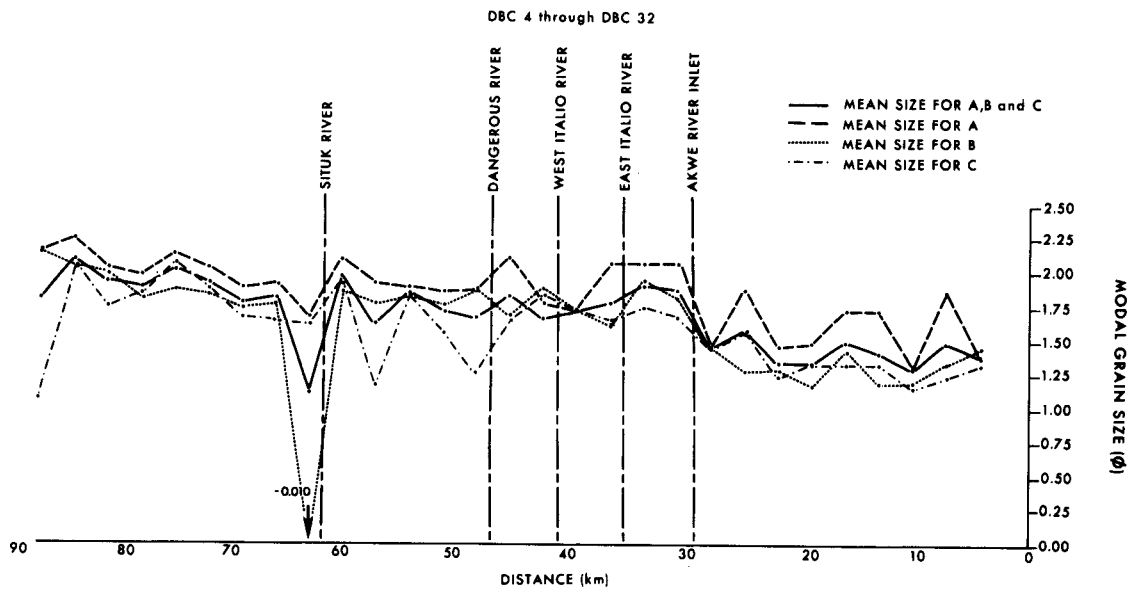
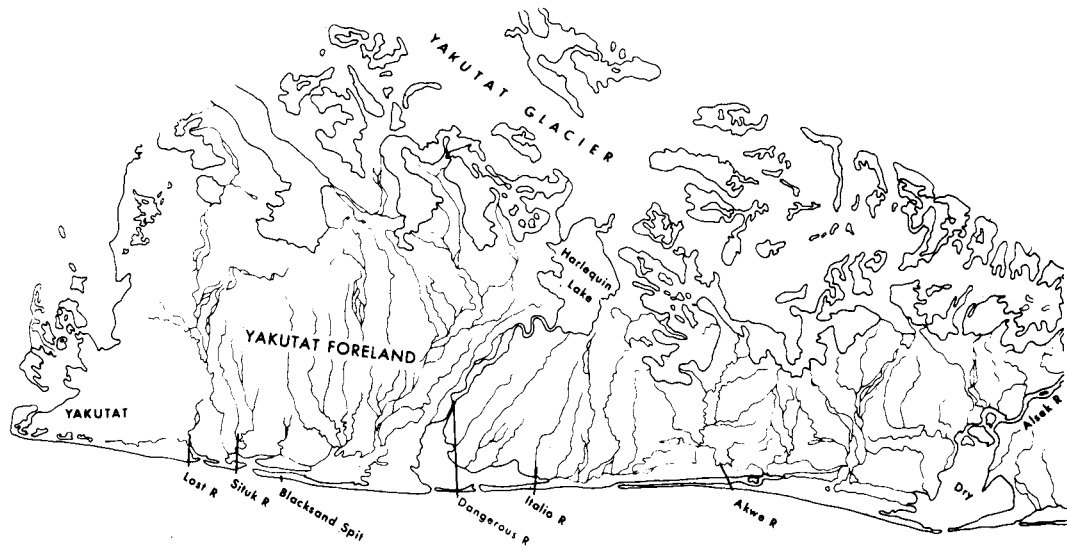


Figure 8. Graph of the mean grain size of Yakutat Foreland samples vs. distance downdrift of Dry Bay. Note that the sediments fine in the downdrift direction.

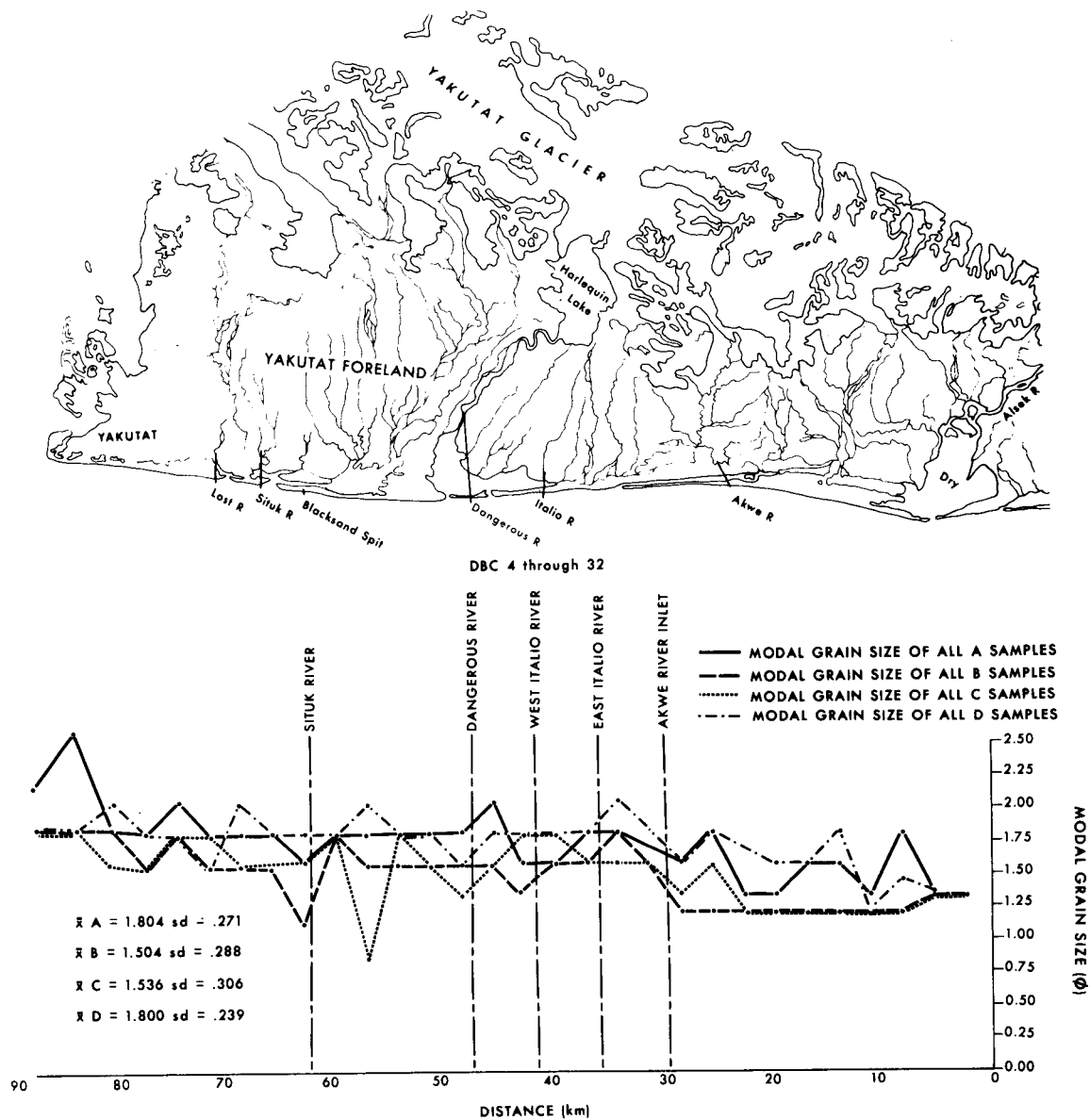


Figure 9. Graph of modal grain size of Yakutat Foreland samples vs. distance downdrift of Dry Bay. Samples show a fining tendency in the downdrift direction.

fine sediment or as a sorting mechanism to eliminate more coarse sediments. Each of the other inlets demonstrate a fine updrift side and a coarser downdrift side, indicating the input of a minor coarse mode. With this in mind, it would seem likely that the Akwe River inlet is sorting out the finer sediments from updrift rather than introducing them itself. This would agree with studies at tidal inlets done by Winkelmoelen and Veestra (1974). Here again, the overall picture is a gradual reduction in grain size from Dry Bay to Yakutat Bay, with the B sample being a more stable indicator than the others.

We have considered taking only one beach face sample on future field studies; thus, we wanted to test the B sample to see how it represented the grain size range on the beaches. Figure 10 shows the modal grain size of the B samples compared to the mean of the modal grain sizes of A, C and D samples. The B sample is generally about 0.2 ϕ coarser than the mean of the A, C and D samples. This is primarily the result of the fine nature of the A and D samples. It follows rather closely the trend of the A, C and D samples and is considered to be the best single sample to use for this type of study.

Finally, a comparison of the D sample taken from dunes located behind the beach face was made with the A, B and C samples taken from the active beach face. Figure 11 shows the result of comparing the major modal grain size of D samples with the mean of the major modal grain size of the A, B and C samples. It is clearly evident that the beach sediments are coarser than the dune sands. This is a well known phenomenon.

Sorting has been used previously by the Coastal Research Division to delineate transport trends (Nummedal et al., 1974). Figure 12 displays the sorting of the A, B, C and D samples graphed against distance from Dry Bay. Unfortunately, no clear trend is evident from this graph. Calculating the mean sorting of A, B, C and D samples taken together and then plotting that on the same X axis, Figure 13 still shows no clear trend from Dry Bay to Yakutat Bay. However, the graph does show an interesting tendency for the sediments to be more poorly sorted on the

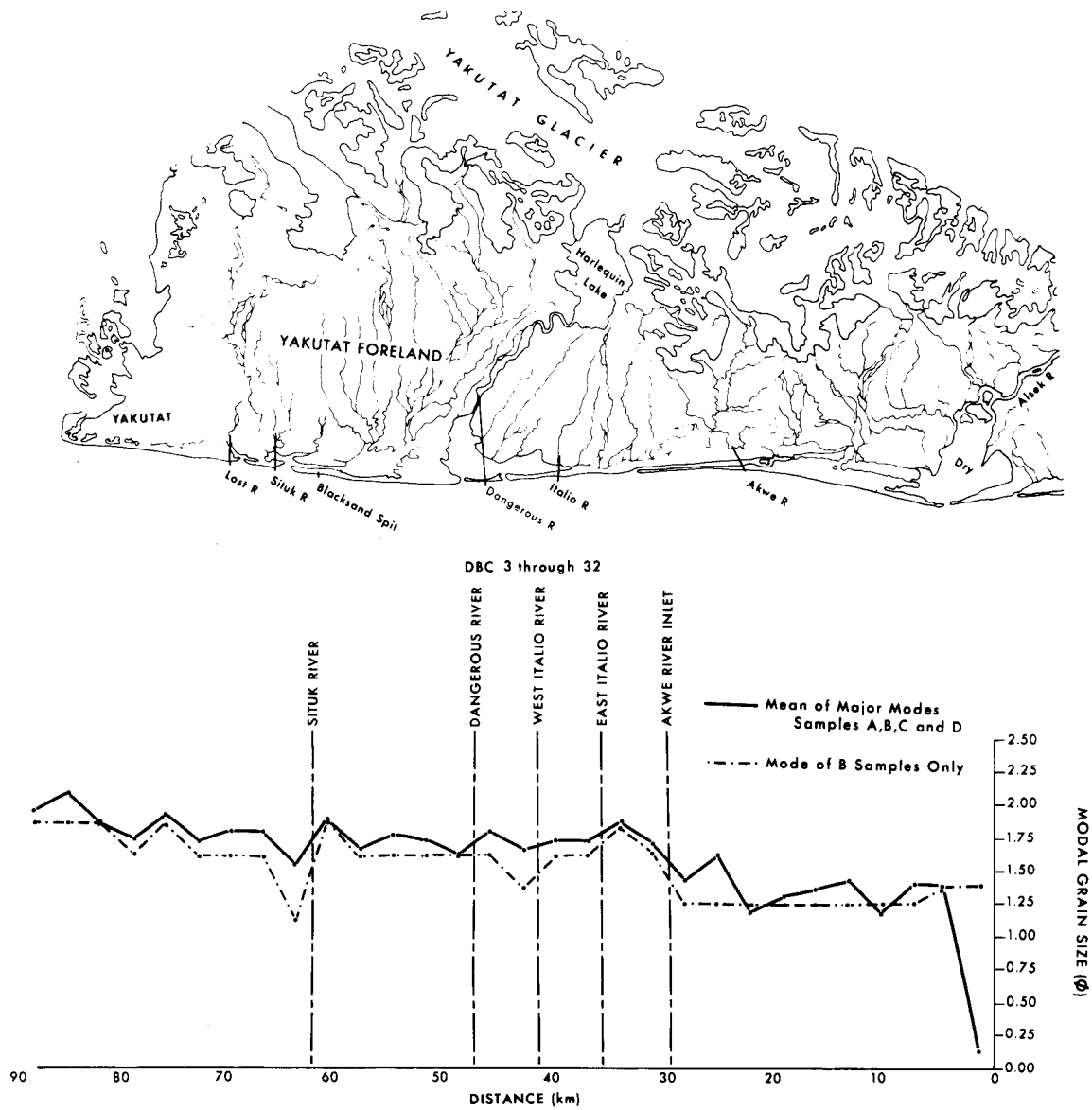


Figure 10. Graph of the modal grain size of "B" samples, and the mean of the modal grain sizes of A, C, and D samples vs. distance downdrift of Dry Bay. The "B" sample is generally slightly finer than the mean of the A, C and D samples. It is also a more stable indicator.

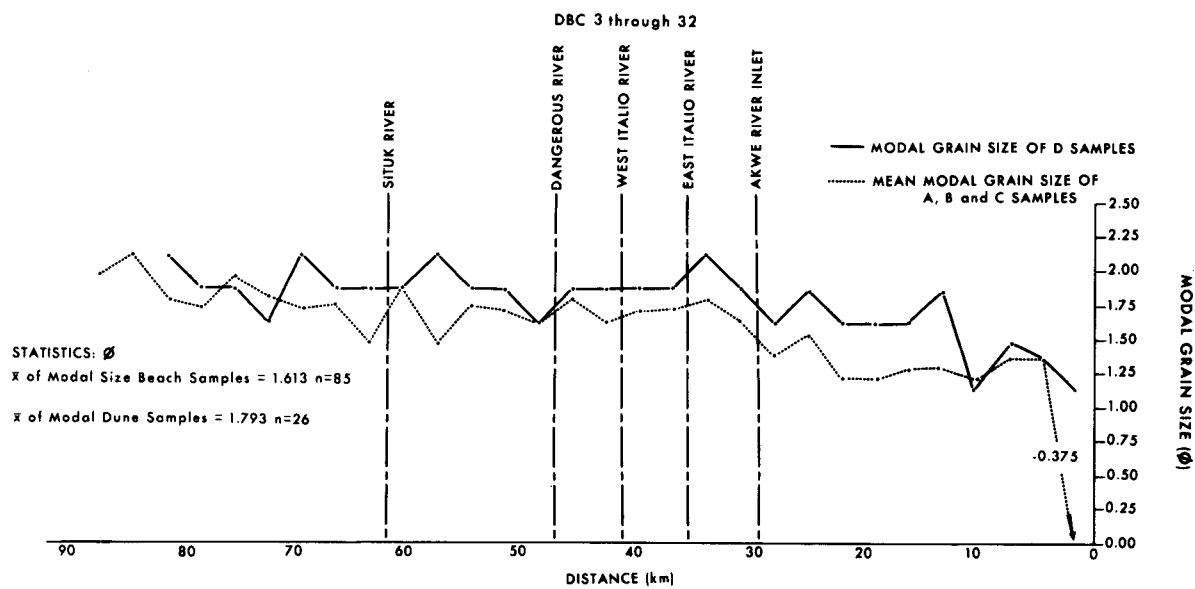
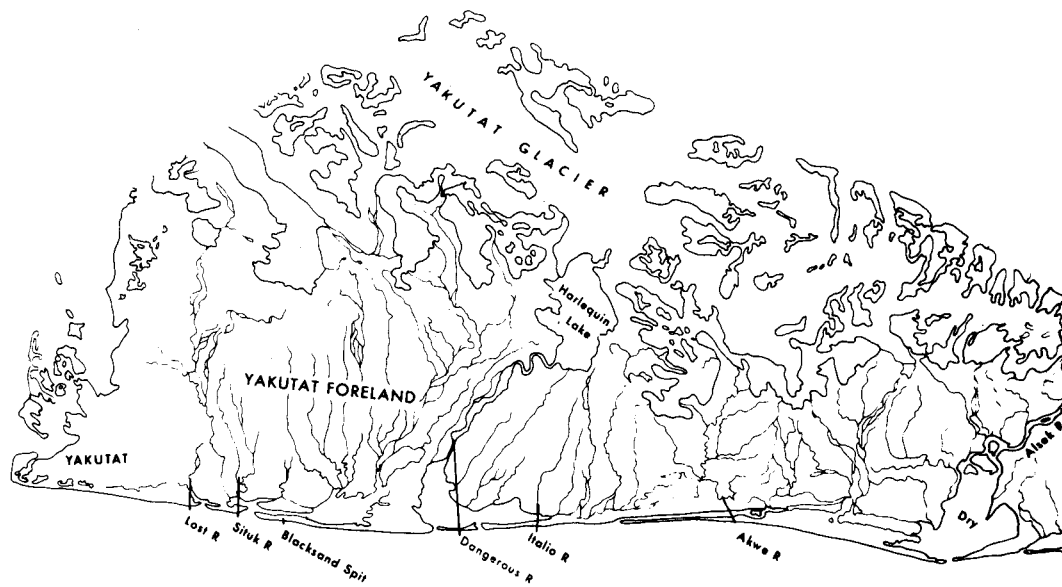


Figure 11. Graph of modal grain size of "D" samples and the mean of the modal grain size of A, B, and C samples vs. distance downdrift of Dry Bay. The "D" sample is consistently finer than the A, B, and C sample means.

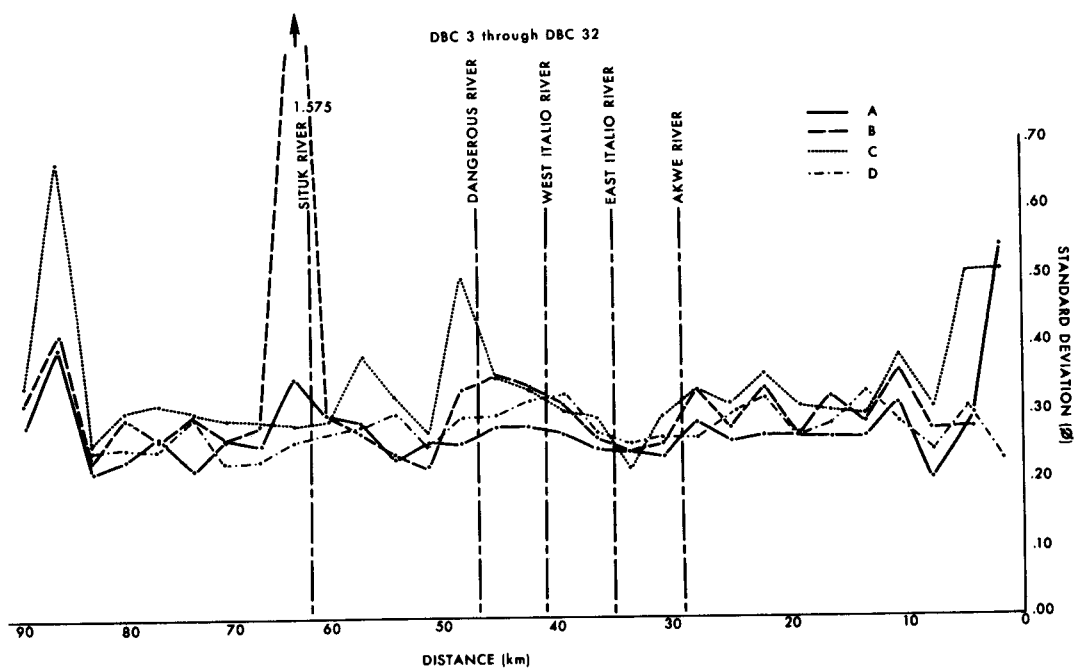
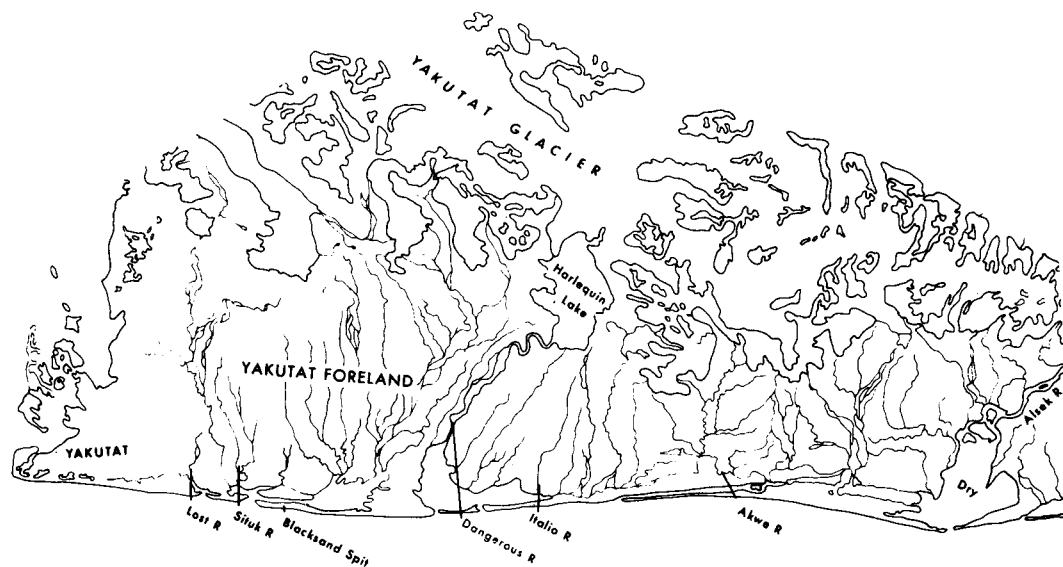


Figure 12. Graph of the standard deviation (sorting) of the Yakutat Foreland samples vs. distance downdrift of Dry Bay. No clear trend is evident; however, most variation occurs at river inlets.

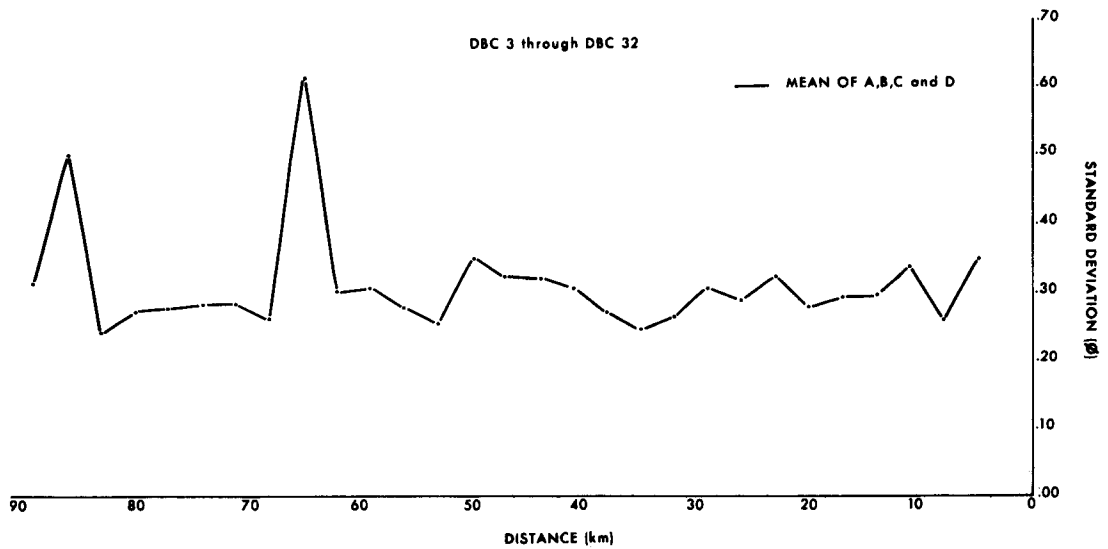
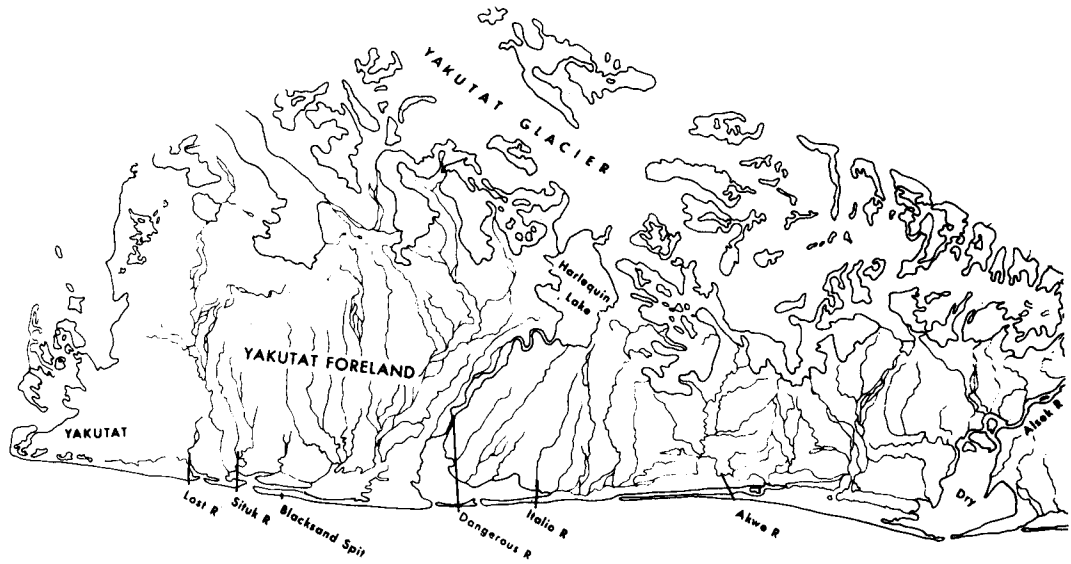


Figure 13. Graph of the mean sorting of A, B, C and D samples vs. distance downdrift of Dry Bay. No clear trend is evident.

downdrift side of the river inlets. This tends to support the hypothesis that the rivers are transporting a slightly coarser minor grain size mode, discussed earlier in this section.

In summary, grain size parameters can be used to delineate sediment transport trends. Even on a coastline, such as the one between Dry Bay and Yakutat Bay, interrupted by numerous rivers, classic concepts relating to sediment maturing can be detailed with careful laboratory analysis of the sediments.

1975 Data (Yana River to Riou Spit). - A second section of shoreline, between the Yana River Spit and Riou Spit in Icy Bay (Fig. 1) was selected to do a visual grain size analysis. This 32 km shoreline was divided into 32 sample sites located at a one km interval. At each site, the active beach face was subdivided into 8 equal sections, and a sample was taken from the center of each section. Thus, a total of 256 samples were analyzed, using a $\frac{1}{4}\phi$ interval hand-held visual size estimator. Sorting, gravel size, and % gravel were also analyzed visually for each sample. Figure 14 graphically displays some of the results of that study. The sections at the top, bottom, and midpoint of the beach were selected for this graph. The mean of the three samples has been used in the plots. A number of trends are evident.

The inflection point on Riou Spit (where it turns 90° into Icy Bay) is acting as a sediment sorting locus. Note that the sand grain size at that point is the coarsest on the graph. Also, the % gravel is high, although the relative gravel grain size (calculated visually on a scale from 1 to 7 ranging from granule to cobbles) is rather fine. From that point to the end of the spit (downdrift), the sand size decreases, as does the % gravel. This conforms to the general rule of sediment fining in the direction of dominant sediment transport. The gravel grain size increases, however, due to a glacial platform underlying the spit near its downdrift end. This glacial till platform has formed a boulder and cobble low-tide terrace over which the spit is prograding. Thus, the inflection point is acting to sort out coarser grain sizes (gravels and coarse sands) while bypassing

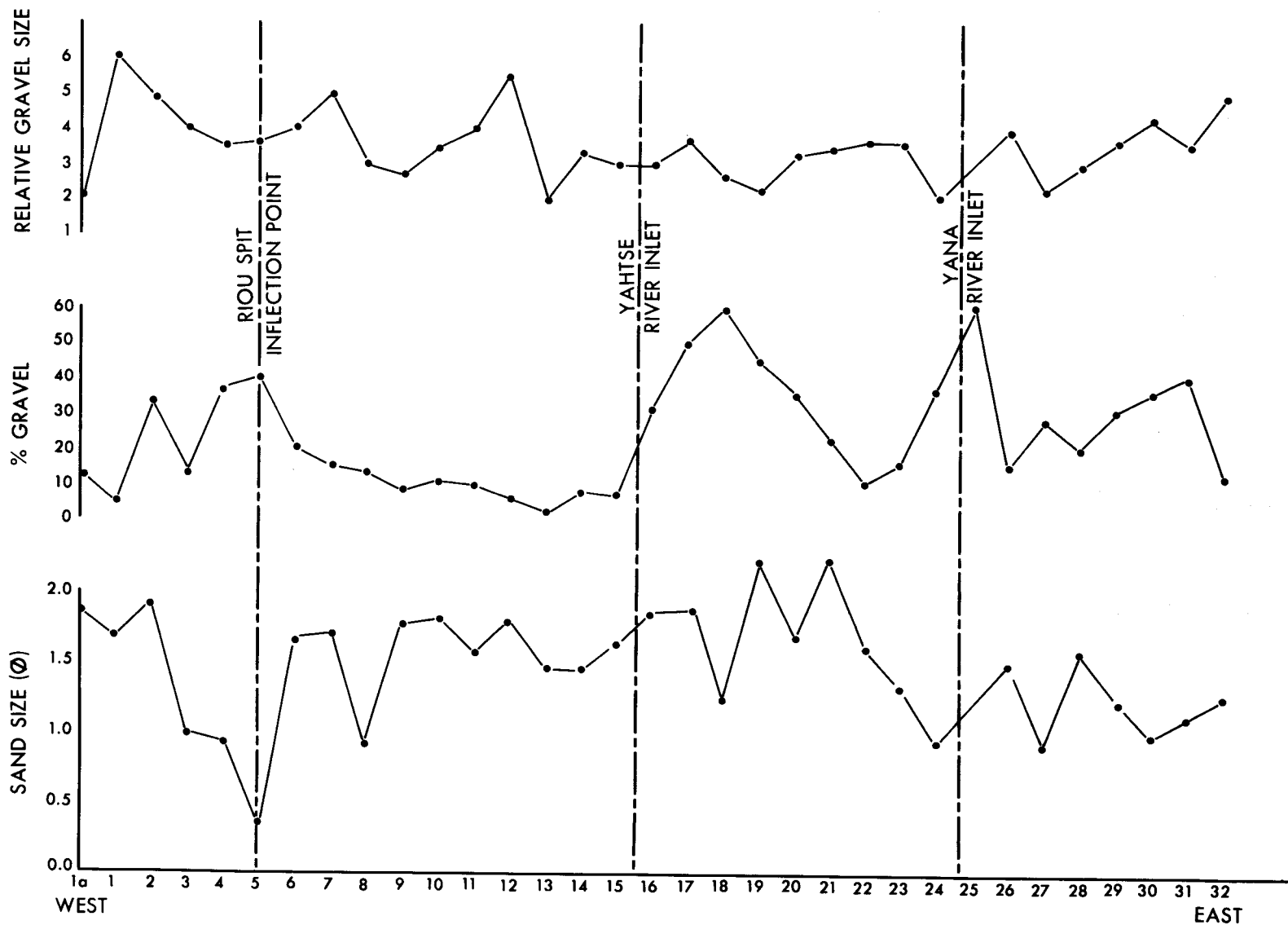


Figure 14. The parameters of sand grain size, % gravel, and relative gravel grain size are graphed vs. distance on the West Malaspina Foreland. Stations on the "x" axis are 1 km apart. Trends are explained in the text.

the finer sediments. At the inflection point, the spit is prograding into deeper water (Nummedal and Stephen, 1976). Much of the sediment moving along the spit is deposited here, including the vast majority of the coarser sediments. However, the progradation of this particular portion of the Riou Spit acts to shelter the glacial platform behind it. This sheltering results in considerably smaller waves which are, therefore, only capable of carrying the finer sediments. Thus, the spit is also prograding into the bay, over the platform, by the addition of fine sand.

Another trend, evident from Figure 14, is a pronounced deposition of gravels at the updrift (east) side of the river inlets. In conjunction with this trend is a coarsening of the sand grain size from the updrift to the downdrift side of the inlets. This agrees with the trends on the Yakutat Foreland.

Finally, the means of the grain size parameters for each section from the top to the bottom of the beach were calculated. Figure 15 shows that the % gravel increases as the toe of the beach is approached. This is the result of the increased exposure of the lower parts of the beach face to wave action. Relatively large waves are required to move the gravels. Thus, most of the gravel is moving at the base of the beach while the sand fraction is moving throughout the beach face. The sand size graph in Figure 15 also shows a sharp increase in sand size at the base of the beach face, probably the result of the same process.

1975 Data (Malaspina Foreland). - A final grain size trend analysis was done on the Malaspina Foreland. This area is dominated by the Malaspina Glacier, which is drained by a number of very active glacial outwash streams with sources close to the shoreline. It contrasts well with the Yakutat Foreland. Fifteen sites were sampled either visually (for very coarse sediments) or using standard sieving techniques. Figure 16 graphically displays the results of this analysis. The graph shows the mean of A, B, and C samples taken at the 15 sites in 1970 (Hayes et al., 1970). It is immediately obvious that there is a fining of sediments both to the east and to the west of Sitkagi Bluffs. In their earlier report,

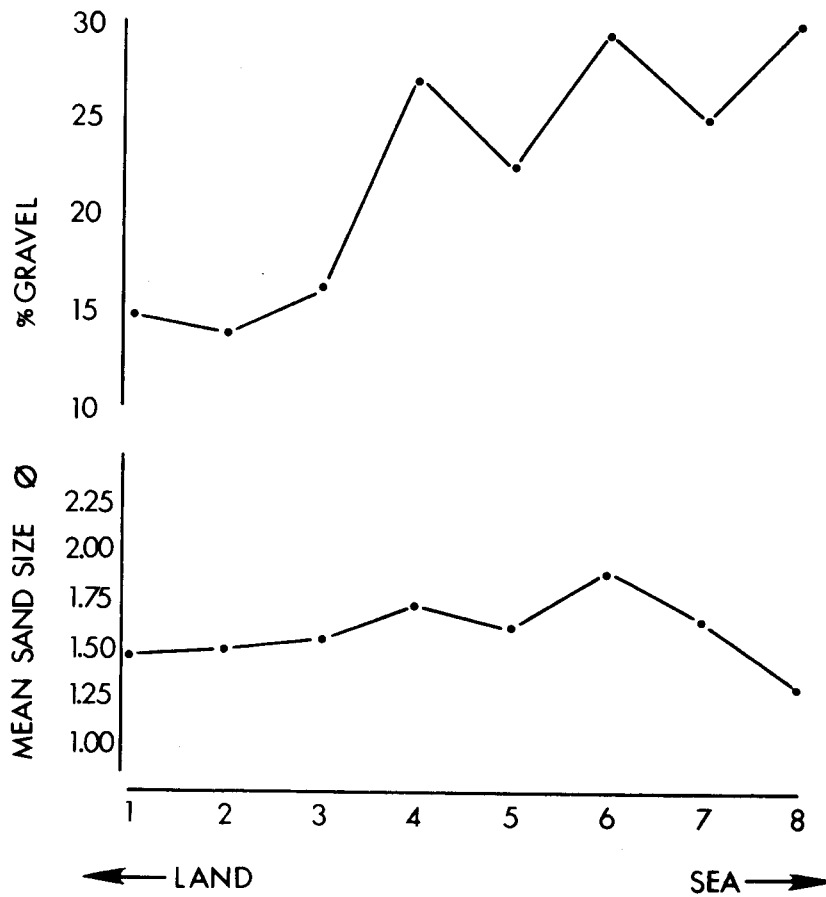


Figure 15. Graph of % gravel and sand size vs. position of beach face. Gravel % increases and sand size increases as the toe of the beach is approached.

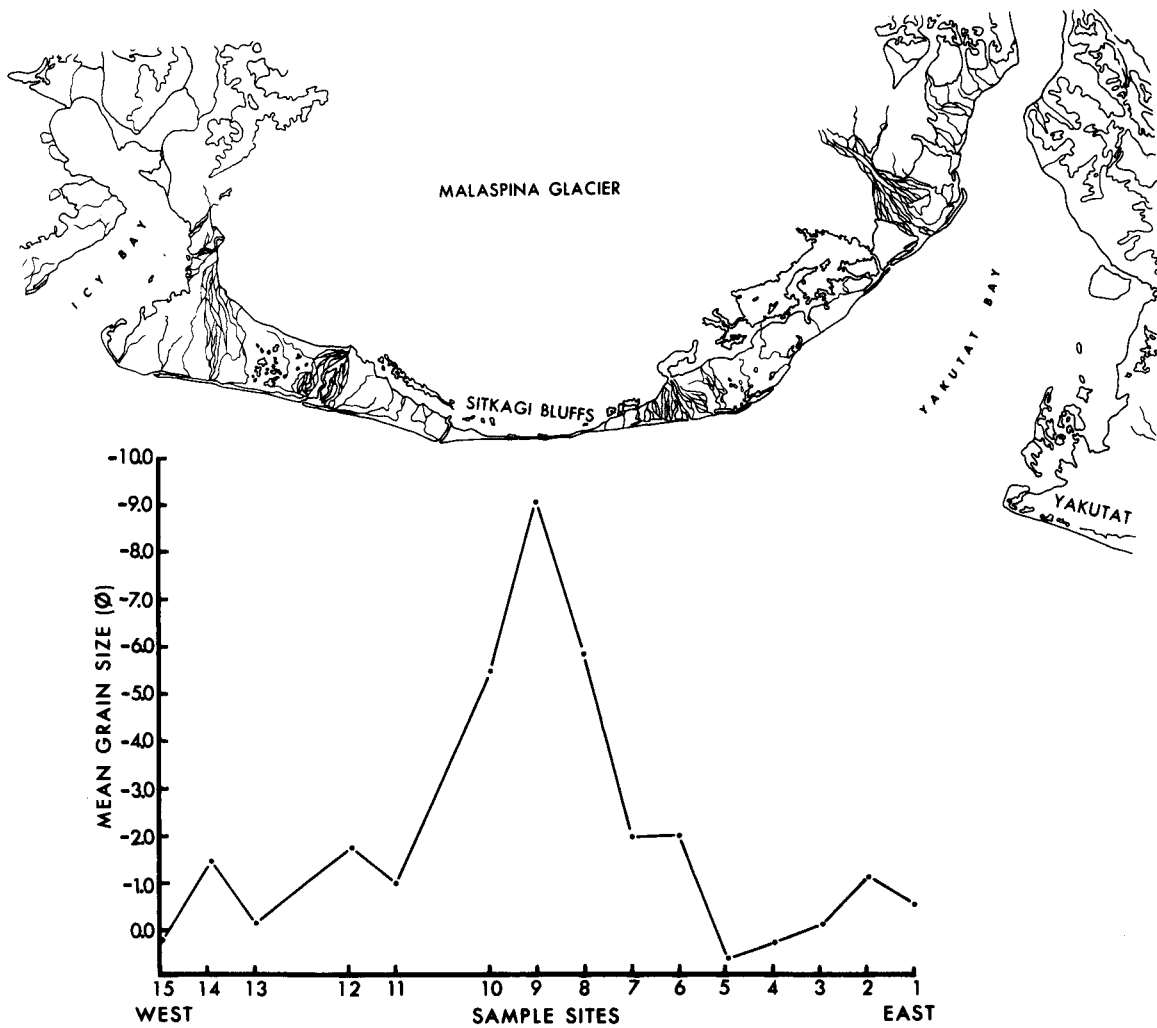


Figure 16. Graph of sediment grain size vs. position on the Malaspina Foreland. Note the fining trends to the east and west of Sitkagi Bluffs, a nodal point for sediment transport.

Nummedal and Stephen (1976) indicated that the bluffs are located at a point for transport direction. Sediments are transported both east and west from that area. Figure 16 supports that concept completely. Each of the other peaks on the graph coincides with an outwash stream outlet. These outwash systems are carrying abundant gravels, as indicated by the graph.

Discussion. - The three separate areas described above demonstrate that sediment grain size analysis can be useful in determining sediment transport trends in radically different geomorphic areas. These studies can be used to verify geomorphic indicators of transport trends as well as calculated trends using marine process parameters.

The shoreline from Cape Yakataga to Dry Bay (DBC-series area, Fig. 1) has been sub-divided into three separate areas for further discussion.

- 1) Cape Yakataga to Icy Cape (DBC-92 through DBC-80).
- 2) Pt. Riou to Grand Wash (DBC-68 through DBC-33).
- 3) Yakutat Bay to Dry Bay (DBC-32 through DBC-1).

For each of these areas, the A, B, C and D sample major and minor grain size modes were calculated and graphed. The results are shown in Figure 17. The areas are easily separated from one another using this method.

In Figure 17A, the graph for the Yakutat Foreland area, the sediments are clustered very tightly around the 1.0ϕ to 2.0ϕ size. There are few minor modes and more than $\frac{1}{2}$ of them are fine. This agrees with the positive skewness displayed in Figure 7. This is very close to a mono-modal distribution. This is to be expected, given the relatively constant sediment source for the area.

In Figure 17B, the graph for the Malaspina Foreland area, the sediments are far more varied with major modes occurring over the range from -3.5ϕ to $+3.0\phi$. Minor modes display even more range of grain size. This distribution is polymodal with medium sand and fine gravel making up most of the distribution. This is to be expected across the Malaspina Foreland because of the active outwash streams carrying an abundance of mixed sand and gravel modes.

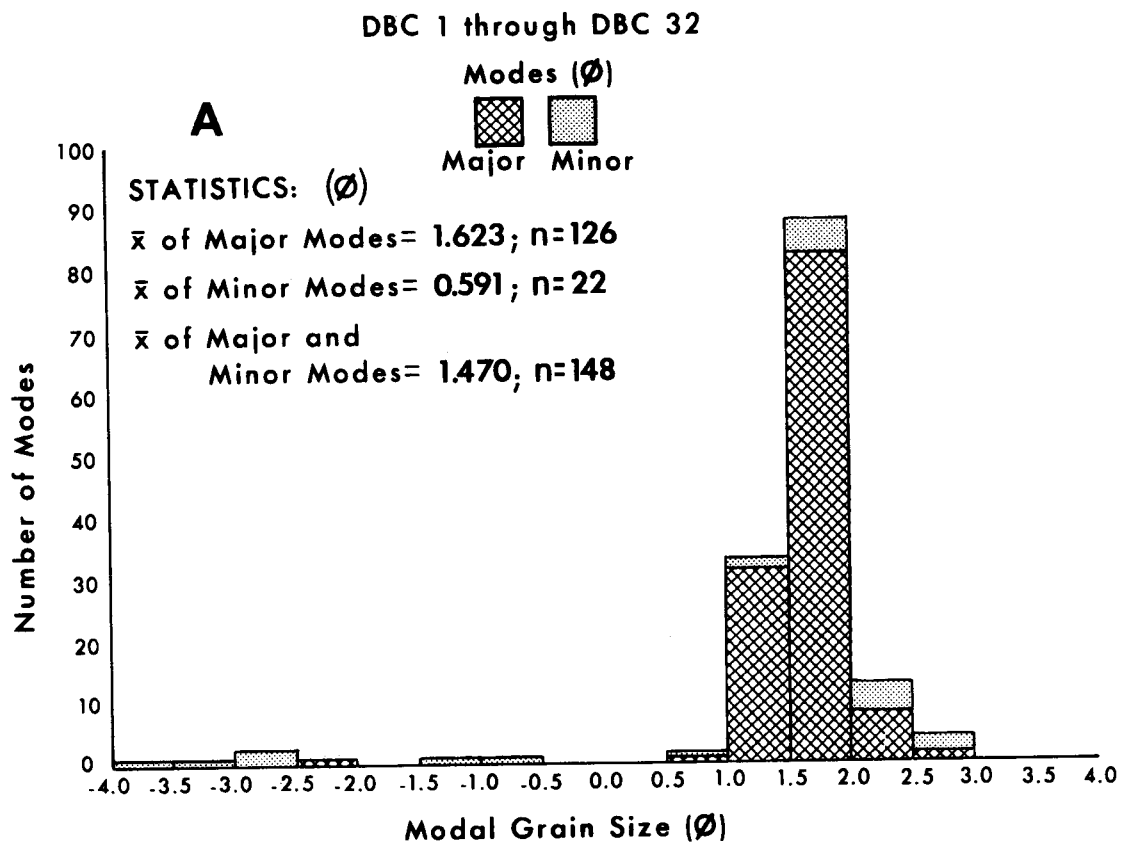
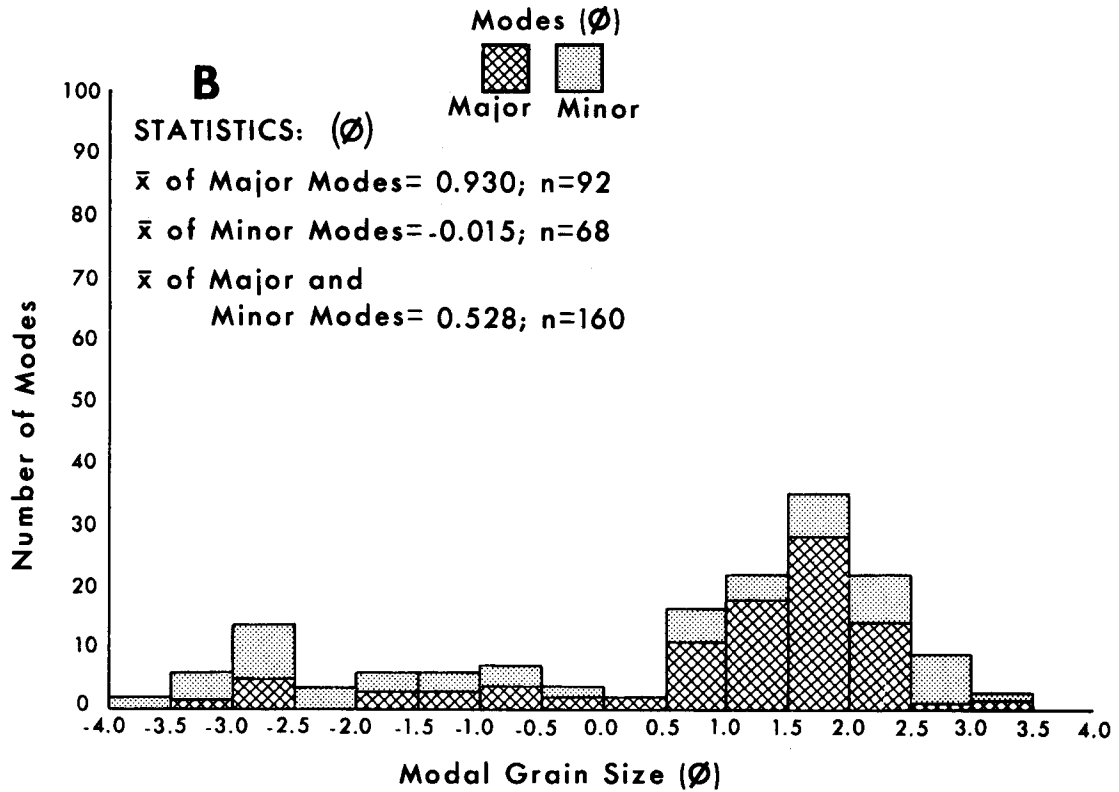


Figure 17. A. Modal grain size analysis of samples from the Yakutat Foreland. Note the bimodal nature of these sediments.

B. Modal grain size analysis of samples from the Malaspina Foreland. These samples are bimodal with a fine and coarse mode.

C. Modal grain size analysis of samples from the Yakataga - Icy Cape area. These show a highly polymodal distribution.

DBC33 through DBC 68



DBC80 through DBC92

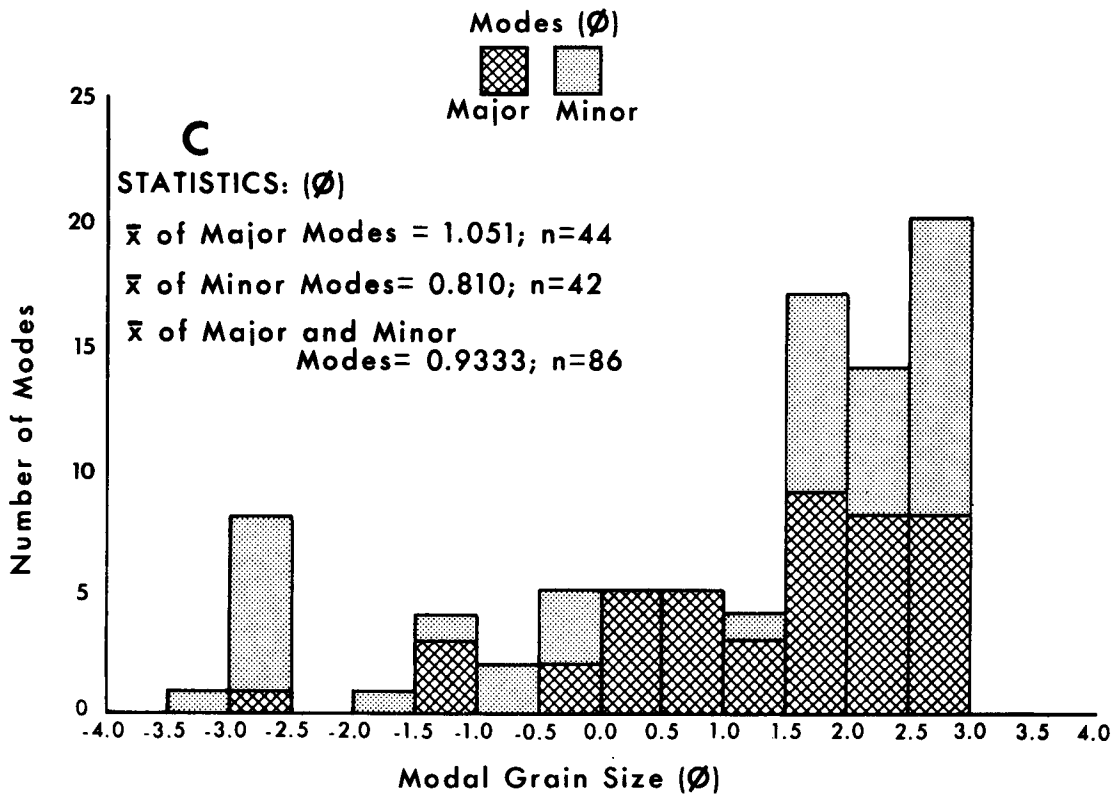


Figure 17C, the graph for the area between Icy Cape and Cape Yakataga, displays another polymodal distribution. There are almost as many minor modes as there are major modes. There are a number of active outwash streams within the area supplying coarse sediment to the system, resulting in the coarse mode. There are also areas where the beach is eroding into older beach ridge plains, thus reworking sediments, resulting in a fine sand mode. Figure 18 shows the relationship between the mean grain size of the DBC-79 through DBC-92 samples and the sorting of those samples as well as their skewness.

Thus, Figure 17 demonstrates that these areas can be distinguished from one another on the basis of grain size. The variability of the grain size is primarily a function of recent glacial history, present glacial position and drainage characteristics.

COMPOSITION

During the 1969-1970 field studies, a sample network was set up from Hinchinbrook Island to Dry Bay. At these sites, samples were taken from the middle of the beach face. These samples were later analyzed for composition. Composition was determined by analyzing 100 grains randomly selected and placing them in one of five categories:

- 1) Feldspar
- 2) Quartz
- 3) Rock fragments
- 4) Mica
- 5) Opaque heavy minerals.

The results of this analysis are given in Table 3 in the Appendix.

The sample sites have been divided into 5 separate provinces based on relatively similar geomorphic and physical process settings. They are as follows:

- 1) Copper River Delta Province: all barrier islands forming the delta as well as the spit on the east side of Hinchinbrook Island.
- 2) Controller Bay Province: Katak Island and Okalee Spit.

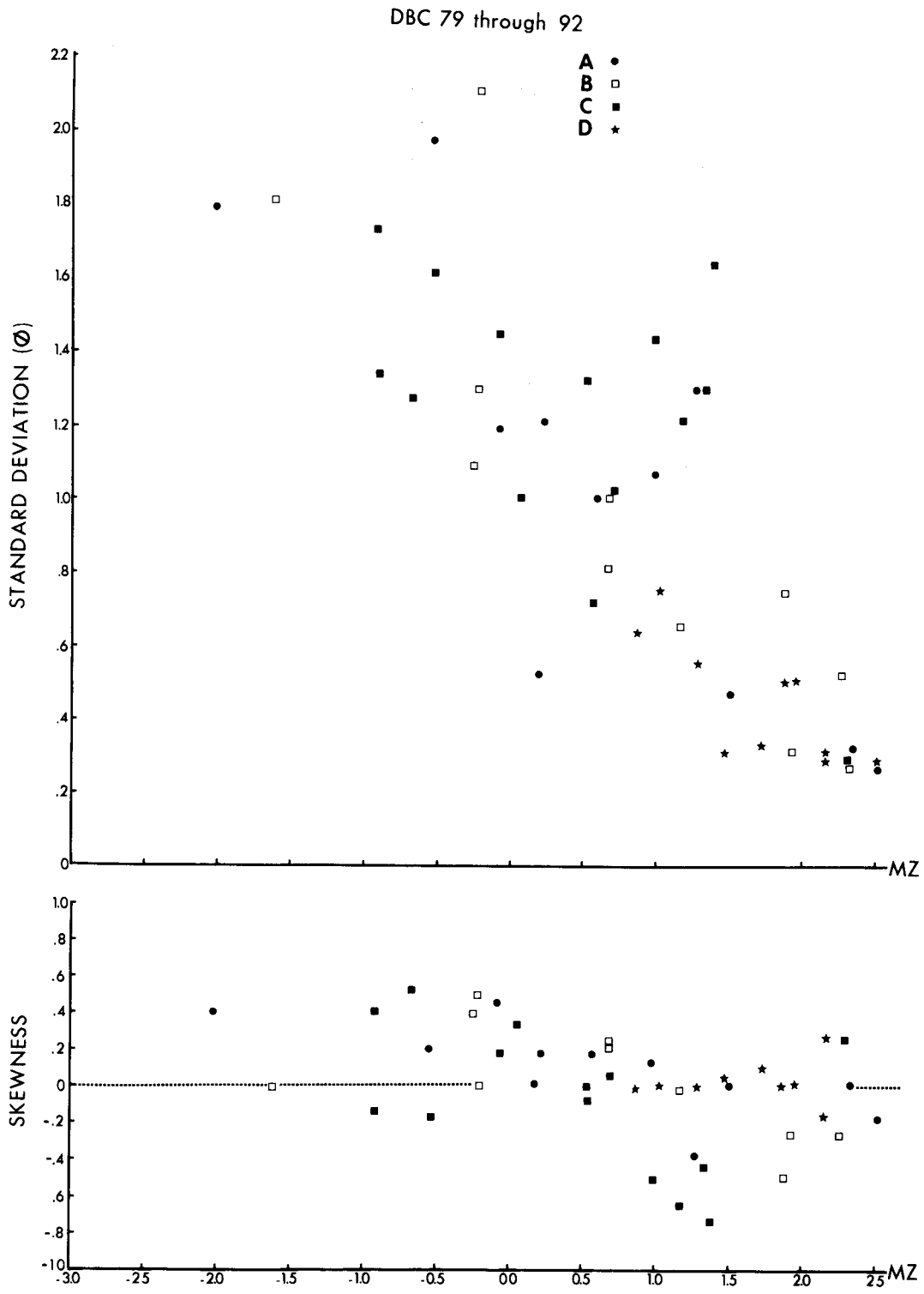


Figure 18. Graph of grain size vs. skewness and sorting for samples from the Yakataga - Icy Cape area. These samples show a high degree of variability in size and skewness.

3) Bering Foreland-Robinson Mountain Province: From Cape Suckling to Icy Bay.

4) Malaspina Foreland Province: All beaches bordering the Malaspina Glacier.

5) Yakutat Foreland Province: From Yakutat Bay to Dry Bay.

The results of the compositional analysis are given in Figure 19. This diagram is a modification from Folk (1974), using Pettijohn's (1975) maturity and provenance indexes. In this diagram, the relative percentages of quartz, feldspar, and rock fragments are used. The relative percentage of quartz to the combined feldspar and rock fragment percentage is called the maturity index.* The relative percentage of feldspar to rock fragments is called the provenance index (the lack of feldspar in these samples rendered this index non-discriminatory). It is obvious from the diagram that the provinces have distinct compositional suites.

The Copper River delta province sediments, as indicated in an earlier section, have a higher percentage of quartz than the sediments from other provinces, thus giving them a higher maturity index. They are all very similar compositionally. The Controller Bay province sediments are slightly less mature. The sediments of the Yakutat Foreland province contain still less quartz and are thus less mature than either the Copper River or Controller Bay sediments. They also show considerable variability. Using the maturity index, plotted against distance downdrift of Dry Bay, they were tested to see if they would follow the same maturing patterns demonstrated by the grain size data. Figure 20 shows the results. Note the increase in the maturity index with greater distance from Dry Bay. This agrees perfectly with the grain size trends given previously in this section. Finally, referring back to Figure 19, the Bering Glacier-Robinson Mountain sediments and the Malaspina Foreland sediments appear to have a strong compositional similarity.

* Table 4 in the Appendix presents the maturity indices for these samples.

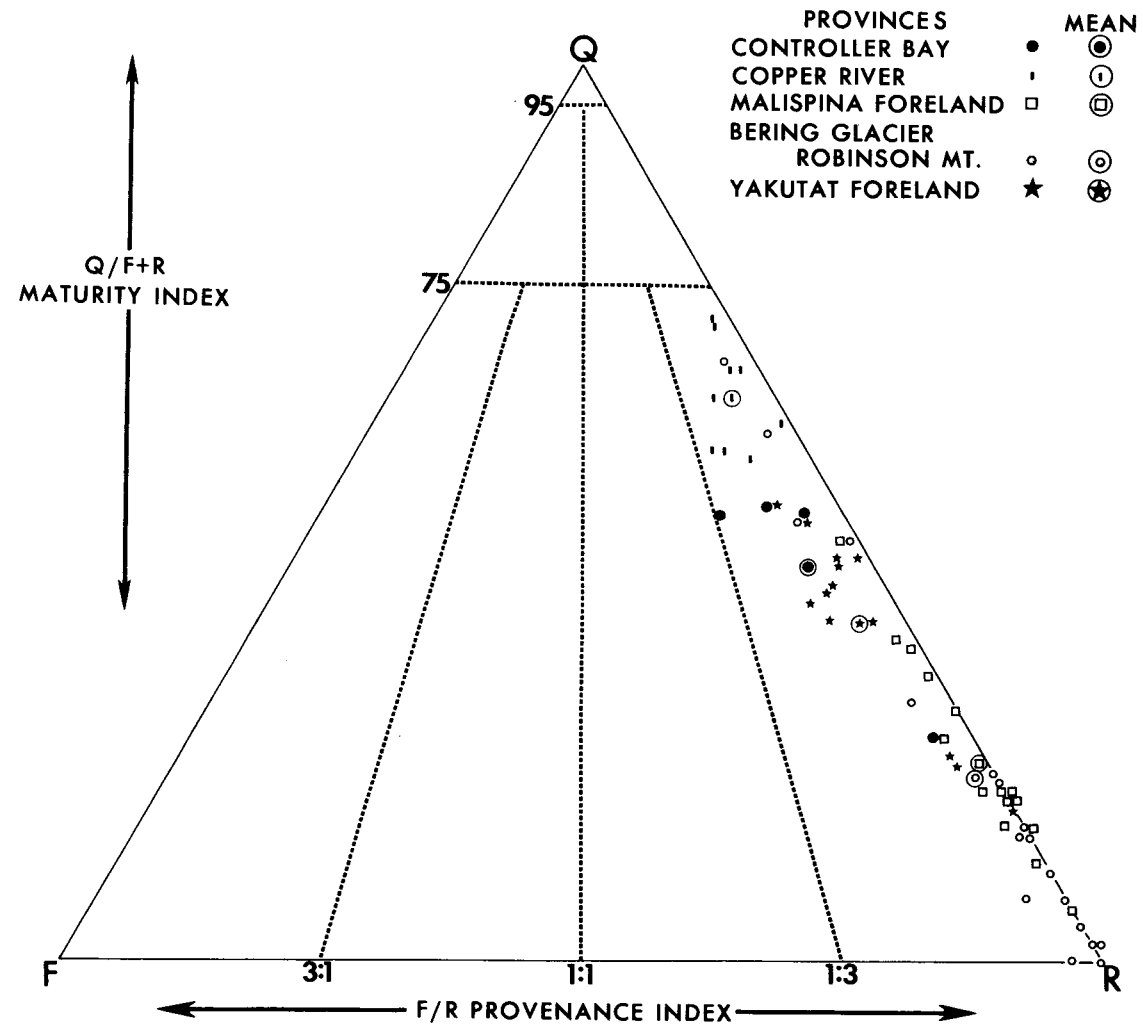


Figure 19. Compositional diagram of sediment samples from 5 areas in the Northern Gulf study area. Most samples cluster at certain points on the graph.



Figure 20. Graph of maturity index vs. distance down-drift of Dry Bay. Note the increase in the index with increased transport distance from the bay.

They show considerable scatter.

Figure 21 shows just the sediments from the Malaspina Foreland Province. They have been divided on the basis of distance downdrift of probable sediment sources. Note the very good correlation of increased sediment maturity with increased transport distance from sediment source. This corresponds well with concepts regarding sediment maturing compositionally with increased distance from source areas and explains the high variability of these samples.

Figure 22 shows the maturity index for the Bering Glacier - Robinson Mountain Province samples. Some interesting trends are evident. Refer to Figure 2 for locations. Moving from east to west on the diagram, a very low maturity index is located at site 29. This site is just downdrift of a glacial till exposed at Icy Cape and the Big River, both sediment suppliers. This is followed by a maturity index increase with increased distance from these sources. The White River, which is located updrift of site 26, introduces immature sediment into the system; these sediments mature with increasing distance downdrift of the river, finally terminating with a high maturity index at the end of the Duktoth River Spit. From there to Cape Suckling, the outwash streams draining the Bering Glacier introduce an immature sediment suite to the coast.

This section has analyzed the sediment samples collected during two separate field studies. This analysis follows closely accepted patterns for sediment dispersal and maturing. The study area is extremely diverse with regard to coastal geomorphology and the balance between marine and terrestrial processes. However, even with this complexity, trends in sediment transport are present which verify geomorphic and process indicators of dominant sediment transport direction as well as visual estimates of sediment sources.

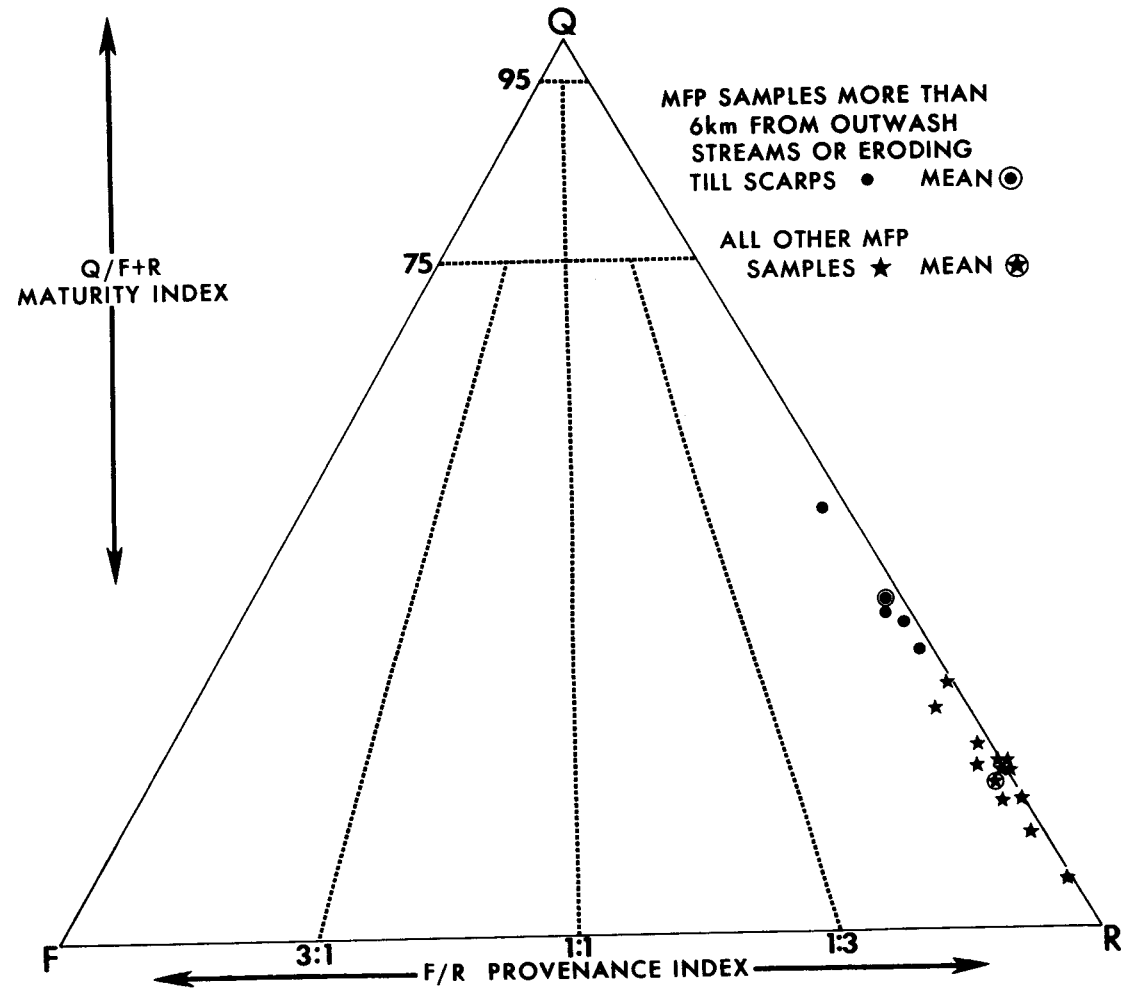


Figure 21. Compositional graph of Malaspina Foreland Province samples separated on the basis of distance from sediment sources. The samples 6 km or more from their sediment sources have a higher percentage of quartz.

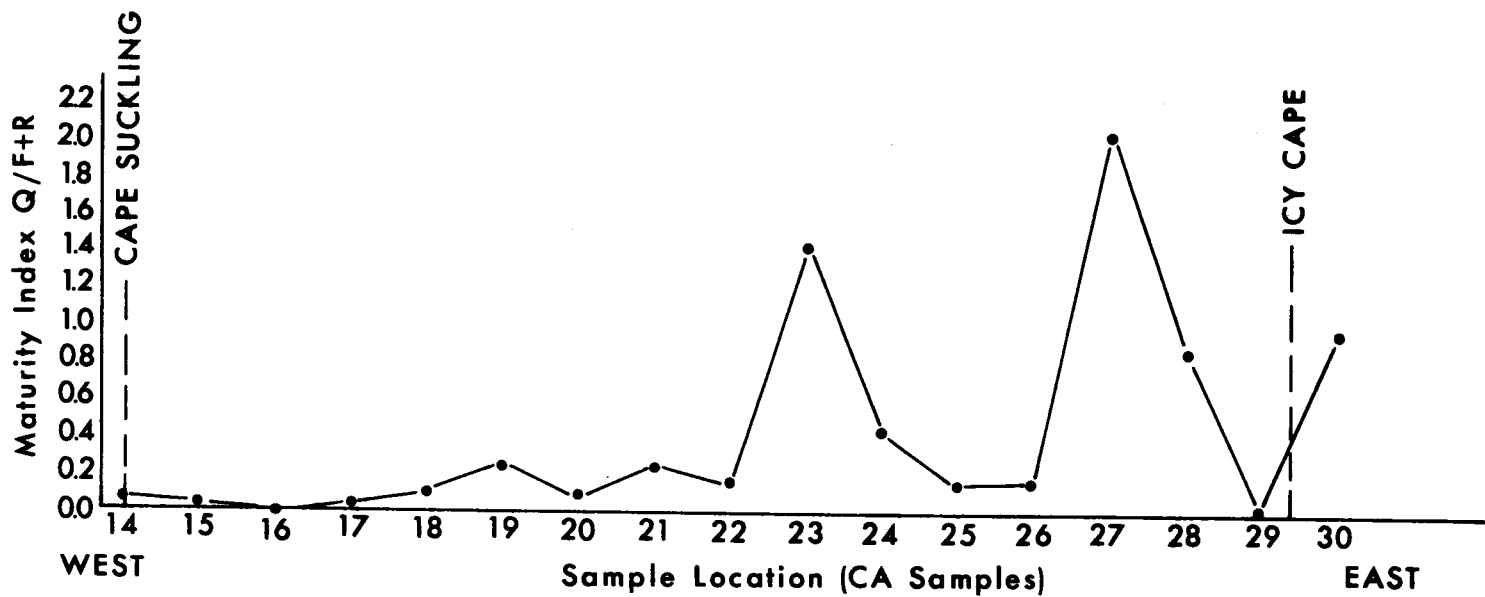


Figure 22. Graph of maturity index vs. position on the Bering Glacier - Robinson Mountain Province. The more mature sediments are at the ends of spits far from sediment sources. See discussion in text.

REFERENCES CITED

- Folk, R. L., 1968, Petrology of sedimentary rocks: Hemphill's, Austin, Texas, 170 p.
- Folk, R. L., 1974, Petrology of sedimentary rocks, Hemphill Publishing Company, Austin, Texas 182 p.
- Folk, R. L., and Ward, W. C., 1957, Brazos River point bar: a study in the significance of grain size parameters: Jour. Sed. Pet., v. 27, No. 1, p. 3-26.
- Hayes, M. O., et al., 1969-1970, Field work done in the Northern Gulf of Alaska.
- Nummedal, D., et al., 1974, Recent migrations of the Skeidararsandur shoreline, southeast Iceland, Final Rept. to Naval Ordnance Laboratory, Univ. of Mass, 182 p.
- Nummedal, D., and Stephen, M. F., 1976, Coastal dynamics and sediment transportation, Northeast Gulf of Alaska, Tech. Rept. No. 9-CRD, Dept. of Geo., U.S.C., 148 p.
- NODC (National Ocean Data Center) 707 A Street, Anchorage, Alaska, 99501
- Pettijohn, F. J., 1975, Sedimentary rocks, 3rd ed., Harper and Row, Publishers, N. Y., N. Y., 628 p.
- Winkelmolen, A. M. and Veenstra, H. J., 1974, Size and shape sorting in a Dutch tidal inlet, Sedimentology, v. 21, No. 1, p. 107-126.

Project 2. Shoreline of Kotzebue Sound (Cape Prince of Wales to Point Hope)

a) Field and Laboratory Activities

No field work has been carried out on this project since the 1976 summer field season. Laboratory analysis of sediment samples is underway as well as computer storage of each profile measured during July - August, 1976. Additionally, Christopher H. Ruby and Larry G. Ward, both members of the 1976 field team, traveled to the Buzzards Bay, Massachusetts oil spill. Detailed descriptive data regarding oil spills in ice bound environments was collected. Shortly after that spill, the Ethyl H., a barge carrying #6 fuel oil, was holed in the Hudson River. Since there was considerable ice on the river at that time, C. H. Ruby and Erich Gundlach spent a few days in the field analyzing the interaction of the oil and ice as well as the constraints placed on the clean up operation by the oil. These two field studies supported by USC funds, have provided considerable insight into oil spills in arctic and near arctic areas. This information will be used to formulate an oil spill vulnerability scheme for Kotzebue Sound, after the ice studies we have planned for the Sound this year are completed.

APPENDIX

- Table 1 -- Grain Size Parameters
- Table 2 -- Modal Grain Size Parameters
- Table 3 -- Compositional Data
- Table 4 -- Maturity Indices

TABLE 1

<u>Photo</u>	<u>Mean (ϕ)</u>	<u>Standard Deviation (ϕ)</u>	<u>Skewness (ϕ)</u>
DBC-1			
A-U.B.F.	1.590	0.287	0.056
B-L.H.T.S.	1.370	0.233	0.059
C-Neap Berm	0.394	1.162	0.567
D-W.S. Dune	1.640	0.264	0.116
DBC-2			
A-Spring H.T.B.F.	1.535	0.271	0.147
B-L.H.T.S.	0.177	1.747	-0.687
C-M.B.F.	0.380	1.398	-0.436
D-W.S. Dune	1.645	0.313	-0.061
DBC-3			
A-Berm Runnel	1.627	0.546	0.277
B-Neap Berm	0.401	1.542	-0.577
C-L.B.F.	-0.700	1.137	-0.026
D-W.S. Dune	1.244	0.232	0.154
DBC-4			
A-Berm Top	1.397	0.294	0.071
B-Berm Crest	1.446	0.278	-0.002
C-L.B.F.	1.312	0.509	-0.157
D-W.S. Dune	1.459	0.306	0.038
DBC-5			
A-Berm Top	1.862	0.197	-0.003
B-Berm Crest	1.335	0.275	0.095
C-L.B.F.	1.236	0.308	0.187
D-W.S. Dune	1.412	0.243	-0.086
DBC-6			
A-Berm Top	1.306	0.315	-0.049
B-Berm Crest	1.192	0.363	0.070
C-L.B.F.	1.155	0.382	-0.046
D-W.S. Dune	1.193	0.285	-0.059
DBC-7			
A-Runnel	1.719	0.263	0.086
B-Berm Top	1.194	0.289	0.094
C-L.B.F.	1.303	0.295	0.157
D-W.S. Dune	1.620	0.334	-0.087
DBC-8			
A-U.B.F.	1.735	0.257	0.127
B-Berm Runnel	1.418	0.323	0.206
C-Neap Berm Top	1.339	0.301	0.181
D-W. S. Dune	1.734	0.282	0.073
DBC-9			
A-U.B.F.	1.489	0.263	0.122
B-Runnel	1.169	0.263	0.135
C-L.B.F.	1.324	0.310	0.236
D-W.S. Dune	1.803	0.270	0.058

	<u>Mean (ϕ)</u>	<u>Standard Deviation (ϕ)</u>	<u>Skewness (ϕ)</u>
DBC-10			
A-U.B.F.	1.458	0.269	0.088
B-Neap Berm	1.276	0.336	0.172
C-Runnel	1.241	0.356	0.176
D-Low Dune Ridge	1.907	0.323	0.018
DBC-11			
A-U.B.F.	1.880	0.258	0.127
B-Runnel	1.284	0.277	0.139
C-L.B.F.	1.581	0.313	0.048
D-High Dune Ridge	1.802	0.298	0.037
DBC-12; Hq-2			
A-M.B.F.	1.446	0.287	0.006
B-Runnel Edge	1.437	0.333	0.214
C-Ridge Crest	1.432	0.329	0.116
D-Flat Dune	1.878	0.265	0.025
DBC-13			
A-U.B.F.	2.083	0.239	0.158
B-M.B.F.	1.832	0.253	0.223
C-L.T.T.	1.679	0.299	0.120
D-High Dune Ridge	1.970	0.263	0.052
DBC-14			
A-U.B.F.	2.065	0.245	0.308
B-M.B.F.	1.928	0.246	0.099
C-L.T.T.	1.742	0.219	0.229
D-W.S. Dune	2.128	0.256	0.114
DBC-15			
A-Runnel	2.072	0.247	0.246
B-M.B.F.	1.619	0.263	0.174
C-L.B.F.	1.630	0.292	0.166
D-W.S. Dune	2.071	0.269	0.093
DBC-16			
A-U.B.F.	1.701	0.270	0.126
B-Ridge Crest	1.741	0.312	0.082
C-L.B.F.	1.724	0.301	-0.058
D-W.S. Dune	1.893	0.329	0.232
DBC-17			
A-U. Ridge Top	1.779	0.281	0.161
B-L. Ridge Top	1.389	0.340	0.055
C-L.B.F.	1.833	0.336	0.078
D-W.S. Dune	1.909	0.320	0.191
DBC-18			
A-U.B.F.	2.135	0.280	0.200
B-Ridge Top	1.695	0.352	0.066
C-Ridge Top	1.651	0.353	0.096
D-W.S. Dune	2.037	0.296	0.101

	<u>Mean (ϕ)</u>	<u>Standard Deviation (ϕ)</u>	<u>Skewness (ϕ)</u>
DBC-19			
A-U.B.F.	1.872	0.258	0.141
B-Ridge Top	1.861	0.338	0.230
C-L.B.F.	1.267	0.503	-0.270
D-W. S. Dune	1.905	0.299	0.169
DBC-20			
A-U.B.F.	1.871	0.260	0.118
B-L.T.T.	1.751	0.220	0.168
C-L.T.T.	1.560	0.268	0.063
D-Dune Ridge	2.079	0.251	0.073
DBC-21			
A-U.B.F.	1.891	0.232	-0.064
B-L.B.F.	1.813	0.239	0.216
C-Ridge	1.860	0.327	0.209
D-Dune	1.940	0.301	0.115
DBC-22			
A-U.B.F.	1.929	0.285	0.117
B-L.B.F.	1.765	0.271	0.188
C-L.T.T.	1.152	0.385	0.210
D-High Dune Ridge	2.065	0.280	0.083
DBC-23			
A-U.B.F.	2.151	0.299	0.206
B-Runnel	1.890	0.303	0.178
C-Ridge Top	1.926	0.291	0.097
DBC-24			
A-U.B.F.	1.663	0.351	0.140
B-L.B.F.	-0.010	1.575	-0.371
C-L.T.T.	1.629	0.287	0.146
D-W.S. Dune	1.918	0.262	0.014
DBC-25			
A-U.B.F.	1.902	0.253	0.088
B-Ridge Top	1.755	0.281	0.114
D-Flat Dune	2.024	0.233	0.145
DBC-26			
A-U.B.F.	1.894	0.266	0.160
B-L.B.F.	1.743	0.262	0.153
C-Ridge Top	1.661	0.293	0.101
D-W.S. Dune	2.094	0.227	0.065
DBC-27			
A-U.B.F.	2.030	0.218	0.247
B-L.B.F.	1.832	0.298	0.138
C-Ridge Top	1.881	0.305	0.225
D-W.S. Dune	1.826	0.303	0.138

<u>Photo</u>	<u>Mean (ϕ)</u>	<u>Standard Deviation (ϕ)</u>	<u>Skewness (ϕ)</u>
DBC-28			
A-U.B.F.	2.136	0.270	0.182
B-L.T.T.	1.868	0.265	0.144
C-Ridge Top	2.054	0.319	0.122
D-W.S. Dune	1.936	0.249	0.079
DBC-29			
A-U.B.F.	1.994	0.235	0.179
B-L.T.T.	1.799	0.296	0.231
C-L.T.T.	1.843	0.303	0.181
D-W.S. Dune	1.893	0.253	0.086
DBC-30			
A-U.B.F.	2.002	0.220	0.145
B-M.B.F.	1.998	0.235	0.157
C-Low Ridge	1.749	0.257	0.119
D-W.S. Dune	2.190	0.249	0.113
DBC-31			
A-U.B.F.	2.245	0.405	0.073
B-M.B.F.	2.023	0.421	0.103
C-L.B.F.	2.025	0.681	-0.176
DBC-32			
A-Runnel	2.132	0.288	0.191
B-M.B.F.	2.125	0.317	0.278
C-Ridge	1.045	0.342	0.195
DBC-33			
A-M.B.F.	2.179	0.525	-0.004
B-L.T.T.	2.587	0.415	0.151
C-L.T.T.	2.545	0.266	0.383
D-W.S. Dune	-0.291	2.117	-0.079
DBC-34			
A-M.B.F.	2.116	0.801	-0.592
B-L.T.T.	2.819	0.393	0.132
C-L.T.T.	2.332	0.995	-0.533
D-Low Dune	1.346	0.718	-0.319
DBC-35			
A-M.B.F.	1.405	0.788	-0.248
B-L.T.T.	2.241	0.670	-0.369
C-L.T.T.	2.313	0.599	-0.054
D-W.S. Dune	2.377	0.526	0.166
DBC-36			
A-U.B.F.	1.983	0.367	0.116
C-L.T.T.	0.166	1.726	0.063
D-W.S. Dune	1.021	0.698	0.043

	<u>Photo</u>	<u>Mean (ϕ)</u>	<u>Standard Deviation (ϕ)</u>	<u>Skewness (ϕ)</u>
DBC-37				
	A-Berm Crest	1.517	0.374	-0.057
	B-M.B.F.	1.364	0.542	0.177
	C-L.B.F.	1.667	0.693	0.004
DBC-38				
	A-Berm Top *	1.337	0.523	0.175
	B-M.B.F.	0.114	2.006	-0.044
	C-Ridge Top	1.739	0.468	0.008
DBC-39				
	A-U.B.F. *	1.813	0.517	0.016
	B-M.B.F.	1.985	0.492	0.047
DBC-40				
	A-M.B.F.	1.484	0.575	-0.078
	B-L.B.F.	2.002	0.395	0.119
	C-L.B.F.	2.189	0.411	0.166
	D-W.S. Dune	0.613	0.794	0.110
DBC-41				
	A-U.B.F.	1.689	0.434	0.077
	B-M.B.F.	1.885	0.855	-0.322
	C-L.B.F. *	2.084	0.511	-0.037
	D-W.S. Dune	1.636	0.522	-0.077
DBC-42				
	A-Berm *	1.966	0.367	0.060
	B-M.B.F.	1.733	0.486	0.086
	C-L.B.F.	-0.113	0.987	0.002
	D-W.S. Dune	0.663	0.636	-0.036
DBC-43				
	A-Berm Crest *	2.268	0.783	-0.251
	B-U.B.F.	0.226	1.886	-0.490
	C-L.B.F.	1.686	0.524	0.125
	D-W.S. Dune	1.169	0.793	-0.206
DBC-44				
	A-Berm Top	0.421	1.687	-0.301
	B-L.B.F.	1.986	0.553	0.017
	C-L.B.F.	0.893	1.237	-0.175
	D-Dune Ridge *	1.494	0.371	0.040
DBC-45				
	A-U.B.F.	1.649	0.370	0.027
	B-Neap Berm	1.572	0.515	0.103
	C-L.B.F.	0.634	0.843	0.071
	D-W.S. Dune	1.508	0.265	0.100

	<u>Photo</u>	<u>Mean (ϕ)</u>	<u>Standard Deviation (ϕ)</u>	<u>Skewness (ϕ)</u>	
DBC-46					
	A-U.B.F.	*	-1.948	1.309	0.068
	B-Runnel		1.625	0.077	-0.000
	C-Ridge		2.228	0.461	0.252
	D-Dune Ridge		1.619	0.377	0.098
DBC-47					
	A-Berm Crest		1.165	0.392	0.013
	C-L.B.F.	*	-1.032	1.541	0.226
DBC-48; Mal-3					
	A-Storm Beach	*	0.629	0.657	0.015
	B-Berm Top		0.629	0.657	0.015
	C-L.B.F.	*	-2.183	1.044	0.122
	D-W.S. Dune		-1.329	0.591	0.422
DBC-49					
	A-Berm Top		1.322	0.498	0.283
	B-U.B.F.		0.854	0.324	-0.002
	C-L.B.F.	*			
DBC-50					
	A-U.B.F.	*	1.208	0.461	0.318
	B-M.B.F.	*			
	C-L.B.F.		-1.343	1.717	0.146
	D-W.S. Dune		1.194	0.452	0.309
DBC-51					
	A-U.B.F.	*			
	B-M.B.F.	*			
	C-L.B.F.	*			
DBC-52					
	A-U.B.F.	*			
	B-M.B.F.	*			
	C-L.B.F.	*	0.769	1.054	-0.006
DBC-57					
	A-U.B.F.		1.240	0.518	0.235
	B-M.B.F.	*			
	C-L.B.F.	*	0.339	1.708	-0.292
	D-W.S. Dune		1.268	0.301	0.207
DBC-58					
	A-U.B.F.	*	1.495	0.363	0.154
	B-M.B.F.	*			
	C-Berm Face	*	-2.597	1.585	0.546
	D-Dune Ridge		1.031	0.363	0.128

	<u>Photo</u>	<u>Mean (ϕ)</u>	<u>Standard Deviation (ϕ)</u>	<u>Skewness (ϕ)</u>
DBC-59				
	A-Storm Berm Face	*		
	B-M.B.F.	*	-0.424	1.176
	C-L.B.F.	*	-0.753	1.562
DBC-60; Mal-2				
	A-Spring Berm	*		
	B-M.B.F.	*	1.650	0.441
	C-Neap Berm	*		-0.105
	D-Grassy Dunes		1.142	0.441
DBC-61				
	A-U.B.F.	*		
	B-Berm	*	0.351	1.380
	C-L.B.F.	*	0.128	1.449
	D-W.S. Dune		1.419	0.679
DBC-62				
	A-U.B.F.	*		
	B-Berm	*		
	C-L.B.F.	*	0.525	1.488
	D-W.S. Dune		1.898	0.354
DBC-63				
	A-High Berm	*	0.348	1.522
	B-Mid Berm	*		-0.227
	C-L.B.F.	*	0.028	1.517
DBC-64				
	A-High Berm	*	1.305	1.080
	B-Low Berm	*		-0.383
	C-L.B.F.	*		
DBC-65				
	A-Berm Top		1.721	0.650
	B-Low Berm	*		-0.054
	C-L.B.F.	*	-1.022	2.163
DBC-66				
	A-U.B.F.	*		
	B-M.B.F.	*		
	C-L.B.F.	*	0.483	1.607
DBC-67				
	A-Berm Runnel	*	0.662	1.158
	B-Low Berm Crest	*	1.187	1.068
	C-Berm Cusp	*		0.103
DBC-68				
	A-Berm Top	*	-1.557	1.137
	B-Lower Berm	*		-0.304
	C-L.B.F.	*	-2.232	1.365

	<u>Photo</u>	<u>Mean (ϕ)</u>	<u>Standard Deviation (ϕ)</u>	<u>Skewness (ϕ)</u>
DBC-69				
A-U.B.F.	*			
B-Berm Runnel	*			
C-L.B.F.	*			
DBC-71				
A-U.B.F.	*	1.694	0.487	0.047
B-M.B.F.	*	0.069	1.757	-0.434
C-L.B.F.	*	1.533	0.634	-0.115
D-Wind Lag		1.215	0.658	-0.112
DBC-72				
A-Berm Top		1.439	0.518	-0.058
B-Berm Crest	*	1.588	0.533	-0.028
C-L.B.F.	*	0.691	1.234	-0.336
D-W.S. Dune		1.723	0.540	-0.041
DBC-73				
A-L.H.T.S.		2.200	0.535	-0.240
B-M.B.F.		2.439	0.350	-0.323
C-Low Berm Cusp	*	2.271	0.469	-0.225
DBC-75				
A-L.H.T.S.		0.355	1.641	-0.343
B-L.T.T.		0.987	1.380	-0.564
C-L.T.T.		2.097	0.555	-0.126
D-W.S. Dune		1.819	0.610	-0.106
DBC-76				
A-Berm Top		1.169	0.517	-0.047
B-Spring Berm Crest	*	1.484	1.113	-0.378
C-Spring Berm Base	*	0.534	0.982	-0.155
D-W.S. Dune		2.651	0.479	-0.052
DBC-77				
A-U.B.F.	*			
B-M.B.F.	*			
C-L.B.F.	*	-0.437	1.156	-0.149
DBC-78				
A-U.B.F.	*			
B-Gravel Horn	*			
C-L.B.F.	*	-0.782	1.750	-0.191
DBC-79				
A-U.B.F.	*	-2.022	1.798	0.401
B-L.T.T.	*	-1.626	1.811	-0.081
C-L.T.T.	*	-0.914	1.738	-0.148
D-W.S. Dune		1.297	0.558	-0.017

	<u>Photo</u>	<u>Mean (ϕ)</u>	<u>Standard Deviation (ϕ)</u>	<u>Skewness (ϕ)</u>
DBC-80				
	A-L.H.T.S.	0.238	1.211	0.186
	C-L.T.T.	-0.062	1.441	0.175
	D-Dune Ridge	1.719	0.309	0.095
DBC-81				
	A-L.H.T.S.	*		
	B-M.B.F.	*		
	C-L.B.F.	*	-0.528	1.614
	D-W.S. Dune		1.488	0.304
DBC-82				
	A-Berm Top	0.574	0.999	0.185
	B-M.B.F.	1.933	0.306	-0.259
	C-Ridge Top	0.514	1.325	0.016
	D-W.S. Dune	1.016	0.754	-0.002
DBC-83				
	A-L.H.T.S.	*	2.340	0.320
	B-Runnel Edge		1.870	0.740
	C-Ridge Top		0.996	1.438
	D-Low Dune		2.518	0.284
DBC-84				
	B-L.B.F.	2.318	0.264	0.361
	C-L.T.T.	2.300	0.287	0.264
	D-W.S. Dune	2.156	0.294	-0.167
DBC-85; YKG-3				
	A-H.T.S.	*		
	B-Welded Ridge	*		
	C-Ridge Top	*	1.169	1.212
	D-W.S. Dune		2.165	0.307
DBC-86				
	A-U.B.F.	*	2.506	0.263
	B-Ridge Top	*	-0.233	2.102
	C-Ridge Top	*	1.387	1.628
DBC-87				
	A-M.B.F.	*	0.171	0.538
	B-Ridge Crest		2.257	0.524
	C-Ridge Top		1.328	1.299
DBC-88				
	A-Gravel Cusp	-0.098	1.194	0.467
	B-M.B.F. Horn	0.537	1.015	0.230
	C-L.B.F.	-0.059	0.983	0.328
DBC-89				
	A-Berm Top	-0.536	1.968	0.201
	B-Berm Face	-0.276	1.081	0.409
	C-Low Berm Face	-0.684	1.272	0.524

	<u>Photo</u>	<u>Mean (ϕ)</u>	<u>Standard Deviation (ϕ)</u>	<u>Skewness (ϕ)</u>	
DBC-90					
	A-U.B.F.	*	1.278	1.287	-0.386
	B-Berm Top	*	-0.230	1.289	0.552
	C-L.B.F.	*	-0.914	1.347	0.405
	D-W.S. Dune		1.960	0.514	0.029
DBC-91					
	A-U.B.F.		0.982	0.926	0.127
	B-M.B.F.		0.655	0.806	0.241
	C-L.B.F.		0.688	1.002	0.063
	D-W.S. Dune		0.867	0.637	-0.014
DBC-92					
	A-U.B.F.	*	1.503	0.469	-0.027
	B-L.T.T. Runnel	*	1.165	0.645	-0.052
	C-L.T.T. Ridge	*	0.546	0.708	-0.077
	D		1.883	0.505	-0.004
DBC-93					
	A-L.H.T.S.	*	2.409	0.386	-0.171
DBC-101					
	A-High Berm Crest	*			
	B-Mid Berm Crest	*			
	C-Neap Berm Crest	*	-1.279	0.743	-0.319
DBC-102					
	A-L.H.T.S.	*	-0.397	2.244	-0.779
	B-Berm Face	*			
	C-Berm Crest	*	-2.094	1.185	-0.193
DBC-103					
	A-H.H.T.S.	*	2.352	0.485	-0.074
	B-M.B.F.	*	2.297	0.516	-0.149
	C-L.B.F.	*	-0.074	2.520	-0.621
DBC-104					
	A-H. Berm Top	*			
	B-M.B.F.	*			
	C-L.B.F.	*	-0.528	2.675	0.098
DBC-105					
	A-H. Berm Crest	*			
	B-M.B.F.	*			
	C-L.B.F.	*			
DBC-106					
	A-M.B.F.		-2.328	1.373	0.365
	B-L.T.T.	*			
	C-L.T.T.	*			

PERMANENT PROFILES

	<u>Mean</u>	<u>St. Dev.</u>	<u>Skew</u>
Eg1 A	2.320	0.254	0.100
B	2.356	0.280	0.187
D	2.306	0.367	0.079
Eg3 C	2.270	0.296	0.282
D	2.293	0.249	0.354
Eg4 A	2.094	0.288	0.070
B	2.305	0.240	0.292
Eg8 A	2.106	0.564	0.115
B	2.324	0.448	0.213
C	1.675	0.748	0.049
Sr1 A	2.323	0.316	0.315
B	1.525	0.991	-0.226
C	1.813	0.452	0.032
D	2.031	0.420	0.096
Knk1 A	2.809	0.382	0.016
B	1.351	0.383	-0.104
C	2.992	0.307	-0.170
D	2.911	0.302	0.030
Ok1 A	2.110	0.374	0.163
Seal A	1.498	0.410	0.042
B	1.813	0.394	-0.027
C	0.996	0.445	0.182
Ykg2 C	1.344	0.979	-0.379
D	2.047	0.358	0.219
Ykg3 C	1.169	1.212	-0.668
D	2.165	0.307	0.266
Ma12 B	1.650	0.441	-0.105
D	1.142	0.441	-0.058
Ma13 A	0.629	0.657	0.015
B	-2.183	1.044	0.122
C	-0.823	1.268	-0.283
D	-1.329	0.591	0.422
Hq2 A	1.446	0.287	0.006
B	1.437	0.333	0.214
C	1.472	0.329	0.116
D	1.878	0.265	0.025

TABLE 2

MODES (ϕ)

	<u>Major</u>	<u>Major</u>	<u>Minor</u>	<u>Minor</u>
DBC-1A	1.625			
B	1.375			
C	1.625			
DBC-2A	1.375			
B	1.125		-3.375	
C	1.375		-2.625	0.875
D	1.625			
DBC-3B	1.375			
C	-2.125		-2.625	1.875
D	1.125		-1.125	0.625
DBC-4A	1.375			
B	1.375			
C	1.375			
D	1.375			
DBC-5A	1.875			
B	1.125			
C	1.125		1.625	
D	1.500			
DBC-6A	1.375			
B	1.125			
C	1.125			
D	1.125			
DBC-7A	1.625			
B	1.125			
C	1.125			
D	1.875		1.375	
DBC-8A	1.625			
B	1.125			
C	1.125			
D	1.625			
DBC-9A	1.375			
B	1.125			
C	1.125			
D	1.625			
DBC10A	1.375			
B	1.125			
C	1.125			
D			1.625	2.125

	<u>Major</u>	<u>Major</u>	<u>Minor</u>	<u>Minor</u>
DBC-11A	1.875			
B	1.125			
C	1.625			
D	1.875	1.625		
DBC-12;				
HQ2A	1.625			
B	1.125		1.875	
C	1.375			
D	1.625		2.125	
DBC-13A			2.125	1.875
B	1.625			
C	1.625			
D	1.875			
DBC-14A	1.875			
B	1.875			
C	1.625			
D	2.125			
DBC-15A	1.875			
B	1.625			
C	1.625			
D	1.875			
DBC-16A	1.625			
B	1.625			
C	1.875			
D	1.875		2.375	
DBC-17A	1.625			
B	1.375			
C	1.875	1.625		
D	1.875	1.625		
DBC-18A	2.125			
B	1.625			
C	1.625			
D	1.875			
DBC-19A	1.875			
B	1.625			
C	1.375			
D	1.625			
DBC-20A	1.875			
B	1.625			
C	1.625			
D	1.875			
DBC-21A	1.875			
B	1.625			
C	1.875	1.625		
D	1.875			

	<u>Major</u>	<u>Major</u>	<u>Minor</u>	<u>Minor</u>
DCB-22A	1.875			
B	1.625			
C	0.875			
D	2.125	1.875		
DBC-23A	1.875			
B	1.875			
C	1.875			
DBC-24A	1.625		2.125	
B	1.125		-3.625	-2.625
C	1.625			
D	1.875			
DBC-25A	1.875			
B	1.625			
D	1.875			
DBC-26A	1.875			
B	1.625			
C	1.625			
D	2.125			
DBC-27A	1.875			
B	1.625			
C	1.875			
D	1.625			
DBC-28A	2.125			
B	1.875			
C	1.875			
D	1.875			
DBC-29A	1.875			
B	1.625			
C	1.625			
D	1.875			
DBC-30A	1.875			
B	1.875			
C	1.625			
D	2.125			
DBC-31A	2.625	2.125		
B	1.875		2.625	
C	1.875		2.625	
DBC-32A	2.125			
B	1.875		2.875	
C	1.875			
DBC-33A	2.625		1.875	
B	2.375			
C	2.375			
D	1.875		-0.875	-3.125

	<u>Major</u>	<u>Major</u>	<u>Minor</u>	<u>Minor</u>
DBC-34A	2.375		1.375	
B	2.625			
C	2.375		-2.125	
D	1.625		0.375	
DBC-35A	1.700		.700	
B	2.375		1.875	-3.875
C	2.125			
D	2.125			
DBC-36A	1.875			
C	-0.375		2.375	-3.125
D	1.125		0.375	
DBC-37A	1.625			
B	1.125			
C	1.125		2.125	
DBC-38A	1.125			
B	-0.875		-2.625	2.625
C	1.375	1.875		
DBC-39A	2.125			
B	1.875			
DBC-40A	1.625		0.875	
B	1.875			
C	2.125			
D	0.625		0.125	
DBC-41A	1.625			
B	2.125		2.625	
C	2.125			
D	1.875		2.375	
DBC-42A	1.875			
B	1.625			
C	0.125	0.625	-2.125	2.375
D	0.625			
DBC-43A	2.375		0.625	
B	1.375		-2.625	
C	1.625			
D	1.875		0.450	-3.875
DBC-44A	1.625	0.875	-0.875	-2.625
B	2.125			
C	1.375	0.875	2.625	-2.625
D	1.375			
DBC-45A	1.625			
B	1.625	1.125		
C	0.625		2.375	
D	1.375			

	<u>Major</u>	<u>Major</u>	<u>Minor</u>	<u>Minor</u>
DBC-46A	-2.625		-1.375	-3.125
B	1.625			
C	2.125	-1.875	3.125	
D	1.625			
DBC-47A	1.125		1.625	
B	-1.375		1.375	-2.625
DBC-48;				
Mal 3 A	0.625			
B	-2.625		-2.125	0.875
C	0.125	-0.875	-2.125	-3.375
D	-1.625		1.375	
DBC-49A	1.125			
B	0.875			
DBC-50A	1.950		2.125	
C	-1.625		0.875	-2.625
D	0.875			
DBC-52C	0.375		1.625	
DBC-57A	1.125			
C	0.875		-1.875	-2.875
D	1.125			
DBC-58A	1.375			
C	-2.625		-3.125	-1.625
D	-0.875			
DBC-59B	-0.625		-1.875	
C	-0.875		-2.625	
DBC-60;				
Mal 2 B	1.875			
D	1.125			
DBC-61B	-0.625		2.625	
C	-1.125		1.875	2.375
D	1.375		2.625	
DBC-62C	0.875		-0.875	2.625
D	1.875			
DBC-63A	1.600		-2.625	
C	-1.300		1.875	
DBC-64A	1.875		2.625	
DBC-65A	1.625			
C	-3.125		-1.125	1.875
DBC-66C	1.875		-1.375	
DBC-67A	-0.375		1.375	
B	1.875		-0.125	

	<u>Major</u>	<u>Major</u>	<u>Minor</u>	<u>Minor</u>
DBC-68A	-1.625		-2.625	
C	-2.625		3.125	
DBC-71A	1.625			
B	1.125		-1.875	2.875
C	1.625		-3.625	
D	1.375			
DBC-72A	1.375			
B	1.625			
C	1.375		-2.625	
D	1.875			
DBC-73A	2.625		2.125	
B	2.625		2.125	
C	2.625		2.125	
DBC-75A	1.875		-3.875	0.125
B	1.875		-2.625	0.625
C	2.125		2.625	
D	1.875		2.625	
DBC-76A	1.125			
B	1.625		-3.375	-2.625
C	1.375			
D	2.625			
DBC-77C	-0.375		-3.875	
DBC-78C	-0.625		-3.625	
DBC-79A	-3.875		-2.625	0.125
B	-3.875		-2.625	-0.375
C	-0.375		-3.875	-2.625
D	1.375			
DBC-80A	-0.375		1.625	
C	0.900		1.700	-2.625
D	1.625			
DBC-81C	0.375		-1.375	-2.625
D	1.375			
DBC-82A	0.125		1.875	2.375
B	2.125			
C	1.875		-0.375	
D	0.625		1.875	
DBC-83A	2.125		2.625	
B	1.875		2.625	
C	1.875		-2.625	
D	2.625			

	<u>Major</u>	<u>Major</u>	<u>Minor</u>	<u>Minor</u>
DBC-83A	2.125		2.625	
B	1.875		2.625	
C	1.875		-2.625	
D	2.625			
DBC-84B	2.125		2.625	
C	2.125		2.625	
D	2.625			
DBC~85; Ykg-3C	1.875		-0.375	-2.875
D	2.125		1.375	
DBC-86A	2.625			
B	2.125		-0.900	-2.625
C	2.125	2.625	-3.125	
DBC-87A	0.125			
B	2.625		2.125	
C	2.625		2.125	-0.400
DBC-88A	-0.625		2.000	
B	-0.300		1.625	
C	-0.375		1.750	
DBC-89A	-2.625		-1.875	1.875
B	-0.265		2.625	
C	-1.375		2.625	
DBC-90A	2.625		2.000	-0.875
B	-1.125		2.000	
C	-1.375		-2.625	
D	1.875		2.625	
DBC-91A	0.375		1.625	2.625
B	0.375			
C	0.625		2.625	
D	0.875			
DBC-92A	1.375			
B	1.125			
C	0.700			
D	1.875		2.625	
DBC-93A	2.625		2.125	
DBC-101C	0.875		-2.625	
DBC-102A	1.375		-3.875	
C	-1.375		-3.125	
DBC-103A	2.625		2.125	
B	2.625		2.125	
C	2.125		2.625	-3.875
DBC-104C	2.625		-3.125	3.875

		<u>Major</u>	<u>Major</u>	<u>Minor</u>	<u>Minor</u>
DBC-106A		-3.125	-2.625	-1.875	
PERMANENT PROFILES					
EG-1	A	2.125			
	B	2.125			
EG-3	C	2.125			
	D	2.125			
EG-4	A	2.125			
	B	2.125			
EG-8	A	1.625		2.125	3.125
	B	2.000			
	C	1.125	1.625		
Sr-1	A	1.875		1.375	
	B	1.700			
	C	0.875			
Ykg2	C	1.875			
	D	1.875			
Ykg3	C	1.875		-0.375	-2.875
	D	2.125		2.625	
Mal-2	B	1.875			
	D	1.125			
Mal-3	A	0.625			
	B	-2.625		-2.125	0.875
	C	0.125	-0.875	-2.125	-3.375
	D	-1.625		1.375	
Hq2	A	1.625			
	B	1.125		1.875	
	C	1.375			
	D	1.625		2.125	
Knk-1	A	2.625		3.125	
	B	1.375			
	C	3.215			
	D	3.125	2.625		
Ok-1	A	2.125			
Sea-1	A	1.875	1.375		
	B	1.700			
	C	0.875			

TABLE 3

COMPOSITIONAL ANALYSIS*

Copper River Province

	Qtz	F	Mica	Rf	Op
CA 1	56	5	5	28	6
2	57	2	5	27	9
3	53	1	7	34	5
4	48	5	4	32	11
5	60	2	5	23	10
6	60	2	9	23	6
7	55	2	4	27	12
8	53	8	0	31	8
9	54	8	3	33	2

Controller Bay Province

CA 10	44	6	10	37	3
11	45	11	7	35	2
12	24	4	3	68	1
13	46	4	4	44	2

Bering Glacier - Robinson Mountain Province

CA 14	7	4	0	89	0
15	2	0	0	98	0
16	0	0	0	100	0
17	4	0	0	96	0
18	10	0	1	89	0
19	21	0	2	77	0
20	7	0	0	93	0
21	20	1	0	79	0
22	14	1	0	85	0
23	58	3	1	38	0
24	28	4	1	66	1
25	14	0	0	86	0
26	15	0	0	84	1
27	59	3	0	26	12
28	46	1	0	50	3
29	2	0	0	98	0
30	47	5	0	44	4

Malaspina Foreland Province

CA 31	46	2	1	49	2
32	19	2	0	79	0
33	32	1	0	66	1
34	36	2	0	62	0
35	18	0	0	82	0
36	18	0	0	82	0
37	15	2	0	83	0
38	19	0	0	81	0

		Qtz	F	Mica	Rf	Op
CA	39	25	3	0	72	0
	40	11	1	0	88	0
	41	15	0	0	85	0
	42	19	0	0	81	0
	43	35	1	0	64	0
	44	21	1	0	78	0
	45	6	0	0	94	0
	46	28	0	0	72	0

Yakutat Foreland Province

CA	47	45	3	1	51	0
	48	40	6	3	51	0
	49	44	1	2	53	0
	50	45	3	1	51	0
	51	51	6	0	43	0
	52	39	8	0	53	0
	53	37	7	3	53	0
	54	49	4	1	47	0
	55	37	3	3	57	0
	56	41	5	3	49	2
	57	23	3	0	74	0
	58	17	0	0	83	0
	59	22	3	1	74	0

TABLE 4

MATURITY INDEX*

Copper River Province

	% Qtz	% Feld	% Rf	Maturity Index
CA 1	63	6	31	1.70
2	66	3	31	1.94
3	60	1	39	1.50
4	56	6	38	1.27
5	71	2	27	2.45
6	71	2	27	2.45
7	66	2	32	1.94
8	57	9	34	1.33
9	<u>57</u>	<u>8</u>	<u>35</u>	<u>1.33</u>
Mean	63.0	4.3	32.7	1.77
S.D.	5.87	2.95	4.27	0.46

Controller Bay Province

CA 10	51	7	42	1.04
11	50	12	38	1.00
12	25	4	71	0.33
13	<u>50</u>	<u>4</u>	<u>46</u>	<u>1.00</u>
Mean	44.0	6.7	49.3	0.84
S.C.	12.67	3.77	14.86	0.34

Bering Glacier - Robinson Mountain Province

CA 14	7	4	89	0.08
15	2	0	98	0.02
16	0	0	100	0.00
17	4	0	96	0.04
18	10	0	90	0.11
19	21	0	79	0.27
20	7	0	93	0.08
21	20	0	80	0.25
22	14	1	85	0.16
23	59	3	38	1.44
24	29	4	67	0.41
25	14	0	86	0.16
26	15	0	85	0.18
27	67	3	30	2.03
28	47	1	52	0.89
29	2	0	98	0.02
30	<u>49</u>	<u>5</u>	<u>46</u>	<u>0.96</u>
Mean	21.6	1.2	77.2	0.42
S.C.	21.18	1.79	22.33	0.58

Malaspina Foreland Province

	% Qtz	% Feld	% Rf	Maturity Index
CA 31	47	2	51	0.89
32	19	2	79	0.23
33	32	1	67	0.47
34	36	2	62	0.56
35	18	0	82	0.22
36	18	0	82	0.22
37	15	2	83	0.18
38	19	0	81	0.23
39	25	3	72	0.33
40	11	1	88	0.12
41	15	0	85	0.18
42	19	0	81	0.23
43	35	1	64	0.54
44	21	1	78	0.27
45	6	0	94	0.06
46	<u>28</u>	<u>0</u>	<u>72</u>	<u>0.39</u>
Mean	22.8	0.94	76.3	0.32
S.D.	10.52	1.00	10.98	0.21

Yakutat Foreland Province

CA 47	45	3	52	0.82
48	41	6	53	0.69
49	45	1	54	0.81
50	45	3	52	0.81
51	51	6	43	1.04
52	39	8	53	0.64
53	38	7	55	0.61
54	49	4	47	0.96
55	38	3	59	0.61
56	42	5	53	0.72
57	23	3	74	0.30
58	17	0	83	0.20
59	<u>22</u>	<u>3</u>	<u>75</u>	<u>0.28</u>
Mean	38.1	4.0	57.9	0.65
S.D.	10.74	2.30	11.86	0.26

ANNUAL REPORT

Contract #03-5-022-67
Research Unit #87
Reporting Period:
1 April 1976-1 April 1977
Number of Pages: 64

THE INTERACTION OF OIL WITH SEA ICE IN THE ARCTIC OCEAN

Seelye Martin
Department of Oceanography
University of Washington
Seattle, WA 98195

10 March 1977

The Seasonal Variation of Oil Entrainment in First Year Arctic Sea Ice:
A Comparison of NORCOR/OCS Observations

A Report from BLM/NOAA Contract No. 03-5-022-67, Task Order No. 6,
Research Unit #87, Principal Investigator, Seelye Martin

Seelye Martin
Department of Oceanography, WB-10
University of Washington
Seattle, WA 98195

Department of Oceanography Special Report Number 71

10 March 1977

M77-24

ANNUAL REPORT

Because of a field trip beginning 13 March and ending 1 April 1977, we are submitting our annual report both early and without reference to the forthcoming field trip. The attached report summarizes our work during the past year on the oil absorption properties of the first year ice in the Beaufort Sea.

1. Introduction

During the period 1974-1976, the author took a number of field and laboratory observations on oil absorption by sea ice. These observations come from three sources: (1) the NORCOR oil-in-ice experiment conducted at Balaena Bay, N.W.T., during the 1974-75 ice growth season for the Canadian Beaufort Sea Project; (2) field observations of unoiled first-year ice growth made by the author and his colleagues in the Beaufort Sea north of Alaska for the OCS program during the 1975-76 ice growth season; (3) laboratory studies made by the author during the past year on the growth of oiled and unoiled sea ice.

The present paper discusses the types of first-year ice which occur in the Beaufort Sea and the way in which they interact with petroleum over a growing season. Because the specific gravity of petroleum is generally less than that of sea water, oil floats on water, and oil released under ice generally floats to the ice-water interface. From the NORCOR field experiment, we know if brine channels are present in the ice, that oil rises up through the ice channels, then spreads out both on and within the ice surface. Therefore, the properties of the top layer of the ice will determine whether the oil once it reaches the surface will either spread out over the surface as over a glass sheet, or be absorbed within the ice.

In the following, most of our data consists of photographs of ice cores. We used several different photographic techniques, depending on whether the core was oiled or unoiled. In the NORCOR field experiment, we generally placed the oiled core on a sheet of oil absorbant, which is a white, felt-like material, then photographed the core either with a front flash or by natural light. Figure 16a shows a typical oiled ice

core. In the field, we took all of our cores with a SIPRE corer, which yields a core diameter of 71 mm.

In the OCS field experiment, we treated the uncoiled ice cores in the following way. First, we cut the core longitudinally in half. Then, to bring out the crystal structure, we rubbed the flat surface of the half-core with an alcohol-water solution which dissolved the saw cuts and melted away some of the surface so that the crystal structure stood out. Finally, we rubbed the ice surface with an oil-soluble dye which settled in the cracks between the individual crystals, thus greatly increasing the contrast.

To photograph the uncoiled cores, we used both a front and back flash. In the fall 1975 OCS traverse we used a front flash; Figure 3a shows an example. During the winter and spring 1976 traverses we used a back flash, which consisted of a box containing a half cylinder Plexiglas insert with flash tubes beneath it. To photograph the core, we placed the dyed half-core in the box, then took a flash photograph. Figure 10a, a typical photograph, shows that this technique not only shows the crystal structure, but also brings out the presence of air bubbles within the ice.

In the following sections, we describe how the properties of first year sea ice change and interact with oil over a growing season. In Section 2, we discuss the different kinds of ice which we observed in our OCS field traverses, and show how the ice properties change over a growing season. Then in Section 3, we interpret the results from the NORCOR experiment in terms of our discussion in Section 2.

2. Types of Sea Ice

Sea ice occurs in several forms; in the following, we consider four kinds of ice which include three kinds grown from open water, namely columnar ice, frazil ice, and ice grown from sea water mixed with snow. The fourth kind forms at the upper ice surface from recrystallized snow. We next discuss these types in the above order.

a. Columnar Ice

Most ice begins its growth from liquid sea water. Figure 1 is a photograph of a newly opened lead, taken on 7 November 1975, at a station north of Barter Island, Alaska. There was no wind at the ice surface, the air temperature was -30.5°C , and the sea water salinity was approximately $32^{\circ}/\text{oo}$. In the right foreground, the tape measure rests on ice which is 0.38 m thick. Immediately adjacent to the ice on which the tape measure rests, new ice is growing, where the rough surface material is salt flowers. This ice which extends out about 1 m, had a thickness of 35 mm and a salinity of $16^{\circ}/\text{oo}$, while the salt flowers had a salinity of $54^{\circ}/\text{oo}$. Beyond this ice, on what appears to be open water, the lead is covered with a layer of 10 mm thick layer of ice with a salinity of $19^{\circ}/\text{oo}$. (We took this ice sample using an ice chisel, and determined that the lead was ice-covered by throwing bits of snow out onto the surface). From the entire surface, we saw vapor streaming off and diffusing the sunlight at the upper left corner of the photograph. Both the vapor and the salt flowers show that the initial ice growth is characterized by the movement of salt water both up and down within the ice.

Figure 2 shows a close-up photograph of salt flowers made on a separate occasion at an air temperature of -36.4°C . For this case we observed a salt flower salinity of $61^{\circ}/\text{oo}$. The salt flowers occurred on

most of our young ice samples in the fall, and had salinities ranging from 45 to 95⁰/oo. The salt flowers are important evidence of the upward movement of salt during the initial ice growth; further, we show later that the high surface salinities established by this upward salt movement lead to the growth of brine channels in the spring.

Beneath the salt flowers as numerous writers discuss, the ice growth from undisturbed water begins with very small, randomly-oriented crystals in the top 10-20 mm of the core; below this depth long columnar crystals with a horizontal c-axis dominate the growth. Figure 3a, an example of a typical columnar core, shows the long columnar ice platelets separated by thin layers of brine which make up most of the core; and Figure 3b shows a bottom view of columnar sea ice grown in the laboratory; the sample has been rubbed with dye to outline the individual platelets. Examination of Figure 3b shows that some platelets share the same orientation; groups of platelets with the same orientation are called crystals. The bottom 10-40 mm of columnar sea ice is called the skeletal layer; this is a porous, fragil layer which can absorb oil.

Finally, Figure 3c shows the salinity structure of the core in 3a; most of this core has a salinity of 8-10⁰/oo except at the surface, where the salinity jumps to a value of 50⁰/oo. The snow also has a high salinity, presumably also caused by the upward flux of salt.

b. Frazil Ice

Frazil ice grows when a cold wind blows over sea water which is at its freezing point; the wind generates waves which stir the water. The stirring prevents growing ice crystals from organizing themselves into the long columnar platelets, rather as our laboratory observations show, the water column becomes slightly supercooled so that ice crystals form

in the interior and float to the surface. The crystals are platelets with typical thicknesses of 10-100 microns and diameters of 2-4 mm. In salt water, these crystals have rough edges and are possibly hexagonal, unlike the circular disks which Michel (1971) reports for fresh water. Once these crystals reach the surface, they form a porous mass with a random crystal structure. Because in the fall and winter traverse, high winds were often accompanied by blowing snow, we took our best frazil ice cores in May.

Figure 4 is a composite photograph taken on 18 May 1976 of an open frazil ice forming in an open lead with a 50 m fetch. The wind velocity was about 10 m s^{-1} and the air temperature was -13°C . Because of the combination of wind and wave herding of the crystals, they were swept downwind to pile up at the far edge of the lead, where they formed a slushy ice mass which was about 0.1 m thick. Figure 5a shows a core taken on 23 May 1976 through such a lead after it has frozen solid. The top 95 mm of the core in Figure 5a is made up of the small frazil crystals, then at 95 mm, there is an abrupt transition to columnar ice. Figure 5b is a photograph of a core taken from our laboratory wave tank, for ice grown in a wave field at an air temperature of -20°C . The top of this core is also made up of many small platelets with an abrupt transition to columnar ice. Finally, Figure 5c shows the salinity and temperature profile of the core in Figure 5a; even though this ice grows under relatively warm conditions, it still has a relatively high surface salinity. In the Beaufort Sea, we observed frazil ice thicknesses up to 0.13 m; in the Bering, Ramseier *et al.* (1975) observed thicknesses up to 0.35 m.

c. Ice grown from snow mixed with sea water

A third kind of young ice forms when blowing snow accompanies the

wind. Figure 6a shows a core taken on 7 November 1975 north of Barter Island at an air temperature of -30°C ; judging by the bad weather in the days immediately preceding our flight, we suspect that this core formed from snow crystals mixing into the open water during the initial freezing. Figure 6b shows the salinity and temperature profile of the core in Figure 6a; the salinity profile shows both a high surface salinity and that there is no sharp change in salinity at the depth where the columnar ice growth begins.

d. Ice formed from re-crystallized snow

Unlike the preceding three ice types, the present type of ice forms at the ice surface during the arctic winter and spring from the interaction of solar radiation with the snow layer on top of the cold sea ice. The snow which has been previously soaked in salt has its freezing point depressed, for example, a salinity of $100^{\circ}/\text{oo}$ has a solution freezing point of -7°C . The incident solar radiation melts and compacts this salty snow, whereupon the heat flux from the relatively warm snow to the cold ice below refreezes the snow into a hard porous mass. This forms a porous saline layer at the upper ice surface with a thickness of 10-30 mm. Figure 7a shows such porous ice at the top of the ice core, taken in February 1976 at an air temperature of -36°C north of Lonely, Alaska, and Figure 7b shows the salinity and temperature profiles for the core. Comparison of Figure 7b with Figure 3c shows that the high surface salinities now appear to be spread out into the porous snow ice.

Both the high surface salinity caused by the growth of young ice and the porous snow ice help determine the way in which sea ice absorbs oil; the high surface salinity initiates the growth of top-to-bottom brine drainage channels, and the porous ice absorbs the oil which comes up the

channels.

3. Brine Drainage Channels

First-year ice generally grows to a thickness of 1-2 m, with a predominantly columnar crystal structure. For oil entrainment, the most important feature of this ice are the tubes extending up into the ice with diameters ranging up to 10 mm, called brine drainage channels.

Brine channels are observed in all parts of the growing season for first-year ice; however, they are largest and most effective when the ice becomes warm. Lake and Lewis (1970) show that the brine drainage systems form between crystal boundaries with feeder channels coming in between the platelet boundaries. Figure 8 shows an observation made by Robert Lake of the brine tube distribution at the bottom of a 1.6 m thick piece of first-year ice taken in February 1968 at Resolute Bay, N.W.T.; the brine channels have a characteristic spacing of about 0.1 m on a rectangular grid. In the 1.6 m thick ice, these channels extended 0.1 to 0.5 m up into the ice.

In our observations, we observed very few channels in the fall and winter from our ice cores. As an example of a winter channel, which is one of the few which we saw, Figure 9 shows a core taken on 8 November 1975 from ice of 0.31 m thickness. The drainage channel in the core which is at most 3 mm in diameter grows out of the near surface ice and extends to the bottom of the core. From rafted ice in November 1975, we saw indirect evidence of drainage channels. When the ice was rafted, the brine within the channels drained out, leaving desalinated ice above and salty stalactites growing on the ice bottom, which also had about a 0.1 m grid spacing.

The major brine channel growth occurs in the spring, when both the air and the ice temperature warm up toward the freezing point. As an example of a spring brine channel, Figure 10a shows the upper 0.78 m of a core taken in Prudhoe Bay about 2.5 nautical miles south of Cross Island on 21 May 1976 at an air temperature of -8.6°C . In the lower portion of the core, a long brine channel is visible; the break in the channel may be caused by a slight rotation of the core during the longitudinal cutting. For the same core, Figure 10b shows the salinity and temperature structure; the salinity profile shows that the high surface salinities present in the fall and winter cores are now replaced by near-zero values. The downward movement of the surface salt has led to the brine channel growth.

The photograph in Figure 10a shows that the crystal structure of the core is such that below a depth of 0.15 m, the sea ice is columnar; above this depth, tightly grained snow or frazil ice replaces the columnar ice. Also above 0.15 m, the shadows of what are probably air bubbles with diameters of 2-3 mm are visible. Judging from our other shore-fast ice cores, the freeboard of this ice is probably 0.16-0.20 m, so that the vertical extent of the bubbles may be correlated with the freeboard. As we show in the next section, these bubbles tend to absorb the oil which flows up the brine channels.

Figure 11 shows the salinity and temperature profile of another warm core taken on 26 May 1976 at an air temperature of -1.5°C . For this case the surface ice has nearly been completely desalinated. The warming of the ice causes it to become porous and less salty. If the upper part of the ice is frazil ice, then as it warms, the ice becomes slushy. Figure 12 shows the upper portion of a core where the top 30 mm are refrozen

snow, and the next 100 mm are frazil ice. Our laboratory studies show that, because the basic crystal which makes up frazil ice is so much smaller than the elongated columnar ice platelets, the warm frazil ice becomes slushy, whereas columnar ice retains its structural integrity. If the frazil ice is located above the water line, it may serve as an additional sponge for any oil released either under or on top of the sea ice.

The porosity of the near-surface ice may have one additional effect. If there is sufficient snow or desalinated ice above the freeboard to provide a source of fresh or low salinity water; upon melting, this water may percolate down into the porous layer and refreeze, from heat loss either to the colder ice below or to the atmosphere on a cold day. We have observed this refreezing process in the laboratory, and it provides an explanation for some of the observations described in the next section.

4. Oil in Sea Ice: Results from the NORCOR Study

The NORCOR Experiment (1975) was a study carried out in a partially enclosed bay on the Cape Parry Peninsula, N.W.T., Canada, on the behavior of oil released at different times of the year under first year ice. Two kinds of oil were used; a Norman Wells crude with a pour point of -50°C and a specific gravity at 0°C of 0.845 and a Swan Hills crude with a pour point of -5°C and a specific gravity at 0°C of 0.835. A thorough description of the experiment and the oil properties are given in the Beaufort Sea Project Technical Report No. 27 (1975); in this section, we will only look at interaction of these oils with first year ice.

a. A winter spill

As an example of oil behavior under young columnar ice, Figure 13 shows a photograph of a core pulled on 15 November 1974; the oil lens was

located at the second break down in the core from the top. The Norman Wells crude oil in this core was spilled on 24 October 1974 under ice with a thickness of about 0.38 m. Because of lateral variations in the ice thickness, the oil collected in pools under the ice, and the oil lens thickness in the above core was about 10 mm. Examination of Figure 13 shows that, above the oil lens, the oil moved uniformly up 10-20 mm into the skeletal layer; above this height the oil moved an additional 70-80 mm up through four small brine channels. From our examination of the core at the site, we estimated that the first 50 mm of ice above the oil lens held by volume about 5% oil.

Directly under the oil lens, the photograph shows a clear ice 'cap' of about 10 mm thickness. Figure 13b shows a close-up view of this cap; our salinity measurements showed that this ice had a low salinity. There was no evidence of oil penetration through the cap, and beneath it the sea ice abruptly resumed its columnar ice growth. The oil in the ice beneath the cap, we feel, entered the core during the removal of the core from the hole.

The reason this cap forms beneath the oil pool is that the thermal conductivity of sea ice is 19 times that of oil. This means for steady state heat transfer, 10 mm of oil are equivalent to 190 mm of sea ice; so that the release of oil under ice, for a constant surface temperature, greatly reduced the heat flux through the oil-ice mixture. This heat flux reduction means that the new ice growth beneath the oil starts off very slowly, and Weeks and Lofgren (1966) show that when sea ice grows very slowly, it is very nearly salt free. This appears to be a reason for the cap formation. The cap, with the additional buoyancy of the new ice growth underneath it, tends to pressurize the oil lens, so that in

the fall growing season, coring into an oil lens resulted in oil flow up the core hole; in one instance, oil jetted up around the SIPRE corer to a height of 0.3 m above the ice surface. The oil then is ready to flow upward and move out of the lens as soon as a path presents itself.

In summary, when oil is released under young columnar ice sheets, it tends to flow into pools under the ice, where some of it is entrained in between the platelets in the skeletal layer, and some of it flows up into the brine channels. The observations made at the site through March 1975 showed that the oil in the ice remained essentially static, with only a slight rise of oil up the brine channels as the ice began to warm.

For the period 15 February - 22 May, 1975, Figure 14 shows a selection of temperature profiles from a control thermistor chain in unholed sea ice at the test site. The figure shows that there was a warm period in April, where the air temperature increased from -15°C to a maximum of about 10°C , whereupon it cooled off again in May. Because of this strong warming, sometime in late April, top-to-bottom brine channels in the ice opened up and the oil came to the surface under the snow. Once the oil arrived at the surface, it was free to interact with the surface ice.

Beginning to 10 May 1975, the author carried out an intensive coring program at the site. We also investigated the effect of oil released under this relatively warm ice. Before discussing the changes in the winter discharges, we first discuss the spill under warm ice.

b. The 15 May 1975 discharge

At 1700 h on 15 May 1975, we carried out a small oil discharge under 1.95 m of ice. Immediately preceding the experiment, we shoveled the snow from the surface down to the hard sea ice. Figure 15a shows the sur-

face appearance before the discharge. The air temperature was about -8°C ; the ice surface temperature taken from a nearby thermistor chain was -3°C . John Overall and David Lapp carried out the discharge; it consisted of two barrels of Norman Wells crude oil injected in the space of 3 minutes under the cleared area through a slanted discharge pipe.

By 45 minutes after completion of the discharge, a single oil droplet with a 1 mm diameter appeared on the ice surface inside the cleared area. We marked the droplet location with a small nail stuck into the feeder channel. As time went on, the oil spread laterally from this point both over and within the ice surface; at other points on the surface, droplets also appeared and spread laterally. Figure 15b shows the surface appearance at about two hours after the discharge. In the figure, the nail which marks the point of first appearance is slightly above the shadow thrown by the post. The oil which came to the surface and spread laterally gives the ice a mottled appearance. The distance between the centers of the oiled areas varies from 0.1 to 0.5 m and the diameters of these areas range from 0.1 to 0.2 m. The spacing of the oiled blotches on the ice surface in Figure 15b is consistent with Lake's observations in Figure 8.

Between 1500 and 1600 hours on the following day, we pulled cores from the spill. For one of these, we centered the SIPRE barrel around the surface point of first appearance and cored down. Figure 16a shows the resultant core, where the core bottom is to the left and the core length is 1.95 m. Except at the very bottom of the core, the ice was hard to the touch. The photograph clearly shows the oil-filled brine channel running throughout the core length, with smaller feeder channels running diagonally outside of the core. Figure 16b is a close-up of the

large bottom core segment in 16a; the main channel in the ice bottom was large enough to hold a pencil.

To measure the amount of oil contained in this core, we melted it down to recover 85 ml of oil and 7.8 liters of fluid. If we estimate the oil losses caused by oil sticking to the sides of the pails and insides of the plastic bags used to hold the core pieces during the melting-down at 15 ml, then we have 100 ml of oil contained in the core, or a 1.3% oil content. This estimate neglects the flow of oil out of the large brine channel caused by our removal of the core. If we assume that a 4 mm diameter channel runs the length of the core, we only obtain an additional 25 ml of oil within the core, so that the relative oil volume of the core is 1.6%. Finally, since the oil rose through 1.95 m of ice in 50 minutes, its rise velocity was 4 cm min^{-1} or 0.7 mm s^{-1} .

c. Oil and the upper part of the ice

The upper part of the core in Figure 16a illustrates another interesting feature of this spill; namely that the oil at the ice surface is absorbed within the ice, and that the near-surface absorption occurs in horizontal bands. From analogy with our OCS field work, we feel that the cause of these oiled bands at the surface are the layers of snow and frazil ice.

To examine this banded, near-surface structure in detail, Figure 17a shows the top 0.6 m of a core which was pulled on 16 May from the 12 April 1975 Swan Hills crude spill; this core also shows a banded structure in the upper part of the ice for the more viscous Swan Hills crude oil. Figure 17b shows a 20 mm thick section of 17a taken by transmitted light with an adjacent schematic diagram. The figure shows that the upper part of the ice is composed of four parts:

1) The top 15 mm. This ice is nearly clear of oil and overlies a bubbly layer of oil. A similar clear zone occurred in a large number of the cores which we pulled in May, including the surface spill discussed below. We suspect that this clear ice forms from the absorption of solar radiation by the surface oil, which causes melting and collapse of the overlaying snow which then refreezes into clear ice, in a manner similar to the formation of the refrozen snow layer shown in Figure 6a. This layer is absent from the core shown in Figure 16, where the oil was only on the surface for one day.

2) The region between 15 and 80 mm. In this region, the oil is trapped in form of spherical bubbles within the ice. In some cores we observed this layer to be simply oil-soaked ice, rather than trapped droplets. From our field and laboratory observations, this region is either the porous, refrozen snow shown in Figure 7a, where oil has filled the pore holes, or the bubbles in the core in Figure 10 which are now oil filled, or oil-soaked frazil ice such as Figure 12 shows.

3) The region of clear ice between 80 and 180 mm. This ice was apparently frazil ice; when we held the core segment up to the sun, we saw reflections from randomly-oriented crystals within this layer. Also, the ice below this layer is clearly columnar ice, which stops abruptly at 180 mm. The reason that this clear frazil ice zone is not saturated with oil is that the very warm period which occurred in April may have let melt water from the surface move down into the ice to fill the voids, then refreeze during the colder weather in May.

4) The region below 180 mm. This ice is clearly columnar, with the oil outlining the vertical crystals. The abrupt end of the columnar ice at 180 mm also looks like the transition from frazil to columnar ice

in Figures 5a and 5b.

The pattern of clear ice, oiled ice, clear frazil ice, and columnar ice shown in Figure 17b is present in most of the cores which we pulled in May; however, the thicknesses of the different layers varied slightly from core to core.

In the case of the open water spill, we also observed ice growth above the surface oil layer. This spill took place on 1 November 1974 in a 6 m square open area which was cut into the ice. Approximately 0.4 m^2 of Norman Wells crude was poured on this open area to a depth of about 11 mm. By 15 November, the oil had mixed with blowing snow to form a granulated mixture, which could be handled like dirt at -28°C . In the spring, the solar radiation again caused melting, collapse, and refreezing of the snow over the oil. Figure 18 is a photograph of a partial core segment, 0.3 m in length, which we pulled on 15 May from under 0.25 m of snow. The figure shows that over the dark oil-ice matrix, there is about 50 mm of clear ice, and that there is no evidence of oil penetration down into the core. When we melted down the oily portion of this core, we found 10 ml of oil in 140 ml of fluid for a 7% oil volume.

d. The Offshore spill

Additional evidence for both the free rise of oil within the brine channels and the segregation of oil within the upper part of the ice comes from the NORCOR offshore experiment, which the NORCOR report describes in great detail. This experiment took place on 8 April 1975 under a sheet of first-year ice at a location 18 nautical miles north of Cape Parry. There were no cores taken at this site until our return on 28 and 30 May 1975, so that the oil interaction with the ice was unaffected by

people walking and coring in the area.

There were two spills of Norman Wells crude oil at this site; a spill under relatively smooth ice to determine the effects of currents on a spill; and a spill next to a small weathered pressure ridge. The first spill spread out in a sheet; the second was trapped in a cavity to a depth of 0.1 m adjacent to the ridge. For both spills, oil was visible on the ice surface from the air and surface during our May visit.

From the first spill, Figure 19a shows a core which closely resembles the cores from Balaena Bay. In the photograph, an oil lens with a 4 mm thickness was located at the break in the core between the clean and oily ice. The core has oiled brine channels running through it, with some very dark oil-saturated portions. When we melted down a section of the black part of the core which lies between 8 and 14 inches on the tape measure in the photograph, we found 12 ml of oil in 485 ml of fluid for an oil content of 2.5%. The top of the core shows the zonal structure described in the previous section; Figure 19b is a close-up of the upper part of the core and shows that at the top of the core, the oil is segregated into many small droplets with the droplet size increasing with depth. This segregation may be caused by the oil mixing with melting snow. Below this droplet zone there is a region of oil-free clear ice, which may be frazil ice flooded by fresh water, and below this is a zone of large oil droplets not segregated by size. The core length is 1.27 m, so that the freeboard is about 0.13 m; this depth approximately corresponds with the droplet zone depth.

At the second spill near the pressure ridge, the location of the under-ice spill was clearly marked by the oil on the surface. We took three cores on a north-south line across the spill; Figure 20 is a sketch of the

resultant core configuration; and Figure 21 shows the core photographs. The cores confirmed the divers' observations, namely, most of the oil was trapped in a deep cavity with a thin sheet spread out on the sides. When a portion of the core in Figure 21c, which was the blackest core observed in the experiment, was melted down, we found 30 ml of oil in 910 ml of total liquid for an oil concentration of 3.3%. In other words, a relatively small amount of oil produces very dark cores. This particular core was over an oil lens which we measured as 0.1 m thick, and Figure 22, a photograph of the core hole, shows that pure oil from the lens flowed up to the surface. At the adjacent holes, oil did not rise to the surface, and the thin oil lenses were frozen within the cores. Figures 21 a-c also show that the ice beneath the oil lens appears both clean and free of oil. Figure 23, a close-up of the surface of that part of the core which grew beneath the oil lens of the black core, shows a fine wave-like fluting. Tankin and Farhadieh (1971) show that thermal convection causes similar fluting in the growth of sea ice; we suspect that thermal convection within the oil layer also causes the fluting in Figure 23.

e. Oil in feeder channels

The previous figures show that as the ice warms up, the oil beneath the ice flows up into the brine channels and associated feeder channels. In one case, on 21 May 1975, we recovered from the Normal Wells crude oil spill which was done on 15 April, a core which consisted of feeder channels contained in a crystal structure almost entirely made up of parallel ice platelets. Figure 24 shows a schematic diagram of the feeder channels, where the core in 24a is rotated 90° to the core in 24b. The photographs in Figure 25 show the side views of the core; between the

depths of 0.6 and 1.45 m, Figures 24 and 25 show that the core is filled with plane parallel diagonal feeder channels. These feeders have a vertical spacing of 5 to 10 mm, and lie at an angle to the horizontal of approximately 40° .

From the core sections marked 1 and 2 in Figure 24, we cut thin horizontal and vertical sections. Figure 26 shows the two views from section 1; the vertical in 26a and the horizontal in 26b. In the vertical cut, the channels are nearly vertical; while in horizontal, the crystal platelets are oriented in about three directions, with a predominant slope from upper left to lower right. Figure 27 shows a similar horizontal and vertical section from the lower part of the core in section 2. The horizontal cut shows that the crystal platelets almost all lie in the same plane; and the vertical cut, which is taken parallel to the crystal planes, show that the feeder channels have the same slope. The photographs also show that within the ice, the oil is entrained not only in brine channels but also between the crystal platelets. When we melted down an ice sample near section 2, we found 30 ml of oil in 550 ml of fluid for an oil volume of 5.5%. This was the largest oil volume observed within the ice during the experiment, and suggests that large feeder channel systems within plane parallel crystals will be important in the absorption of oil by sea ice.

The data of Campbell and Orange (1974) suggests that the formation of sea ice with plane parallel crystals may not be an isolated occurrence. Using an impulse radar on the sea ice in the Canadian Queen Elizabeth Islands, they made numerous observations of anisotropic sea ice which they feel was caused by the growing ice platelets lining up in the direction of the predominant tidal current. If ice composed of parallel plates

does form in tidal channels, the core described above suggests that this ice could be important as an additional sink for spilled oil.

f. Trapping of oil within the ice

The coring observations show that away from the oil lenses that the low viscosity Norman Wells crude oil tended to spread out in thin sheets, and the high viscosity Swan Hills crude oil formed into small droplets under the ice. As an example of the Norman Wells behavior, Figure 21a shows for the offshore experiment a frozen-in sheet of Norman Wells. Underwater observations at the site confirmed that the low viscosity Norman Wells tended to spread into these sheets. The Swan Hills crude, on the other hand, formed into small droplets. Figure 28 shows two views of droplets in a core taken on 21 May 1975 from the Swan Hills spill of 7 December 1974. These droplets were at a depth of 0.74 m from the surface. Figure 28a shows the side view of the droplets; the largest has a diameter of about 10 mm. Figure 28b, the top view, shows that smallest drop diameters are of the order of microns. The presence of both these small droplets and thin oil sheets within the ice probably means that some spilled oil would remain intact over the summer, rather than rise to the surface through the brine channels.

g. Oil on the surface

When oil came to the surface in the spring, it spread laterally both within and on the ice under the snow. The oil affected the appearance of the snow in two ways. First, the snow color changed from white to a light yellow; second, because of the radiation effects described in the previous sections, the snow subsided and in cases refroze over the oil. Even under snow depths of up to 0.3 m, the color and snow depth change generally marked the oil location under the snow. Because of

the radiation absorption by oil, melt ponds formed earliest over oily surfaces. Figure 29a shows a photograph of an oiled melt pond at the Balaena Bay site taken on 15 May 1975, where there is the possibility that some of this oil came up old core holes. Figure 29b shows an example of one of several small melted-through holes at the Offshore Site, which was taken on 28 May just after our landing at the site. The oily melt ponds, then, formed well in advance of the unoiled melt ponds. On 8 June, Mr. Richard Brown made a final visit to the Offshore Site, and found a dead, partially-eaten bird in an oiled melt pond, whose formation may have been accelerated by our May coring. The premature formation of oiled melt ponds will probably serve to attract migratory birds.

5. Concluding Remarks

The previous two sections describe the growth of young ice, and the role that the initial upward salt migration plays in the later development of the top-to-bottom brine drainage channels. The drainage of the surface salt does at least three things. First, it generates the top-to-bottom brine drainage channels; second, it helps form the porous snow ice at the sea ice surface; third, it generates void spaces above the freeboard of the sea ice. The oiled ice discussion shows that even for the Swan Hills crude oil with its pour point of -5°C , that the oil rises up the warm brine channels, then distributes itself within the brine channels and throughout the porous surface ice. We observed that the amount of oil trapped within the ice varied between 1 and 5% by volume. Both the entrapment of oil within the porous surface ice and the contain-

ment of it within brine and feeder channels means that the release of the oil from the ice may be slow but continuous throughout the summer melt season.

Acknowledgements

This report draws heavily on data taken for the OCS program by the author with the help of Peter Kauffman, Edward Josberger, Terren Niedrauer, and Steven Soltar. I am especially grateful to Peter Kauffman for the design of the photographic techniques. The data on oiled ice comes from my work as a consultant with the NORCOR corporation at Balaena Bay. I thank Richard F. Brown for his invitation to participate in that project, for permission to use several photographs and Figure 14 which appeared in the NORCOR report, and for many useful conversations. I also thank David Dickins, John Overall, and George Greene for useful conversations and support at Balaena Bay; additional support was provided by Sandra Brown, Tom Kitchen, David Lapp, and Oscar Mullerbeck. With regard to the general topic of brine drainage from sea ice, I especially thank Robert Lake for many useful talks, and for the use of his data in Figure 6. Finally, I thank Dr. William Campbell for his help during the preparation of this report. The writing of this report was supported by BLM/NOAA Contract No. 03-5-022-67, Task Order No. 6, RU #87.

Bibliography

- _____ (1975). The interaction of crude oil with Arctic sea ice (NORCOR Engineering and Research Limited), Beaufort Sea Technical Report #27, Beaufort Sea Project, Department of Environment, 512 Federal Building, 1230 Government Street, Victoria, B.C. V8W 1Y4, Canada.
- Campbell, K.J. and Orange, A.S. (1974). The electrical anisotropy of sea ice in the horizontal plane. J. Geophys. Res., 79(33), pp. 5059-5064.
- Lake, R.A. and Lewis, E.L. (1970). Salt rejection by sea ice during growth. J. Geophys. Res., 75(3), pp. 583-597.
- Michel, B. (1971). Winter regime of rivers and lakes, CRREL monograph III-B1A, Cold Regions Research and Engineering Laboratory, United States Army Corp of Engineers, Hanover, New Hampshire.
- Ramseier, R.O., Gloersen, P., Campbell, W.J., and Chang, T.C. (1975). Mesoscale description for the principal Bering Sea Ice Experiment, in USSR/US Bering Sea Experiment (ed. Kondratyev, K. Ya.), Gidrometeoizdat, Leningrad, pp. 234-270.
- Tankin, R.S. and Faradieh, R. (1971). Effects of thermal convection currents on formation of ice. Int. J. Heat Mass Transfer, 14, pp. 953-961.
- Weeks, W.F. and Lofgren, G. (1967). The effective solute distribution coefficient during the freezing of NaCl solutions, in Physics of Snow and Ice (ed: H. Oura), 1, Hokkaido University, pp. 579-598.

Figure Captions

1. A newly opened lead, 7 November 1975.
2. Salt flowers; the chisel blade measures 60 mm across.
3. Columnar ice. (3a) Ice core taken north of Deadhorse on 2 November 1975; core bottom is at left. (3b) The bottom of a columnar ice core; scale is in millimeters. (3c) Salinity and temperature profile of the core shown in (3a); salinity ●, temperature ○.
4. Frazil ice growing in an open lead; 18 May 1976.
5. Frazil ice. (5a) Ice core showing both frazil and columnar ice taken 23 May 1976; core bottom is to right. (5b) A laboratory ice core from ice grown in a wave field; core bottom is to right, scale is in millimeters. (5c) Salinity and temperature profile of the core shown in (5a); salinity ●, temperature ○.
6. Ice grown from snow mixed with sea water. (6a) Ice core taken 7 November 1975, core bottom is at left. (6b) Salinity and temperature profile for core in (6a); salinity ●, temperature ○.
7. Ice formed from re-crystallized snow on sea-ice surface. (7a) Partial photograph of core taken on 20 February 1976; middle gap was caused by flash malfunction. (7b) Salinity and temperature profile for core in (7a); salinity ●, temperature ○; note scale change on salinity between (7b) and (6b).

8. Sketch of the brine channel distribution on the bottom of first-year ice made in February 1968 by Robert Lake. Large circles have a diameter of about 10 mm; large dots, about 5 mm; small dots, about 1 mm.
9. Core taken 8 November 1976 showing brine drainage channel; index card gives scale.
10. Brine drainage channels in the spring. (10a) The top 0.57 m of a core taken on 21 May 1976; top of core is at upper left, segment on right is the lower continuation of segment at left. (10b) Salinity and temperature profile for (10a); salinity ●, temperature ○.
11. The salinity and temperature profile of a very warm core taken 26 May 1976.
12. The upper portion of a core taken 25 May 1976; top is at left.
13. Ice core taken through an oil spill on 15 November 1974. (13a) The whole core; (13b) The ice directly beneath the oil lens.
14. Temperature profiles from the 1975 Balaena Bay test site. 1. 15 February, 2. 28 February, 3. 16 March, 4. 31 March, 5. 15 April, 6. 30 April, 7. 14 May, 8. 22 May.
15. The 15 May 1975 discharge. (15a) Site appearance before spill; (15b) Appearance two hours after spill.
16. Core from 15 May 1975 spill. (16a) The total core with bottom at left. (16b) Close-up of ice bottom in (16a).

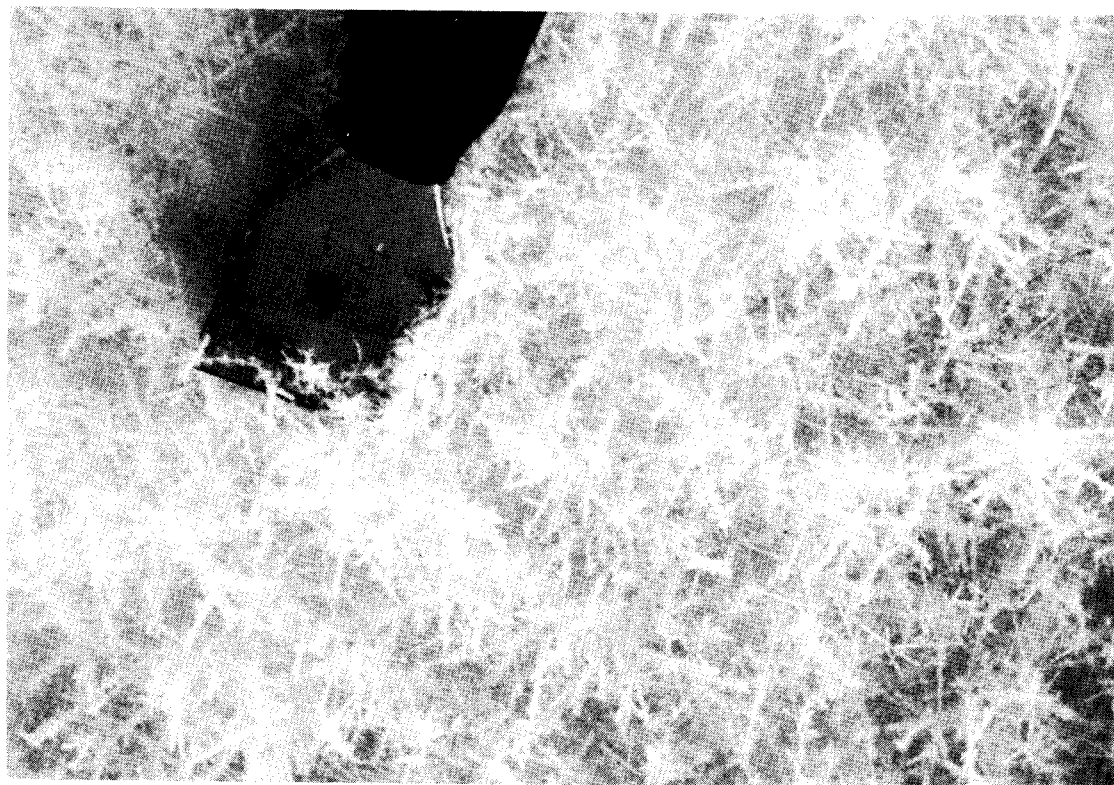
17. Oil and the upper part of the ice. (17a) The top 0.6 m of a core contaminated with Swan Hills crude oil, top of core is at right. (17b) Photograph by transmitted light of 20 mm thick segment of upper part of (17a) plus explanatory diagram; see text for additional description. Break in this core at 80 mm depth occurred during cutting.
18. Core from the surface spill; top is at left. See text for additional description.
19. Core from the Offshore Site. (19a) The total core with the top at left. (19b) Detail by transmitted light of the upper part of the core in (19a). Scale at left is in centimeters.
20. Sketch of the configuration of the three cores pulled near the pressure ridge. Symbols at bottom of each core refer to photographs.
21. Photographs of the three cores shown in Figure 20.
22. Photograph of the core hole for core shown in Figure 21c (OS3).
23. Close-up photograph of the ice beneath the oil lens for core OS3.
24. Schematic diagram of the feeder channel distribution for the core pulled on 21 May 1975. View in (24a) is rotated 90° from the view in (24b).
25. Core photograph of core sketched in Figure 24a. Top of core is at upper left; bottom is at lower right.
26. Detail of core from section marked '1' in Figure 24. (26a) Vertical section. (26b) Horizontal section.

27. Detail of core from section marked '2' in Figure 24. (27a) Vertical section. (27b) Horizontal section.
28. Detail of frozen droplets of Swan Hills crude oil. (28a) Vertical section. (28b) Horizontal section. Scale is in tenths of inches.
29. Oiled melt ponds. (29a) Balaena Bay, 15 May 1975. (29b) Offshore Site, 28 May 1975.

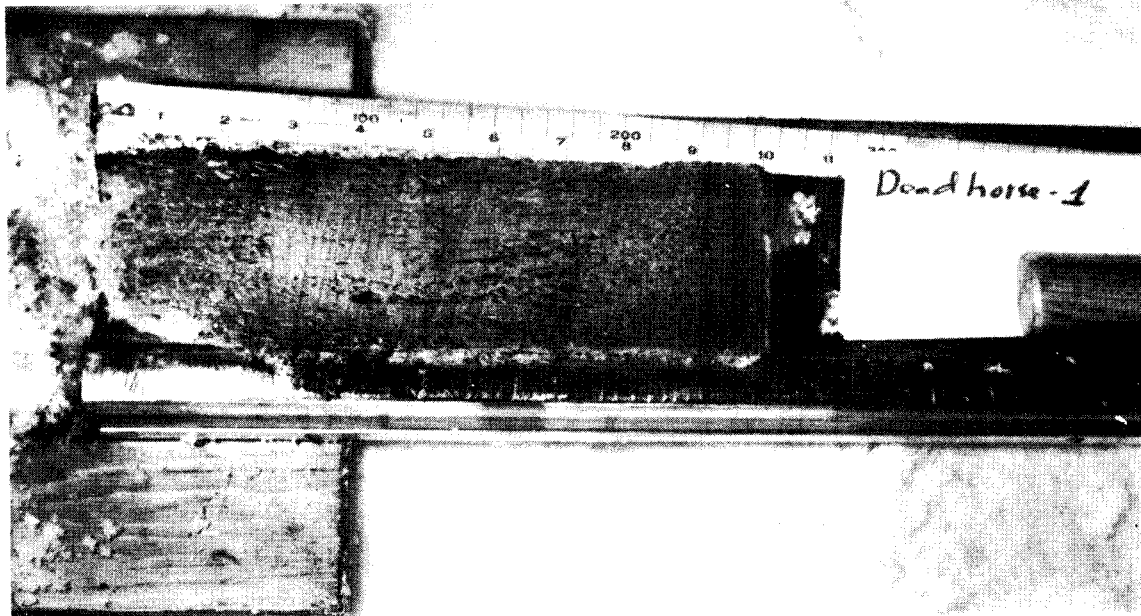
1



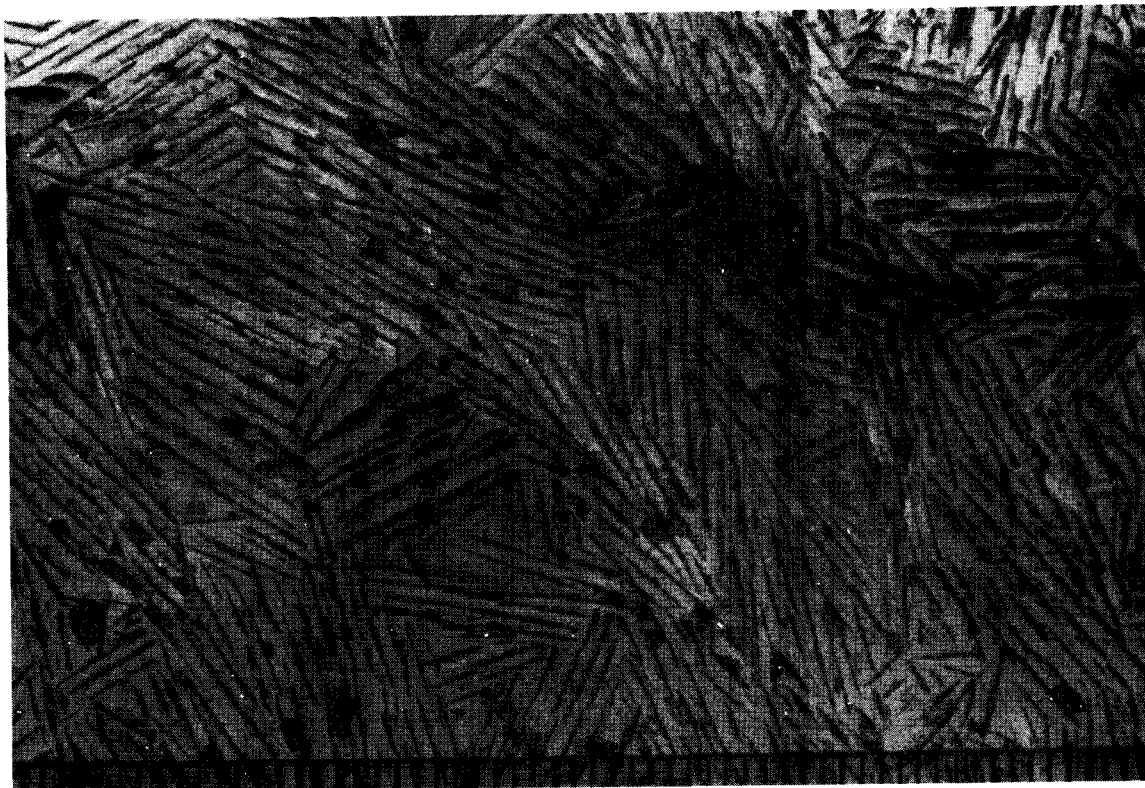
2

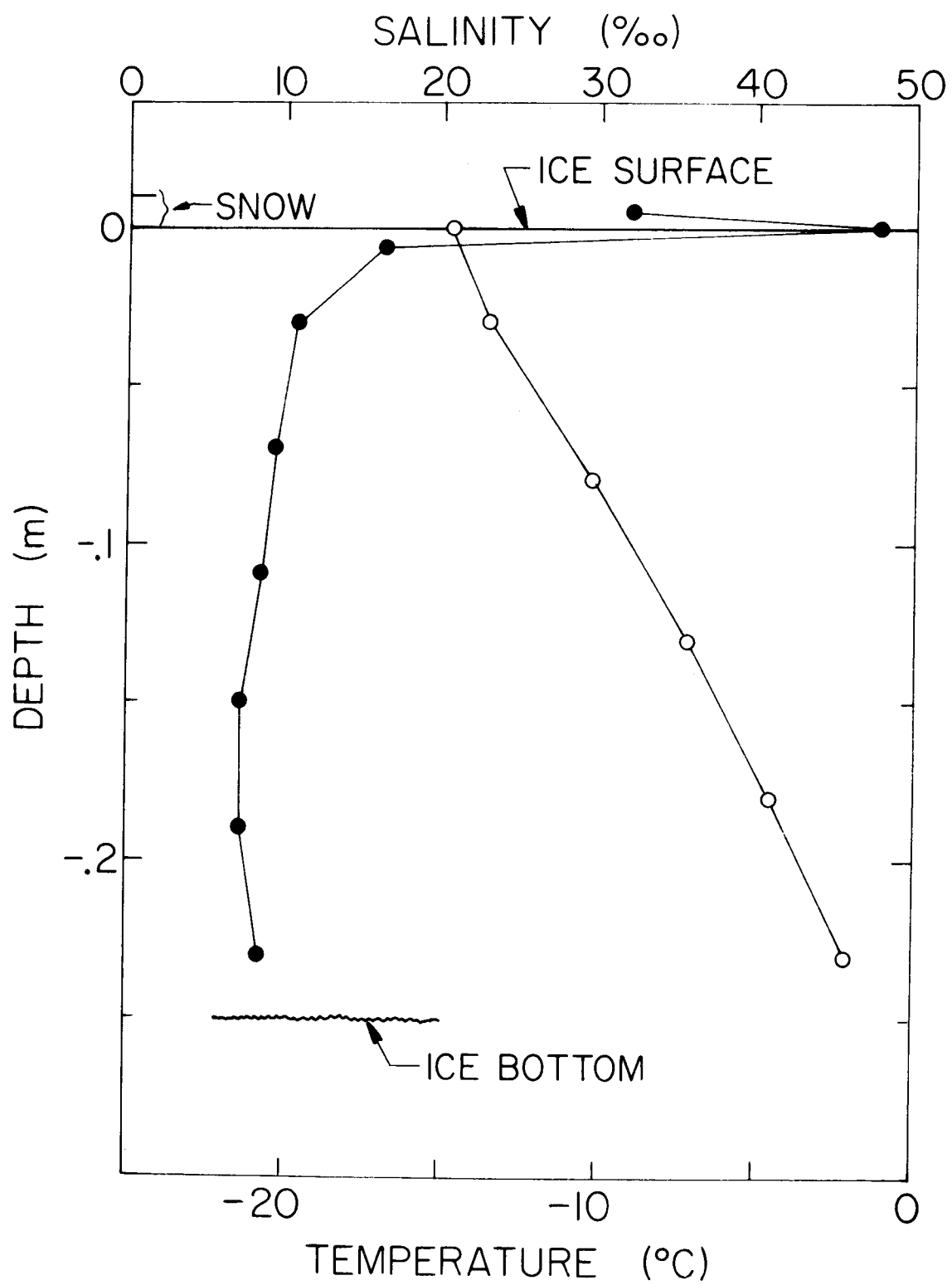


3a

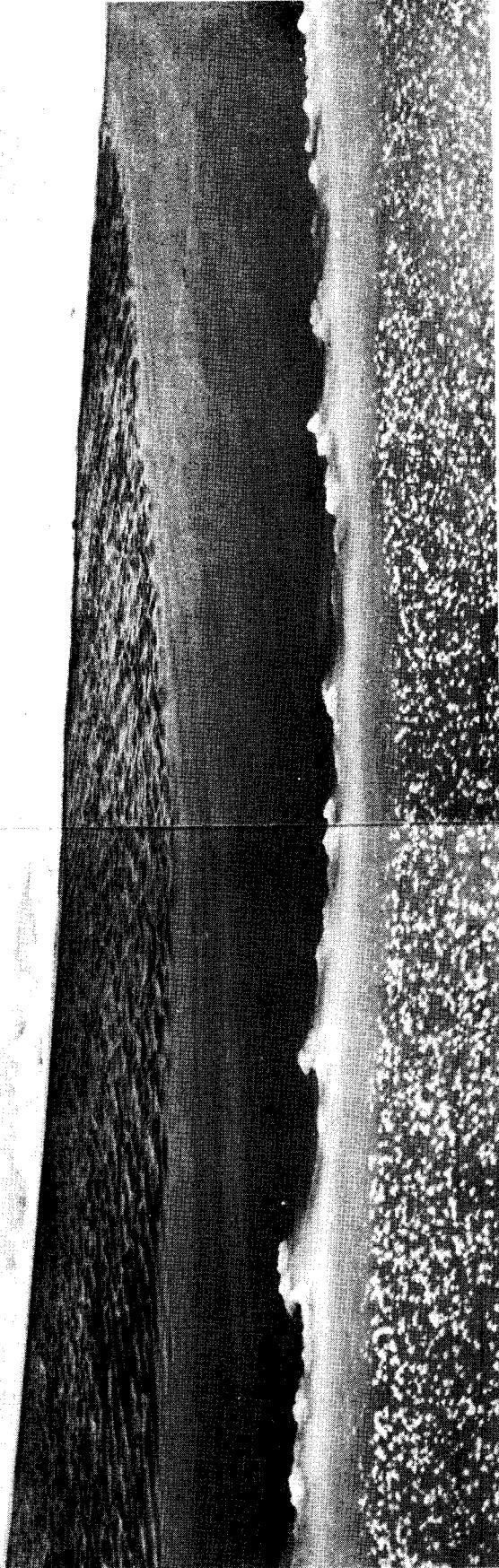


3b



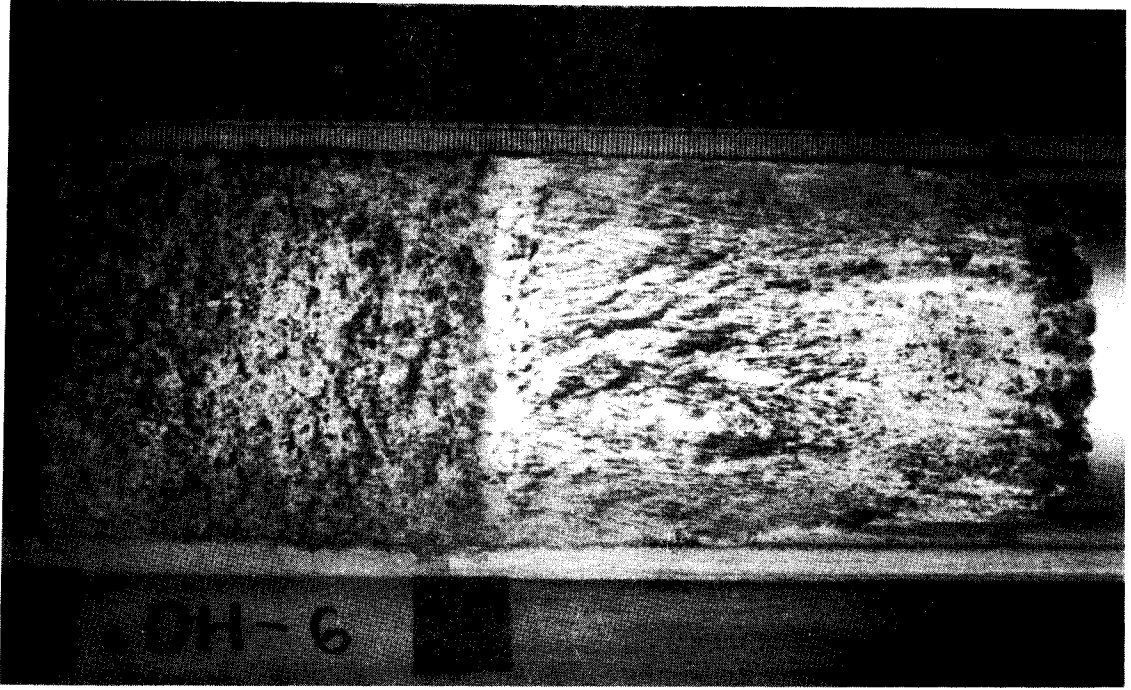


3c

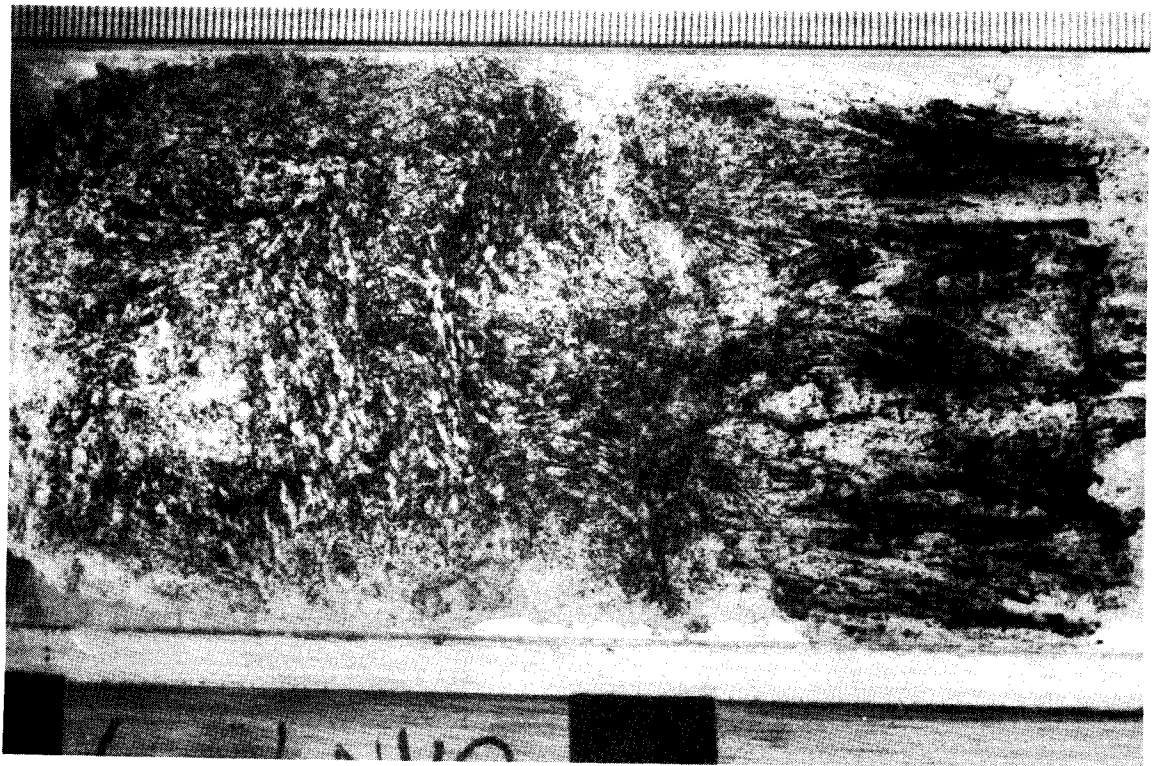


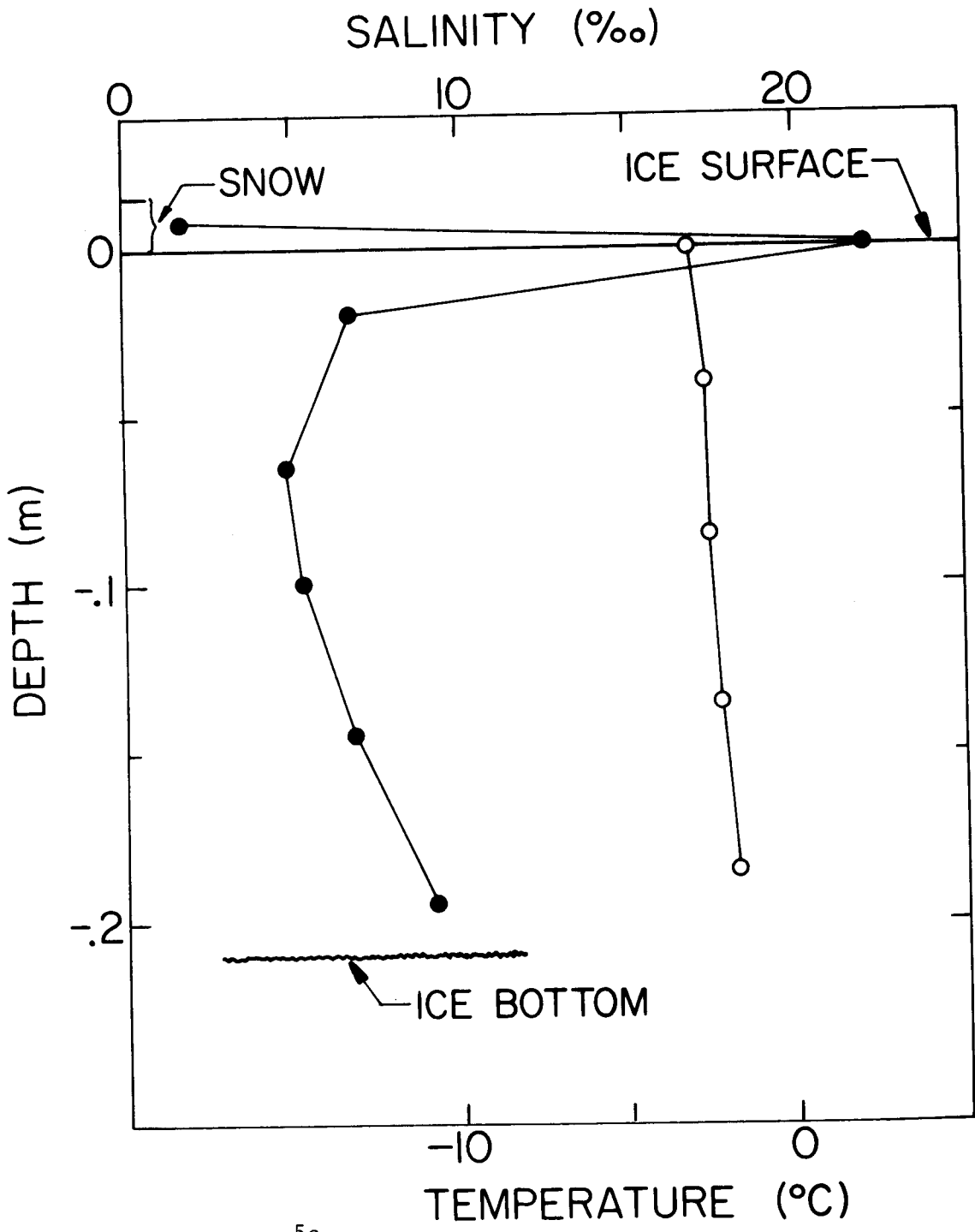
4

5a

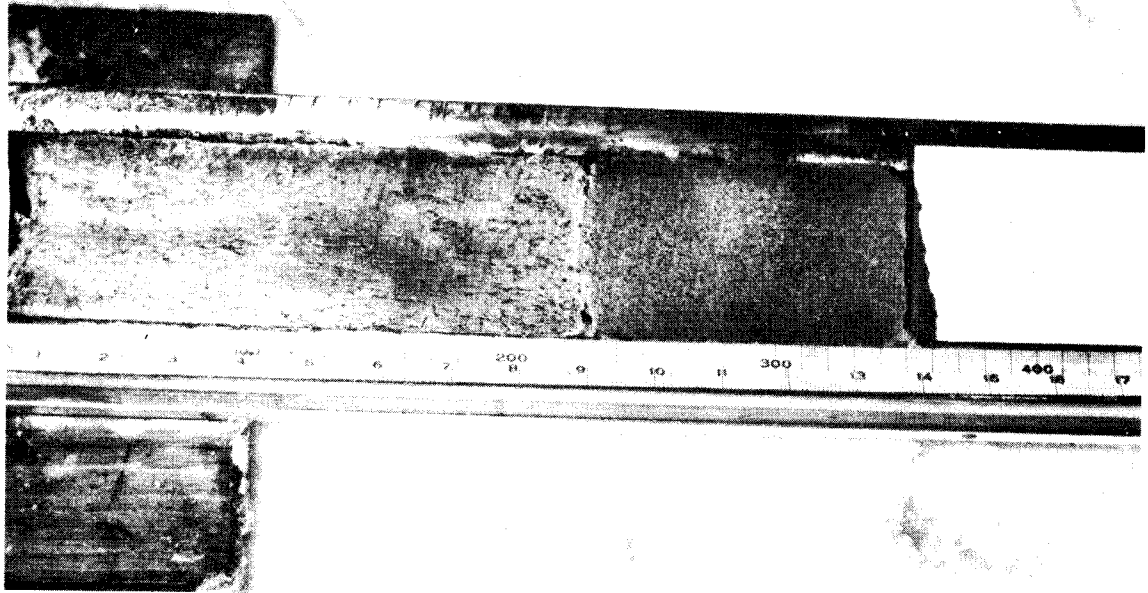


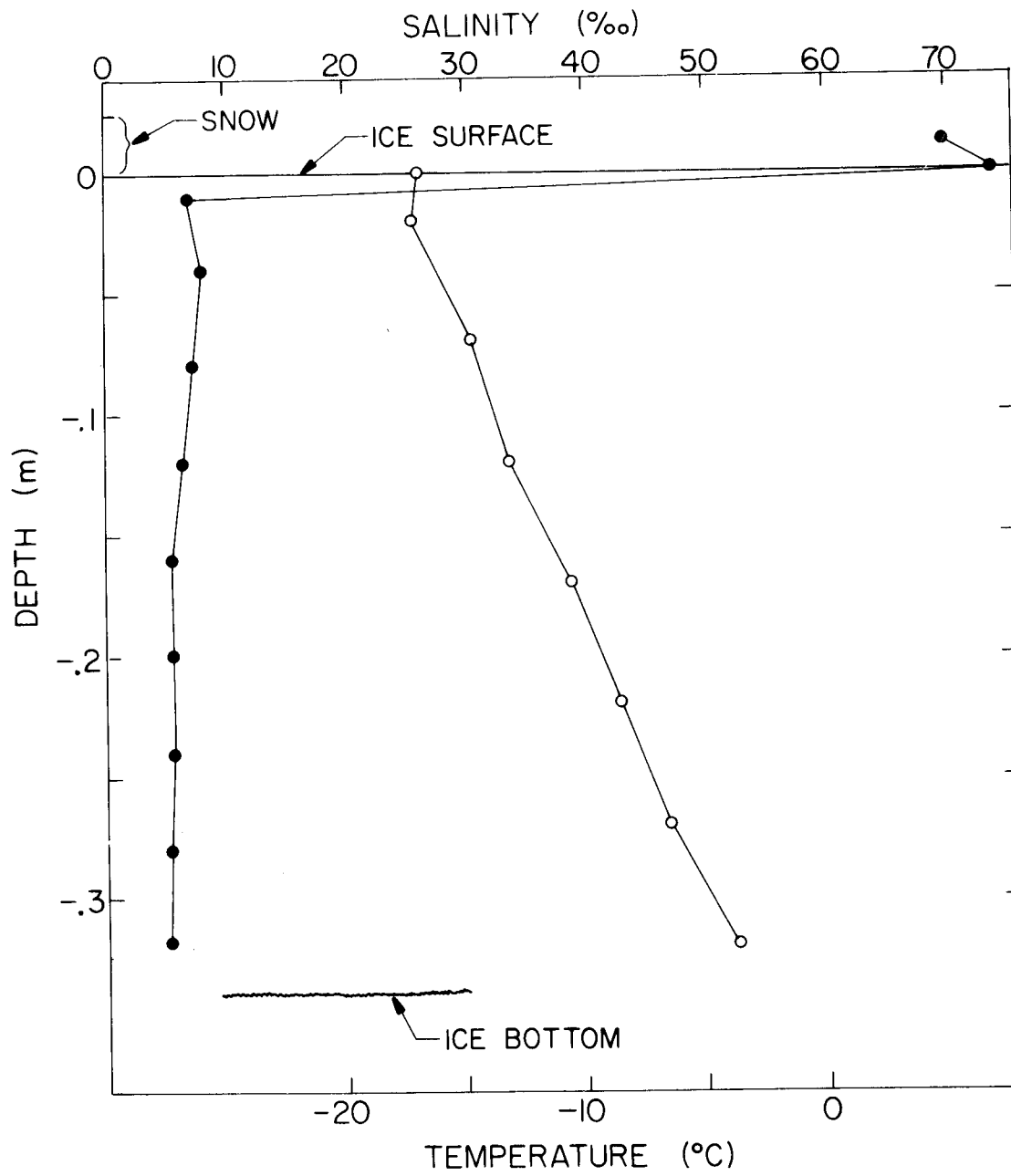
5b



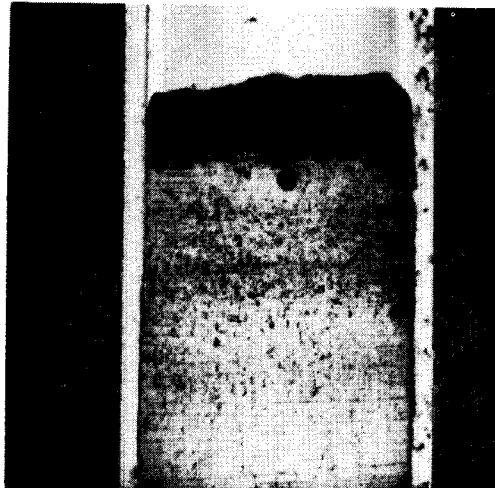


6a





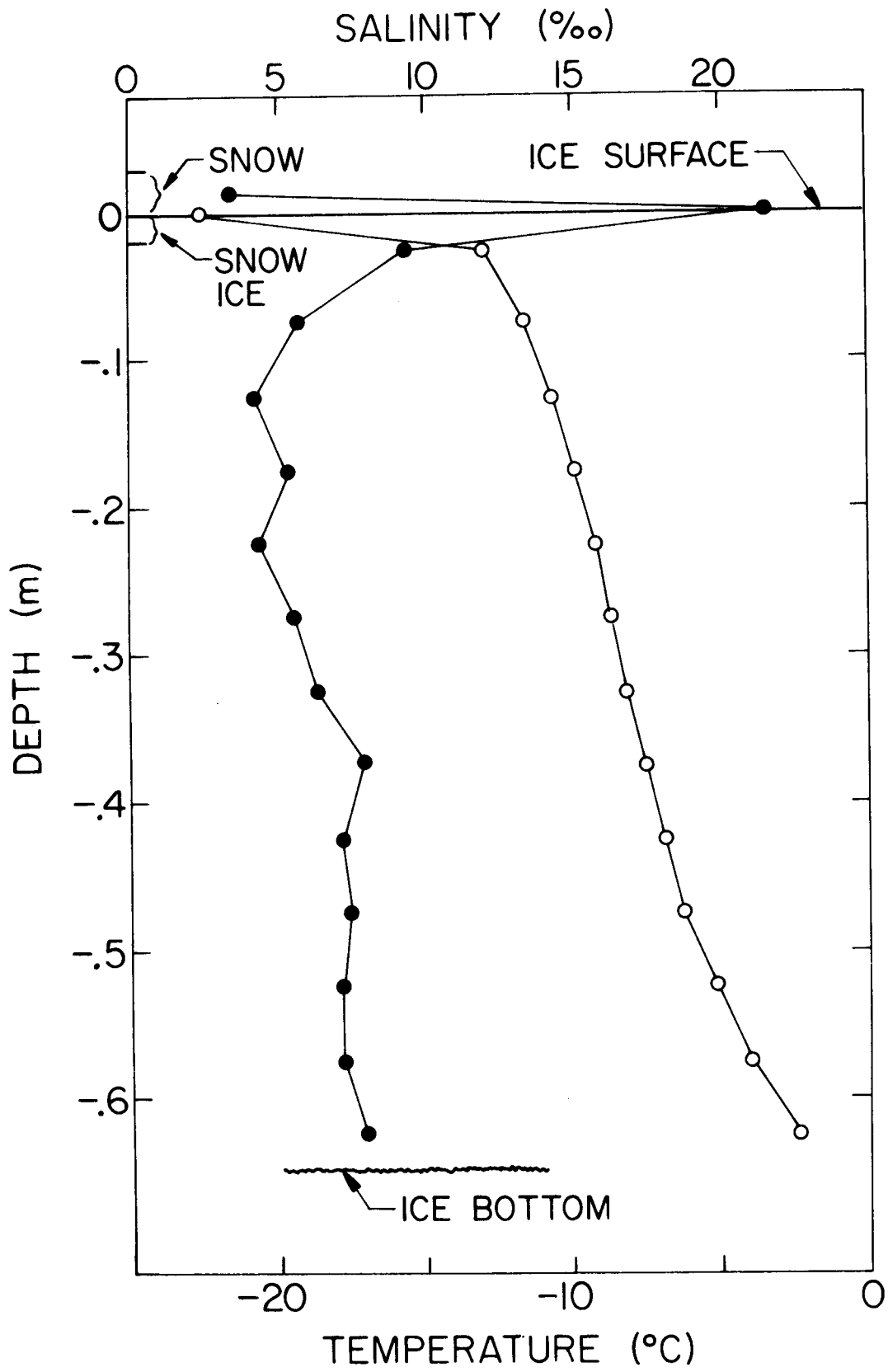
6b



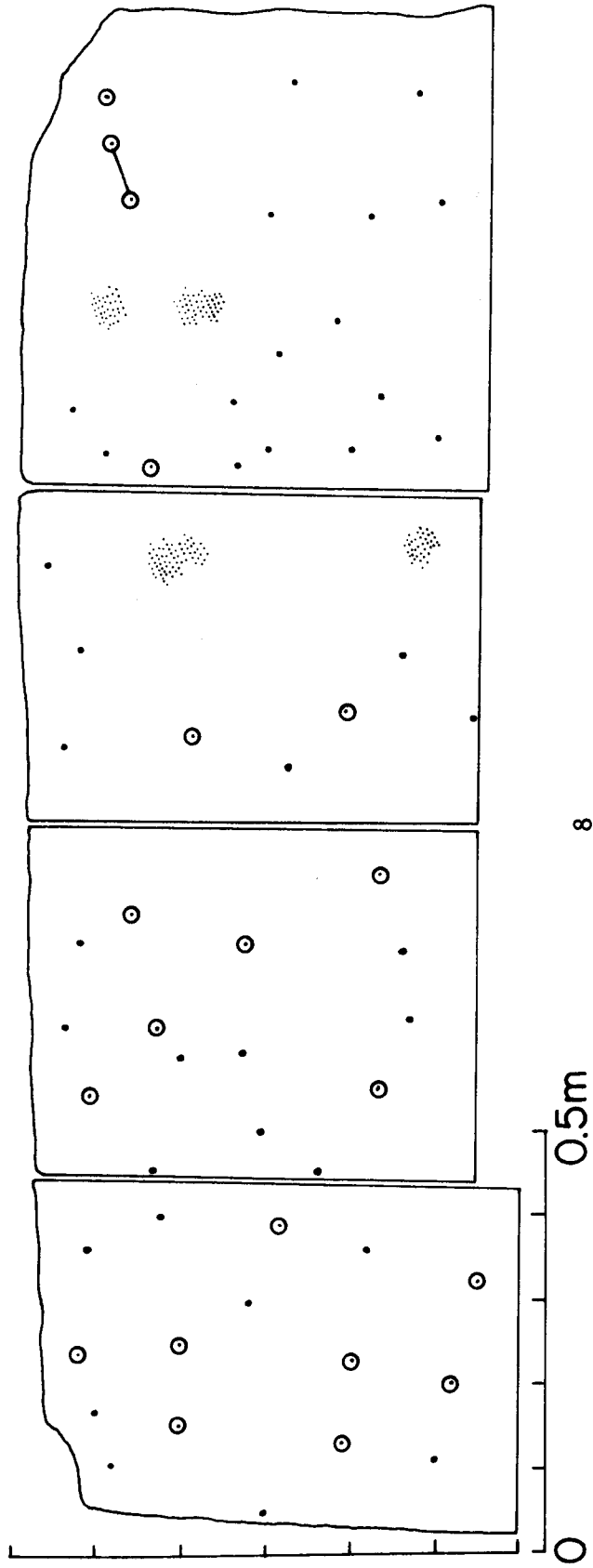
0.13m



7a

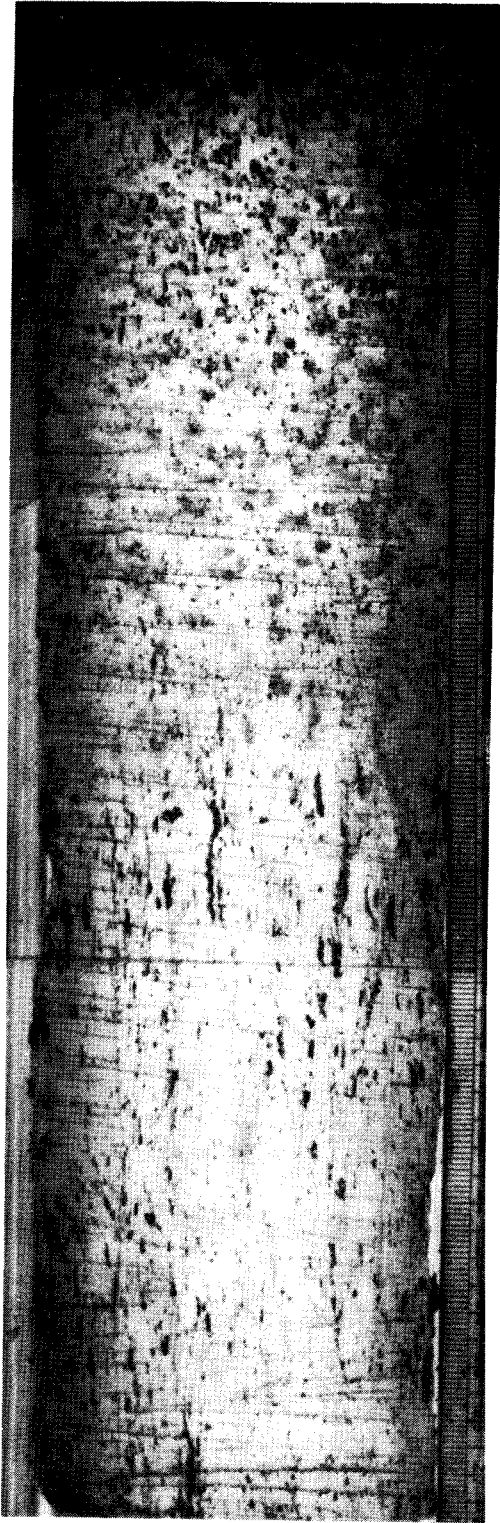


7b



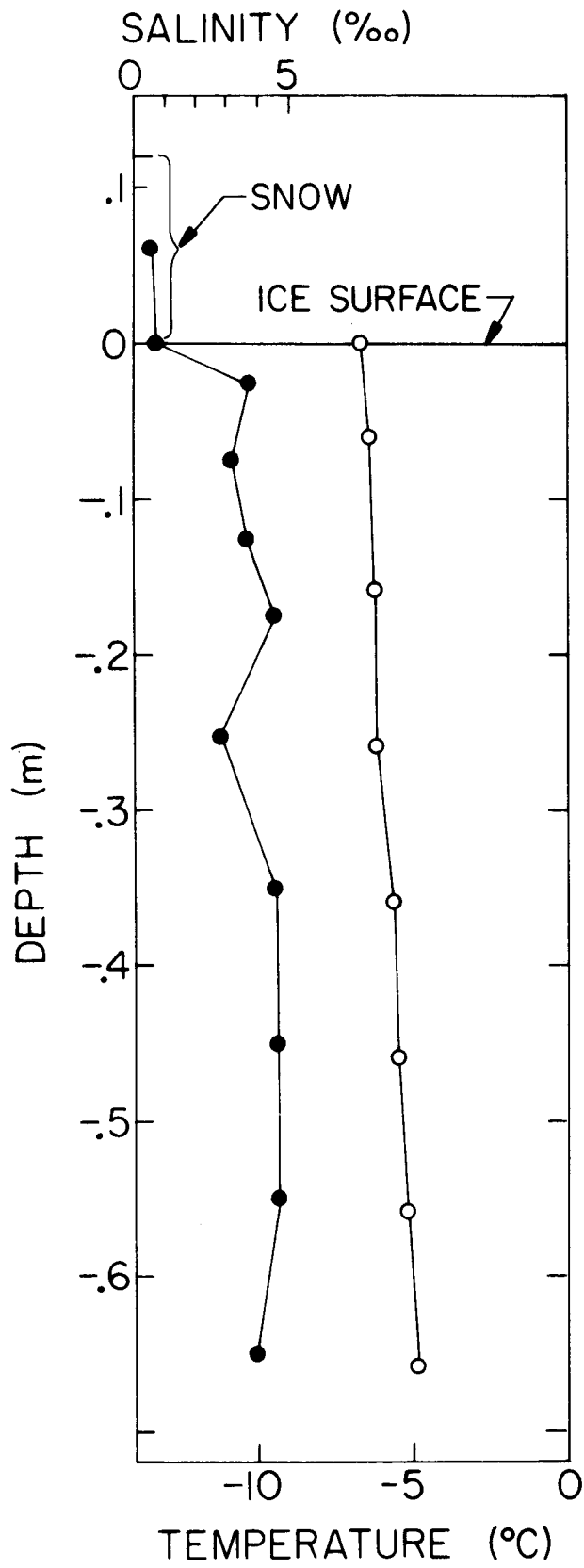


9

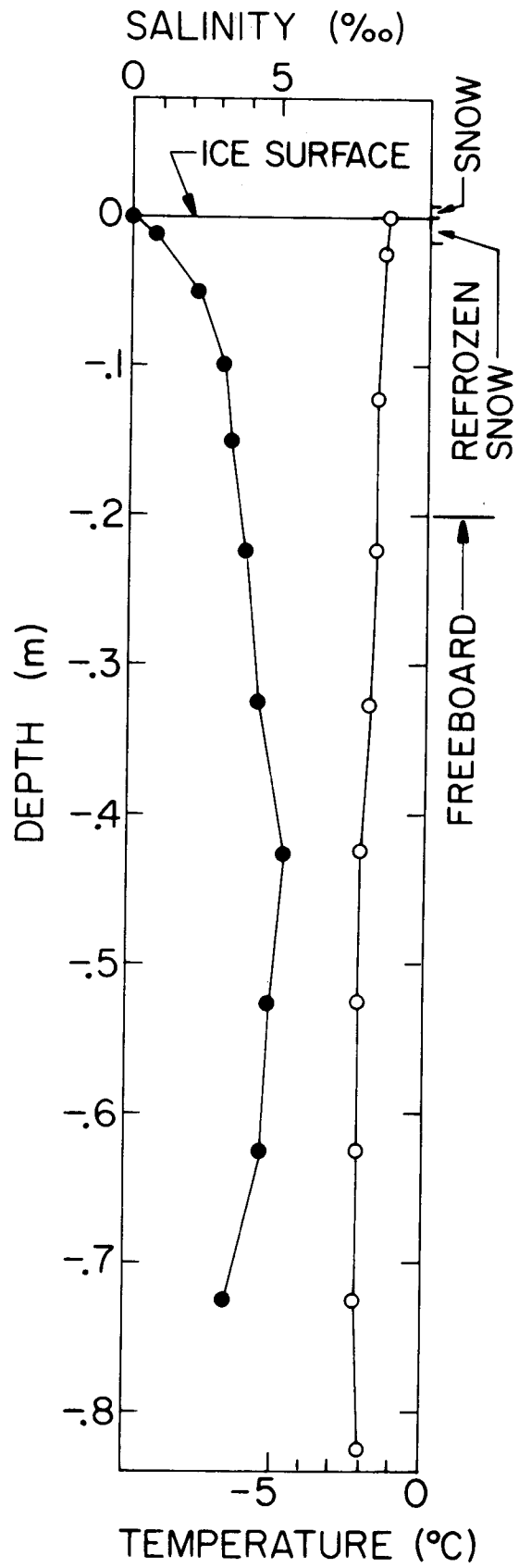


10a

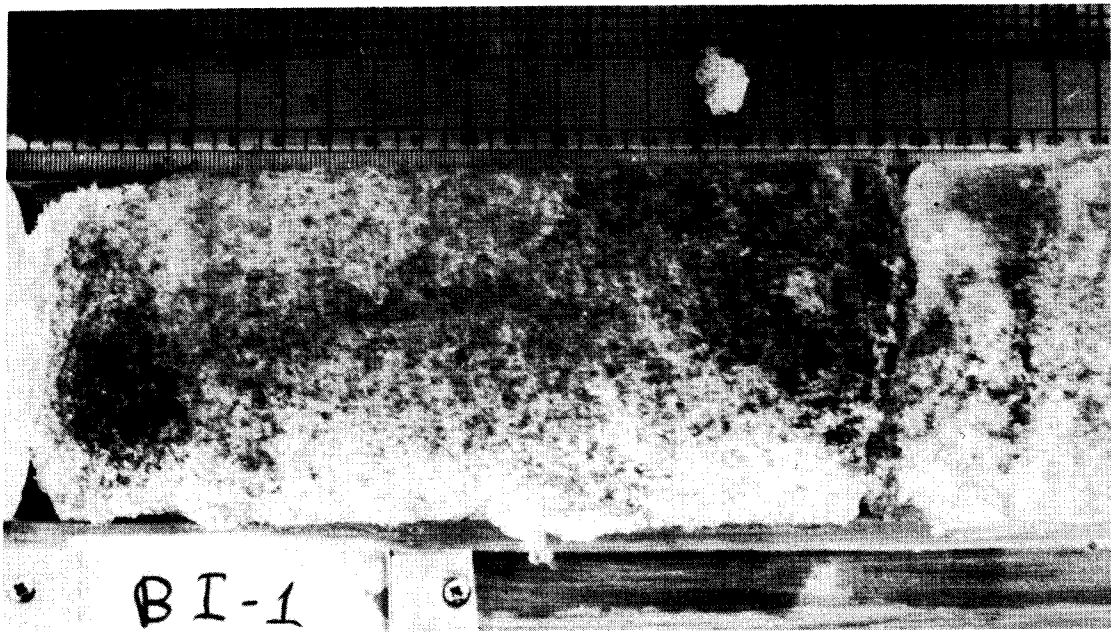
129



10b



11



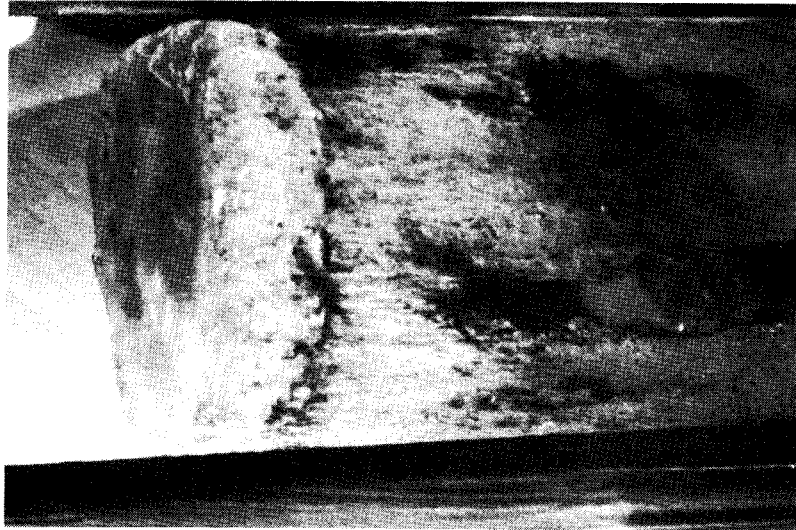
12

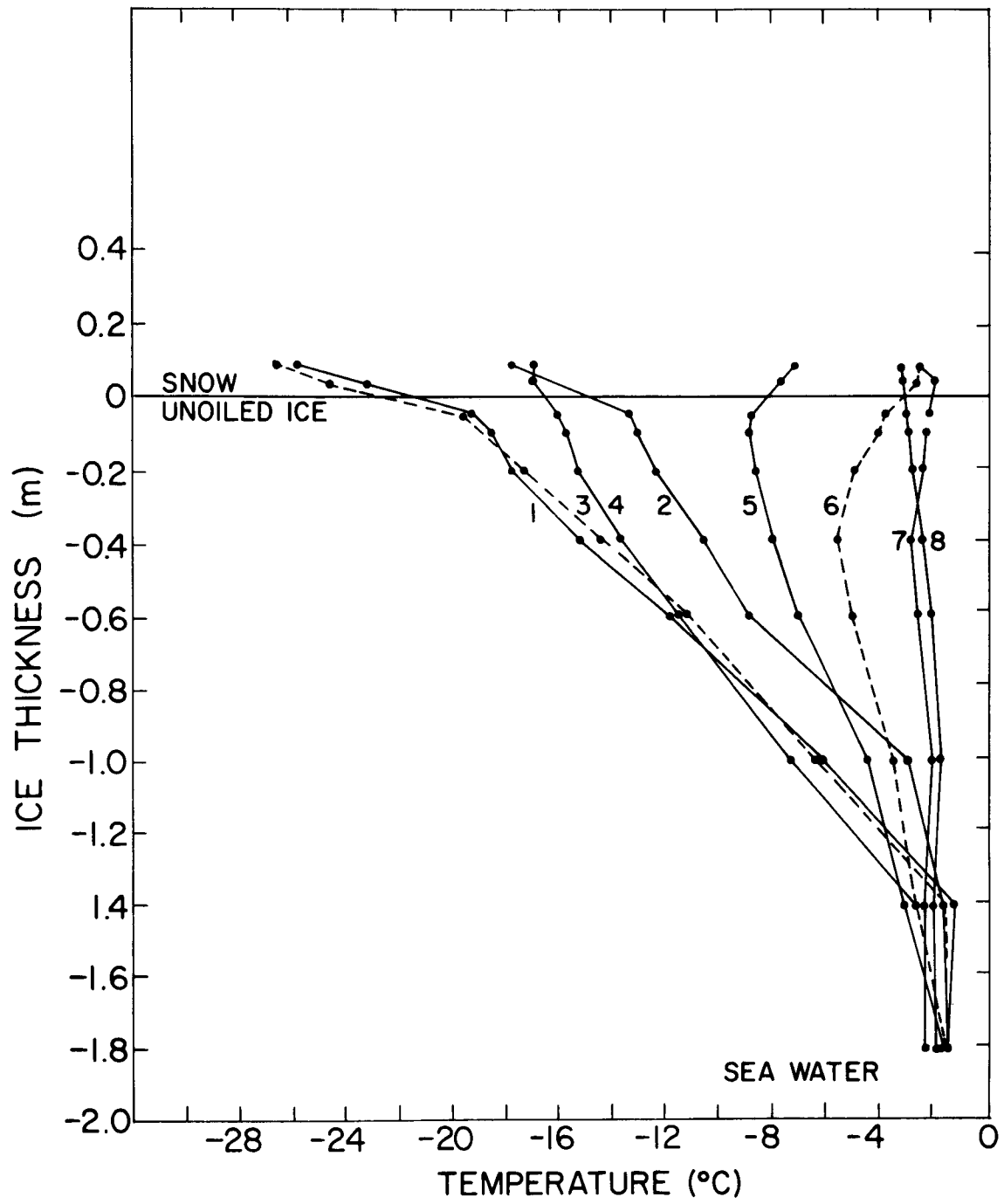
132

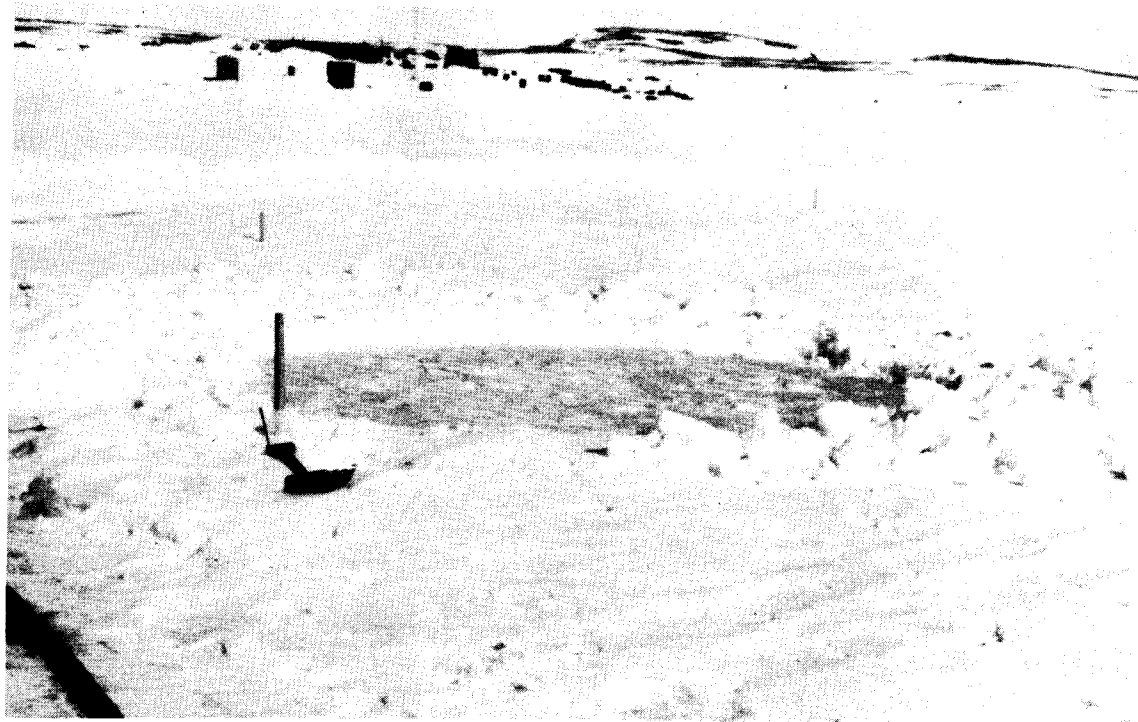
13a



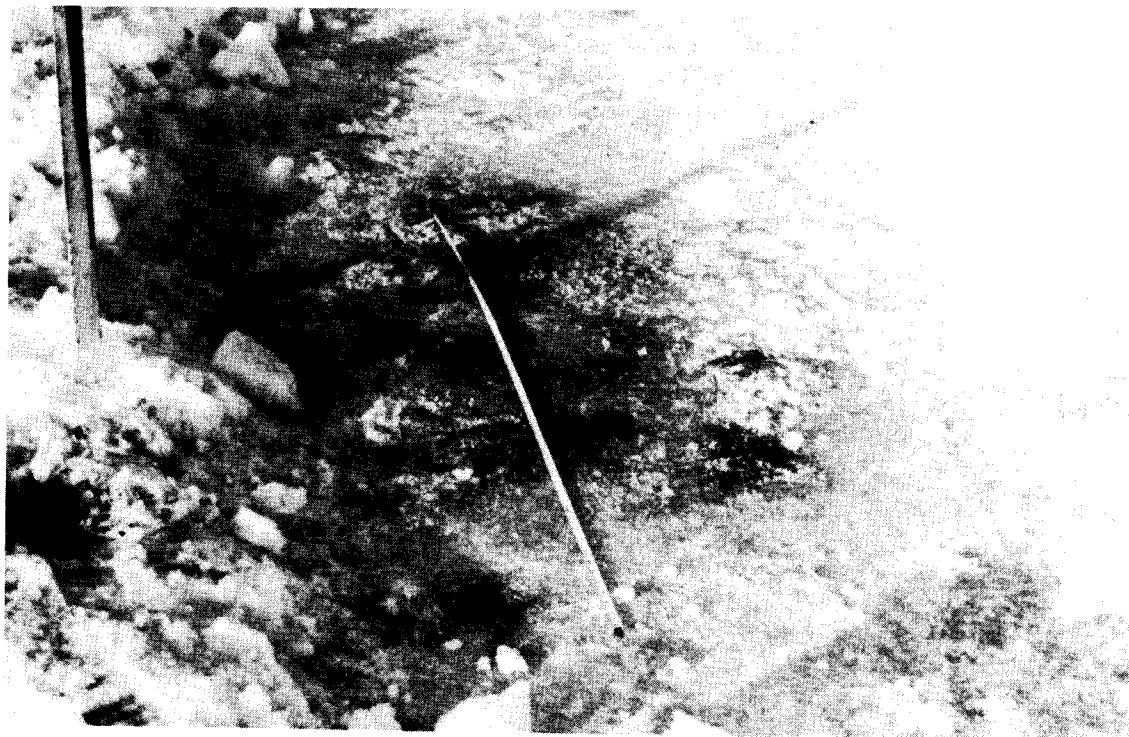
13b



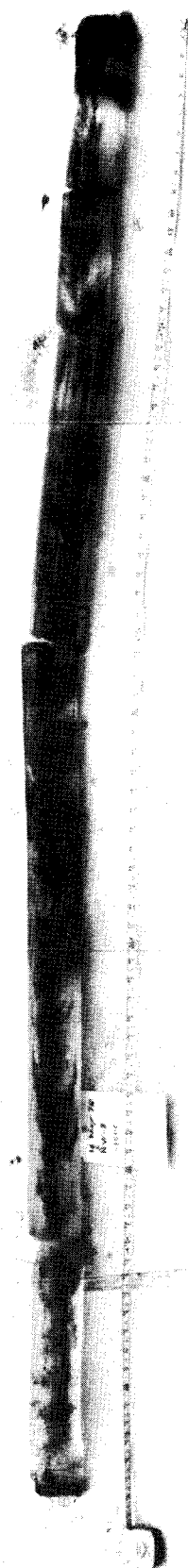




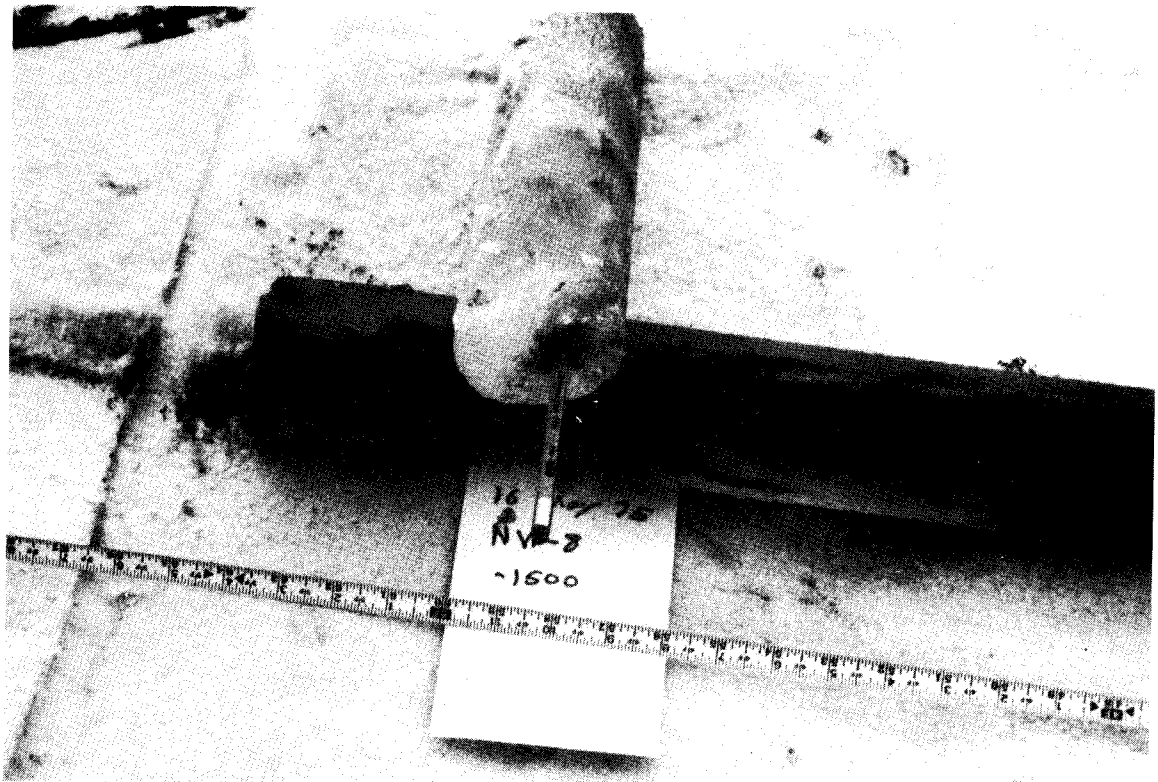
15a



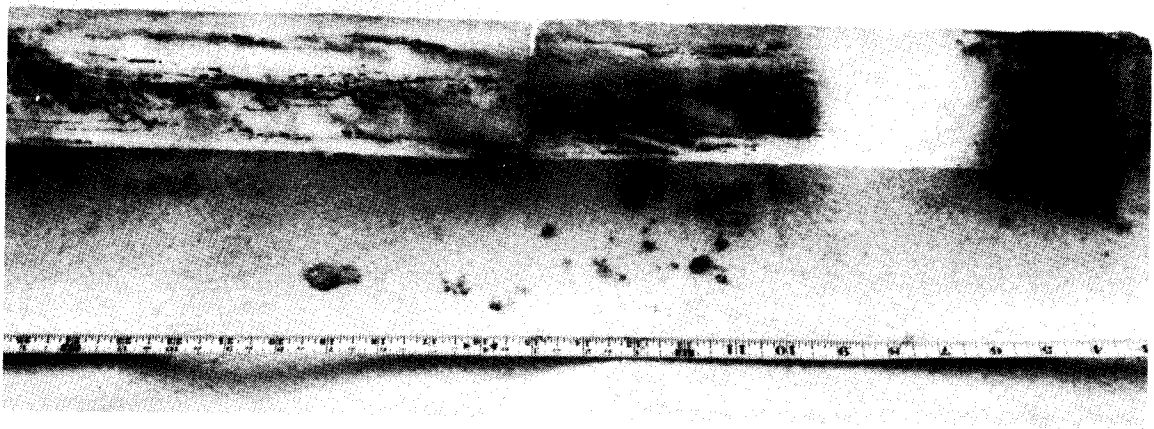
15b



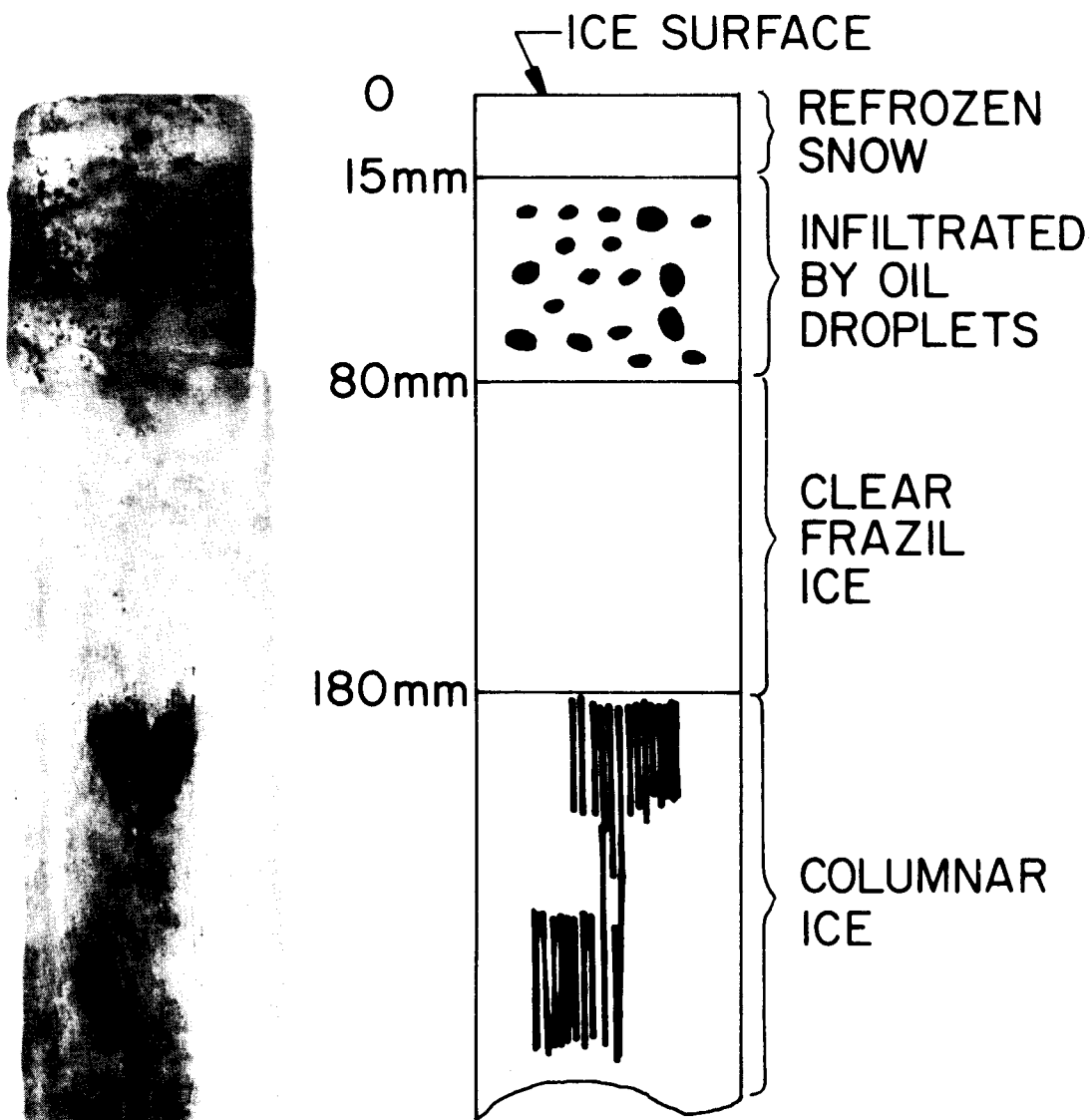
16a



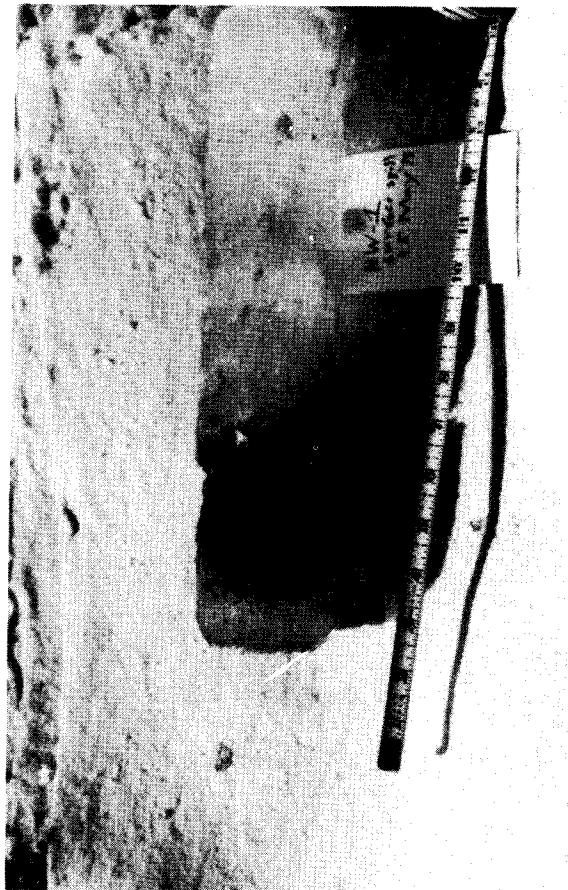
16b



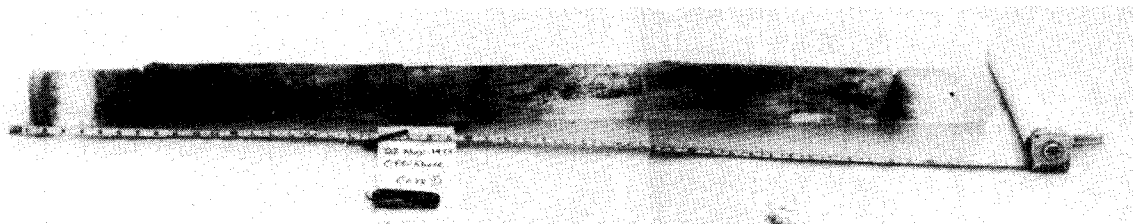
17a



17b



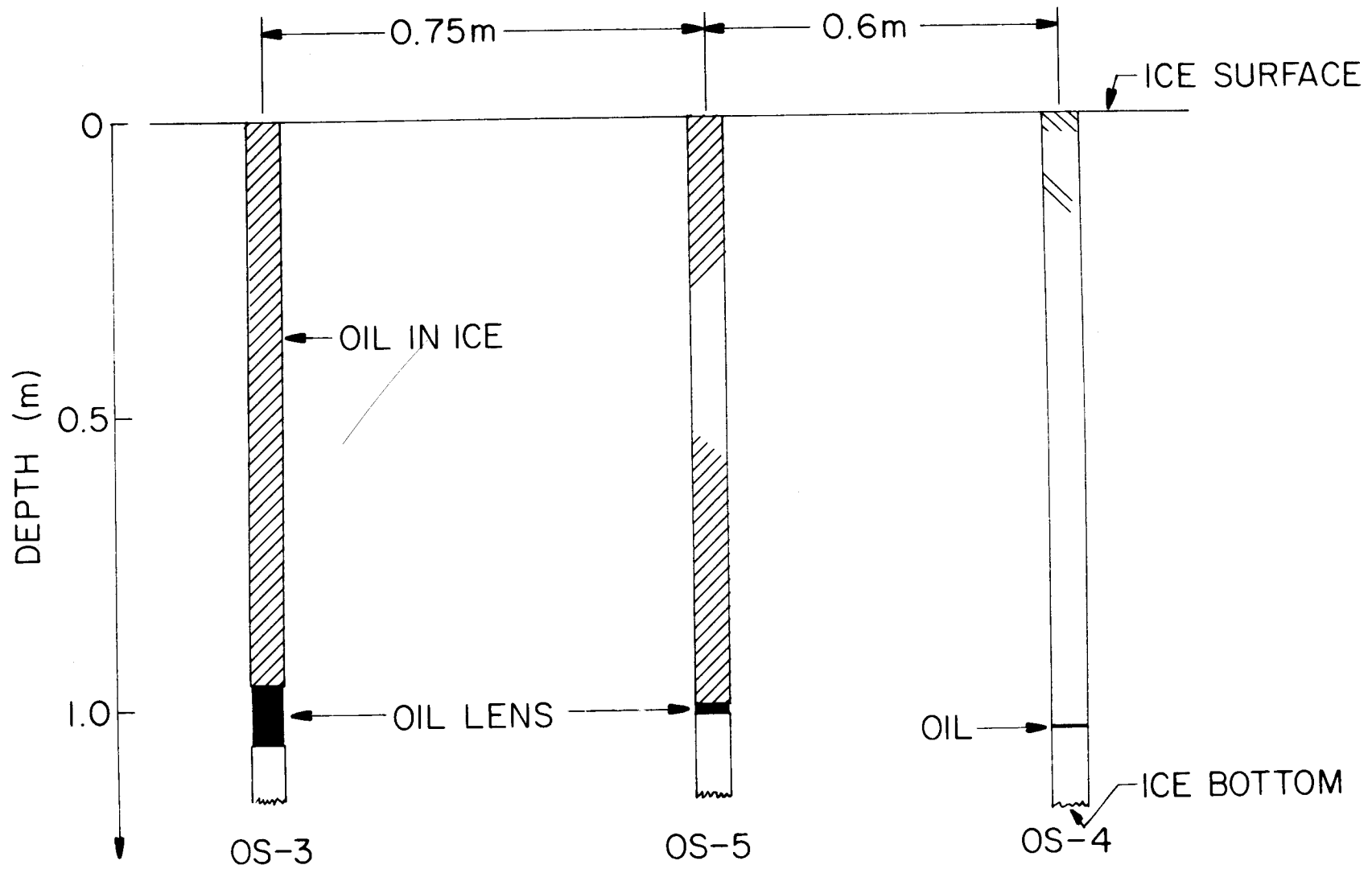
18

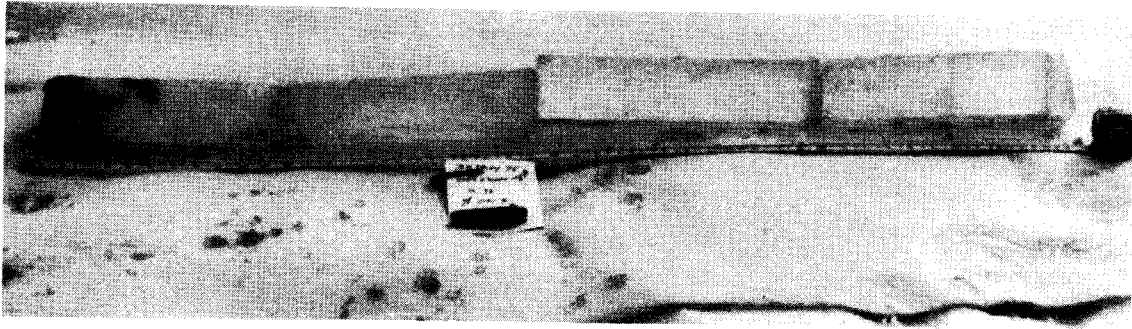


19a



19b

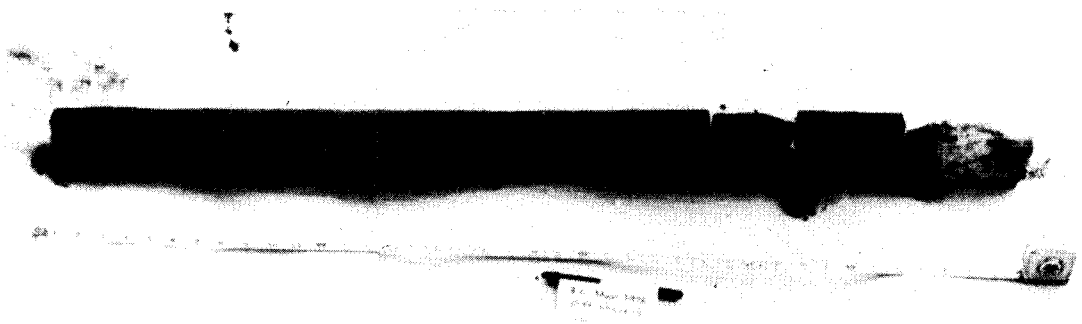




21a



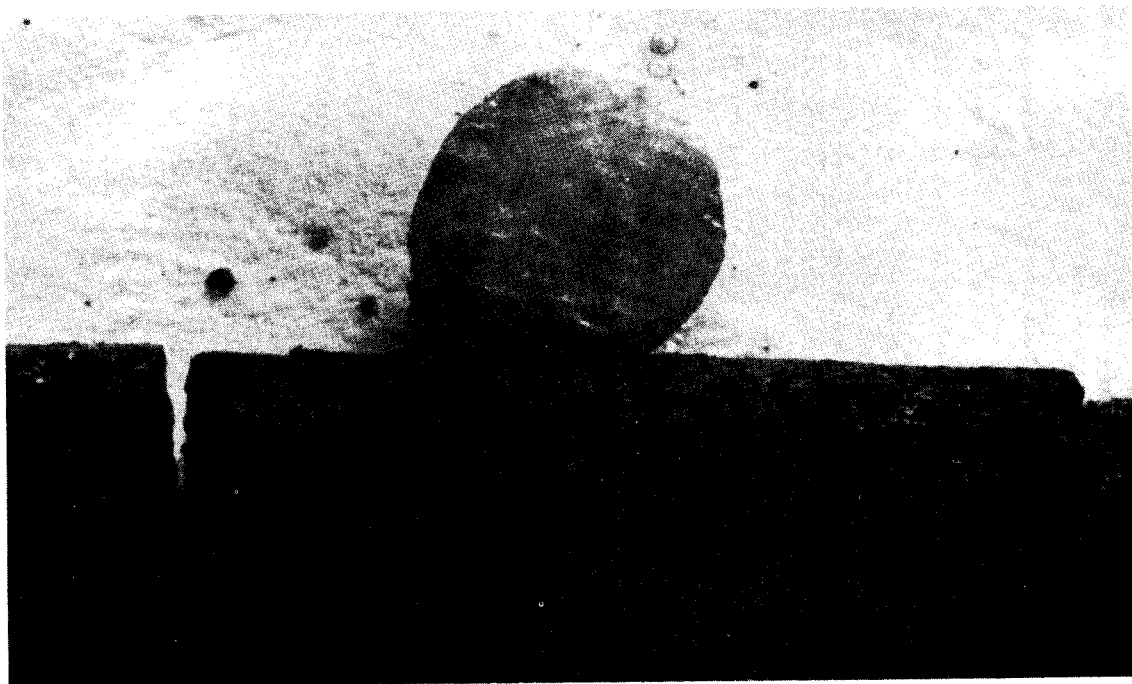
21b



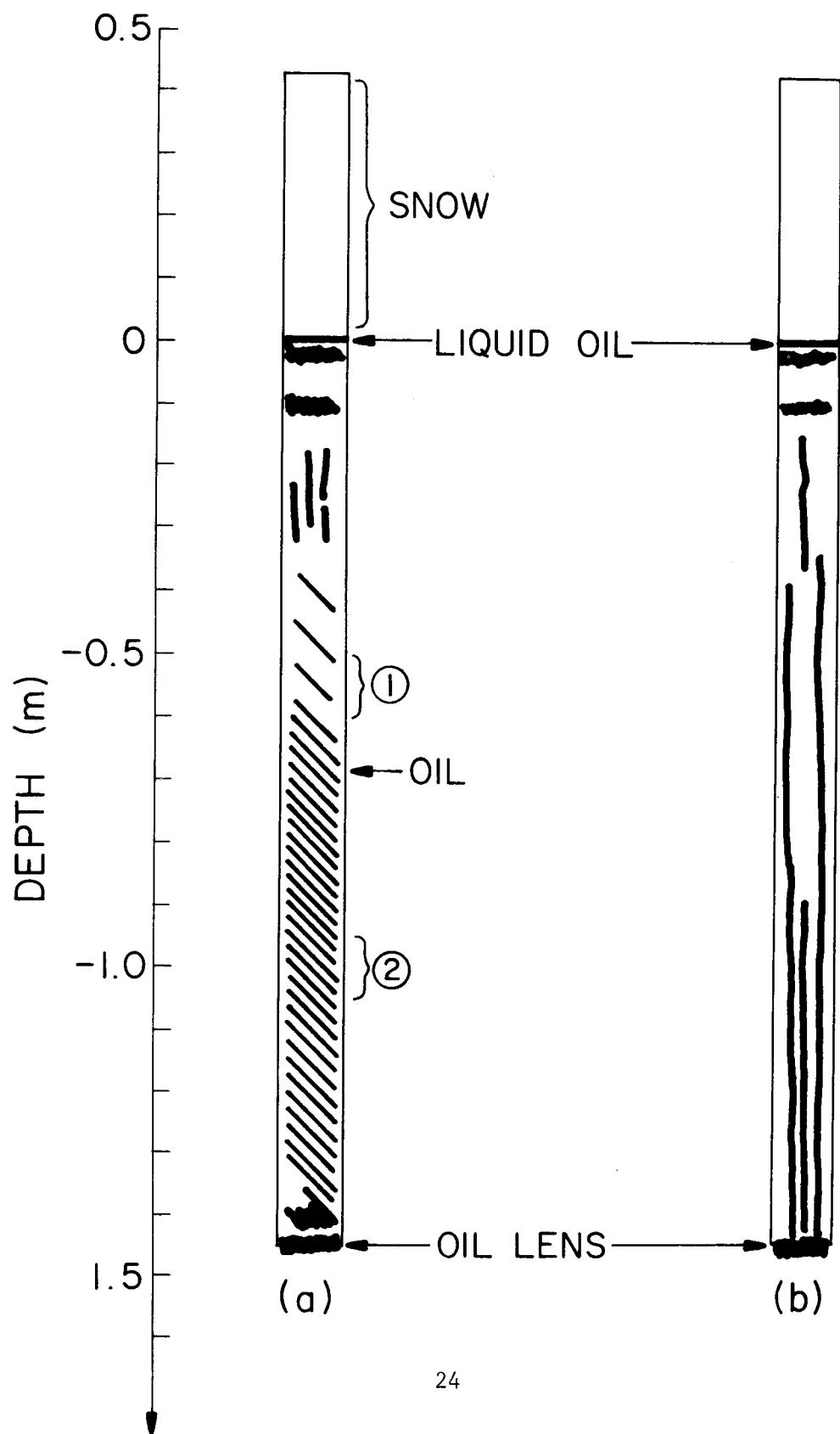
21c

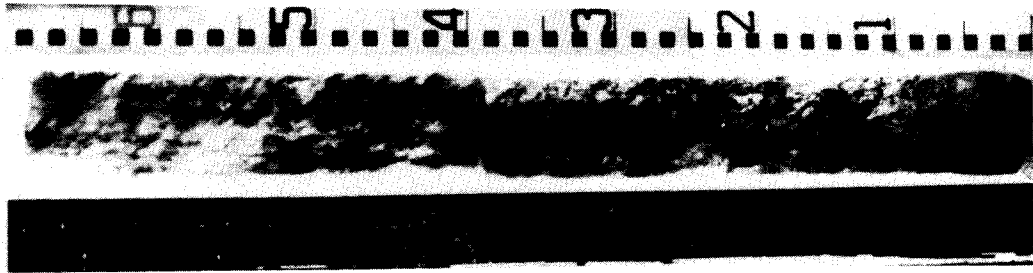


22



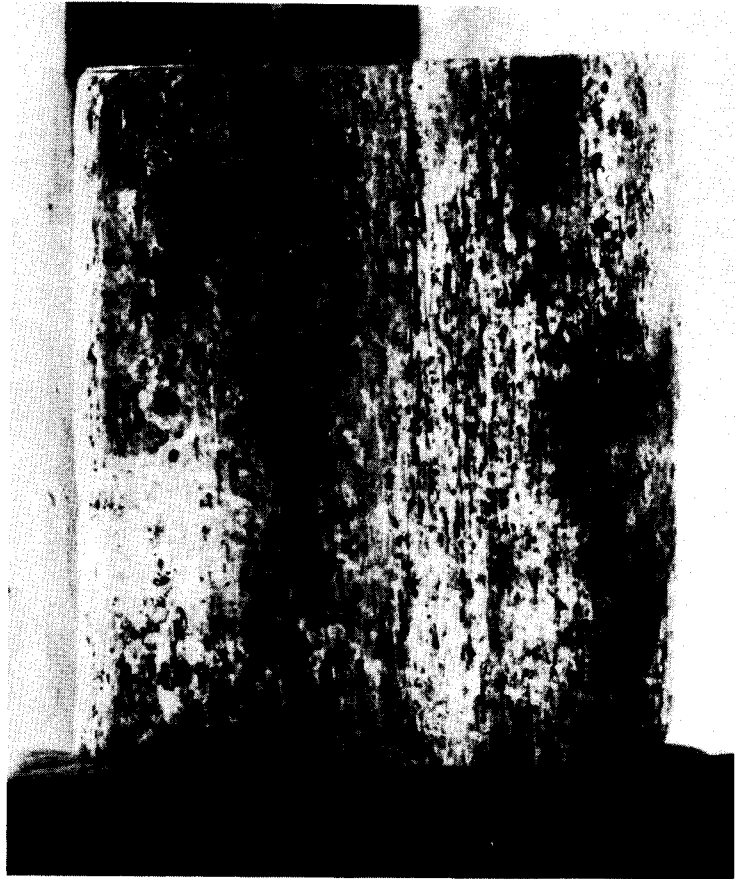
23





25

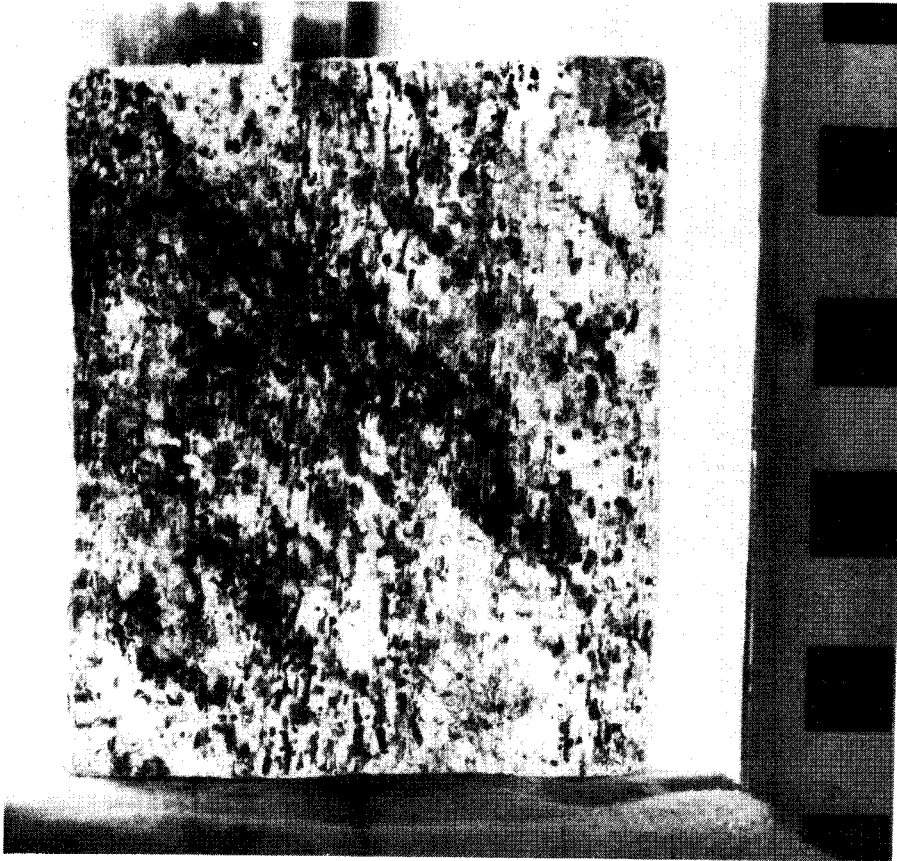
26a



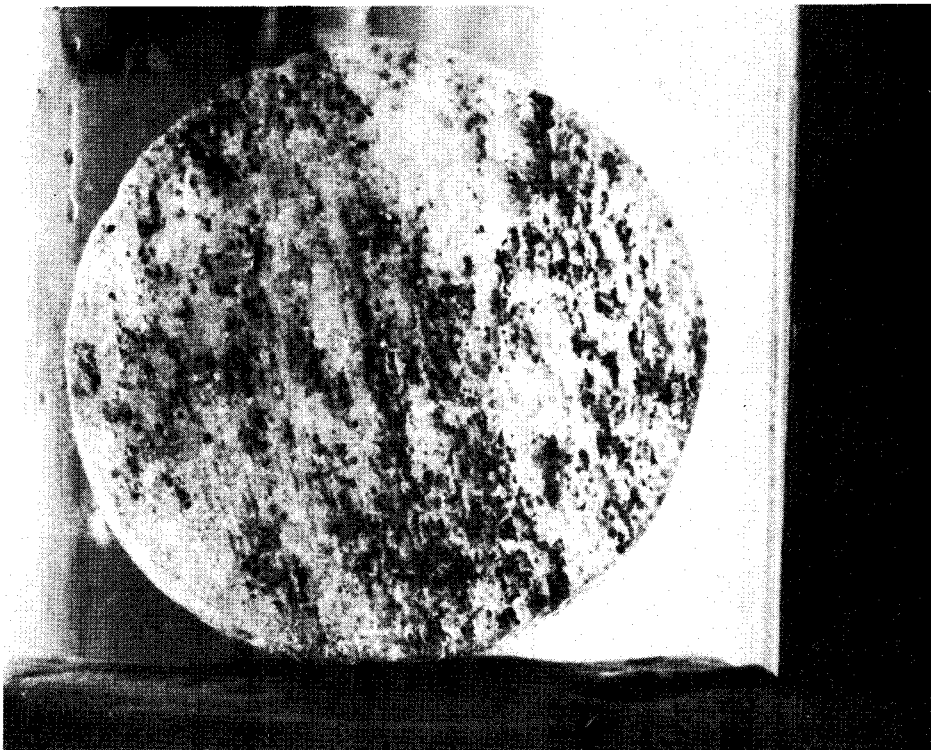
26b

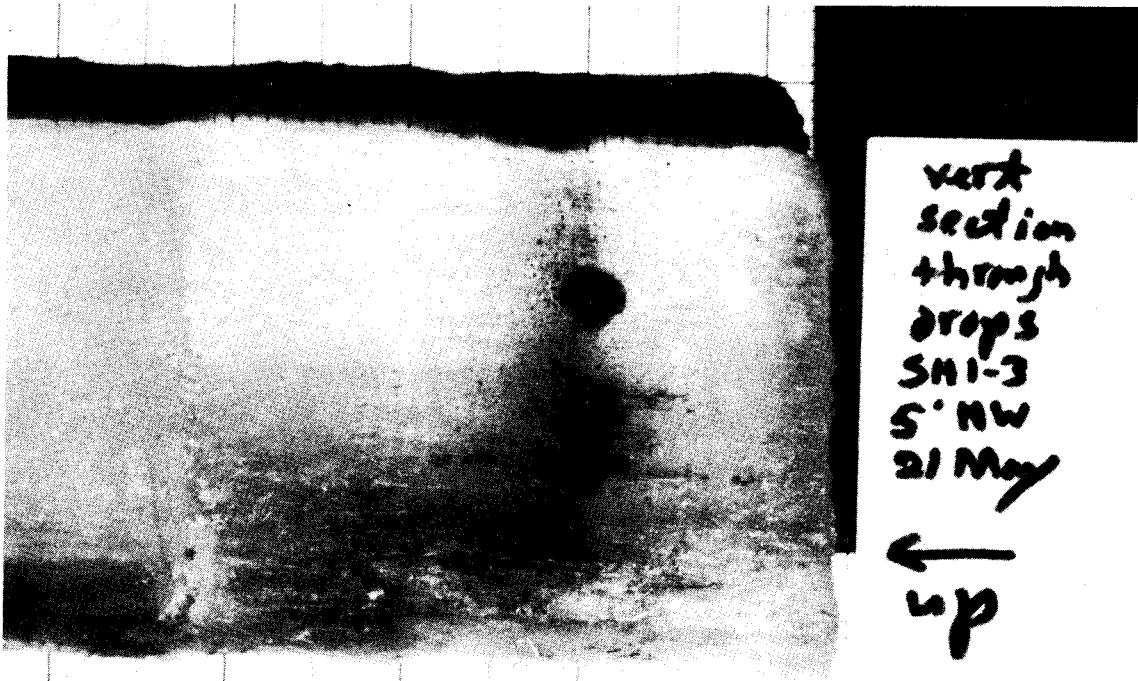


27a



27b

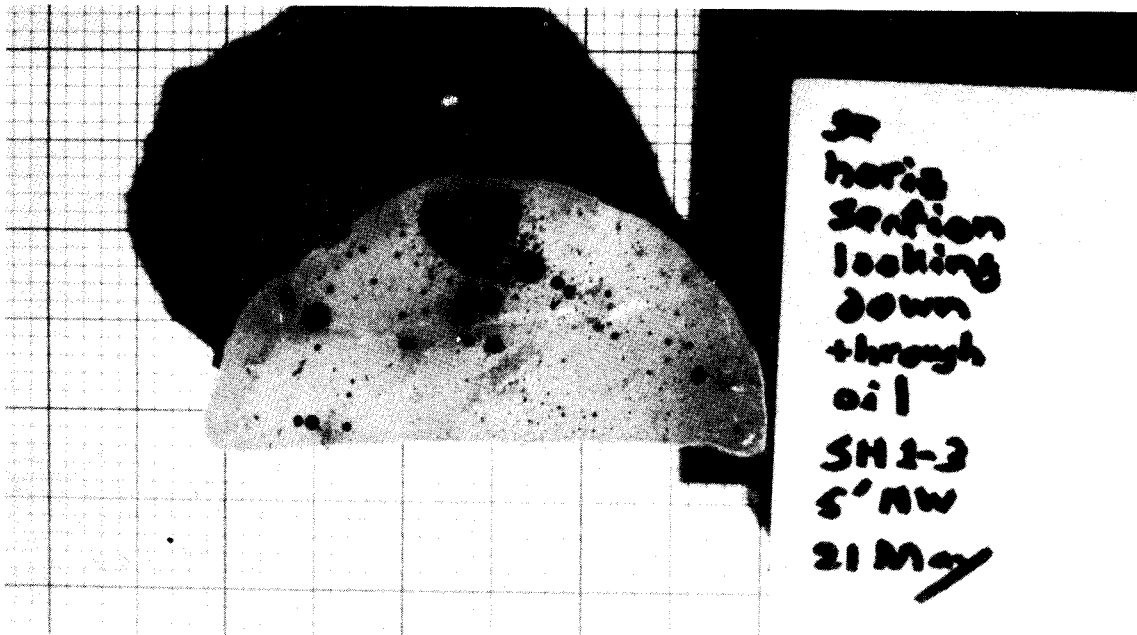




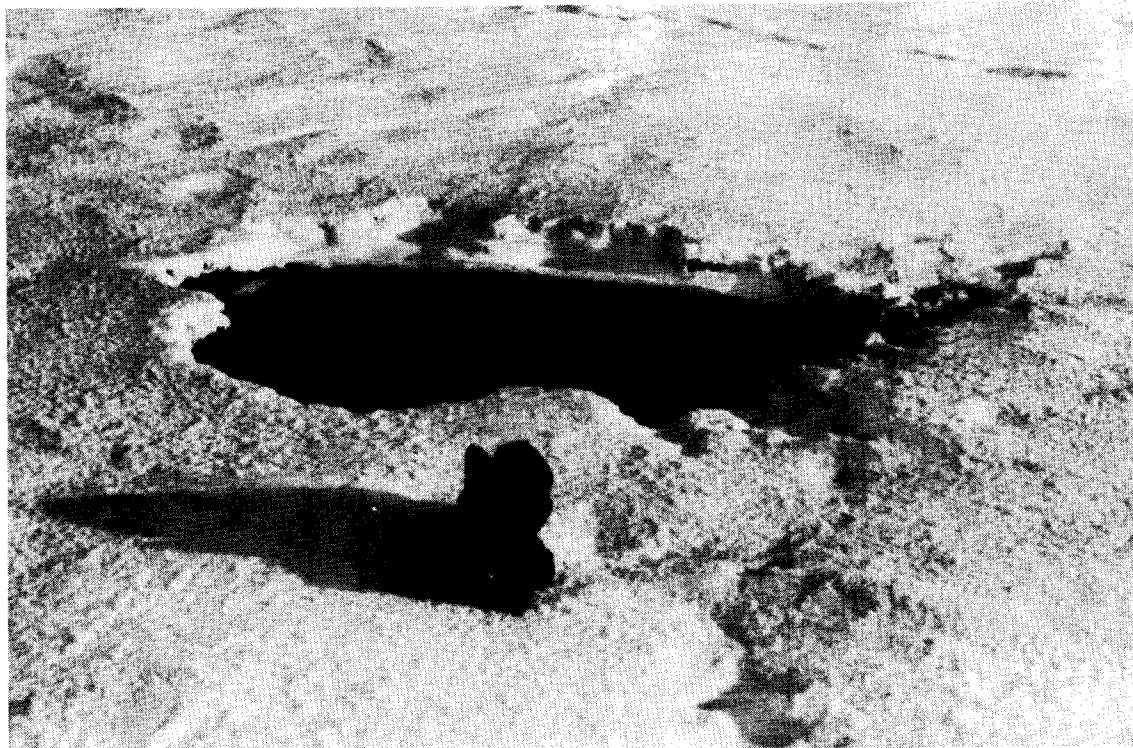
vert
section
through
drops
SH1-3
5' NW
21 May

←
up

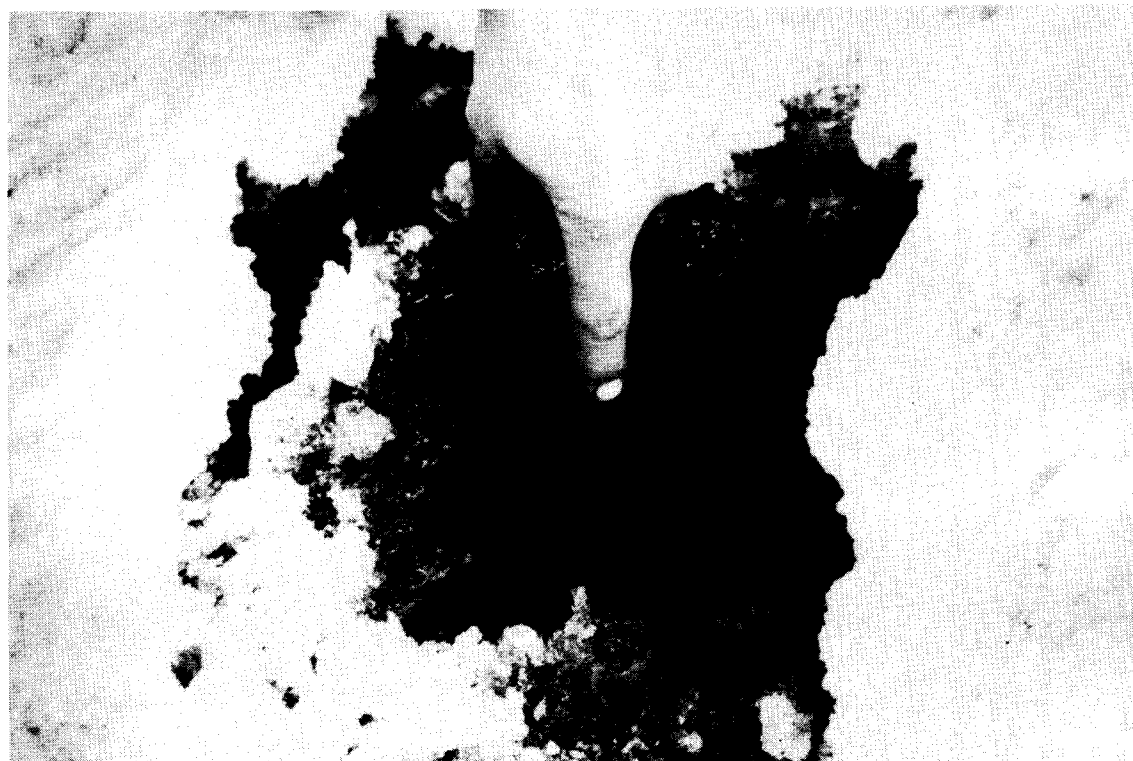
28a



horiz
section
looking
down
through
oil
SH1-3
5' NW
21 May



29a



29b

ANNUAL REPORT

R.U. #88: Dynamics of Near-Shore Ice
P.O.: 01-5-022-1651
Reporting Period: April 1976-March 77
Number of Pages: 12

DYNAMICS OF NEAR - SHORE ICE

Principal Investigators: A. Kovacs
and W. F. Weeks

Cold Regions Research and Engineering Laboratory
Hanover, New Hampshire 03755

20 March 1977

I. SUMMARY OF OBJECTIVES, CONCLUSIONS AND IMPLICATIONS WITH RESPECT TO OCS
OIL AND GAS DEVELOPMENT

The purpose of this project is to:

- a. study the motion of the fast ice and near-shore sea ice north of Prudhoe Bay and in the vicinity of the Bering Strait,
- b. make observations on major ice deformation features that occur near the edge of the pack ice/fast ice boundary,
- c. explore the use of an air-borne pulsed radar system to measure the thickness of sea ice,
- d. study the internal structure of near-shore sea ice,
- e. characterize the spatial and temporal variations in sea ice pressure ridging via the use of laser profilometry and side-looking airborne radar (SLAR).

At the present time our results (discussed more fully later in this report) suggest the following:

- a. during the time period March-May 1976 fast ice motions within the barrier islands are small,
- b. fast ice motions outside the barrier islands increase with increasing distance from shore,
- c. the fast ice/pack ice boundary may be located a considerable distance offshore from the 18 m. depth contour, where it is usually assumed to be located,
- d. locally-formed multiyear pressure ridge systems are a major hazard to offshore development in water depths in excess of 18 m,
- e. impulse radar systems can quite effectively obtain sea ice thickness information when operated from a helicopter,

- f. large areas of fast ice may show the same crystal orientation (if this can be verified it may cause appreciable increases in the effective ice strength used to design offshore structures),
- g. remote sensing studies of ice deformation show a general decrease in the amount of pressure ridging as one moves to the west from Barter Island and/or further north away from the edge of the fast ice.

II. INTRODUCTION

A. General Nature and Scope of Study.

The present program can be considered to be split into three main sub-projects:

1. The Narwhal Island Program

The purpose of this program is to obtain detailed quantitative information on the movement and deformation of both the near-shore pack ice and the fast ice along the coast of the Beaufort Sea (with particular emphasis on the region north of Prudhoe Bay). Using this same field site studies have also been carried out on the nature of the ridge systems located near the edge of the fast ice, on lateral variations in the thickness of first and multiyear ice, and on the internal structure of sea ice.

2. The Bering Strait Program

This program is focused on one task; measuring the flux of sea ice through the Bering Strait in specific and developing theoretical models for the motion of ice through straits in general.

3. The Remote Sensing Program

This program attempts both to gather remote sensing data using a laser profilometer, a SLAR system and standard mapping cameras and to utilize this data to study the nature of pressure ridging and ice conditions along the coast of the Beaufort and Chukchi Seas.

B. Methods and Field Sites

The Narwhal Island Program uses a radar ranging system that utilizes master units installed on 150 foot towers on Narwhal and on Cross Islands. These fixed master units range to remote transponders that are sited on the sea ice. This particular system was chosen because the very low elevations encountered along the coast of the North Slope greatly limit the range of more conventional radar systems. This information is also supplemented by precise strain measurements made using a laser ranging system. The targets in this case are corner reflectors sited on the sea ice at locations near Narwhal Island. The observations made on pressure ridge systems located near Narwhal Island have utilized conventional surveying, ice coring, and side-looking sonar systems. The ice thickness observations have utilized a GSSI pulsed radar system modified so that it can be operated from a helicopter. The studies of the structure of the sea ice in the vicinity of Narwhal Island have utilized conventional petrographic methods modified for ice.

We selected the Narwhal/Cross Island area of the barrier islands northeast of Prudhoe Bay because we believe it to be representative of the large number of barrier islands located north of the North slope. It is also an area of intense interest to oil companies. This makes our data both generally applicable to a type of environmental setting common along the edge of the Arctic Ocean as well as site specificications for certain leasing questions. Narwhal Island also has a number of logistic advantages because of the nearness of the Deadhorse/Prudhoe Bay complex.

The Bering Strait Program uses quite a different type of radar system to study ice motion through the Strait (i.e. a conventional marine X-band system with a P.P.I display. This system is effective at this location because the antenna can be sited on top of Cape Mountain at an elevation of

approximately 700 m. The data consists of time-lapse photographs of the radar screen on which the movement of the ice in the Strait can be observed. The resolution of this system is much less than the system used at Narwhal Island. However, this is not a problem because ice motions in the vicinity of the Bering Strait are very large. Analysis of the photographs will allow us to calculate the flux of ice through the Strait between Wales and Little Diomedes Island. The radar data is also being supplemented using NOAA satellite data.

The selection of the Bering Strait as a study site was based on the fact that during the winter large amounts of sea ice stream through it from the Chukchi Sea into the Bering Sea. Therefore, understanding the nature of its ice conditions is essential to understanding the winter ice regimes in both the Bering and the Chukchi Seas and to some extent even in the Beaufort Sea. Also if there were an oil spill in either the Beaufort or the Chukchi Seas, the oil would move west within the ice until reaching the area north of the Straits. Then depending upon whether conditions favored the Straits acting as a "drain" for ice moving south or as a "block" the oil would move either south into the biologically rich Northern Bering Sea or north over the Pole exiting the Arctic Ocean east of Greenland.

The Remote Sensing Program primarily utilizes data obtained via a laser profilometer. This system is effective in studying the surface roughness of sea ice and is also relatively easy to operate under arctic conditions. These data are obtained on traverses oriented roughly normal to the coast. Each traverse is 200 km long and the starting points are Barter Island, Cross Island, Lonely, Barrow, Wainwright and Point Lay. These points were chosen primarily because they are easy aircraft turning points and are spaced roughly evenly along the coast. The timing of the laser flights is arranged to

sample ice conditions representing the different seasons of the year (fall-winter-spring-summer). The SLAR coverage which has been flown by Fort Huachuka is less frequent and has been restricted to the summer and late winter periods. These flights have usually been made parallel to the coast.

C. Relevance to Problems of Petroleum Development

A knowledge of motion, deformation and physical characteristics of both the near-shore pack ice and the fast ice is essential to adequately designing and estimating the hazards associated with a variety of engineering options that may be considered for offshore operations in the near coastal areas of the Beaufort and Chukchi Seas (e.g. construction of gravel islands, structural platforms, causeways, reinforced ice platforms, buried pipelines, or the utilization of the ice sheet itself to carry large, long-term loads). The present program contributes directly to the solution of this general class of engineering problem in that it will provide much of the geophysical and engineering data upon which sound engineering and regulatory decisions can be made. The Narwhal Island area that is being studied is currently being considered by the petroleum companies because it possesses favorable geologic structures and is a natural extension of the known Prudhoe Bay field. Of all the Alaskan OCS areas it is one that will undoubtedly be developed in the very near future inasmuch as a transportation system is nearing completion (the Alyeska Pipeline) that will enable the operating companies to readily move any offshore oil south to existing markets.

Our interest in observing and in developing methods to predict the drift of pack ice through the Bering Strait is, as mentioned earlier, linked to the fact that ice flow through the Straits would be a key mechanism in dispersing an oil spill occurring along the coastal areas of the Beaufort and Chukchi Seas. We also believe that a knowledge of the ice

conditions in the Strait is essential to developing an adequate ice forecasting model for the Chukchi and Bering Seas. Such a model is required to predict the trajectories of potential oil spills.

The remote sensing program provides the basic information on the distribution of ice types and features and in particular ridges that will be required as one aspect of a risk analysis for the construction of an offshore drilling platform sited on the edge of the Arctic Ocean.

III. CURRENT STATE OF KNOWLEDGE

There has never been a comparable study of the motion of near-shore fast and pack ice as is being carried out at Narwhal Island. The closest study is that of the University of Washington (R.U. #98) using drifting data buoys employed on the ice north of the Alaskan coast. These buoys are located further offshore than our study area. However, this data set may ultimately prove to be useful to us in analyzing our results. The oil companies have also carried out studies of the motion of the fast ice in the vicinity of our operation. However, their results have not been made available to OCS program.

The Bering Strait Program is also quite different than existing programs. The most similar programs are R.U. 250 which uses a radar system to study the formation of near-shore ridges near Barrow, and the Japanese program using radar to study ice motion along the coast of Hokkaido. Neither of these efforts is focused on the problem of the passage of sea ice through restricted channels.

The laser profilometer program is the only such program currently underway. In the past there have been laser flights in the area of the Mackenzie Delta carried out by the Beaufort Sea Program. This data will be most useful to us in making regional comparisons of ridging intensities.

IV. RESULTS

1. Published reports (DB indicates availability in the OCS Data Bank)
 - a) Kovacs, A. (1976) Grounded ice in the fast ice zone along the Beaufort Sea Coast of Alaska. CRREL Report 76-32, 21 pp (DB)
 - b) Kovacs, A. and Gow, A. J. (1976) Some characteristics of grounded floebergs near Prudhoe Bay, Alaska. CRREL Report 76-34, 10 pp (DB)
2. Reports Completed and In Press
 - a) Weeks, W. F., Kovacs, A., Mock, S. H., Tucker, W. B. Hibler, W. D. and Gow, A. J. (1977) Studies of the movement of coastal sea ice near Prudhoe Bay, Alaska. Journal of Glaciology, Vol. 19, No. 81 (DB, available in xerox copy only).
 - b) Kovacs, A. (1977) Sea ice thickness profiling and under-ice oil entrapment. Offshore Technology Conference (DB, available in xerox copy only).
 - c) Schwarz, J. and Weeks, W. F. (1977) Engineering properties of sea ice. Journal of Glaciology, Vol. 19, No. 81 (DB, available in xerox copy only).
 - d) Gow, A. J. and Weeks, W. F. (1977) The internal structure of fast ice near Narwhal Island, Beaufort Sea, Alaska. CRREL Report.
 - e) Sohdi, D. S. (1977) Ice arching and the drift of pack ice through restricted channels. CRREL Report.
3. Reports in Preparation
 - a) Kovacs, A. (1977) The origin of rock debris found on sea ice north of Narwhal Island, Alaska. CRREL Report.

- b) Tucker, W. B. III, Weeks, W. F., Kovacs, A. and Gow, A.J.,
(1977) Near shore ice motion at Prudhoe Bay, Alaska.
AIDJEX Sea Ice Symposium.
- c) Weeks, W. F., Tucker, W. B. III, Frank, M. and Fungcharoen, S.
(1977) Characterization of the surface roughness and floe
geometry of the sea ice over the continental shelves of the
Beaufort and Chukchi Seas. AIDJEX Sea Ice Symposium.

V CONCLUSIONS

A. Narwhal Island

- a) Laser observations of fast ice motion at sites close to Narwhal Island show long term changes in the distance to targets located on the ice that are believed to be primarily the result of the thermal expansion of the sea ice. The main ice motion was outward normal to the coast (in the least-constrained direction). The maximum movement was approximately 1 m with short term changes of 30 cm.
- b) Radar observations of fast ice sites further off-shore from the barrier islands do not permit the study of small motions (as do the laser records) because of insufficient measurement resolution. However, these records show many larger events with the standard deviation of the motion measured parallel to the coast increasing systematically with distance off-shore reaching a value of ± 6.6 m at 31 km. The ice motions show short term displacements of as much as 12 m at the sites furthest from the coast. The observations also show systematic changes in line length (up to 6 m over a distance of 30 km) that are believed to be the result of thermal expansion

- of the ice. Correlations between the wind and the ice movement are only appreciable for movements normal to the coast.
- c) Radar targets located within the pack ice showed large short term movements (up to 2.7 km) but negligible net motion along the coast. There was no significant correlation between the motion of the pack and the local wind suggesting the models for predicting coastal ice movement in the Beaufort Sea during the March-June time period can only succeed if they are handled as part of a regional model which incorporates the lateral transfer of stress through the pack ice.
- d) Off-shore from Narwhal and Cross Islands the fast ice/pack ice boundary was usually located (during March-May 1976) in 30 to 35 m of water as opposed to 18 m of water where the boundary has been observed at sites further west along the Alaskan coast.
- e) The large grounded multiyear shear ridge formations that were studied along Beaufort Sea coast in the Harrison Bay/Prudhoe Bay area must be considered as formidable obstacles in the development of off-shore operations in this region. In the design of off-shore drilling structures significant consideration must be given to not only the forces which can develop when these formations are pushed against the structures, but also to the potential for ice piling up and overriding them. The inner edges of the multiyear shear ridge formations studied north of Cross Island were found to be as high as 12.5 m and to be grounded along the ~ 15 m depth contour. This depth is significantly less than the ~ 19 m contour previously considered

to be the water depth at which grounded shear ridges begin to form. The grounded ice formations studied formed in the fall of 1974 and remained through August 1976. However, they were not present in November 1976.

- f) The dual antenna impulse radar system was highly effective in determining the thickness of both first-year and multiyear sea ice from the air. Good agreement was achieved between calculated and observed ice thicknesses and representative cross-sections of both ice types were obtained. These cross sections reveal characteristic undulating bottom relief in both ice types which could trap significant amounts of oil as the result of an under-ice spill. Preliminary estimates of the entrapped volume of oil are 0.03 m^3 of oil per square meter of ice area for first year ice and 0.3 m^3 of oil per square meter for multiyear ice.
- g) Our observations coupled with published U.S. and Russian results suggest that very large areas (tens of kilometers) of sea ice have sufficiently similar c-axes orientations to act as a large single crystal. If this proves to be the case off-shore structures may have to be designed for "hard-fail" ice strengths which are 2 to 6 times the strength values normally used. The Russian theory that such orientations are aligned parallel to the magnetic field is shown to be doubtful.

B. Bering Strait

- a) The radar system was installed at Top Camp at Tin City on the Bering Strait and is now operating at 15 KW power output.
- b) The theory of the flow of granular media through chutes and

hoppers has been applied with considerable success to ice motion through the Bering Strait. There is good correspondence between observed arching and lead patterns and those predicted by theory. In addition values determined via the theory for the angle of internal friction of pack ice (≈ 30 to 35°) and the cohesive strength ($\approx 2000 \text{ N/m}^3$) are similar to values obtained by other approaches. It is estimated that if the wind velocity parallel to the Bering Strait exceeds $\approx 6 \text{ m/s}$, there will be ice flow through the Strait.

C. Remote Sensing

- a) During the 1975-76 ice season the heaviest ridging occurred at Barter Island and there was a general decrease in the intensity of the ridging as one moves further west into the Chukchi Sea. Ridging also decreases as one moves further offshore. Individual frequency profiles fall off in an exponential manner as ridge height increases. There is no decrease in frequency at low ridge heights as has been suggested from the analysis of sonar profiles.
- b) Analysis of SLAR imagery shows that the area of ridged ice decreases in a linear manner as one moves away (North) of the coast. There is no obvious break corresponding to the boundary of the so-called shear zone.
- c) The most common shape of multiyear ice floes is roughly circular. The largest length to width ratio observed was just over 5. The distribution of floe diameters shows an exponential decrease as floe size increases. The largest floe diameter observed was 3600 m.

d) Although there have been many studies of the engineering properties of sea ice, there still is considerable uncertainty concerning the appropriate values to use in offshore design. This comment is particularly true of the mechanical properties where both the basic experimental measurements and their interpretation are not well resolved.

VI. SUMMARY OF 4th QUARTER OPERATIONS

During this quarter time has been devoted to the following three subjects:

A. Preparation for the 1977 Narwhal Island Program.

All field equipment has been shipped and as of 31 March 1977 Tucker, Weeks and Kelley are in the field.

B. Report Writing

The papers by Gow and Weeks and by Sodhi have been completed.

C. Installation of the X-band Radar System at the Bering Strait.

Frank and Weeks were in the field during most of the month of February completing this installation.

We currently estimate that we have expended one quarter of our funding.

ANNUAL REPORT

Contract: 03-50-022-67, No. 5
Research Unit: 98
Reporting Period: 1 Oct - 31 Dec 1976
Number of Pages:

DYNAMICS OF NEAR SHORE ICE

Norbert Untersteiner
Professor of Atmospheric Sciences and Geophysics
AIDJEX Project Director

Max D. Coon
AIDJEX Research Coordinator
Division of Marine Resources
University of Washington
Seattle, Washington 98195

CONTENTS

SECTION	PAGE
I. SUMMARY	1
II. INTRODUCTION	2
A. General nature and scope of study	2
B. Specific Objectives	2
C. Relevance to problems of petroleum development	3
III. CURRENT STATE OF KNOWLEDGE	4
IV. STUDY AREA	4
V. SOURCES, METHODS AND RATIONALE OF DATA COLLECTION	4
VI. RESULTS	5
VII. DISCUSSION	6
VIII. CONCLUSIONS	7
IX. NEEDS FOR FURTHER STUDY	8
X. SUMMARY OF FOURTH QUARTER OPERATIONS	11
A. Field activities	11
B. Problems encountered/recommended changes	13
C. Estimate of funds expended	13
APPENDICES	
1. Measurements of Sea Ice Motion Determined from OCS Data Buoys - October 1975 to December 1976. Submitted previously.	
2. AIDJEX Met-Ocean Buoys -- Interim Data Report	
3. Winter Ice Dynamics in the Nearshore Beaufort Sea.	

I. SUMMARY

The objectives of NOAA Contract 03-5-022-67, task No. 5, RU 98, can be divided into two groups. First, the objective of the field program was to determine the kinematics of the ice in the Beaufort and Chukchi Seas by satellite tracking of data buoys. In addition to the position, some of these buoys gathered data on ocean currents and barometric pressures. These data are helpful in understanding the causes of the kinematics of the ice. The second objective of this work is to develop an understanding of the dynamics and thermodynamics of nearshore sea ice, which can be converted into computer models to study the forces, motions, and ice state, which will be useful in understanding the behavior of oil spills, sea ice interaction with its environment and manmade objects.

The data from the 20 buoys deployed and analyzed (eight additional buoys have been deployed in March 1977) show that this is a reliable and economical way of determining the trajectories of sea ice. During most of the year oil spilled in the Arctic will be trapped in sea ice and subsequently transported by it. These trajectories being developed by the tracking of data buoys will be the baseline information needed to judge how pollutants delivered to the ice will be transported. From the analysis of this OCS data and the related data from AIDJEX, it appears that during much of the summer the trajectories of ice could be computed from a knowledge of wind conditions only. However, during extended periods in fall, winter and spring the trajectories are influenced by the condition of the pack ice and its internal stress. Model calculations indicate that ice velocities can be determined from the AIDJEX ice model when high quality wind data are available, together with some buoy positions to provide boundary conditions for the calculations. These calculations allow one to find trajectories when they are affected by other than wind conditions alone. In addition, the model calculations provide information about the stress transmitted through the pack ice. Because it is likely that these ice

stresses and severe ice conditions can be the cause of oil spills, the knowledge of ice conditions and ice stress will be important in determining times and locations for safe operations.

II. INTRODUCTION

A. General nature and scope of the study

The work reported here involves studying the dynamics and thermodynamics of nearshore ice along the north coast of Alaska. To understand the response of the ice requires observation of the kinematics of the ice cover in the Beaufort and Chukchi Seas. To this end we have determined the tracks of numerous data buoys drifting with the ice. In several cases ocean currents were measured also. The trajectories provide baseline information needed to find which pollutants could be advected by the moving ice. To develop an understanding of the causes and limitations of these motions also requires a mathematical model of the dynamic and thermodynamic interaction of sea ice with its environment. Solutions to the model we are using are obtained by numerical integration. We are thus able to simulate observed conditions to study the motion, deformation, stress and state of the ice cover. The buoy drift tracks and satellite imagery allow a direct test of the field of motion predicted by the model. These tests allow material parameters to be chosen and show that the model accurately represents ice response. These results will be useful in understanding the behavior of oil or other pollutants spilled into the ice, the interaction of ice with its environment, and the evaluation of the loads that ice may exert on marine structures.

B. Specific objectives

This work performed can be subdivided into three phases. First, drift data taken by four RAMS and sixteen ADRAMS buoys have been processed and analyzed to provide time series of the motion of each station. Second, the AIDJEX model has

used to simulate conditions observed near the north coast of Alaska during 27 January - 4 February, 1976. The results of the simulation have been analyzed to assess how well the model performed. Third, another set of ADRAMS buoys have been deployed in the Chukchi Sea (6) and near Prudhoe Bay (2) to allow determination of ice motions in these regions beginning about March 1977.

C. Relevance to problems in petroleum development

With the increase in oil drilling and shipping activities that are occurring on the North Slope of Alaska and the Mackenzie Bay area of Canada, we must count on the accidental release of oil or other pollutants into the marine environment. The effect of such a spill is one of the primary concerns of the OCSEAP project. The question that we address relates to the transport of the pollutant from the spill area into other regions of the Arctic and also to the forces that the ice may exert on a marine structure. Our efforts represent a multiple attack on the problem of determining the kinematic and kinetic response of the ice-ocean system under a variety of conditions. Although the observation of ice and water trajectories provides an important baseline of information, it is inadequate for describing the most probable conditions that might exist during the next five years, or for delineating the range of conditions that are expected to occur, or for identifying the extremes that could occur. Given 50 or so years we could establish such statistics of ice motions. But the problem of petroleum development is urgent. The only data sets for which such statistical measures exist are observations of barometric pressure and local surface winds. Therefore, we turn to modeling to learn how to relate ice drift to the winds, thereby allowing us to consider the necessarily wide variety of conditions. Fortunately, the AIDJEX model has been developed to the point where it can be used to make the analysis. Since the AIDJEX model has been based on the small-scale physical processes that allow the ice cover to deform, we are able to

understand the response of the model and also obtain important information in addition to ice drift--the deformation, ice thickness distribution, and the loads exerted by the ice. Since these forces cannot be measured without full-scale experiments (a prohibitively expensive project), the modeling effort is identified as a necessary part of the plan.

III. CURRENT STATE OF KNOWLEDGE

The state of development of air-droppable data buoys (ADRAMS) indicates that this is a fully developed technology which can be used to obtain data in arctic surroundings. The present data set from these ADRAMS buoys describes the conditions of ice motion in many locations in the Beaufort Sea for one season.

The AIDJEX ice model has been tested and, although further development will be needed, it appears that when sufficiently high-quality data are available, the motion, deformation, thickness distribution and stress in the arctic ice pack can be determined.

IV. STUDY AREA

The study area is the Beaufort and Chukchi Seas.

V. SOURCES, METHODS AND RATIONALE OF DATA COLLECTION

The data for this program was taken by three types of buoys in the OCS area of the Beaufort and Chukchi Seas.

The meteorological/oceanographic buoy is basically a short (18 ft.) spar buoy which is inserted into the ocean through a 10-inch hole drilled through the ice. Current sensors are suspended from the bottom of the buoy. After installation, the buoys become frozen into the ice but become free-floating in summer. The hulls are 9-inch diameter polyethylene tubes. The designed operating life is in excess of one year.

Data transmission and buoy tracking utilizes the Random Access Measurement System (RAMS) aboard the NIMBUS-6 satellite. Air pressure, air temperature, buoy heading, and ocean current speed and direction at two depths are sampled every three hours. Ten-minute averages are computed for all data. Twenty-four hours of data are contained in memory and transmitted to the satellite. Power is provided by air-cell primary batteries. The communications system is a specifically modified Buoy Transmit Terminal (BTT) developed by the National Data Buoy Office for buoy application.

The air-droppable buoys (ADRAMS) consists of a 22-inch diameter "lexan" sphere mounted on a 15-inch diameter, 12-inch high foam crash pad. The electronics and battery pack form a single unit inside the sphere, which is free to rotate in any direction on its Teflon bearings. The electronics module contains a pendulous weight so that regardless of the final resting position of the sphere after deployment, the antenna will be properly oriented.

The system is powered by newly developed inorganic lithium batteries. These batteries allow operation down to the low temperature limit of the system, -50°C .

A rugged BTT (Buoy Transmit Terminal) was developed to survive the shock of an air drop, as well as the low temperatures of the arctic ice pack.

The third type of buoy is an ADRAMS buoy to which a pressure sensor has been added.

VI. RESULTS

Positions of the 20 drifting data buoys have been edited and interpolated to provide daily values. These results are presented in Appendix 1, titled "Measurements of Sea Ice Motion Determined from OCS Data Buoys - October 1975 to December 1976," by A. S. Thorndike and J. Y. Cheung. This appendix discusses the techniques

used to analyze the raw position fixes. In it are also presented in graphical form the trajectory and the time history of velocity (speed and direction) of each station.

All drift station trajectories have been drawn on the Beaufort Sea and Chukchi Sea base maps supplied by the OCSEAP Project Office. These maps were supplied to Dr. Gunter Weller at the Barrow Synthesis Meeting, 7-11 February 1977.

The results of the oceanographic measurements from the RAMS buoys are presented in Appendix 2, titled "AIDJEX Met-Ocean Buoys--Interim Data Report" by M. G. McPhee, L. Mangum and P. Martin.

The results of the model calculations to simulate the nearshore sea ice dynamics are presented in Appendix 3, titled, "Winter Ice Dynamics in the Nearshore Beaufort Sea," by R. S. Pritchard, M. D. Coon, M. G. McPhee and E. Leavitt.

VII. DISCUSSION

The report in Appendix 3 describes the ice conditions and dynamics in the Beaufort Sea from 27 January through 3 February, 1976. We describe observed response of the atmosphere, ice, and ocean. The time period was chosen because the ice conditions and motion are very interesting and because there is a considerable amount of high quality data from the AIDJEX program taken during this period of time. The motion of the ice during this period is greatly influenced by the internal stress of the ice pack. A flaw lead is developed along the north coast of Alaska, extending from Pt. Barrow to the Mackenzie Delta. Shoreward of the flaw lead the ice showed little motion; seaward of this lead the ice moved appreciably. However, even in the regions where there is appreciable motion the amount and direction of it is greatly influenced by the internal stress.

A simulation of the ice dynamics for the nearshore region of the Beaufort Sea has been made using the AIDJEX ice model. During the simulation, part of the data

from AIDJEX stations are used to drive the model and the remaining data are used to verify the quality of the simulation.

There is no motion during the first two days. When motions begin, they are westward. The ice in the western part of the area moves first with the eastern portion responding later. In the nearshore a fast ice region exists that is separated from the moving pack by a discontinuity. These conditions are verified by NOAA satellite imagery and data from the drifting buoys. The model simulates these features accurately, including the velocity discontinuity. This test of the AIDJEX model shows that we understand how ice responds on the large scale to driving forces and we are able to describe this relationship at times when the ice stress exerts a dominant influence.

VIII. CONCLUSIONS

The technology for building and deploying air-droppable buoys to obtain information on ice trajectories has been developed to a point where it is reliable and economical. The ice trajectory data determined from the buoy motions will be useful in developing an understanding of the trajectory of pollutants spilled under or into the ice.

Thus far the data indicate that the pack ice outside the shear zone on the North Slope of Alaska would transport the oil to the west and that if it were far enough north after moving west of Barrow, it would continue to go north and west. Some of this oil could be trapped in the Beaufort Gyre. Depending on degradation rates, this oil could be transported back to Canadian waters. The remaining oil would apparently enter the transpolar drift stream. However, oil remaining near shore could be transported south into the Chukchi Sea. The possibility of oil moving into the Bering Sea cannot be assessed at this point.

The AIDJEX model has been shown to provide a physically realistic simulation of the dynamic response of sea ice to winds during the winter when ice stress is significant. Furthermore, the motion is seen to compare extremely well with observed motions of buoys and manned camps. In the nearshore regions the plasticity model represents fast ice areas. These areas are separated from the moving pack ice by rapid variations or discontinuities. The location of the flaw lead agrees with satellite images. A close look at deformations and stress shows that we may improve some details of the response by changing the yield surface shape and we expect to pursue that work soon.

IX. NEEDS FOR FURTHER STUDY

The program of work that we are reporting on has been shown as crucial to understanding transport of oil by sea ice, and the upper layer of the ocean, also the forces that the ice may exert on marine structures. We have reported results that describe observed ice and ocean trajectories and have shown how a mathematical model (the AIDJEX model) relates ice motion to the wind field. However, because the OCSEAP program has been operational only for two years, the observed motion data in the nearshore Beaufort Sea are limited to the period from October 1975 to December 1976. Similarly, the modeling program, even when all results developed under the AIDJEX/NSF funding are included, covers only a limited range of time and space where simulations have been tested. In this section, we identify the work that must continue if we are to understand the role played by the ice cover in transporting oil and exerting forces. Our aims are to increase geographic coverage, to obtain data at different times of year, to determine season-to-season variations, to simplify the mathematical model, and to balance the levels of sophistication of ice and ocean models in the nearshore environment. It is obvious from the description that the state of the art of understanding ice motion has not advanced

uniformly. This is true because of the far greater complexity under some conditions. On one hand, in the summer conditions when the ice is wind driven (meaning no ice stress, not that ocean currents are negligible) (McPhee, to be published), we are ready to study the range of ice response using historical wind data. We note that the area-wide barometric pressure may control ocean currents. On the other hand, in the rest of the year when the marginal zone is ice covered, no effort has yet begun to understand the important interaction of ice and ocean on smaller scales.

A most alarming question arises as we consider that oil spilled near Reindeer Island at the end of October would be transported to the west of Pt. Barrow by the following June, as shown by buoy trajectories reported in Appendix 1. Since there is a well-known southerly motion in the Chukchi Sea south from Barrow to Cape Lisburne we must ask, "under what conditions can oil be transported during spring breakup from the Beaufort Sea through the Bering Strait and into the Bering Sea?" The consequence of such transport would be devastating on that rich eco-system. Fortunately, the stage is set to develop a mathematical model of the Chukchi Sea that will allow this "breakout" problem to be analyzed. The AIDJEX model has already been shown to be an accurate simulation tool in similar circumstances. And the ongoing data buoy program will provide drift tracks and barometric pressures in this region beginning in March 1977. Therefore, the important question of understanding large-scale motion in the Chukchi Sea can be addressed immediately. In addition to studying the motions observed with presently deployed buoys, satellite imagery will enhance our knowledge of the ice conditions. Analysis of these data will help to determine parameters of the model and to identify which features are most important. As part of this model development, the ocean must be considered as an important component. Ocean current data are available and must be analyzed to find the relative importance of ocean currents.

As a result of current modeling activities and data analysis we have learned that simpler models may be used to relate winds to ice drift under certain conditions. We have shown theoretically that area-wide wind stress averages control drift rates--with the effect of ice stress being small if the area is large enough (Pritchard, to be published). This result is obtained from the AIDJEX model, but the accuracy with which that model represents ice drift lends confidence to the results. Therefore, we feel that the analysis showing limited effect of internal stress on large scales is reasonable. However, the results show that the distance over which this force becomes negligible depends upon the strength of the ice. During the summer when large amounts of open water are present, the average distance can be quite small--even less than 100 km--so that local wind-driven drift can be used to predict motions. However, in winter when the ice is compact and strong, the distances over which air stress must be averaged increase to the order of 1000 km. This means that the average ice motion within such a region can only be defined at distances more than 500 km from shore. Because of this limitation we feel that additional modeling using the entire AIDJEX model in the nearshore region is necessary. However, for the conditions that satisfy this limitation we feel that the currently described simple model should prove useful in correlating winds and ice trajectories. This will allow statistical evaluation of historical wind data and a confident prediction of mean ice trajectories and the range of variations of these trajectories.

The OCS data buoy program that has been in progress during 1975-1977 should be continued to fill several data gaps. The most significant is the need to deploy buoys in the same areas as before to ascertain the year-to-year variability that occurs because of different atmospheric and ice conditions. In addition, buoys deployed in separate local regions, such as the high speed flume off the Alaskan coast of the Chukchi Sea, can answer specific questions. Identification of these

areas and times of year at which deployment should be made also depends on other ongoing programs. The decision should receive strong input from investigators who are testing air, ice and/or ocean models that are being developed.

Finally, more thought must enter the understanding of ice and ocean dynamics on space scales less than 100 km. At times when the ice cover may deform, the response of the ice-ocean system is unknown on these scales. On these scales it is important to understand how loads are transmitted to structures and to learn how to protect these structures from storm surges or from the impinging pack ice. Such a study could allow the barrier islands to be used as protective structures if the manmade structures were properly designed and located. It is obvious that final results of this work will be at least several years in coming, but it is desirable to begin a pilot program soon.

X. SUMMARY OF FOURTH QUARTER OPERATIONS

A. Field Activities.

1. Field trip schedule

The field party arrived at NARL on 25 February and worked there until 23 March. NARL aircraft support as follows: Twin Otter, 25 February; C-117, 2 & 7 March; C-180, 14, 17 & 22 March. NOAA helicopter support on 9, 17, 18, 19 and 20 March. Chartered Volpar aircraft support from Arctic Guide in Barrow on 13 March.

2. Scientific party

In addition to the aircraft crews the personnel involved in the work were: Pat Martin, who coordinated the various activities; Mel Clarke, who took care of electronic troubleshooting and repair and handled the data processing and analysis; and Dave Bell, who assisted in the assembly and deployment of the buoys.

3. Methods

The buoys mentioned in this report are sampled by the Random Access Measurement System on board NIMBUS-VI. Position and barometric pressure are determined 6-12 times per day.

4. Sample localities

The deployment sites of the buoys are as follows:

<u>Buoy ID</u>	<u>Date</u>	<u>Latitude</u>	<u>Longitude</u>
1064	2 March	67°05'N	168°00'W
1035	2 March	68°50'N	168°59'W
1052	2 March	70°40'N	165°40'W
1617	7 March	72°20'N	166°00'W
1023	13 March	69°40'N	173°40'W
1305	13 March	70°55'N	173°45'W
0632	22 March	70°37'N	147°15'W
1601	22 March	70°50'N	147°00'W

5. Data collected or analyzed

There have been no significant new data collected during the fourth quarter 1976. Data analysis from earlier periods are presented in the appendices.

6. Milestone chart and data submission schedule

- a. October 1976 Buoy deployment (in agreement with Gunter Weller, this deployment was held off until March 1977, and has been completed).
- b. January 1977. Complete data analysis of buoys in the Beaufort Sea. Data report complete (See Appendix 1).
- c. June 1977. Data report completed (See Appendices 1 and 2).

- d. June 1977. Model calculation in progress (See Appendix 3).
- e. October 1977. Model report (see preliminary report, Appendix 3).

B. Problems encountered/recommended changes.

The principal problem encountered with the spring field work was with arrangements to deploy buoys west of 169° west longitude. Though written notification of the need for such arrangements was given on 3 November, it was apparently impossible for the OCS office to obtain the necessary clearances on time. Therefore, the mission was flown by charter aircraft on March 13. This charter flight was conducted by an operator unfamiliar with and unequipped for air navigation techniques necessary for the safe conduct of such flights. These facts were known in advance and were weighed carefully by the participants who decided to accept the risks and proceed with the mission. In the future such operations should be planned well in advance with non-military aircraft.

All the buoys deployed stand a good chance of drifting to positions where the data will no longer be of use to the proposed study, but where recovery of the buoys for reuse will be feasible. Such missions are not a part of the proposed work, but should be considered by OCS.

C. Estimate of funds expended.

As of 28 February 1977, actual expenditures under this contract totaled \$150,609. The estimated obligations for March are anticipated to be approximately \$38,239.

MEASUREMENTS OF SEA ICE MOTION DETERMINED FROM OCS DATA BUOYS
OCTOBER 1975 TO DECEMBER 1976

by

A. S. Thorndike and J. Y. Cheung
AIDJEX
4059 Roosevelt Way N.E.
Seattle, WA 98105

Contents

ABSTRACT	1
1. INTRODUCTION	1
2. THE RAW MEASUREMENTS	1
3. PREPROCESSING	2
4. KALMAN SMOOTHING	3
ACKNOWLEDGMENTS	5
REFERENCES	6
APPENDICES	
1. 80-character format for RAMS buoys	7
2. Kalman smoothing equations	8
3. Conversion table from AIDJEX days to calendar days	9
4. Tape format of final smoothed position and velocities, from AIDJEX Data Bank	12
5. Coordinate systems	13
FIGURES	
1. Raw data from RAMS buoy R1003 (station 10)	14
2. Edited raw data and smoothed position estimates from Fig. 1	15
3. Approximate response function for data processing scheme	16
4. Bar graph, times of usable data collection, by station	17
5. Trajectories of each station	18-38
6. Speed and direction plotted for RAMS buoys	39-55
TABLES	
1. Estimation errors	56
2. Estimated positions of RAMS buoys	57-72

MEASUREMENTS OF SEA ICE MOTION DETERMINED FROM OCS DATA BUOYS

OCTOBER 1975 TO DECEMBER 1976

by

A. S. Thorndike and J. Y. Cheung
AIDJEX

ABSTRACT

During 1975 and 1976 measurements of sea ice motion were made as part of AIDJEX, and the Outer Continental Shelf project. The raw data from the 20 platforms deployed in the continental shelf region have been edited and interpolated for presentation in this report.

1. INTRODUCTION

The objective of the Arctic Ice Dynamics Joint Experiment, as set forth in its most general statement, was to reach an understanding of the dynamic and thermodynamic interaction between the ice cover and its environment [Maykut et al., 1972]. One component of the experiment was an array of drifting stations at which frequent measurements of position were made. For the present report those measurements have been edited and interpolated using Kalman smoothing techniques to give position and velocity estimates at evenly spaced time points. (The raw measurements themselves are not reported here, but are available through the AIDJEX Data Bank.)

This report is limited to buoys deployed in the continental shelf region. For data from other platforms which were tracked during AIDJEX, we refer the reader to Thorndike and Cheung [1977].

2. THE RAW MEASUREMENTS

The measurements were made with the Random Access Measurement System (RAMS), which uses the techniques of Doppler Satellite navigation. The

raw measurement is the frequency of a signal transmitted from the ice station to the satellite. The measured frequency is affected by a Doppler shift related to the rate of change in distance between the satellite and the ice station, which is itself related to the unknown ice coordinates and the known satellite orbit. During each satellite orbit several frequency measurements were made and from them an over-determined solution was found for the unknown coordinates. The Doppler counts were made for discrete 1-second bursts transmitted from the buoy each minute. Typically, 20 measurements per pass were collected, stored, and transmitted to a receiving station on the ground. Fix calculations were done at NASA and the results passed to AIDJEX on magnetic tape. The best of these buoys got about 15 fixes per day. A few RAMS buoys operated for only part of each day and had a much lower data rate, approximately 4 fixes per day. (See Brown and Kerut [1976], Burke and Buck [1975], and Martin and Gillespie [1976], for details of the hardware systems.)

3. PREPROCESSING

The first step in preprocessing was to reduce each position fix to an abbreviated format containing 80 characters which summarize the fix. Only the fix itself, the time of the fix, and several parameters relating to the quality of the fix were included in the summary format. Raw data--the Doppler counts, say--are contained only in the original data tapes. The abbreviated format is summarized in Appendix 1.

The raw data sequence from RAMS platforms is seriously contaminated with bad fixes. A glance at a plot of the raw time series (Figure 1) illustrates the problem. Because outlying fixes have a deleterious effect on the Kalman filtering results, an attempt was made to remove them during preprocessing. The algorithm employed compares each fix latitude with the median of the latitude of the 10 fixes preceding and the 10 fixes following it. When the differences exceeded a preset tolerance, the fix was eliminated. The algorithm was applied twice, with a smaller tolerance the second time. The same procedure was then applied for longitude. The tolerances used were 20 km and 5 km for buoys with a high data rate and 40 km and 10 km for buoys with a low data rate.

Data were filtered in 20-day blocks. Some overlap was provided to give continuity at the end points of each block, so actually the raw data were prepared for filtering in overlapping 26-day chunks, and are available from the AIDJEX Data Bank in that form.

Visual checks were an important part of the procedure. Plots of the data points were produced before and after preprocessing. At times it seemed from the plots that we were not detecting certain bad fixes, or that we were throwing out good ones, and it was necessary to adjust the tolerance levels. This was especially true for buoys with a low data rate. The final data plots (Figure 2) provided assurance that the data were ready for filtering.

4. KALMAN SMOOTHING

In the smoothing scheme used here an assumption is made regarding the motion of the ice. If the state of the ice at time t_n is represented by a vector X_n , containing, say, the position, velocity, and acceleration of each point in the ice pack, then the state at some future time is assumed to be partially determined by X_n :

$$X_{n+1} = \Phi X_n + \Gamma W_{n+1} \quad (1)$$

where Φ and Γ are known from the physics of the situation, and W_{n+1} represents an unknown random perturbation. In Kalman's formulation, which we follow, the random effects are assumed to be Gaussian and *white*:

$$\text{cov}(W_n, W_m) = \begin{cases} Q & \text{if } n = m, \text{ and} \\ 0 & \text{if } n \neq m. \end{cases} \quad (2)$$

We have chosen $Q = 100 \text{ m}^2 \text{ hr}^{-6}$ [Thorndike, 1973]. Qualitatively choosing a small value of Q is equivalent to assuming that the ice moves in a completely predetermined way. (See from equations 1 and 2 that $Q = 0$ would imply that $X_{n+1} = \Phi X_n$.) A large value of Q corresponds to assuming that

the ice experiences large sudden changes in its acceleration. For this problem we have defined $\Delta = t_{n+1} - t_n$ and

$$X = \begin{pmatrix} x \text{ position} \\ x \text{ velocity} \\ x \text{ acceleration} \end{pmatrix}, \quad \Phi = \begin{pmatrix} 1 & \Delta & \Delta^2/2 \\ 0 & 1 & \Delta \\ 0 & 0 & 1 \end{pmatrix}, \quad (3)$$

and

$$\Gamma = \begin{pmatrix} \Delta^3/6 \\ \Delta^2/2 \\ \Delta \end{pmatrix}. \quad (4)$$

An identical equation can be written for the y -coordinates. The two coordinates are treated independently. Treating the stations one at a time in this way is equivalent to assuming that different stations experience *independent* random perturbations in acceleration. We know that this is not true [see Thorndike, 1974, p. 114, Fig. 5]. But since an objective of the program was to study the differences in motion between the stations, we chose not to build into the data processing scheme any physical coupling between the stations. Otherwise, interpretation of, say, strain estimates would be clouded by an underlying assumption that one station knew what the other was doing.

The variance Q affects the high frequency response of the processing scheme. Figure 3 shows the approximate response. Fluctuation with periods of less than about two days cannot be resolved with these measurements and this processing scheme.

Each measurement, Z_n , is related to X by a matrix H which picks out of X the position element:

$$Z_n = H X_n + V_n$$

where V_n is a measurement error with assumed variance R .

The structure of R reflects our understanding of the measurement process. In the equations (Appendix 2) which give the smoothed estimates of X , data points are weighted according to the measurement error variance assigned in R .

Important for our application of the RAMS system is the presence of several RAMS platforms at fixed sites on land. For each satellite pass it is possible to determine the error at the fixed reference platforms and to apply a correction to the fixes obtained from the same pass by our moving buoys.

The algorithm used finds the fix error in the direction of satellite motion at the reference point and subtracts that error in the direction of the satellite motion at the buoy. The application of this translocation principle improves the accuracy of the RAMS fixes and allows us to process data from the RAMS buoys one buoy at a time. A constant value of $R = (2 \text{ km})^2$ has been used in processing the RAMS data.

The general smoothing problem is to estimate X at time t_n using the entire set of observations $\{Z_i\}$ $i = 1, \dots, M$, and to give the error variance of that estimate. The solution equations, due to Kalman, are reproduced in Appendix 2. Tables and plots which follow summarize the results of our calculations. Typical estimation error variances for each quantity are summarized in Table 1. When measurements were scarce the variances increased, of course. Figure 4 shows the time periods for which the variance exceeded a nominal limit, at which times the results must not be taken too seriously.

ACKNOWLEDGMENTS

The authors want to emphasize that the work reported on here, for which they were responsible, is only a part of the total effort involved in this buoy program. Pat Martin had the responsibility for monitoring the design and production of the buoys and for their deployment. Max Coon and others from the AIDJEX modeling group made decisions about *where* the buoys were to be deployed. Gillespie wrote the software to read the data from the NASA tapes and got them into a form suitable for our processing.

Finally Bill Seechuk at NASA provided important support and was remarkably patient in dealing with our many requests for near real time data.

The work was supported by the National Science Foundation Grant Arctic Sea Ice Study number OPP76-10801, and by the National Oceanographic and Atmospheric Administration Outer Continental Shelf contract 03-5-022-67 entitled Near Shore Ice.

REFERENCES

- Brown, W. P., and E. G. Kerut. 1976. Air droppable RAMS (ADRAMS) buoy. In *Ocean 76, Proceedings of the 1976 International Conference on Engineering in the Ocean Environment*. IEEE Publ. No. 76 CHO 1118-9 OEC, section 14, D1-6.
- Burke, S. P., and B. M. Buck. 1975. The SYNRAMS ice station. In *Ocean 75, Proceedings of the 1975 IEEE International Conference on Engineering in the Ocean Environment*. IEEE Publ. No. 75 995-1 OEC, pp. 413-417.
- Martin, P., and C. R. Gillespie. 1976. Arctic odyssey--five years of data buoys in AIDJEX. In *Proceedings of the Symposium on Meteorological Observations from Space, Their Contribution to the First GARP Global Experiment*, National Center for Atmospheric Research, Boulder, CO, pp. 328-334.
- Maykut, G. A., A. S. Thorndike, and N. Untersteiner. AIDJEX scientific plan. *AIDJEX Bulletin*, 15, 67 pp.
- Meditch, J. S. 1969. *Stochastic Optimal Linear Estimation and Control*. McGraw-Hill, New York.
- Thorndike, A. S. 1973. An integrated system for measuring sea ice motions. In *Ocean 73, Proceedings of the 1973 IEEE International Conference on Engineering in the Ocean Environment*. IEEE Publ. No. 73 CHO 774-0 OEC, pp. 490-499.
- Thorndike, A. S. 1974. Strain calculations using AIDJEX 1972 position data. *AIDJEX Bulletin*, 24, 107-129.
- Thorndike, A. S., and J. Y. Cheung. 1977. AIDJEX measurements of sea ice motion, 11 April 1975 to 14 May 1976. *AIDJEX Bulletin*, 35, 1-149.

APPENDIX 1
80-CHARACTER FORMAT FOR RAMS BUOYS

Field Number	Columns	Format	Description
1	1	--	Blank.
2	2-6	F6.0	Orbit number.
3	7,8	F2.0	Platform i.d.
4	9,10	F2.0	
5	11,12	F2.0	Year
6	13-15	F3.0	Day of year
7	16,17	F2.0	Hour
8	18,19	F2.0	Minute
9	20,21	F2.0	Second
10	22,23	F2.0	Along-track correction; divide by 10 to get kilometers.
11	24-27	F4.0	Change in latitude in meters for 1 km along-track correction.
12	28	F1.0	Numerical 1.
13	29-32	F4.0	1 for single pass, 2 for two-pass solution.
14	33-36	F4.0	Error index for two-pass, F value for one-pass solutions.
15	37-47	F11.6	Fix latitude, corrected for along-track error.
16	48-58	F11.6	Fix longitude, corrected for along-track error.
17	59	F1.0	Numerical 9.
18	60,61	F2.0	Minute (same as field no. 8).
19	62,63	F2.0	Number of messages used for fix.
20	64-72	F9.2	Frequency bias, in Hz.
21	73-77	F5.0	Change in longitude in meters for 1 km along-track correction.
22	78-79	F2.0	Elevation angle (largest value).
23	80	F1.0	Numerical 1.

APPENDIX 2

KALMAN SMOOTHING EQUATIONS

Symbols

X = state vector ($n \times 1$)
 ϕ = transition matrix ($n \times n$)
 Γ = coefficient matrix for random perturbations to physical model ($n \times m$)
 W = white noise driving the physical process ($m \times 1$)
 Q = covariance matrix for W ($m \times m$)
 Z = measurement vector ($l \times 1$)
 H = matrix relating measurement to state vector ($l \times n$)
 V = measurement error vector ($l \times 1$)
 R = measurement error covariance ($l \times l$)
 P = prediction, filtering and smoothing error covariance matrix ($n \times n$)
 K = Kalman gain matrix for filtering ($n \times l$)
 A = smoothing gain matrix ($n \times n$)
 N = number of measurements in the data sequence
 k = index for the data sequence
 t = time

The superscript T denotes the transpose operation. The symbol $\hat{X}(i|j)$ means the estimate of X at time t_j given observations $\{Z_1, Z_2, \dots, Z_j\}$. The notation here follows Meditch [1969].

Prediction

Given observations $\{Z_1, \dots, Z_k\}$, predict the state at the future time t_{k+1} , and find the prediction error covariance.

$$\hat{X}(k+1|k) = \phi(k+1, k)\hat{X}(k|k), \quad A(1)$$

$$P(k+1|k) = \phi(k+1, k)P(k|k)\phi^T(k+1, k) + \Gamma(k+1, k)Q(k)\Gamma^T(k+1, k). \quad A(2)$$

Filtering

Given observations $\{Z_1, \dots, Z_k\}$ and a new observation Z_{k+1} , estimate the present state at time t_{k+1} and find the filtering error covariance.

$$\hat{X}(k+1|k+1) = \hat{X}(k+1|k) + K(k+1)[Z(k+1) - H(k+1)\hat{X}(k+1|k)], \quad A(3)$$

$$P(k+1|k+1) = [I - K(k+1)H(k+1)]P(k+1|k), \quad A(4)$$

where

$$K(k+1) = P(k+1|k)H^T(k+1)[H(k+1)P(k+1|k)H^T(k+1) + R(k+1)]^{-1} \quad A(5)$$

Smoothing

Given the complete data set $\{Z_1, \dots, Z_N\}$, estimate the state at any point t_k , and find the smoothing error covariance.

$$\hat{X}(k|N) = \hat{X}(k|k) + A(k)[\hat{X}(k+1|N) - \hat{X}(k+1|k)] \quad A(6)$$

$$P(k|N) = P(k|k) + A(k)[P(k+1|N) - P(k+1|k)]A^T(k), \quad \text{where} \quad A(7)$$

$$A(k) = P(k|k)\Phi^T(k+1, k)P^{-1}(k+1|k). \quad A(8)$$

Implementation of the filter algorithm

Starting from an initial condition $X(0|0)$, $P(0|0)$, a prediction is made to time t_1 . The prediction error covariance matrix $P(1|0)$ is used to obtain the Kalman gain $K(1)$. The filtered estimate $\hat{X}(1|1)$ is then found by adding to the predicted $\hat{X}(1|0)$ a quantity which is proportional to the difference between the observation $Z(1)$ and $H(1)\hat{X}(1|0)$. $H(1)\hat{X}(1|0)$ is the value the measurement would have if the true state were actually $\hat{X}(1|0)$ and no measurement errors were made. The algorithm is repeated as each new data point is entered until the last filtered quantities $\hat{X}(N|N)$ and $P(N|N)$ are produced.

The smoothing algorithm, proceeding backward in time, utilizes results from the prediction and filtering calculations. The first step is to find $\hat{X}(N-1|N)$ and $P(N-1|N)$ from equations A(6), A(7), and A(8). No direct use of the measurements is made in smoothing. The algorithm simply corrects the filtered vector $X(k|k)$ by a quantity proportional to the difference between the prediction vector at time t_{k+1} and the smoothed value at time t_{k+1} .

In the calculations done for this application, the CDC 6400 computer time required to do the prediction, filtering, and smoothing is about 0.5 second per data point, nearly half of which is absorbed in the matrix inversion in A(8). Because of the recursive nature of the filter, demands on central memory storage space are very modest.

Reproduced from Thorndike, A. S., 1973, An integrated system for measuring sea ice motions. In *Ocean '73, IEEE International Conference on Engineering in the Ocean Environment*, IEEE publ. no. 73 CHO 774-0 OEC, pp. 490-499.

APPENDIX 3
CONVERSION TABLE FROM AIDJEX DAYS TO CALENDAR DAYS

For the main experiment the AIDJEX convention was to number days consecutively beginning with day 1 = 1 January 1975. The table given here continues through day 900 = 18 June 1977. The first column is the AIDJEX day; the second column is the corresponding day of 1975, 1976, or 1977; and the third entry is the calendar date.

APPENDIX 4
TAPE FORMAT OF FINAL SMOOTHED POSITION AND VELOCITIES
FROM AIDJEX DATA BANK

I. File Structure. One file per station for all stations.

File 1 = station 0

⋮

File 40 = station 39

Files 31, 41, 42, 43, and 44 are empty.

File 45 - station 44

File 46 - station 66

II. Record Structure. One record per time point at 3-hour intervals.

III. Reading Instructions. The tape is odd parity, CDC display code characters.

```
READ (1, 10) ISTA, TIME, X, Y, VARX, U, V, VARU
```

```
10 FORMAT (I10, 3F10.3, F10.5, 2F10.3, F10.5)
```

ISTA = station number.

TIME = time in days with decimal fraction.

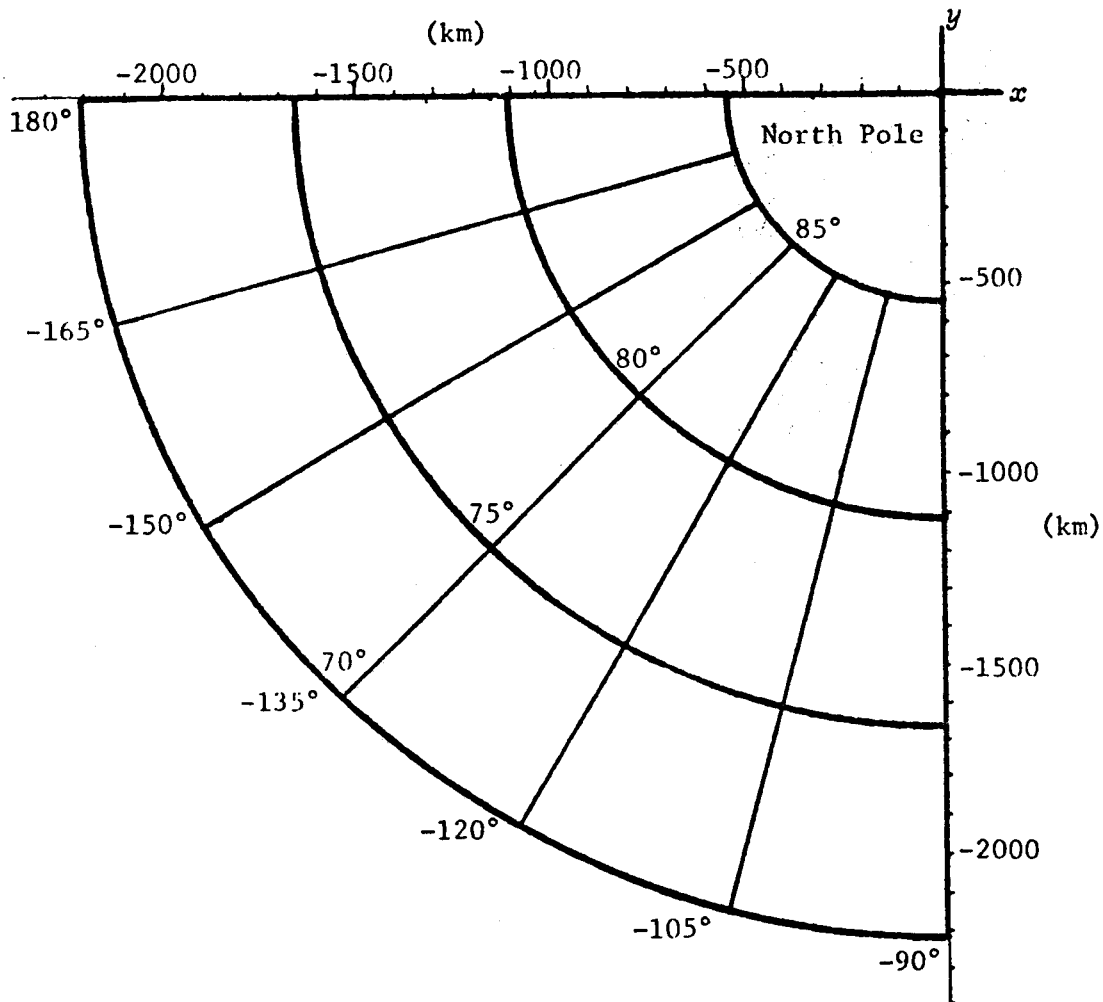
X, Y = position coordinates in km (see Appendix 7).

VARX = variance of the errors in X and Y in km².

U, V = velocity estimates in cm sec⁻¹ (see Appendix 7).

VARU = variance of the errors in U and V in cm² sec⁻².

APPENDIX 5
COORDINATE SYSTEMS



Position measurements were made in geographical coordinates (latitude north, longitude east). The smoothing operation was done in a Cartesian system (x, y) , where

$$x = 110.494 (90^\circ - \text{latitude}) \cos (\text{longitude}) \quad (\text{km})$$

$$y = 110.949 (90^\circ - \text{latitude}) \sin (\text{longitude}) \quad (\text{km})$$

Velocities u and v refer to the positive x and y directions.

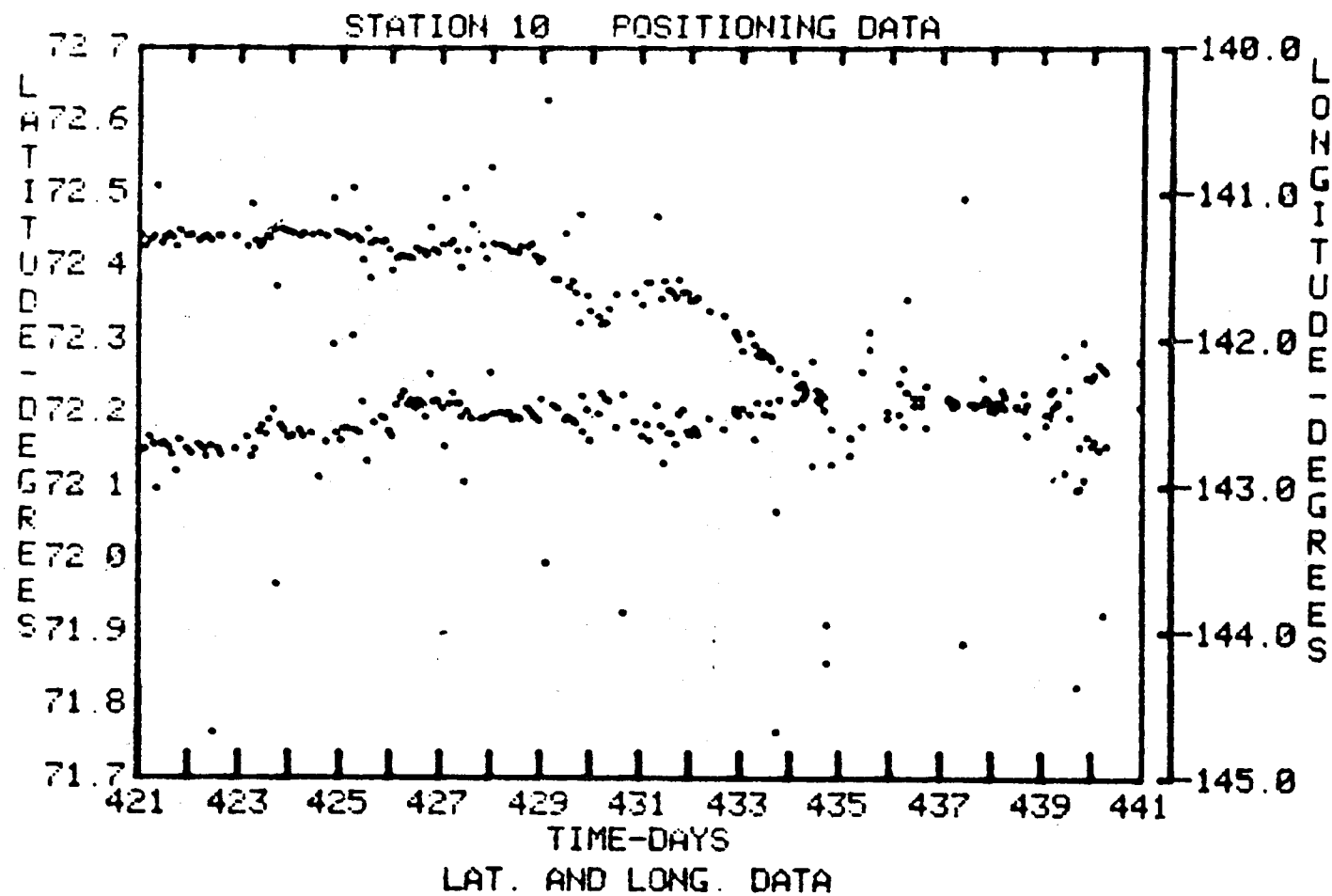


Fig. 1. Raw data from RAMS buoy R1003 (station 10). Latitude and longitude are plotted versus time. Outlying points were eliminated in preprocessing.

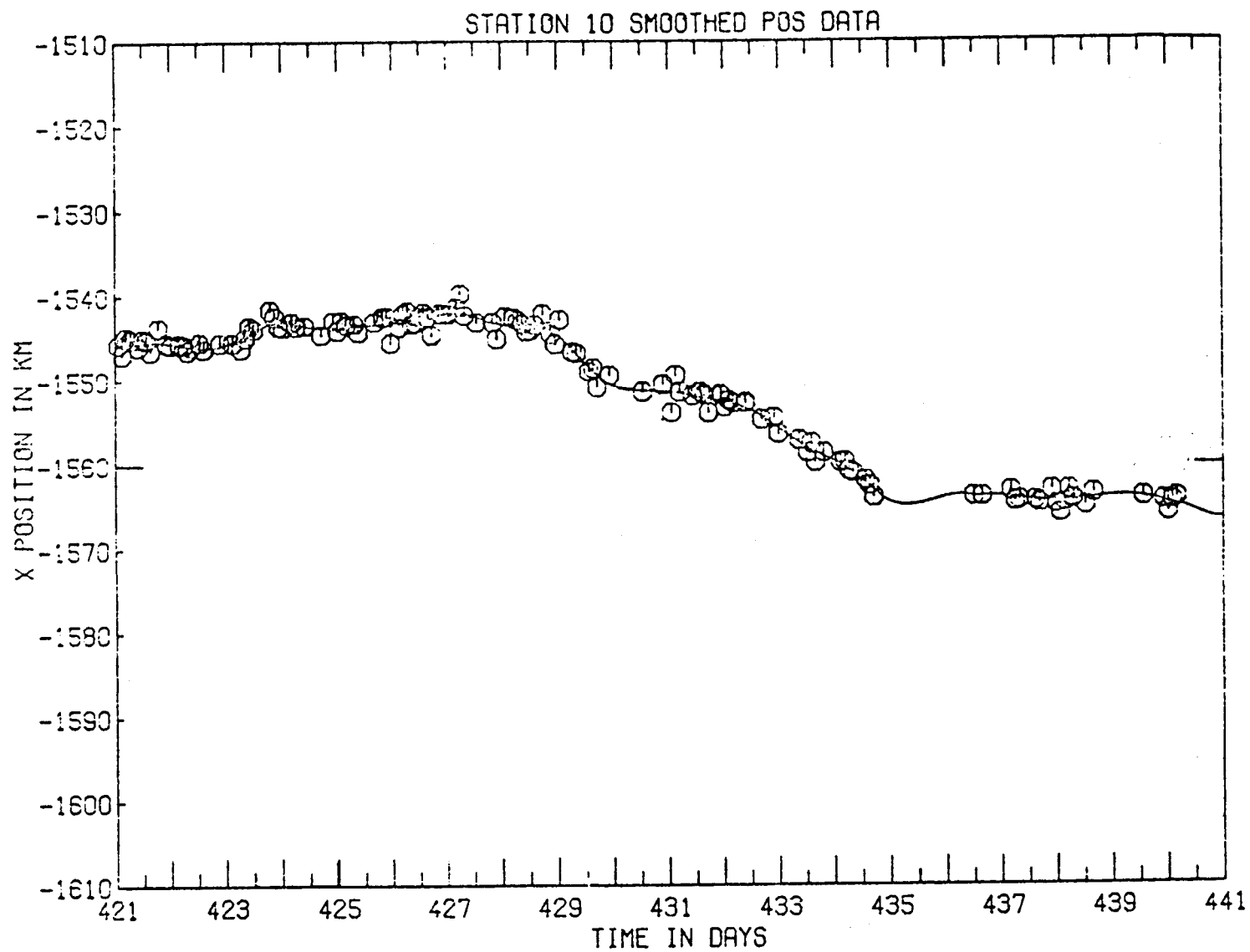


Fig. 2. Edited raw data (symbols) and smoothed position estimate (solid line) corresponding to the data in Figure 1. (Coordinates have been changed from latitude, longitude to x, y ; see Appendix 7.)

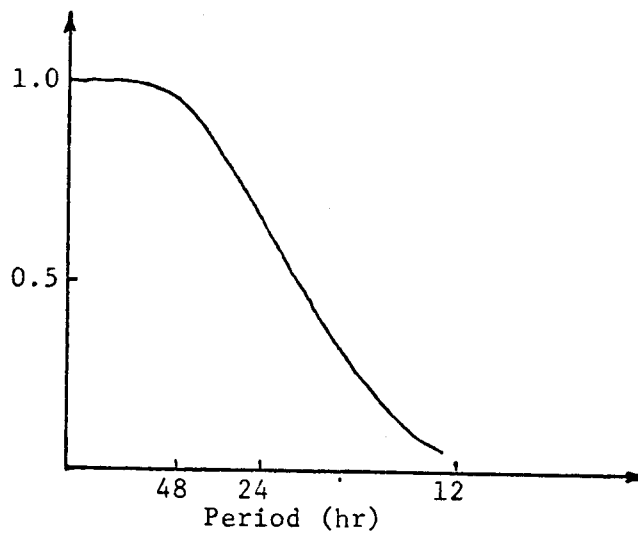


Fig. 3. Approximate response function for data processing scheme. Using measurements from RAMS hardware, an oscillation with a 24 hr period would be attenuated to about 60% of its amplitude.

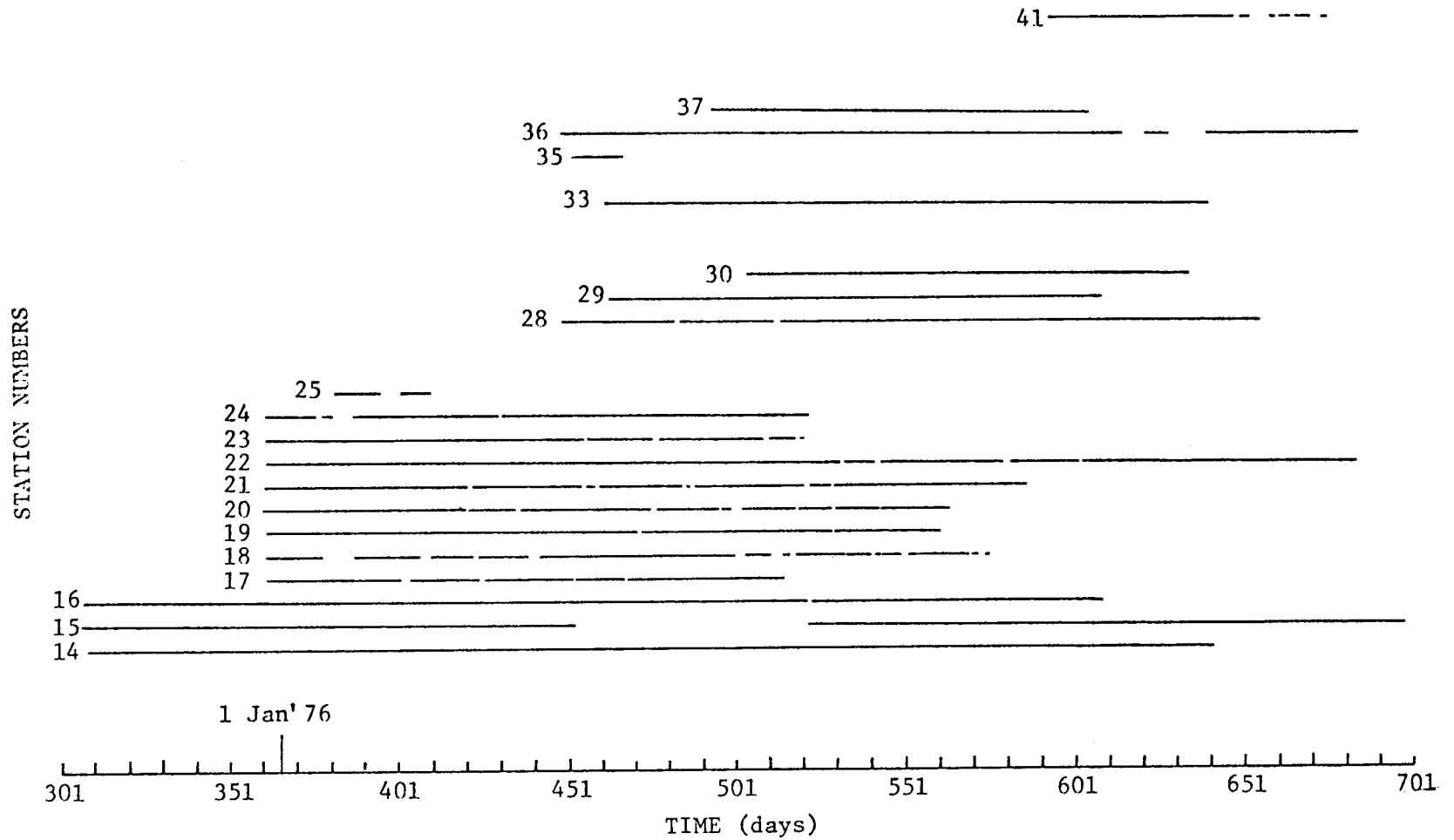
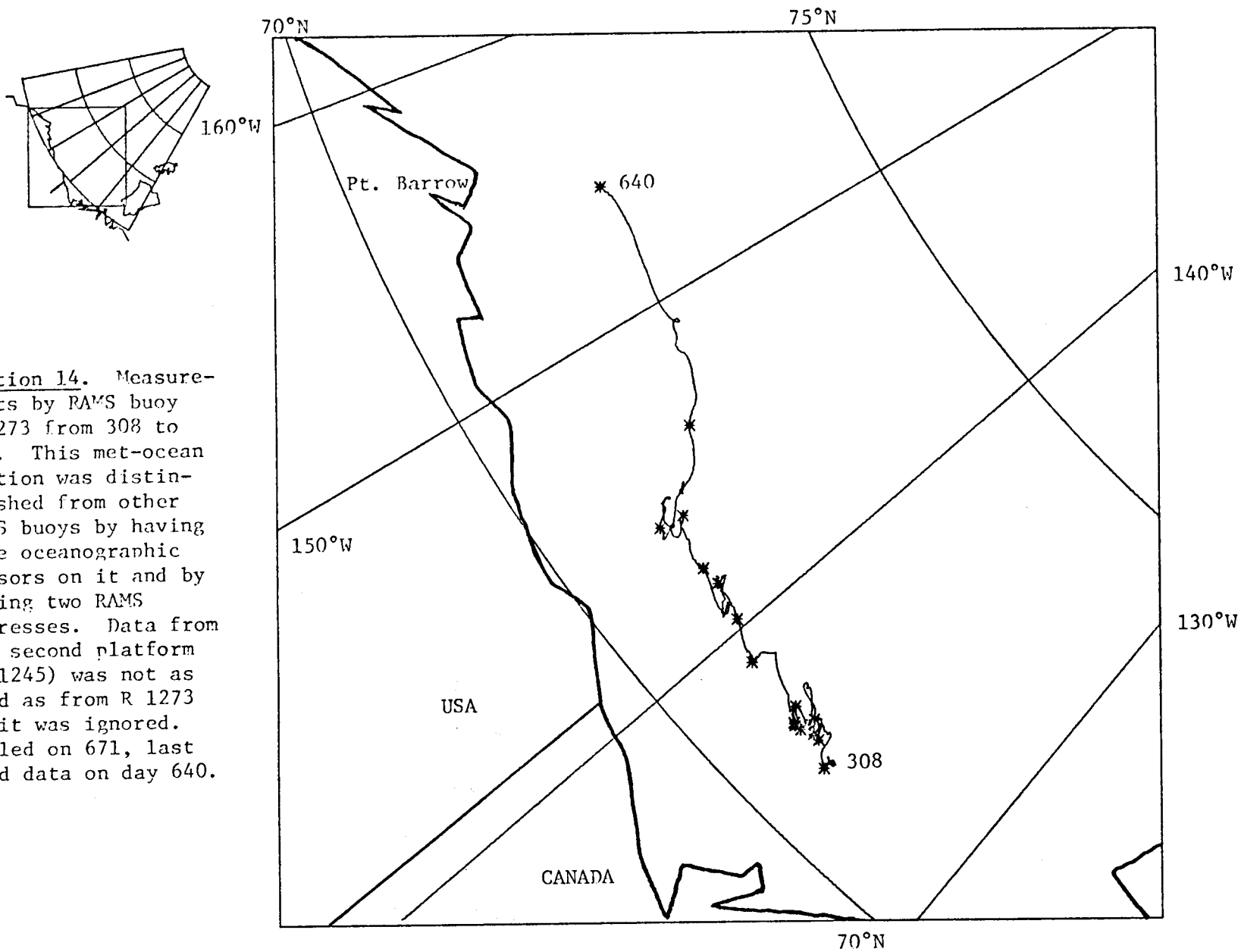


Fig. 4. Bar graph showing when usable data were collected at each RAMS station. Solid lines indicate good data. Goodness criteria were somewhat subjective; roughly speaking, data gaps of a day or more appear as gaps in the graph.

Fig. 5. The trajectory of each station is plotted. A thumbnail sketch locates the plotted region with respect to the Alaskan and Canadian coast. Asterisks indicate the positions at integral multiples of 20 days. The beginning and ending days are noted for each trajectory. A dashed line indicates a long period of missing data. The region is 1000 km \times 1000 km aligned with the x,y coordinate system shown in Appendix 5.

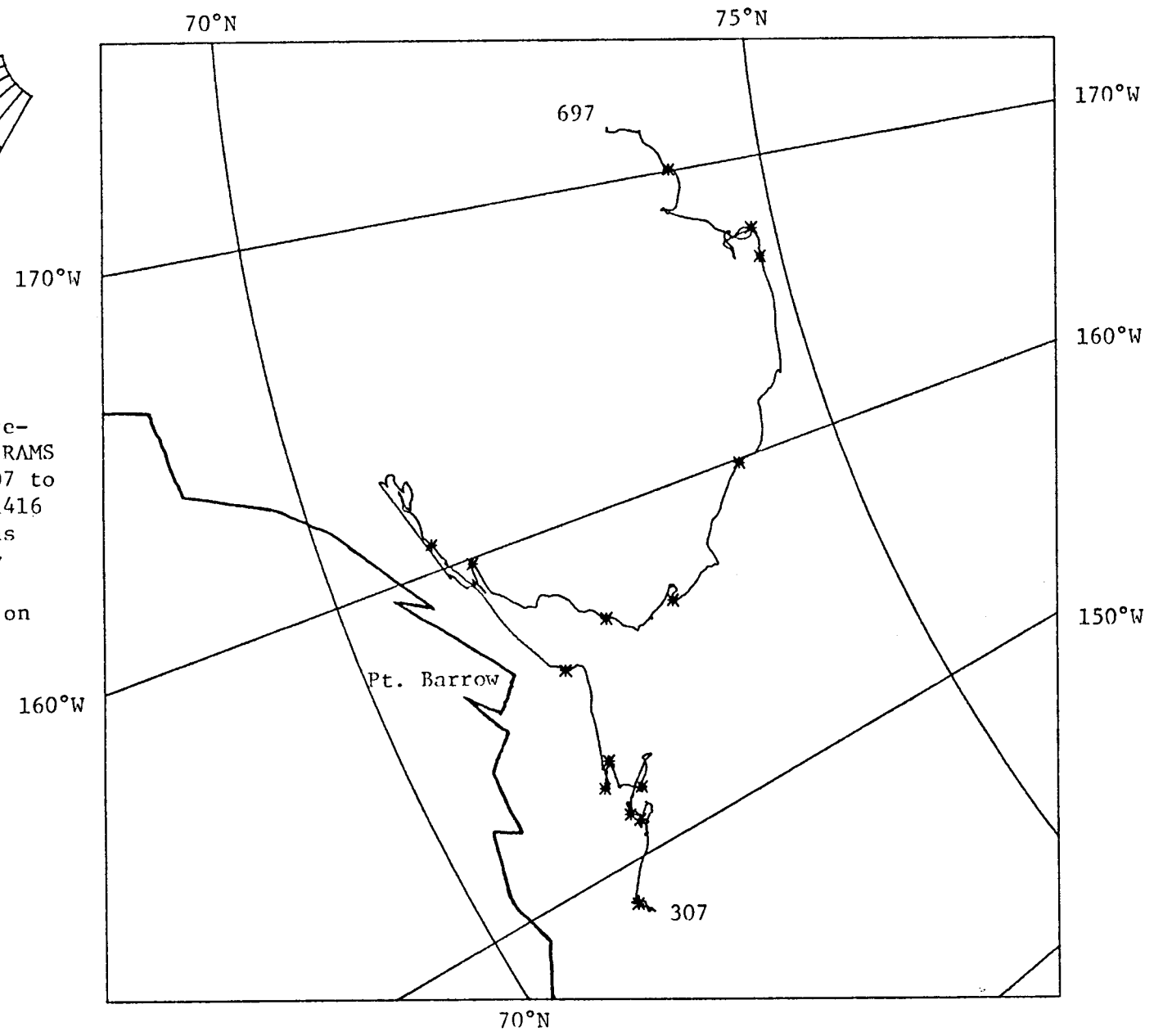
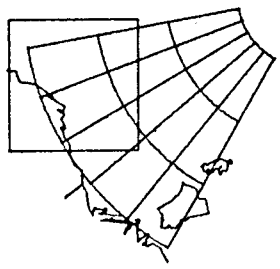
198

Station 14. Measurements by RAMS buoy R 1273 from 308 to 640. This met-ocean station was distinguished from other RAMS buoys by having some oceanographic sensors on it and by having two RAMS addresses. Data from the second platform (R 1245) was not as good as from R 1273 so it was ignored. Failed on 671, last good data on day 640.



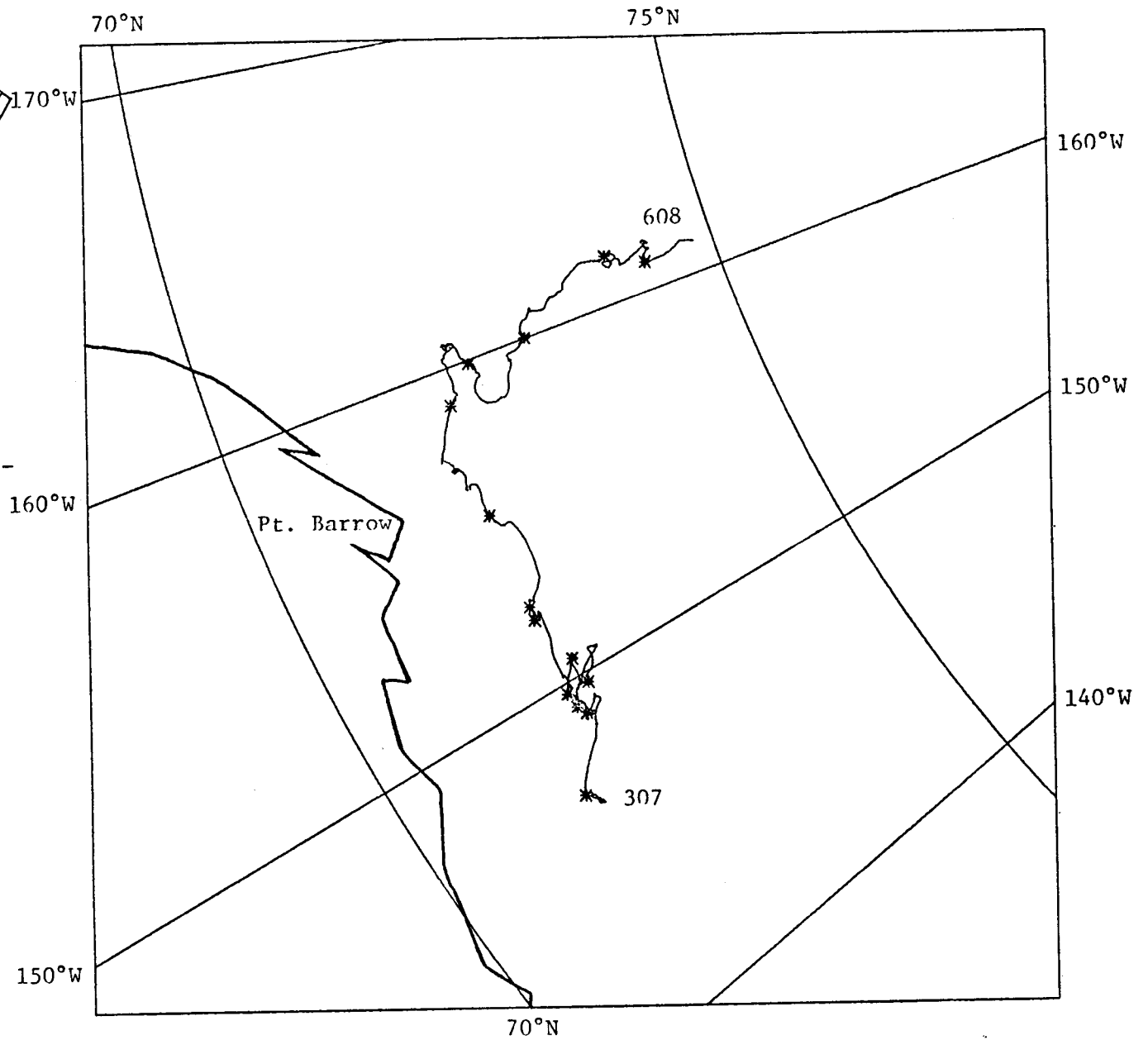
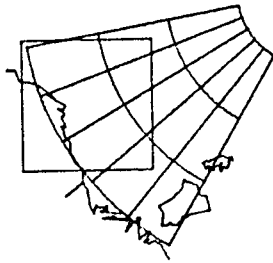
199

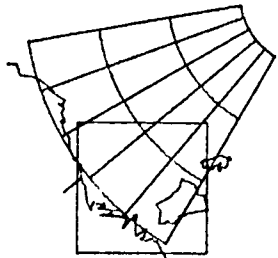
Station 15. Measurements by met-ocean RAMS buoy R 1420 from 307 to 452. Data from R 1416 at the same site was not used. The buoy was revived around day 520 and failed on day 697.



200

Station 16. Measurements by met-ocean RAMS buoy R 1467 from 307 to 608. Data from R 1451 at the same site was not used.

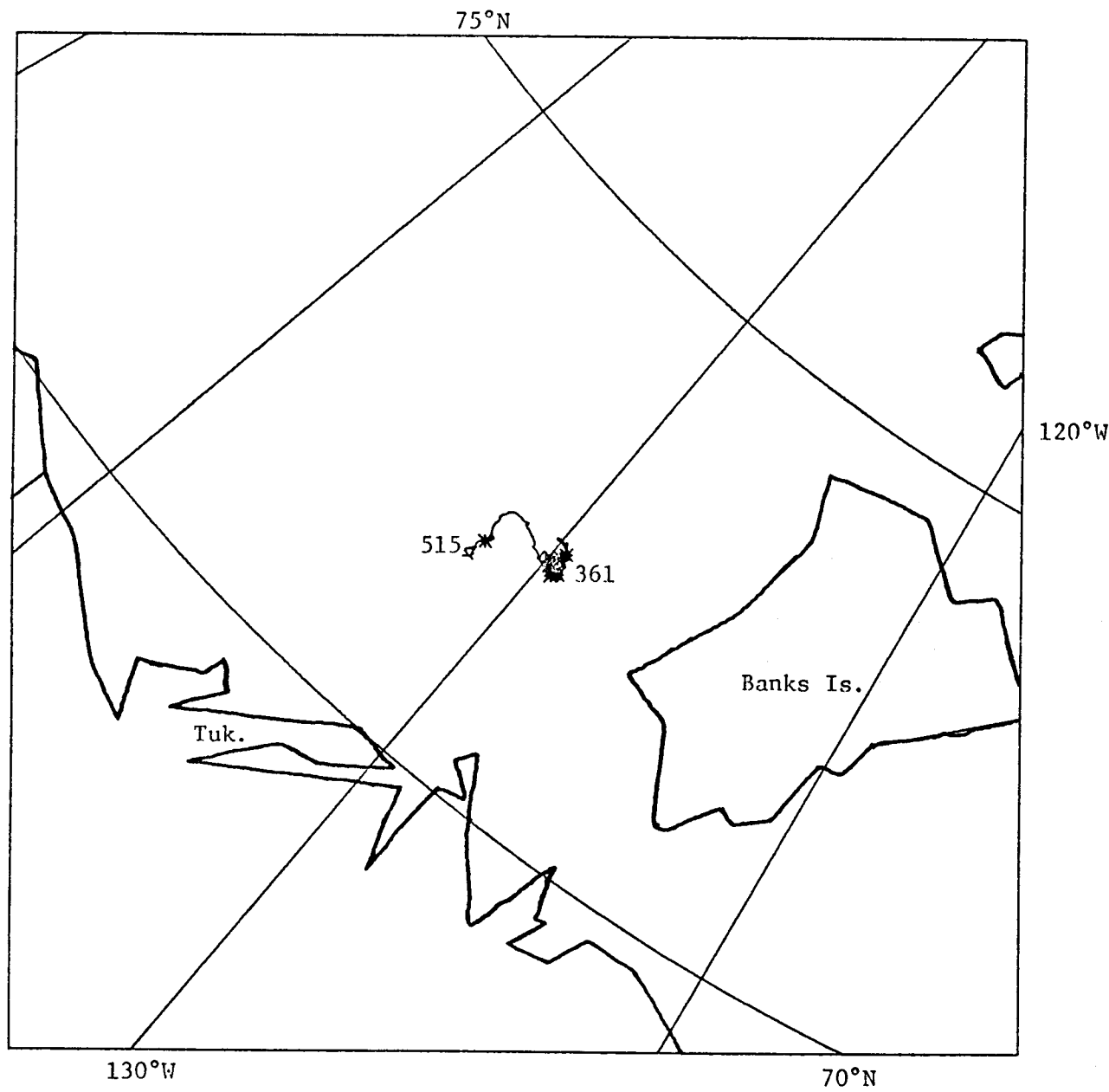




201

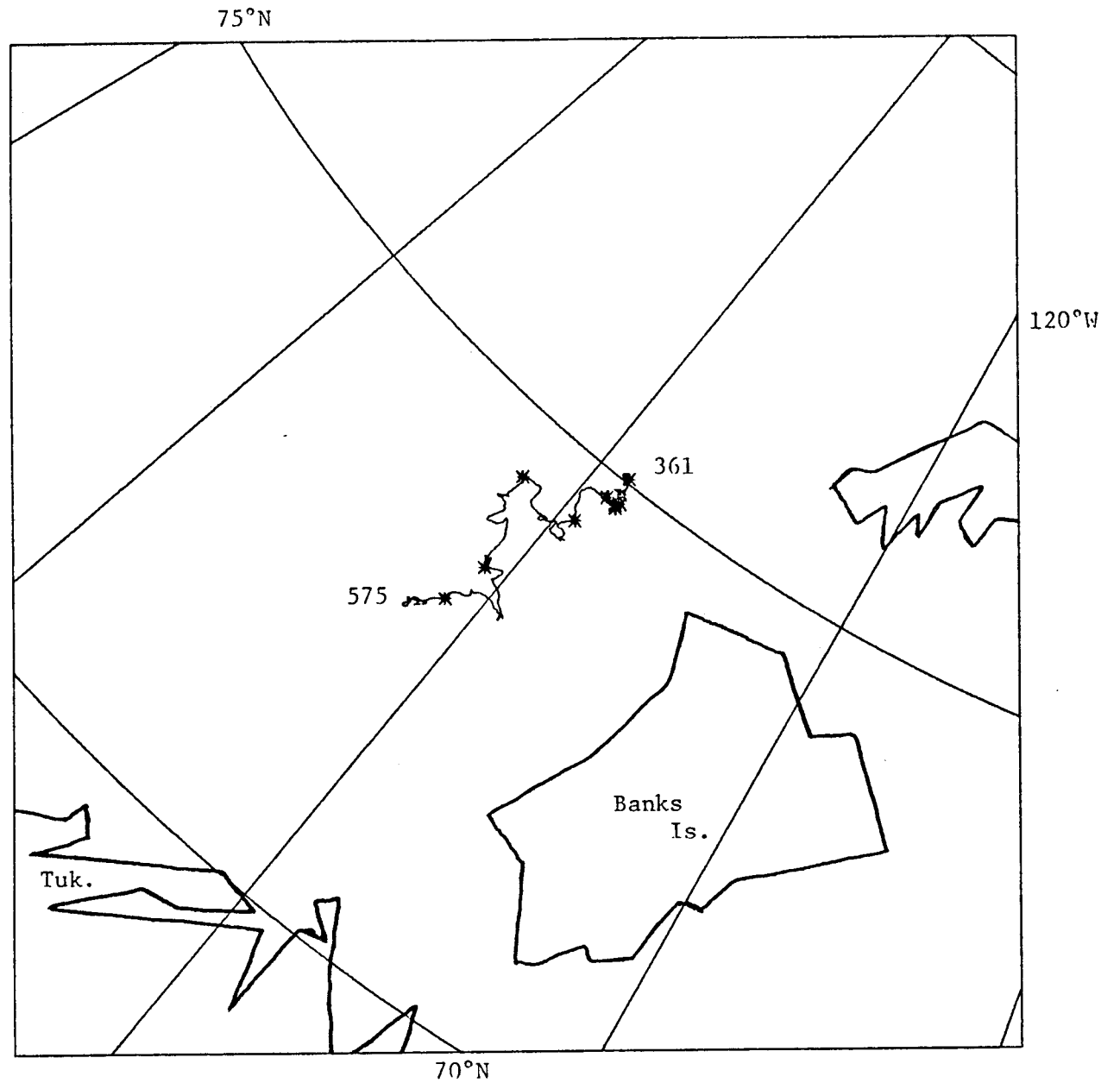
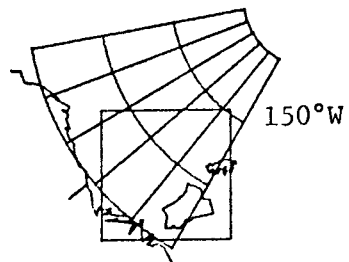
Station 17. Measurements by RAMS buoy R 10 from 361 to 515.

140°W



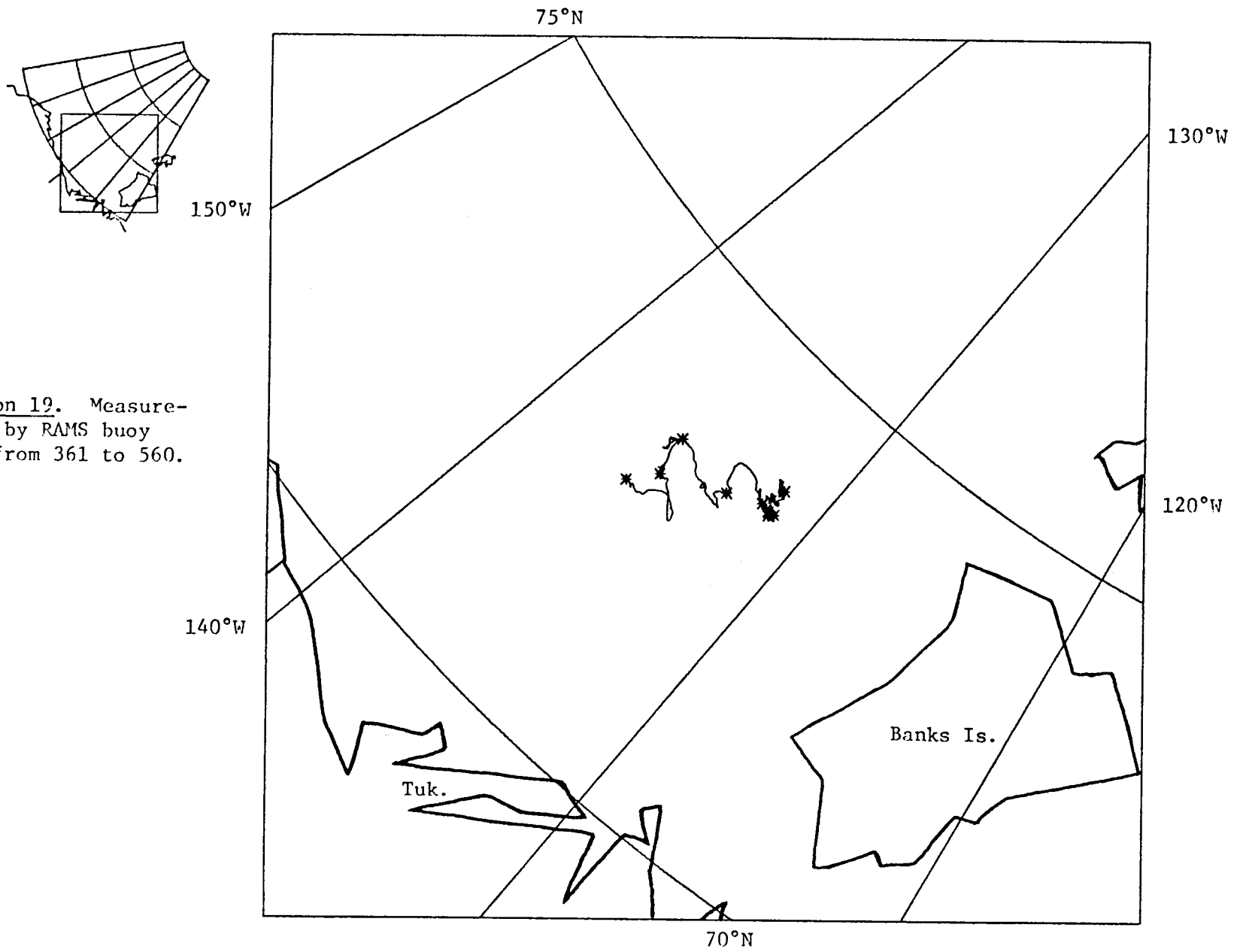
202

Station 18. Measurements by RAMS buoy R 26 from 361 to 575, with a gap from 381 to 387. Failed on 575.

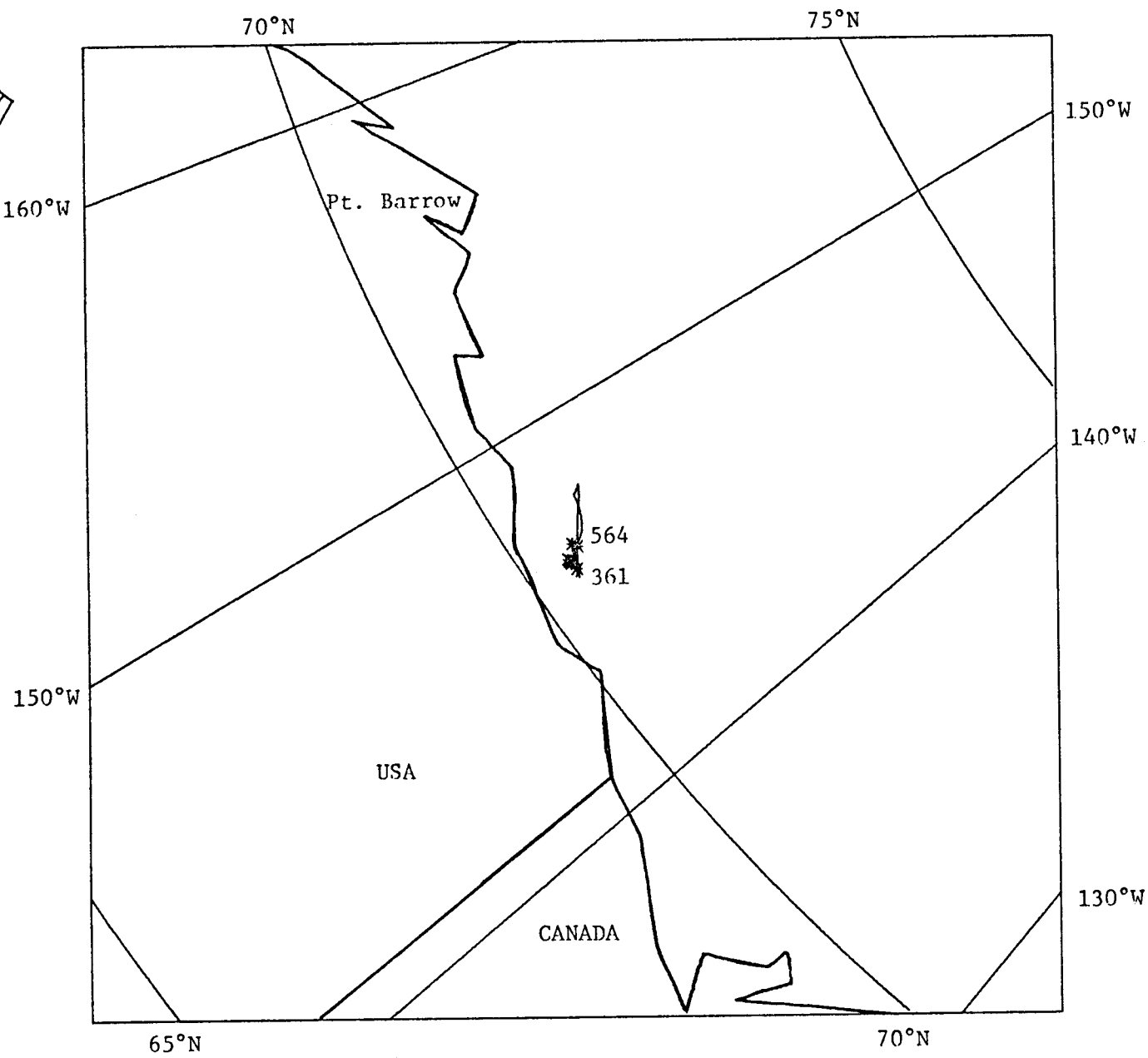
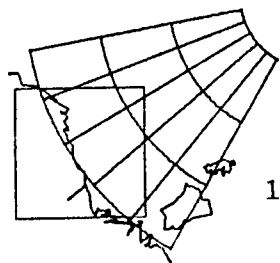


203

Station 19. Measurements by RAMS buoy R 57 from 361 to 560.

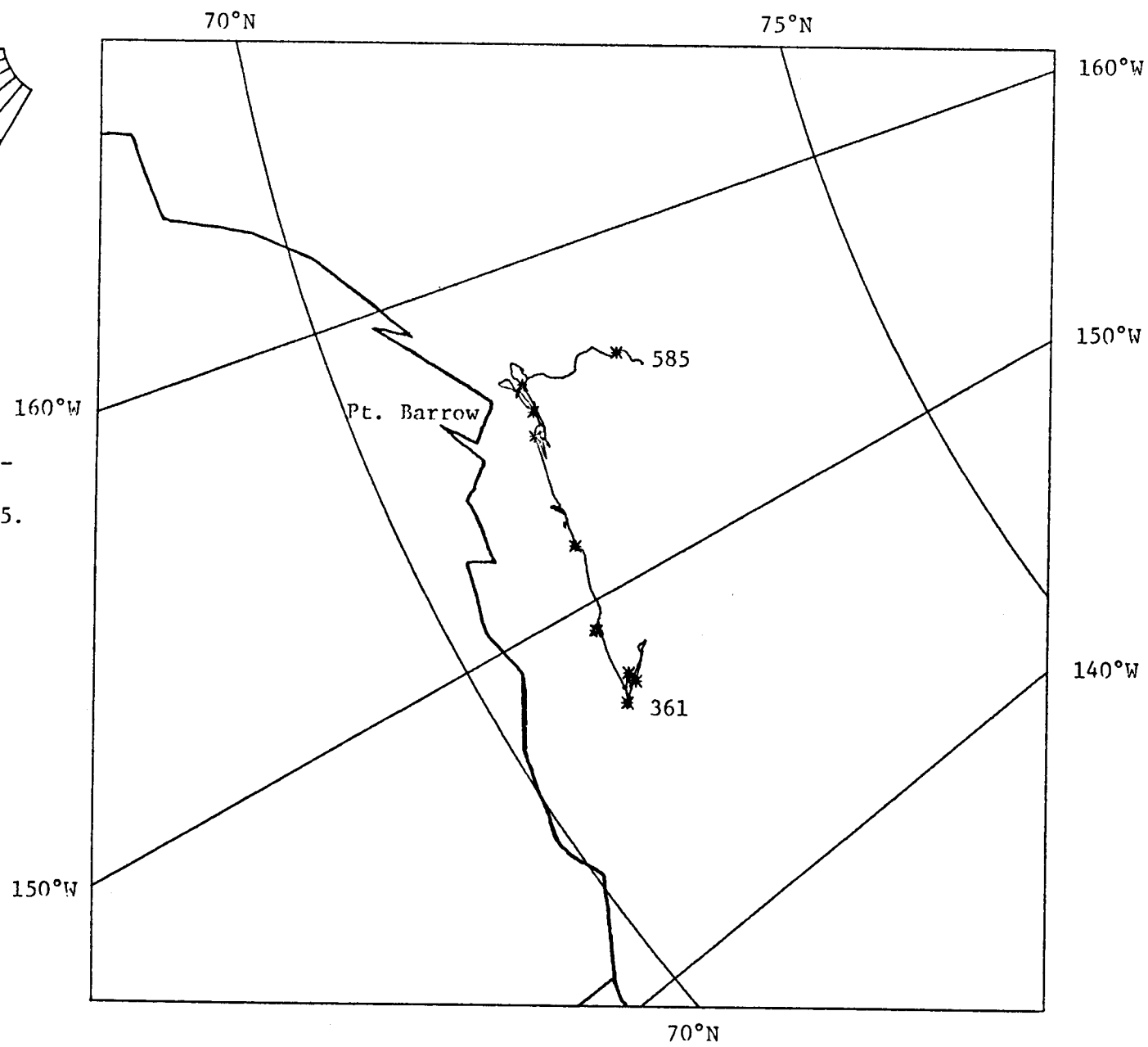
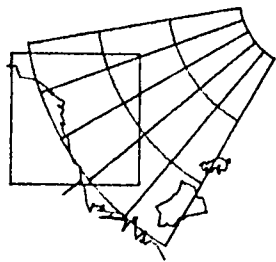


204 Station 20. Measure-
ments by RAMS buoy
R 61 from 361 to 564.



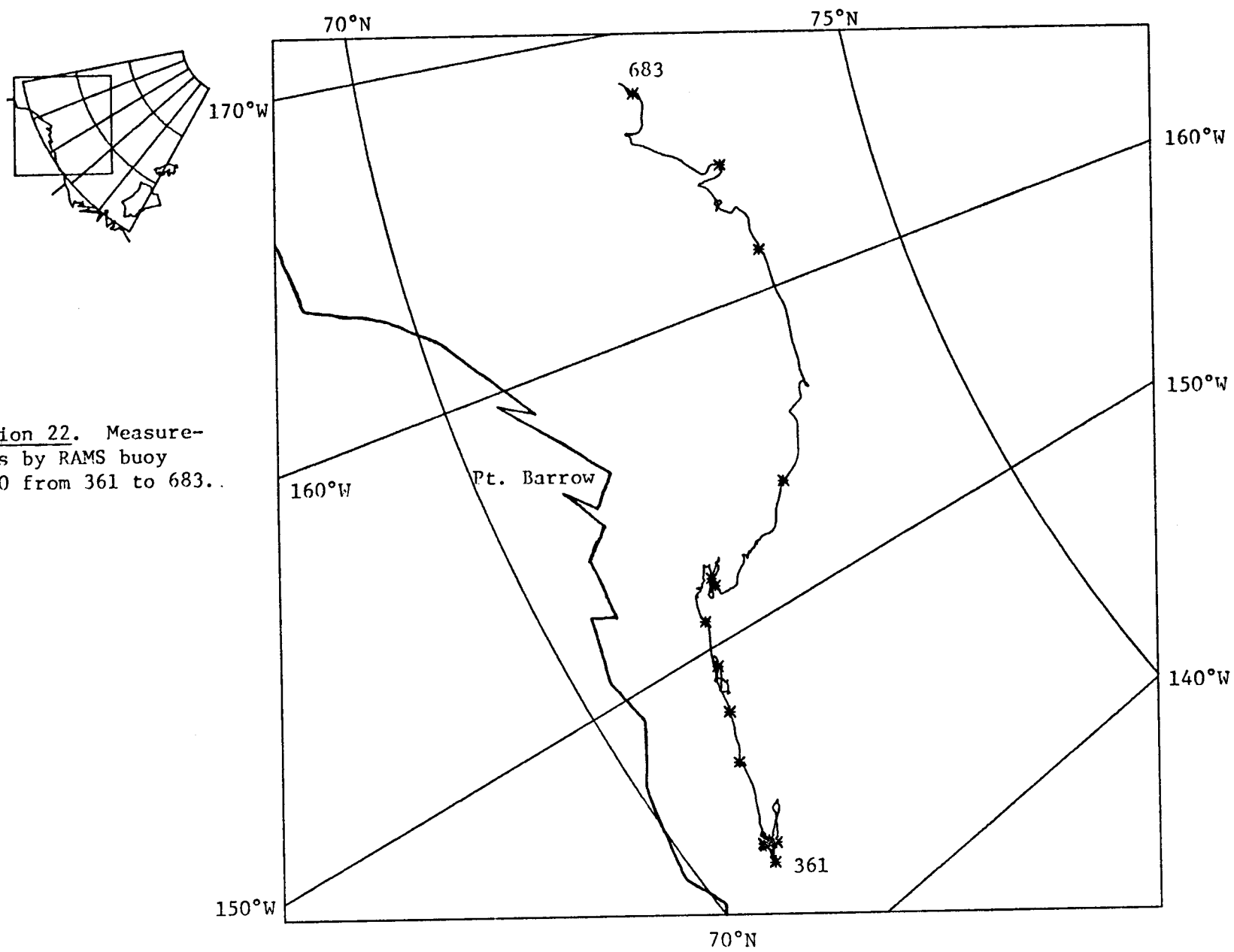
205

Station 21. Measure-
ments by RAMS buoy
R 316 from 361 to 585.



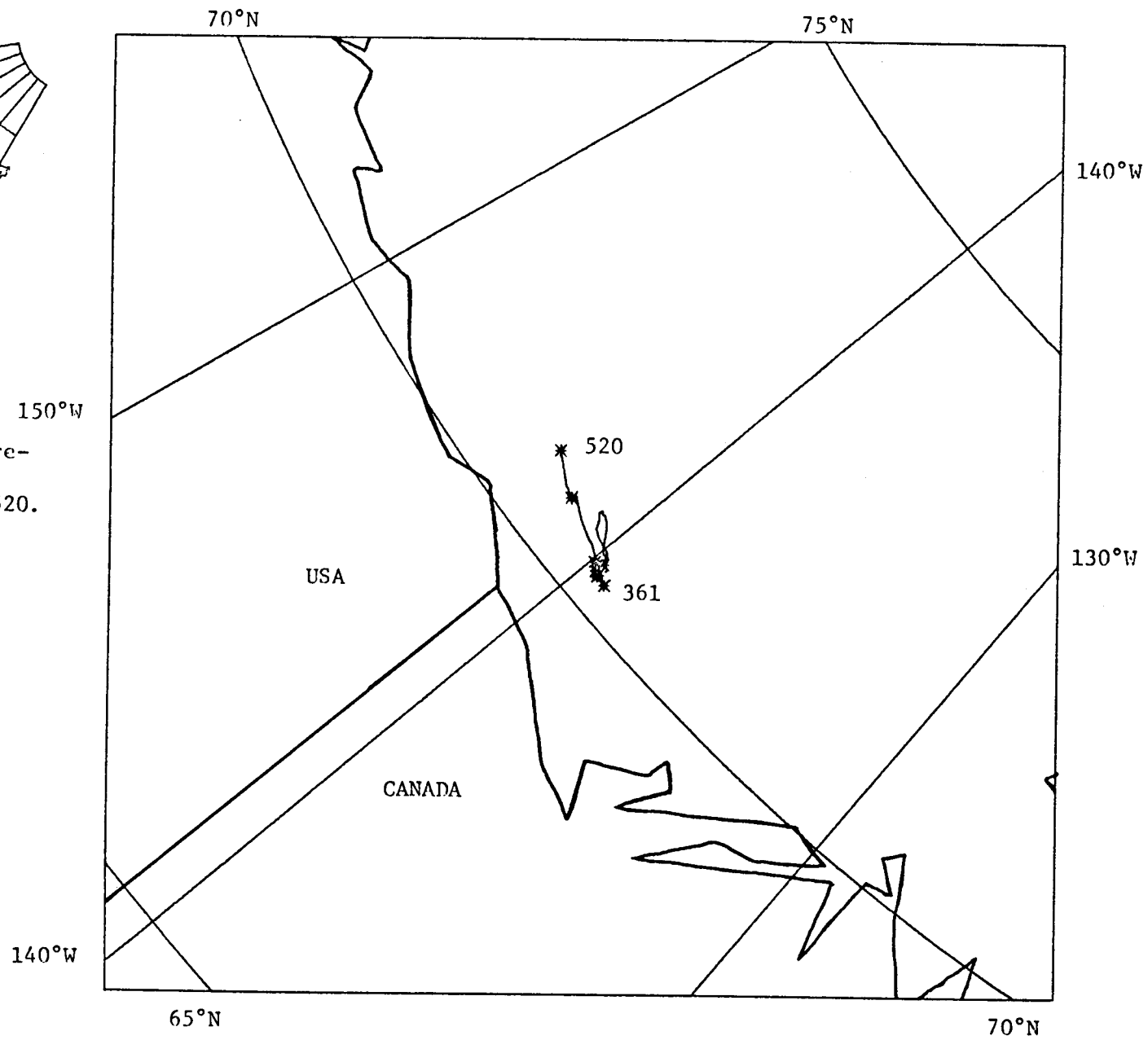
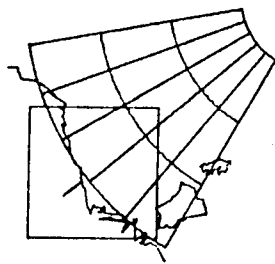
206

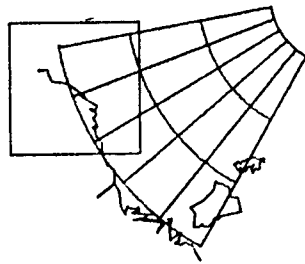
Station 22. Measure-
ments by RAMS buoy
R 320 from 361 to 683..



207

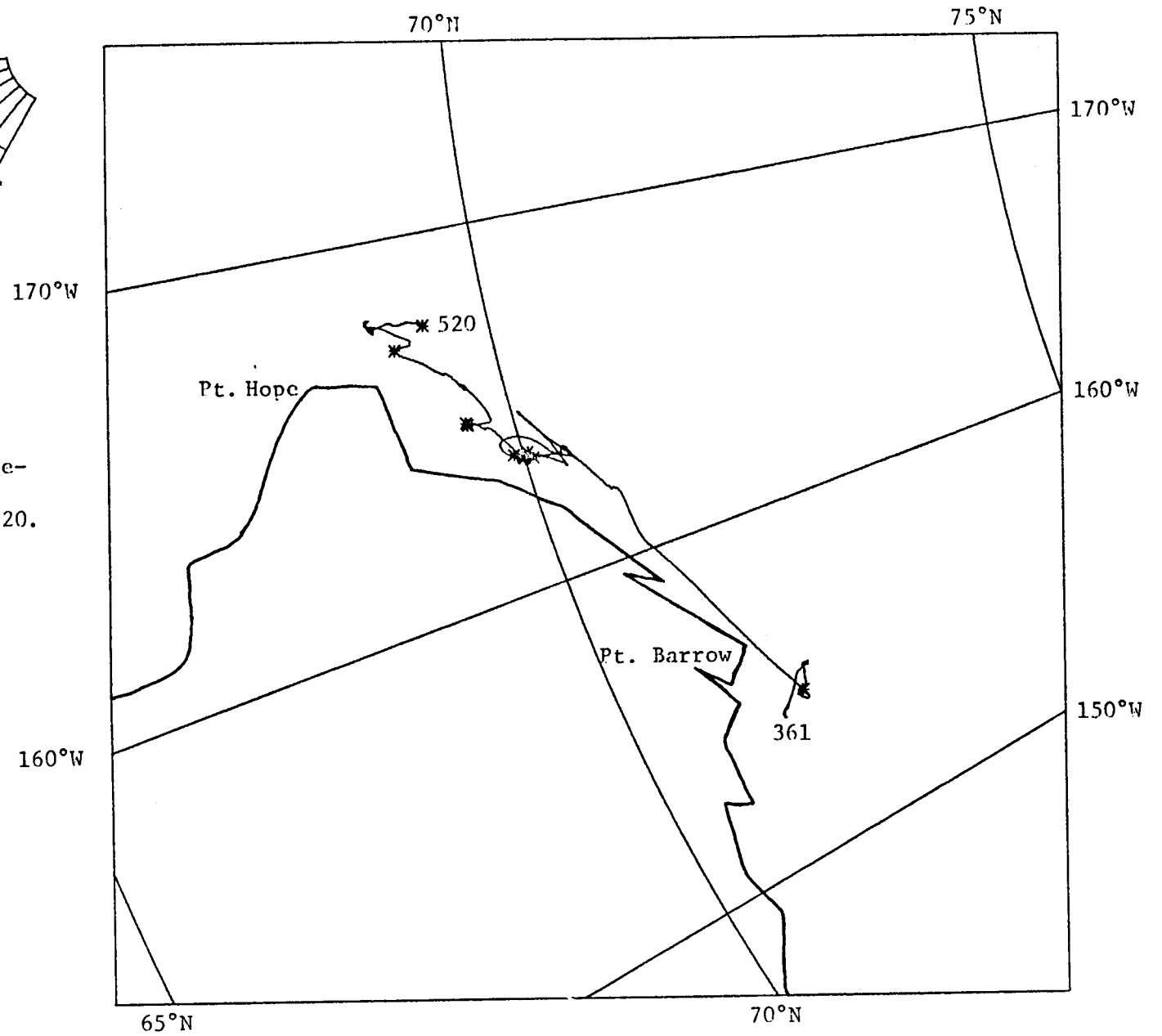
Station 23. Measure-
ments by RAMS buoy
P. 502 from 361 to 520.





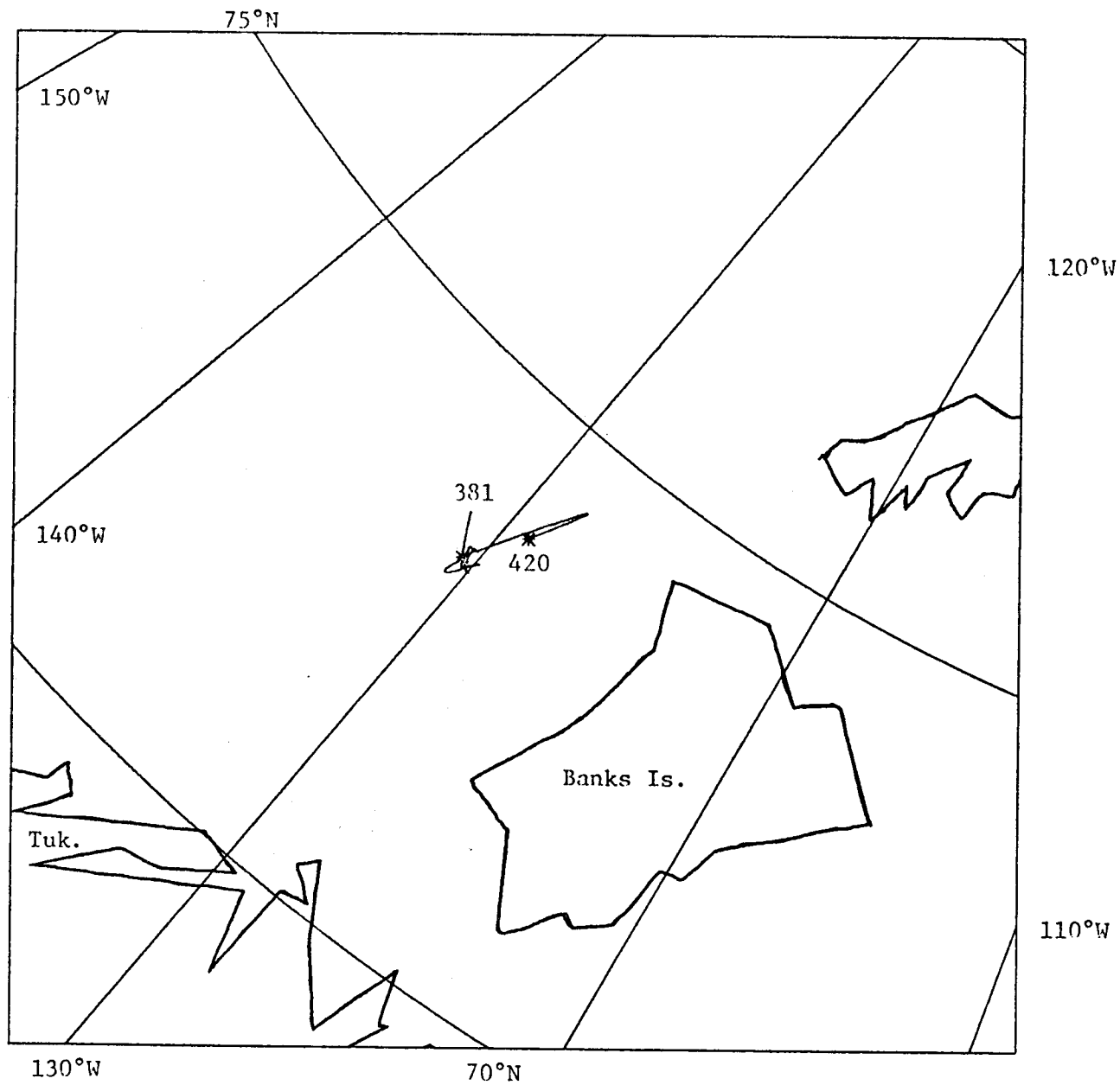
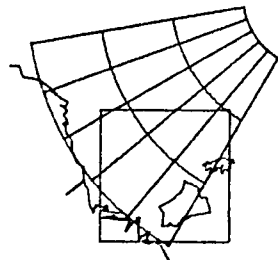
208

Station 24. Measurements by RAMS buoy R 534 from 361 to 520.



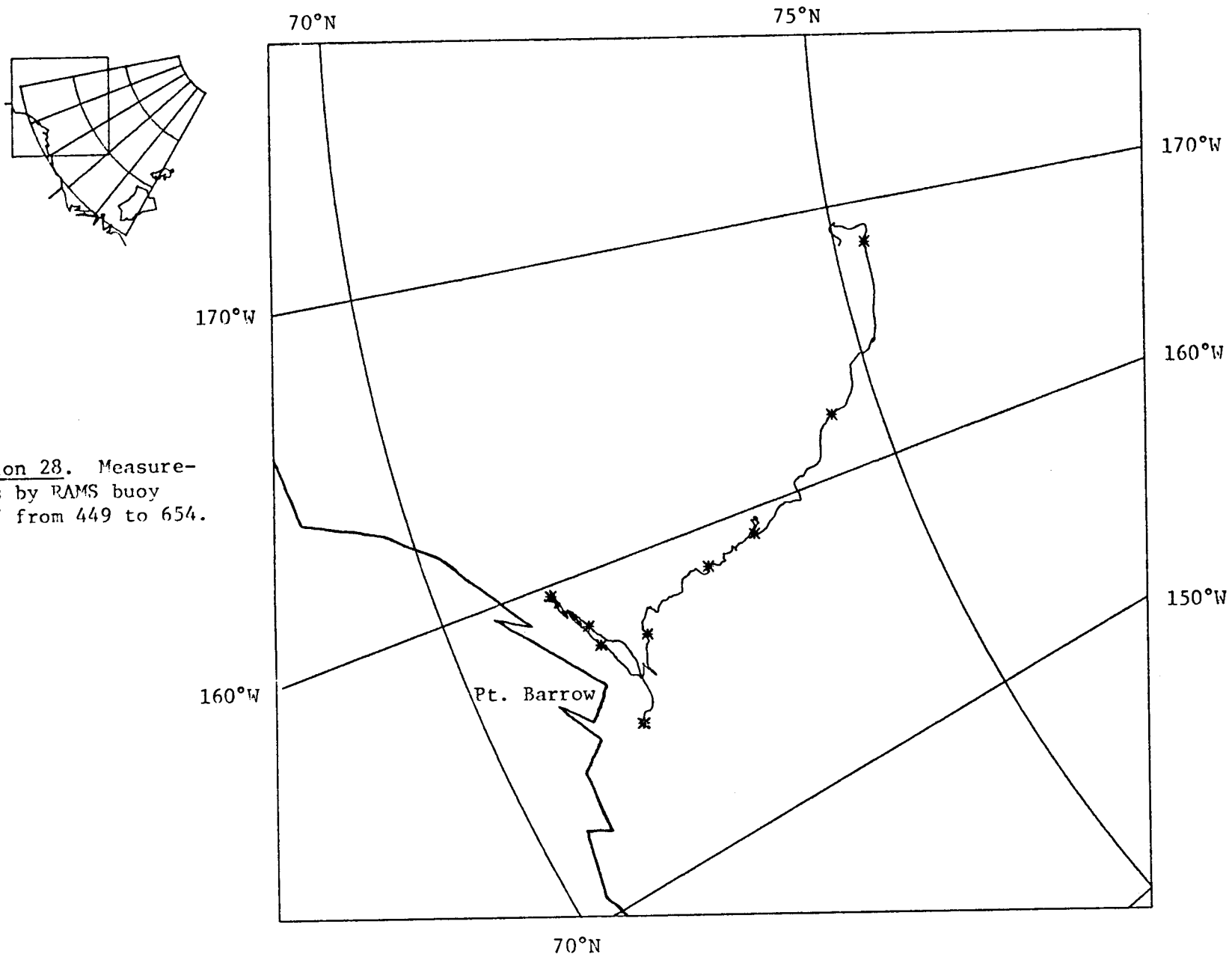
209

Station 25. Measurements by met-ocean RAMS buoy R 1143 from 381 to 420. Very poor data. The data from R 1175 at the same site was also very poor.



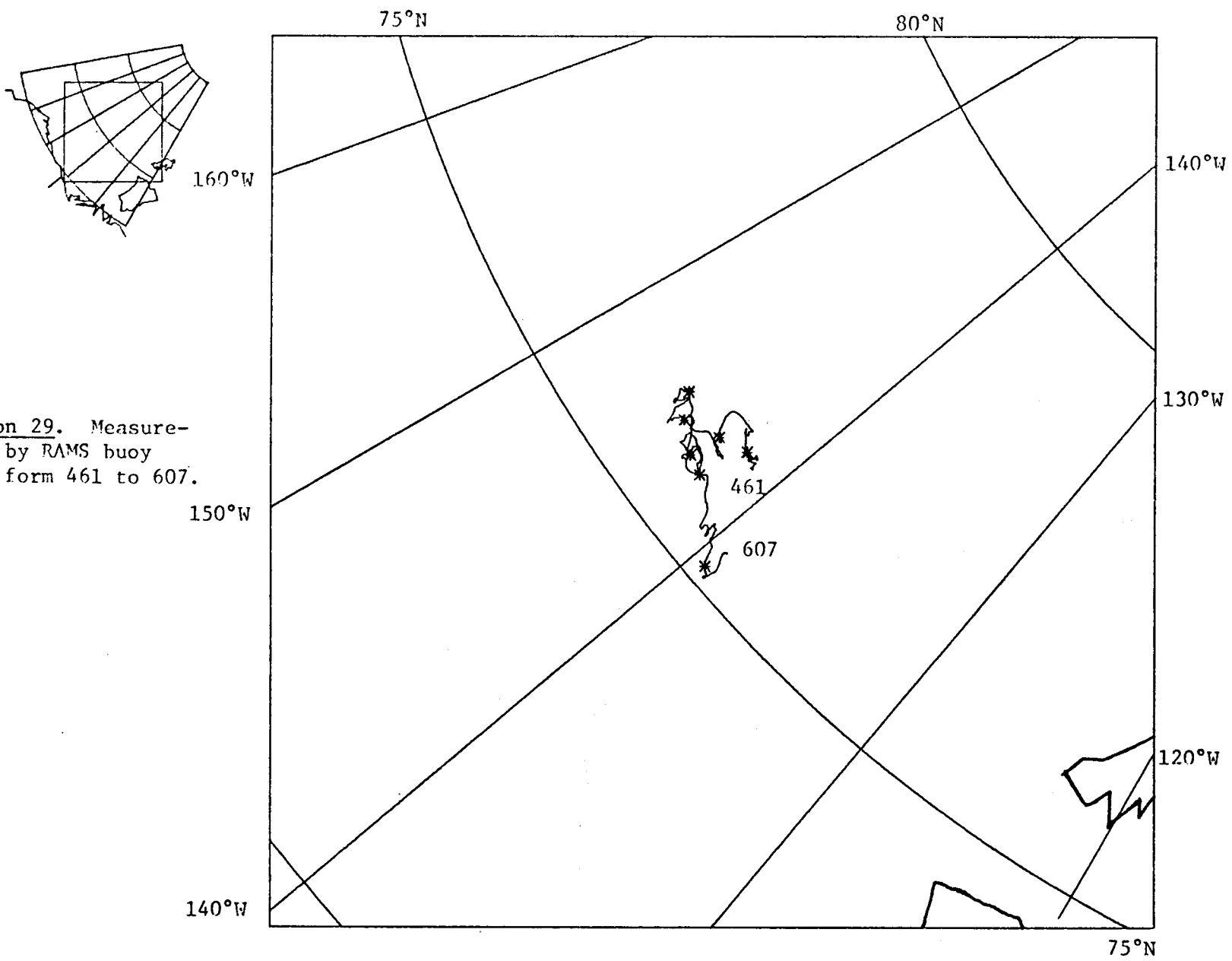
210

Station 28. Measure-
ments by RAMS buoy
R 137 from 449 to 654.



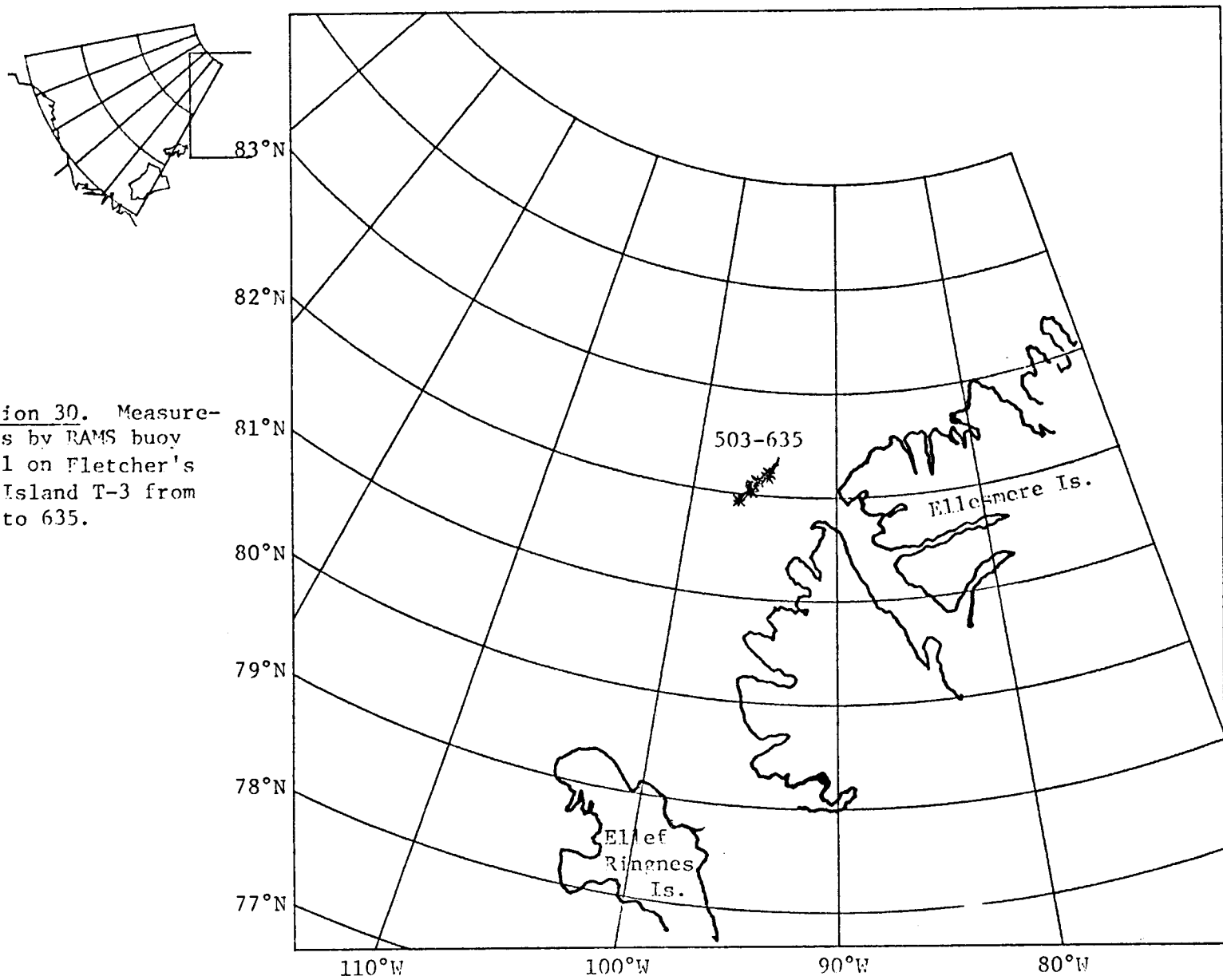
211

Station 29. Measure-
ments by RAMS buoy
R 207 form 461 to 607.



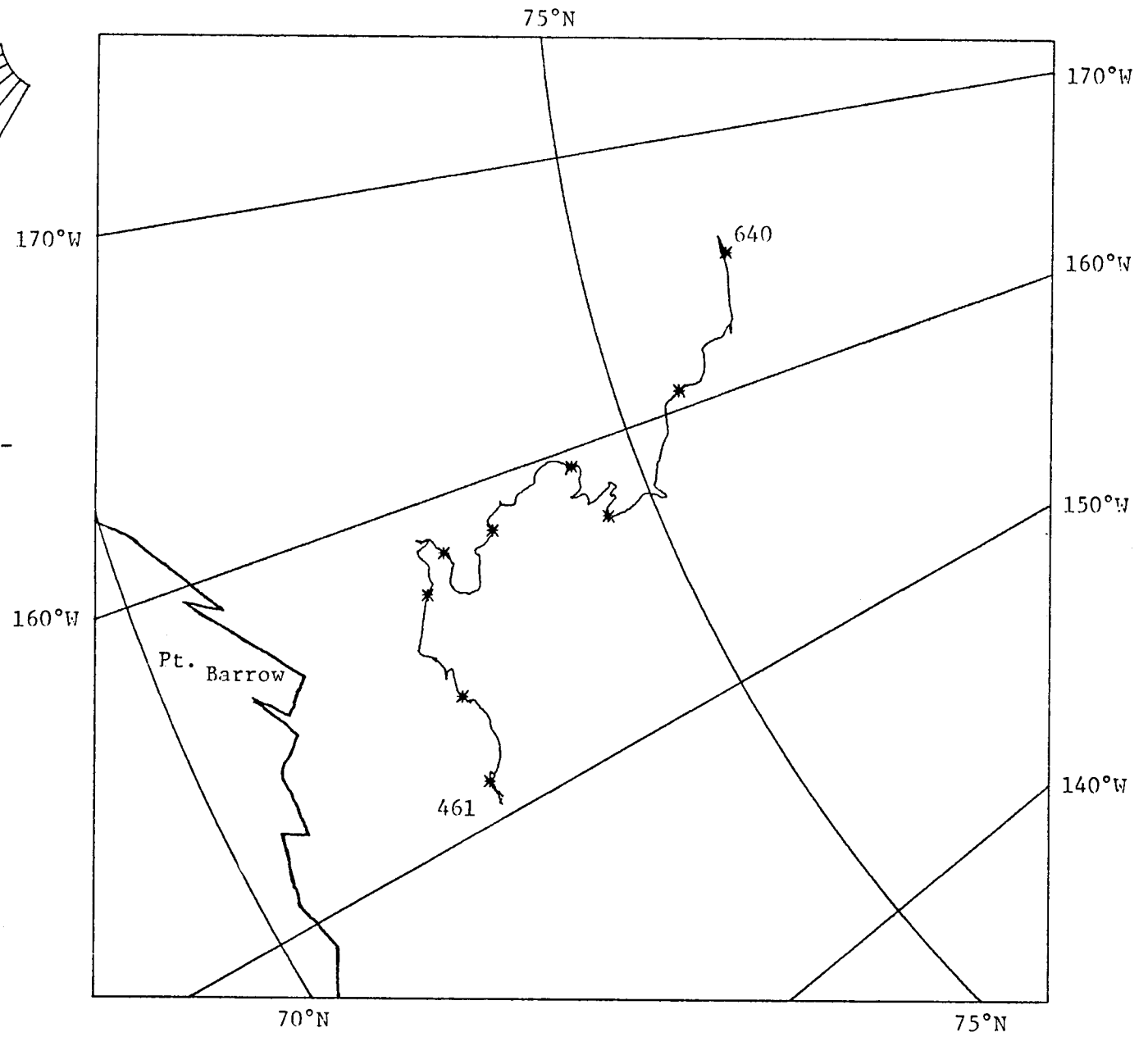
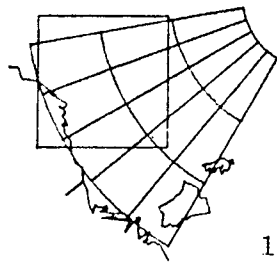
212

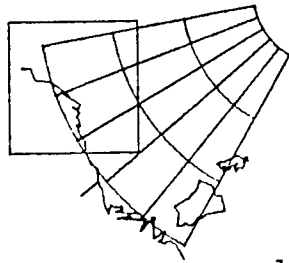
Station 30. Measurements by RAMS buoy R 231 on Fletcher's Ice Island T-3 from 503 to 635.



213

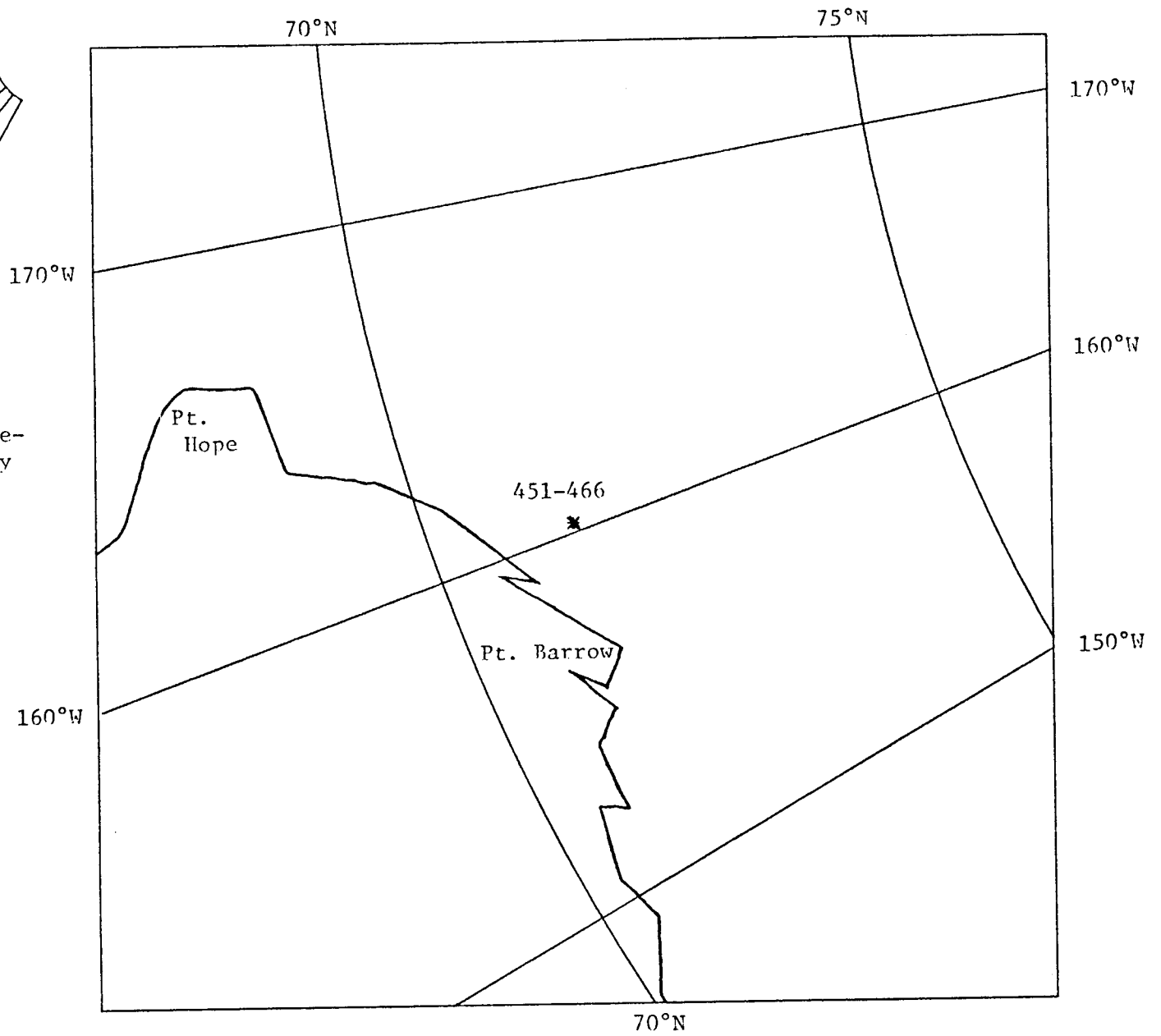
Station 33. Measurements from RAMS buoy R 1015 from 461 to 641.

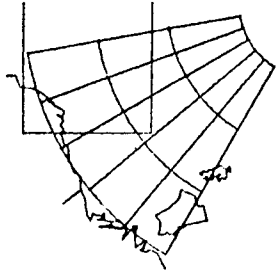




214

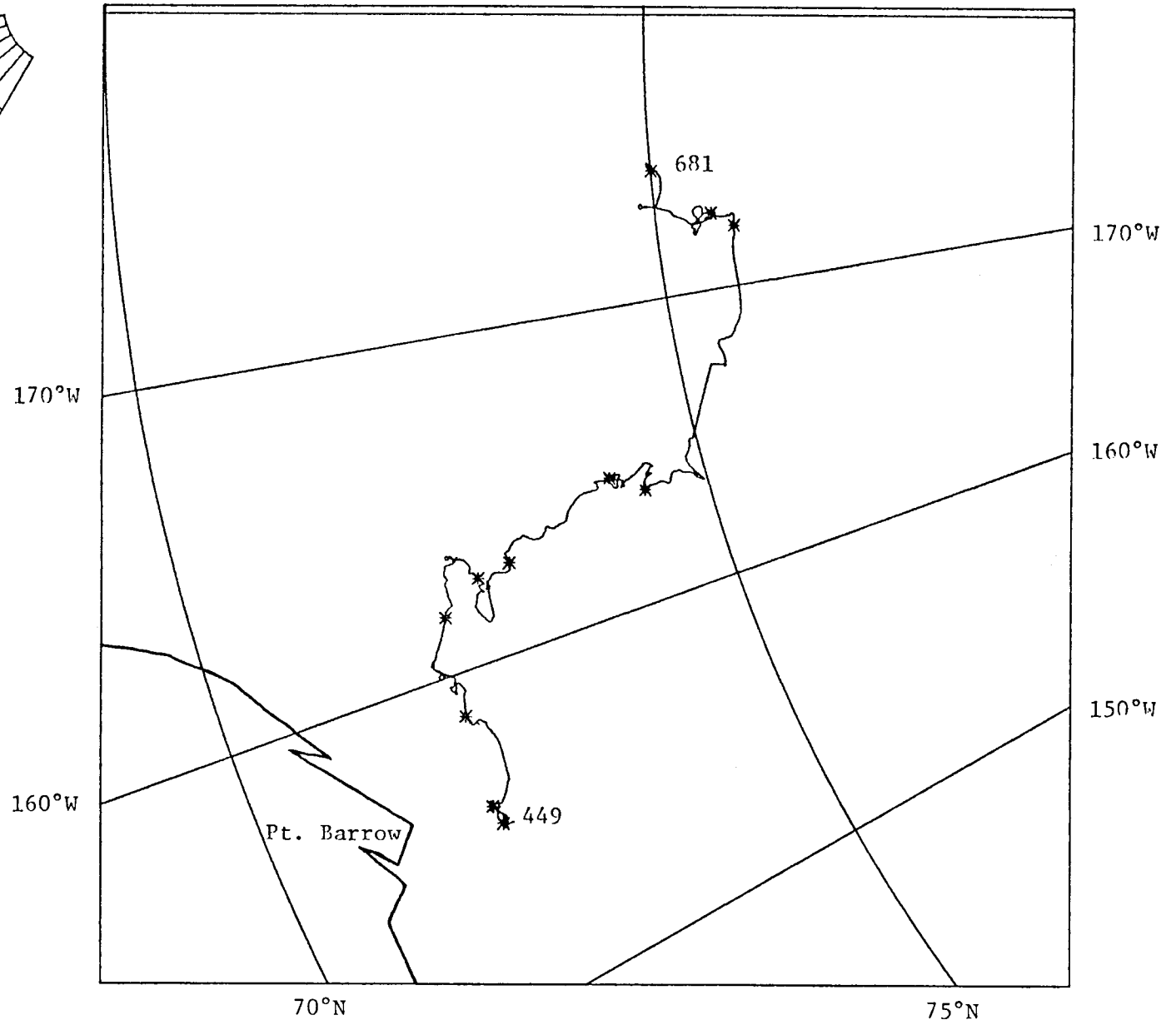
Station 35. Measurements from RAMS buoy R 1757 from 451 to 466. This station had radio call name APLIS.





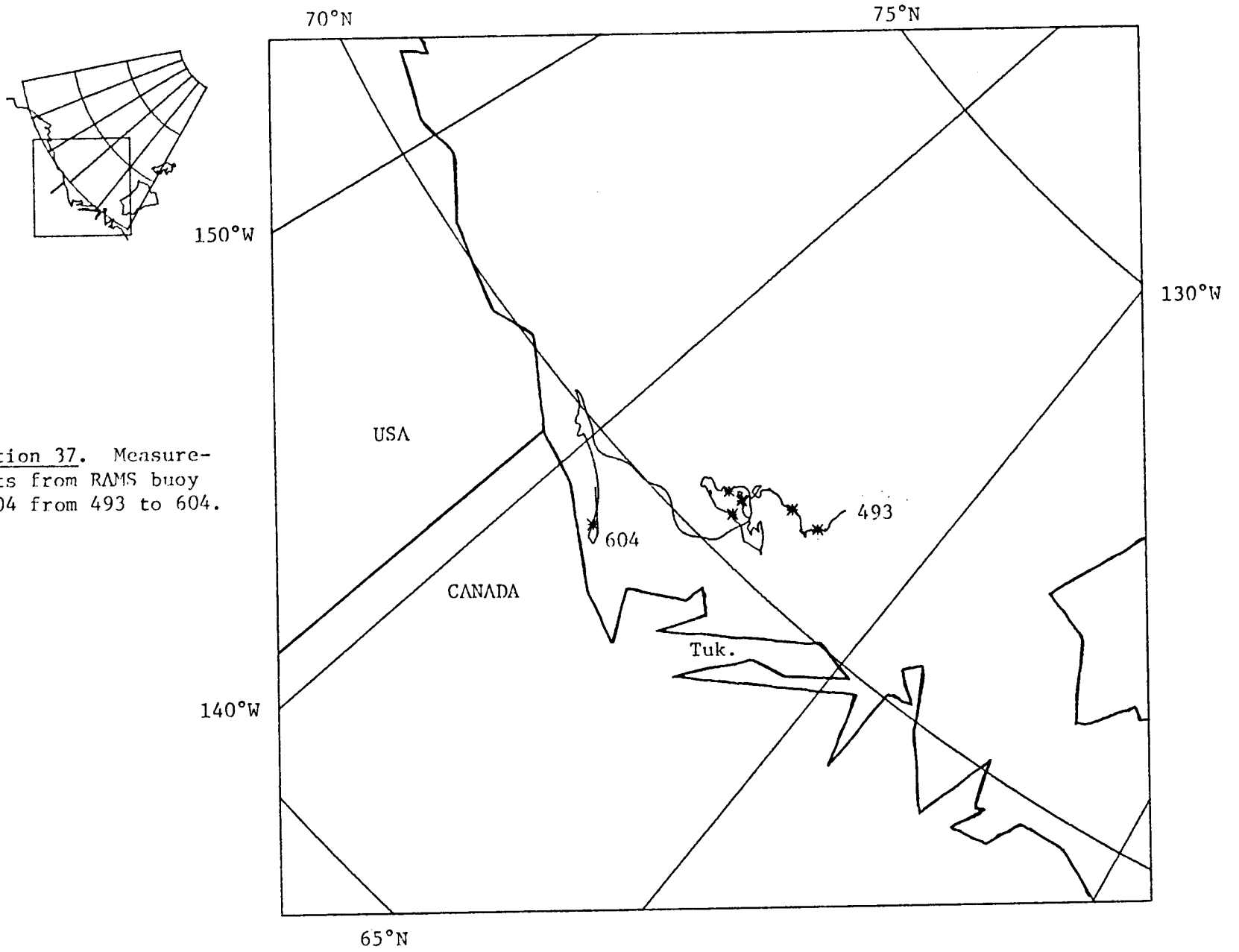
215

Station 36. Measurements from RAMS buoy R 1761 from 449 to 681.

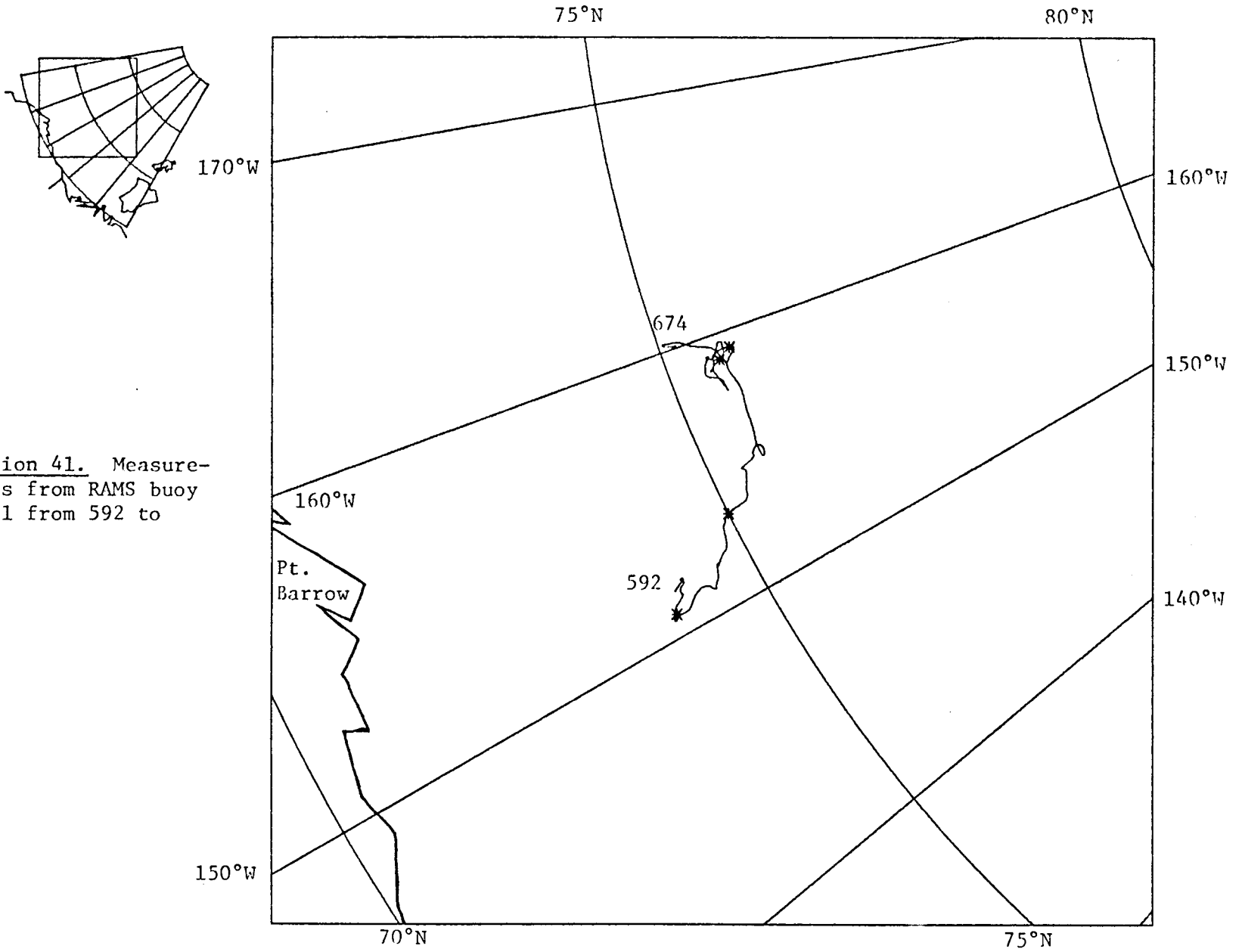


216

Station 37. Measurements from RAMS buoy R 604 from 493 to 604.



Station 41. Measurements from RAMS buoy R 101 from 592 to 674.



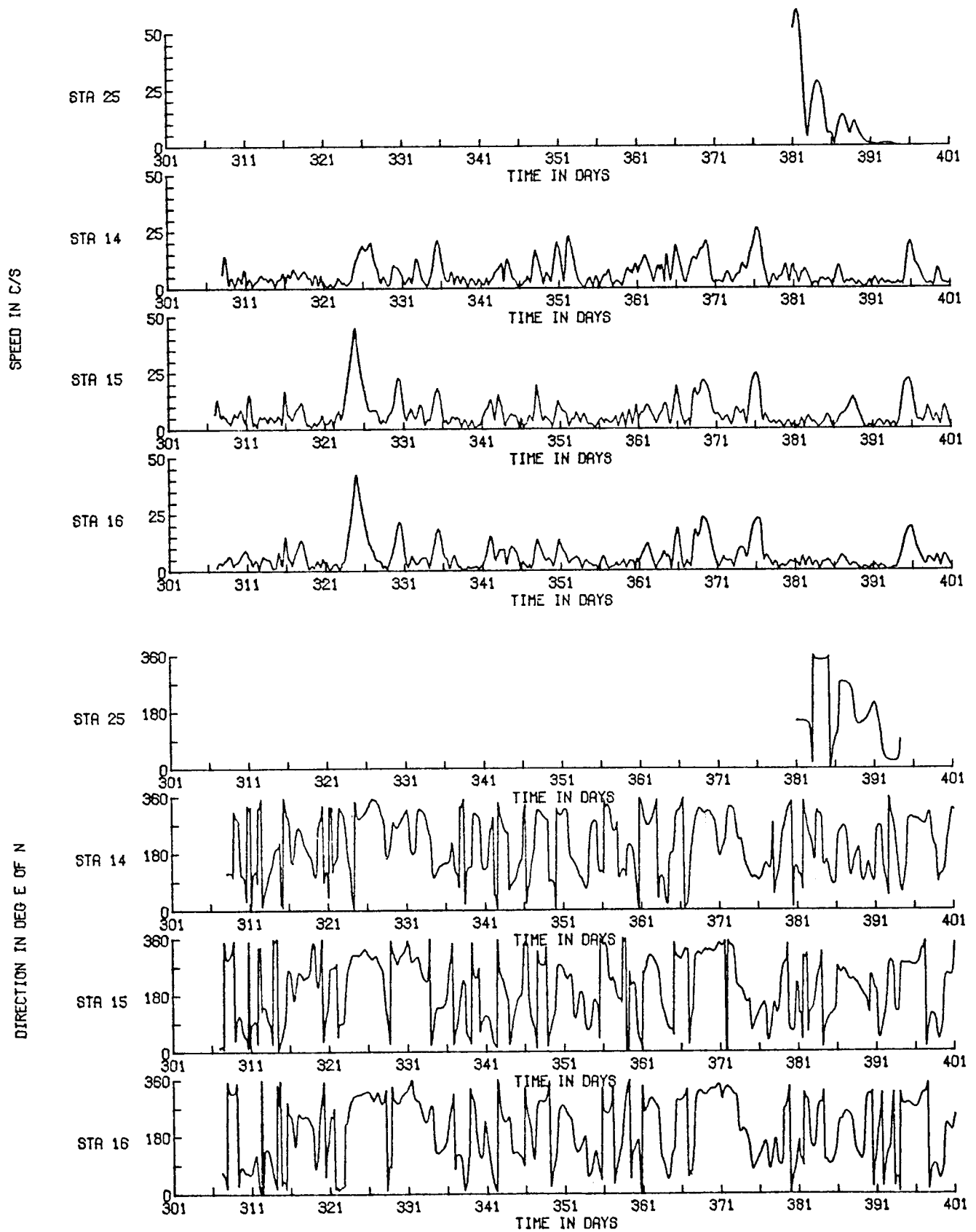


Fig. 6. Speed and direction plotted for RAMS buoys, by station and day.

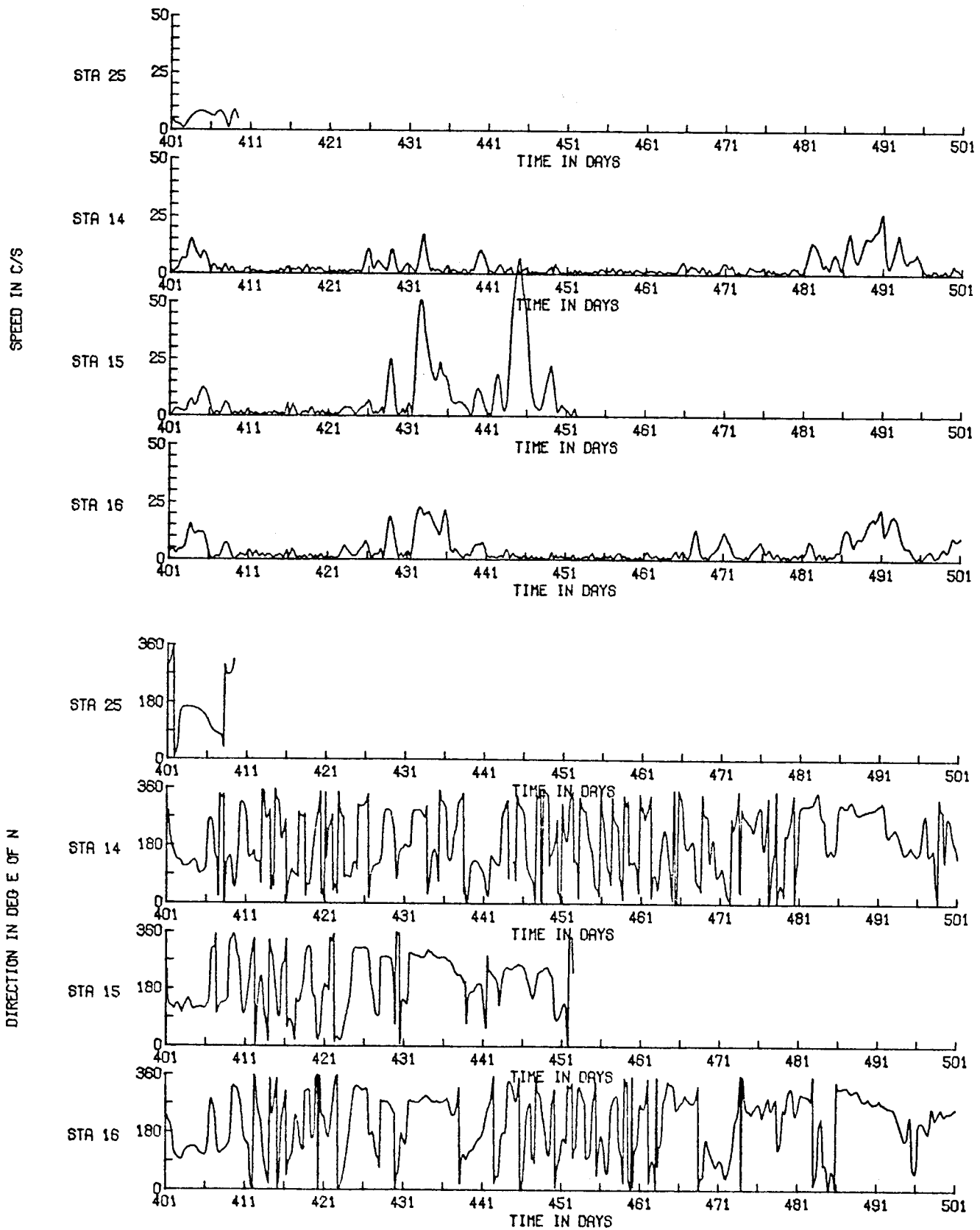


Fig. 6 -- continued.

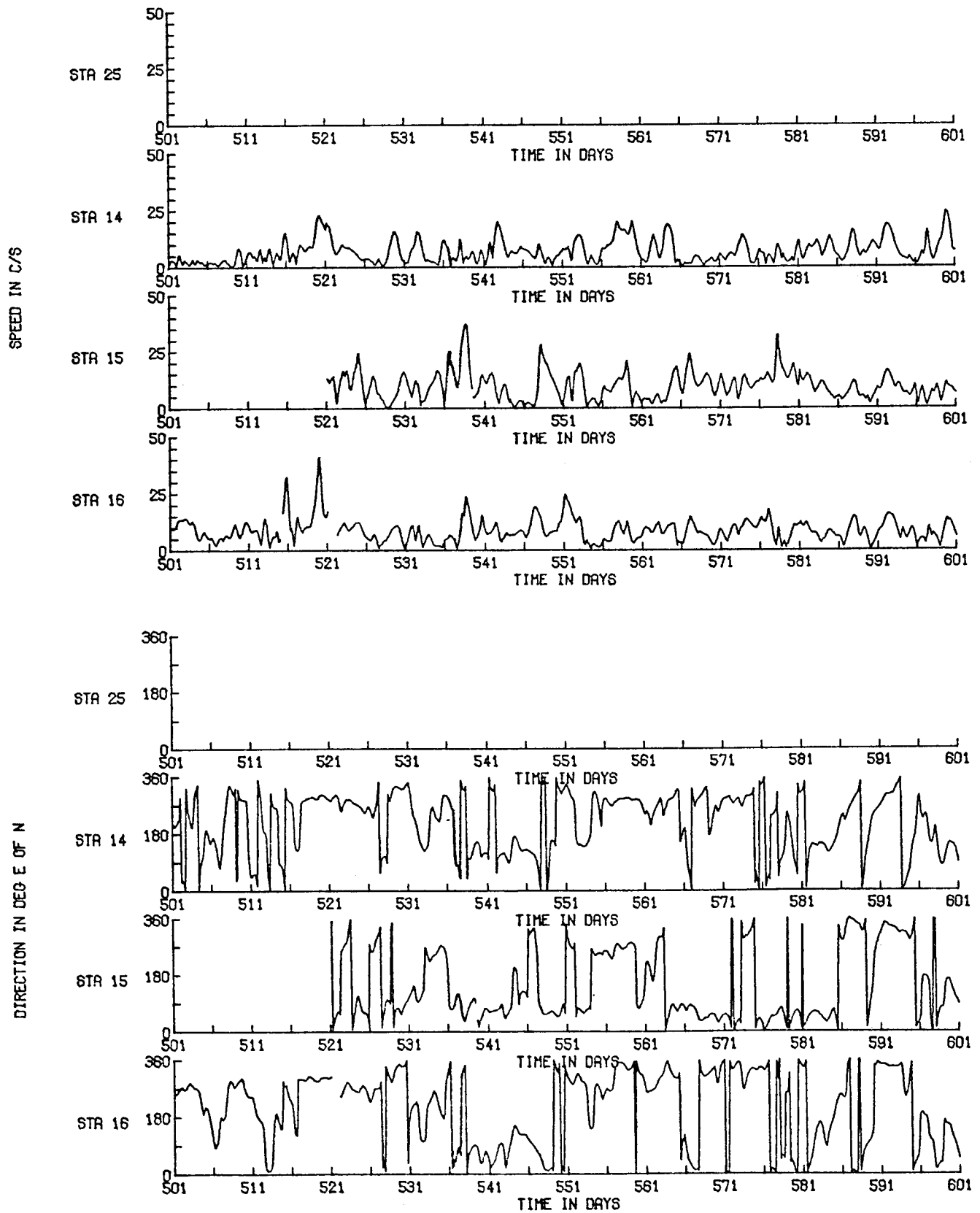


Fig. 6 -- continued

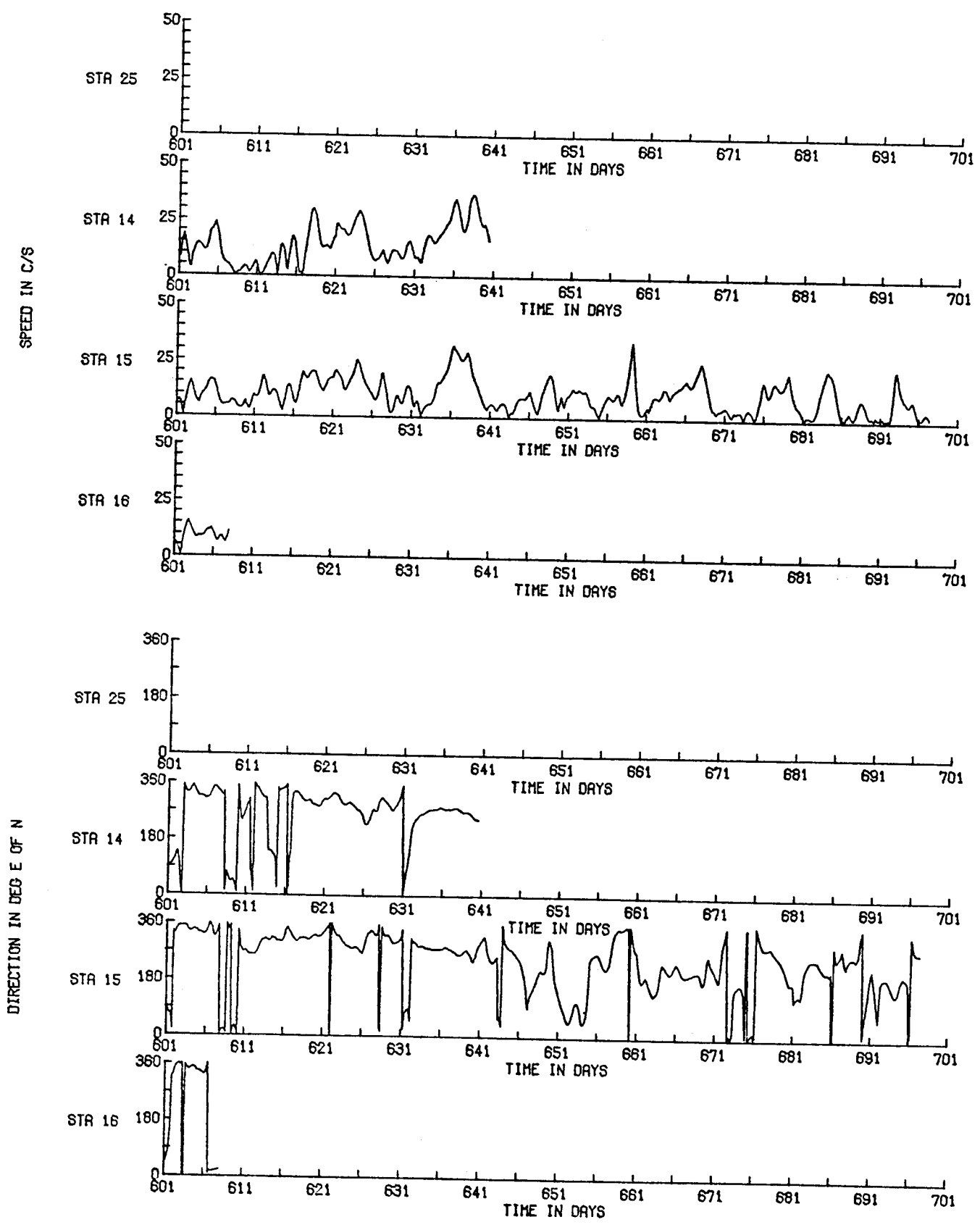


Fig. 6 -- continued

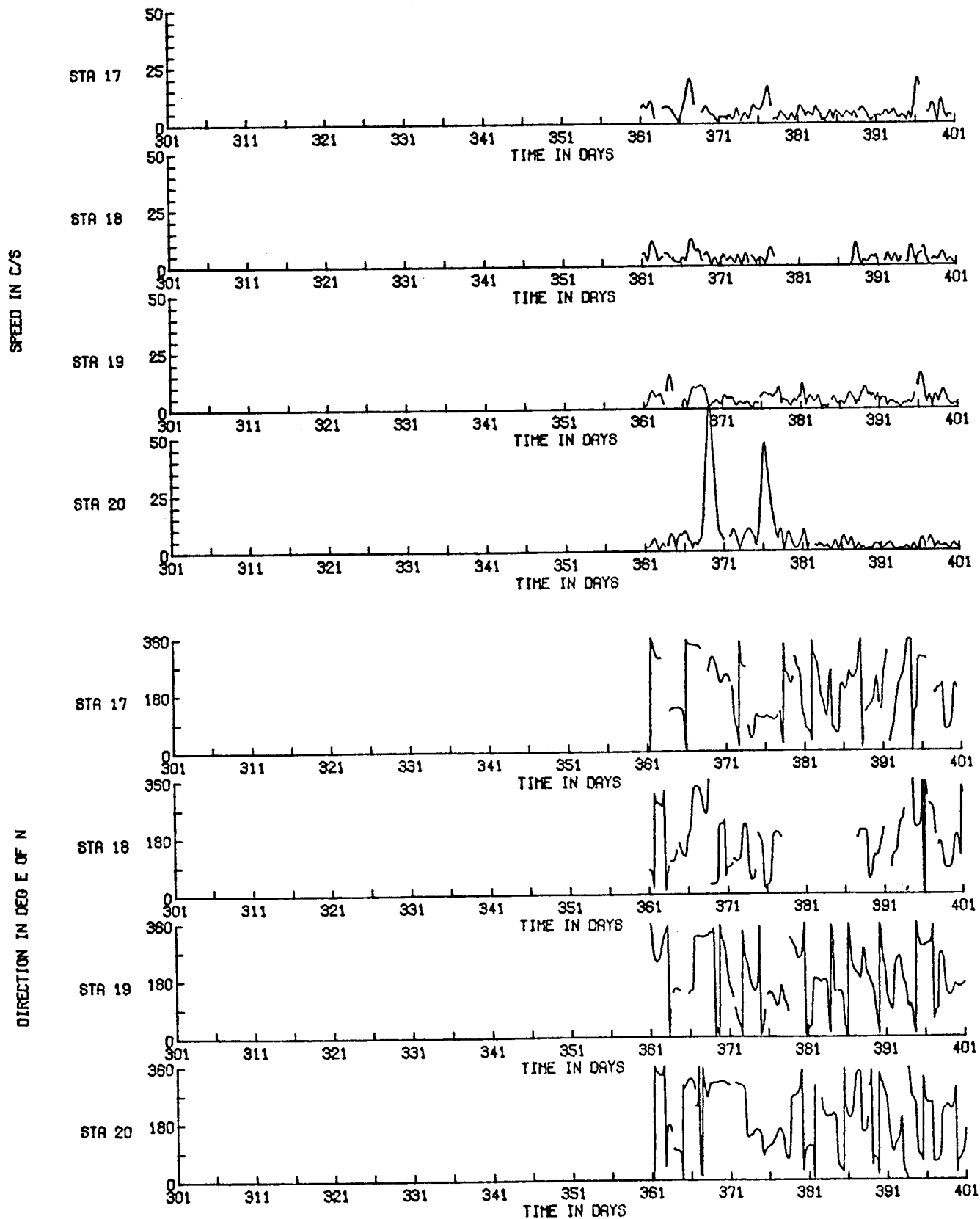


Fig. 6 -- continued

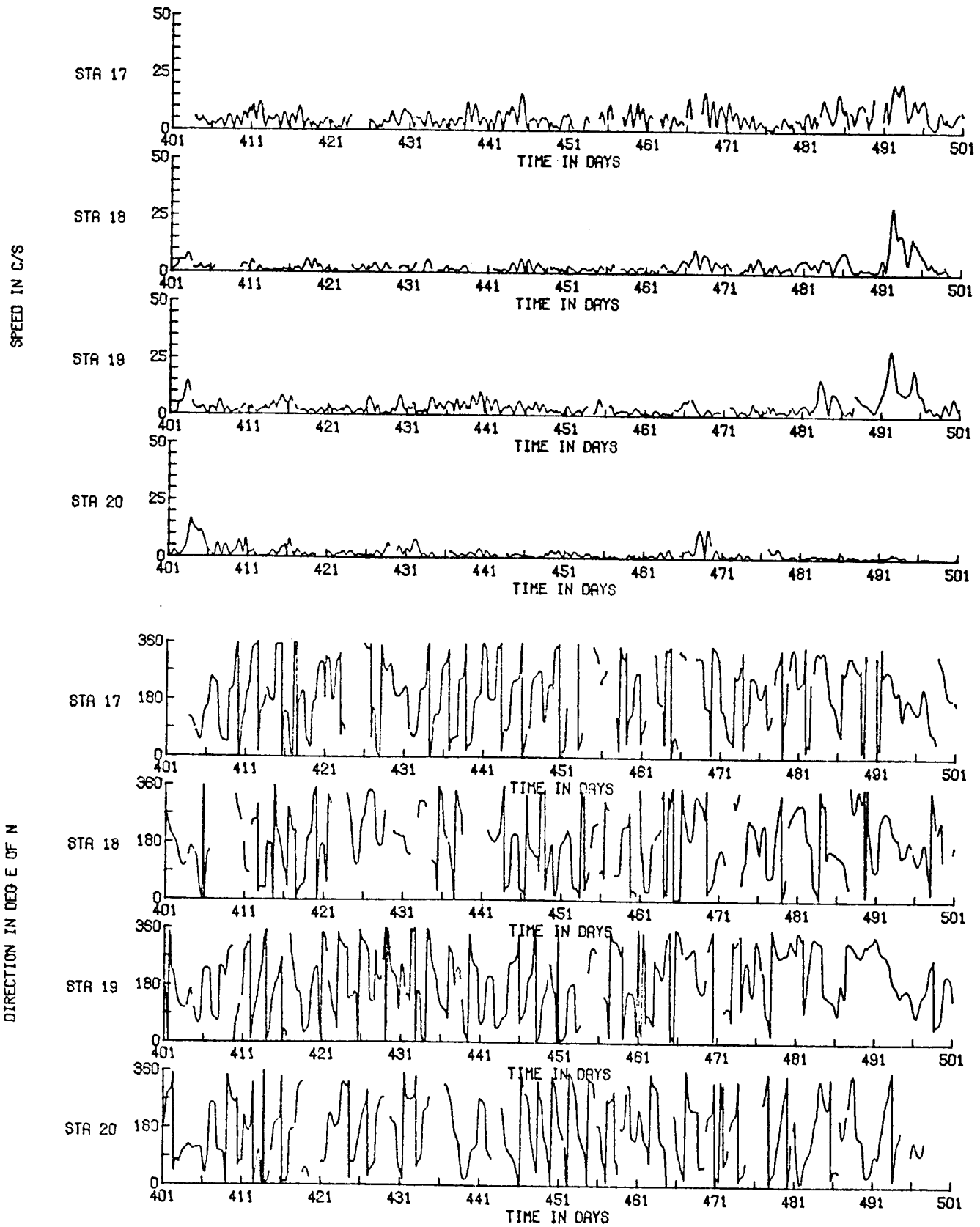


Fig. 6 -- continued

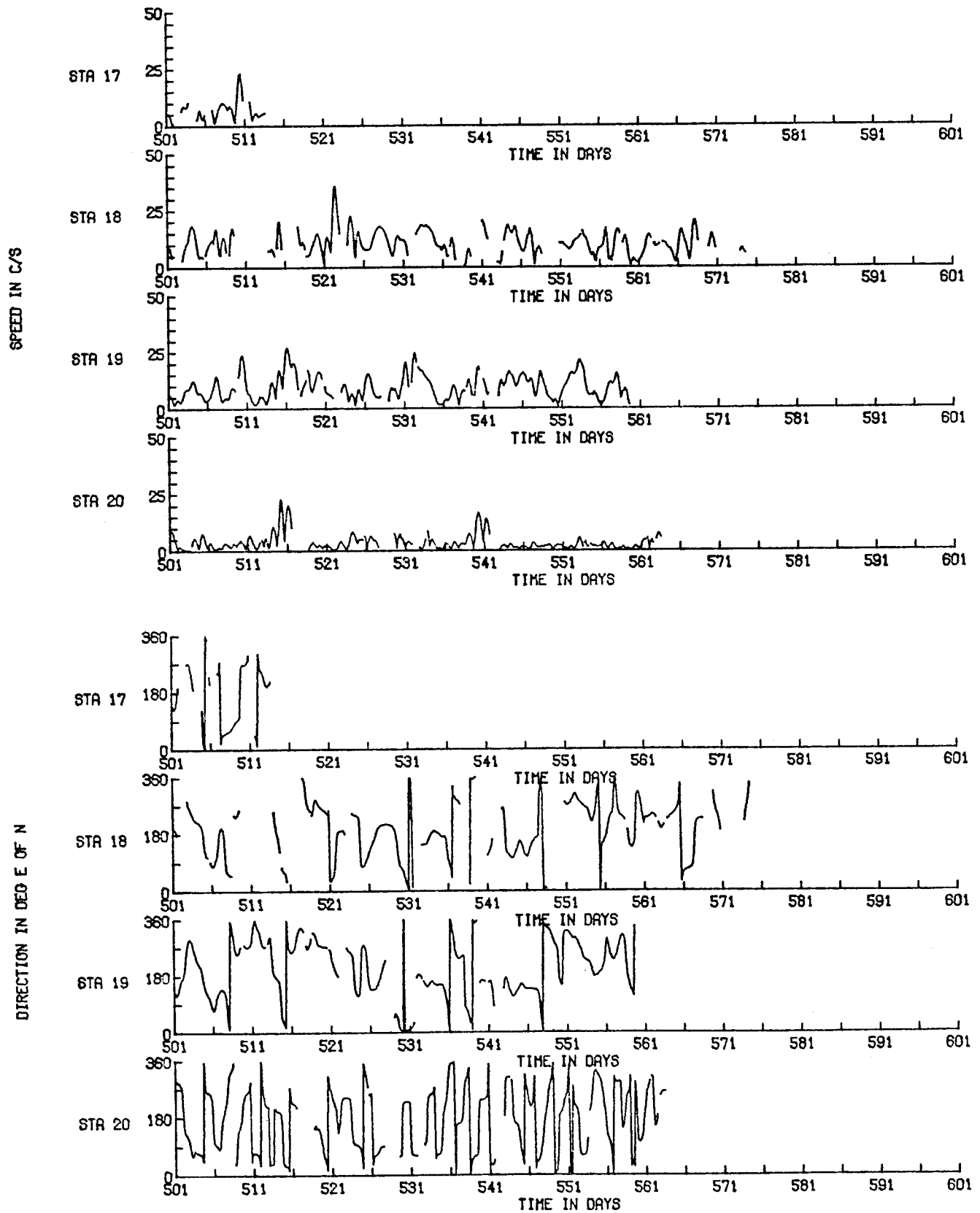


Fig. 6 -- continued

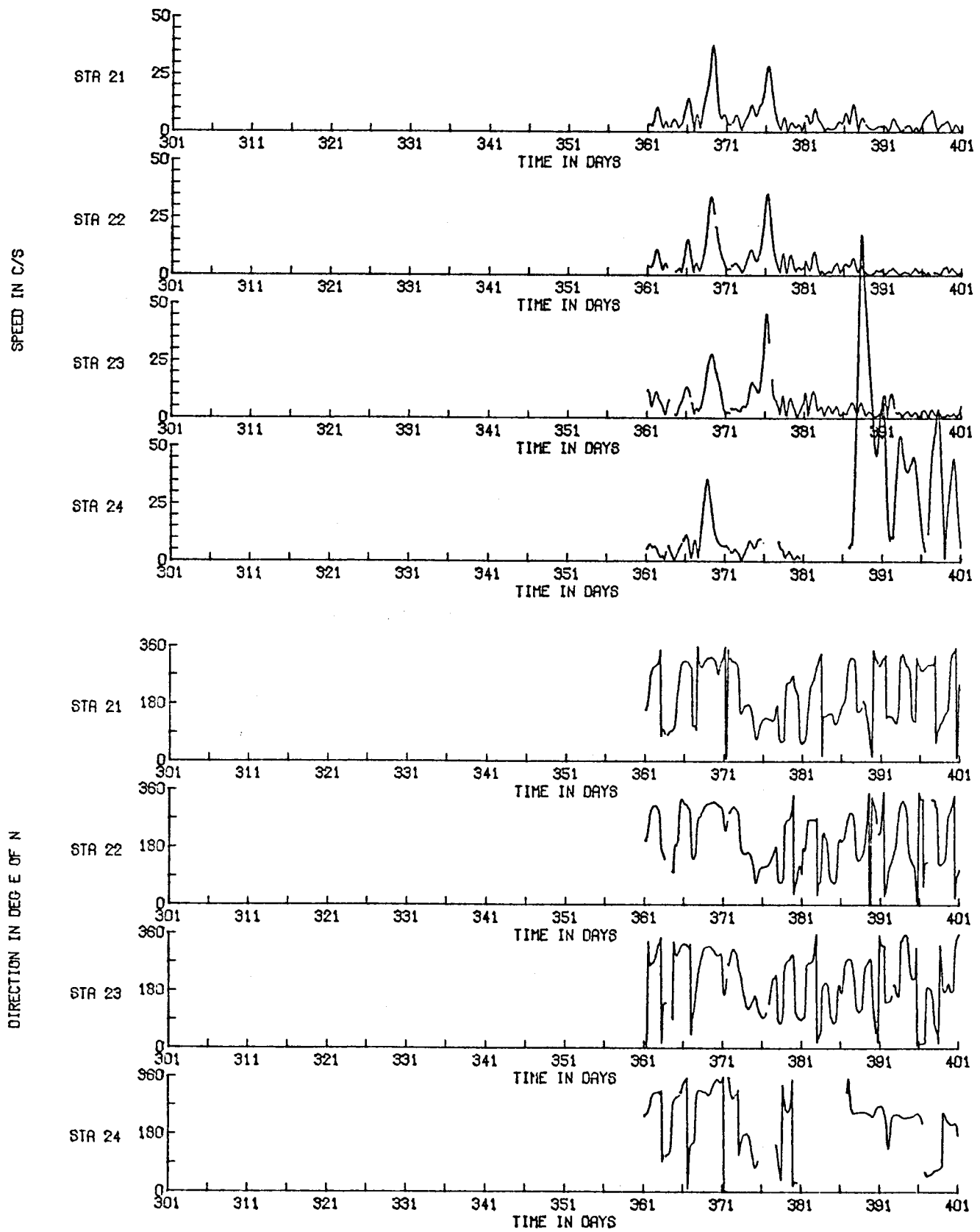


Fig. 6 -- continued

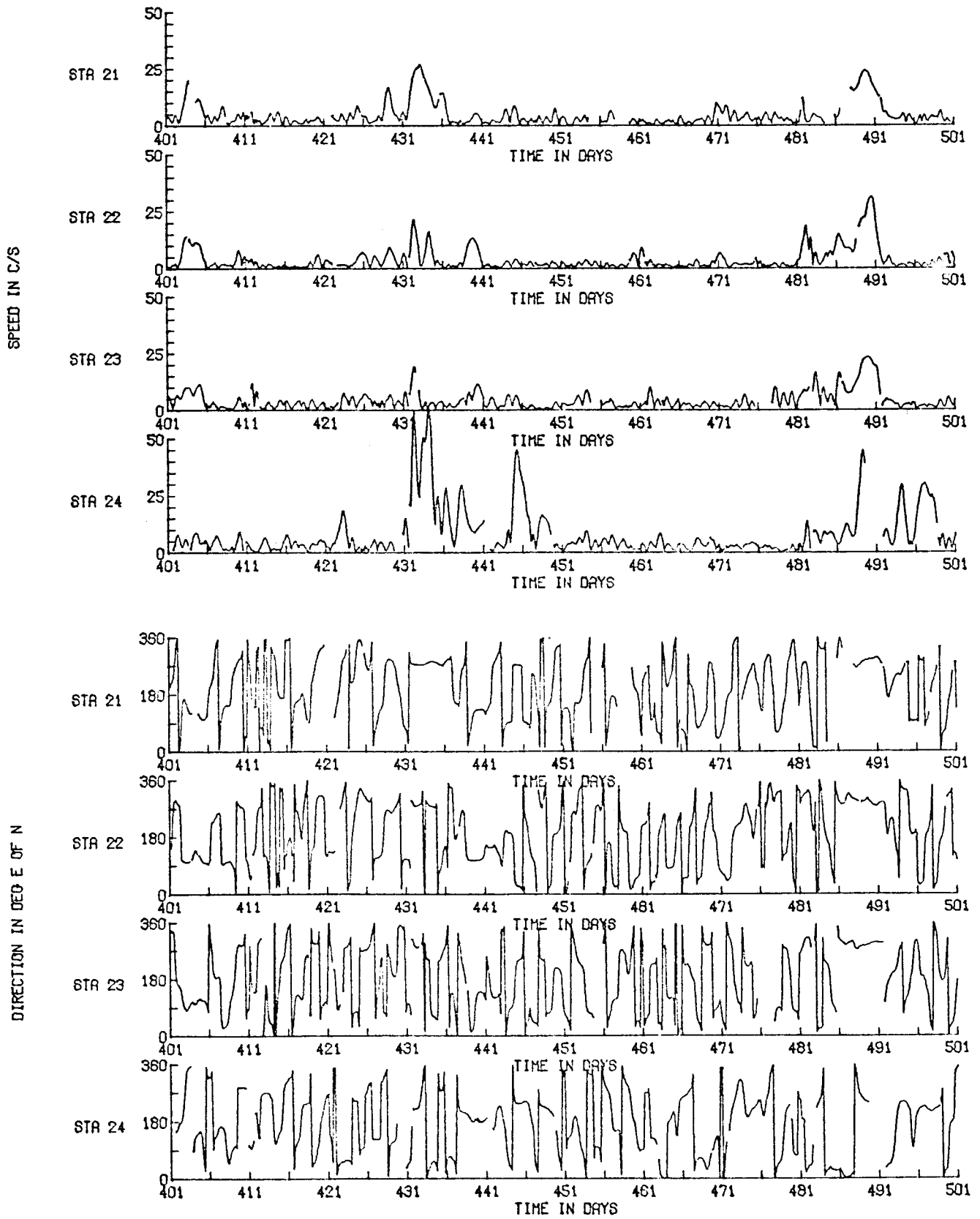


Fig. 6 -- continued

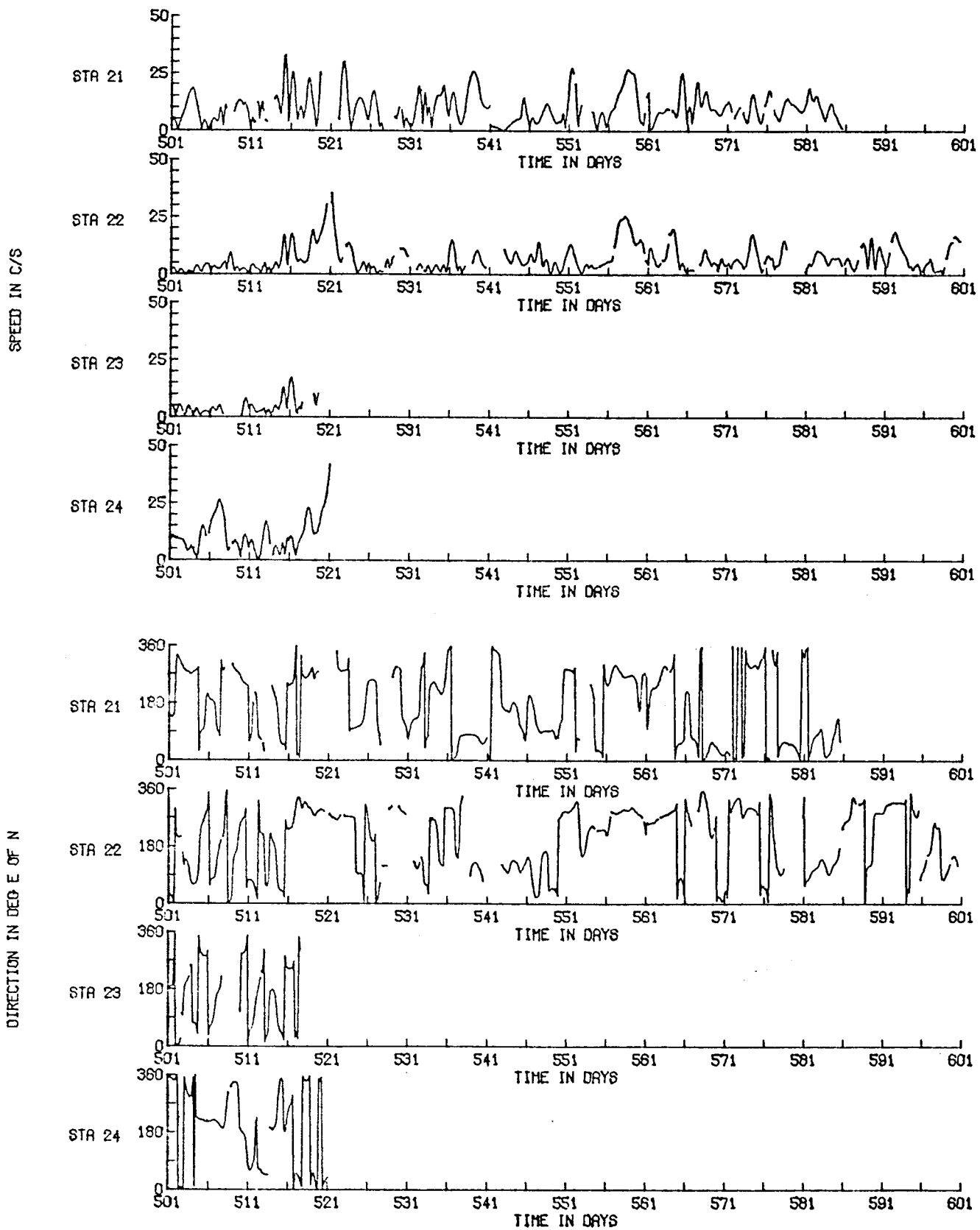


Fig. 6 -- continued

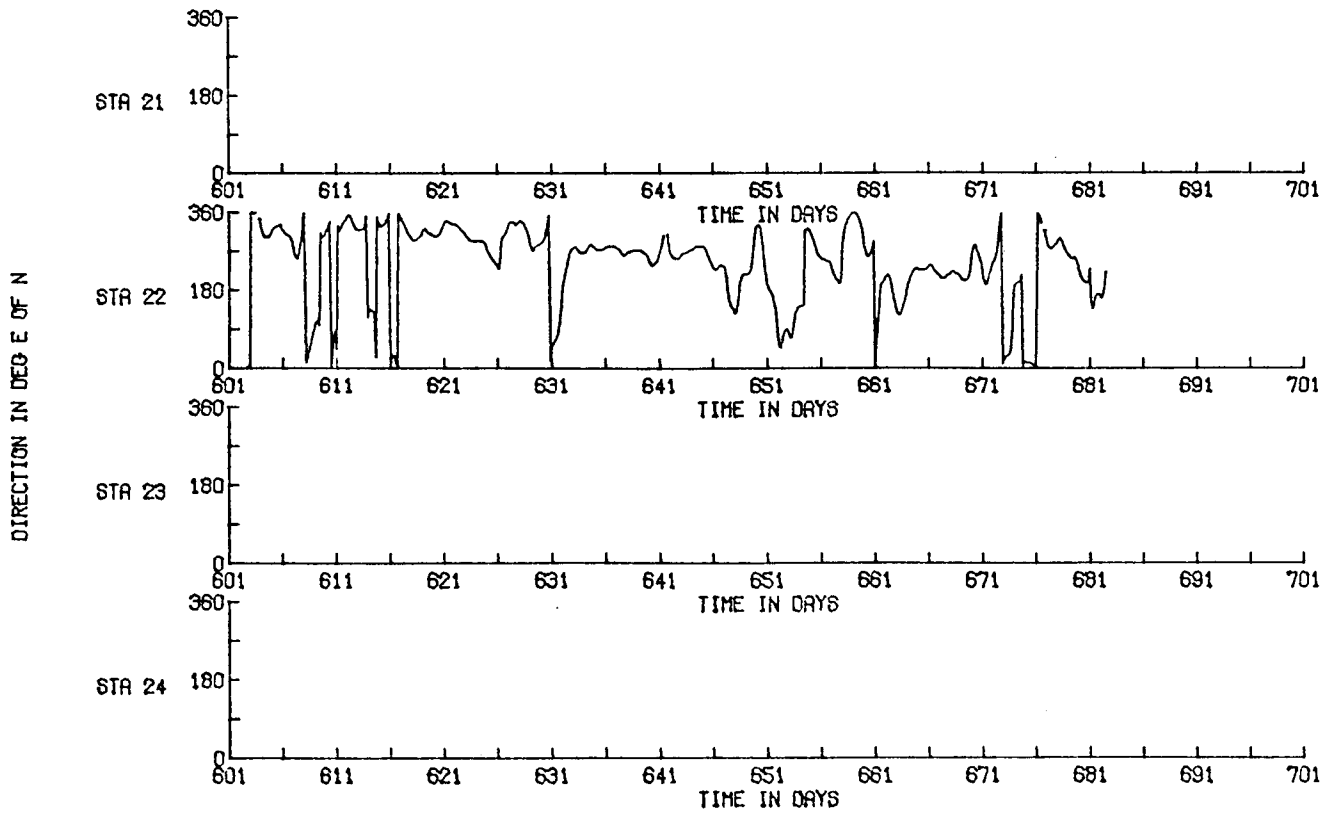
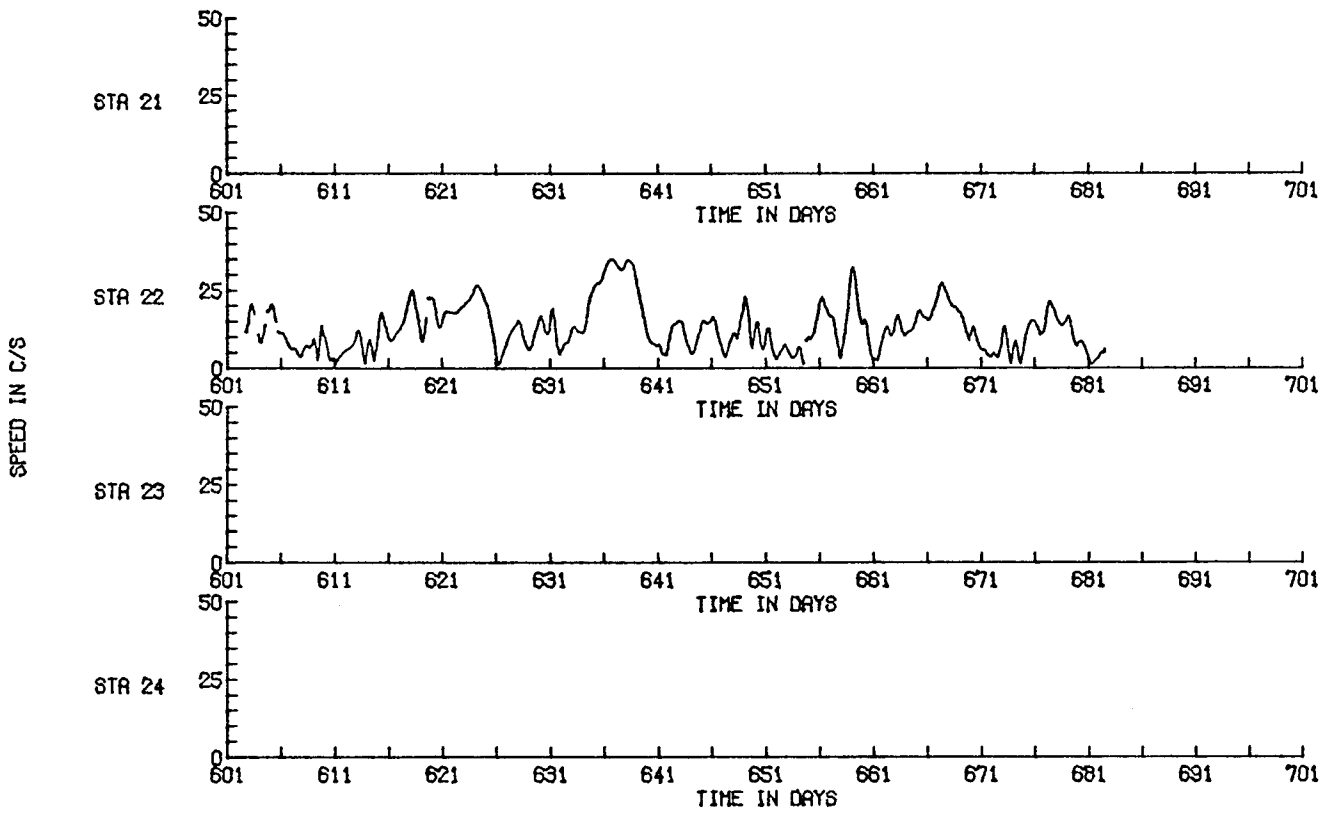


Fig. 6 -- continued

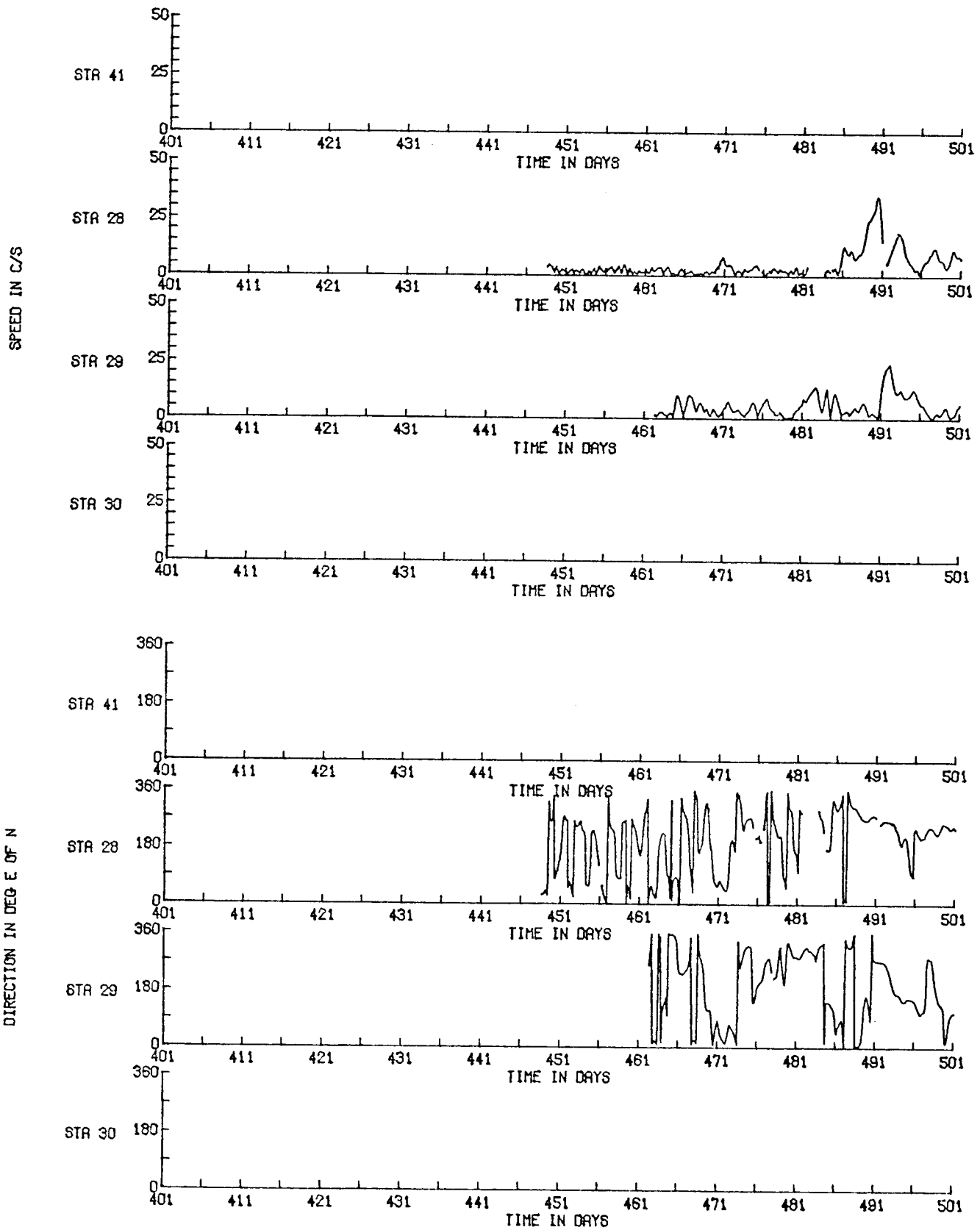


Fig. 6 -- continued

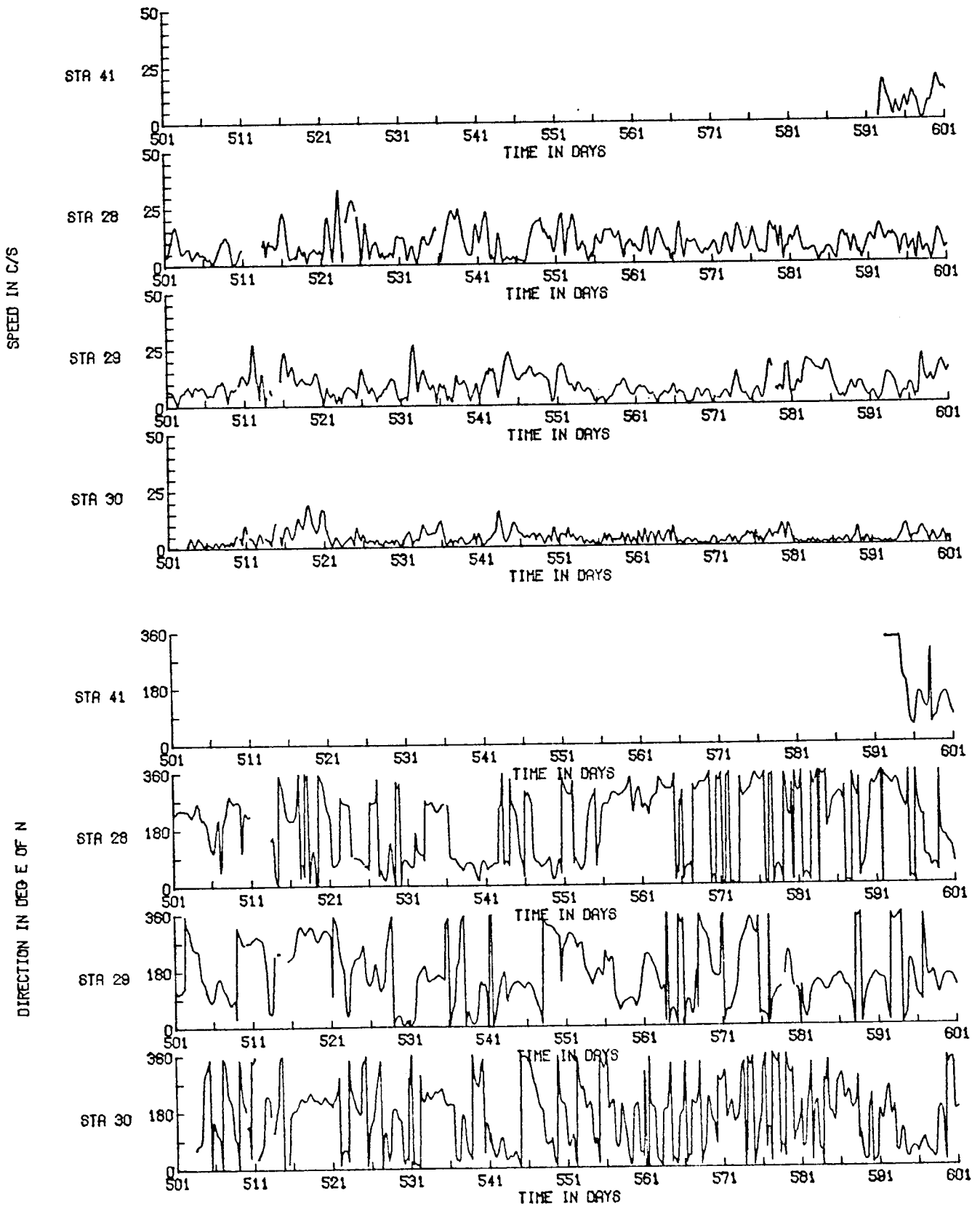


Fig. 6 -- continued

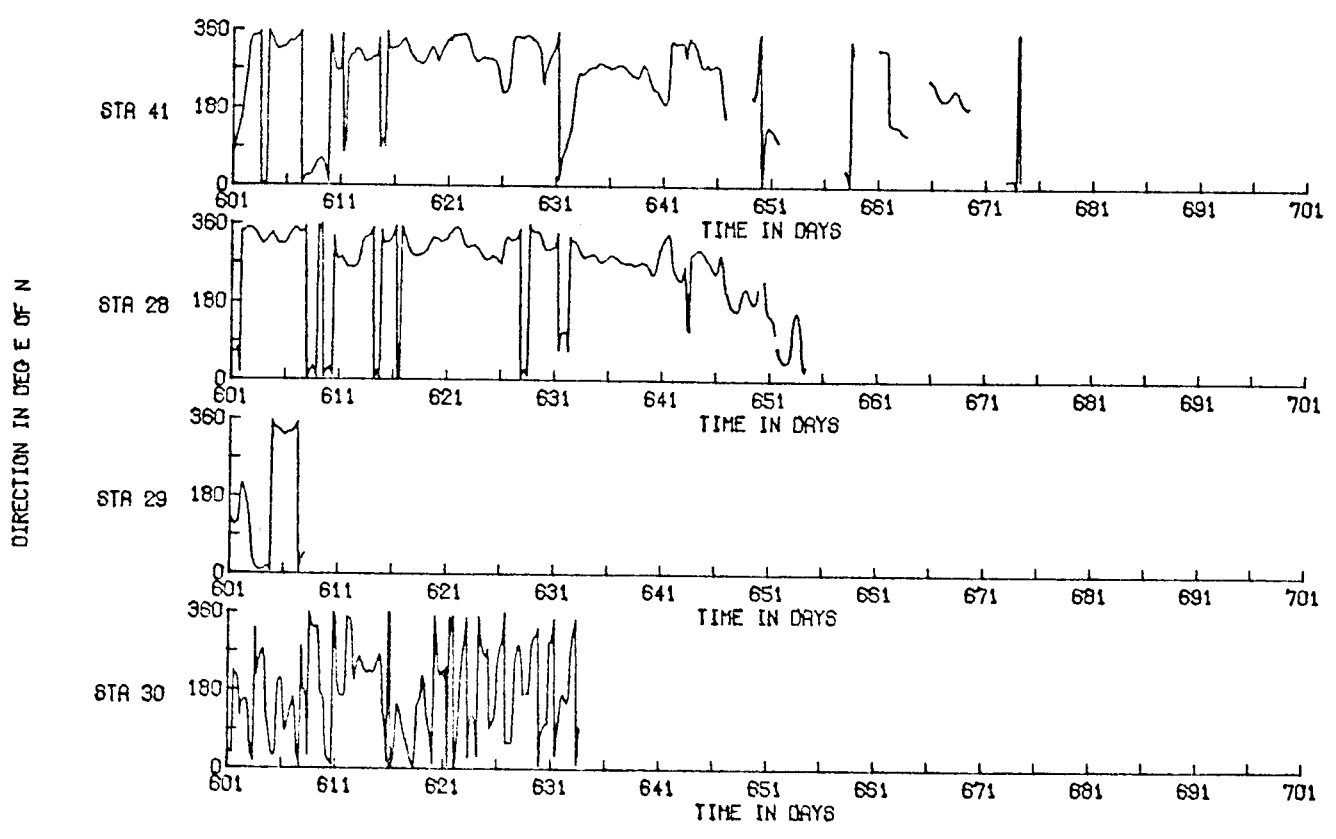
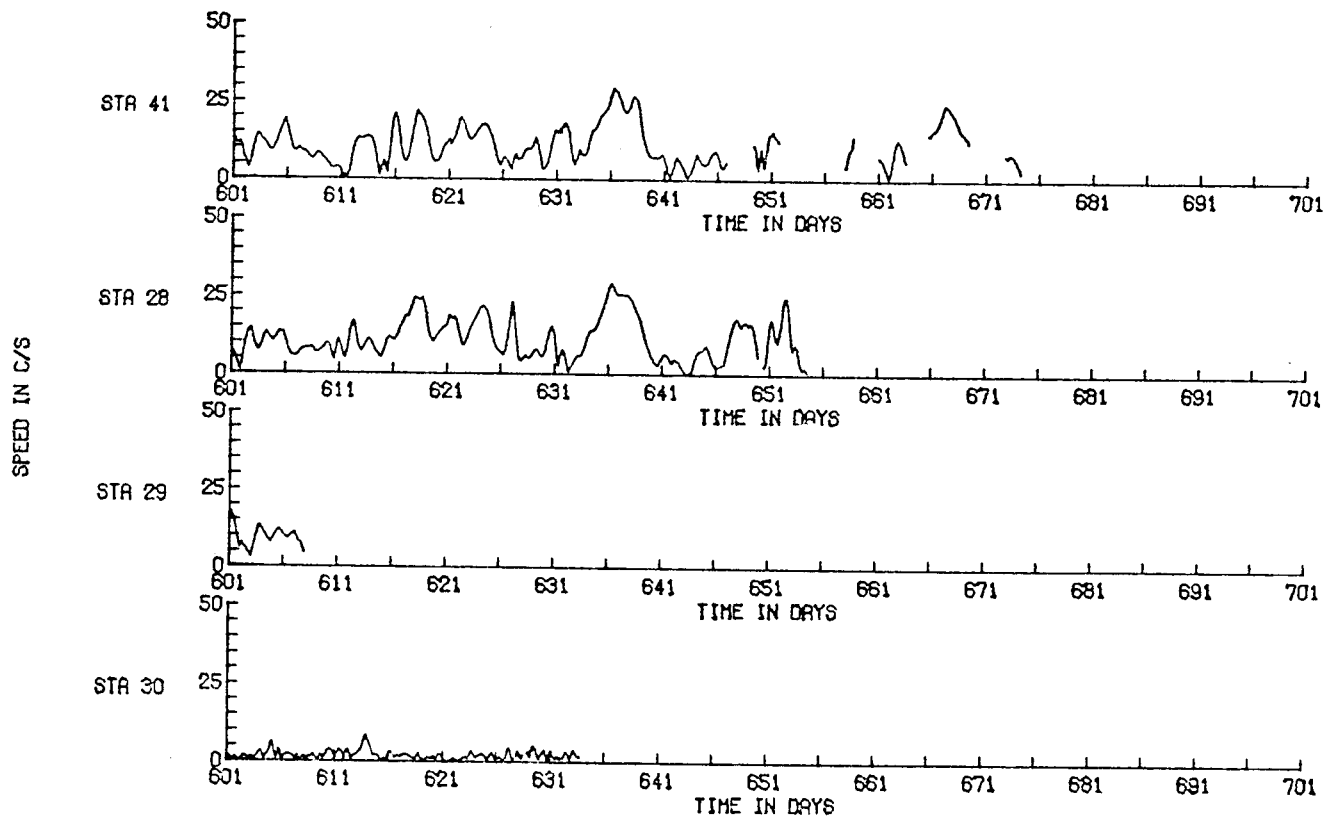


Fig. 6 -- continued

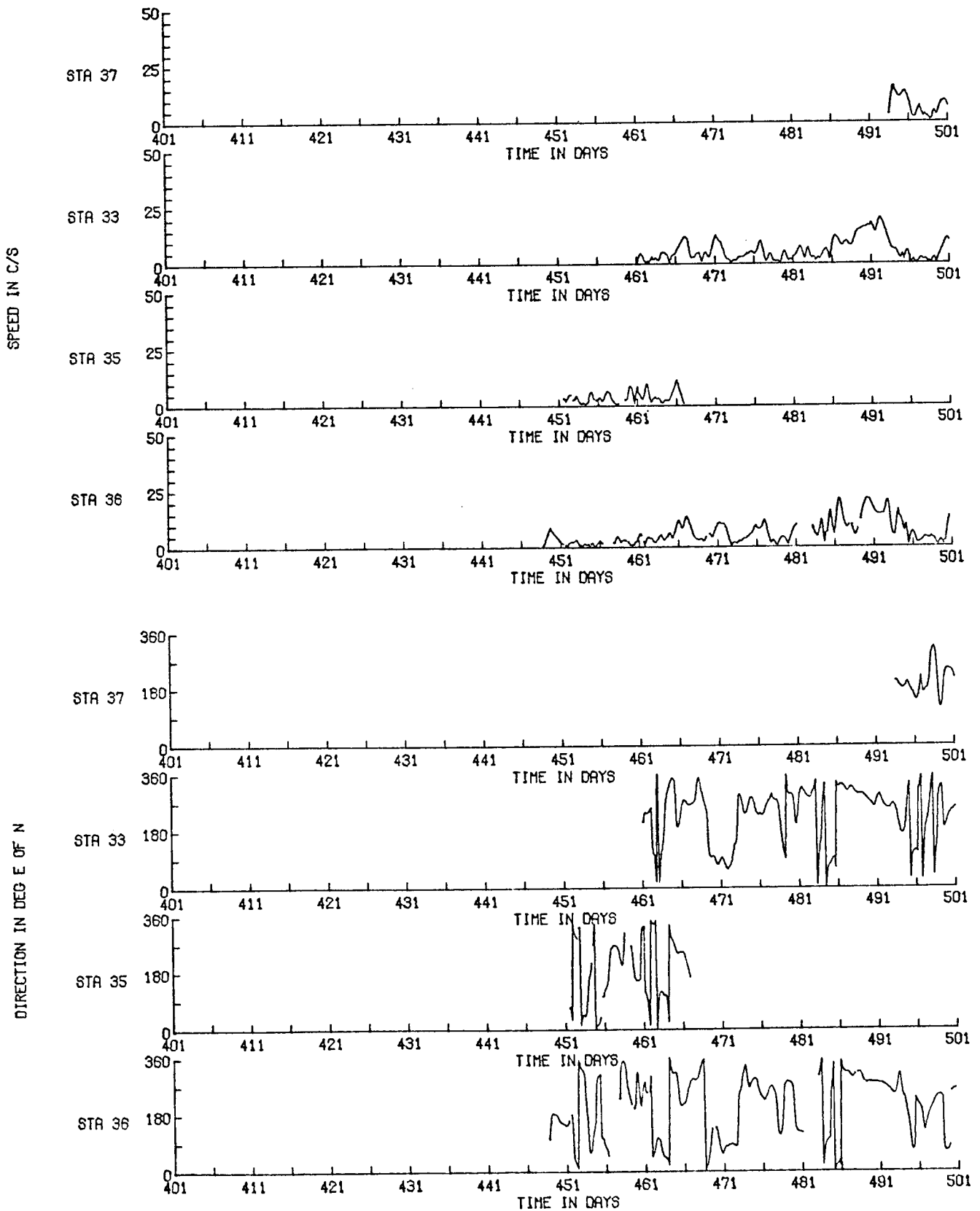


Fig. 6 -- continued

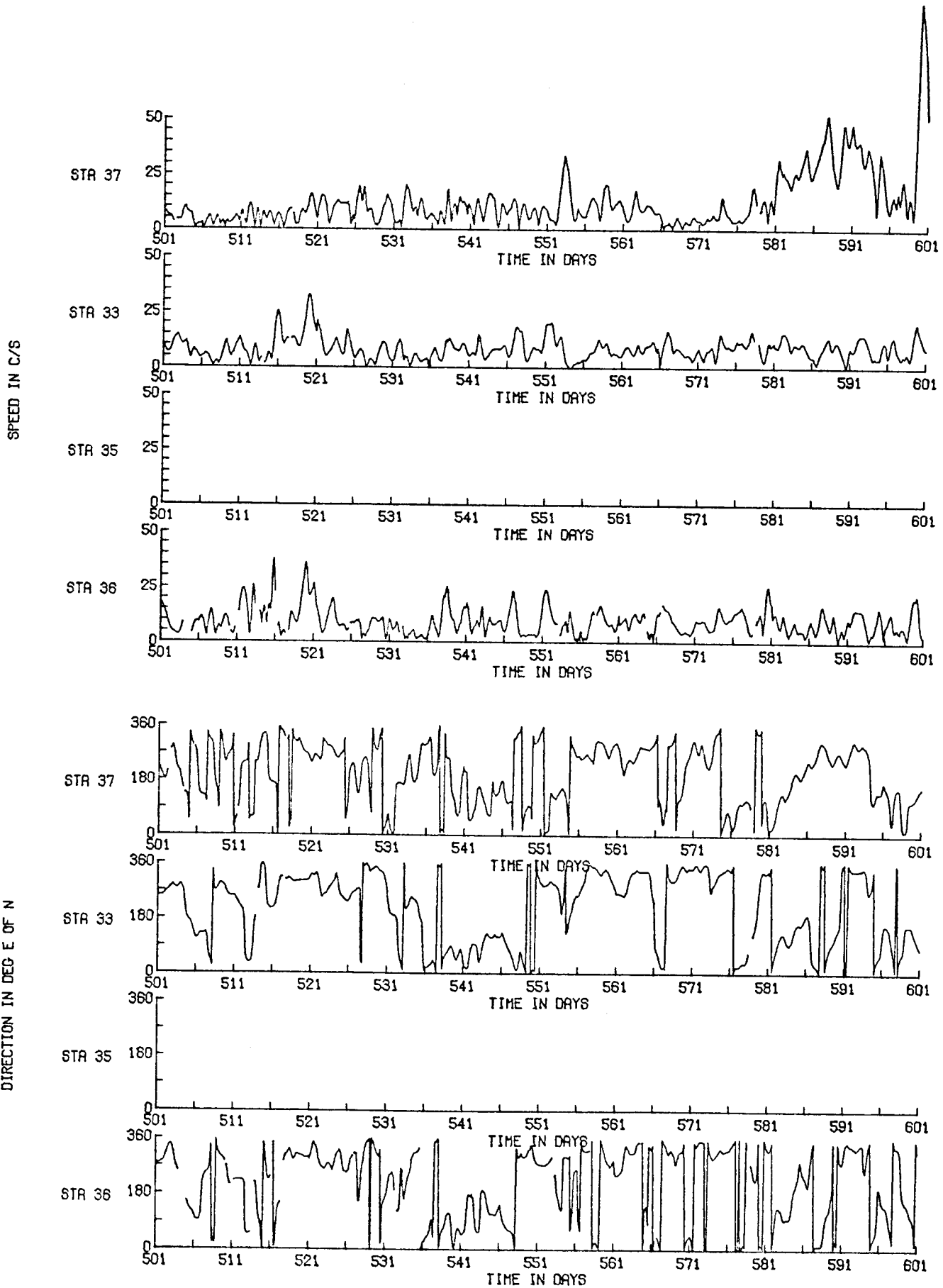


Fig. 6 -- continued

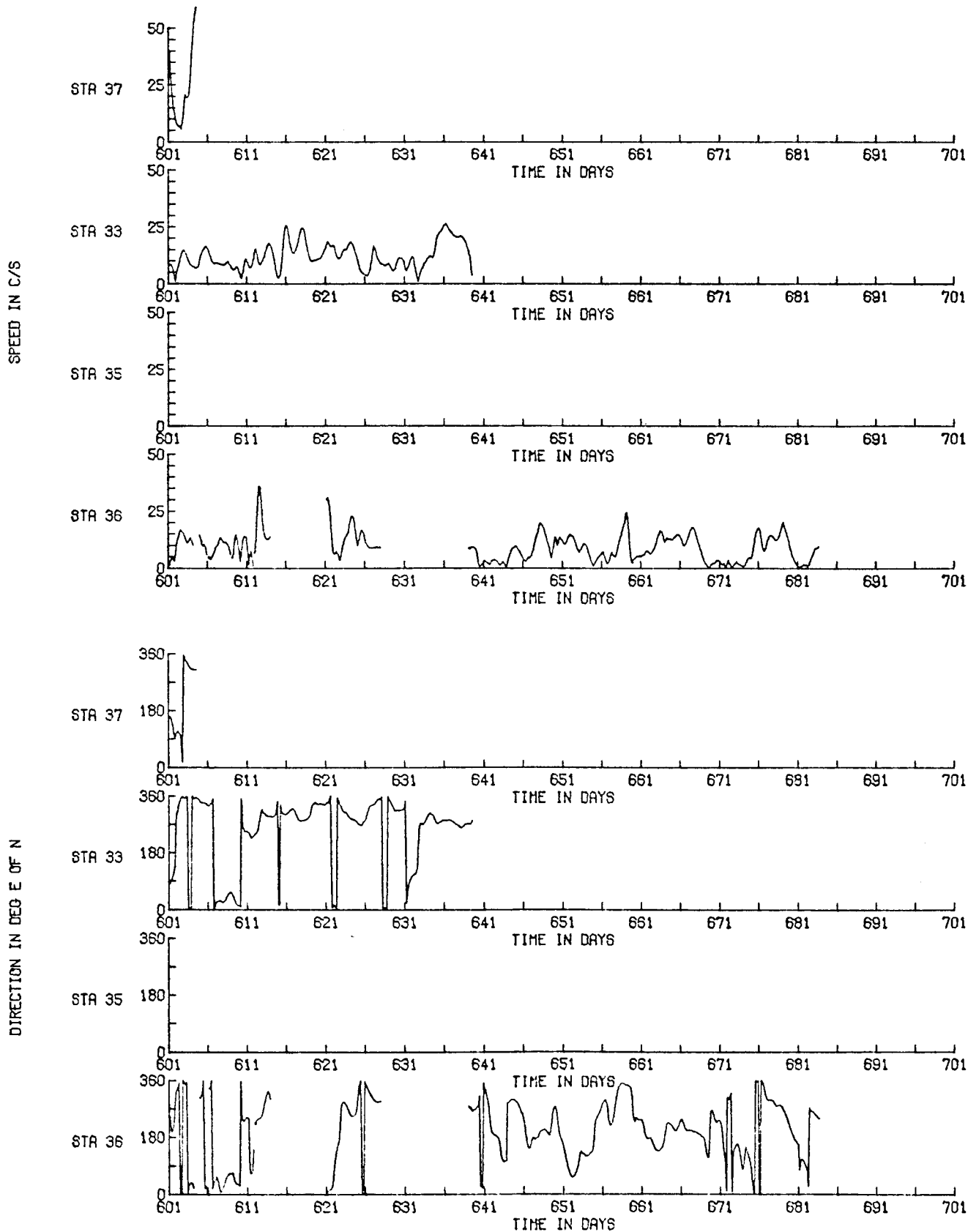


Fig. 6 -- continued

TABLE 1

ESTIMATION ERRORS (standard error = $\sqrt{\text{variance}}$)

	Fixes per Day	Assumed Measurement Error	Errors	
			Position	Velocity
RAMS buoys	10	2000 m	1000 m	3 cm sec ⁻¹
RAMS buoys	4	2000 m	1500 m	4 cm sec ⁻¹

Note: Approximate standard deviations are given for the position and velocity estimates. These values represent the performance of the system during normal operation. When data are sparse (see Fig. 4) the error variances increase.

TABLE 2

ESTIMATED POSITIONS OF RAMS BLOYS, BY STATION

RAMS 1273 / STA 14														
DAY	LAT	LONG	DAY	LAT	LONG	DAY	LAT	LONG	DAY	LAT	LONG	DAY	LAT	LONG
301			371	71.244	-137.230	441	70.903	-136.736	511	71.017	-139.071	581	71.414	-143.927
302			372	71.256	-137.287	442	70.895	-136.709	512	71.027	-139.065	582	71.388	-143.827
303			373	71.269	-137.356	443	70.888	-136.687	513	71.009	-139.061	583	71.328	-143.694
304			374	71.226	-137.363	444	70.886	-136.686	514	71.010	-139.152	584	71.289	-143.577
305			375	71.193	-137.128	445	70.881	-136.673	515	71.027	-139.112	585	71.221	-143.429
306			376	71.155	-136.633	446	70.884	-136.699	516	71.043	-139.315	586	71.192	-143.490
307			377	71.070	-136.402	447	70.885	-136.683	517	71.032	-139.340	587	71.186	-143.585
308	70.878	-135.145	378	71.064	-136.348	448	70.890	-136.695	518	71.053	-139.530	588	71.237	-143.841
309	70.880	-135.156	379	71.052	-136.390	449	70.896	-136.683	519	71.080	-139.720	589	71.243	-143.775
310	70.876	-135.093	380	71.095	-136.462	450	70.885	-136.676	520	71.144	-140.087	590	71.207	-143.895
311	70.891	-135.090	381	71.059	-136.329	451	70.884	-136.681	521	71.190	-140.466	591	71.203	-144.103
312	70.897	-135.079	382	71.066	-136.411	452	70.886	-136.666	522	71.218	-140.672	592	71.265	-144.405
313	70.906	-134.987	383	71.044	-136.457	453	70.886	-136.682	523	71.229	-140.871	593	71.347	-144.612
314	70.880	-134.968	384	71.044	-136.471	454	70.883	-136.694	524	71.239	-141.064	594	71.387	-144.595
315	70.892	-134.975	385	71.030	-136.414	455	70.885	-136.672	525	71.233	-141.190	595	71.377	-144.545
316	70.884	-134.998	386	71.024	-136.428	456	70.886	-136.685	526	71.225	-141.268	596	71.372	-144.581
317	70.863	-135.120	387	71.015	-136.577	457	70.884	-136.668	527	71.224	-141.301	597	71.330	-144.614
318	70.825	-135.169	388	71.001	-136.545	458	70.882	-136.686	528	71.221	-141.264	598	71.285	-144.570
319	70.796	-135.108	389	70.991	-136.532	459	70.887	-136.691	529	71.263	-141.367	599	71.275	-144.350
320	70.800	-135.156	390	70.989	-136.514	460	70.880	-136.662	530	71.343	-141.540	600	71.143	-144.071
321	70.798	-135.116	391	70.985	-136.526	461	70.884	-136.678	531	71.358	-141.575	601	71.120	-143.870
322	70.794	-135.112	392	70.980	-136.519	462	70.889	-136.691	532	71.309	-141.581	602	71.082	-143.644
323	70.797	-135.164	393	70.988	-136.537	463	70.890	-136.671	533	71.241	-141.393	603	71.158	-143.718
324	70.803	-135.151	394	70.985	-136.515	464	70.883	-136.679	534	71.229	-141.433	604	71.248	-143.830
325	70.840	-135.362	395	70.992	-136.575	465	70.898	-136.672	535	71.223	-141.466	605	71.347	-144.114
326	70.947	-135.583	396	71.039	-136.948	466	70.915	-136.699	536	71.250	-141.659	606	71.443	-144.438
327	71.072	-135.677	397	71.049	-137.136	467	70.891	-136.700	537	71.252	-141.654	607	71.486	-144.489
328	71.084	-135.768	398	71.051	-137.176	468	70.892	-136.675	538	71.250	-141.717	608	71.498	-144.508
329	71.069	-135.791	399	71.039	-137.106	469	70.894	-136.701	539	71.275	-141.635	609	71.511	-144.464
330	71.075	-135.984	400	71.024	-137.075	470	70.890	-136.690	540	71.256	-141.585	610	71.520	-144.484
331	71.092	-136.070	401	71.026	-137.098	471	70.887	-136.597	541	71.249	-141.527	611	71.521	-144.574
332	71.078	-136.097	402	71.003	-137.052	472	70.898	-136.574	542	71.263	-141.464	612	71.542	-144.583
333	71.127	-136.264	403	70.969	-136.873	473	70.899	-136.585	543	71.210	-141.113	613	71.590	-144.711
334	71.122	-136.283	404	70.920	-136.643	474	70.897	-136.635	544	71.188	-141.006	614	71.541	-144.576
335	71.057	-136.077	405	70.904	-136.463	475	70.891	-136.679	545	71.148	-140.924	615	71.581	-144.592
336	70.973	-135.923	406	70.867	-136.428	476	70.892	-126.710	546	71.109	-140.776	616	71.656	-144.652
337	70.949	-135.860	407	70.889	-136.445	477	70.894	-136.714	547	71.095	-140.655	617	71.701	-144.738
338	70.959	-135.869	408	70.933	-136.459	478	70.895	-136.704	548	71.144	-140.674	618	71.839	-145.225
339	70.957	-135.823	409	70.896	-136.437	479	70.893	-136.705	549	71.136	-140.645	619	71.908	-145.600
340	70.966	-135.976	410	70.898	-136.441	480	70.894	-136.742	550	71.151	-140.683	620	71.938	-145.903
341	70.952	-135.847	411	70.900	-136.461	481	70.904	-136.784	551	71.194	-140.778	621	72.016	-146.235
342	70.959	-135.864	412	70.895	-136.449	482	70.954	-137.004	552	71.193	-140.854	622	72.139	-146.551
343	70.975	-136.005	413	70.895	-136.446	483	71.013	-137.101	553	71.112	-140.673	623	72.227	-146.974
344	70.973	-135.955	414	70.896	-136.451	484	71.006	-137.143	554	71.082	-140.636	624	72.313	-147.606
345	70.960	-135.825	415	70.900	-136.466	485	70.953	-137.097	555	71.089	-140.687	625	72.335	-148.049
346	70.961	-135.818	416	70.896	-136.474	486	70.973	-137.198	556	71.099	-140.816	626	72.307	-148.222
347	70.947	-135.802	417	70.895	-136.430	487	71.035	-137.450	557	71.108	-141.047	627	72.298	-148.452
348	71.007	-136.025	418	70.896	-136.471	488	71.057	-137.603	558	71.151	-141.417	628	72.335	-148.642
349	71.015	-136.043	419	70.898	-136.439	489	71.090	-137.948	559	71.194	-141.758	629	72.366	-148.875
350	71.039	-136.074	420	70.896	-136.468	490	71.147	-138.324	560	71.228	-142.110	630	72.398	-149.161
351	71.114	-136.336	421	70.894	-136.444	491	71.236	-138.690	561	71.223	-142.220	631	72.457	-149.145
352	71.013	-136.227	422	70.896	-136.442	492	71.216	-138.770	562	71.204	-142.343	632	72.408	-149.237
353	70.970	-136.021	423	70.899	-136.450	493	71.144	-139.000	563	71.207	-142.545	633	72.375	-149.658
354	70.971	-136.000	424	70.899	-136.422	494	71.099	-138.996	564	71.229	-142.842	634	72.379	-150.091
355	70.973	-136.055	425	70.903	-136.440	495	71.042	-138.961	565	71.276	-143.061	635	72.401	-150.656
356	70.966	-136.013	426	70.944	-136.571	496	71.015	-138.930	566	71.266	-143.056	636	72.439	-151.445
357	70.981	-136.113	427	70.935	-136.482	497	71.012	-138.936	567	71.271	-143.065	637	72.467	-152.056
358	70.976	-136.110	428	70.926	-136.468	498	71.008	-138.926	568	71.284	-143.149	638	72.489	-152.824
359	70.960	-136.104	429	70.945	-136.636	499	71.010	-138.940	569	71.285	-143.166	639	72.477	-153.612
360	70.927	-136.078	430	70.938	-136.630	500	71.002	-138.986	570	71.277	-143.227	640	72.424	-154.129
361	70.978	-136.172	431	70.911	-136.625	501	70.988	-138.999	571	71.286	-143.318	641		
362	70.989	-136.400	432	70.916	-136.704	502	70.993	-139.001	572	71.294	-143.418	642		
363	71.011	-136.407	433	70.944	-136.964	503	70.991	-139.033	573	71.302	-143.565	643		
364	71.018	-136.266	434	70.945	-136.963	504	70.999	-139.058	574	71.338	-143.827	644		
365	70.972	-136.292	435	70.941	-136.959	505	70.990	-139.037	575	71.356	-143.872	645		
366	71.064	-136.451	436	70.950	-136.990	506	70.978	-139.024	576	71.395	-143.893	646		
367	71.080	-136.428	437	70.943	-136.982	507	70.973	-138.994	577	71.396	-143.914	647		
368	71.112	-136.633	438	70.950	-136.999	508	70.981	-139.037	578	71.393	-143.855	648		
369	71.143	-136.901	439	70.948	-136.963	509	70.987	-139.053	579	71.371	-143.843	649		
370	71.261	-137.207	440	70.905	-136.806	510	70.997	-139.146	580	71.370	-143.808	650		

TABLE 2 (continued)

RAMS 1420 / STA 15														
DAY	LAT	LONG	DAY	LAT	LONG	DAY	LAT	LONG	DAY	LAT	LONG	DAY	LAT	LONG
301			381	71.939	-151.824	461			541	71.060	-160.624	621	74.103	-159.948
302			382	71.945	-151.850	462			542	71.092	-160.360	622	74.226	-160.025
303			383	71.922	-151.822	463			543	71.117	-160.240	623	74.313	-160.321
304			384	71.923	-151.825	464			544	71.118	-160.151	624	74.376	-160.927
305			385	71.910	-151.736	465			545	71.111	-160.125	625	74.401	-161.356
306			386	71.904	-151.742	466			546	71.109	-160.111	626	74.410	-161.630
307	71.355	-148.984	387	71.889	-151.873	467			547	71.116	-160.122	627	74.507	-161.627
308	71.384	-149.071	388	71.833	-152.060	468			548	71.183	-159.778	628	74.551	-161.914
309	71.392	-149.033	389	71.767	-152.145	469			549	71.250	-159.405	629	74.597	-162.039
310	71.409	-148.696	390	71.756	-152.140	470			550	71.269	-159.219	630	74.635	-162.273
311	71.422	-148.701	391	71.754	-152.140	471			551	71.300	-159.296	631	74.682	-162.392
312	71.425	-148.643	392	71.751	-152.093	472			552	71.310	-159.339	632	74.690	-162.320
313	71.428	-148.544	393	71.753	-152.128	473			553	71.364	-158.968	633	74.707	-162.468
314	71.438	-148.531	394	71.751	-152.150	474			554	71.369	-158.924	634	74.730	-162.802
315	71.455	-148.455	395	71.770	-152.570	475			555	71.360	-158.967	635	74.750	-162.331
316	71.426	-148.600	396	71.782	-152.972	476			556	71.345	-159.120	636	74.789	-164.142
317	71.400	-148.700	397	71.803	-153.019	477			557	71.331	-159.296	637	74.830	-164.928
318	71.361	-148.893	398	71.789	-152.856	478			558	71.329	-159.580	638	74.816	-165.711
319	71.365	-148.921	399	71.804	-152.763	479			559	71.346	-159.931	639	74.813	-166.195
320	71.367	-148.920	400	71.780	-152.913	480			560	71.352	-159.877	640	74.799	-166.405
321	71.360	-148.906	401	71.772	-152.945	481			561	71.336	-159.865	641	74.817	-166.544
322	71.362	-148.916	402	71.759	-152.888	482			562	71.317	-159.879	642	74.817	-166.673
323	71.348	-148.893	403	71.744	-152.819	483			563	71.336	-159.958	643	74.803	-166.771
324	71.445	-149.361	404	71.713	-152.718	484			564	71.347	-159.881	644	74.821	-166.837
325	71.538	-150.001	405	71.671	-152.487	485			565	71.376	-159.558	645	74.828	-167.091
326	71.732	-150.293	406	71.646	-152.363	486			566	71.389	-159.306	646	74.795	-167.338
327	71.760	-150.470	407	71.650	-152.374	487			567	71.422	-158.674	647	74.768	-167.269
328	71.750	-150.518	408	71.625	-152.267	488			568	71.485	-158.704	648	74.660	-167.217
329	71.776	-150.565	409	71.626	-152.284	489			569	71.553	-158.471	649	74.565	-167.418
330	71.842	-150.599	410	71.628	-152.304	490			570	71.600	-158.320	650	74.571	-167.570
331	71.913	-151.033	411	71.621	-152.277	491			571	71.655	-158.110	651	74.519	-167.377
332	71.935	-151.181	412	71.623	-152.288	492			572	71.708	-158.006	652	74.560	-167.059
333	71.904	-151.341	413	71.618	-152.266	493			573	71.768	-157.968	653	74.561	-166.743
334	71.909	-151.324	414	71.624	-152.292	494			574	71.826	-158.209	654	74.574	-166.591
335	71.833	-151.110	415	71.620	-152.283	495			575	71.891	-158.178	655	74.569	-166.635
336	71.785	-151.061	416	71.622	-152.307	496			576	71.977	-158.091	656	74.557	-166.598
337	71.795	-151.012	417	71.625	-152.264	497			577	72.055	-157.875	657	74.503	-167.104
338	71.775	-151.018	418	71.615	-152.260	498			578	72.115	-157.438	658	74.544	-167.282
339	71.786	-150.993	419	71.623	-152.298	499			579	72.231	-157.254	659	74.736	-167.438
340	71.782	-151.015	420	71.626	-152.280	500			580	72.299	-156.929	660	74.782	-167.459
341	71.772	-150.922	421	71.618	-152.278	501			581	72.372	-156.842	661	74.773	-167.545
342	71.830	-150.792	422	71.625	-152.278	502			582	72.435	-156.574	662	74.702	-167.567
343	71.790	-150.954	423	71.646	-152.225	503			583	72.471	-156.390	663	74.626	-167.379
344	71.780	-150.928	424	71.639	-152.194	504			584	72.536	-156.235	664	74.560	-167.469
345	71.744	-150.866	425	71.654	-152.253	505			585	72.562	-156.117	665	74.473	-167.695
346	71.750	-150.876	426	71.678	-152.349	506			586	72.580	-156.200	666	74.392	-168.046
347	71.753	-150.795	427	71.671	-152.344	507			587	72.621	-156.216	667	74.271	-168.238
348	71.773	-151.068	428	71.677	-152.431	508			588	72.655	-156.291	668	74.115	-168.496
349	71.791	-151.042	429	71.701	-152.851	509			589	72.729	-156.216	669	74.046	-168.612
350	71.768	-151.065	430	71.707	-152.858	510			590	72.723	-156.305	670	74.027	-168.682
351	71.770	-151.280	431	71.687	-152.801	511			591	72.764	-156.432	671	73.995	-168.749
352	71.755	-151.328	432	71.758	-153.436	512			592	72.862	-156.567	672	74.002	-168.796
353	71.719	-151.308	433	71.831	-154.425	513			593	72.935	-156.739	673	74.020	-168.783
354	71.725	-151.206	434	71.894	-154.884	514			594	72.984	-156.906	674	73.990	-168.761
355	71.715	-151.185	435	71.930	-155.356	515			595	73.014	-157.003	675	74.015	-168.749
356	71.735	-151.206	436	71.946	-155.691	516			596	73.037	-156.946	676	74.112	-168.718
357	71.720	-151.264	437	71.934	-155.832	517			597	73.002	-156.931	677	74.166	-168.057
358	71.697	-151.256	438	71.905	-155.918	518			598	73.042	-156.884	678	74.202	-168.445
359	71.723	-151.263	439	71.875	-155.910	519			599	73.039	-156.756	679	74.184	-168.927
360	71.698	-151.301	440	71.794	-155.920	520			600	72.983	-156.630	680	74.137	-170.057
361	71.717	-151.321	441	71.780	-155.929	521	70.787	-162.878	601	72.982	-156.452	681	74.120	-170.042
362	71.751	-151.509	442	71.715	-155.141	522	70.821	-162.741	602	73.025	-156.493	682	74.108	-170.028
363	71.749	-151.607	443	71.669	-158.192	523	70.855	-163.003	603	73.117	-156.599	683	74.083	-170.268
364	71.737	-151.452	444	71.541	-157.012	524	70.904	-162.873	604	73.176	-156.647	684	74.027	-170.797
365	71.755	-151.422	445	71.370	-158.422	525	70.943	-162.461	605	73.271	-156.824	685	73.940	-171.072
366	71.809	-151.699	446	71.268	-159.230	526	70.953	-162.470	606	73.353	-156.999	686	73.933	-171.103
367	71.818	-151.690	447	71.222	-159.240	527	70.999	-162.678	607	73.391	-157.057	687	73.932	-171.177
368	71.872	-151.862	448	71.187	-159.360	528	71.010	-162.608	608	73.439	-157.039	688	73.919	-171.337
369	71.978	-152.189	449	71.123	-159.732	529	71.014	-162.583	609	73.473	-157.045	689	73.914	-171.493
370	72.075	-152.445	450	71.109	-159.722	530	71.029	-162.415	610	73.505	-157.035	690	73.921	-171.481
371	72.122	-152.505	451	71.102	-159.658	531	70.996	-162.124	611	73.505	-157.264	691	73.910	-171.487
372	72.155	-152.531	452	71.111	-159.662	532	70.971	-161.947	612	73.482	-157.653	692	73.897	-171.479
373	72.143	-152.585	453			533	70.955	-161.904	613	73.509	-157.916	693	73.755	-171.642
374	72.088	-152.589	454			534	70.924	-162.057	614	73.544	-158.078	694	73.675	-171.582
375	72.079	-152.413	455			535	70.915	-162.386	615	73.590	-158.297	695	73.613	-171.650
376	71.974	-151.985	456			536	70.916	-162.365	616	73.635	-158.454	696	73.610	-171.667
377	71.955	-151.872	457			537	70.897	-161.995	617	73.734	-158.725	697	73.615	-171.745
378	71.944	-151.819	458			538	70.995	-161.565	618	73.826	-159.124	698		
379	71.940	-151.881	459			539	70.990	-161.020	619	73.909	-159.466	699		
380	71.946	-151.821	460			540	71.023	-160.894	620	73.990	-159.715	700		

TABLE 2 (continued)

RAMS 1467 / STA 16														
DAY	LAT	LONG	DAY	LAT	LONG	DAY	LAT	LONG	DAY	LAT	LONG	DAY	LAT	LONG
301			371	72.368	-150.428	441	72.013	-152.084	511	71.980	-157.132	581	74.033	-161.625
302			372	72.400	-150.482	442	72.015	-152.106	512	71.935	-157.105	582	74.081	-161.450
303			373	72.402	-150.535	443	72.013	-152.085	513	71.988	-157.053	583	74.038	-161.352
304			374	72.335	-150.591	444	72.003	-152.093	514	71.958	-157.040	584	74.022	-161.242
305			375	72.326	-150.357	445	72.010	-152.115	515	71.962	-157.242	585	73.959	-161.278
306			376	72.227	-149.945	446	72.016	-152.111	516	71.880	-157.483	586	73.952	-161.405
307	71.584	-146.867	377	72.182	-149.809	447	72.015	-152.120	517	71.904	-157.623	587	73.997	-161.403
308	71.610	-146.895	378	72.166	-149.752	448	72.017	-152.127	518	71.945	-157.815	588	74.095	-161.378
309	71.636	-146.932	379	72.167	-149.756	449	72.012	-152.108	519	71.998	-158.146	589	74.106	-161.182
310	71.649	-146.811	380	72.179	-149.727	450	72.015	-152.117	520	72.122	-158.752	590	74.107	-161.140
311	71.659	-146.653	381	72.159	-149.694	451	72.011	-152.099	521	72.251	-159.149	591	74.161	-161.190
312	71.676	-146.625	382	72.165	-149.753	452	72.016	-152.110	522	72.235	-159.279	592	74.260	-161.333
313	71.655	-146.534	383	72.146	-149.738	453	72.017	-152.112	523	72.253	-159.537	593	74.353	-161.471
314	71.672	-146.489	384	72.148	-149.759	454	72.017	-152.106	524	72.247	-159.785	594	74.358	-161.620
315	71.699	-146.441	385	72.143	-149.663	455	72.017	-152.104	525	72.251	-160.062	595	74.404	-161.598
316	71.667	-146.568	386	72.132	-149.569	456	72.010	-152.087	526	72.233	-160.186	596	74.400	-161.555
317	71.644	-146.675	387	72.119	-149.800	457	72.011	-152.082	527	72.235	-160.307	597	74.375	-161.480
318	71.600	-146.909	388	72.105	-149.815	458	72.014	-152.113	528	72.254	-160.335	598	74.405	-161.366
319	71.591	-146.904	389	72.099	-149.778	459	72.017	-152.106	529	72.300	-160.452	599	74.388	-161.313
320	71.596	-146.936	390	72.104	-149.797	460	72.018	-152.100	530	72.367	-160.516	600	74.327	-161.068
321	71.579	-146.947	391	72.096	-149.797	461	72.014	-152.131	531	72.351	-160.548	601	74.344	-160.898
322	71.594	-146.933	392	72.096	-149.774	462	72.018	-152.140	532	72.309	-160.597	602	74.385	-160.941
323	71.592	-146.974	393	72.096	-149.771	463	72.018	-152.119	533	72.294	-160.517	603	74.490	-160.952
324	71.668	-147.329	394	72.104	-149.811	464	72.019	-152.128	534	72.278	-160.638	604	74.559	-161.004
325	71.865	-147.944	395	72.124	-150.134	465	72.033	-152.160	535	72.265	-160.653	605	74.637	-161.102
326	71.930	-148.290	396	72.134	-150.548	466	72.031	-152.220	536	72.290	-160.681	606	74.703	-161.234
327	72.017	-148.457	397	72.169	-150.570	467	72.036	-152.359	537	72.308	-160.603	607	74.768	-161.176
328	72.023	-148.508	398	72.176	-150.580	468	72.044	-152.522	538	72.384	-160.526	608		
329	72.037	-148.558	399	72.191	-150.482	469	72.045	-152.505	539	72.397	-160.168	609		
330	72.103	-148.884	400	72.159	-150.538	470	72.036	-152.415	540	72.431	-160.017	610		
331	72.169	-149.025	401	72.138	-150.524	471	72.046	-152.189	541	72.475	-159.852	611		
332	72.184	-149.120	402	72.121	-150.539	472	72.067	-152.079	542	72.495	-159.830	612		
333	72.165	-149.205	403	72.103	-150.373	473	72.060	-152.077	543	72.510	-159.511	613		
334	72.159	-149.273	404	72.037	-150.139	474	72.065	-152.094	544	72.482	-159.383	614		
335	72.036	-149.034	405	71.984	-149.910	475	72.050	-152.203	545	72.445	-159.232	615		
336	72.027	-149.032	406	71.971	-149.815	476	72.043	-152.337	546	72.424	-159.667	616		
337	72.016	-148.987	407	71.968	-149.830	477	72.039	-152.408	547	72.453	-158.699	617		
338	72.017	-148.941	408	71.946	-149.714	478	72.038	-152.448	548	72.536	-158.541	618		
339	72.019	-148.953	409	71.935	-149.683	479	72.031	-152.450	549	72.588	-158.522	619		
340	72.013	-148.933	410	71.942	-149.717	480	72.039	-152.485	550	72.656	-158.550	620		
341	72.000	-148.898	411	71.924	-149.696	481	72.037	-152.533	551	72.745	-158.924	621		
342	72.078	-148.790	412	71.938	-149.695	482	72.058	-152.691	552	72.805	-159.282	622		
343	72.056	-148.934	413	71.931	-149.702	483	72.070	-152.681	553	72.837	-159.543	623		
344	72.026	-148.959	414	71.936	-149.692	484	72.065	-152.678	554	72.822	-159.527	624		
345	71.986	-148.770	415	71.943	-149.702	485	72.077	-152.638	555	72.822	-159.575	625		
346	71.981	-148.778	416	71.943	-149.720	486	72.126	-152.741	556	72.818	-159.663	626		
347	71.975	-148.780	417	71.938	-149.684	487	72.186	-152.906	557	72.853	-159.738	627		
348	72.004	-149.024	418	71.933	-149.680	488	72.228	-153.074	558	72.933	-159.792	628		
349	72.034	-149.041	419	71.936	-149.699	489	72.260	-153.374	559	72.996	-159.893	629		
350	72.028	-149.051	420	71.942	-149.699	490	72.281	-153.805	560	73.023	-159.941	630		
351	72.022	-149.305	421	71.939	-149.690	491	72.288	-154.249	561	73.024	-160.133	631		
352	71.997	-149.335	422	71.939	-149.698	492	72.277	-154.639	562	73.024	-160.356	632		
353	71.963	-149.268	423	71.970	-149.662	493	72.242	-155.011	563	73.073	-160.548	633		
354	71.967	-149.210	424	71.964	-149.635	494	72.198	-155.058	564	73.133	-160.661	634		
355	71.962	-149.154	425	71.985	-149.593	495	72.179	-155.044	565	73.170	-160.827	635		
356	71.960	-149.215	426	72.014	-149.769	496	72.178	-155.033	566	73.179	-160.742	636		
357	71.961	-149.253	427	72.031	-149.778	497	72.154	-155.061	567	73.269	-160.654	637		
358	71.950	-149.228	428	72.031	-149.818	498	72.144	-155.091	568	73.322	-160.743	638		
359	71.963	-149.259	429	72.006	-150.189	499	72.128	-155.187	569	73.357	-160.801	639		
360	71.944	-149.218	430	72.002	-150.222	500	72.096	-155.366	570	73.374	-160.915	640		
361	71.956	-149.293	431	71.986	-150.201	501	72.077	-155.404	571	73.431	-160.930	641		
362	71.989	-149.515	432	71.998	-150.528	502	72.077	-155.411	572	73.479	-160.992	642		
363	71.990	-149.560	433	72.021	-151.039	503	72.098	-155.232	573	73.530	-161.103	643		
364	72.003	-149.431	434	72.059	-151.469	504	72.092	-155.482	574	73.589	-161.337	644		
365	71.995	-149.416	435	72.081	-151.602	505	72.048	-155.545	575	73.661	-161.485	645		
366	72.047	-149.715	436	72.096	-152.185	506	72.028	-155.455	576	73.746	-161.643	646		
367	72.052	-149.674	437	72.087	-152.268	507	72.002	-155.430	577	73.853	-161.601	647		
368	72.115	-148.851	438	72.067	-152.277	508	72.003	-155.545	578	73.886	-161.542	648		
369	72.229	-150.190	439	72.077	-152.207	509	72.022	-155.753	579	73.892	-161.565	649		
370	72.343	-150.389	440	72.040	-152.104	510	72.023	-156.938	580	73.952	-161.546	650		

TABLE 2 (continued)

			RAMS			10 / STA 17								
DAY	LAT	LONG	DAY	LAT	LONG	DAY	LAT	LONG	DAY	LAT	LONG	DAY	LAT	LONG
361	72.320	-129.685	401	72.338	-129.662	441	72.197	-129.587	481	72.203	-129.885	521		
362	72.350	-129.806	402	72.263	-129.717	442	72.167	-129.595	482	72.217	-129.878	522		
363	72.351	-129.784	403	72.219	-129.654	443	72.198	-129.576	483	72.242	-130.053	523		
364	72.329	-129.673	404	72.200	-129.546	444	72.199	-129.405	484	72.284	-130.167	524		
365	72.310	-129.596	405	72.207	-129.455	445	72.164	-129.580	485	72.217	-130.187	525		
366	72.346	-129.629	406	72.194	-129.441	446	72.179	-129.557	486	72.194	-130.064	526		
367	72.449	-129.792	407	72.182	-129.507	447	72.176	-129.506	487	72.203	-130.220	527		
368	72.455	-129.863	408	72.195	-129.433	448	72.172	-129.594	488	72.244	-130.448	528		
369	72.461	-129.999	409	72.187	-129.451	449	72.161	-129.573	489	72.264	-130.545	529		
370	72.452	-130.084	410	72.209	-129.435	450	72.181	-129.593	490	72.342	-131.003	530		
371	72.444	-130.121	411	72.166	-129.411	451	72.210	-129.576	491	72.376	-131.088	531		
372	72.437	-130.102	412	72.203	-129.470	452	72.154	-129.601	492	72.372	-131.443	532		
373	72.444	-130.163	413	72.198	-129.449	453	72.162	-129.576	493	72.295	-131.762	533		
374	72.454	-130.122	414	72.156	-129.472	454	72.141	-129.494	494	72.236	-131.786	534		
375	72.444	-130.015	415	72.179	-129.492	455	72.176	-129.532	495	72.143	-131.771	535		
376	72.429	-129.854	416	72.174	-129.432	456	72.160	-129.667	496	72.066	-131.625	536		
377	72.409	-129.570	417	72.211	-129.410	457	72.171	-129.612	497	72.048	-131.646	537		
378	72.405	-129.542	418	72.193	-129.419	458	72.169	-129.557	498	72.058	-131.542	538		
379	72.399	-129.618	419	72.198	-129.384	459	72.189	-129.600	499	72.074	-131.622	539		
380	72.389	-129.665	420	72.191	-129.429	460	72.152	-129.597	500	72.035	-131.667	540		
381	72.383	-129.595	421	72.179	-129.438	461	72.147	-129.555	501	71.984	-131.652	541		
382	72.401	-129.537	422	72.180	-129.464	462	72.154	-129.561	502	71.963	-131.657	542		
383	72.379	-129.599	423	72.192	-129.454	463	72.141	-129.579	503	71.957	-131.795	543		
384	72.370	-129.551	424	72.195	-129.345	464	72.152	-129.589	504	71.859	-131.734	544		
385	72.377	-129.489	425	72.187	-129.446	465	72.174	-129.552	505	71.850	-131.695	545		
386	72.349	-129.534	426	72.216	-129.441	466	72.222	-129.642	506	71.804	-131.750	546		
387	72.335	-129.607	427	72.219	-129.427	467	72.183	-129.616	507	71.778	-131.869	547		
388	72.342	-129.547	428	72.242	-129.452	468	72.222	-129.750	508	71.808	-131.723	548		
389	72.316	-129.552	429	72.245	-129.590	469	72.191	-129.734	509	71.813	-131.610	549		
390	72.295	-129.534	430	72.199	-129.642	470	72.222	-129.764	510	71.814	-131.848	550		
391	72.290	-129.538	431	72.161	-129.695	471	72.205	-129.745	511	71.884	-131.797	551		
392	72.303	-129.486	432	72.170	-129.587	472	72.214	-129.609	512	71.905	-131.775	552		
393	72.278	-129.509	433	72.148	-129.602	473	72.215	-129.671	513	71.877	-131.829	553		
394	72.287	-129.547	434	72.150	-129.626	474	72.219	-129.631	514	71.845	-131.904	554		
395	72.299	-129.541	435	72.137	-129.581	475	72.210	-129.680	515	71.893	-131.759	555		
396	72.326	-129.823	436	72.142	-129.629	476	72.197	-129.696	516			556		
397	72.330	-129.990	437	72.161	-129.577	477	72.191	-129.674	517			557		
398	72.287	-130.024	438	72.154	-129.649	478	72.191	-129.729	518			558		
399	72.294	-129.927	439	72.189	-129.614	479	72.200	-129.728	519			559		
400	72.284	-129.895	440	72.180	-129.588	480	72.216	-129.800	520			560		

TABLE 2 (continued)

RAMS 26 / STA 18														
DAY	LAT	LONG	DAY	LAT	LONG	DAY	LAT	LONG	DAY	LAT	LONG	DAY	LAT	LONG
361	74.981	-128.833	411	74.808	-128.617	461	74.760	-128.640	511	74.314	-129.884	561	73.163	-131.079
362	75.001	-129.092	412	74.806	-128.626	462	74.764	-128.626	512	74.307	-130.052	562	73.118	-131.303
363	75.011	-129.070	413	74.810	-128.618	463	74.746	-128.656	513	74.285	-130.292	563	73.053	-131.450
364	74.999	-128.933	414	74.808	-128.616	464	74.752	-128.664	514	74.260	-130.416	564	72.996	-131.637
365	74.979	-128.891	415	74.807	-128.621	465	74.771	-128.475	515	74.290	-130.195	565	72.980	-131.783
366	74.958	-128.895	416	74.804	-128.610	466	74.803	-128.093	516	74.293	-130.710	566	73.016	-131.601
367	75.020	-129.000	417	74.803	-128.640	467	74.766	-128.813	517	74.423	-130.941	567	73.030	-131.403
368	75.035	-129.151	418	74.821	-128.581	468	74.782	-128.913	518	74.476	-131.112	568	72.964	-131.603
369	75.064	-129.093	419	74.807	-128.602	469	74.802	-129.018	519	74.475	-131.290	569	72.983	-131.606
370	75.059	-129.109	420	74.818	-128.615	470	74.822	-128.935	520	74.461	-131.619	570	73.000	-131.793
371	75.059	-129.049	421	74.809	-128.616	471	74.799	-128.873	521	74.464	-131.620	571	72.948	-131.726
372	75.052	-128.962	422	74.810	-128.626	472	74.796	-128.840	522	74.316	-131.651	572	72.964	-131.926
373	75.038	-129.974	423	74.820	-128.598	473	74.803	-128.855	523	74.232	-131.622	573	72.909	-131.789
374	75.046	-128.919	424	74.834	-128.625	474	74.805	-128.815	524	74.191	-131.886	574	72.891	-131.897
375	75.023	-128.927	425	74.828	-128.589	475	74.790	-128.927	525	74.182	-131.742	575	72.947	-131.773
376	75.039	-128.894	426	74.830	-128.629	476	74.777	-128.954	526	74.152	-131.550	576		
377	75.006	-128.915	427	74.849	-128.651	477	74.773	-128.948	527	74.104	-131.453	577		
378	74.978	-128.929	428	74.833	-128.652	478	74.772	-128.933	528	74.008	-131.617	578		
379	75.005	-128.829	429	74.834	-128.692	479	74.783	-128.951	529	73.956	-131.617	579		
380	75.031	-128.839	430	74.822	-128.722	480	74.781	-129.020	530	73.994	-131.293	580		
381			431	74.809	-128.728	481	74.805	-129.170	531	74.066	-131.210	581		
382			432	74.781	-128.656	482	74.800	-129.233	532	74.036	-131.085	582		
383			433	74.781	-128.579	483	74.811	-129.185	533	73.926	-130.863	583		
384			434	74.781	-128.707	484	74.842	-129.215	534	73.792	-130.872	584		
385			435	74.791	-128.694	485	74.817	-129.171	535	73.699	-130.867	585		
386			436	74.785	-128.714	486	74.781	-129.036	536	73.675	-130.764	586		
387			437	74.782	-128.708	487	74.750	-128.966	537	73.700	-130.944	587		
388	74.927	-128.797	438	74.792	-128.746	488	74.756	-128.988	538	73.665	-130.780	588		
389	74.921	-128.784	439	74.780	-128.684	489	74.768	-129.006	539	73.709	-130.769	589		
390	74.905	-128.727	440	74.791	-128.714	490	74.769	-128.991	540	73.664	-130.811	590		
391	74.902	-128.767	441	74.773	-128.684	491	74.761	-128.950	541	73.666	-130.183	591		
392	74.893	-128.711	442	74.764	-128.702	492	74.769	-129.475	542	73.582	-130.291	592		
393	74.886	-128.744	443	74.758	-128.713	493	74.716	-129.855	543	73.571	-130.302	593		
394	74.912	-128.718	444	74.771	-128.691	494	74.657	-129.857	544	73.530	-129.452	594		
395	74.890	-128.785	445	74.752	-128.723	495	74.562	-129.747	545	73.445	-129.691	595		
396	74.899	-128.850	446	74.767	-128.695	496	74.514	-129.618	546	73.406	-129.494	596		
397	74.906	-128.983	447	74.756	-128.687	497	74.491	-129.574	547	73.321	-129.376	597		
398	74.893	-128.949	448	74.751	-128.666	498	74.493	-129.552	548	73.364	-129.388	598		
399	74.895	-128.832	449	74.761	-128.662	499	74.482	-129.590	549	73.376	-129.372	599		
400	74.883	-128.807	450	74.758	-128.649	500	74.471	-129.497	550	73.375	-129.372	600		
401	74.881	-128.822	451	74.746	-128.647	501	74.423	-129.471	551	73.367	-129.632	601		
402	74.853	-128.830	452	74.741	-128.658	502	74.433	-129.384	552	73.413	-129.846	602		
403	74.831	-128.682	453	74.751	-128.643	503	74.427	-129.506	553	73.421	-130.170	603		
404	74.818	-128.643	454	74.757	-128.635	504	74.353	-129.768	554	73.380	-130.480	604		
405	74.813	-128.511	455	74.750	-128.662	505	74.316	-129.761	555	73.380	-130.575	605		
406	74.816	-128.500	456	74.750	-128.656	506	74.313	-129.568	556	73.323	-130.578	606		
407	74.797	-128.501	457	74.751	-128.677	507	74.246	-129.464	557	73.301	-130.769	607		
408	74.794	-128.676	458	74.751	-128.634	508	74.253	-129.321	558	73.255	-131.001	608		
409	74.810	-128.608	459	74.744	-128.668	509	74.232	-129.511	559	73.183	-130.999	609		
410	74.817	-128.650	460	74.754	-128.656	510	74.239	-129.864	560	73.178	-131.015	610		

TABLE 2 (continued)

			RAPS			57 / STA 19								
DAY	LAT	LONG	DAY	LAT	LONG	DAY	LAT	LONG	JAY	LAT	LONG	DAY	LAT	LONG
361	73.749	-131.622	401	73.614	-131.766	441	73.524	-131.486	481	73.544	-132.019	521	73.415	-135.613
362	73.739	-131.755	402	73.598	-131.785	442	73.501	-131.503	482	73.547	-132.039	522	73.387	-135.623
363	73.768	-131.815	403	73.558	-131.553	443	73.503	-131.469	483	73.591	-132.208	523	73.384	-135.770
364	73.715	-131.673	404	73.538	-131.439	444	73.507	-131.407	484	73.629	-132.327	524	73.364	-135.788
365	72.716	-131.628	405	73.538	-131.374	445	73.500	-131.500	485	73.573	-132.189	525	73.358	-135.882
366	73.712	-131.513	406	73.530	-131.400	446	73.504	-131.486	486	73.555	-132.101	526	73.304	-135.769
367	73.744	-131.729	407	73.528	-131.358	447	73.485	-131.477	487	73.548	-132.113	527	73.252	-135.699
368	73.798	-131.907	408	73.527	-131.349	448	73.498	-131.485	488	73.588	-132.272	528	73.230	-135.802
369	73.833	-131.973	409	73.526	-131.376	449	73.492	-131.470	489	73.597	-132.416	529	73.248	-135.775
370	73.849	-132.007	410	73.528	-131.350	450	73.484	-131.490	490	73.614	-132.487	530	73.301	-135.748
371	73.829	-131.984	411	73.523	-131.345	451	73.501	-131.483	491	73.668	-132.637	531	73.398	-135.668
372	73.839	-131.888	412	73.530	-131.343	452	73.500	-131.476	492	73.703	-132.224	532	73.309	-135.617
373	73.839	-131.918	413	73.518	-131.344	453	73.498	-131.454	493	73.648	-132.532	533	73.189	-135.440
374	73.823	-131.901	414	73.542	-131.332	454	73.503	-131.377	494	73.572	-132.476	534	73.102	-135.320
375	73.827	-131.885	415	73.501	-131.327	455	73.511	-131.470	495	73.459	-132.377	535	73.075	-135.260
376	73.801	-131.773	416	73.512	-131.336	456	73.497	-131.502	496	73.424	-132.179	536	73.083	-135.262
377	73.782	-131.633	417	73.529	-131.362	457	73.488	-131.468	497	73.404	-132.119	537	73.061	-135.416
378	73.755	-131.509	418	73.520	-131.348	458	73.498	-131.505	498	73.394	-132.142	538	73.065	-135.400
379	73.765	-131.567	419	73.528	-131.322	459	73.497	-131.514	499	73.404	-132.066	539	73.130	-135.383
380	73.765	-131.623	420	73.518	-131.345	460	73.479	-131.485	500	73.375	-132.102	540	73.070	-135.306
381	73.788	-131.576	421	73.536	-131.355	461	73.485	-131.498	501	73.352	-132.066	541	72.993	-135.163
382	73.761	-131.569	422	73.526	-131.343	462	73.497	-131.474	502	73.333	-132.061	542	73.038	-134.955
383	73.734	-131.560	423	73.537	-131.337	463	73.488	-131.467	503	73.341	-132.216	543	72.997	-134.850
384	73.736	-131.552	424	73.541	-131.362	464	73.487	-131.488	504	73.295	-132.417	544	72.941	-134.572
385	73.717	-131.490	425	73.529	-131.336	465	73.510	-131.493	505	73.256	-132.371	545	72.868	-134.364
386	73.730	-131.478	426	73.558	-131.401	466	73.542	-131.551	506	73.253	-132.264	546	72.787	-134.119
387	73.700	-131.534	427	73.557	-131.419	467	73.542	-131.752	507	73.202	-132.058	547	72.734	-133.915
388	72.678	-131.576	428	73.554	-131.427	468	73.540	-131.800	508	73.200	-132.007	548	72.802	-133.941
389	73.627	-131.559	429	73.559	-131.444	469	73.527	-131.793	509	73.192	-132.175	549	72.846	-134.079
390	73.647	-131.488	430	73.529	-131.528	470	73.536	-131.818	510	73.208	-132.529	550	72.839	-134.116
391	73.630	-131.499	431	73.515	-131.520	471	73.536	-131.724	511	73.242	-132.748	551	72.876	-134.234
392	73.626	-131.471	432	73.501	-131.491	472	73.520	-131.623	512	73.256	-132.811	552	72.920	-134.549
393	73.617	-131.510	433	73.504	-131.481	473	73.536	-131.620	513	73.261	-132.931	553	72.870	-134.958
394	73.618	-131.475	434	73.526	-131.482	474	73.537	-131.655	514	73.211	-132.910	554	72.794	-135.149
395	73.636	-131.516	435	73.528	-131.542	475	73.523	-131.710	515	73.263	-132.846	555	72.751	-135.105
396	73.661	-131.793	436	73.512	-131.457	476	73.519	-131.742	516	73.272	-134.302	556	72.743	-135.223
397	73.680	-131.843	437	73.515	-131.462	477	73.506	-131.733	517	73.351	-134.593	557	72.719	-135.427
398	73.674	-131.894	438	73.492	-131.513	478	73.517	-131.743	518	73.373	-134.786	558	72.743	-135.668
399	73.642	-131.794	439	73.503	-131.462	479	73.518	-131.801	519	73.427	-135.044	559	72.705	-135.623
400	73.624	-131.771	440	73.513	-131.582	480	73.527	-131.878	520	73.436	-135.402	560	72.730	-135.805

TABLE 2 (continued)

			RAMS			01 / STA 20								
DAY	LAT	LONG	DAY	LAT	LONG	DAY	LAT	LONG	DAY	LAT	LONG	DAY	LAT	LONG
361	70.405	-145.841	411	70.452	-145.966	461	70.437	-146.215	511	70.437	-146.167	561	70.437	-146.297
362	70.431	-145.876	412	70.442	-145.984	462	70.432	-146.204	512	70.438	-146.157	562	70.436	-146.324
363	70.424	-145.855	413	70.443	-145.975	463	70.441	-146.228	513	70.435	-146.166	563	70.425	-146.441
364	70.421	-145.792	414	70.455	-145.971	464	70.431	-146.200	514	70.402	-146.203	564	70.426	-146.460
365	70.436	-145.839	415	70.440	-145.968	465	70.438	-146.207	515	70.476	-146.079	565		
366	70.470	-145.962	416	70.446	-145.963	466	70.435	-146.182	516	70.442	-146.211	566		
367	70.474	-145.000	417	70.447	-145.974	467	70.448	-146.171	517	70.423	-146.174	567		
368	70.499	-146.193	418	70.445	-145.986	468	70.424	-146.302	518	70.444	-146.250	568		
369	70.708	-147.118	419	70.450	-145.976	469	70.448	-146.190	519	70.435	-146.223	569		
370	70.830	-147.600	420	70.453	-145.990	470	70.436	-146.211	520	70.438	-146.197	570		
371	70.851	-147.704	421	70.455	-145.954	471	70.442	-146.214	521	70.436	-146.234	571		
372	70.880	-147.652	422	70.450	-145.957	472	70.441	-146.211	522	70.431	-146.245	572		
373	70.876	-147.871	423	70.437	-145.977	473	70.430	-146.224	523	70.420	-146.297	573		
374	70.821	-147.767	424	70.449	-145.009	474	70.436	-146.219	524	70.417	-146.196	574		
375	70.755	-147.639	425	70.451	-145.955	475	70.436	-146.194	525	70.435	-146.201	575		
376	70.712	-146.913	426	70.445	-145.954	476	70.431	-146.139	526	70.434	-146.250	576		
377	70.591	-146.552	427	70.450	-145.976	477	70.424	-146.233	527	70.439	-146.170	577		
378	70.569	-146.423	428	70.450	-145.956	478	70.443	-146.210	528	70.435	-146.230	578		
379	70.565	-146.520	429	70.452	-145.954	479	70.439	-146.199	529	70.444	-146.202	579		
380	70.570	-146.544	430	70.432	-146.125	480	70.442	-146.209	530	70.439	-146.201	580		
381	70.552	-146.447	431	70.437	-146.115	481	70.435	-146.195	531	70.434	-146.205	581		
382	70.576	-146.557	432	70.439	-146.239	482	70.441	-146.187	532	70.440	-146.153	582		
383	70.563	-146.591	433	70.443	-146.264	483	70.436	-146.174	533	70.436	-146.177	583		
384	70.550	-146.604	434	70.440	-146.273	484	70.435	-146.195	534	70.435	-146.226	584		
385	70.563	-146.580	435	70.447	-146.252	485	70.434	-146.215	535	70.426	-146.205	585		
386	70.537	-146.620	436	70.435	-146.239	486	70.443	-146.192	536	70.444	-146.214	586		
387	70.546	-146.565	437	70.443	-146.275	487	70.435	-146.194	537	70.431	-146.203	587		
388	70.536	-146.555	438	70.437	-146.269	488	70.436	-146.213	538	70.437	-146.219	588		
389	70.541	-146.560	439	70.446	-146.248	489	70.435	-146.210	539	70.454	-146.156	589		
390	70.549	-146.675	440	70.443	-146.205	490	70.437	-146.202	540	70.422	-146.311	590		
391	70.547	-146.702	441	70.441	-146.222	491	70.438	-146.187	541	70.464	-146.254	591		
392	70.542	-146.549	442	70.439	-146.221	492	70.424	-146.189	542	70.445	-146.196	592		
393	70.541	-146.545	443	70.433	-146.225	493	70.440	-146.220	543	70.445	-146.207	593		
394	70.543	-146.543	444	70.433	-146.248	494	70.439	-146.202	544	70.441	-146.219	594		
395	70.544	-146.544	445	70.435	-146.221	495	70.444	-146.215	545	70.438	-146.206	595		
396	70.538	-146.693	446	70.440	-146.218	496	70.443	-146.205	546	70.426	-146.231	596		
397	70.548	-146.543	447	70.441	-146.227	497	70.441	-146.193	547	70.443	-146.213	597		
398	70.544	-146.629	448	70.441	-146.225	498	70.440	-146.193	548	70.439	-146.206	598		
399	70.531	-146.655	449	70.435	-146.228	499	70.438	-146.226	549	70.448	-146.229	599		
400	70.538	-146.648	450	70.446	-146.214	500	70.436	-146.218	550	70.442	-146.242	600		
401	70.537	-146.641	451	70.437	-145.219	501	70.432	-146.193	551	70.442	-146.267	601		
402	70.543	-146.569	452	70.442	-145.207	502	70.431	-145.223	552	70.439	-146.271	602		
403	70.541	-146.558	453	70.446	-146.218	503	70.430	-146.215	553	70.447	-146.211	603		
404	70.494	-146.275	454	70.433	-146.192	504	70.437	-146.159	554	70.437	-146.238	604		
405	70.459	-146.061	455	70.443	-145.200	505	70.437	-146.225	555	70.443	-146.272	605		
406	70.453	-145.984	456	70.439	-145.159	506	70.432	-146.217	556	70.433	-146.253	606		
407	70.448	-145.027	457	70.440	-145.157	507	70.428	-146.212	557	70.439	-146.267	607		
408	70.442	-145.982	458	70.441	-145.202	508	70.437	-146.238	558	70.436	-146.277	608		
409	70.448	-145.956	459	70.437	-146.206	509	70.424	-146.216	559	70.438	-146.293	609		
410	70.450	-145.954	460	70.440	-145.218	510	70.426	-145.252	560	70.436	-146.262	610		

TABLE 2 (continued)

RAMS 316 / STA 21														
DAY	LAT	LONG	DAY	LAT	LONG	DAY	LAT	LONG	DAY	LAT	LONG	DAY	LAT	LONG
361	71.192	-147.010	411	71.173	-147.026	461	71.260	-149.235	511	71.502	-152.859	561	71.634	-156.765
362	71.211	-147.156	412	71.155	-146.986	462	71.259	-149.248	512	71.474	-152.824	562	71.608	-156.883
363	71.220	-147.148	413	71.152	-146.957	463	71.263	-149.231	513	71.498	-152.820	563	71.619	-157.046
364	71.219	-147.080	414	71.181	-146.979	464	71.262	-149.248	514	71.443	-152.994	564	71.640	-157.255
365	71.215	-147.099	415	71.159	-146.987	465	71.263	-149.277	515	71.513	-152.852	565	71.715	-156.999
366	71.269	-147.291	416	71.169	-146.989	466	71.268	-149.231	516	71.498	-152.838	566	71.703	-156.956
367	71.272	-147.281	417	71.165	-146.976	467	71.267	-149.239	517	71.518	-152.910	567	71.749	-156.671
368	71.315	-147.452	418	71.157	-146.960	468	71.267	-149.207	518	71.506	-152.266	568	71.852	-156.654
369	71.486	-147.852	419	71.153	-146.948	469	71.263	-149.179	519	71.518	-153.505	569	71.909	-156.513
370	71.551	-148.083	420	71.165	-146.946	470	71.270	-149.219	520	71.566	-154.512	570	71.961	-156.391
371	71.587	-148.151	421	71.165	-146.970	471	71.302	-149.069	521	71.630	-155.270	571	72.041	-156.266
372	71.619	-148.236	422	71.157	-146.983	472	71.271	-149.030	522	71.673	-155.413	572	72.098	-156.220
373	71.605	-148.246	423	71.163	-146.941	473	71.300	-149.038	523	71.705	-155.945	573	72.161	-156.302
374	71.537	-148.216	424	71.160	-146.979	474	71.263	-149.064	524	71.677	-155.889	574	72.204	-156.533
375	71.523	-148.026	425	71.195	-147.029	475	71.274	-149.155	525	71.669	-155.808	575	72.236	-156.675
376	71.419	-147.616	426	71.206	-147.110	476	71.259	-149.162	526	71.637	-156.187	576	72.334	-156.734
377	71.353	-147.396	427	71.211	-147.097	477	71.267	-149.243	527	71.623	-156.295	577	72.357	-156.787
378	71.352	-147.342	428	71.201	-147.098	478	71.268	-149.203	528	71.626	-156.303	578	72.446	-156.636
379	71.348	-147.377	429	71.223	-147.350	479	71.263	-149.169	529	71.625	-156.457	579	72.503	-156.414
380	71.341	-147.416	430	71.210	-147.437	480	71.273	-149.210	530	71.635	-156.566	580	72.564	-156.302
381	71.356	-147.332	431	71.216	-147.398	481	71.269	-149.243	531	71.622	-156.471	581	72.637	-156.358
382	71.332	-147.416	432	71.229	-147.731	482	71.276	-149.385	532	71.562	-156.265	582	72.701	-156.114
383	71.345	-147.436	433	71.244	-148.307	483	71.302	-149.385	533	71.597	-156.346	583	72.711	-155.916
384	71.337	-147.467	434	71.270	-148.743	484	71.321	-149.417	534	71.558	-156.544	584	72.773	-155.823
385	71.322	-147.418	435	71.284	-149.002	485	71.319	-149.388	535	71.465	-156.783	585	72.781	-155.708
386	71.285	-147.408	436	71.292	-149.267	486	71.340	-149.476	536	71.517	-156.880	586		
387	71.317	-147.523	437	71.299	-149.318	487	71.397	-149.711	537	71.559	-156.841	587		
388	71.303	-147.525	438	71.294	-149.326	488	71.407	-150.094	538	71.578	-156.862	588		
389	71.287	-147.517	439	71.295	-149.310	489	71.428	-150.527	539	71.607	-156.867	589		
390	71.298	-147.523	440	71.276	-149.240	490	71.480	-151.014	540	71.643	-155.812	590		
391	71.308	-147.560	441	71.268	-149.208	491	71.519	-151.371	541	71.696	-155.140	591		
392	71.288	-147.509	442	71.265	-149.223	492	71.499	-151.517	542	71.702	-155.135	592		
393	71.282	-147.480	443	71.274	-149.225	493	71.473	-151.560	543	71.688	-155.103	593		
394	71.293	-147.515	444	71.274	-149.132	494	71.466	-151.635	544	71.655	-155.073	594		
395	71.291	-147.512	445	71.276	-149.233	495	71.468	-151.651	545	71.627	-154.910	595		
396	71.303	-147.593	446	71.276	-149.223	496	71.468	-151.634	546	71.617	-154.856	596		
397	71.333	-147.751	447	71.272	-149.224	497	71.470	-151.637	547	71.599	-154.788	597		
398	71.337	-147.746	448	71.279	-149.211	498	71.469	-151.670	548	71.597	-154.549	598		
399	71.317	-147.659	449	71.272	-149.193	499	71.479	-151.662	549	71.596	-154.407	599		
400	71.325	-147.703	450	71.288	-149.244	500	71.474	-151.643	550	71.593	-154.320	600		
401	71.321	-147.737	451	71.288	-149.227	501	71.464	-151.633	551	71.625	-154.710	601		
402	71.335	-147.748	452	71.284	-149.213	502	71.478	-151.693	552	71.649	-154.886	602		
403	71.294	-147.642	453	71.289	-149.203	503	71.498	-152.016	553	71.671	-154.576	603		
404	71.227	-147.342	454	71.275	-149.232	504	71.507	-152.344	554	71.647	-154.692	604		
405	71.196	-147.110	455	71.280	-149.207	505	71.508	-152.345	555	71.673	-154.696	605		
406	71.175	-147.051	456	71.274	-149.290	506	71.484	-152.363	556	71.661	-154.784	606		
407	71.185	-147.363	457	71.252	-149.274	507	71.471	-152.302	557	71.694	-155.106	607		
408	71.157	-146.975	458	71.262	-149.217	508	71.498	-152.404	558	71.695	-155.066	608		
409	71.149	-148.982	459	71.267	-149.240	509	71.526	-152.595	559	71.691	-156.229	609		
410	71.161	-147.039	460	71.257	-149.260	510	71.513	-152.641	560	71.660	-156.389	610		

TABLE 2 (continued)

RAMS 320 / STA 22														
DAY	LAT	LONG	DAY	LAT	LONG	DAY	LAT	LONG	DAY	LAT	LONG	DAY	LAT	LONG
361	70.738	-143.599	431	70.744	-143.662	501	71.031	-146.534	571	71.643	-151.851	641	73.593	-161.548
362	70.773	-143.741	432	70.764	-143.930	502	71.027	-146.545	572	71.671	-151.952	642	73.594	-161.755
363	70.767	-143.774	433	70.781	-144.097	503	71.024	-146.537	573	71.695	-152.034	643	73.574	-162.120
364	70.772	-143.684	434	70.796	-144.325	504	71.030	-146.495	574	71.745	-152.306	644	73.573	-162.311
365	70.766	-143.694	435	70.802	-144.378	505	71.026	-146.527	575	71.769	-152.438	645	73.588	-162.645
366	70.827	-143.842	436	70.797	-144.365	506	71.035	-146.545	576	71.804	-152.346	646	73.534	-162.961
367	70.826	-143.825	437	70.799	-144.373	507	71.023	-146.515	577	71.816	-152.364	647	73.499	-163.097
368	70.849	-143.939	438	70.795	-144.394	508	71.024	-146.553	578	71.797	-152.125	648	73.439	-163.976
369	70.997	-144.453	439	70.782	-144.309	509	71.031	-146.535	579	71.765	-151.973	649	73.337	-163.246
370	71.094	-144.687	440	70.758	-144.099	510	71.026	-146.554	580	71.777	-151.928	650	73.373	-163.426
371	71.107	-144.777	441	70.747	-144.057	511	71.031	-146.497	581	71.782	-151.961	651	73.328	-163.499
372	71.123	-144.868	442	70.738	-144.071	512	71.033	-146.462	582	71.772	-151.796	652	73.320	-163.406
373	71.118	-144.900	443	70.734	-144.061	513	71.022	-146.502	583	71.733	-151.625	653	73.322	-163.254
374	71.055	-144.835	444	70.720	-144.072	514	71.005	-146.513	584	71.718	-151.496	654	73.303	-163.196
375	71.037	-144.657	445	70.734	-144.050	515	71.056	-146.377	585	71.665	-151.386	655	73.340	-163.309
376	70.938	-144.139	446	70.736	-144.054	516	71.035	-146.542	586	71.667	-151.489	656	73.304	-163.864
377	70.864	-143.938	447	70.732	-144.026	517	71.053	-146.657	587	71.678	-151.560	657	73.227	-164.185
378	70.862	-143.830	448	70.740	-144.050	518	71.085	-146.611	588	71.732	-151.726	658	73.239	-164.287
379	70.861	-143.915	449	70.749	-144.048	519	71.134	-147.171	589	71.716	-151.587	659	73.422	-164.351
380	70.876	-143.914	450	70.733	-144.057	520	71.197	-147.656	590	71.719	-151.699	660	73.474	-164.641
381	70.841	-143.859	451	70.740	-144.058	521	71.267	-148.469	591	71.739	-151.638	661	73.477	-164.703
382	70.857	-143.946	452	70.739	-144.061	522	71.270	-148.732	592	71.827	-152.103	662	73.408	-164.505
383	70.853	-144.012	453	70.746	-144.071	523	71.282	-148.990	593	71.896	-152.299	663	73.332	-164.614
384	70.851	-144.014	454	70.744	-144.024	524	71.285	-149.111	594	71.927	-152.345	664	73.255	-164.622
385	70.856	-143.938	455	70.740	-144.043	525	71.286	-149.057	595	71.936	-152.415	665	73.175	-164.926
386	70.833	-143.976	456	70.740	-144.052	526	71.287	-149.112	596	71.927	-152.354	666	73.092	-165.260
387	70.835	-144.089	457	70.736	-144.038	527	71.287	-149.111	597	71.899	-152.323	667	72.944	-165.604
388	70.823	-144.052	458	70.738	-144.038	528	71.277	-149.059	598	71.893	-152.330	668	72.804	-165.953
389	70.817	-144.025	459	70.735	-144.041	529	71.313	-149.182	599	71.860	-152.103	669	72.689	-166.181
390	70.823	-144.103	460	70.757	-143.986	530	71.356	-149.393	600	71.786	-151.869	670	72.657	-166.394
391	70.819	-144.126	461	70.732	-144.044	531	71.301	-149.522	601	71.779	-151.510	671	72.630	-166.521
392	70.818	-144.084	462	70.737	-144.054	532	71.350	-149.457	602	71.794	-151.364	672	72.621	-166.602
393	70.813	-144.087	463	70.736	-144.050	533	71.349	-149.458	603	71.909	-151.355	673	72.677	-166.551
394	70.819	-144.104	464	70.735	-144.049	534	71.348	-149.504	604	71.988	-151.471	674	72.658	-166.553
395	70.811	-144.076	465	70.734	-144.055	535	71.340	-149.502	605	72.084	-151.776	675	72.685	-166.560
396	70.820	-144.077	466	70.735	-144.040	536	71.372	-149.674	606	72.152	-151.944	676	72.768	-166.602
397	70.820	-144.074	467	70.733	-144.048	537	71.372	-149.720	607	72.165	-152.060	677	72.616	-166.937
398	70.822	-144.076	468	70.742	-144.032	538	71.402	-149.731	608	72.194	-152.092	678	72.655	-167.348
399	70.809	-144.043	469	70.738	-144.037	539	71.393	-149.594	609	72.200	-151.975	679	72.845	-167.710
400	70.816	-144.066	470	70.732	-144.040	540	71.379	-149.477	610	72.245	-152.124	680	72.608	-167.656
401	70.817	-144.076	471	70.744	-143.949	541	71.394	-149.406	611	72.257	-152.109	681	72.778	-167.869
402	70.819	-144.094	472	70.755	-143.911	542	71.392	-149.295	612	72.299	-152.150	682	72.751	-167.878
403	70.804	-143.902	473	70.746	-143.931	543	71.357	-149.104	613	72.354	-152.283	683	72.715	-168.196
404	70.760	-143.653	474	70.743	-143.964	544	71.327	-148.967	614	72.349	-152.235	684		
405	70.726	-143.445	475	70.735	-143.993	545	71.305	-148.856	615	72.420	-152.335	685		
406	70.722	-143.397	476	70.738	-144.017	546	71.273	-148.744	616	72.504	-152.334	686		
407	70.717	-143.429	477	70.741	-144.031	547	71.320	-148.620	617	72.596	-152.422	687		
408	70.715	-143.398	478	70.748	-144.056	548	71.314	-148.562	618	72.658	-152.677	688		
409	70.715	-143.378	479	70.744	-144.044	549	71.326	-148.518	619	72.708	-153.166	689		
410	70.720	-143.473	480	70.742	-144.049	550	71.336	-148.556	620	72.857	-153.575	690		
411	70.722	-143.399	481	70.749	-144.114	551	71.364	-148.791	621	72.958	-153.782	691		
412	70.712	-143.396	482	70.811	-144.317	552	71.367	-148.899	622	73.060	-154.009	692		
413	70.711	-143.357	483	70.796	-144.375	553	71.369	-148.897	623	73.178	-154.419	693		
414	70.722	-143.390	484	70.789	-144.358	554	71.353	-148.961	624	73.256	-155.015	694		
415	70.725	-143.386	485	70.785	-144.316	555	71.334	-149.039	625	73.282	-155.551	695		
416	70.720	-143.374	486	70.822	-144.527	556	71.312	-149.158	626	73.265	-155.718	696		
417	70.720	-143.379	487	70.857	-144.736	557	71.348	-149.549	627	73.318	-156.834	697		
418	70.720	-143.332	488	70.890	-144.923	558	71.418	-150.034	628	73.410	-156.981	698		
419	70.717	-143.369	489	70.949	-145.328	559	71.479	-150.460	629	73.441	-156.159	699		
420	70.730	-143.424	490	71.019	-145.915	560	71.505	-150.763	630	73.461	-156.488	700		
421	70.722	-143.384	491	71.043	-146.404	561	71.497	-150.699	631	73.550	-156.346	701		
422	70.714	-143.369	492	71.044	-146.476	562	71.486	-151.034	632	73.529	-156.330	702		
423	70.720	-143.389	493	71.029	-146.522	563	71.494	-151.226	633	73.534	-156.622	703		
424	70.722	-143.391	494	71.035	-146.530	564	71.531	-151.615	634	73.539	-156.981	704		
425	70.743	-143.449	495	71.033	-146.543	565	71.552	-151.661	635	73.571	-157.640	705		
426	70.769	-143.555	496	71.034	-146.537	566	71.557	-151.667	636	73.604	-158.459	706		
427	70.762	-143.507	497	71.031	-146.536	567	71.553	-151.686	637	73.637	-159.369	707		
428	70.753	-143.491	498	71.037	-146.531	568	71.600	-151.756	638	73.619	-160.264	708		
429	70.747	-143.648	499	71.025	-146.539	569	71.603	-151.654	639	73.626	-161.019	709		
430	70.751	-143.724	500	71.042	-146.603	570	71.615	-151.872	640	73.604	-161.337	710		

TABLE 2 (continued)

RAMS 502 / STA 23														
DAY	LAT	LONG	DAY	LAT	LONG	DAY	LAT	LONG	DAY	LAT	LONG	DAY	LAT	LONG
361	70.445	-139.491	401	70.417	-139.697	441	70.337	-139.667	481	70.346	-139.618	521		
362	70.448	-139.672	402	70.391	-139.863	442	70.220	-139.596	482	70.376	-139.793	522		
363	70.458	-139.713	403	70.383	-139.894	443	70.323	-139.569	483	70.423	-139.888	523		
364	70.434	-139.599	404	70.367	-139.502	444	70.327	-139.514	484	70.424	-139.929	524		
365	70.450	-139.563	405	70.335	-139.308	445	70.311	-139.557	485	70.410	-139.888	525		
366	70.513	-139.812	406	70.332	-139.284	446	70.312	-139.557	486	70.445	-140.038	526		
367	70.526	-139.835	407	70.316	-139.291	447	70.318	-139.548	487	70.474	-140.251	527		
368	70.529	-139.981	408	70.323	-139.273	448	70.319	-139.551	488	70.493	-140.455	528		
369	70.670	-140.361	409	70.321	-139.271	449	70.319	-139.543	489	70.530	-140.843	529		
370	70.744	-140.670	410	70.331	-139.237	450	70.308	-139.563	490	70.596	-141.221	530		
371	70.745	-140.731	411	70.226	-139.295	451	70.309	-139.538	491	70.652	-141.657	531		
372	70.752	-140.811	412	70.303	-139.260	452	70.319	-139.552	492	70.636	-141.653	532		
373	70.743	-140.873	413	70.315	-139.275	453	70.300	-139.615	493	70.613	-141.688	533		
374	70.685	-140.733	414	70.330	-139.244	454	70.307	-139.509	494	70.613	-141.705	534		
375	70.602	-140.543	415	70.321	-139.268	455	70.318	-139.529	495	70.602	-141.701	535		
376	70.537	-139.643	416	70.335	-139.291	456	70.328	-139.602	496	70.605	-141.736	536		
377	70.450	-139.675	417	70.330	-139.252	457	70.325	-139.535	497	70.597	-141.726	537		
378	70.442	-139.633	418	70.319	-139.225	458	70.322	-139.535	498	70.606	-141.722	538		
379	70.442	-139.717	419	70.326	-139.270	459	70.317	-139.559	499	70.592	-141.729	539		
380	70.447	-139.745	420	70.328	-139.264	460	70.329	-139.554	500	70.606	-141.715	540		
381	70.447	-139.648	421	70.329	-139.263	461	70.339	-139.526	501	70.594	-141.697	541		
382	70.448	-139.810	422	70.323	-139.248	462	70.322	-139.562	502	70.610	-141.690	542		
383	70.470	-139.811	423	70.325	-139.285	463	70.329	-139.573	503	70.596	-141.696	543		
384	70.445	-139.832	424	70.340	-139.299	464	70.325	-139.588	504	70.596	-141.691	544		
385	70.443	-139.764	425	70.343	-139.327	465	70.323	-139.537	505	70.602	-141.714	545		
386	70.431	-139.782	426	70.354	-139.451	466	70.339	-139.538	506	70.610	-141.705	546		
387	70.434	-139.896	427	70.365	-139.450	467	70.324	-139.560	507	70.593	-141.670	547		
388	70.416	-139.897	428	70.364	-139.458	468	70.328	-139.550	508	70.601	-141.729	548		
389	70.409	-139.898	429	70.341	-139.521	469	70.326	-139.588	509	70.588	-141.710	549		
390	70.411	-139.867	430	70.349	-139.540	470	70.339	-139.553	510	70.586	-141.691	550		
391	70.444	-139.897	431	70.357	-139.494	471	70.343	-139.524	511	70.611	-141.681	551		
392	70.414	-139.865	432	70.386	-139.734	472	70.346	-139.531	512	70.603	-141.662	552		
393	70.399	-139.854	433	70.403	-139.872	473	70.339	-139.487	513	70.602	-141.663	553		
394	70.414	-139.874	434	70.402	-139.883	474	70.327	-139.541	514	70.584	-141.664	554		
395	70.409	-139.901	435	70.406	-139.882	475	70.326	-139.530	515	70.619	-141.546	555		
396	70.420	-139.894	436	70.411	-139.928	476	70.299	-139.581	516	70.602	-141.725	556		
397	70.409	-139.838	437	70.407	-139.901	477	70.329	-139.669	517	70.612	-141.787	557		
398	70.407	-139.876	438	70.394	-139.937	478	70.340	-139.559	518	70.642	-142.092	558		
399	70.403	-139.884	439	70.400	-139.882	479	70.341	-139.626	519	70.686	-142.330	559		
400	70.395	-139.892	440	70.372	-139.755	480	70.337	-139.569	520	70.759	-142.748	560		

TABLE 2 (continued)

RAMS 534 / STA 24														
DAY	LAT	LONG	DAY	LAT	LONG	DAY	LAT	LONG	DAY	LAT	LONG	DAY	LAT	LONG
361	71.378	-154.057	401			441	70.016	-163.433	481	69.549	-164.812	521		
362	71.389	-154.172	402	69.981	-163.541	442	70.006	-163.436	482	69.586	-164.729	522		
363	71.395	-154.184	403	69.997	-163.579	443	69.985	-163.463	483	69.548	-164.821	523		
364	71.381	-154.086	404	69.983	-163.521	444	70.007	-163.438	484	69.581	-164.829	524		
365	71.394	-154.241	405	69.983	-163.450	445	69.882	-163.996	485	69.635	-164.744	525		
366	71.446	-154.285	406	69.981	-163.484	446	69.765	-164.527	486	69.674	-164.705	526		
367	71.428	-154.228	407	69.944	-163.424	447	69.723	-164.514	487	69.752	-164.683	527		
368	71.507	-154.471	408	69.934	-163.394	448	69.676	-164.657	488	69.796	-164.773	528		
369	71.652	-155.010	409	69.934	-163.375	449	69.593	-164.814	489	69.704	-165.452	529		
370	71.723	-155.115	410	69.945	-163.482	450	69.580	-164.788	490	69.608	-165.849	530		
371	71.772	-155.143	411	69.939	-163.410	451	69.582	-164.783	491	69.598	-165.812	531		
372	71.797	-155.198	412	69.935	-163.413	452	69.556	-164.760	492	69.639	-165.715	532		
373	71.798	-155.226	413	69.934	-163.507	453	69.552	-164.690	493	69.622	-165.721	533		
374	71.742	-155.212	414	69.928	-163.530	454	69.592	-164.725	494	69.530	-166.129	534		
375	71.737	-155.344	415	69.824	-163.539	455	69.593	-164.670	495	69.481	-166.212	535		
376	71.710	-154.796	416	69.953	-163.622	456	69.627	-164.730	496	69.378	-166.311	536		
377	71.688	-154.580	417	69.943	-163.592	457	69.578	-164.721	497	69.228	-166.772	537		
378	71.637	-154.474	418	69.935	-163.645	458	69.573	-164.714	498	69.082	-167.049	538		
379	71.637	-154.532	419	69.841	-163.615	459	69.582	-164.790	499	69.075	-167.114	539		
380	71.644	-154.538	420	69.920	-163.607	460	69.570	-164.776	500	69.063	-167.101	540		
381	71.642	-154.569	421	69.911	-163.644	461	69.570	-164.812	501	69.115	-167.129	541		
382	71.642	-154.566	422	69.941	-163.606	462	69.562	-164.760	502	69.186	-167.195	542		
383	71.666	-154.385	423	70.001	-163.357	463	69.582	-164.747	503	69.230	-167.180	543		
384	71.641	-154.259	424	70.007	-163.349	464	69.584	-164.748	504	69.242	-167.255	544		
385	71.599	-154.349	425	70.006	-163.332	465	69.571	-164.766	505	69.182	-167.391	545		
386	71.601	-154.517	426	70.007	-163.356	466	69.564	-164.838	506	69.092	-167.581	546		
387	71.615	-154.771	427	69.982	-163.299	467	69.567	-164.857	507	68.940	-167.825	547		
388	71.317	-156.988	428	70.011	-163.347	468	69.564	-164.775	508	68.853	-167.922	548		
389	71.012	-158.226	429	70.003	-163.297	469	69.600	-164.710	509	68.893	-168.002	549		
390	70.808	-160.455	430	70.004	-163.357	470	69.591	-164.609	510	68.870	-168.017	550		
391	70.759	-161.797	431	70.034	-163.260	471	69.605	-164.609	511	68.861	-167.911	551		
392	70.878	-162.013	432	69.830	-163.814	472	69.598	-164.611	512	68.858	-167.845	552		
393	70.910	-162.851	433	69.987	-164.118	473	69.598	-164.664	513	68.919	-167.863	553		
394	70.811	-163.449	434	70.275	-163.401	474	69.582	-164.691	514	68.898	-167.673	554		
395	70.124	-164.348	435	70.363	-163.482	475	69.580	-164.749	515	68.909	-167.708	555		
396	70.058	-164.736	436	70.433	-163.222	476	69.549	-164.764	516	68.874	-167.807	556		
397	70.151	-164.333	437	70.458	-163.115	477	69.554	-164.838	517	68.911	-167.783	557		
398	70.339	-163.217	438	70.319	-163.319	478	69.564	-164.823	518	69.035	-167.825	558		
399	70.330	-163.068	439	70.268	-163.388	479	69.561	-164.826	519	69.131	-167.754	559		
400	70.102	-163.523	440	70.130	-163.408	480	69.560	-164.814	520	69.285	-167.736	560		

RAMS 1143 / STA 25

DAY	LAT	LONG	DAY	LAT	LONG	DAY	LAT	LONG	DAY	LAT	LONG	DAY	LAT	LONG
381	73.614	-130.907	391	73.388	-130.241	401	73.395	-130.458	411	73.437	-129.905	421		
382	73.382	-130.420	392	73.386	-130.234	402	73.410	-130.456	412	73.364	-130.061	422		
383	73.325	-130.210	393	73.391	-130.226	403	73.408	-130.418	413	73.231	-130.367	423		
384	73.474	-130.322	394	73.393	-130.226	404	73.365	-130.363	414	73.189	-130.544	424		
385	73.505	-130.244	395	73.345	-130.233	405	73.322	-130.274	415	73.273	-130.529	425		
386	73.512	-130.169	396	73.387	-130.239	406	73.314	-130.143	416	73.374	-130.425	426		
387	73.508	-130.340	397	73.376	-130.251	407	73.312	-129.990	417	73.502	-130.230	427		
388	73.480	-130.432	398	73.358	-130.270	408	73.315	-129.982	418	73.974	-129.267	428		
389	73.426	-130.307	399	73.369	-130.324	409	73.300	-130.145	419	74.365	-128.362	429		
390	73.389	-130.257	400	73.383	-130.400	410	73.359	-130.138	420	74.262	-128.488	430		

TABLE 2 (continued)

RAMS 137 / STA 28														
DAY	LAT	LONG	DAY	LAT	LONG	DAY	LAT	LONG	DAY	LAT	LONG	DAY	LAT	LONG
441			491	71.713	-156.823	541	71.478	-157.618	591	73.176	-158.993	641	75.333	-168.441
442			492	71.700	-157.048	542	71.525	-157.266	592	73.270	-159.067	642	75.337	-168.548
443			493	71.656	-157.448	543	71.530	-157.225	593	73.343	-159.272	643	75.330	-168.583
444			494	71.605	-157.507	544	71.541	-157.114	594	73.379	-159.527	644	75.347	-168.693
445			495	71.561	-157.618	545	71.532	-157.122	595	73.393	-159.601	645	75.364	-168.725
446			496	71.556	-157.650	546	71.537	-157.123	596	73.431	-159.631	646	75.359	-168.818
447			497	71.514	-157.774	547	71.540	-157.022	597	73.411	-159.634	647	75.299	-168.958
448			498	71.473	-157.979	548	71.586	-156.745	598	73.427	-159.472	648	75.174	-169.011
449	71.525	-154.815	499	71.447	-158.078	549	71.629	-156.369	599	73.423	-159.418	649	75.068	-169.192
450	71.525	-154.812	500	71.420	-158.276	550	71.690	-156.188	600	73.354	-159.220	650	75.047	-169.329
451	71.521	-154.824	501	71.392	-158.442	551	71.742	-156.355	601	73.358	-159.068	651	74.984	-169.158
452	71.524	-154.831	502	71.343	-158.724	552	71.776	-156.515	602	73.403	-159.090	652	75.042	-168.755
453	71.524	-154.845	503	71.306	-158.882	553	71.843	-156.137	603	73.487	-159.165	653	75.061	-168.505
454	71.524	-154.841	504	71.287	-159.010	554	71.826	-156.171	604	73.554	-159.351	654	75.056	-168.441
455	71.515	-154.863	505	71.254	-159.053	555	71.823	-156.219	605	73.630	-159.525	655		
456	71.514	-154.832	506	71.234	-158.982	556	71.807	-156.382	606	73.692	-159.711	656		
457	71.522	-154.845	507	71.232	-158.992	557	71.827	-156.654	607	73.739	-159.753	657		
458	71.513	-154.818	508	71.215	-159.157	558	71.862	-156.667	608	73.600	-159.737	658		
459	71.517	-154.822	509	71.210	-159.181	559	71.914	-157.158	609	73.857	-159.717	659		
460	71.517	-154.839	510	71.201	-159.424	560	71.923	-157.306	610	73.916	-159.645	660		
461	71.507	-154.840	511	71.171	-159.517	561	71.926	-157.463	611	73.932	-159.859	661		
462	71.518	-154.852	512	71.180	-159.472	562	71.918	-157.689	612	73.917	-160.189	662		
463	71.525	-154.822	513	71.170	-159.356	563	71.948	-157.859	613	73.946	-160.396	663		
464	71.512	-154.845	514	71.179	-159.289	564	72.012	-158.100	614	74.015	-160.461	664		
465	71.514	-154.822	515	71.183	-159.414	565	72.052	-158.166	615	74.084	-160.546	665		
466	71.519	-154.801	516	71.192	-159.618	566	72.072	-158.148	616	74.148	-160.650	666		
467	71.518	-154.823	517	71.084	-159.644	567	72.117	-157.942	617	74.262	-160.644	667		
468	71.518	-154.817	518	71.121	-159.626	568	72.164	-158.108	618	74.322	-161.469	668		
469	71.514	-154.828	519	71.129	-159.565	569	72.216	-158.106	619	74.392	-161.926	669		
470	71.507	-154.803	520	71.162	-159.527	570	72.253	-158.184	620	74.471	-162.127	670		
471	71.527	-154.671	521	71.161	-159.639	571	72.311	-158.220	621	74.561	-162.331	671		
472	71.528	-154.625	522	71.194	-159.306	572	72.356	-158.219	622	74.648	-162.419	672		
473	71.523	-154.628	523	71.172	-159.551	573	72.420	-158.214	623	74.756	-162.712	673		
474	71.526	-154.576	524	71.169	-159.562	574	72.464	-158.506	624	74.826	-163.235	674		
475	71.532	-154.742	525	71.208	-158.990	575	72.512	-158.637	625	74.891	-163.478	675		
476	71.522	-154.779	526	71.230	-158.941	576	72.595	-158.752	626	74.871	-163.671	676		
477	71.530	-154.796	527	71.240	-159.071	577	72.640	-158.761	627	74.978	-164.141	677		
478	71.530	-154.828	528	71.281	-158.972	578	72.685	-158.989	628	75.019	-164.131	678		
479	71.524	-154.823	529	71.284	-158.924	579	72.758	-158.515	629	75.070	-164.173	679		
480	71.531	-154.847	530	71.307	-158.899	580	72.763	-158.602	630	75.113	-164.356	680		
481	71.526	-154.931	531	71.332	-158.627	581	72.816	-158.740	631	75.159	-164.548	681		
482	71.528	-154.926	532	71.334	-158.494	582	72.898	-158.583	632	75.151	-164.431	682		
483	71.544	-154.809	533	71.328	-158.444	583	72.934	-158.631	633	75.176	-164.550	683		
484	71.541	-154.829	534	71.313	-158.679	584	72.974	-158.644	634	75.204	-164.676	684		
485	71.509	-154.837	535	71.277	-158.925	585	72.955	-158.700	635	75.229	-165.386	685		
486	71.570	-155.107	536	71.263	-159.079	586	72.976	-158.846	636	75.265	-166.165	686		
487	71.541	-155.132	537	71.256	-158.699	587	73.010	-158.851	637	75.214	-166.939	687		
488	71.689	-155.293	538	71.359	-158.235	588	73.081	-158.963	638	75.313	-167.669	688		
489	71.709	-155.758	539	71.404	-157.924	589	73.115	-158.880	639	75.313	-168.158	689		
490	71.704	-156.442	540	71.433	-157.828	590	73.111	-158.873	640	75.303	-168.336	690		

TABLE 2 (continued)

RAMS 207 / STA 29														
DAY	LAT	LONG	DAY	LAT	LONG	DAY	LAT	LONG	DAY	LAT	LONG	DAY	LAT	LONG
461	76.193	-141.161	491	76.430	-142.709	521	76.152	-145.369	551	75.889	-143.354	581	75.751	-142.278
462	76.187	-141.236	492	76.422	-143.405	522	76.150	-145.469	552	75.917	-143.762	582	75.778	-142.044
463	76.199	-141.237	493	76.353	-143.642	523	76.153	-145.426	553	75.895	-143.964	583	75.673	-141.643
464	76.197	-141.218	494	76.276	-143.562	524	76.107	-145.546	554	75.841	-143.888	584	75.609	-141.223
465	76.243	-141.235	495	76.203	-143.356	525	76.030	-145.666	555	75.795	-143.851	585	75.522	-140.385
466	76.246	-141.325	496	76.198	-143.297	526	76.002	-145.448	556	75.780	-143.879	586	75.427	-140.723
467	76.214	-141.559	497	76.150	-143.180	527	75.952	-145.352	557	75.770	-143.885	587	75.409	-140.622
468	76.240	-141.576	498	76.150	-143.230	528	75.957	-145.374	558	75.783	-143.745	588	75.439	-140.667
469	76.240	-141.543	499	76.128	-143.191	529	76.013	-145.320	559	75.787	-143.450	589	75.472	-140.511
470	76.234	-141.577	500	76.125	-143.136	530	76.054	-145.218	560	75.796	-143.234	590	75.431	-140.355
471	76.249	-141.484	501	76.111	-142.962	531	76.107	-145.201	561	75.766	-143.291	591	75.402	-140.304
472	76.280	-141.414	502	76.103	-142.870	532	76.030	-145.117	562	75.718	-143.397	592	75.400	-140.265
473	76.294	-141.341	503	76.113	-143.025	533	75.920	-145.110	563	75.695	-143.318	593	75.475	-140.377
474	76.295	-141.407	504	76.084	-143.181	534	75.834	-144.921	564	75.709	-143.281	594	75.549	-140.266
475	76.312	-141.490	505	76.050	-142.981	535	75.783	-144.845	565	75.742	-143.216	595	75.535	-140.396
476	76.269	-141.518	506	76.045	-142.789	536	75.832	-144.846	566	75.753	-143.232	596	75.523	-140.209
477	76.291	-141.643	507	76.012	-142.661	537	75.825	-144.806	567	75.796	-143.117	597	75.488	-140.140
478	76.241	-141.701	508	76.017	-142.354	538	75.869	-144.766	568	75.801	-143.126	598	75.396	-139.974
479	76.239	-141.715	509	76.033	-142.328	539	75.958	-144.692	569	75.812	-143.265	599	75.393	-139.915
480	76.251	-141.769	510	76.033	-142.664	540	75.948	-144.598	570	75.774	-143.226	600	75.234	-139.513
481	76.264	-141.966	511	76.047	-143.033	541	75.967	-144.533	571	75.780	-143.211	601	75.150	-139.166
482	76.310	-142.242	512	76.062	-143.575	542	76.011	-144.258	572	75.794	-143.103	602	75.114	-139.109
483	76.348	-142.498	513	76.069	-143.494	543	75.942	-144.100	573	75.783	-143.100	603	75.131	-139.030
484	76.393	-142.672	514	76.047	-143.619	544	75.874	-143.736	574	75.826	-143.259	604	75.219	-138.960
485	76.363	-142.549	515	76.029	-143.668	545	75.760	-143.332	575	75.848	-143.439	605	75.290	-139.004
486	76.358	-142.441	516	75.958	-144.048	546	75.697	-143.052	576	75.872	-143.373	606	75.358	-139.169
487	76.370	-142.411	517	76.009	-144.403	547	75.684	-142.626	577	75.898	-143.293	607	75.429	-139.258
488	76.398	-142.478	518	76.062	-144.672	548	75.775	-142.540	578	75.859	-142.902	608		
489	76.437	-142.450	519	76.089	-144.907	549	75.853	-142.807	579	75.805	-142.773	609		
490	76.426	-142.411	520	76.130	-145.269	550	75.876	-142.982	580	75.739	-142.446	610		

RAMS 231 / STA 30														
DAY	LAT	LONG	DAY	LAT	LONG	DAY	LAT	LONG	DAY	LAT	LONG	DAY	LAT	LONG
501			531	82.045	-95.902	561	82.088	-95.852	591	82.136	-95.559	621	82.176	-94.882
502			532	82.067	-95.991	562	82.072	-95.873	592	82.130	-95.583	622	82.180	-94.881
503	82.280	-94.530	533	82.044	-96.054	563	82.058	-95.830	593	82.129	-95.561	623	82.183	-94.888
504	82.283	-94.415	534	82.010	-96.366	564	82.076	-95.870	594	82.133	-95.510	624	82.182	-94.832
505	82.299	-94.514	535	81.979	-96.641	565	82.092	-95.776	595	82.155	-95.234	625	82.181	-94.864
506	82.294	-94.459	536	81.920	-96.799	566	82.050	-95.763	596	82.180	-95.052	626	82.179	-94.958
507	82.301	-94.460	537	81.926	-96.761	567	82.073	-95.782	597	82.198	-94.822	627	82.186	-94.771
508	82.294	-94.474	538	81.921	-96.687	568	82.076	-95.791	598	82.219	-94.709	628	82.184	-94.842
509	82.298	-94.455	539	81.927	-96.710	569	82.074	-95.779	599	82.201	-94.696	629	82.175	-94.981
510	82.274	-94.410	540	81.940	-96.796	570	82.072	-95.782	600	82.224	-94.769	630	82.176	-94.820
511	82.315	-94.406	541	81.933	-96.719	571	82.074	-95.897	601	82.216	-94.770	631	82.155	-94.853
512	82.323	-94.337	542	81.941	-96.561	572	82.062	-95.890	602	82.212	-94.771	632	82.175	-94.811
513	82.302	-94.330	543	81.969	-96.209	573	82.051	-95.882	603	82.212	-94.739	633	82.185	-94.855
514	82.304	-94.275	544	82.016	-96.057	574	82.062	-95.914	604	82.208	-94.828	634	82.174	-94.762
515	82.378	-94.221	545	82.079	-96.023	575	82.062	-95.824	605	82.220	-94.703	635	82.157	-94.887
516	82.342	-94.234	546	82.122	-96.120	576	82.083	-95.811	606	82.210	-94.701	636		
517	82.301	-94.447	547	82.109	-96.305	577	82.087	-95.758	607	82.204	-94.640	637		
518	82.245	-94.897	548	82.092	-96.190	578	82.115	-95.764	608	82.202	-94.640	638		
519	82.148	-95.431	549	82.102	-96.052	579	82.146	-95.756	609	82.211	-94.680	639		
520	82.083	-95.745	550	82.097	-96.138	580	82.147	-95.618	610	82.216	-94.642	640		
521	82.019	-96.050	551	82.090	-96.010	581	82.137	-95.554	611	82.217	-94.635	641		
522	82.023	-96.035	552	82.111	-95.923	582	82.135	-95.570	612	82.217	-94.641	642		
523	82.030	-95.986	553	82.098	-96.082	583	82.132	-95.553	613	82.209	-94.755	643		
524	82.007	-96.033	554	82.035	-96.083	584	82.134	-95.579	614	82.176	-94.985	644		
525	82.038	-96.077	555	82.093	-96.056	585	82.127	-95.565	615	82.171	-95.045	645		
526	82.026	-95.996	556	82.094	-96.079	586	82.128	-95.646	616	82.184	-95.021	646		
527	82.037	-96.056	557	82.056	-96.027	587	82.119	-95.703	617	82.180	-94.935	647		
528	82.039	-95.980	558	82.078	-95.936	588	82.108	-95.711	618	82.188	-94.869	648		
529	82.024	-95.974	559	82.092	-95.861	589	82.132	-95.600	619	82.180	-94.871	649		
530	82.030	-95.912	560	82.030	-95.865	590	82.139	-95.583	620	82.184	-94.857	650		

TABLE 2 (continued)

RAMS 1015 / STA 33														
DAY	LAT	LONG	DAY	LAT	LONG	DAY	LAT	LONG	DAY	LAT	LONG	DAY	LAT	LONG
461	72.468	-150.437	501	72.595	-154.006	541	73.000	-158.212	581	74.431	-159.416	621	75.651	-160.725
462	72.460	-150.478	502	72.589	-154.239	542	73.017	-157.988	582	74.459	-159.092	622	75.772	-160.681
463	72.468	-150.452	503	72.610	-154.560	543	73.027	-157.845	583	74.417	-158.817	623	75.851	-160.905
464	72.473	-150.500	504	72.624	-154.798	544	72.998	-157.670	584	74.395	-158.551	624	75.906	-161.390
465	72.490	-150.527	505	72.576	-154.798	545	72.963	-157.472	585	74.325	-158.442	625	75.920	-161.744
466	72.480	-150.543	506	72.554	-154.693	546	72.934	-157.305	586	74.290	-158.439	626	75.930	-161.372
467	72.473	-150.918	507	72.534	-154.612	547	72.965	-156.948	587	74.325	-158.267	627	76.014	-157.034
468	72.485	-151.045	508	72.540	-154.614	548	73.041	-156.794	588	74.414	-158.370	628	76.089	-162.057
469	72.485	-151.121	509	72.557	-154.827	549	73.083	-156.745	589	74.440	-158.121	629	76.149	-162.102
470	72.485	-151.019	510	72.555	-155.003	550	73.148	-156.733	590	74.420	-157.965	630	76.193	-162.305
471	72.494	-150.765	511	72.523	-155.264	551	73.210	-157.072	591	74.468	-157.991	631	76.248	-162.397
472	72.516	-150.609	512	72.499	-155.327	552	73.255	-157.475	592	74.557	-158.113	632	76.233	-162.100
473	72.512	-150.599	513	72.526	-155.237	553	73.285	-157.767	593	74.652	-158.257	633	76.229	-162.214
474	72.505	-150.655	514	72.512	-155.270	554	73.281	-157.759	594	74.673	-158.360	634	76.266	-162.537
475	72.503	-150.752	515	72.512	-155.357	555	73.267	-157.809	595	74.710	-158.323	635	76.290	-163.096
476	72.479	-150.857	516	72.409	-155.634	556	73.262	-157.904	596	74.703	-158.151	636	76.329	-163.895
477	72.474	-151.034	517	72.434	-155.849	557	73.300	-158.002	597	74.650	-157.965	637	76.358	-164.619
478	72.475	-151.105	518	72.492	-156.147	558	73.383	-158.056	598	74.682	-157.917	638	76.343	-165.286
479	72.471	-151.097	519	72.540	-156.435	559	73.447	-158.184	599	74.654	-157.746	639	76.346	-165.748
480	72.481	-151.180	520	72.644	-157.009	560	73.487	-158.284	600	74.558	-157.492	640	76.357	-165.676
481	72.486	-151.230	521	72.736	-157.349	561	73.490	-158.460	601	74.554	-157.224	641		
482	72.503	-151.365	522	72.773	-157.515	562	73.478	-158.680	602	74.578	-157.249	642		
483	72.527	-151.414	523	72.766	-157.739	563	73.526	-158.819	603	74.683	-157.278	643		
484	72.527	-151.415	524	72.795	-157.968	564	73.587	-158.917	604	74.747	-157.282	644		
485	72.534	-151.293	525	72.771	-158.275	565	73.654	-159.064	605	74.827	-157.372	645		
486	72.580	-151.391	526	72.748	-158.420	566	73.657	-159.080	606	74.930	-157.564	646		
487	72.633	-151.570	527	72.747	-158.586	567	73.751	-158.899	607	74.998	-157.510	647		
488	72.676	-151.750	528	72.766	-158.596	568	73.800	-159.033	608	75.057	-157.385	648		
489	72.715	-152.038	529	72.803	-158.639	569	73.837	-159.159	609	75.098	-157.219	649		
490	72.723	-152.444	530	72.873	-158.735	570	73.874	-159.192	610	75.134	-157.202	650		
491	72.741	-152.862	531	72.867	-158.803	571	73.926	-159.241	611	75.106	-157.438	651		
492	72.716	-153.313	532	72.802	-158.912	572	73.971	-159.284	612	75.067	-157.724	652		
493	72.692	-153.644	533	72.816	-158.772	573	74.020	-159.341	613	75.112	-157.999	653		
494	72.650	-153.673	534	72.793	-158.876	574	74.068	-159.624	614	75.165	-158.430	654		
495	72.652	-153.657	535	72.773	-158.921	575	74.133	-159.748	615	75.197	-158.533	655		
496	72.647	-153.634	536	72.800	-158.983	576	74.212	-159.829	616	75.294	-159.065	656		
497	72.643	-153.642	537	72.836	-158.916	577	74.291	-159.724	617	75.368	-159.416	657		
498	72.647	-153.658	538	72.904	-158.779	578	74.357	-159.488	618	75.408	-160.065	658		
499	72.652	-153.678	539	72.930	-158.543	579	74.323	-159.220	619	75.459	-160.407	659		
500	72.621	-153.775	540	72.967	-158.333	580	74.360	-159.314	620	75.538	-160.541	660		

RAMS 1757 / STA 35

DAY	LAT	LONG	DAY	LAT	LONG	DAY	LAT	LONG	DAY	LAT	LONG	DAY	LAT	LONG
451	71.342	-160.121	461	71.336	-160.184	471			481			491		
452	71.355	-160.151	462	71.379	-160.221	472			482			492		
453	71.370	-160.155	463	71.384	-160.186	473			483			493		
454	71.370	-160.150	464	71.385	-160.162	474			484			494		
455	71.392	-160.129	465	71.379	-160.233	475			485			495		
456	71.382	-160.089	466	71.346	-160.345	476			486			496		
457	71.375	-160.174	467			477			487			497		
458	71.371	-160.212	468			478			488			498		
459	71.379	-160.263	469			479			489			499		
460	71.348	-160.246	470			480			490			500		

TABLE 2 (continued)

RAMS 1761 / STA 36

DAY	LAT	LONG	DAY	LAT	LONG	DAY	LAT	LONG	DAY	LAT	LONG	DAY	LAT	LONG
441			491	72.371	-157.600	541	72.727	-162.398	591	74.262	-164.195	641	75.732	-172.230
442			492	72.355	-157.974	542	72.697	-162.320	592	74.367	-164.332	642	75.713	-172.255
443			493	72.325	-158.295	543	72.713	-162.111	593	74.448	-164.503	643	75.701	-172.220
444			494	72.272	-158.510	544	72.654	-162.098	594	74.460	-164.572	644	75.710	-172.295
445			495	72.261	-158.395	545	72.623	-161.954	595	74.528	-164.470	645	75.732	-172.553
446			496	72.229	-158.446	546	72.598	-161.742	596	74.507	-164.368	646	75.715	-172.648
447			497	72.209	-158.439	547	72.648	-161.383	597	74.469	-164.181	647	75.667	-172.597
448			498	72.190	-158.499	548	72.697	-161.167	598	74.508	-164.199	648	75.539	-172.686
449	72.179	-155.298	499	72.184	-158.521	549	72.704	-161.209	599	74.479	-164.165	649	75.450	-172.794
450	72.130	-155.270	500	72.180	-158.574	550	72.725	-161.277	600	74.412	-163.757	650	75.427	-173.049
451	72.114	-155.245	501	72.211	-159.230	551	72.742	-161.652	601	74.419	-163.745	651	75.358	-172.878
452	72.119	-155.239	502	72.229	-159.323	552	72.753	-162.054	602	74.486	-163.825	652	75.407	-172.917
453	72.129	-155.266	503	72.248	-159.473	553	72.774	-162.221	603	74.594	-163.842	653	75.396	-172.276
454	72.125	-155.242	504	72.223	-159.703	554	72.747	-162.181	604	74.668	-163.777	654	75.359	-172.052
455	72.127	-155.254	505	72.196	-159.716	555	72.771	-162.317	605	74.728	-164.051	655	75.347	-172.076
456	72.130	-155.215	506	72.170	-159.527	556	72.767	-162.340	606	74.774	-164.051	656	75.254	-172.235
457	72.127	-155.244	507	72.143	-159.537	557	72.800	-162.438	607	74.826	-163.918	657	75.336	-172.335
458	72.130	-155.282	508	72.137	-159.694	558	72.894	-162.528	608	74.900	-163.757	658	75.395	-172.456
459	72.120	-155.327	509	72.182	-159.772	559	72.988	-162.479	609	74.933	-163.588	659	75.535	-172.606
460	72.112	-155.347	510	72.195	-159.932	560	73.013	-162.635	610	74.968	-163.547	660	75.535	-172.702
461	72.098	-155.437	511	72.146	-160.058	561	73.023	-162.837	611	74.939	-163.730	661	75.507	-172.802
462	72.100	-155.403	512	72.055	-160.324	562	73.012	-163.047	612	74.894	-163.963	662	75.454	-172.771
463	72.104	-155.333	513	72.120	-160.063	563	73.082	-163.223	613	74.890	-164.516	663	75.381	-172.527
464	72.131	-155.311	514	72.068	-160.089	564	73.153	-163.354	614	74.928	-164.674	664	75.293	-172.555
465	72.135	-155.402	515	72.101	-160.110	565	73.171	-163.249	615			665	75.205	-172.761
466	72.085	-155.552	516	72.040	-160.474	566	73.241	-163.350	616			666	75.132	-173.017
467	72.107	-155.508	517	72.040	-160.442	567	73.345	-163.177	617			667	75.029	-173.165
468	72.132	-155.908	518	72.079	-160.611	568	73.409	-163.299	618			668	74.924	-173.262
469	72.139	-155.874	519	72.134	-160.874	569	73.430	-163.411	619			669	74.896	-173.247
470	72.115	-155.777	520	72.255	-161.451	570	73.497	-163.465	620			670	74.891	-173.286
471	72.142	-155.565	521	72.342	-161.923	571	73.509	-163.360	621	75.370	-167.312	671	74.877	-173.328
472	72.150	-155.380	522	72.385	-162.023	572	73.580	-163.426	622	75.419	-167.156	672	74.832	-173.352
473	72.151	-155.385	523	72.351	-162.348	573	73.627	-163.456	623	75.431	-167.295	673	74.871	-173.326
474	72.158	-155.438	524	72.383	-162.453	574	73.682	-163.750	624	75.407	-167.888	674	74.865	-173.269
475	72.163	-155.555	525	72.413	-162.786	575	73.742	-163.935	625	75.444	-168.162	675	74.890	-173.211
476	72.127	-155.720	526	72.403	-162.973	576	73.822	-164.126	626	75.536	-168.239	676	75.008	-173.225
477	72.109	-155.925	527	72.433	-163.126	577	73.924	-164.169	627	75.578	-168.460	677	75.054	-173.462
478	72.100	-155.932	528	72.441	-163.181	578	73.990	-164.167	628	75.618	-168.673	678	75.083	-173.861
479	72.099	-155.972	529	72.519	-163.211	579	73.997	-164.363	629	75.649	-168.917	679	75.074	-174.360
480	72.096	-156.016	530	72.565	-163.349	580	74.056	-164.404	630	75.669	-169.207	680	75.018	-174.501
481	72.066	-155.833	531	72.523	-163.334	581	74.166	-164.437	631	75.680	-169.532	681	75.010	-174.483
482	72.055	-155.902	532	72.492	-163.403	582	74.217	-164.366	632	75.654	-169.580	682	75.010	-174.467
483	72.054	-156.126	533	72.472	-163.345	583	74.190	-164.224	633	75.684	-170.238	683	74.993	-174.654
484	72.083	-155.985	534	72.453	-163.405	584	74.174	-164.043	634	75.682	-170.594	684		
485	72.133	-155.985	535	72.465	-163.443	585	74.146	-164.105	635	75.681	-170.938	685		
486	72.212	-156.062	536	72.464	-163.393	586	74.116	-164.265	636	75.682	-171.257	686		
487	72.279	-156.330	537	72.520	-163.298	587	74.145	-164.344	637	75.690	-171.541	687		
488	72.322	-156.520	538	72.623	-163.149	588	74.233	-164.260	638	75.705	-171.778	688		
489	72.337	-156.740	539	72.636	-162.809	589	74.218	-164.045	639	75.716	-172.024	689		
490	72.359	-157.201	540	72.666	-162.703	590	74.233	-164.020	640	75.716	-172.211	690		

TABLE 2 (continued)

RAMS 604 / STA 37														
DAY	LAT	LONG	DAY	LAT	LONG	DAY	LAT	LONG	DAY	LAT	LONG			
491			521	70.855	-134.290	551	70.527	-134.676	581	70.634	-135.919	611		
492			522	70.831	-134.536	552	70.540	-134.638	582	70.653	-135.424	612		
493	71.225	-132.964	523	70.858	-134.707	553	70.425	-134.230	583	70.542	-135.046	613		
494	71.135	-133.013	524	70.861	-134.978	554	70.302	-133.985	584	70.354	-135.040	614		
495	71.044	-132.950	525	70.857	-135.172	555	70.323	-134.070	585	70.115	-135.226	615		
496	70.922	-132.987	526	70.814	-135.242	556	70.311	-134.222	586	69.983	-135.676	616		
497	70.952	-132.985	527	70.721	-135.202	557	70.290	-134.517	587	69.916	-134.452	617		
498	70.447	-133.022	528	70.692	-135.327	558	70.302	-134.726	588	70.076	-137.313	618		
499	70.937	-132.005	529	70.698	-135.371	559	70.374	-135.053	589	70.015	-137.809	619		
500	70.909	-133.121	530	70.768	-135.513	560	70.379	-135.306	590	69.975	-138.721	620		
501	70.865	-133.226	531	70.810	-135.438	561	70.409	-135.491	591	69.840	-139.568	621		
502	70.841	-133.270	532	70.774	-135.403	562	70.371	-135.621	592	69.957	-140.301	622		
503	70.830	-133.375	533	70.660	-135.357	563	70.333	-135.884	593	70.055	-140.990	623		
504	70.773	-133.388	534	70.612	-135.466	564	70.349	-136.105	594	70.052	-141.296	624		
505	70.763	-133.366	535	70.567	-135.524	565	70.369	-136.201	595	69.944	-140.809	625		
506	70.760	-133.380	536	70.587	-135.623	566	70.387	-136.337	596	69.849	-140.685	626		
507	70.749	-133.333	537	70.561	-135.693	567	70.392	-136.341	597	69.859	-140.451	627		
508	70.755	-133.381	538	70.627	-135.664	568	70.407	-136.414	598	69.782	-140.260	628		
509	70.754	-133.390	539	70.565	-135.721	569	70.403	-136.376	599	69.824	-140.077	629		
510	70.750	-133.477	540	70.595	-135.913	570	70.355	-136.438	600	69.519	-138.546	630		
511	70.773	-133.426	541	70.525	-135.574	571	70.396	-136.519	601	69.172	-137.908	631		
512	70.748	-133.499	542	70.550	-135.406	572	70.402	-136.612	602	69.147	-137.706	632		
513	70.760	-133.446	543	70.491	-135.260	573	70.377	-136.714	603	69.246	-137.774	633		
514	70.756	-133.536	544	70.444	-134.989	574	70.443	-136.825	604	69.449	-138.411	634		
515	70.723	-133.598	545	70.456	-134.876	575	70.477	-136.784	605			635		
516	70.758	-133.589	546	70.399	-134.784	576	70.499	-136.703	606			636		
517	70.793	-133.641	547	70.378	-134.929	577	70.498	-136.565	607			637		
518	70.822	-133.723	548	70.439	-134.694	578	70.466	-136.302	608			638		
519	70.858	-133.659	549	70.456	-134.558	579	70.514	-136.195	609			639		
520	70.870	-134.122	550	70.475	-134.561	580	70.518	-136.065	610			640		

RAMS 101 / STA 41														
DAY	LAT	LONG	DAY	LAT	LONG	DAY	LAT	LONG	DAY	LAT	LONG	DAY	LAT	LONG
591			611	74.548	-151.013	631	75.602	-155.148	651	75.376	-158.875	671	75.048	-160.245
592	74.152	-151.595	612	74.582	-151.169	632	75.588	-154.742	652	75.368	-158.522	672	75.078	-160.173
593	74.243	-151.771	613	74.634	-151.493	633	75.567	-154.938	653	75.465	-158.282	673	75.130	-160.112
594	74.285	-151.869	614	74.667	-151.749	634	75.569	-155.319	654	75.504	-157.964	674	75.166	-160.077
595	74.258	-151.865	615	74.675	-151.702	635	75.599	-155.913	655	75.510	-157.747	675		
596	74.266	-151.835	616	74.779	-152.015	636	75.617	-156.733	656	75.464	-158.381	676		
597	74.205	-151.519	617	74.830	-152.193	637	75.644	-157.495	657	75.423	-158.644	677		
598	74.202	-151.468	618	74.879	-152.857	638	75.607	-158.249	658	75.440	-158.656	678		
599	74.181	-151.257	619	74.925	-153.018	639	75.597	-158.727	659	75.485	-159.155	679		
600	74.070	-151.012	620	74.981	-153.187	640	75.565	-158.916	660	75.609	-159.347	680		
601	74.047	-150.669	621	75.050	-153.326	641	75.530	-158.973	661	75.717	-159.145	681		
602	74.010	-150.872	622	75.187	-153.408	642	75.562	-159.044	662	75.682	-159.037	682		
603	74.086	-150.742	623	75.265	-153.659	643	75.581	-159.086	663	75.621	-158.798	683		
604	74.183	-150.745	624	75.317	-154.132	644	75.613	-159.219	664	75.596	-158.814	684		
605	74.263	-150.944	625	75.393	-154.478	645	75.618	-159.413	665	75.565	-159.146	685		
606	74.363	-151.185	626	75.326	-154.813	646	75.618	-159.629	666	75.504	-159.544	686		
607	74.434	-151.235	627	75.393	-154.691	647	75.607	-159.571	667	75.349	-159.826	687		
608	74.488	-151.146	628	75.413	-154.752	648	75.499	-159.145	668	75.219	-160.172	688		
609	74.521	-150.968	629	75.493	-154.855	649	75.427	-159.138	669	75.111	-160.296	689		
610	74.547	-150.973	630	75.507	-155.089	650	75.440	-159.195	670	75.052	-160.296	690		

APPENDIX 2

AIDJEX MET-OCEAN BUOYS

Interim Data Report

by

M. McPhee
L. Mangum
P. Martin
AIDJEX Office

I. INTRODUCTION

This document presents current measurements made from ice-bound drifting data buoys in the Arctic Ocean. It is intended as a "first-look" compilation of the data; interpretation and conclusions have been kept to a minimum.

Four meteorological/oceanographic (M/O) data buoys were deployed in November, 1975, at locations chosen along the 1000 m isobath in the continental shelf break north of Alaska and Western Canada. It was anticipated that the buoys, each of which was equipped to measure relative current speed and direction at 2 m and 30 m below the ice, would add to our meager knowledge of how near-surface currents in the most intense part of the anticyclonic Pacific Gyre interact with the continental shelf regime. In addition, the boundary layer structure inferred from the measured currents could be compared with similar measurements made at manned ice stations to estimate momentum exchange between the ice and upper ocean within the shear zone.

II. BUOY PERFORMANCE AND RAW DATA

A brief summary of M/O buoy performance is listed in Table 1. In conformance with AIDJEX notation we have listed time in days from the beginning of calendar 1975, e.g., day 366 is 1 January 1976.

Environmental data were collected from M/O 1 for 145 days and from M/O 4 for 332 days as shown. The other two buoys furnished no oceanographic data.

Each buoy consists of a tube 6 m long and 0.3 m in diameter frozen into a hole drilled through the ice. Savonius-rotor current meters with current following vanes (manufactured by Hydro-products) are attached to a suspended pipe mast fixed rigidly to the buoy chassis. The magnetic bearing of a reference azimuth for the buoy is sensed with a compass housed in the tube. Samples of current speed and direction, magnetic azimuth, and meteorological parameters are taken every three hours. The current speed is averaged for 10 minutes, while direction samples are instantaneous

in order to avoid 0°-360° crossover ambiguity. The buoy's memory holds a full day's samples, which are repeatedly transmitted so that when the Nimbus VI weather satellite is within view, the data are received and stored for later playback to a tracking station. NASA performs basic processing of the raw data and furnishes the results to our office on magnetic tape. Geographic positions are computed by NASA based on Doppler frequency measurements made by the spacecraft. The position data are further enhanced by processing developed at AIDJEX (see Thorndike and Cheung, 1977).

The buoys were built by the Applied Physics Laboratory, University of Washington, under contract for NOAA Environmental Research Laboratory, monitored by the NOAA Data Buoy Office and AIDJEX. Deployment was from helicopter and required approximately two hours on the ice per installation.

Figures 1 and 2 (adapted from Thorndike and Cheung, 1977) show drift tracks for the two buoys from which oceanographic data were received. M/O 1 left the air on day 452, but began transmitting again about two months later. Environmental data during the later period appear to be garbled; this was unfortunate since buoy drift in the vicinity of Barrow Canyon is often anomalously swift and it would have been particularly useful to have surface current measurements there.

Figures 3 and 4 show the magnetic azimuth data required for defining true current directions. In order to get the actual magnetic azimuth, the raw data shown require a correction, unique to each buoy, that is dependent on the compass direction and the local horizontal field strength. Correction curves were obtained by extrapolating from errors measured at Seattle and Barrow where the field strength is known.

Raw data from the current meter sensors are received as integer counts and converted to dimensional units using calibration data supplied by the designer. Figures 5 through 8 show calibrated data samples (8 per day) as they were received.

The current bearing shown is the apparent direction of the current relative to the buoy azimuth. The scatter is large but not unexpected, particularly since no provision for vector averaging was made. From previous work under ice we expect turbulent eddies with time scales of from 5 to 10 minutes and these would introduce large variations in directions sampled instantaneously even with steady drift. This would be especially true for the 2 m measurements. Another source for large variations on scales of a few hours is inertial oscillation of the ice cover and upper ocean. We found at the manned stations that it was not uncommon for the apparent direction at 30 m to swing full circle in one inertial period. Thus the extreme scatter exhibited in Figures 7 and 8 for the 30 m direction is expected. It does not show up in the 2 m direction because the water at that level is oscillating in phase with ice. An interesting aspect of these oscillations is that their onset is apparently about two months earlier than was observed at the manned camps the previous summer. Presumably the oscillations are damped when the ice is thick, but occur freely when the ice can no longer support internal stress gradients.

III. PROCESSED DATA

For useful results it was clear that some sort of filtering of the current data was required, and as a first attempt we applied a "cosine bell" running mean, i.e., each smoothed sample was calculated by averaging the corresponding unsmoothed sample with the 12 preceding and succeeding samples, all with the proper cosine weighting. The effect in the frequency domain is a low-pass filter with little energy content at periods shorter than 12 hours. The filter attenuates most of the energy at the inertial period, which is 12.6 hours at 72°N.

The filter was applied to the zonal and meridional velocity components. These were obtained by subtracting the corrected magnetic heading from the current direction, then adding the magnetic declination at the buoys' positions. Also, from

intercomparison between the ice motion and the 2 m and 30 m currents, we believe that the 30 m sensor of M/O 1 and both sensors of M/O 2 were installed backward, so that 180° is added to each of those bearings. It should be pointed out that installation requires coupling current meters to the pipe in the field and the design permitted a 180° misalignment.

Results of the calculations described above are shown in Figures 9 through 12. We have reconverted the smooth components to speed and bearing and have shown them compared to the ice speed and bearing as determined from the smoothed satellite data. The reference frame is chosen such that the actual current at either level is obtained from the vector addition of the ice velocity and the measured current. In other words, if the water at 30 m were still, the 30 m current would (ideally) have the same speed as the ice and its bearing would be 180° out of phase with that of the ice.

With this in mind, the speed plots show many of the characteristics we have seen at the manned camp, i.e., the 30 m speed is usually close to and shows many of the same fluctuations as the ice speed. The 2 m speed also follows, but at a reduced magnitude, indicating that the water at 2 m is following the ice (causing reduced shear). An interesting event is apparent beginning about day 360 in the 30 m speed at M/O 1 (Figure 9). Note that the current speed is sustained at a level appreciably higher than the ice speed for several days. A similar event occurs at buoy M/O 4 about 10 days later. It is possible to conjecture that the events are from the same baroclinic disturbance which is propagating eastward at about 40 cm/s (the buoys are approximately 400 km apart). There is also a sustained current during February, March, and April 1976 at M/O 4 in the absence of much ice drift. It apparently sets west as would be expected in the southern part of the gyre.

The intent of this report has not been an exhaustive analysis of the buoy data, and much remains to be done. In view of the fact that the buoys pioneered in having current measuring capability, the results are encouraging. We have had trouble interpreting the directional measurements and consider some of the directional data suspect; however, this may be more due to prejudice from previous ice station experience rather than the actual evidence. We do point out that when a towing velocity is provided by the ice, the directional measurement requires higher precision to determine the actual current direction to the same accuracy than if the current meter were fixed. This is something that should be considered in design of future buoys. It also seems well within present technical capability to provide vector averaging electronics. A sensitive temperature sensor seems feasible and would be useful, particularly during the summer months, to indicate the amount of stratification.

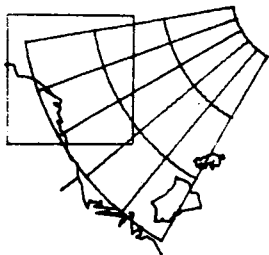
IV. REFERENCES

Thorndike, A. S. and J. Y. Cheung. 1977. Measurements of sea ice motion determined from OCS data buoys - October 1975 to December 1976. Appendix 1, Annual Report, "Dynamics of Near Shore Ice."

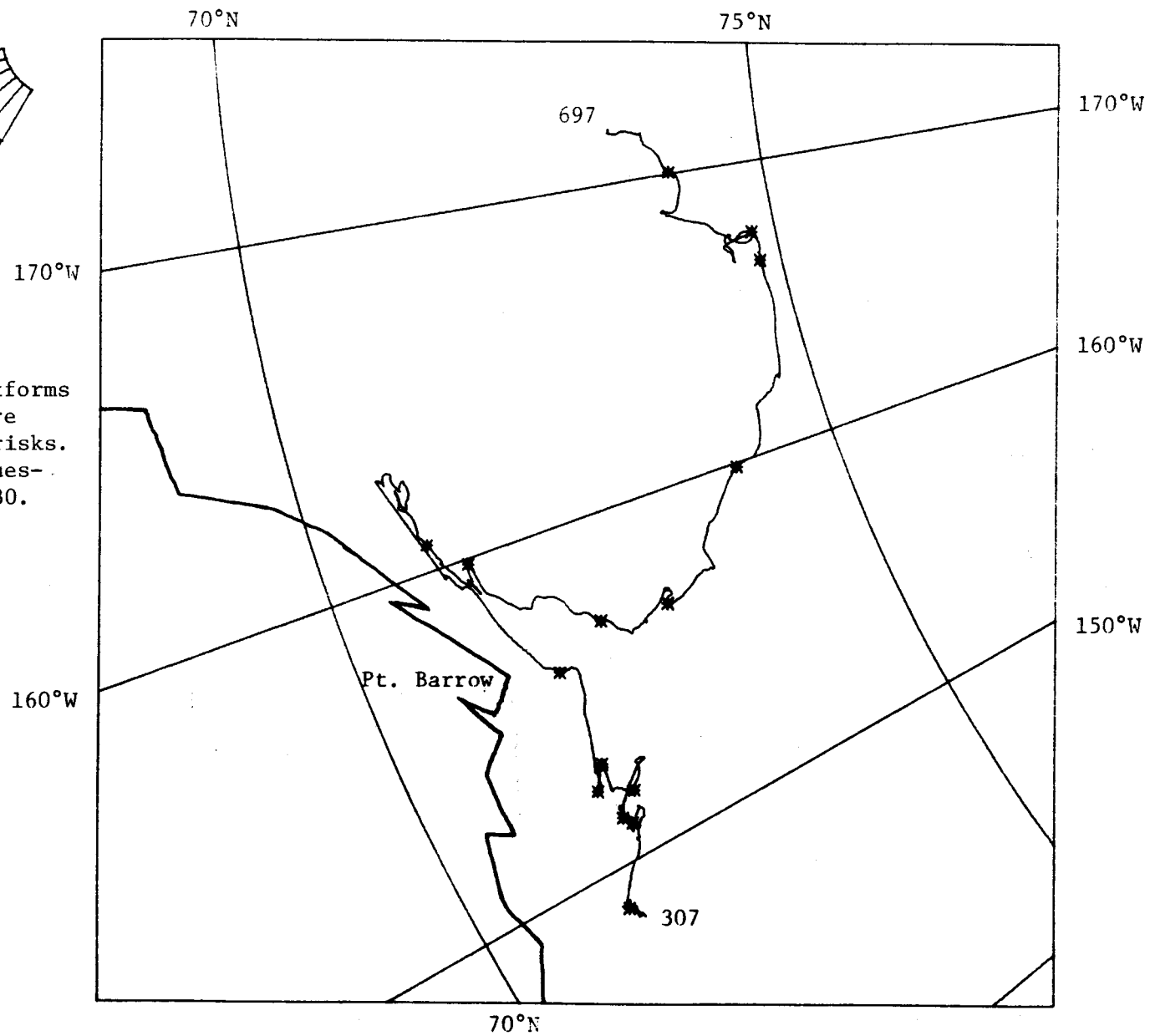
TABLE 1

MET-OCEAN BUOY PERFORMANCE

M/O Buoy	RAMS Platform	Deployed		Position Data	Environmental Data	Remarks
		Position	Date			
1	1416/1420	71°32'N 147°W	2 Nov 75 (306)	307-452 519-697	307-452	Env. data poor quality after 430
2	1451/1467	71°20'N 149°W	2 Nov 75 (306)	307-608	none	Position data only
3	1143/1175	73°44'N 130°W	5 Nov 75 (309)	none	none	Failed soon after deployment
4	1245/1273	71°N 135°W	3 Nov 75 (307)	308-640	308-640	



259
Figure 1. M/O Buoy
Trajectory (RAMS Platforms
1416/1420). There are
20 days between asterisks.
Oceanographic data ques-
tionable after day 430.



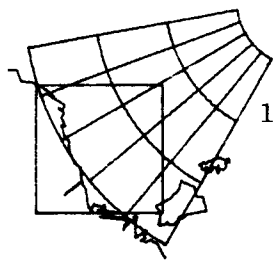
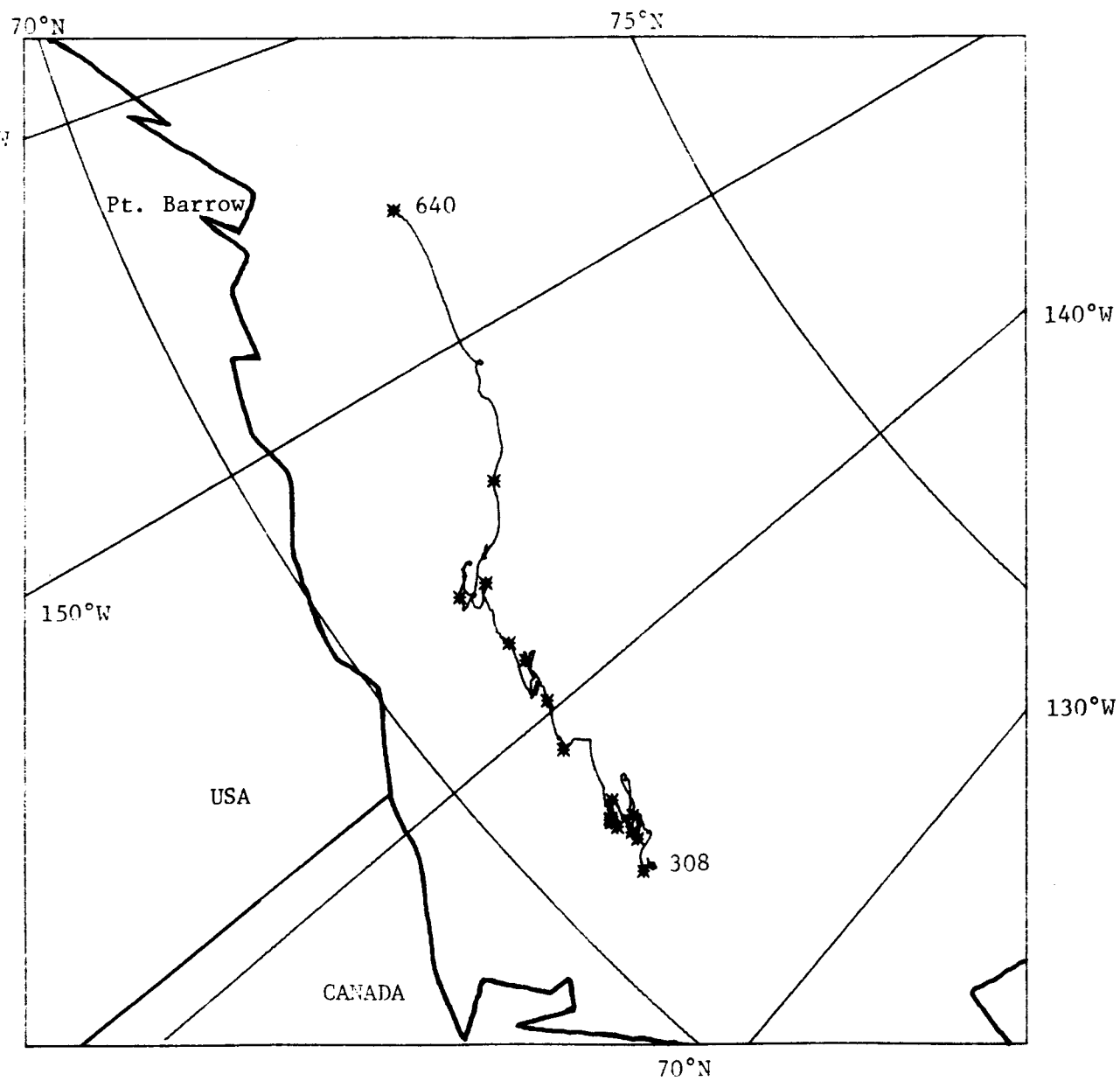


Figure 2. M/O Buoy
Trajectory (RAMS Platform
1245/1273).

260



8

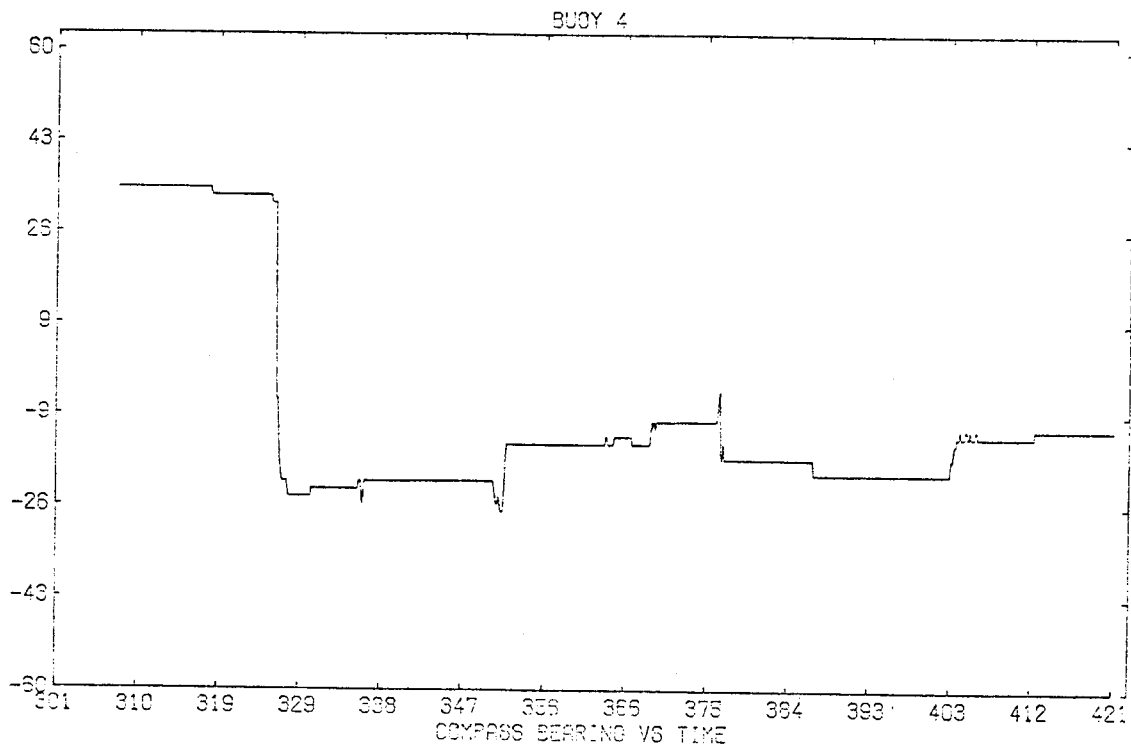
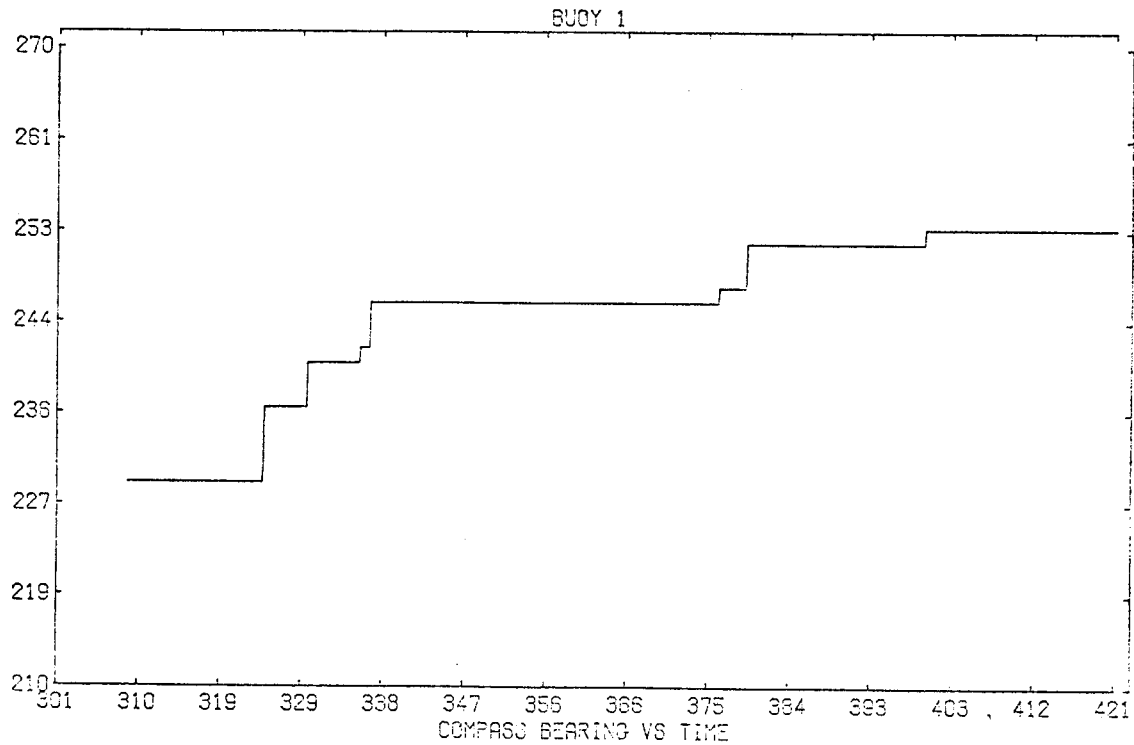


Figure 3. Magnetic Azimuth Buoys 1 and 4, Day 301 to 421 (28 Oct. 75 to 25 Feb. 75).

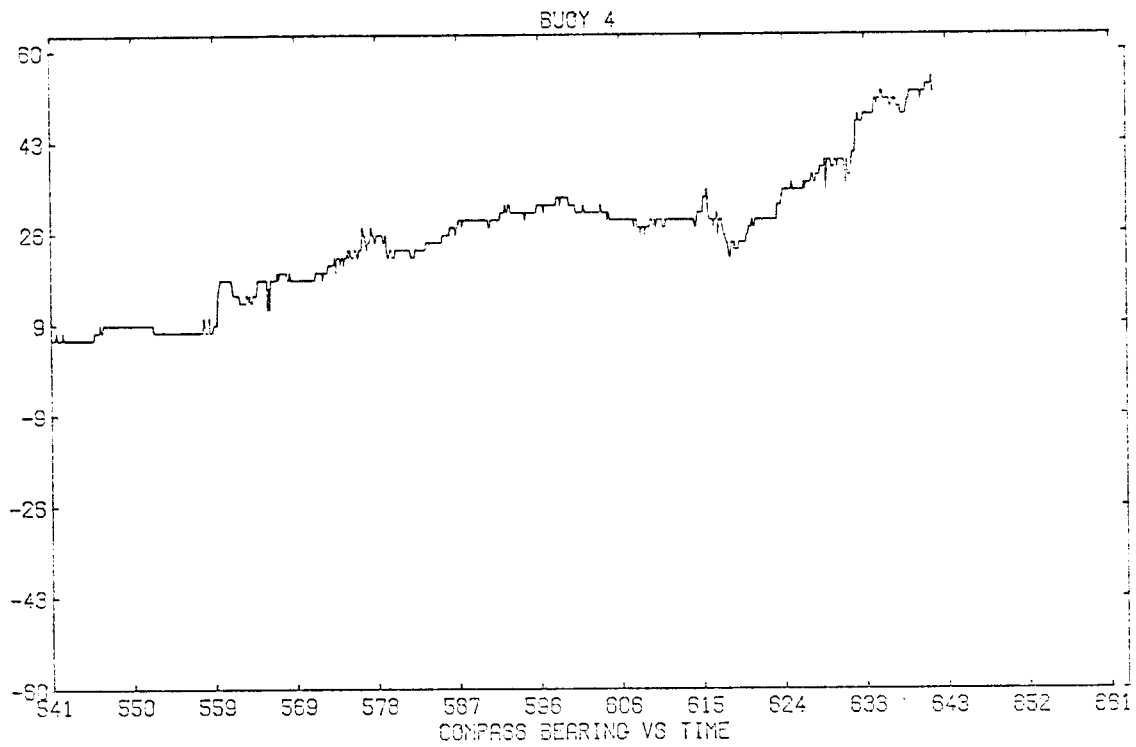
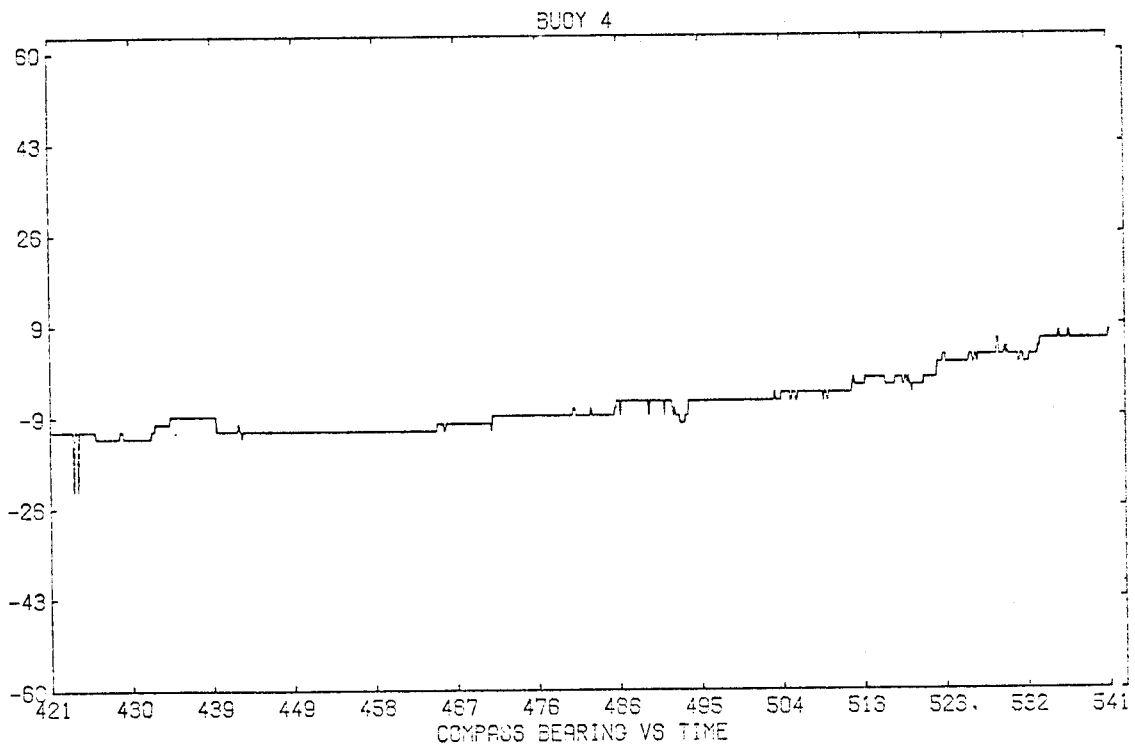


Figure 4. Magnetic Azimuth Buoy 4, Day 421-661 (25 February 76 to 22 October 76).

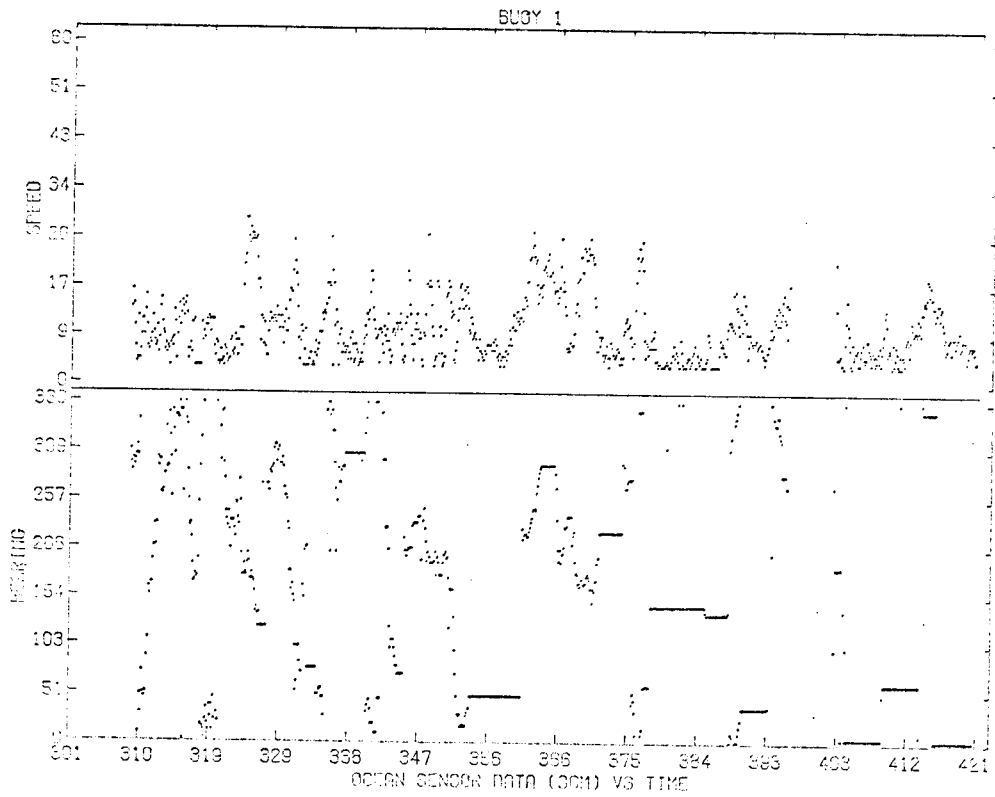
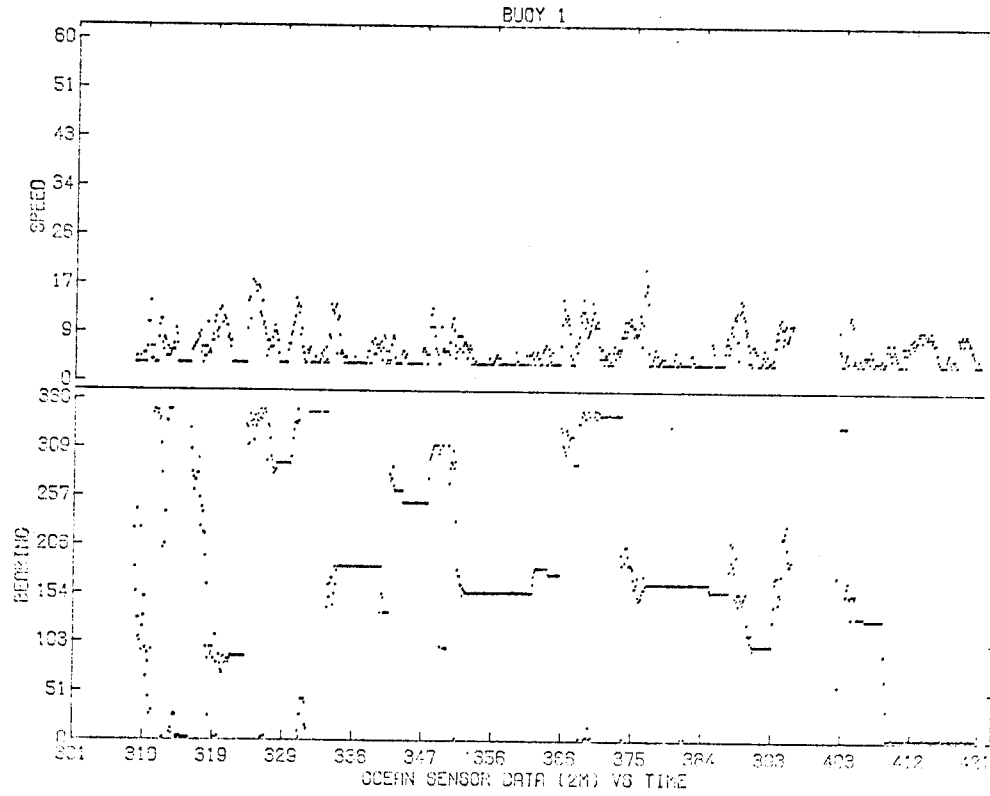


Figure 5. Current Meter Data from Buoy M/O 1, 28 October 75 to 25 February 76. Speed is in cm/s, bearing is degrees clockwise from buoy azimuth.

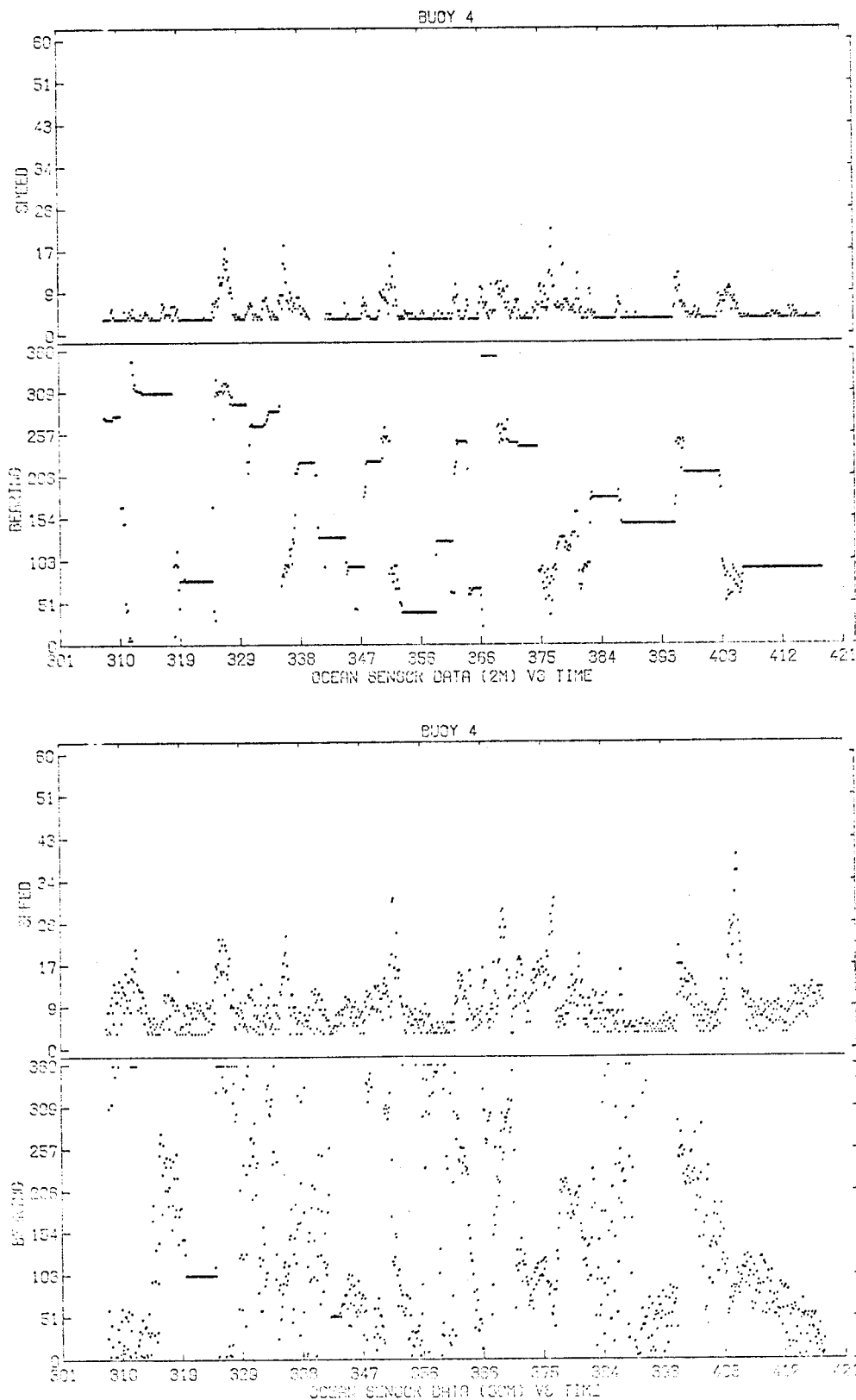


Figure 6. Current Meter Data from Buoy M/O 4, 28 October 75 to 25 February 76.

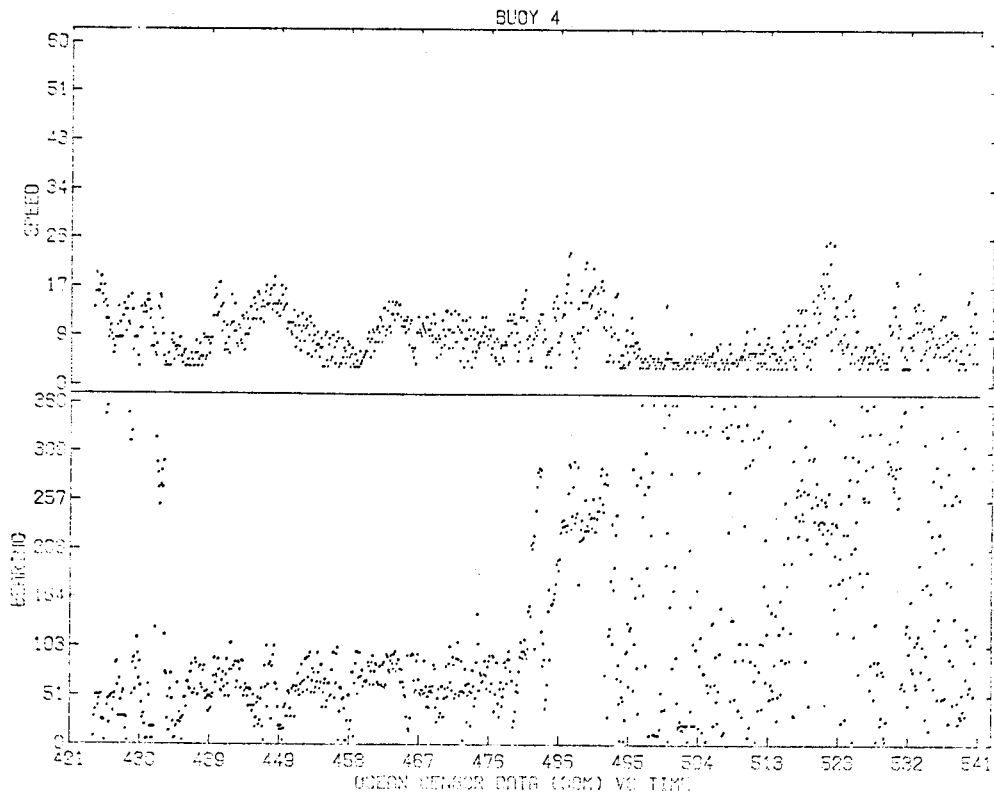
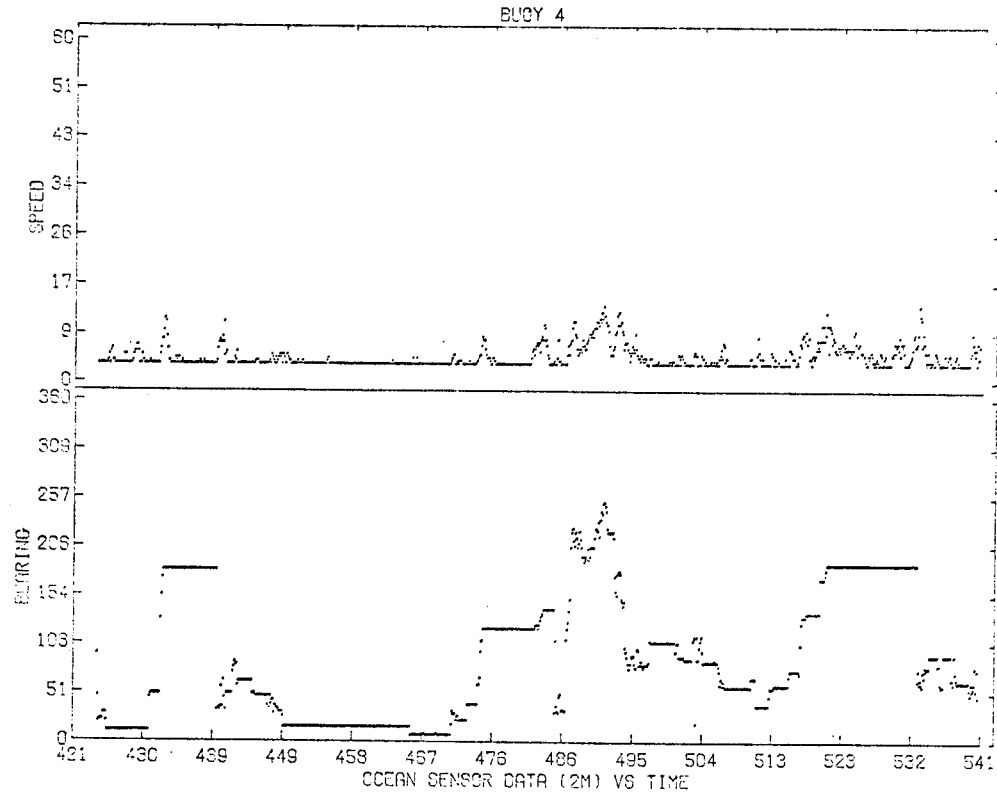


Figure 7. Current Meter Data from Buoy M/O 4, 25 February 76 to 24 June 76.

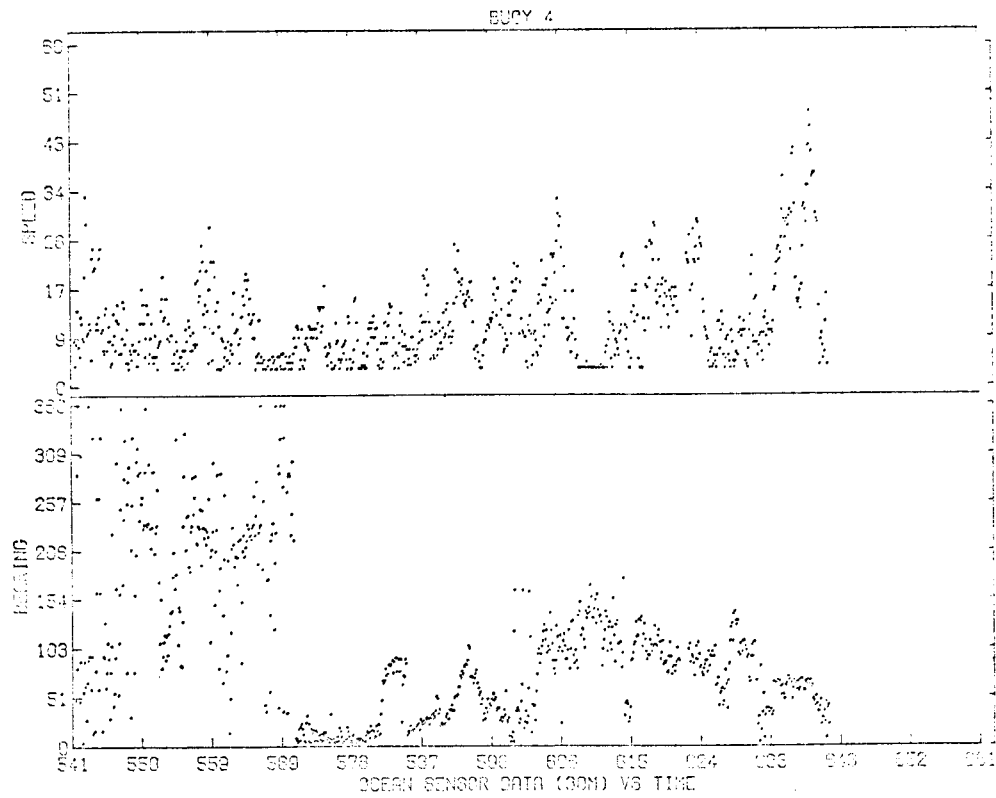
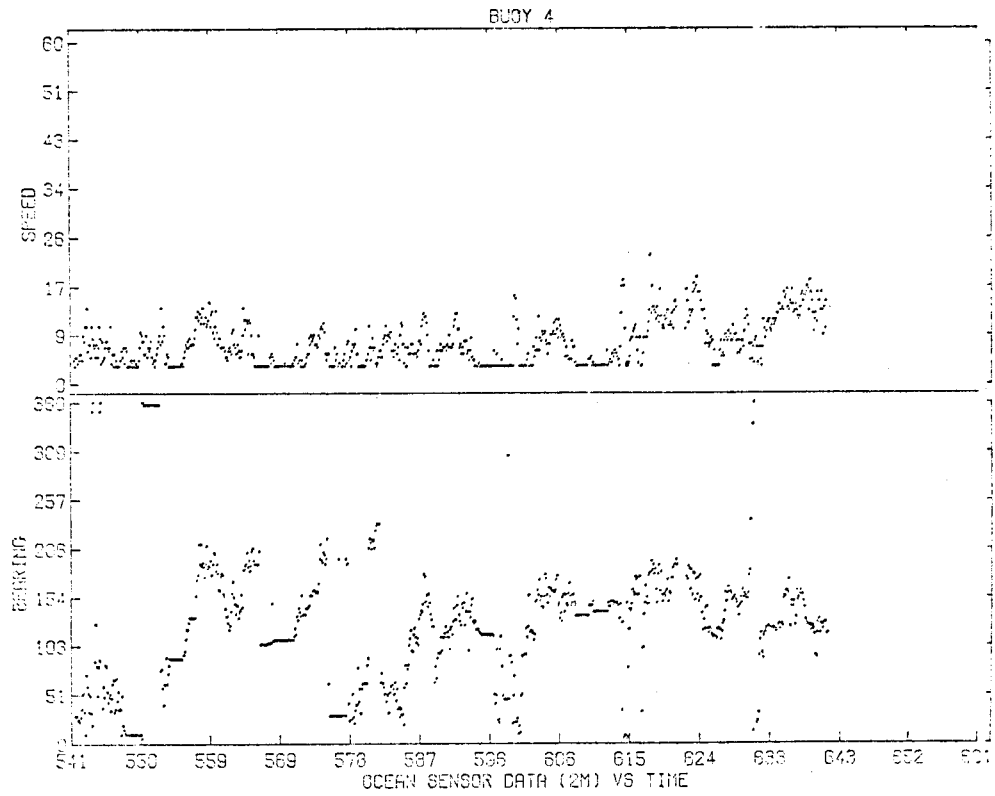


Figure 8. Current Meter Data from Buoy M/O 4, 24 June 76 to 22 October 76.

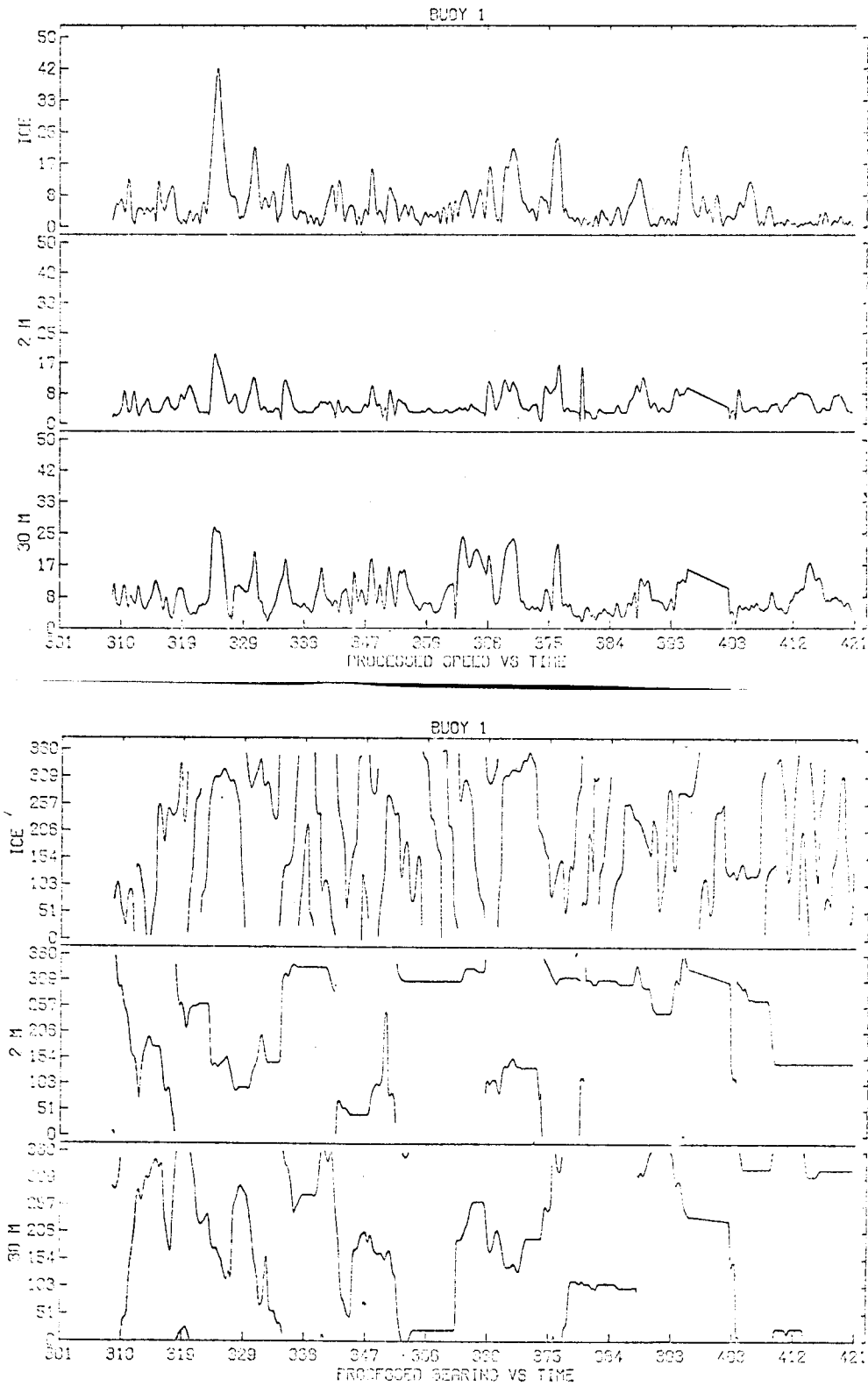


Figure 9. Smoothed and Corrected Data, Buoy M/O 1. Speed is cm/s, bearing is degrees clockwise from true north. Current data are apparent speed and direction relative to the drifting buoy.

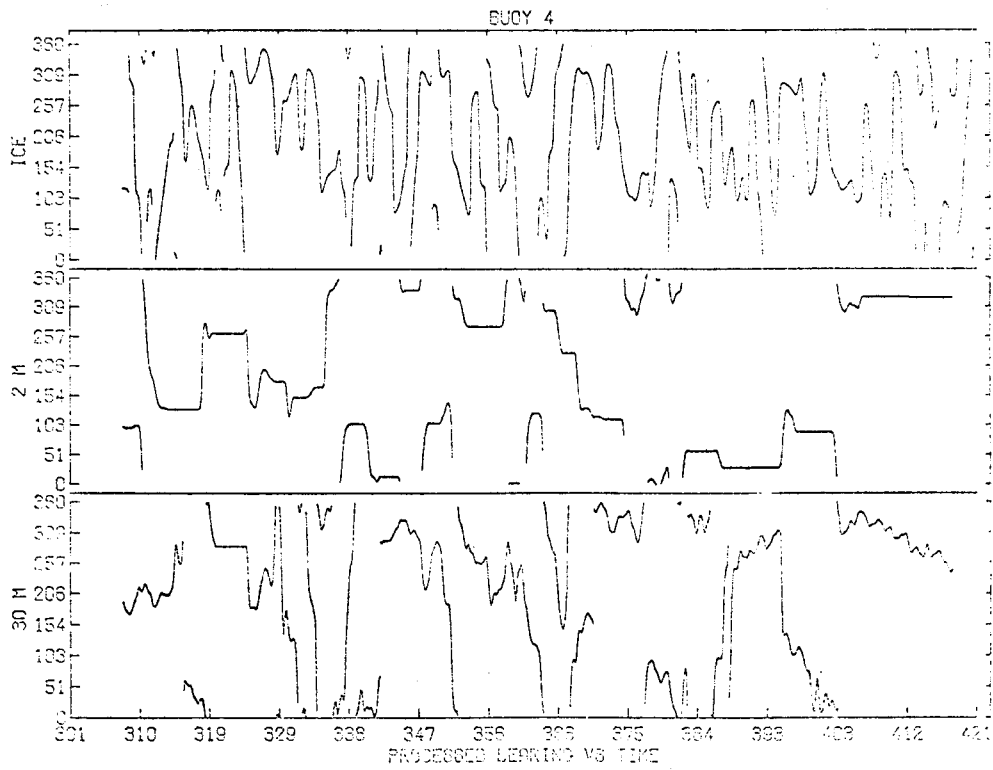
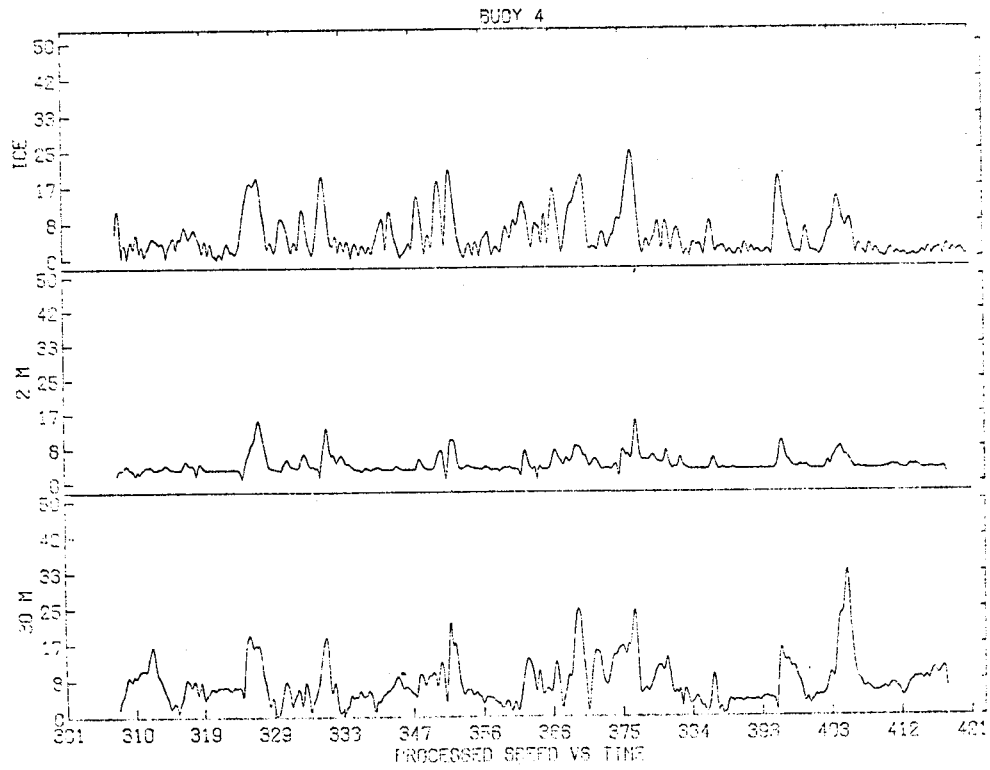


Figure 10. Smoothed and Corrected Data, Buoy M/O 4.

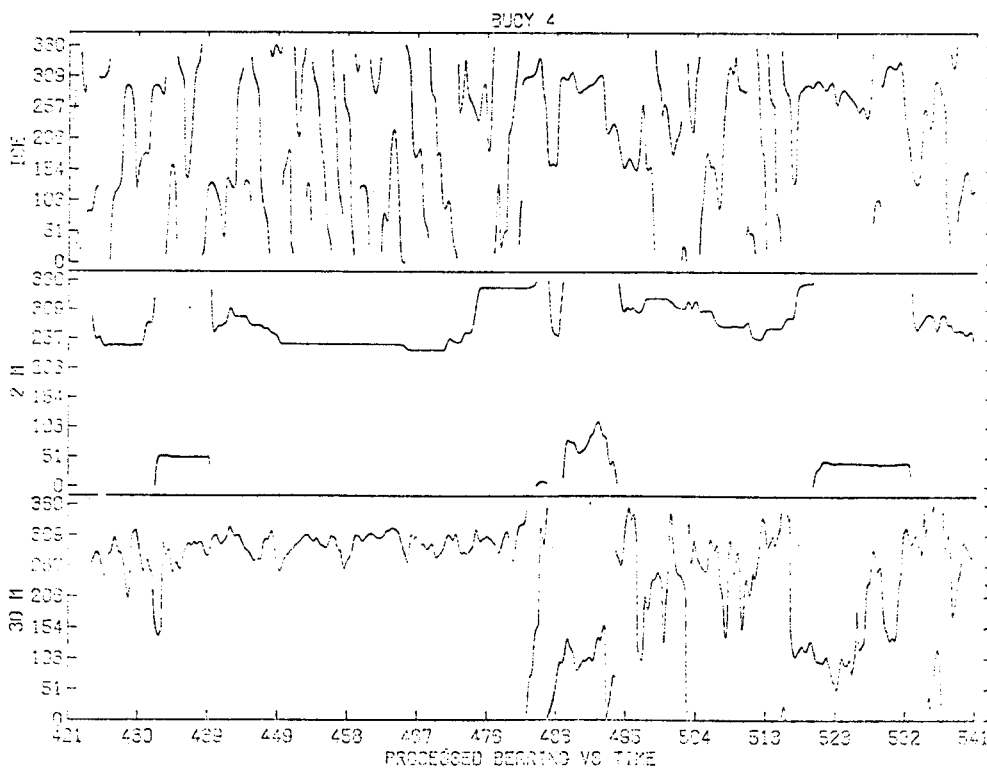
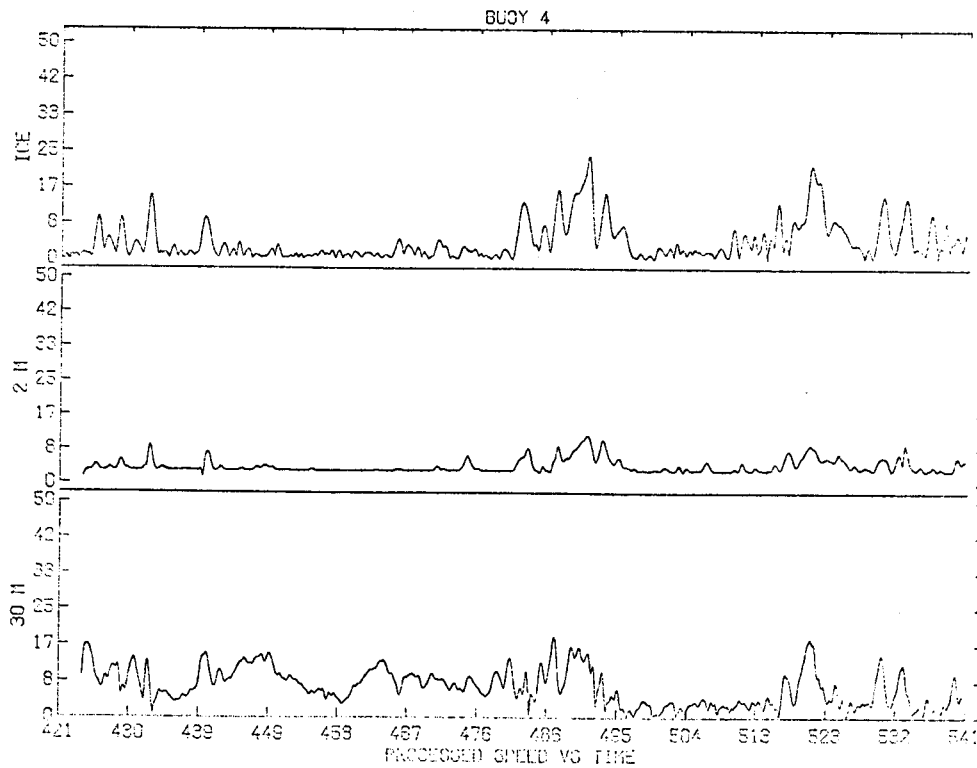


Figure 11. Smoothed and Corrected Data, Buoy M/O 4.

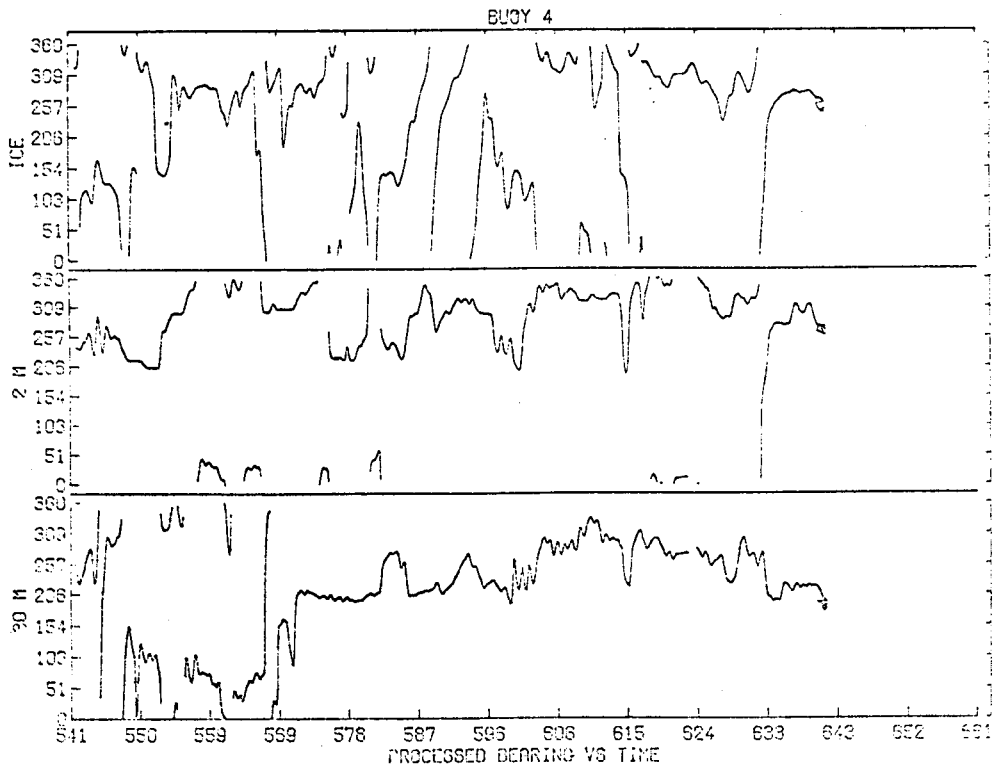
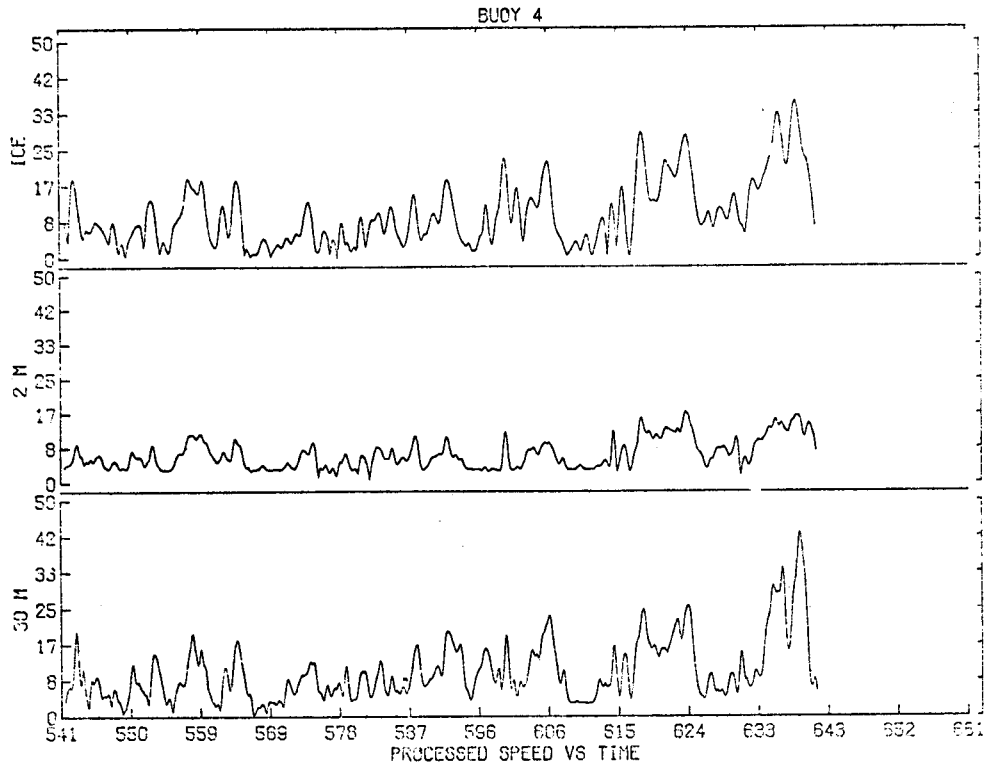


Figure 12. Smoothed and Corrected Data, Buoy M/O 4.

APPENDIX 3

WINTER ICE DYNAMICS IN THE NEARSHORE BEAUFORT SEA

by

Robert S. Pritchard

Max D. Coon

Miles G. McPhee

Eric Leavitt

March 1977

ABSTRACT

Ice conditions and motion in the nearshore Beaufort Sea from 27 January to 3 February, 1976 were strongly affected by ice stresses. We chose to simulate this response using the AIDJEX model. There is no motion during the first two days. When motions begin, they are westward. There is a time lag with ice in the eastern portion responding later. In the nearshore a fast ice region exists that is separated from the moving pack by a discontinuity. These conditions are verified by NOAA satellite imagery and data from drifting buoys and AIDJEX manned camps. The model is shown to simulate these features accurately, including the velocity discontinuity. This test of the AIDJEX model shows that we understand how ice responds on the large scale to driving forces and are able to describe this relationship at times when the ice stress exerts a dominant influence on the response. This model allows us to use winds (including the large set of historical winds) to determine ice velocity (and trajectories) and to estimate the large-scale average forces that pack ice may exert.

INTRODUCTION

This report describes the ice conditions and dynamics in the Beaufort Sea from January 27 through February 3, 1976. In addition to describing observed response of the atmosphere, ice, and ocean, we present a simulation of the ice conditions using the AIDJEX ice model. The time period was chosen because the ice dynamics conditions and motion are very interesting and because there is a considerable amount of high quality data from the AIDJEX program taken during this period of time. The motion of the ice during this period is greatly influenced by the internal stress in the ice pack. A flaw lead is developed along the north coast of Alaska, extending from Pt. Barrow to the Mackenzie Delta. Shoreward of the flaw lead the ice has very little motion; however, seaward of this lead the ice shows

appreciable motion. However, even in the regions where there is appreciable motion the amount and direction of it is greatly influenced by the internal stress. A detailed description of these conditions is given in this report.

In Figure 1 we show the region of interest together with the position of data stations for the AIDJEX program [the data station numbers shown in Figure 1 are the same as those used by Thorndike and Cheung (1977) and in Appendix 1 to report on sea ice motions observed during AIDJEX and as part of this work]. Stations numbered 1, 3 and 2 were manned camps where extensive measurements in the atmospheric and oceanic boundary layers were taken. These camps are also identified by radio call names of Caribou, Snow Bird and Blue Fox, respectively. We have used directly the positions and barometric pressure measured at each camp. The data from the AIDJEX stations and NOAA satellite imagery are used in the next section of this report to describe the ice conditions during the time period in question.

A simulation of the ice dynamics for the region shown in Figure 1 has been made using the AIDJEX ice model. In the simulation, part of the data from AIDJEX stations is used to drive the model and the remaining data are used to verify the quality of the simulation.

ICE CONDITIONS

Daily velocity (average velocity during a day) is shown for eight days for all stations in Figure 2. On January 27 and 28 there is essentially no motion of any station. As will be shown later, there is appreciable air stress applied to the ice during those days. On January 29 the westernmost stations begin to move and over days January 30 and 31 there is a predominantly western motion of all stations except for those in the Alaskan nearshore area, where the stations have essentially no motion. During February 1, 2 and 3 the ice motion reverses. To obtain a more detailed view of how the ice motion develops during this time, velocity time

histories are shown for several of the stations in Figures 3 and 4. Figure 3 indicates the north-south and east-west components of the velocity for stations 3 (Snow Bird) and 2 (Blue Fox). The major velocity component during the time period is directed east-west. We also see that the east-west motion of station 3 begins a half day before station 2. This indicates that the disturbance that causes the motion travels from west to east across the Beaufort Sea and this disturbance produces motion in the ice which is predominantly in the east-west direction. This fact is supported by motions of other stations, e.g., 66 and 17, shown in Figure 2. Figure 4 shows the velocity time history for stations 44, 1 (Caribou), and 22. From Figure 1 it can be seen that these stations are aligned more or less north-south. The largest velocity component at stations 44 and 1 are directed in the east-west direction. We also see that station 1 and 44 begin their motion at essentially the same time (even though the peak occurs later). Again, the disturbance moves west to east. Station 22 shows no appreciable motion during the time period. This indicates that there is a large velocity difference between stations 1 and 22, which is, of course, what was seen in Figure 2 with the average daily velocities.

The characterization of the motion that emerges from Figures 2, 3 and 4 is also indicated clearly in NOAA satellite imagery for the period shown in Figures 5 through 8. All figures show the locations of the AIDJEX stations, and Figure 5 shows the outline of the area of interest. The NOAA images show a development of a series of cracks in the ice running essentially north-south from the flaw lead to the northernmost boundary of the area of interest. The flaw lead is not apparent in the earlier imagery, but by 2 February it is fully developed. It is at the flaw lead that the velocity discontinuity apparent in Figures 2 through 4 arises. It is the opening of cracks running north-south that produces the east-west motion of the stations indicated in Figures 2 through 4. The progression of these cracks occurring in time sequence from west to east across the area is consistent with the

velocity time histories shown in Figure 3.

In addition to examining the kinematics of the sea ice, it is important to look at forces acting on the sea ice. We begin by discussing the atmospheric boundary layer model used in the AIDJEX model simulation. Specifically, we discuss the procedure for determining the drag coefficient and turning angle from observed conditions. A similar discussion follows in the oceanic boundary layer. Finally, we study the forces acting on the ice and the resulting motions of the manned camps (Caribou and Blue Fox).

The barometric pressure field defines the atmospheric geostrophic flow \underline{U} . The planetary boundary layer relates the surface traction exerted by the atmosphere on the upper ice surface $\underline{\tau}_a$ to the geostrophic flow [Brown, 1976]. The air stress is computed as a quadratic function of $\|\underline{U}\|$ applied at an angle α counterclockwise from \underline{U} :

$$\underline{U} = \frac{1}{\rho_a f_c} \underline{k} \times \nabla p \quad (1)$$

$$\underline{\tau}_a = \rho_a C_D \|\underline{U}\| \underline{E}_a \underline{U} \quad (2)$$

where

ρ_a = air density,

$f_c = 14.15 \times 10^{-5} \text{ sec}^{-1}$ is the Coriolis parameter at 76°N latitude,

C_D = a dimensionless drag coefficient,

$$\underline{E}_a = \begin{pmatrix} \cos \alpha & -\sin \alpha \\ \sin \alpha & \cos \alpha \end{pmatrix},$$

\underline{k} = unit vector upward and orthogonal to plane of motion, and

∇p = horizontal gradient of barometric pressure p .

The surface air stress can also be related to the square of the mean wind speed measured at 10 meters above the ice surface

$$\tau_a = \rho_a C_{10} U_{10}^2 \quad (3)$$

where C_{10} is the 10 meter drag coefficient. Combining (2) and (3) we can express C_D as a function of C_{10} and the ratio U_{10}/G .

$$C_D = C_{10} (U_{10}/G)^2 \quad (4)$$

Some measurements of C_{10} from a site near camp Big Bear in spring 1975 are reported by Leavitt et al. (1977). The mean value of C_{10} was 1.3×10^{-3} but the measurements showed a variation with wind direction, from 1.0×10^{-3} to 1.5×10^{-3} . These measurements were taken over smooth floes and do not include the effect of "form" drag due to pressure ridges or rubble fields. For typical ice conditions in the Beaufort Sea Arya (1975) predicts that the drag due to ridges would be approximately equal to that over the smoother ice; for example, this would suggest $C_{10} = 2.6 \times 10^{-3}$. Carney and Leavitt (1977) have calculated air stress by integrating wind profiles through the boundary layer. These wind profiles were obtained by tracking the motion of balloons (pibals) as they ascended through the boundary layer. A preliminary estimate of U_{10} from these data is 2.7×10^{-3} , which agrees with Arya. The confidence limit on this estimate is 0.7×10^{-3} .

Preliminary analysis of pibal data and recorded surface winds for this period suggest $(U_{10}/G)^2 = .3$ and a turning angle $\alpha = 28^\circ$. These values are used to compute the drag coefficient

$$C_D = 0.8 \times 10^{-3} \quad (5)$$

which is used to compute air stress from the geostrophic wind for the simulation. Further comparisons between surface and geostrophic winds suggest that the mean turning angle for this period is 35° rather than 28° , but the standard deviation in this estimate is 15° . The value used is therefore within the range of uncertainty.

A comparison between geostrophic and surface wind derived stresses at each of the manned camps is shown in Figures 9-11. The agreement is excellent except for 30 and 31 January, when the east-west component of air stress obtained from geostrophic velocity exceeds the value determined from surface winds. Barometric pressures at the manned camps have been found to be in error by 0.1 mb at this time. Corrected values reduce the air stress by about 20%. The corrected air stress is shown in Figures 9-11. The uncorrected value has been used in the simulation presented later in this report.

Figure 12 shows a balance of dynamic forces derived from smoothed records of measured quantities at station Caribou sampled at 1200 GMT on 30 January. The force balance is a sum of air stress τ_a , water stress τ_w , Coriolis force f_c and a residual R where

$$\tau_a + \tau_w + f_c + R = 0 \quad (6)$$

The water stress is related to ice velocity by

$$\tau_w = \rho_w C_w \|v\| B v \quad (7)$$

$$B = \begin{pmatrix} \cos(\pi+\beta) & -\sin(\pi+\beta) \\ \sin(\pi+\beta) & \cos(\pi+\beta) \end{pmatrix}$$

and Coriolis force is

$$f_c = -m f_c k \times v$$

where ρ_w is the water density, m is the ice mass per unit area (300 gm cm^{-2}), f_c is the Coriolis parameter and β is the angle of turning. The resultant vector R is required to balance the equation and represents internal ice forces, sea tilt, and ice inertia. We have used summer conditions when the ice is not compact enough to support appreciable internal stress (i.e., R is small) to evaluate the water stress constants. The best results were obtained with $C_w = 0.0055$ and $\beta = 23^\circ$ using

observed surface winds and a drag coefficient $C_{10} = 0.0027$. During 30 January it is clear that \vec{R} is an appreciable force acting on the ice. Therefore, ice stress is an important factor in any simulation of this period.

Figures 13, 14 and 15 show time series of forces and velocities as measured at the three manned camps. In the top segment of each plot are shown the air stress component as determined from the 10-meter wind ($\tau_a = \rho_a C_{10} |\underline{U}_{10}| \underline{U}_{10}$), along with the negative component of the resultant vector, \vec{R} . From (6) and (7), it is clear that \vec{R} and τ_a will be equal and opposite when there is no ice motion, thus the plotted curves coincide for the first few days. When the ice velocity increases, the water drag and Coriolis force become increasingly important. We further analyze the forces by considering how the ice would behave if it were too weak to support an internal stress gradient. Then $\vec{R} = 0$ and (6) can be solved for the wind-driven velocity, \underline{v}_{wd} . Solutions for wind-driven drift are shown along with the measured velocities as the lower traces of each plot. Observed motions are constrained to an east-west direction by the ice stress. Wind-driven drift has a larger north-south component. This is also indicated by the sizable southward components of internal force on 30 January at Caribou (Figure 12) and Snow Bird even though there was practically no north-south component of surface wind.

An important question to ask is how much does the internal ice stress affect the trajectory of a given point? To this end, Figure 16 indicates the observed trajectory of station 1 (Caribou) and the wind-driven trajectory. It can be seen clearly that the difference between these trajectories is very large. At the end of the eight-day period there is a difference in position of approximately 25 kilometers. The internal ice stress has retarded the motion of the ice by this amount.

MATHEMATICAL MODEL

Conservation of momentum in this system accounts for air stress τ_a , water stress τ_w , divergence of ice stress $\nabla \cdot \sigma$ (σ is the Cauchy stress in excess of iso-static equilibrium integrated through the thickness in this two-dimensional material model), Coriolis acceleration $-mf_c \hat{k} \times \underline{v}$ and sea surface tilt ($mf_c \hat{k} \times \underline{v}_g$)

$$m\dot{\underline{v}} = \tau_a + \tau_w + \nabla \cdot \sigma - mf_c \hat{k} \times (\underline{v} - \underline{v}_g) \quad (8)$$

where m = mass per unit area, and $f_c = 14.15 \times 10^{-5} \text{ sec}^{-1}$ is the Coriolis parameter at 76°N latitude. The notation $(\dot{\quad})$ implies differentiation along the particle path and ∇ is the spatial gradient operator.

The oceanic boundary layer is represented by a quadratic drag law similar to that used in the oceanic boundary layer as shown in equation (7). Water drag, however, is a function of the ice velocity relative to the geostrophic current \underline{v}_g . The relationship is

$$\tau_w = \rho_w C_w \|\underline{v} - \underline{v}_g\| \underline{B} (\underline{v} - \underline{v}_g) \quad (9)$$

where all variables except \underline{v}_g have been defined previously. The geostrophic flow is assumed to be given by long-term mean observed values. In Figure 17 we present the values. Values at intermediate locations are computed by linear interpolation between values defined on the 75 km square grid.

The elastic-plastic constitutive law developed by the AIDJEX modeling group (Coon et al., 1974; Coon and Pritchard, 1974; Pritchard, 1975) relates stress to the deformations. We assume a stiff linear elastic response.

$$\underline{\sigma} = (M_1 - M_2) \hat{1} \text{ tr } \underline{\epsilon} + 2M_2 \underline{\epsilon} \quad (10)$$

where $\underline{\epsilon}$ is the elastic strain. Moduli used in each simulation are presented in Table 1. The moduli are large enough so that elastic strain cannot exceed 0.2

percent. The rate of change of elastic strain is determined from

$$\dot{\underline{e}} - \underline{W}\underline{e} + \underline{e}\underline{W} = \underline{D} - \underline{D}_p \quad (11)$$

where stretching $\underline{D} = 1/2(\underline{L} + \underline{L}^T)$ and spin $\underline{W} = 1/2(\underline{L} - \underline{L}^T)$ are obtained from the velocity gradient $\underline{L} = \nabla \underline{v}$. The plastic stretching \underline{D}_p is defined by the normal flow rule

$$\underline{D}_p = \lambda \frac{\partial \phi}{\partial \underline{g}} \quad (12)$$

where λ is a positive multiplier. Finally, the yield criterion

$$\phi(\underline{g}, p^*) \leq 0 \quad (13)$$

completes the description. The yield surface has been assumed to have the shape of a "squished teardrop" as shown in Figure 18. The family of curves has been normalized by p^* . The surfaces are defined by

$$\phi = \sigma_{II} + \tan b \sigma_I (1 + \sigma_I/p^*)^{1/2} \quad (14)$$

where b is the angle at which the curve approaches the origin ($\underline{g} = 0$). We have chosen $b = 30^\circ$ since this value has been found to be reasonable in previous simulations (Pritchard, Coon and McPhee, 1977). Yield strength p^* determines the size of the surface given by equation (14). For the set of simulations we have varied p^* as a parameter, setting it to a constant in each calculation. Thus, we have used a perfect plasticity model.

An important feature of the AIDJEX ice model is the ice thickness distribution. It is this variable that distinguishes ice conditions by describing the relative area covered by ice of each thickness. One of the properties of the ice model that depends on thickness distribution is the yield strength p^* . In our current state of thinking we believe that strengths found from thickness distributions are too low to allow realistic simulation of ice motion and deformation (Pritchard, 1977).

Therefore, we have bypassed this part of the model in favor of varying p^* as an arbitrary input parameter. The results of this work provide critical information on strength needed to simulate ice response and shall provide direction as we reformulate the redistribution function and the energetics argument that enable us to determine strength from the thickness distribution.

QUASI-STEADY NUMERICAL INTEGRATION

In previous simulations (Coon et al., 1976; Pritchard, Coon and McPhee, 1976) we have input air stress fields each six hours and boundary velocities each three hours with values determined at intermediate times by linear interpolation. Solutions were then obtained using a difference approximation known as the leapfrog scheme (Pritchard and Colony, 1976). This scheme requires numerical time steps on the order of 2 minutes for cells that are 40 km wide using typical elastic parameters, say $M_1 = 1/2 \times 10^{11}$ dyn cm^{-1} and $M_2 = 1/4 \times 10^{11}$ dyn cm^{-1} and an area mass density of $m = 300$ gm cm^{-2} . The Courant condition is assumed to give $c \Delta t / \Delta x \leq 1/2$ where $c = [(M_1 + M_2) / m]^{1/2}$. See Table 1 for values used in the simulation.

The fundamental concept of the AIDJEX model is that the physical processes of ridge building and lead formation are the mechanisms that provide deformation. The model further assumes that a large-scale spatial average (~ 100 km) is being described. We feel it is consistent with these ideas that temporal variations be resolved on scales of the order 1 day. To be more compatible with these concepts, we have modified the numerical scheme. We have averaged the air stress and the boundary velocity over each one-day interval and now seek to find the steady state response of the model to the constant driving forces. The ice acceleration may be rewritten

$$\dot{\vec{v}} = \vec{v}_t + \vec{L} \vec{v} \quad (15)$$

where \underline{v}_t is the partial derivative of velocity $\underline{v}(\underline{x}, t)$ with time and $\underline{L} \underline{v}$ represents advection. Since we seek steady solutions (by which we mean that velocity is constant, not zero), we see that an Eulerian formulation is simpler to visualize. In that case $\underline{v}_t = 0$. The contribution of advection to the momentum balance is an apparent force

$$\underline{f}_a = m \underline{L} \underline{v} \quad (16)$$

The magnitude is on the order of

$$\|f_a\| \leq m \|L\| \cdot \|v\| \quad (17)$$

where velocity gradient $\|L\| \approx 1 \times 10^{-5} \text{ sec}^{-1}$ in the marginal ice zone and velocity $\|v\| \approx 20 \text{ cm sec}^{-1}$ in the pack ice so that as a worst case

$$\|f_a\| \approx .06 \text{ dyn cm}^{-2} \quad (18)$$

which is an order of magnitude smaller than significant forces in equation (8).

Therefore, we neglect advection in the simulations.

For completeness, we must similarly evaluate the advection of elastic strain in equation (11). However, we have no accurate estimate of the spatial gradient of elastic strain. Therefore, without proof we neglect this advection term also, but note that the elastic response is as much a numerical artifact as a physical reality. Furthermore, elastic strains are constrained to be less than .2% by choosing moduli (M_1 and M_2) to be large. From these arguments we feel that the assumption is valid.

Our results show that some variations still occur during the last cycle of iteration. It is at this time that we are assuming the solution to have reached steady state. Forces appear to vary less than 0.1 dyn cm^{-2} during the last hour of iteration (approximately 60 cycles) and this difference is acceptable. Since the

quasi-steady concept is a new one, we have not felt justified in developing a criterion to decide when the solution has covered because we have only begun to decide whether or not we should continue the quasi-steady solution method. Present indications are that the method is an improvement over our previous scheme in which solutions vary continuously and we shall begin to look into the convergence question in more detail.

PROBLEM CONFIGURATION

The locations of 17 data buoys and three manned camps have been shown in Figure 1. We have chosen to use the four northernmost and the two westernmost buoys (one buoy common to both) to provide boundary conditions for the simulation. The boundary is assumed fixed to shore along the North Slope from Pt. Barrow east to Banks Island. The motion of each of the other two section of boundary is obtained using a spline interpolation polynomial with zero second derivatives at the end points. For example, a spline interpolation polynomial using four data buoys and a fixed point provides velocities at each grid point lying along the northern boundary of the grid. A generally rectangular grid is set up in the interior of the region. The interior points are chosen so that each additional buoy or camp lies either on a grid point or on a line to simplify interpolation of solutions for comparison. The fifteen interior stations allow us to test the performance of the model at reproducing observed motions. We have regenerated a grid for each day of the calculation because of the motion that occurs. This detail is necessary so that the computed results can be interpolated properly for direct comparison with observations.

RESULTS

Wind-driven drift velocity is presented in Figure 19. This velocity is obtained as a balance between all forces considered in the complete AIDJEX model except for

ice stress divergence. The wind-driven velocity is calculated at each point independent of information at surrounding points using the air stress fields shown in Figure 20. During 27 and 28 January when air stress was quite small over much of the domain and was less than about 2 dyn cm^{-2} near the Alaskan North Slope, the wind-driven velocity ranged from a low of about 5 cm sec^{-1} that reflected transport on the geostrophic ocean current to high speeds on the order of 25 cm sec^{-1} where the winds are largest. These results may be compared with the observed ice drift (Figure 2) which is essentially zero during these two days. During the next three days (29, 30 and 31 January) the winds rise and the air stress increases to a range of values on the order of $2\text{-}5 \text{ dyn cm}^{-2}$. The air stress is more nearly homogenous on each day blowing toward the west. The wind-driven drift shows most of the domain moving to the northwest at about $20\text{-}30 \text{ cm sec}^{-1}$. During the last two days the wind pattern within about 100 km of the Alaskan North Slope shows a steep gradient with wind-driven drift results either zero or turned northward. The speeds are larger than observed at these times but more striking is the fact that the ice was observed to drift westward but the wind-driven drift is to the northwest. During the last three days (1, 2 and 3 February) the winds fall off and turn northward and finally to the northeast. At these times the wind-driven drift generally follows the direction of the observed motion but speeds are typically twice as high as observed speeds. The most striking feature that is modeled poorly by wind-driven drift is the nearshore behavior when ice is motionless in a band nearly 200 km wide along the North Slope and separated by the flaw lead that appears as a velocity discontinuity in the observed motions (Figure 2) and the satellite imagery (Figures 5-8). Instead, the wind driven drift varies smoothly everywhere with spatial gradients dictated by gradients in the air stress field.

The ice model is included in the simulation so that the effect of ice stress divergence may be considered. We have performed the simulation three times during

the time interval 27 January - 3 February. During each of these simulations the yield strength p^* was held at a different constant value throughout the domain. The values are shown in Table 1. The intermediate yield strength of $p^* = 10^8$ dyn cm^{-1} was chosen to agree with the lower bound estimate of Pritchard (1977) during the time interval 10-24 February 1977, just 7 days after the simulation time chosen for the present study. Although a lower bound, the estimate is thought to be a reasonable estimate of the actual value. We have also used values an order of magnitude smaller and larger to see how sensitive the resulting motions are to such variations. For convenience of presentation, we shall first discuss the velocity calculated using the intermediate yield strength (Run 3C). Then we shall show the effect on the velocity field due to changing yield strength. Finally, we shall return to the best estimate to look in more detail at the deformation and stress fields that are obtained.

The sequence of modeled ice velocities determined with yield strength $p^* = 10^8$ dyn cm^{-1} is presented in Figure 21. The accuracy with which we have simulated velocity seems remarkable. The simulated velocity is to be compared with observed velocity at each available station as shown in Figure 2. During 27 and 28 January the model velocity is nearly zero throughout the domain, which agrees with observed motions. During 29 January as the winds rise we find motion to the northwest in the western half of the domain, which agrees with observed motions. Except for the two buoys at approximately 150 km northeast of Pt. Barrow, the velocity of each interior check buoy and manned camp is accurate to within a few centimeters per second. The discrepancy between the two nearshore buoys and model results is caused at least in part by the velocity profile assumed as a boundary condition. We have interpolated the boundary velocities between the five buoys along the boundary to input the velocity of each grid point. Furthermore, all points along the fixed shore have zero velocity. Therefore, the boundary velocity

smoothly approaches zero as we approach shore. This does not allow the large velocity gradients that are observed to appear near these regions. During 30 January the ice speed increases to about 20 cm sec^{-1} with the wind and the flow to the west. In the Alaska nearshore region steep gradients normal to the shoreline appear. The velocity out to about 80 km is small, comparing well with observed motions. To the east we find that the modeled velocity field continues to move with a lead opening along the shore at Banks Island. The observed velocity decays rapidly in the last 200 km of this region. It is possible that either inaccuracies in the winds, incorrect yield surface shape or the lack of tensile strength of the ice model could cause this error in the approximation. During 31 January, winds are similar to 30 January with the velocities being comparable also. By this day the region off Banks Island is observed to be moving at the same velocity as the area to the west. The most striking feature of the velocity field during 31 January is the region of fast ice along the U.S.-Canada north slope that is separated from the moving pack ice by an abrupt change in velocity--a discontinuity. As seen in Figure 2e, the three buoys within this region are stationary and nearby ones are moving rapidly. We interpret this discontinuity as the flaw lead reaching from Pt. Barrow to Banks Island. We have simulated the existence and location of this discontinuity accurately. Furthermore, the smooth velocity field in the pack ice is simulated accurately also. During the last three days of the simulation (1, 2 and 3 February) the details of the velocity field become less interesting but we find that the modeled velocity does come around and match the observed motions accurately. The comparison is accurate throughout the domain with negligible motions in the Alaskan nearshore correctly represented.

It is important to point out that while it is true that the prescribed boundary velocity has a strong influence on the resulting velocity field, the accurate representation of the velocity field throughout the interior of the domain could only

be achieved by a model that represents sea ice response correctly in a variety of deformation states. We shall demonstrate this point by simulating the response using the same plasticity model but with different values of yield strength.

In Figure 22 we present the set of eight velocity fields that result when a yield strength $p^* = 10^7$ dyn cm^{-1} is used (Run 3B). A comparison with wind-driven drift velocities (Figure 19) shows that velocities modeled by the low-strength yield surfaces are similar. In the interior the velocities compare within a few centimeters per second in magnitude and are oriented in approximately the same direction but turned consistently to the left by ice stress divergence by 10-20 degrees. Therefore, as with wind-driven drift, the weak ice model does not provide an accurate simulation of observed buoy and manned camp motions. For example, during the first two days when winds are too low to move the ice we find that the weak ice model instead allows motion. Furthermore, at the boundaries where the velocity is specified by the buoy motions, we find the weak ice model allows a discontinuity to develop in the velocity field. The jump in velocity persists at almost all boundary locations for the entire eight-day period. Finally, the behavior of the weak ice model in the nearshore does not simulate the discontinuous behavior that is observed to exist. The modeled velocity field instead varies smoothly to the zero boundary value specified at the shore. This is not a reasonable representation of the fast ice zone seen in satellite imagery, in the buoy motions and in the modeled results with yield strength $p^* = 10^8$ dyn cm^{-1} (Run 3C).

To learn how sensitive modeled velocities are to changes in yield strength we felt it to be worthwhile also to perform a simulation with $p^* = 10^9$ dyn cm^{-1} (Run 3D), an order of magnitude larger than the estimated value. However, we felt it unnecessary to simulate all eight days. During the first two days (27 and 28 January) when winds were low and boundary velocities motionless, the model predicted

no motion with a yield strength of $p^* = 10^8$ dyn cm^{-1} . It is therefore not possible to change this velocity field by increasing yield strength. Since sea ice conditions were similar during the next three days (29, 30 and 31 January), we felt it necessary to simulate only one day. We have chosen 30 January as representative. The modeled velocity field during 30 January is presented in Figure 23 for the high yield strength $p^* = 10^9$ dyn cm^{-1} . Although the nearshore region has zero velocity it is seen that the width is far larger than the fast ice region defined by buoy motions (Figure 2). Approximately half of the entire domain is predicted to be at rest. As expected, the strength is so high that no discontinuous behavior is exhibited at boundaries, but in the interior modeled velocities do not compare closely with observed velocities. Results similar to those for the days 27-31 January are expected if the last three days are simulated (1-3 February).

In summary, we find that the perfect plasticity model may be used to simulate the observed velocity field quite accurately when the yield strength is estimated correctly. In particular, fast ice regions in the nearshore are accurately delineated and pack ice motion is accurately represented. The interface between these regions is narrow and is approximated by a discontinuity in the theoretical model (and by a rapid variation across 2-3 cells in the difference approximation). Furthermore, we have learned how sensitive modeled velocity fields are to variations in yield strength. Variations of an order of magnitude provide modeled velocities that are similar to wind-driven if too weak, and strongly dominated by boundary conditions if too strong.

Our attention turns back to the intermediate strength simulation (Run 3C). We now present a more detailed view of the results since the velocity field has been shown to be accurate.

The deformation is shown in Figure 24 for each of the eight days simulated using the strength estimated at $p^* = 10^8$ dyn cm^{-1} (Run 3C). We have presented

the stretching \underline{D} which is the symmetric part of the velocity gradient $\underline{L} = \nabla \underline{v}$. This is the variable considered as strain rate in small deformation theories and is the variable most descriptive of velocity differences throughout the domain. Within each cell of the numerical grid we have displayed the principal values of stretching oriented in the correct directions. Opening and closing in each direction are differentiated by dashed and solid lines, respectively. A line of 1 cm length on the figure represents a stretching value of 8×10^{-7} sec (approximately 8% per day). During the first two days (27 and 28 January) deformations are negligible as were the motions. During 29 January deformations begin to occur around the nearshore with opening at Banks Island and with both shearing and opening north of Alaska. We note that principal values of equal magnitude and opposite sign represent pure shearing--that is, shearing accompanied by no dilatation (area changes). During 30 and 31 January a similar pattern of deformation occurs but principal values are larger. Maximum shearing ($D_{II} = D_1 - D_2$, the difference between principal values) in the two cells approximately 100 km north of the U.S.-Canada land mass is about 16×10^{-7} sec ($\sim 16\%$ per day). This larger deformation is calculated in a narrow band about two computational cells wide (~ 80 km) and represents the velocity discontinuity that we discussed earlier (Figure 2). Since the numerical technique does not predict discontinuities explicitly, we must interpret these features by studying both the velocity and the deformation fields. It is seen that deformation in the center of the domain is an order of magnitude smaller than in the nearshore region. It should be pointed out that we had expected a region of uniaxial opening to occur along a line running generally northward from the shear zone. This is seen in the satellite images (Figures 5-8) in the form of leads running north to south. This feature of the observed conditions is not represented in the simulation. We shall return to the discrepancy later. During the last three days (1-3 February) the deformations do not show a simple and significant

pattern until 3 February when the northwest corner is seen to undergo shearing of about 6% per day, whereas the entire part of the domain near shore is not deforming.

The stress states simulated during the eight-day period are presented in Figure 25. At each node point we have determined the stress state as the average value found in the surrounding nodes. The principal stress values are shown proportional to line length in the directions in which they occur. A line length of 1 cm represents a value of stress equal to the yield strength of 10^8 dyn cm^{-1} . While we cannot test the stress state by direct comparison with observations, we can learn at least to some extent whether the stress state is physically reasonable. For example, we see that during 28 January - 1 February when ice is blown away from Banks Island that the stress is small in that region. This result is desirable since we expect little ice stress to arise in regions that are undergoing opening. Similarly, where the ice is being blown into a region the stress is seen to be larger (e.g., the western boundary on 30 January). However, we are not satisfied that principal values of stress in the center of the domain during 30 January are on the order of 5×10^7 dyn cm^{-1} . It is in this region that we have seen the leads opening in a generally north-south direction. We find it difficult to understand how stress may be transmitted across these leads in an east-west direction. We believe the shape of the yield surface must be modified to correct the stress state in this region. We have preliminary results of such a simulation using the triangular yield curve shown in Figure 26. Using the triangular yield curve allows the stress state to be uniaxial where plastic flow occurs. Preliminary results indicate that the principal values are aligned with the leads and a zero stress occurs normal to the leads. We further believe that the uniaxial opening deformation that is not observed in the present simulation (with a squished teardrop) will probably occur when the triangle yield surface is used. In summary, we find the stress fields to be reasonable except for one detail and we understand how that problem may be eliminated.

The force balance at each location provides important insights relating response to the driving forces. In Figure 27 we present the sequence of plots showing the forces acting at the node nearest the location of manned camp Caribou. In Figure 28 we present similar results for the node nearest the location of manned camp Blue Fox. The differences between the two plots depict spatial variations that occur between points that are about 150 km apart. During each day the results are similar but can vary by the order of 25 percent. In each plot of force balance we present the calculated ice drift as a dashed vector. The air stress τ_a , water stress τ_w , ice stress divergence f_G and Coriolis force f_c are also shown. In addition, we show a vector \underline{E} that is required to sum forces to zero. It is composed of sea surface tilt, of inertia which is a measure of the lack of convergence to steady state conditions and of plotting errors on the order of 0.1 dyn cm^{-2} . During 30 and 31 January when winds and ice motion are highest, the force balance plots are especially useful. Since these two days are similar we concentrate on results of only one day--30 January.

We confine our further attention to the Figure 27 and consider results at Caribou because these may be checked directly with Figure 12. It should be noted that during 30 January (see Figure 2d) the observed motion of the two manned camps Caribou and Snow Bird appear to be about 20-30 degrees counterclockwise from other nearby points. This appears from satellite images to occur because the camps are on a large single floe that is surrounded by several leads and is rotating. Therefore, we do not want to be confused by this anomalous motion. The comparison between modeled and observed forces is reasonably accurate. Many of the differences can be explained. First, we have already shown (Figure 9) that the geostrophic air stress input to the model is about 20% too large. This is shown also in the force balance. It is a cause of a large difference between f_G and \underline{R} (we note that stress divergence should be the largest contributor to \underline{R}) because a reduction of τ_a by 20% would cause

that vector difference to be subtracted from f_{σ} . Furthermore, the anomalous observed velocity of Caribou means that the modeled velocity is a better representation of large-scale motion than the motion measured at the camp. This observed velocity in turn is used to compute f_c and τ_w in Figure 12. Rotating each clockwise would better align the "observed" forces with computed results. The water stress computed from observations neglects geostrophic ocean currents which are about 5 cm sec^{-1} in the direction of motion. This accounts for the fact that the water stress in Figure 12 is about twice as large as modeled. The consequence of this neglect of v_g is to reduce R . Thus, halving τ_w automatically adds the vector difference to R because $R(\equiv -\tau_a - \tau_w - f_c)$. Consideration of these three corrections to the "observed" force balance reduces the discrepancy to about 0.5 dyn cm^{-2} . In that case f_{σ} and R are aligned to within about 20° . This comparison is felt to be excellent considering the uncertainty in each of the many components.

SUMMARY

The AIDJEX model has been shown to provide a physically realistic simulation of the dynamic response of sea ice to winds during the winter when ice stress is significant. Furthermore, the motion is seen to compare extremely well with observed motions of buoys and manned camps. In the nearshore regions the plasticity model represents fast ice areas. These areas are separated from the moving pack ice by rapid variations or discontinuities. The location of the flaw lead agrees with satellite images. A close look at deformations and stress shows that we may improve some details of the response by changing the yield surface shape and we expect to pursue that work soon.

In addition to gaining a greater scientific understanding by studying the results of this simulation, we are a large step closer to answering a question of more immediate concern. That is, how can we relate the ice drift to given wind

conditions? We have shown that the AIDJEX model, including air, ice and ocean components, allows the large-scale ice drift to be determined. Thus, it is now possible to use the large set of historical winds data to drive a model and determine what ice drift occurs in the wide variety of conditions. Since the amount of ice drift data is very sparse, this provides a dramatic increase in our knowledge of ice trajectories.

Ice trajectories are not the only variables that become better known as a result of this modeling effort. The stress state in the ice cover is also important and our model also allows stress to be studied. The stress in the AIDJEX model is interpreted as the large-scale average of the forces that are transmitted between ice floes on the small scale. Although much work remains to relate the large-scale stress to forces that may be exerted on an individual ship or marine structure, we are sure that the large-scale stress is an indicator of relative size of those forces.

ACKNOWLEDGEMENTS

We thank R. T. Hall and A. S. Thorndike for help in preparing NOAA satellite images and manned camp motion data. In addition, the help of D. R. Thomas and L. Harris in making the computer calculations and graphics is appreciated.

REFERENCES

- Arya, S. P. S. 1975. A drag partition theory for determining the large-scale roughness parameter and wind stress on arctic pack ice. *AIDJEX Bull. No. 28*: 29-47.
- Brown, R. A. 1976. The resistance law. *AIDJEX Bull. No. 31*:21-31.
- Carsey, F. D. and E. Leavitt. 1977. Pibal acoustic radar data measurements and computation of air stress over pack ice. To appear in *AIDJEX Bull. No. 36*.
- Coon, M. D., R. Colony, R. S. Pritchard and D. A. Rothrock. 1976. Calculations to test a pack ice model. In *Numerical methods in geomechanics*, Vol. II., ed. C. S. Desai, pp. 1210-1227. New York: American Society of Civil Engineers.
- Coon, M. D., G. A. Maykut, R. S. Pritchard, D. A. Rothrock and A. S. Thorndike. 1974. Modeling the pack ice as an elastic-plastic material. *AIDJEX Bull. No. 24*:1-106.
- Coon, M. D. and R. S. Pritchard. 1974. Application of an elastic-plastic model of arctic pack ice. In *Coast and Shelf of the Beaufort Sea*, ed. J. C. Reid and J. E. Sater, pp. 173-193. Arlington, Virginia: Arctic Institute of North America.
- Leavitt, E., D. Bell, M. Clarke, R. Andersen and C. Paulson. 1977. Computations of air stress and sensible heat fluxes from surface layer profile data, AIDJEX 1975. To appear in *AIDJEX Bull. No. 36*.
- Pritchard, R. S. 1975. An elastic-plastic constitutive law for sea ice. *Journ. Appl. Mech.*, Vol. 42, No. 2:379-384.
- _____. 1977. An estimate of the strength of arctic pack ice. *AIDJEX Bull. No. 34*:94-113.
- Pritchard, R. S. and R. Colony. 1976. A difference scheme for the AIDJEX sea ice model. In *Numerical methods in geomechanics*, Vol. II, ed. C. S. Desai, pp. 1194-1209. New York: American Society of Civil Engineers.
- Pritchard, R. S., M. D. Coon and M. G. McPhee. 1977. Simulation of sea ice dynamics during AIDJEX. *AIDJEX Bull. No. 34*:73-93.
- Thorndike, A. S. and J. Y. Cheung. 1977. AIDJEX measurements of sea ice motion, 11 April 1975 to 14 May 1976. *AIDJEX Bull. No. 35*:1-149.

TABLE 1. MODEL PARAMETERS FOR VARIOUS SIMULATIONS

Parameter		Run Identifier		
Name	Symbol (Units)	Run 3B	Run 3C	Run 3D
Strength	p^* (dyn cm ⁻¹)	10^7	10^8	10^9
Bulk Modulus	M_1 (dyn cm ⁻¹)	0.5×10^{10}	0.5×10^{11}	0.5×10^{12}
Shear Modulus	M_2 (dyn cm ⁻¹)	0.25×10^{10}	0.25×10^{10}	0.25×10^{12}
Time Step	Δt (sec)	300	120	40
Mean Thickness	m (gm cm ⁻²)	300	300	300

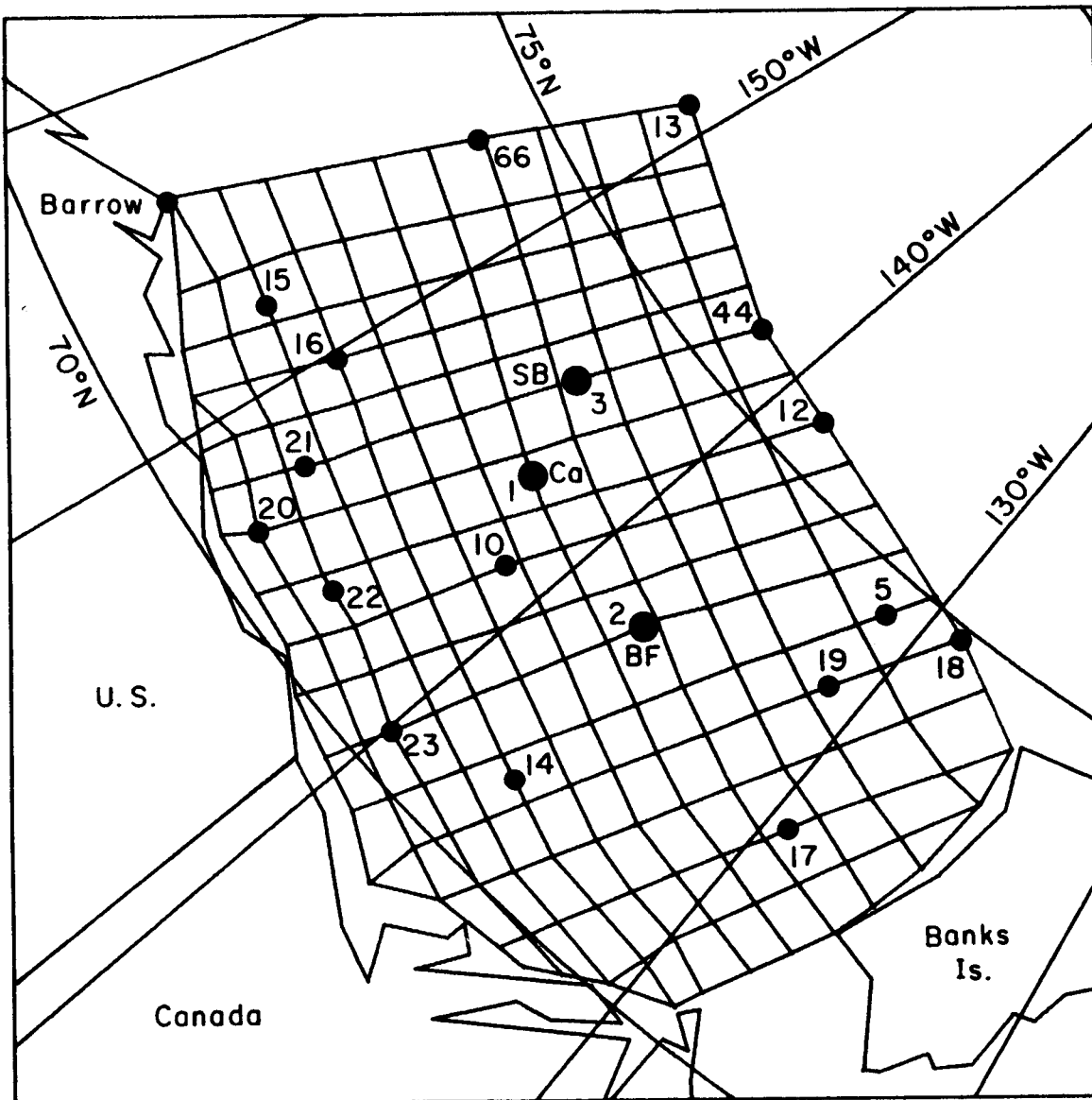
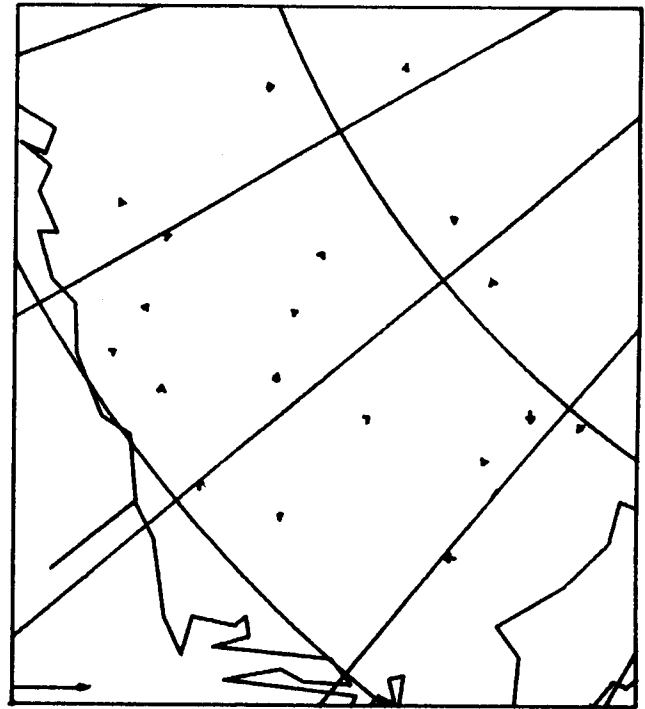


Figure 1. Numerical Grid with Manned Camp and Buoy Locations. Station numbers are consistent with Thronkide and Cheung (Appendix 1). Manned camps are identified with the following station numbers: 1 - Caribou; 3 - Snow Bird; 2 - Blue Fox.



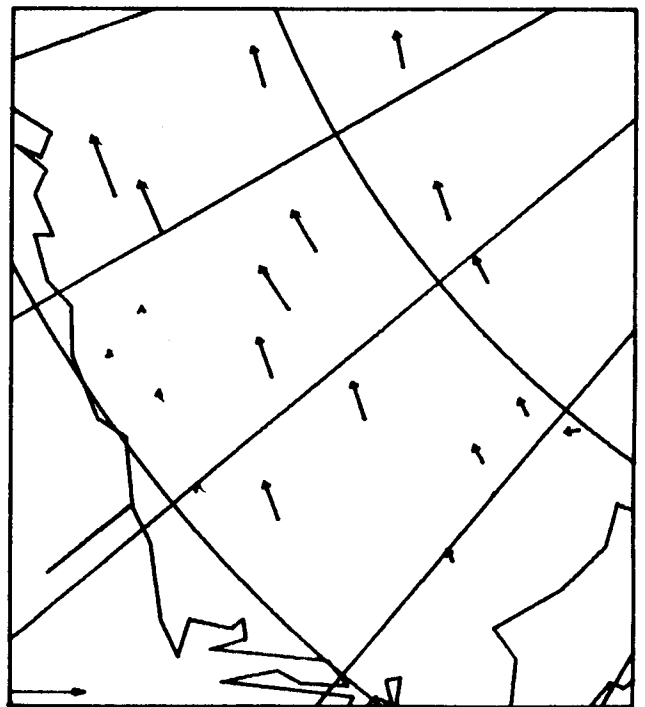
a) 27 January



b) 28 January

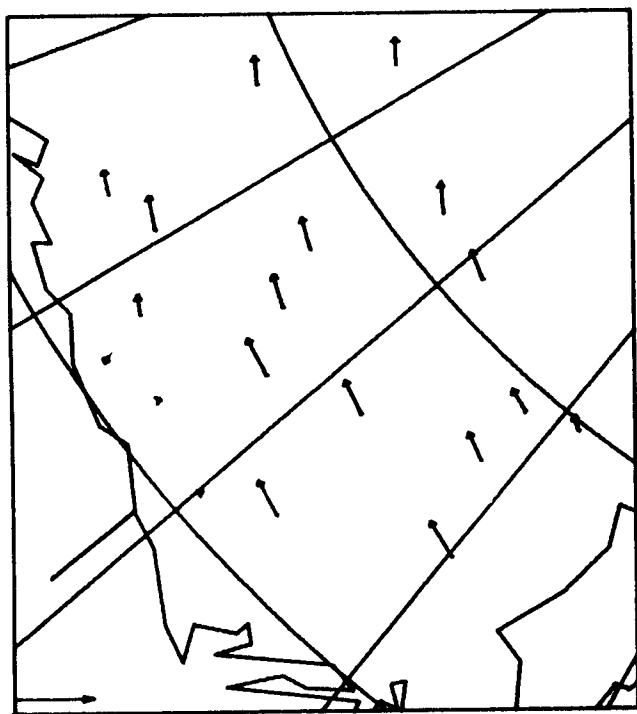


c) 29 January



d) 30 January

Figure 2. Daily Averages of Data Buoy and Manned Camp Velocities. Scale vector is 25 cm sec^{-1} . The U.S. and Canadian coastline compares with the model boundary.



e) 31 January



f) 1 February



g) 2 February



h) 3 February

Figure 2.(cont.) Daily Averages of Data Buoy and Manned Camp Velocities. Scale vector is 25 cm sec^{-1} . The U.S. and Canadian coastline compares with the model boundary.

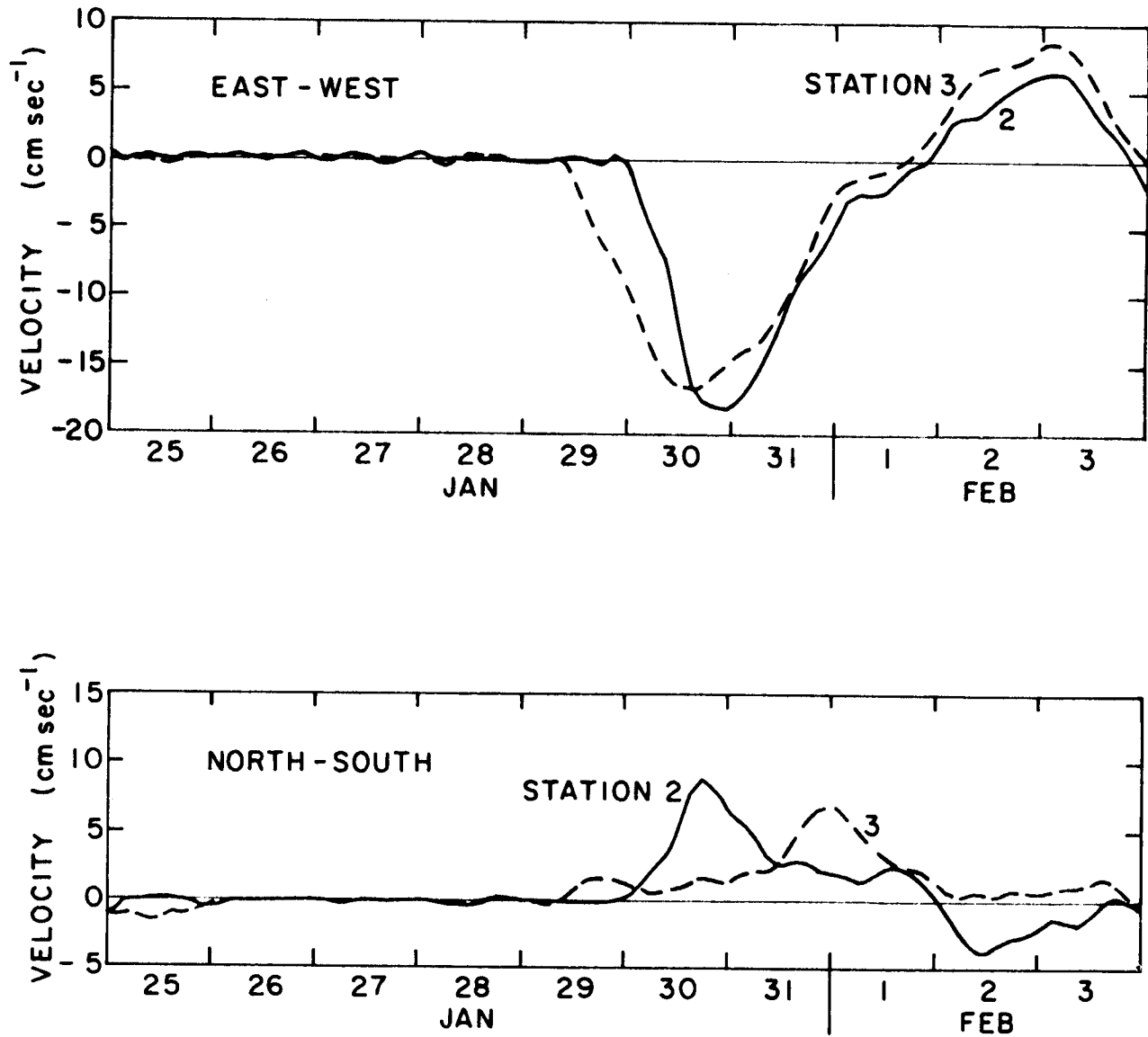


Figure 3. Time History of Observed Velocity from Data Buoys at Stations 3 (Snow Bird) and 2 (Blue Fox). Components at each location are east and north.

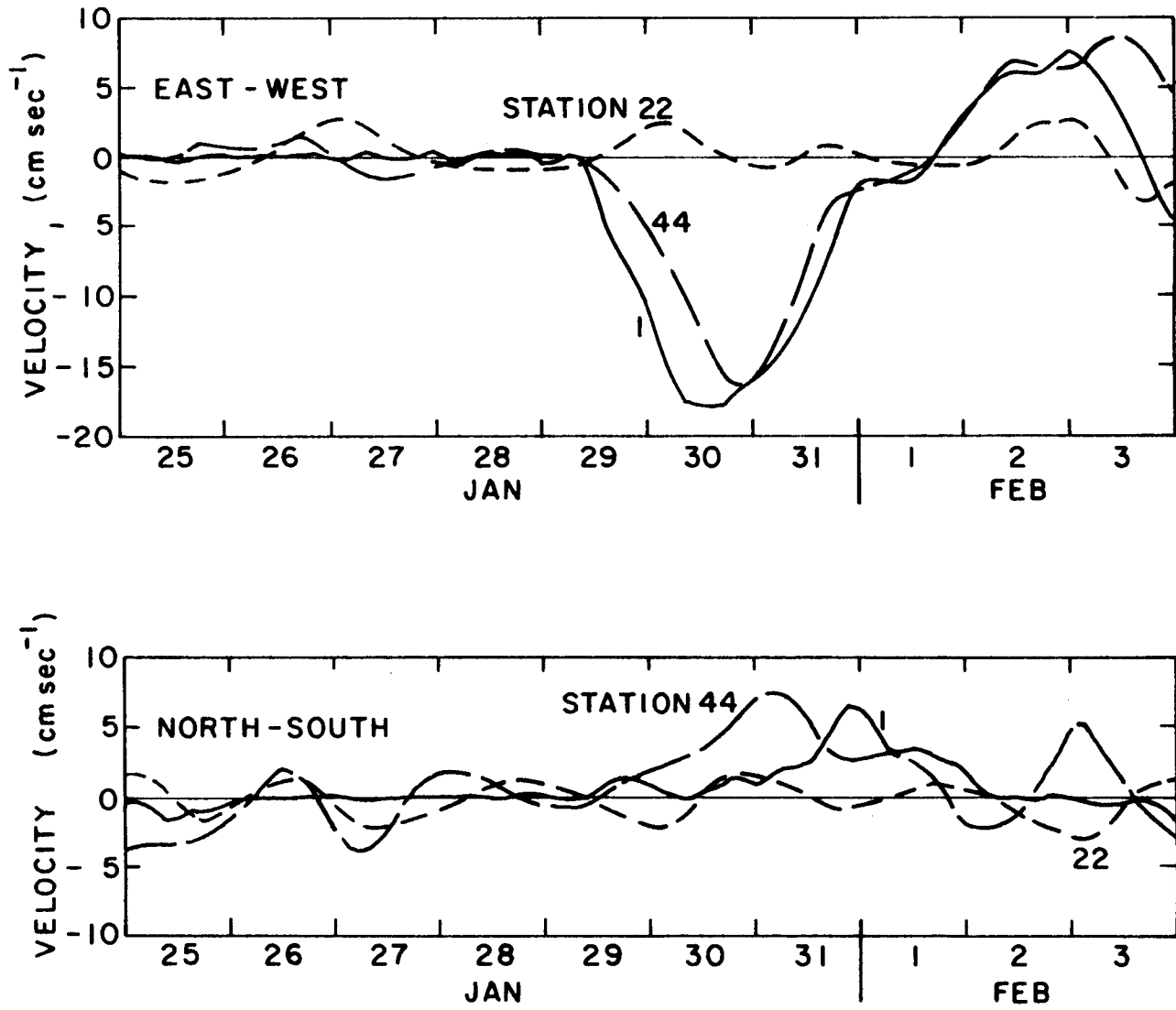


Figure 4. Time History of Observed Velocity from Data Buoys at Stations 1 (Caribou), 22 and 44. Components at each location are east and north.

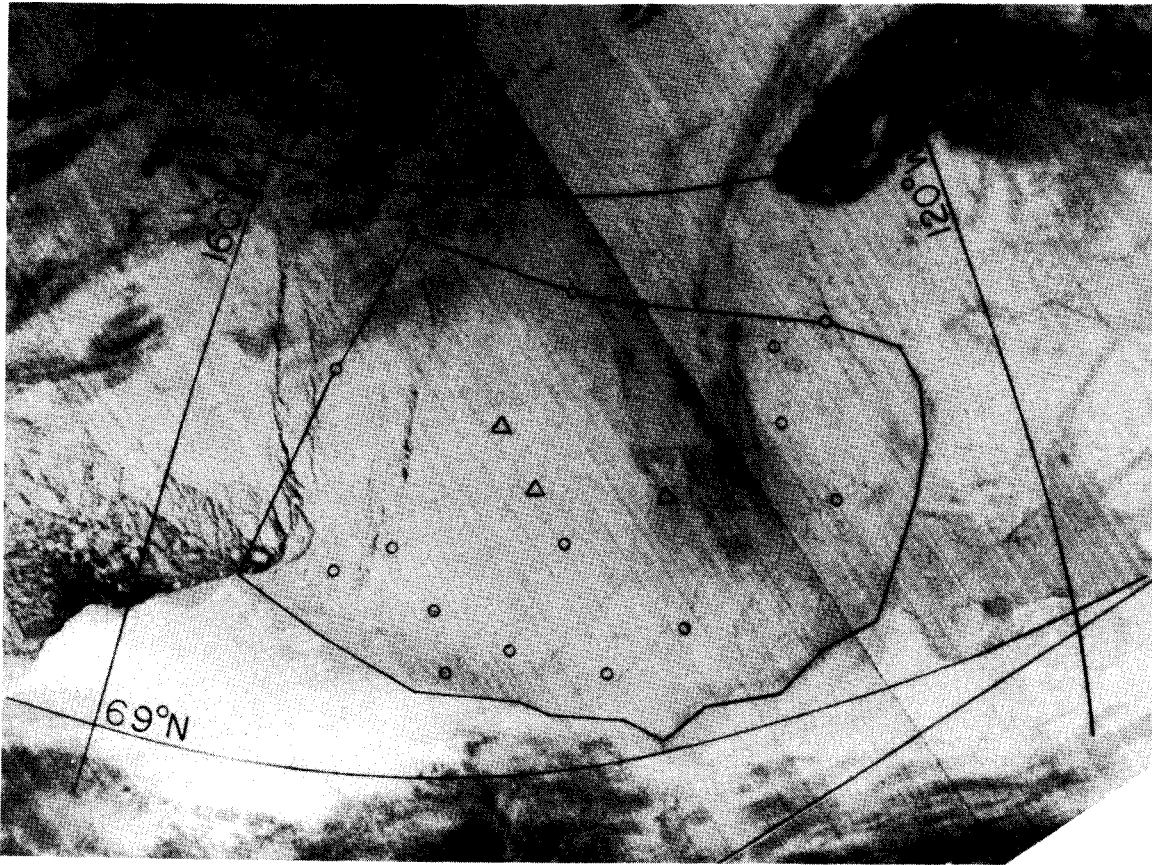


Figure 5. Reproduction of NOAA 4, IR-VHRR Images (orbit number 5487, frames I1F0001 and I2F2238) Covering the Simulation Region on 27 January 1976 at Approximately 2100 GMT. The boundary of the numerical grid (Figure 1) is shown. Triangles and circles indicate locations of manned camps and data buoys, respectively.

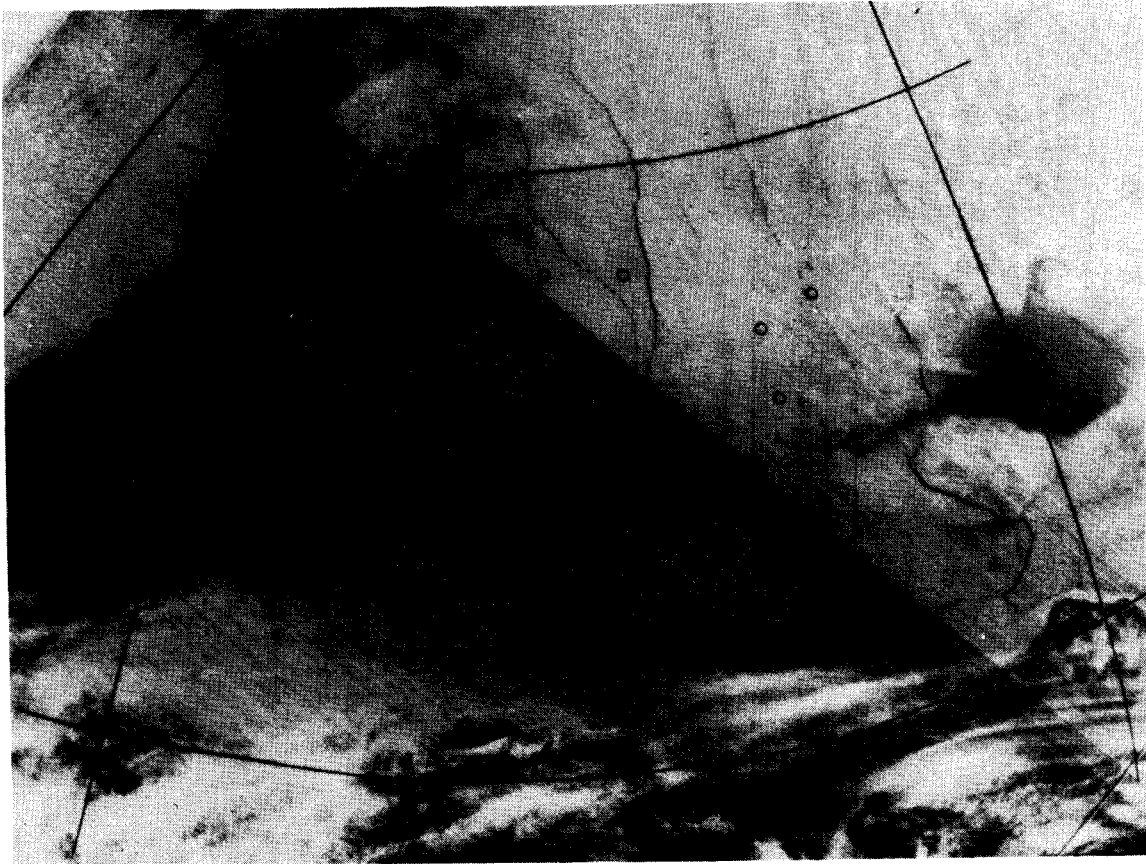


Figure 6. Reproduction of NOAA 4, IR-VHRR Images (orbit number 5524, frames I1F0001 and I2F2238) Covering the Simulation Region on 30 January 1976 at Approximately 2100 GMT. Triangles and circles indicate locations of manned camps and data buoys, respectively.



Figure 7. Reproduction of NOAA 4, IR-VHRR Images (orbit number 5549, frames 11F0001 and 12F2238) Covering the Simulation Region on 1 February 1976 at Approximately 2100 GMT. Triangles and circles indicate locations of manned camps and data buoys, respectively.

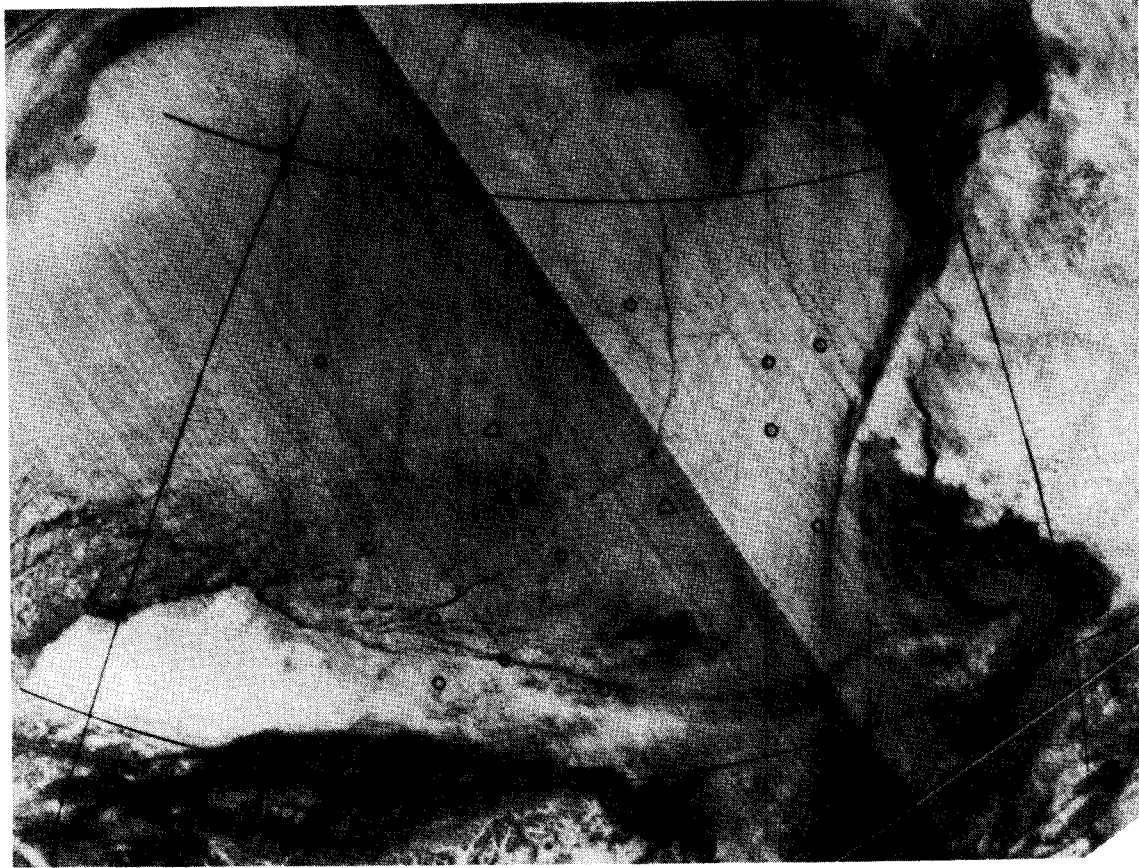


Figure 8. Reproductions of NOAA 4, IR-VHRR Images (orbit number 5562, frames I1F0001 and I2F2238) Covering the Simulation Region on 2 February 1976 at Approximately 2100 GMT. Triangles and circles indicate locations of manned camps and data buoys, respectively.

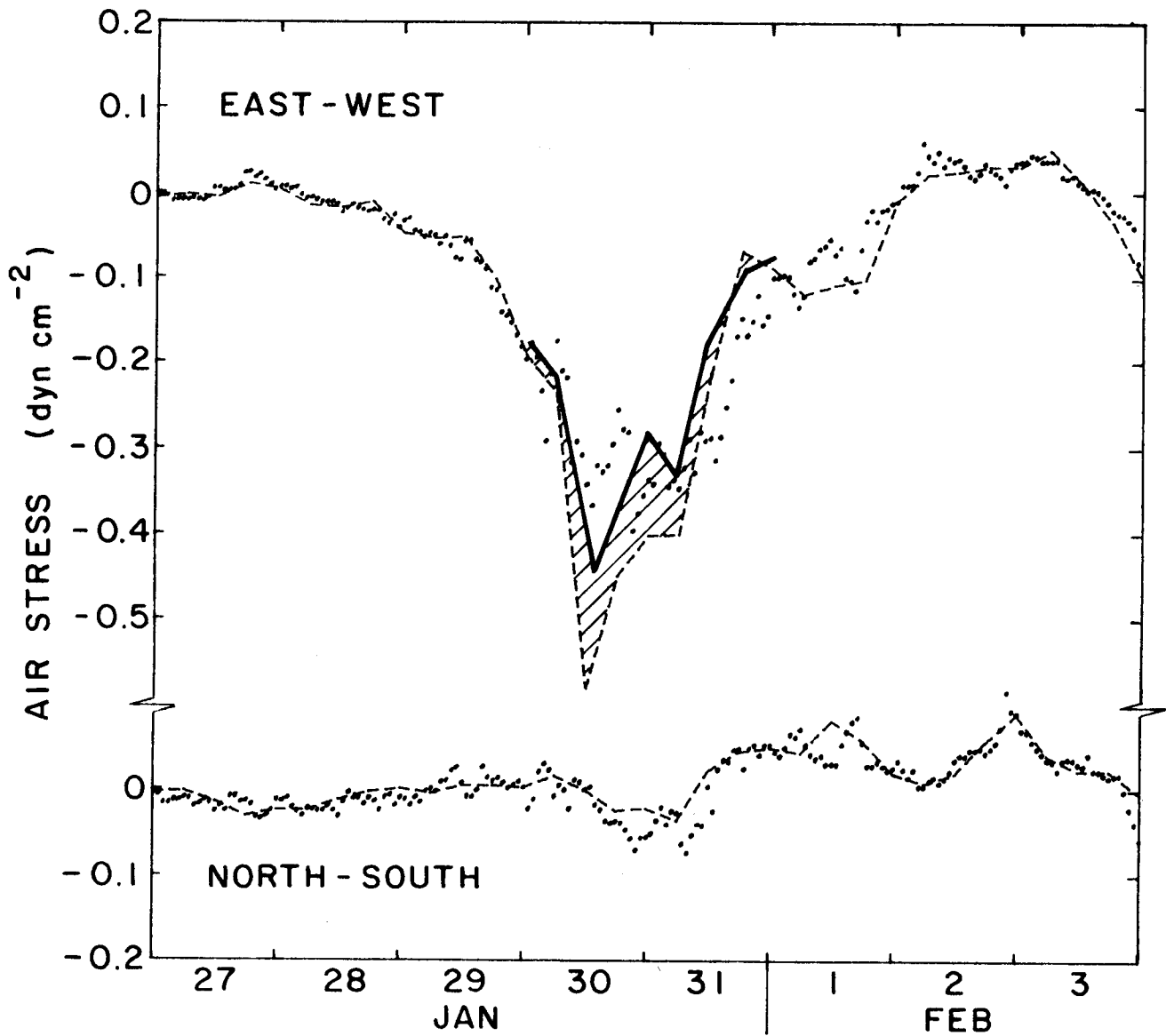


Figure 9. Air Stress Time History at Station 1 (Caribou). Components are shown in east and north directions. The dotted lines (...) represent the best estimate from 10-meter winds, while the dashed lines (---) represent values from geostrophic winds. The latter are linearly interpolated between data points each six hours. The bold line (—) represents modified values after barometric pressures were corrected.

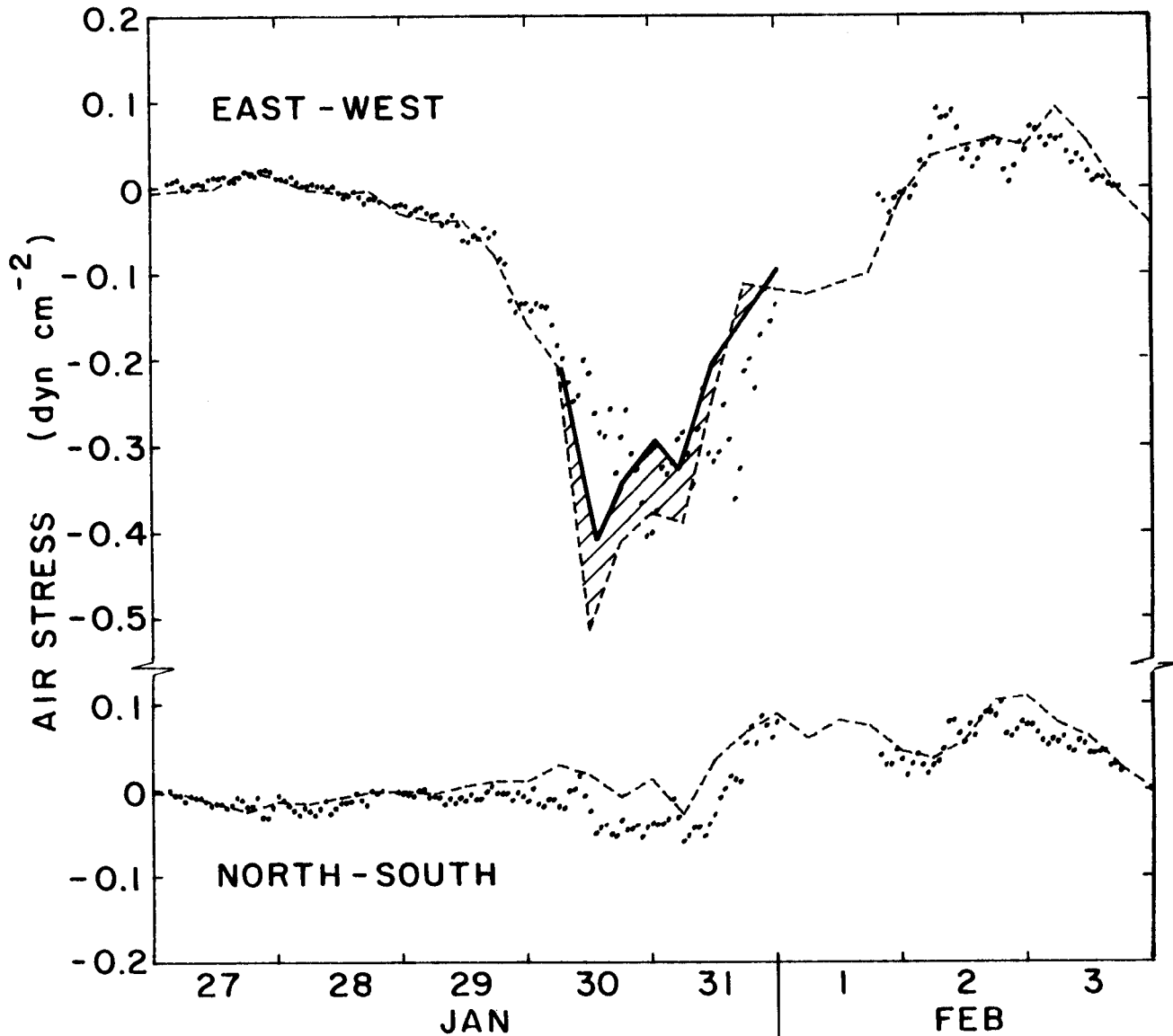


Figure 10. Air Stress Time History at Station 3 (Snow Bird). Components are shown in east and north directions. The dotted lines (...) represent the best estimate from 10-meter winds, while the dashed lines (---) represent values from geostrophic winds. The latter are linearly interpolated between data points each six hours. The bold line (—) represents modified values after barometric pressures were corrected.

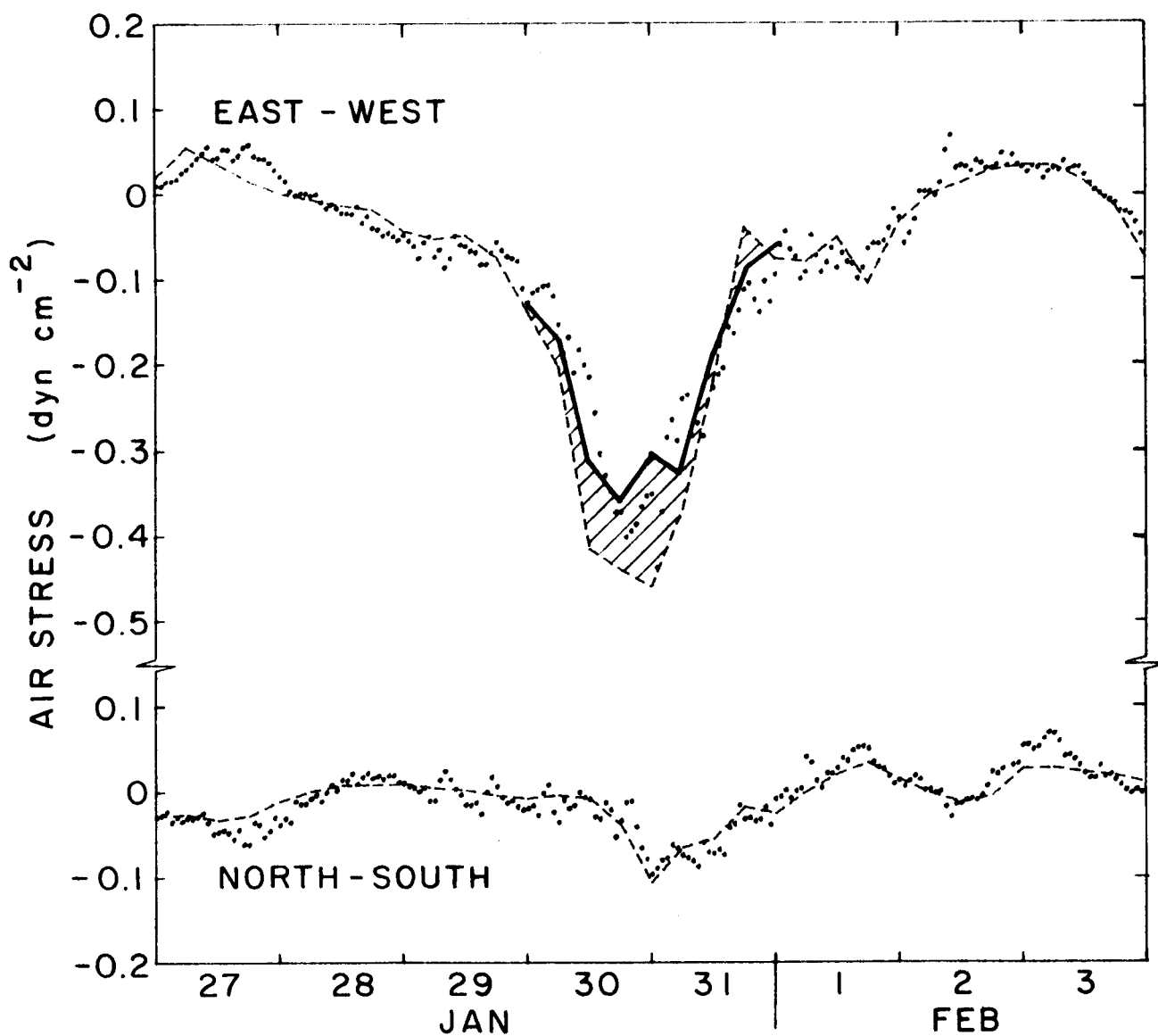


Figure 11. Air Stress Time History at Station 2 (Blue Fox). Components are shown in east and north directions. The dotted lines (...) represent the best estimate from 10-meter winds, while the dashed lines (---) represent values from geostrophic winds. The latter are linearly interpolated between data points each six hours. The bold line (—) represents modified values after barometric pressures were corrected.

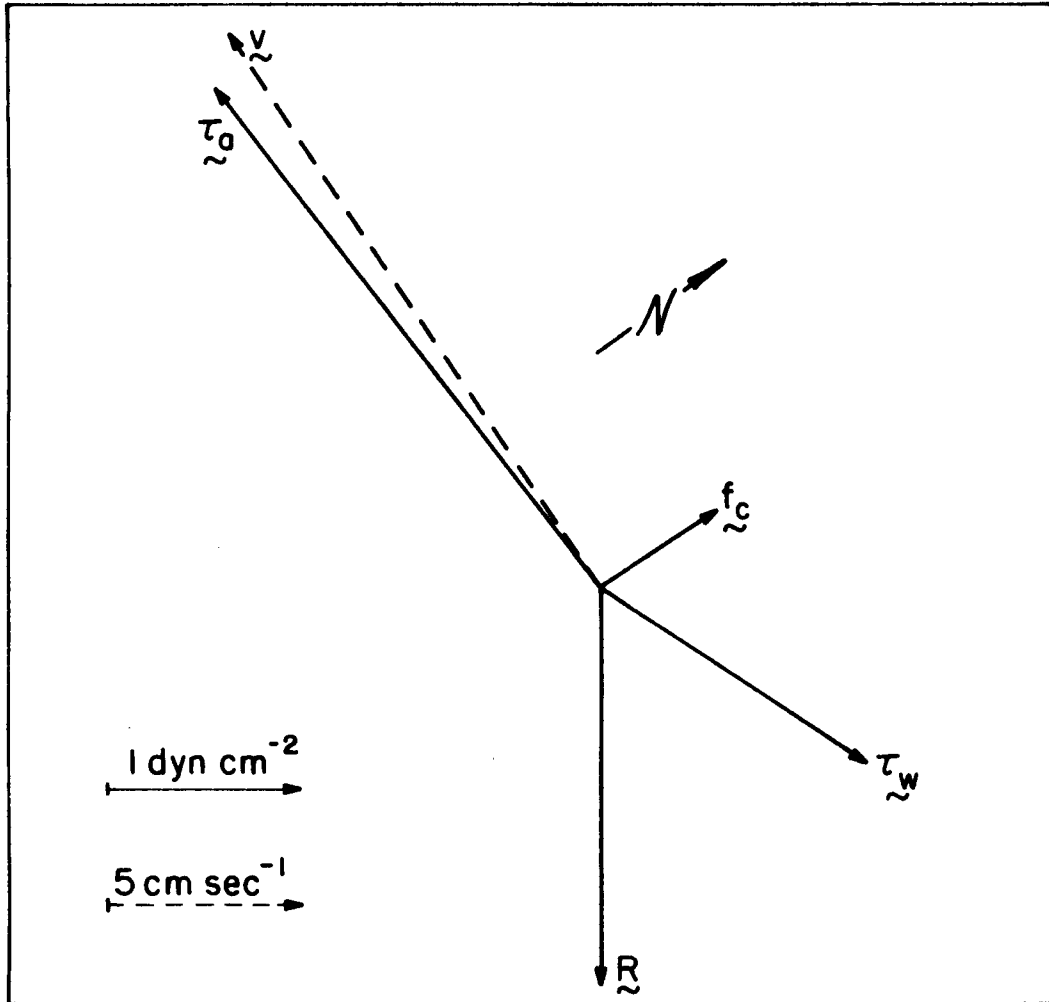


Figure 12. Force Balance at Station 1 (Caribou) at 1200 GMT on 30 January.

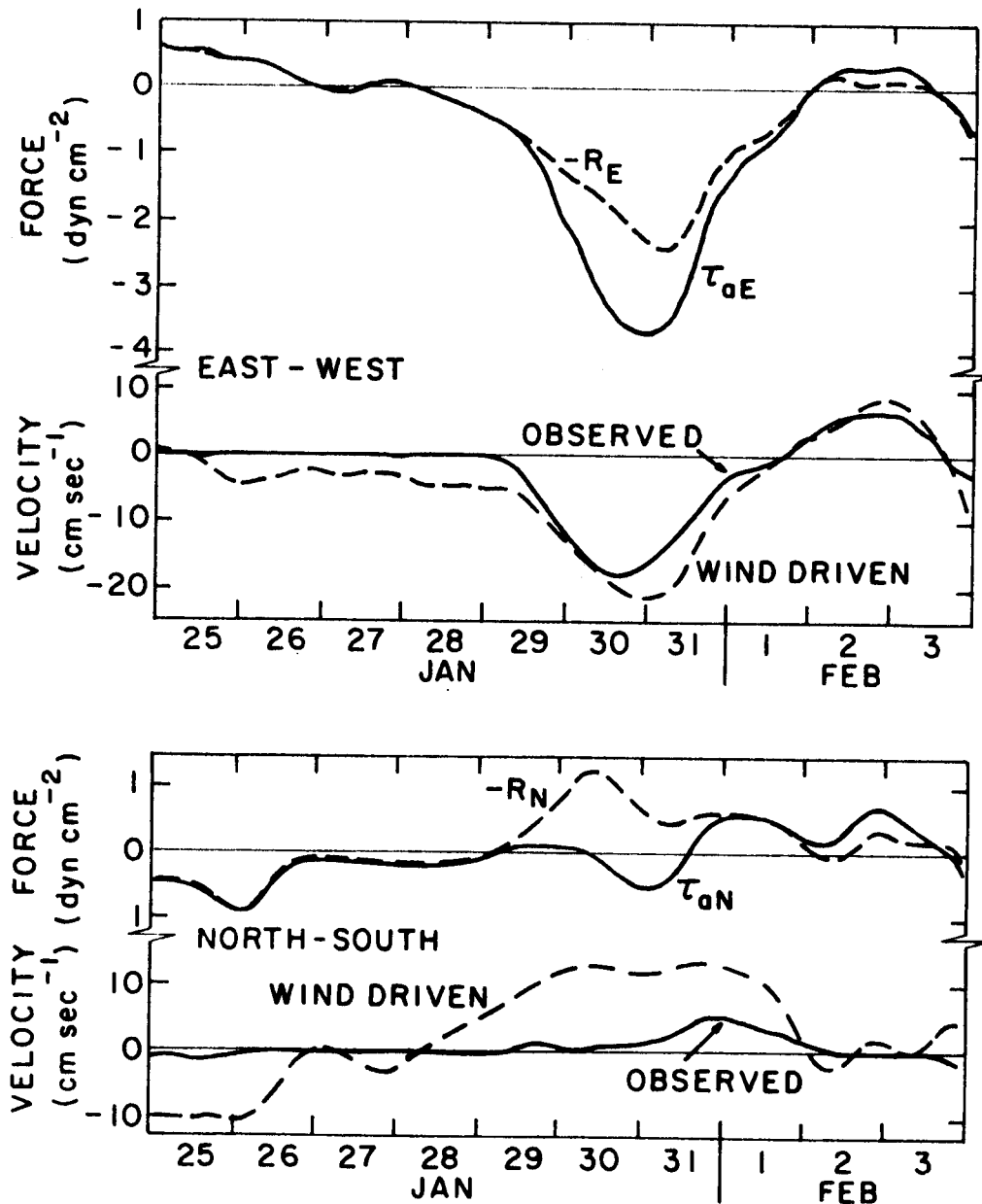


Figure 13. Time History of Driving Forces and Resulting Velocity at Station 1 (Caribou). Components are given in geographic coordinates. Subscript E and N indicate positive values of the component to the east and north, respectively. Air stress τ_a and the residual R (composed largely of ice stress divergence) are shown as are the observed and wind-driven velocities.

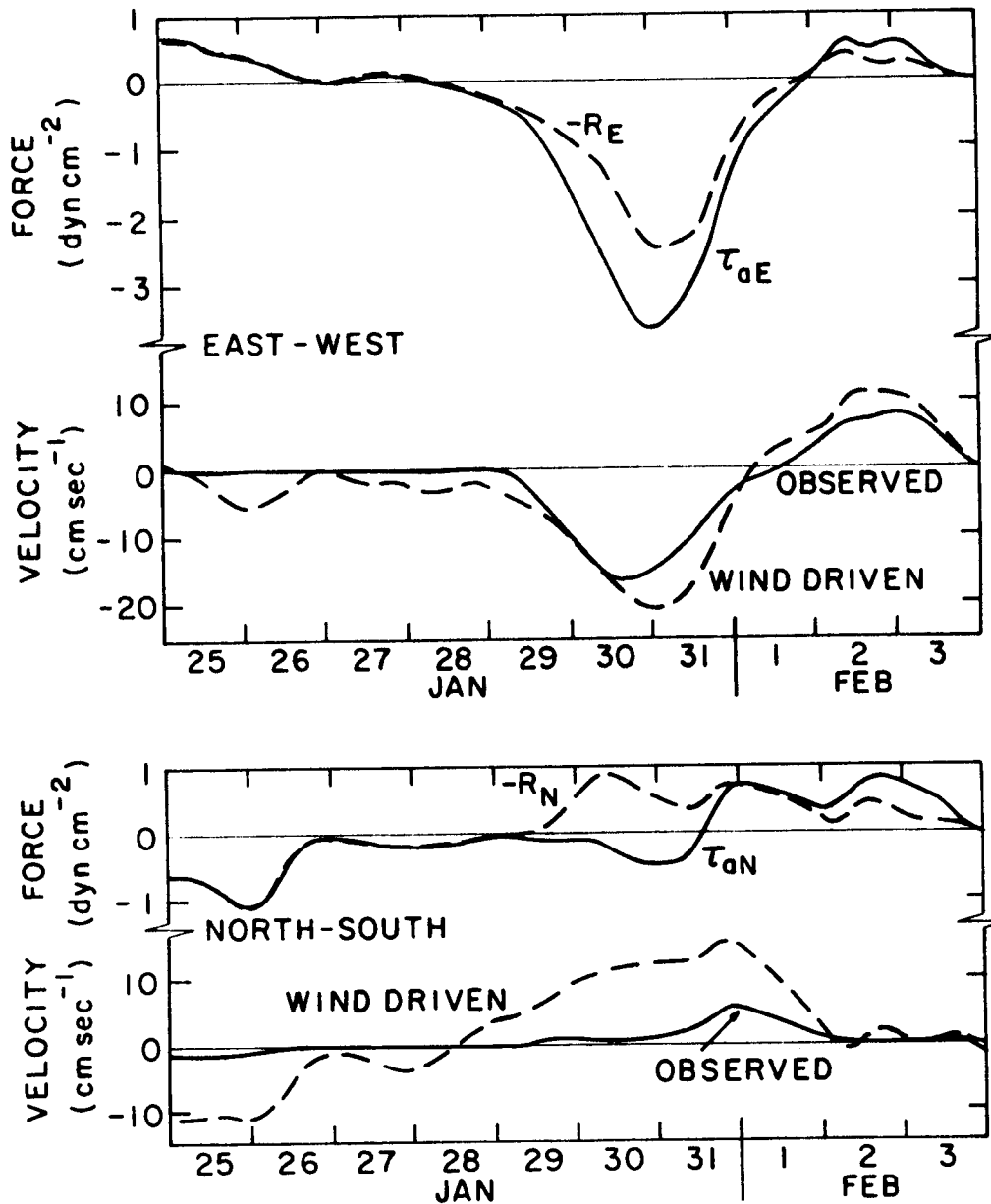


Figure 14. Time History of Driving Forces and Resulting Velocity at Station 3 (Snow Bird). Components are given in geographic coordinates. Subscript E and N indicate positive values of the component to the east and north, respectively. Air stress τ_a and the residual R (composed largely of ice stress divergence) are shown as are the observed and wind-driven velocities.

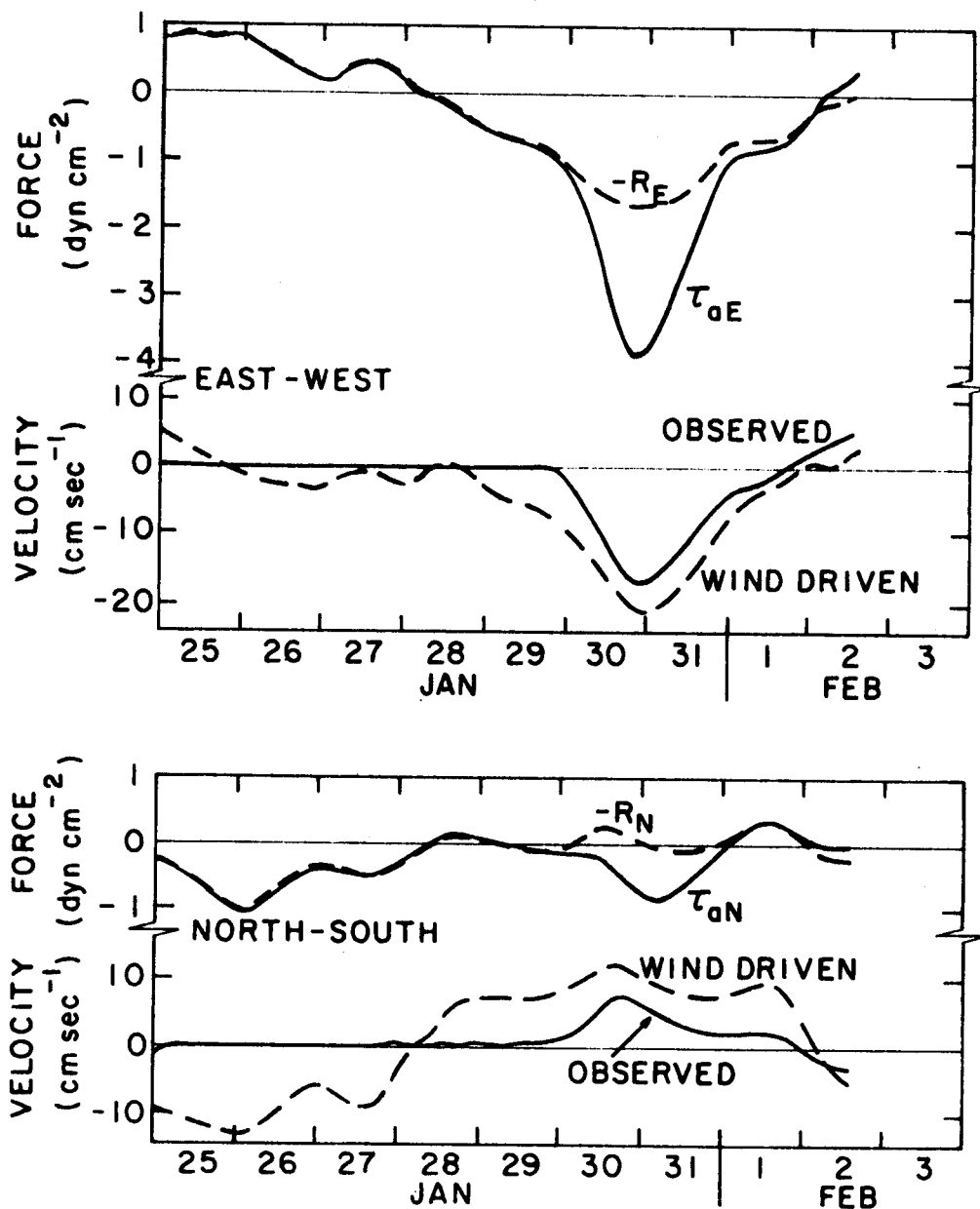


Figure 15. Time History of Driving Forces and Resulting Velocity at Station 2 (Blue Fox). Components are given in geographic coordinates. Subscript E and N indicate positive values of the components to the east and north, respectively. Air stress τ_a and the residual R (composed largely of ice stress divergence) are shown as are the observed and wind-driven velocities.

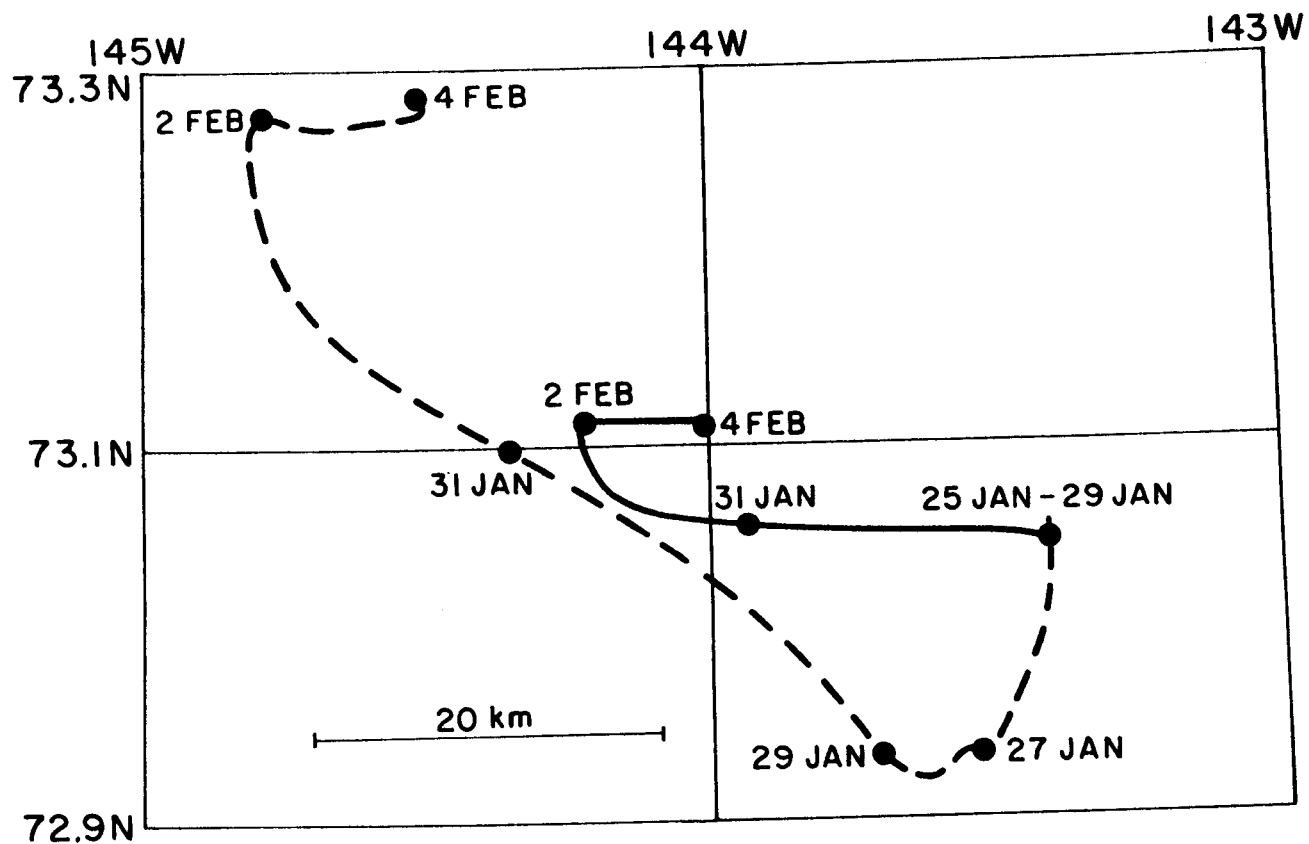


Figure 16. Trajectory of Station 1 (Caribou). Observed drift track shown as (—) and wind-driven shown as (---). Circles indicate location on indicated data at 0000 GMT.

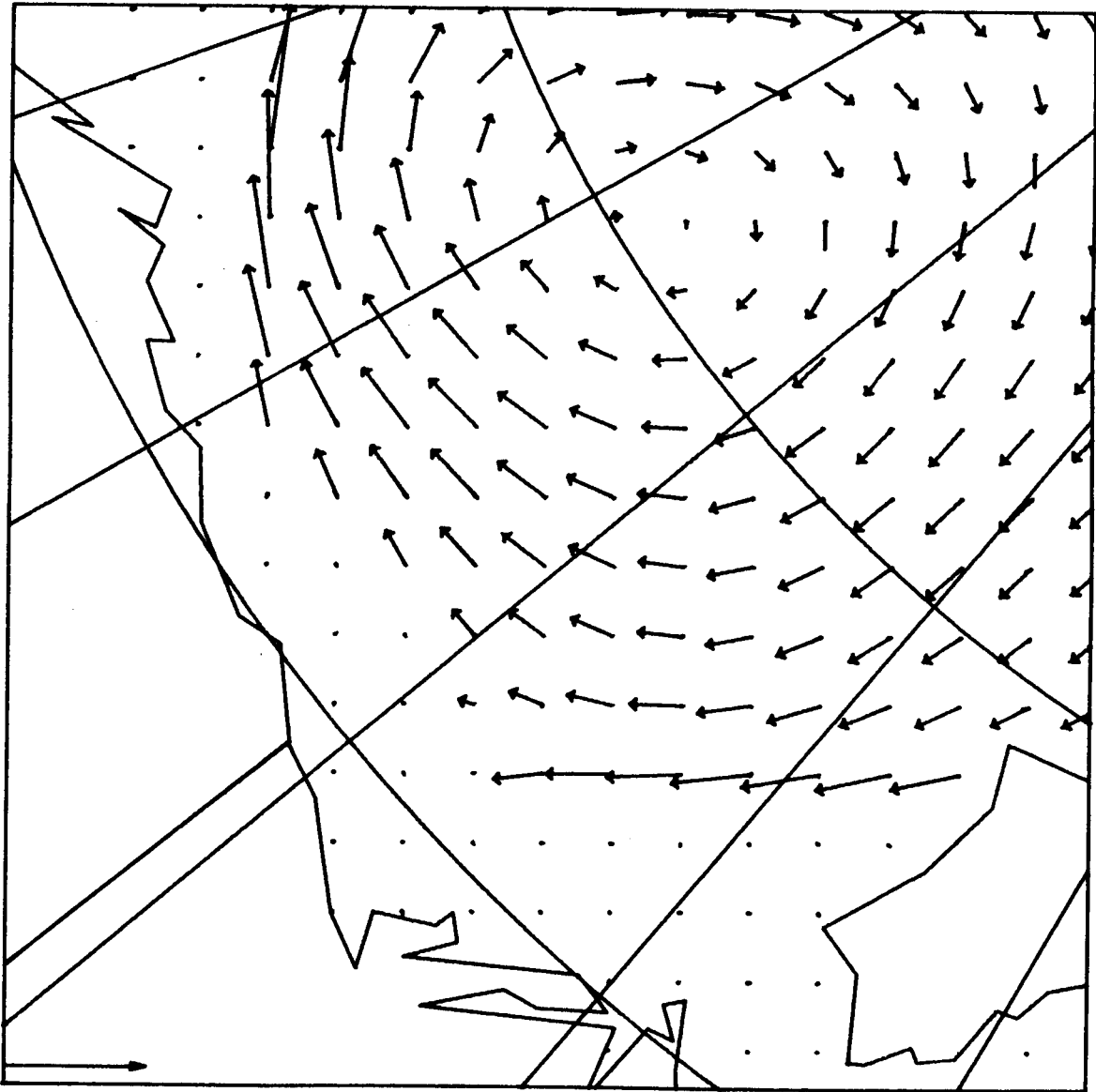


Figure 17. Geostrophic Ocean Current from Long-Term Dynamic Topography. Scale arrow is 10 cm sec^{-1} . Dots represent zero current.

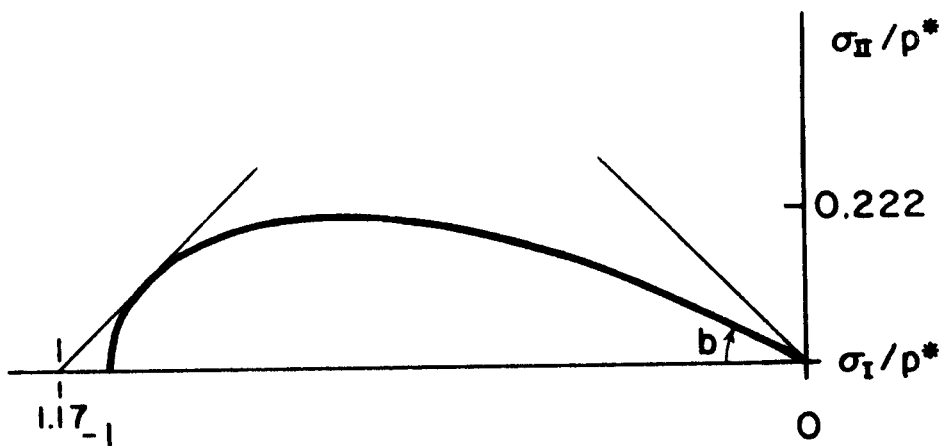
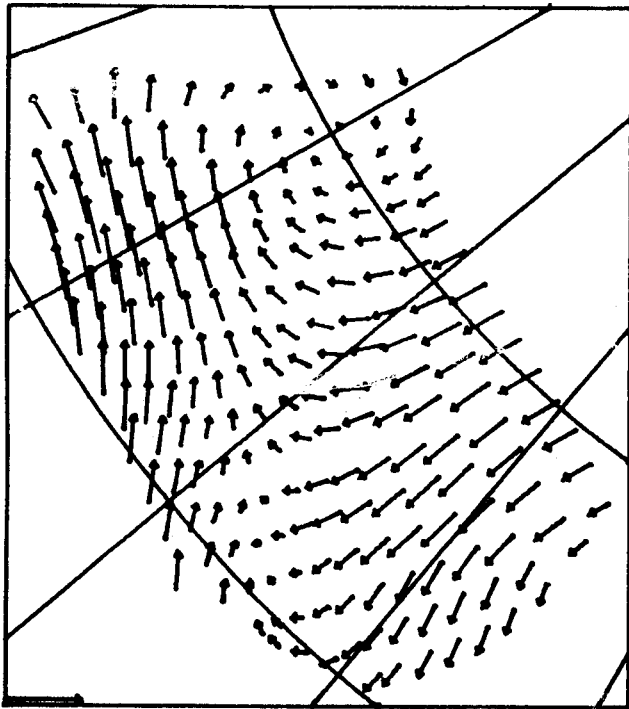
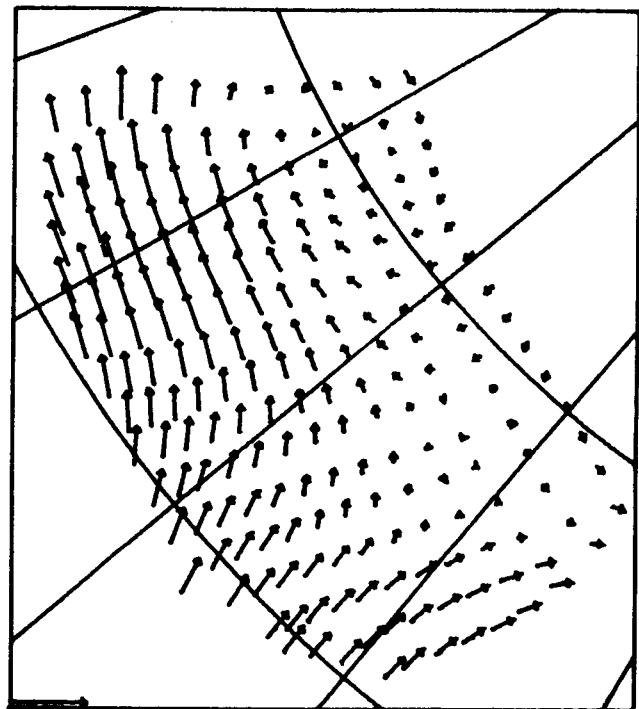


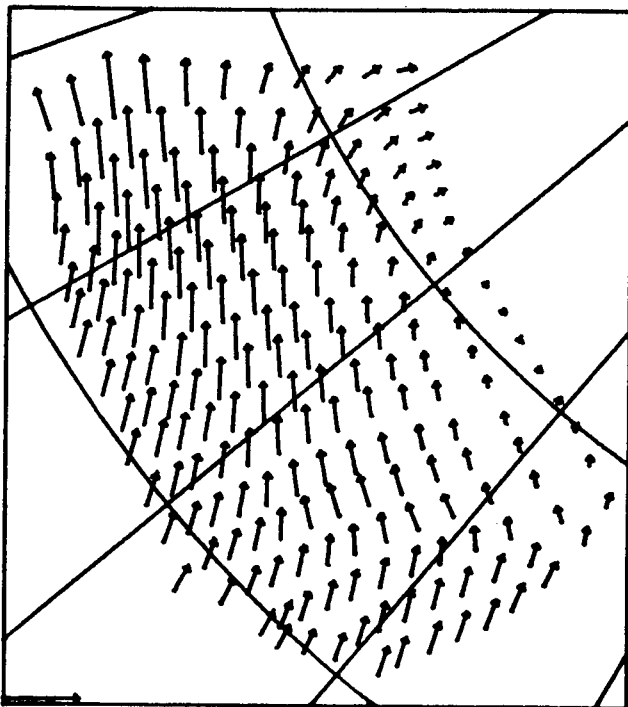
Figure 18. Squished Teardrop Yield Curve.



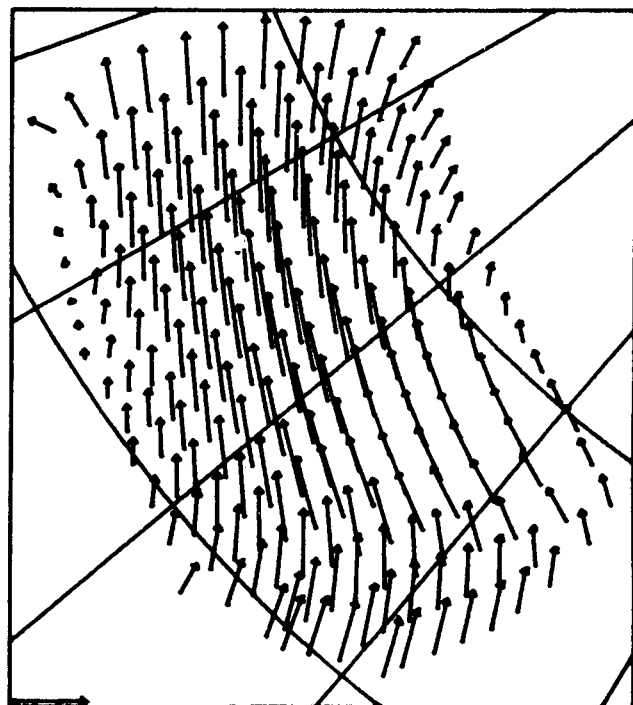
a) 27 January



b) 28 January

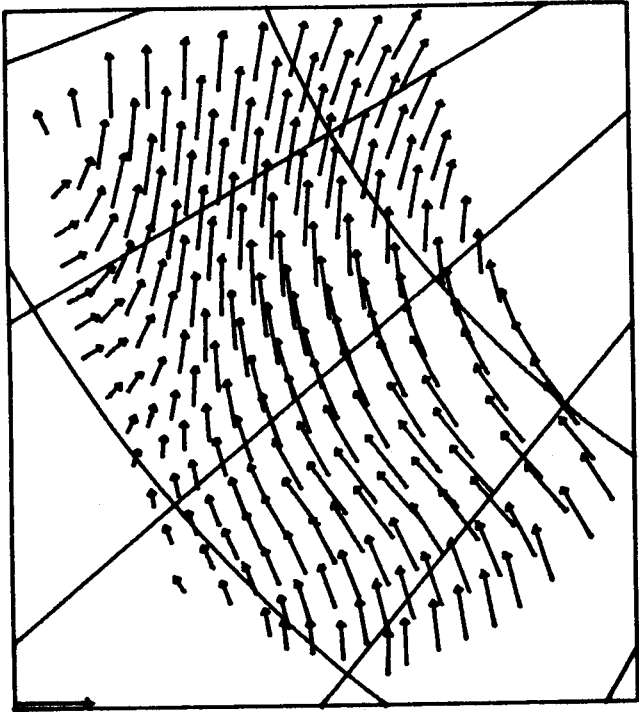


c) 29 January

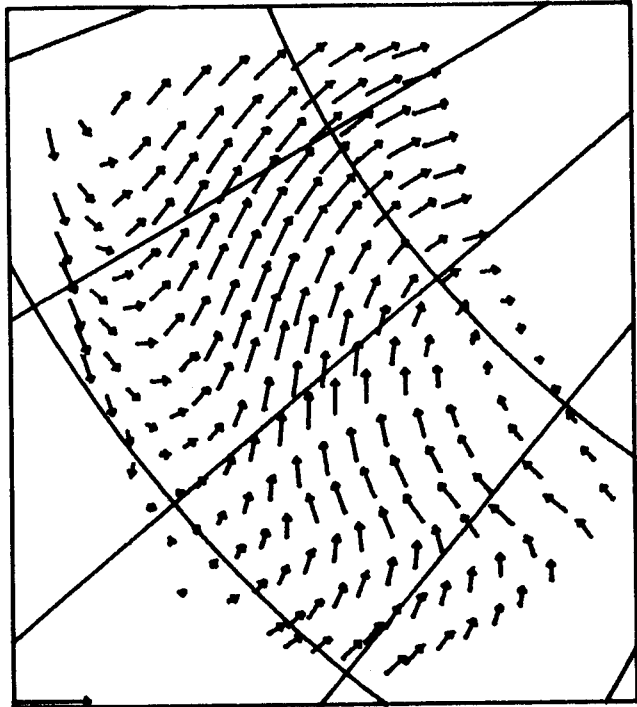


d) 30 January

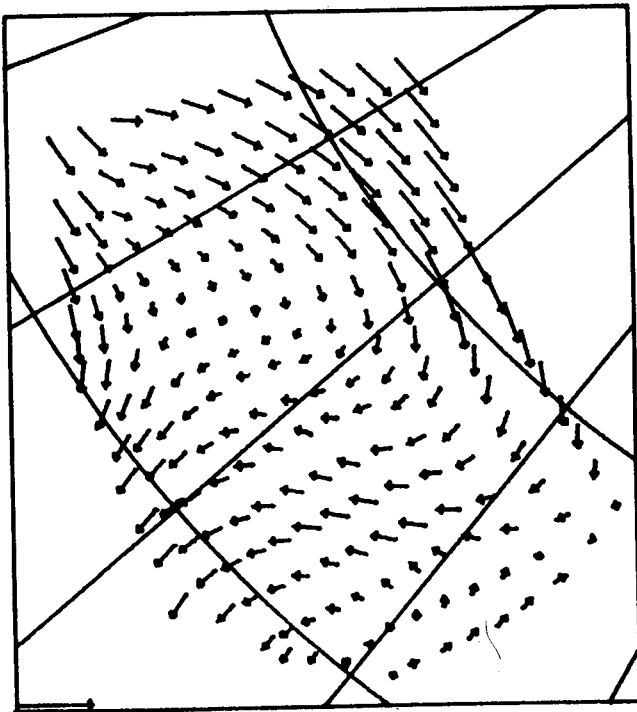
Figure 19. Wind-Driven (Free-Drift) Ice Velocity. Scale vector is 25 cm sec^{-1} .



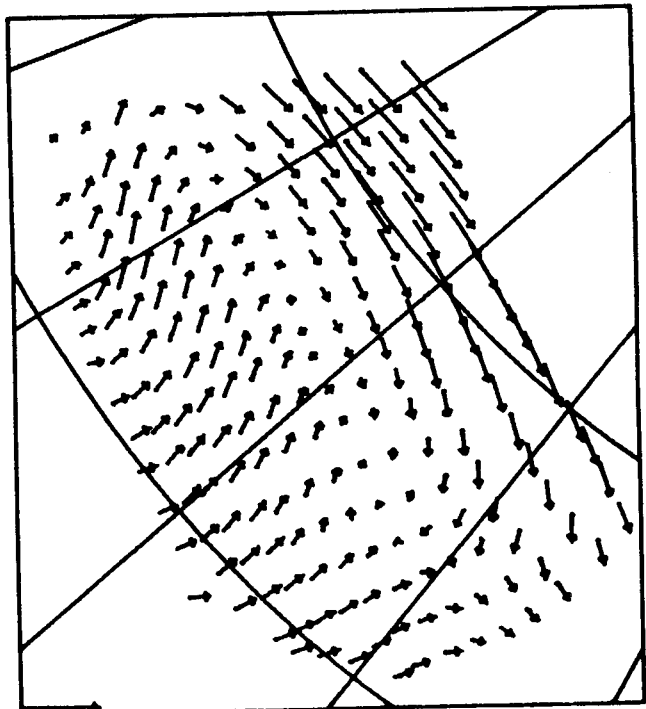
e) 31 January



f) 1 February

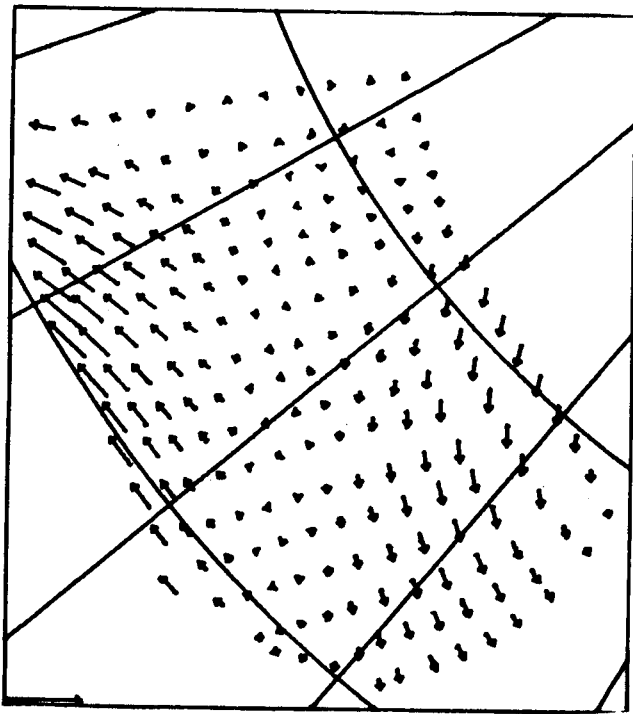


g) 2 February

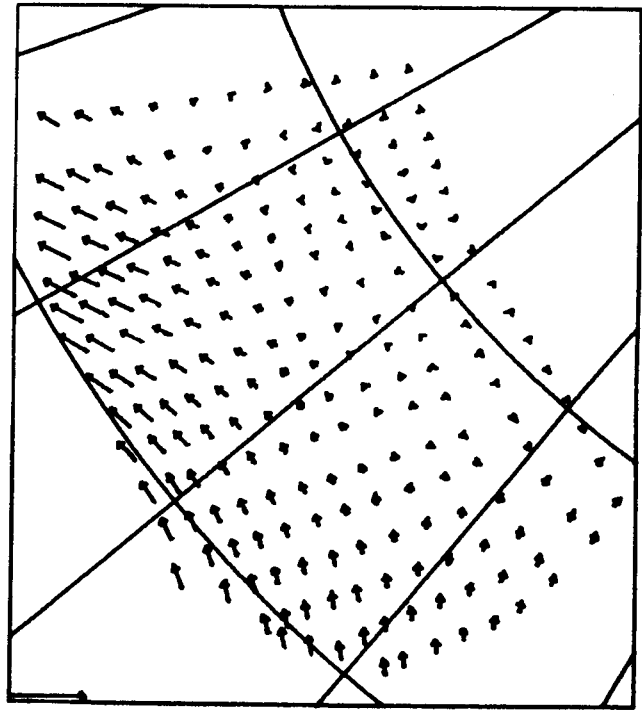


h) 3 February

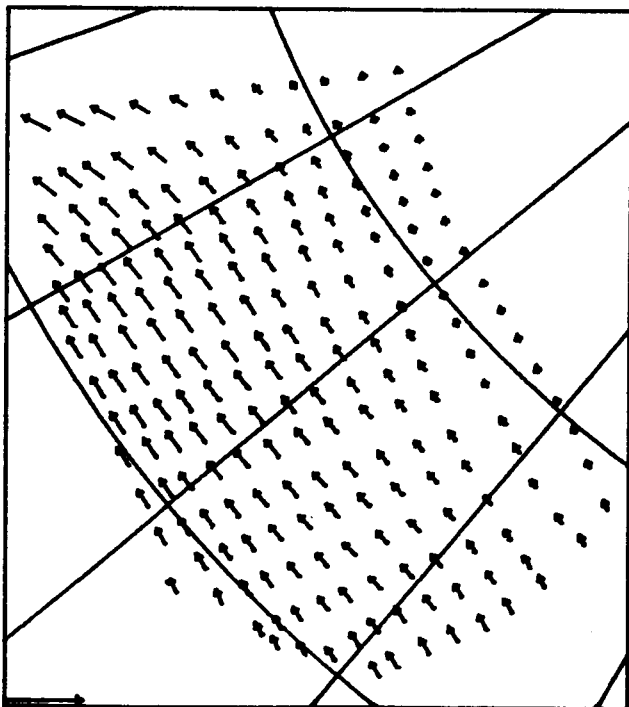
Figure 19.(cont.) Wind-Driven (Free-Drift) Ice Velocity. Scale vector is 25 cm sec^{-1} .



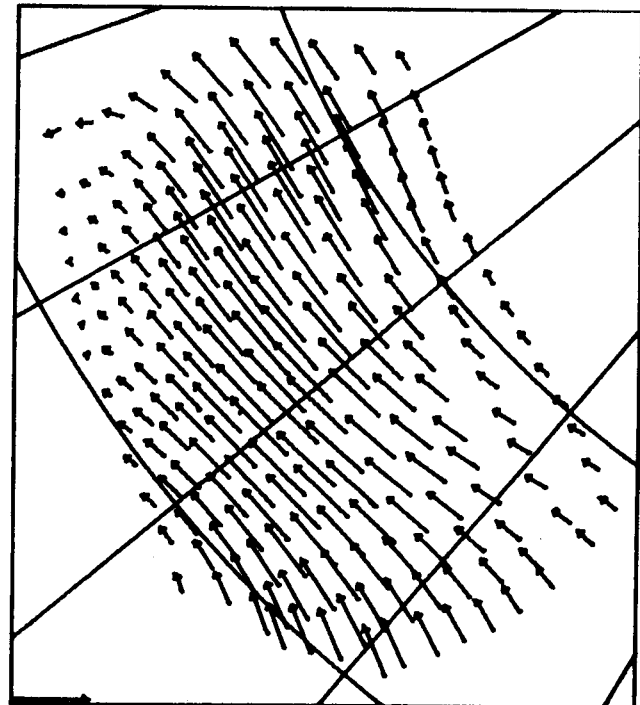
a) 27 January



b) 28 January

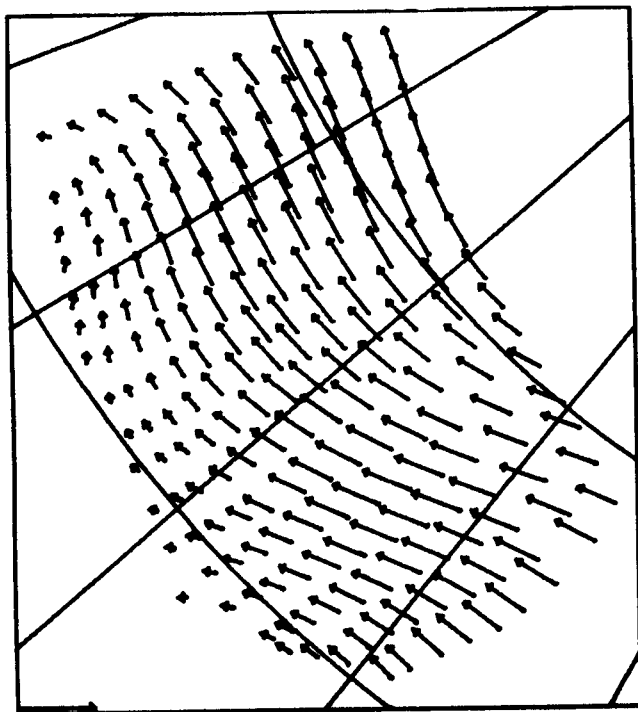


c) 29 January

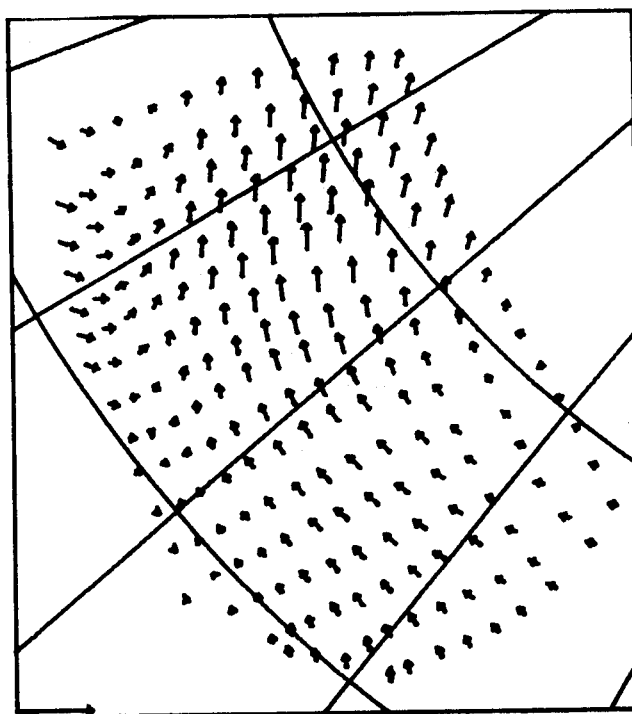


d) 30 January

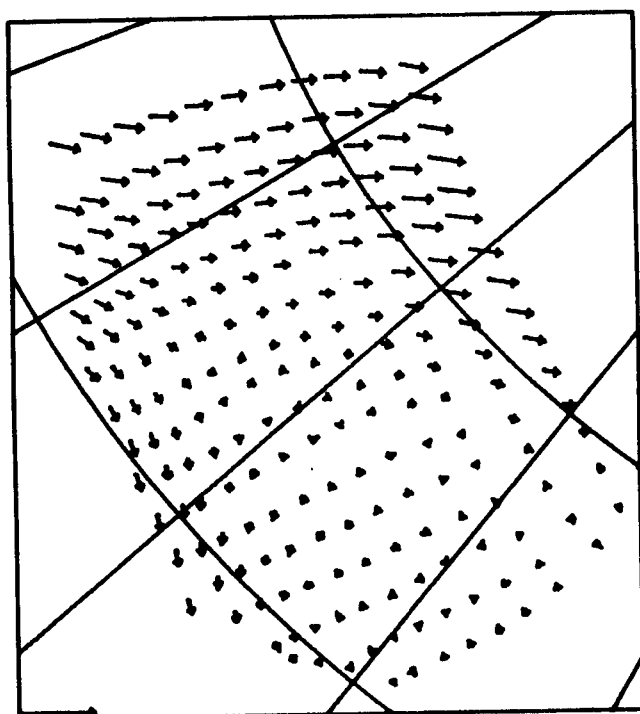
Figure 20. Daily Average of Air Stress Field. Scale vector is 4 dyn cm^{-1} .



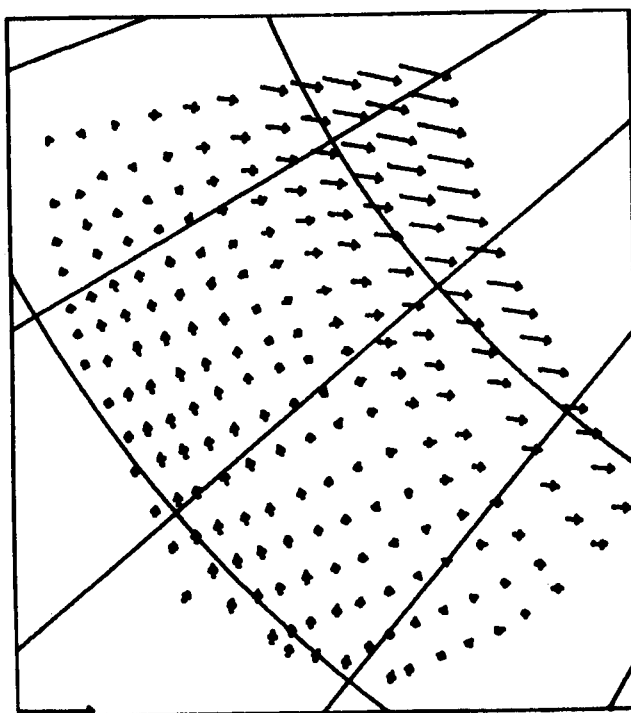
e) 31 January



f) 1 February

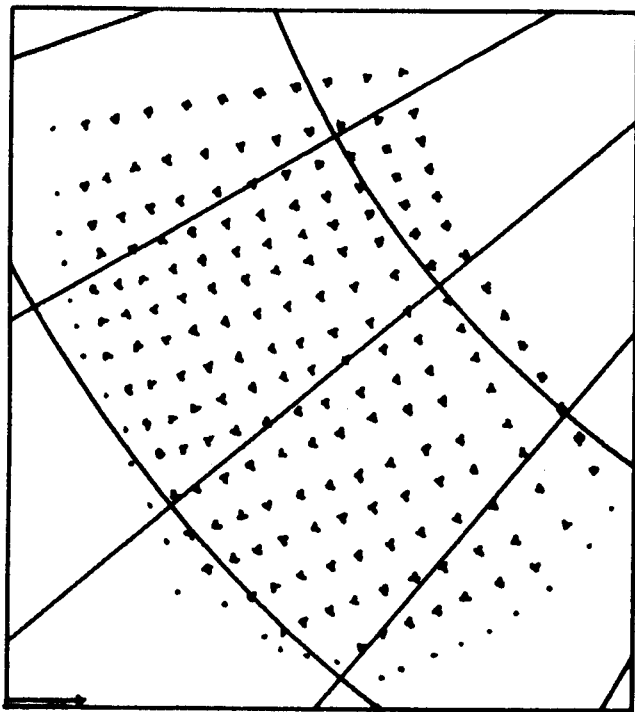


g) 2 February

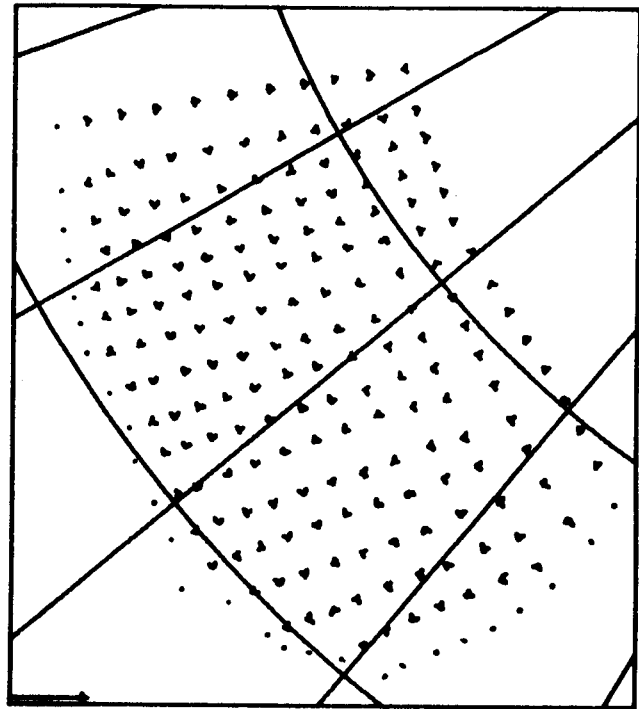


h) 3 February

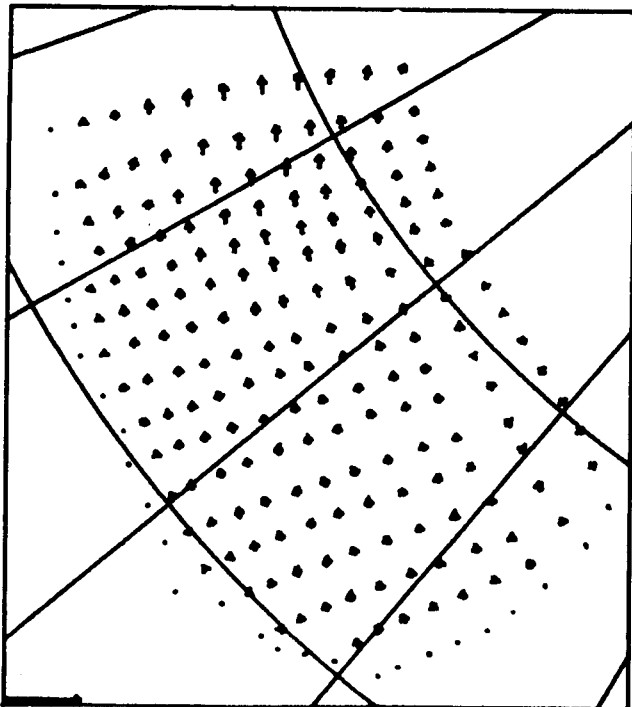
Figure 20. (cont.) Daily Average of Air Stress Field. Scale vector is 4 dyn cm^{-1} .



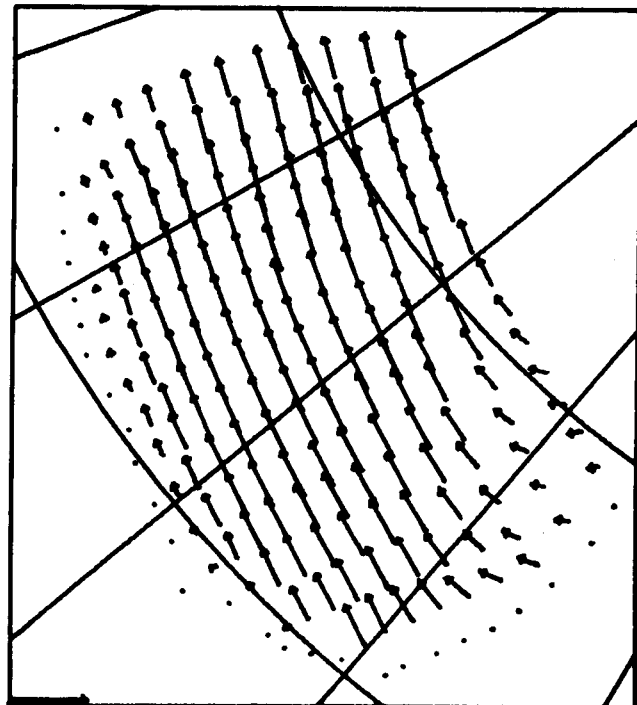
a) 27 January



b) 28 January

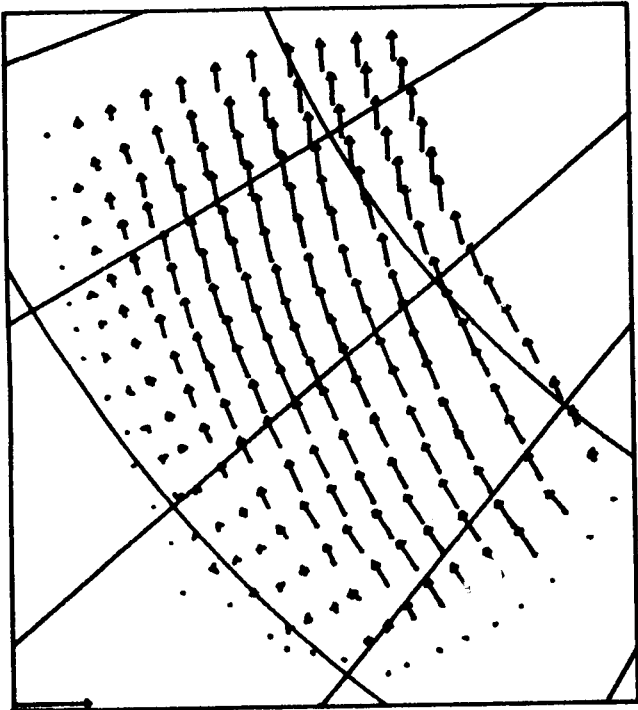


c) 29 January

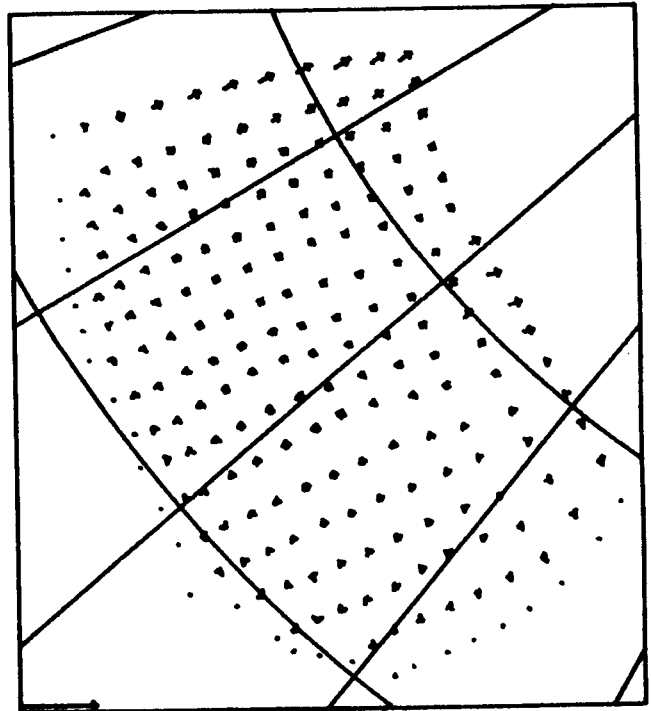


d) 30 January

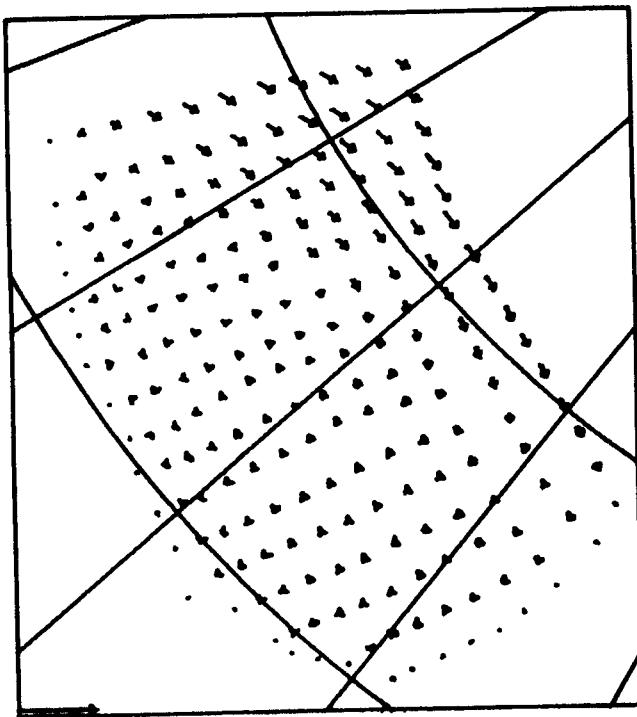
Figure 21. Modeled Ice Velocity Field with Yield Strength $p^* = 10^8 \text{ dyn cm}^{-1}$. Scale vector is 25 cm sec^{-1} .



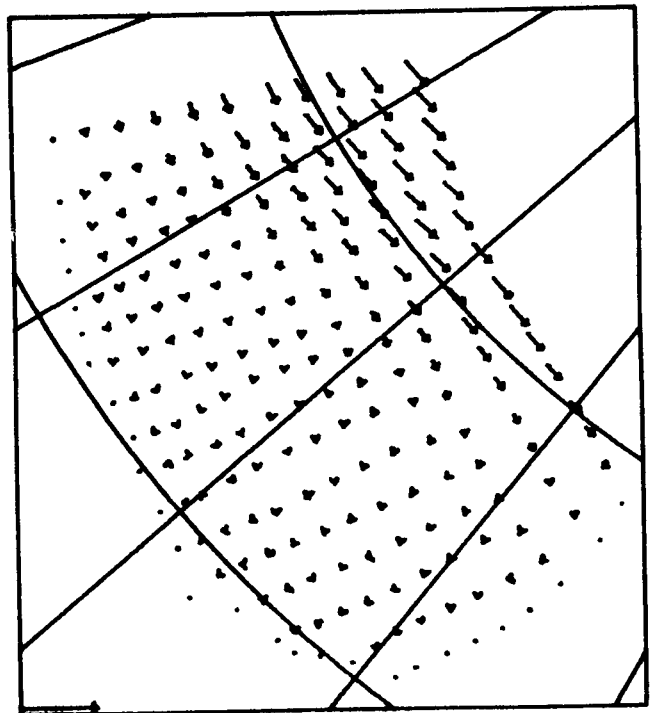
e) 31 January



f) 1 February

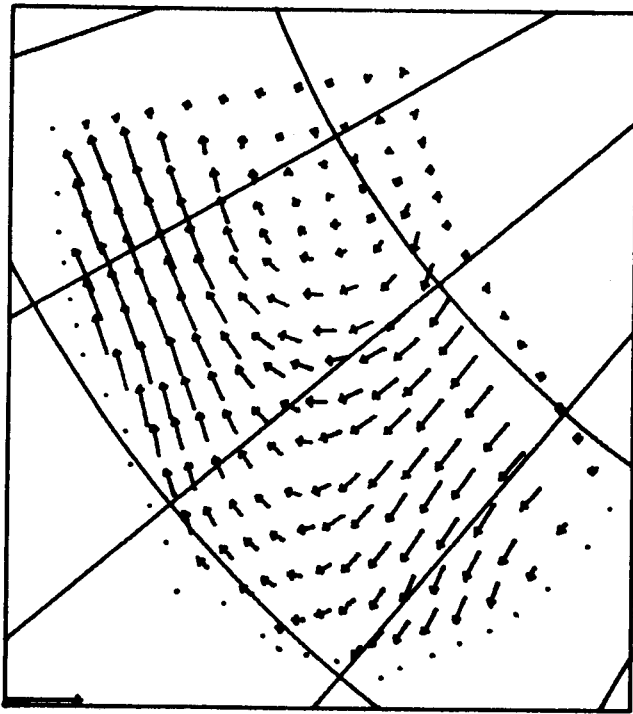


g) 2 February

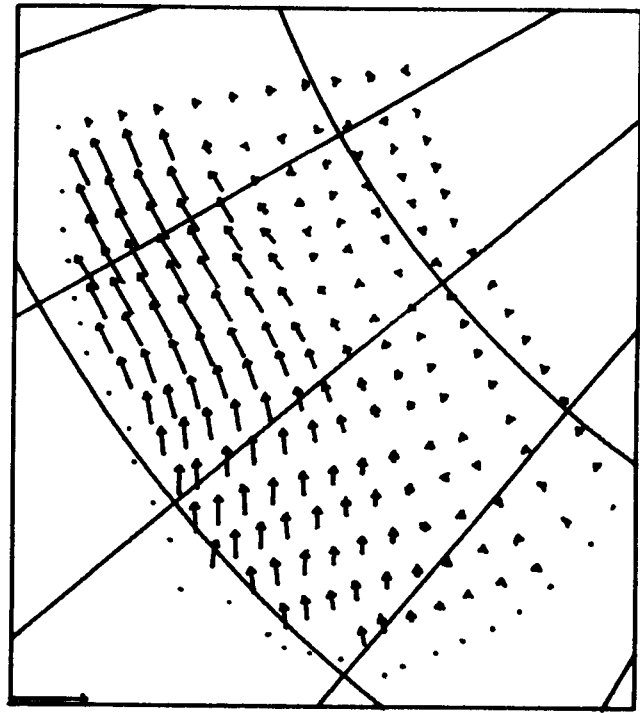


h) 3 February

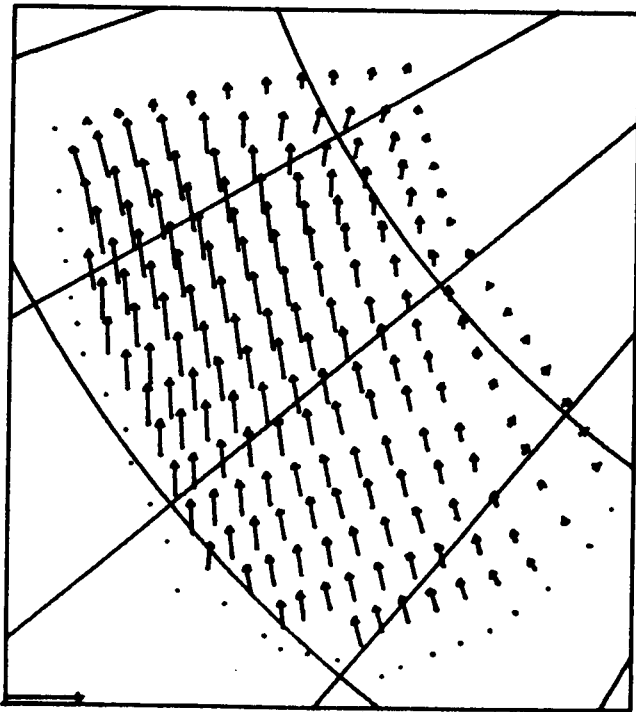
Figure 21.(cont.) Modeled Ice Velocity Field with Yield Strength $p^* = 10^8 \text{ dyn cm}^{-1}$.
Scale vector is 25 cm sec^{-1} .



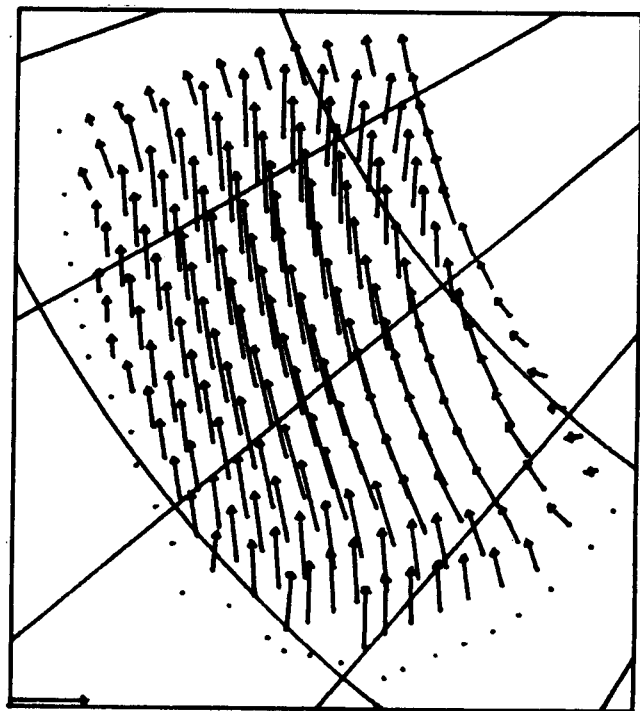
a) 27 January



b) 28 January

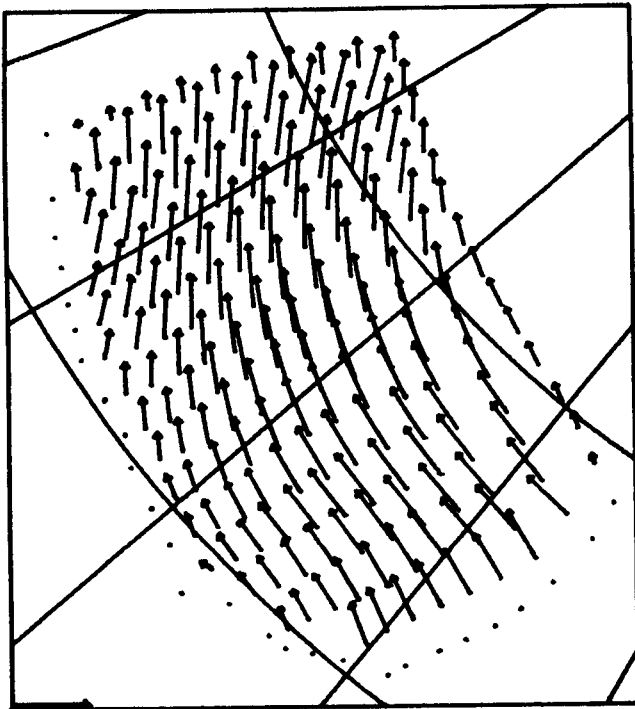


c) 29 January

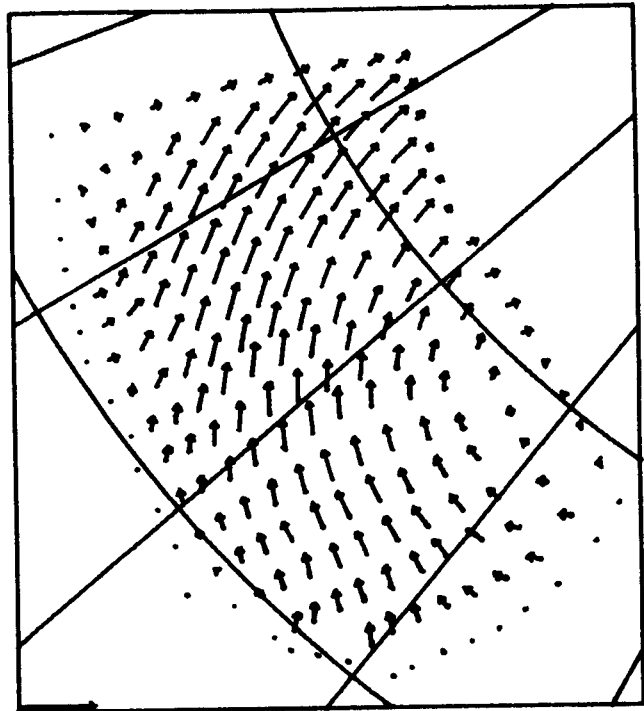


d) 30 January

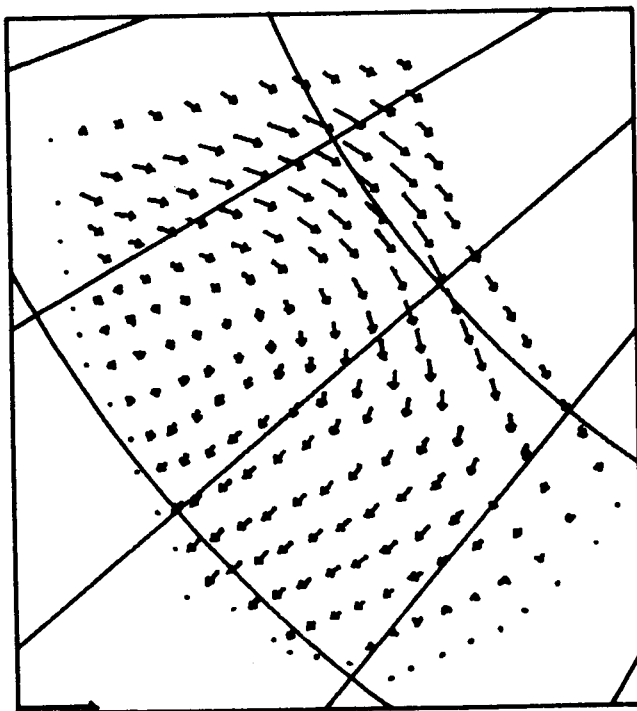
Figure 22. Modeled Ice Velocity Field with Yield Strength $p^* = 10^7 \text{ dyn cm}^{-1}$. Scale vector is 25 cm sec^{-1} .



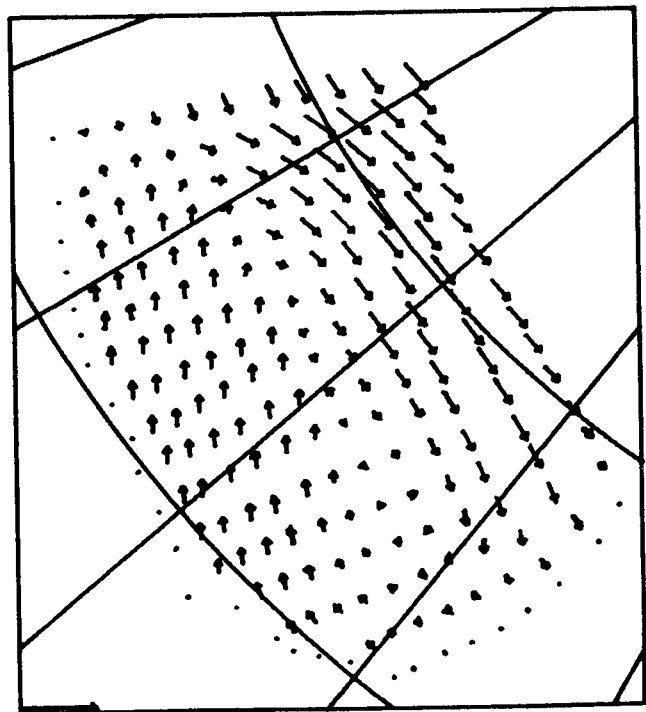
e) 31 January



f) 1 February

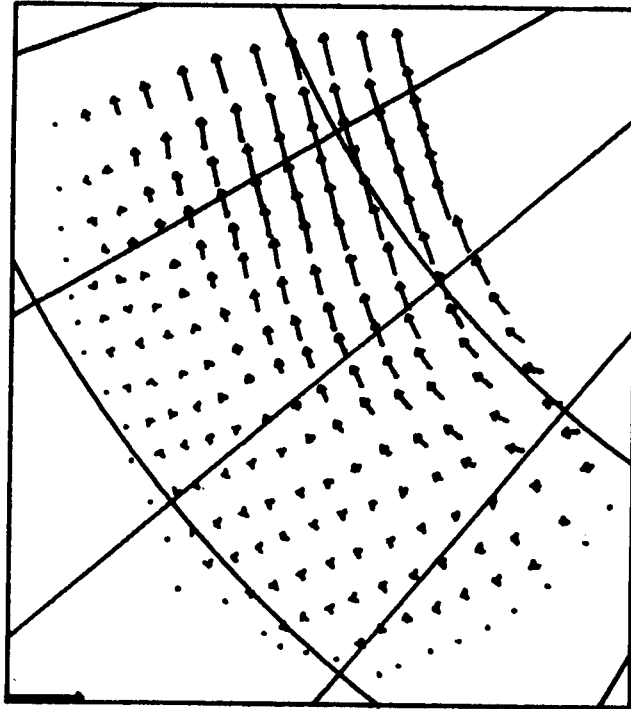


g) 2 February



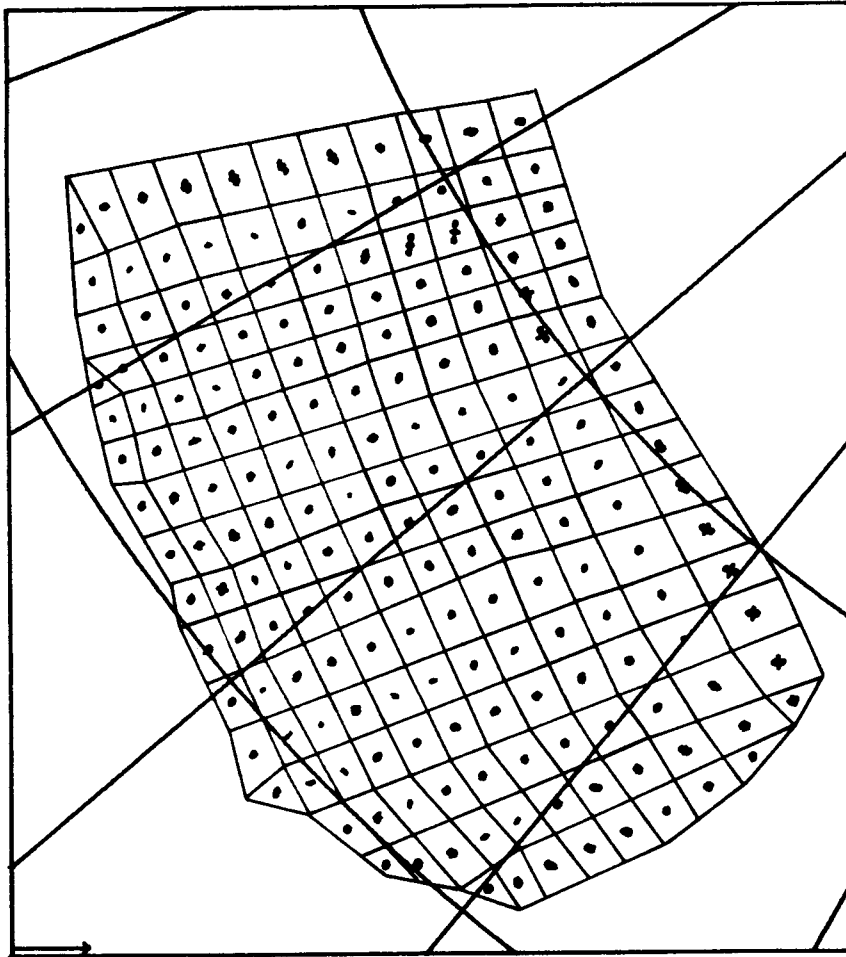
h) 3 February

Figure 22.(cont.) Modeled Ice Velocity Field with Yield Strength $p^* = 10^7 \text{ dyn cm}^{-1}$. Scale vector is 25 cm sec^{-1} .

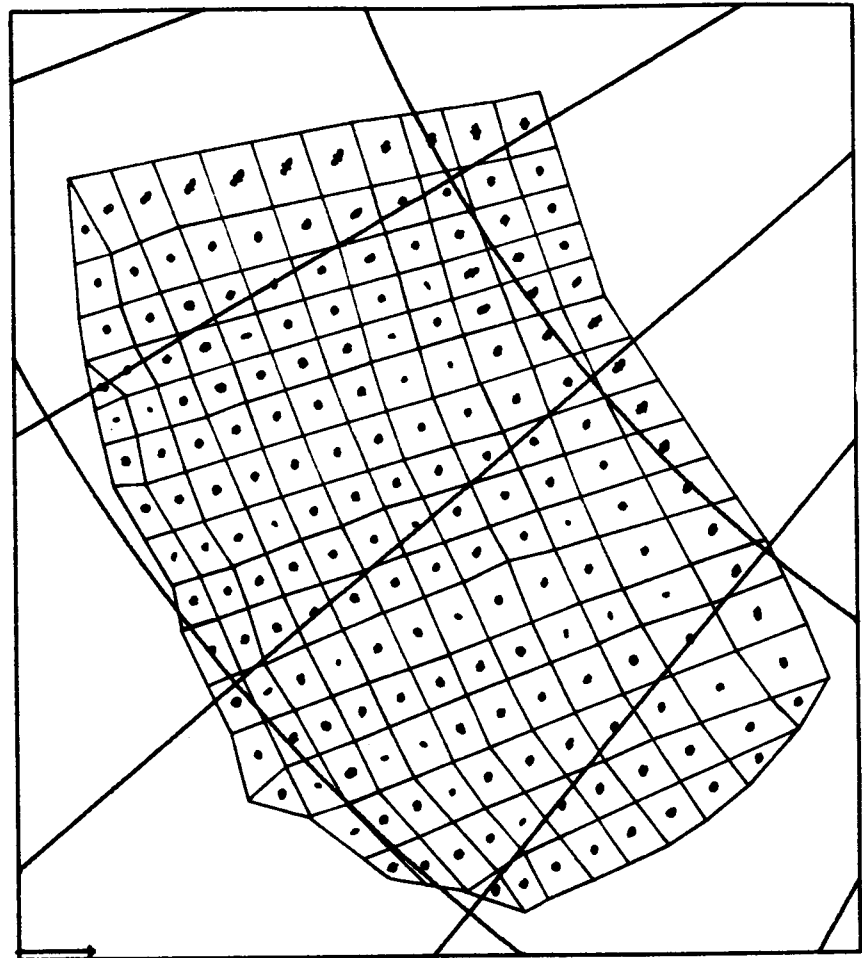


30 January

Figure 23. Modeled Ice Velocity Field with Yield Strength $p^* = 10^9 \text{ dyn cm}^{-1}$. Scale vector is 25 cm sec^{-1} .

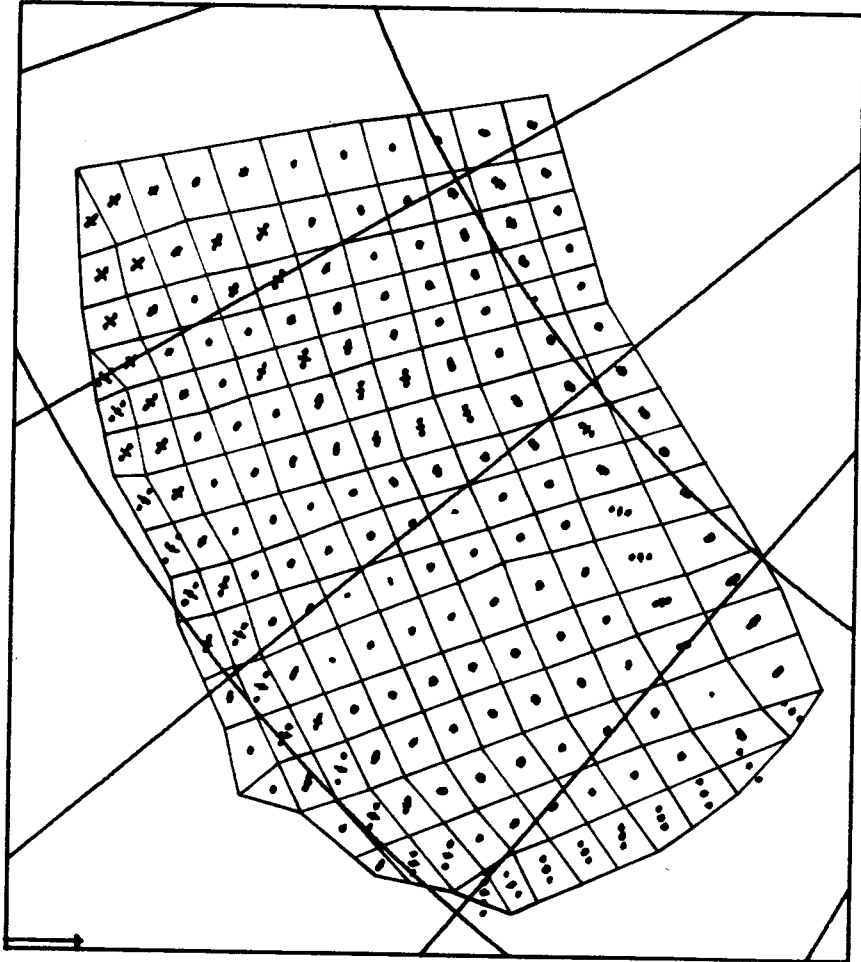


a) 27 January

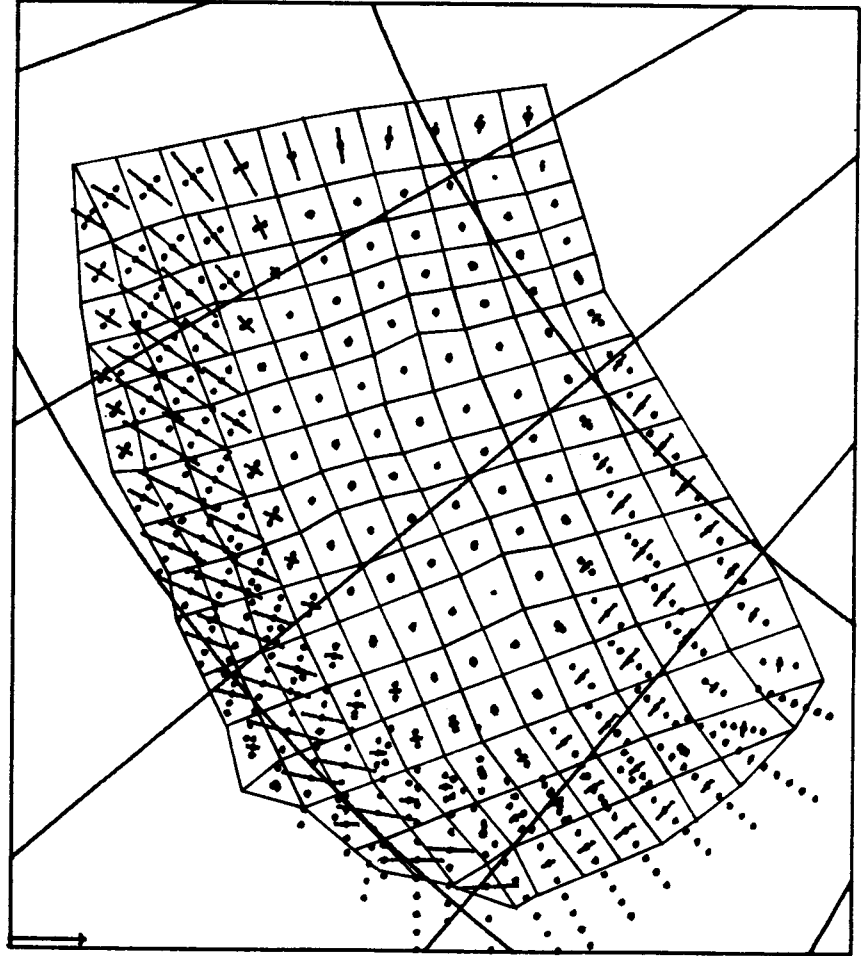


b) 28 January

Figure 24. Stretching Tensor Field (Daily Strain) with Principal Values Proportional to Line Length in Directions Shown. Dashed lines indicate opening and solid lines closing. Scale vector is $8 \times 10^{-7} \text{ sec}^{-1}$ (approximately 8% per day).

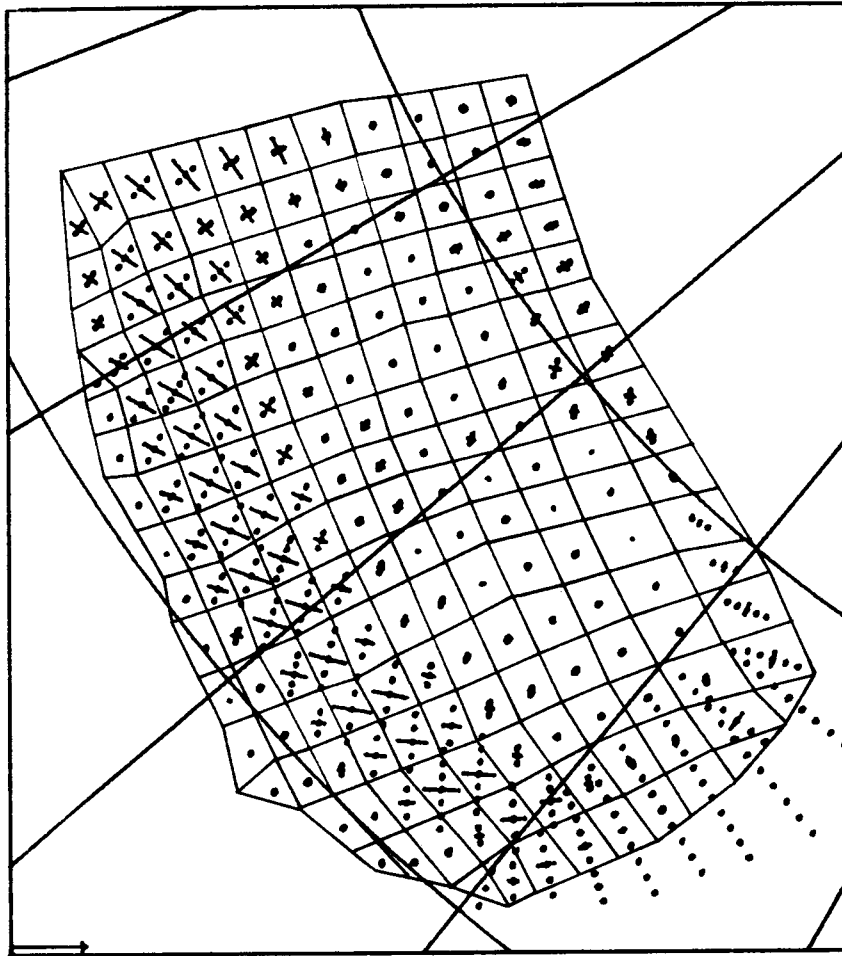


c) 29 January

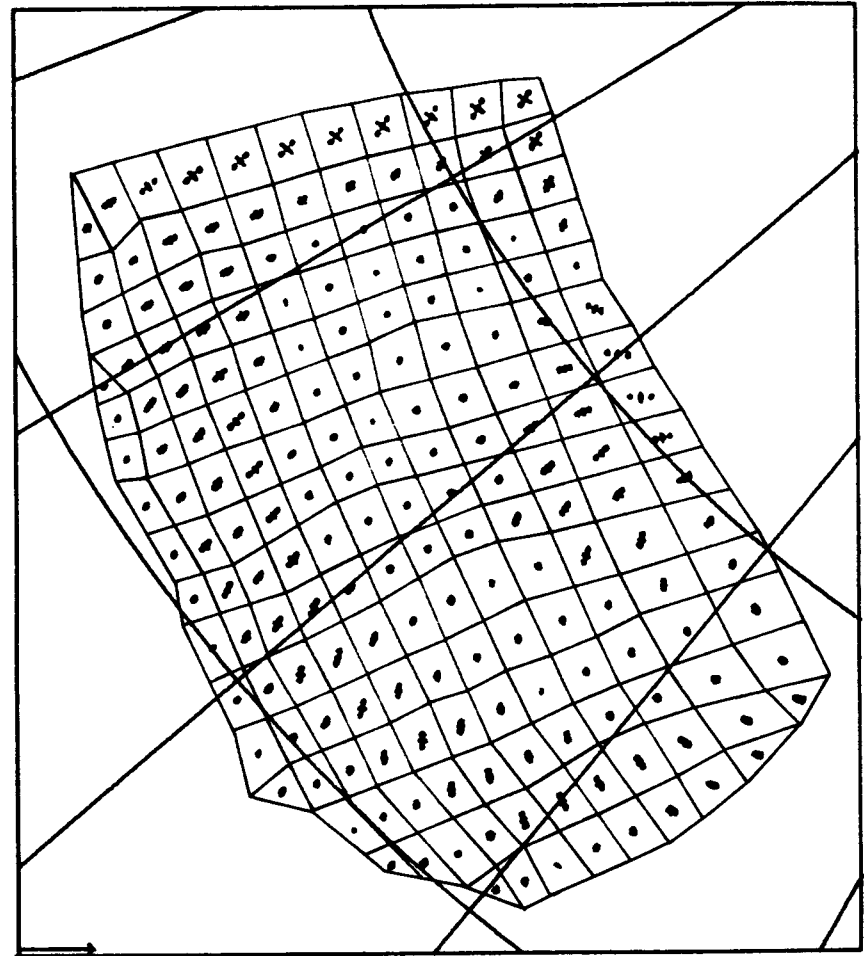


d) 30 January

Figure 24.(cont.) Stretching Tensor Field (Daily Strain) with Principal Values Proportional to Line Length in Directions Shown. Dashed lines indicate opening and solid lines closing. Scale vector is $8 \times 10^{-7} \text{ sec}^{-1}$ (approximately 8% per day).

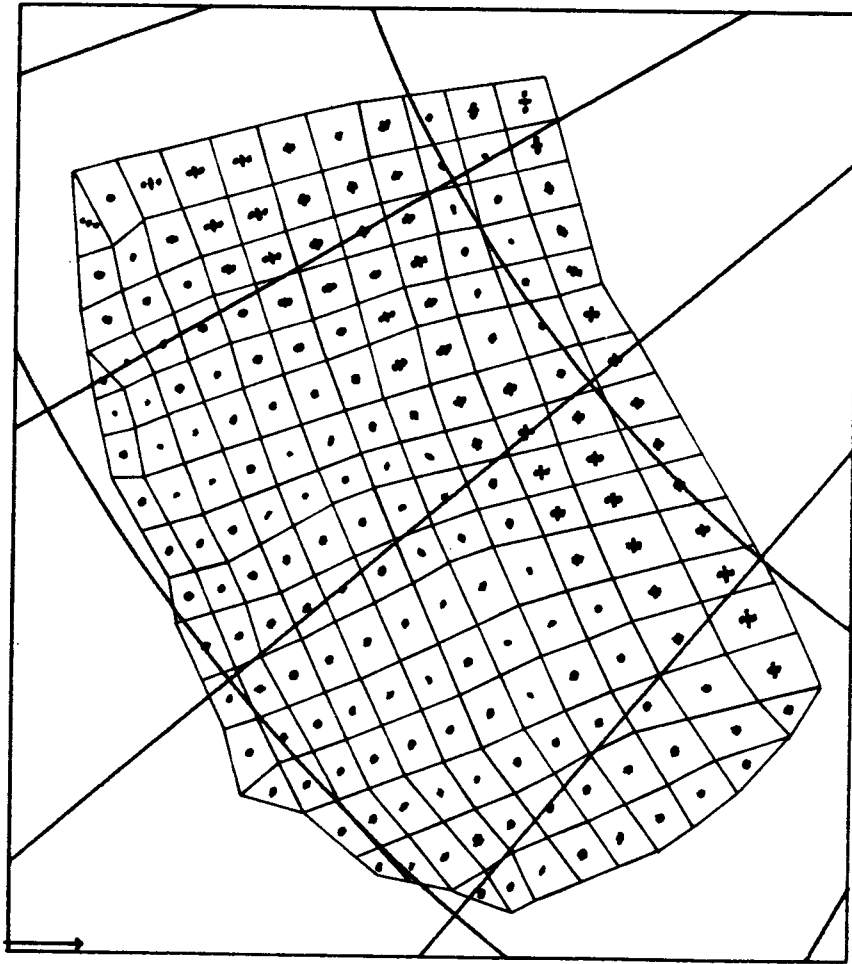


e) 31 January

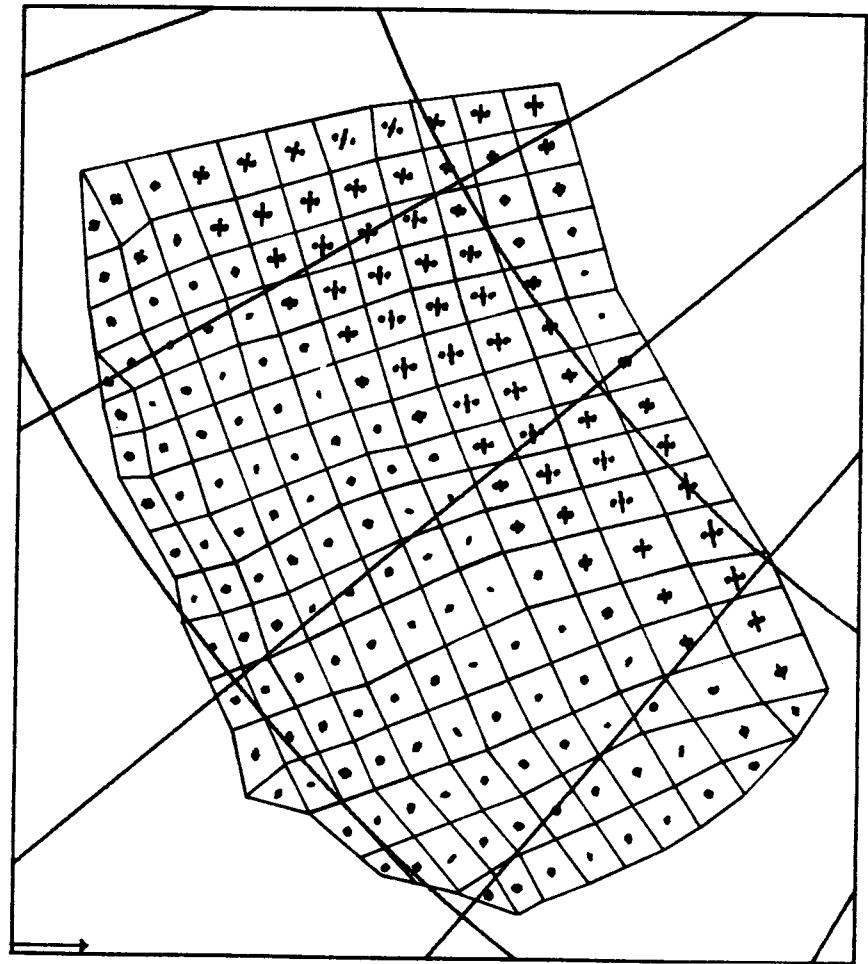


f) 1 February

Figure 24.(cont.) Stretching Tensor Field (Daily Strain) with Principal Values Proportional to Line Length in Directions Shown. Dashed lines indicate opening and solid lines closing. Scale vector is $8 \times 10^{-7} \text{ sec}^{-1}$ (approximately 8% per day).

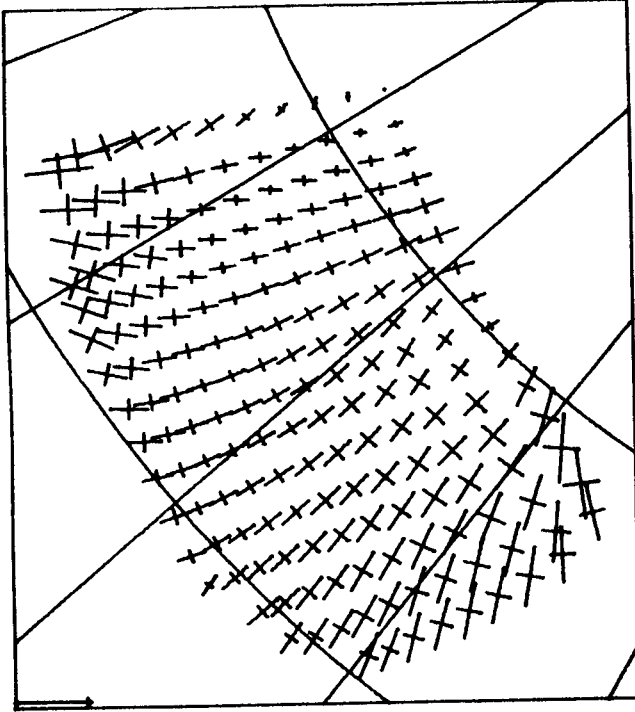


g) 2 February

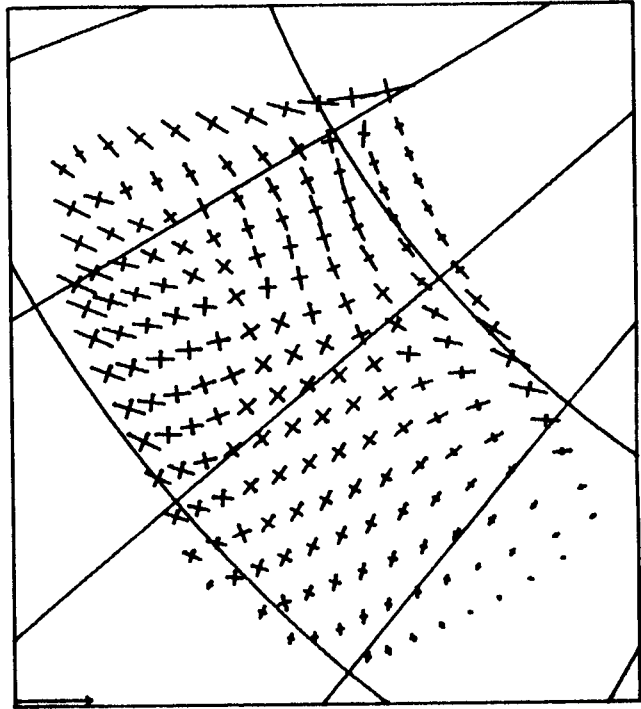


h) 3 February

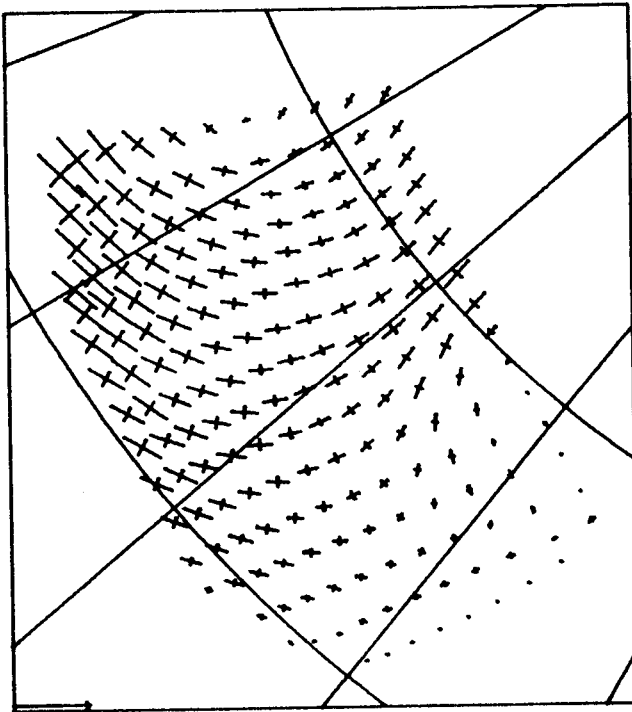
Figure 24.(cont.) Stretching Tensor Field (Daily Strain) with Principal Values Proportional to Line Length in Directions Shown. Dashed lines indicate opening and solid lines closing. Scale vector is $8 \times 10^{-7} \text{ sec}^{-1}$ (approximately 8% per day).



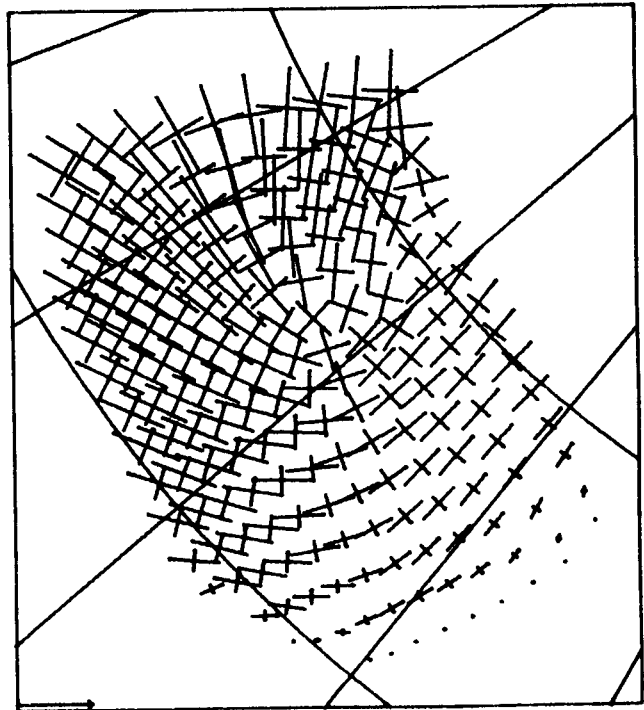
a) 27 January



b) 28 January

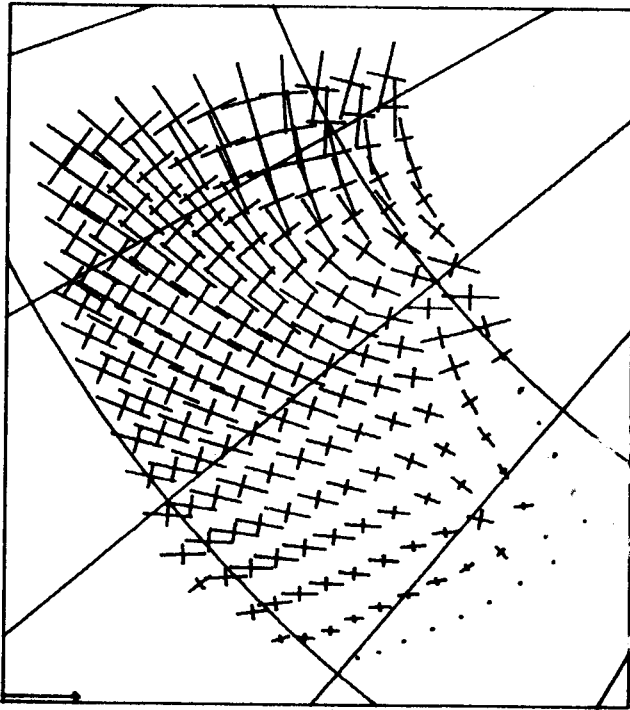


c) 29 January

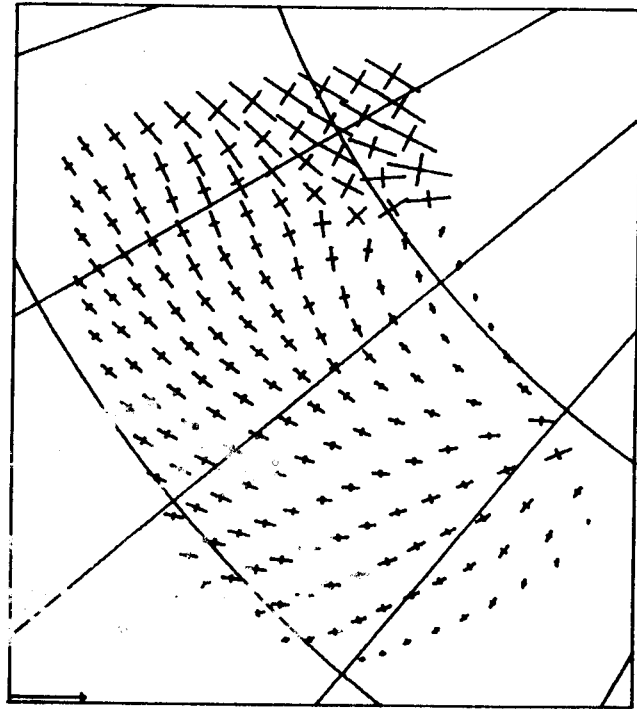


d) 30 January

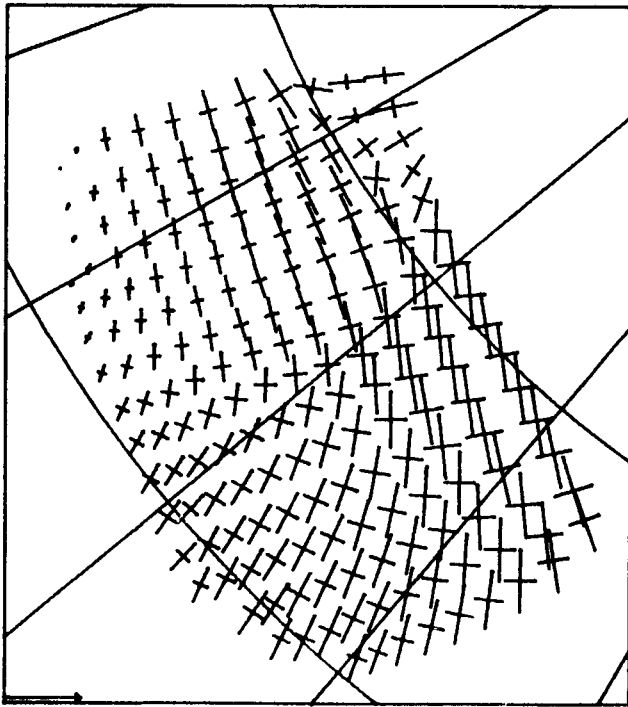
Figure 25. Stress Tensor Field with Principal Values (all compressive) Proportional to Line Lengths in Directions Shown. Scale vector is 10^8 dyn cm^{-1} .



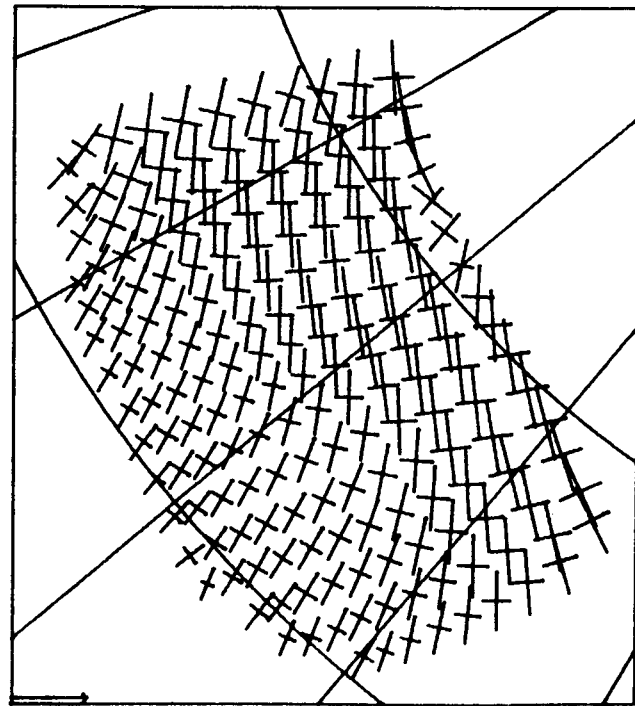
e) 31 January



f) 1 February



g) 2 February



h) 3 February

Figure 25. (cont.) Stress Tensor Field with Principal Values (all compressive)
 Proportional to Line Lengths in Directions Shown. Scale vector is 10^8 dyn cm^{-1} .

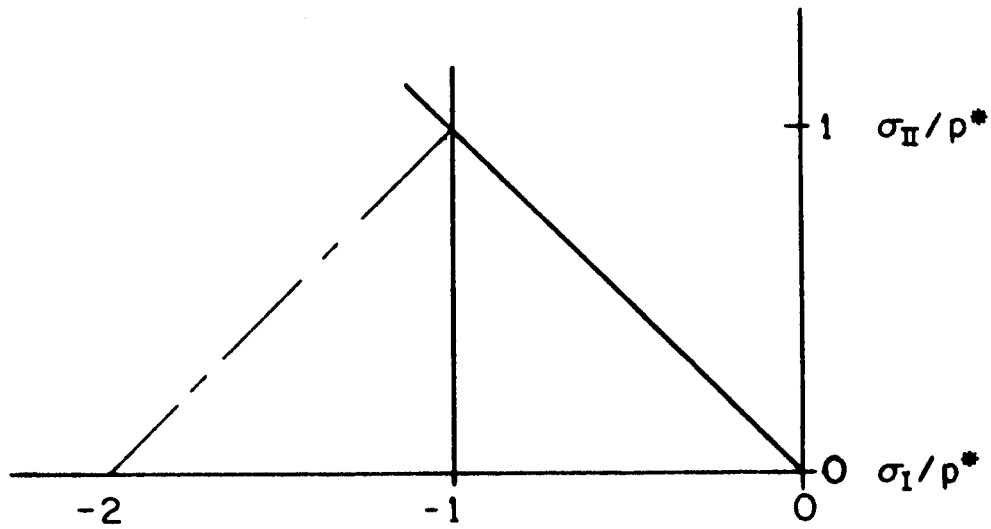


Figure 26. Triangle Yield Curve.

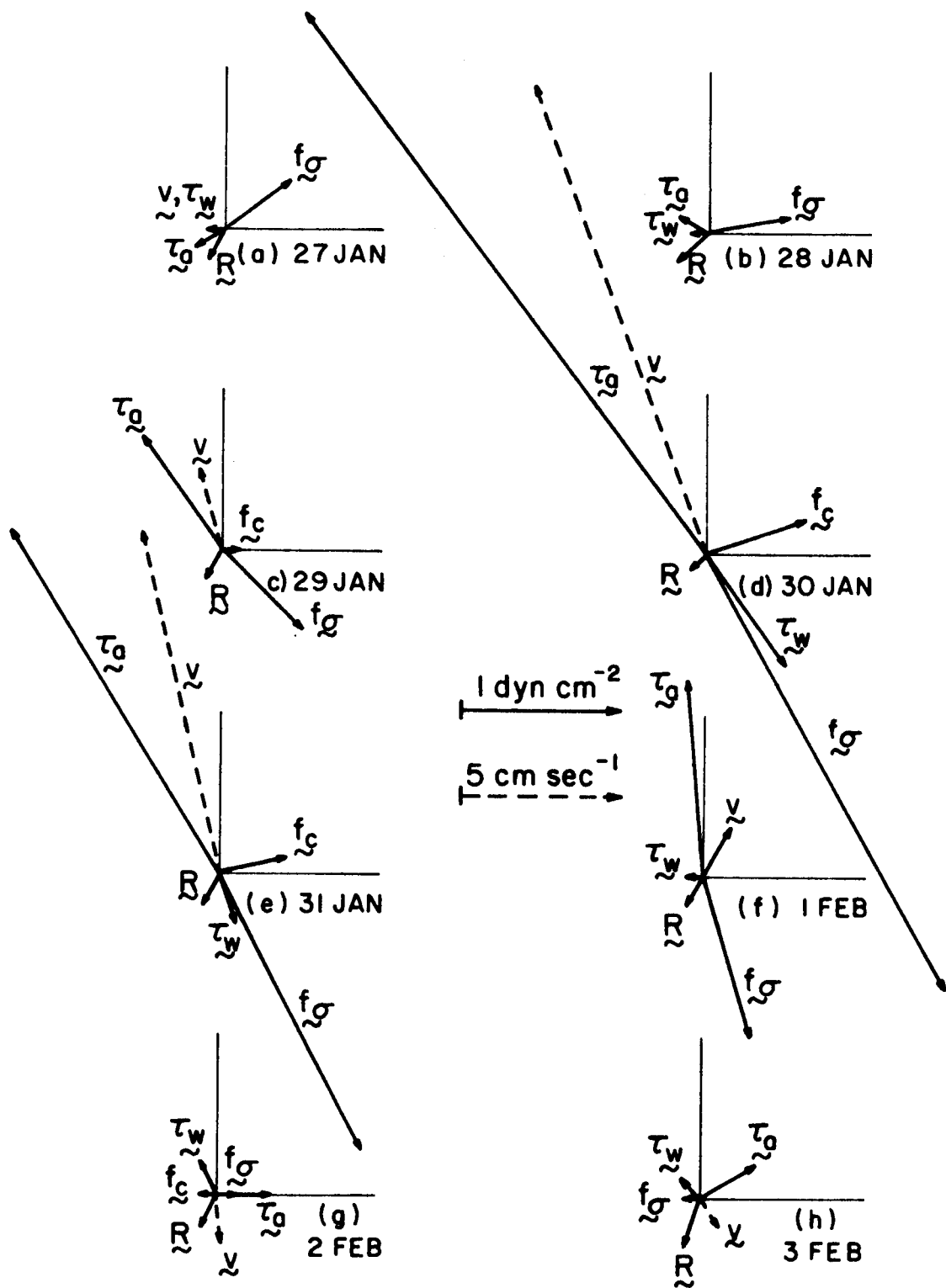


Figure 27. Force Balance at Node Nearest Caribou for Each Day. Scale vectors show magnitude of forces (per unit area) and velocity (dashed). Air stress τ_a , water stress τ_w , ice stress divergence f_σ , Coriolis force f_c and ice velocity v are each shown. If any vector is missing, then it is zero on that day. Cartesian axes are aligned with all other axes in this report.

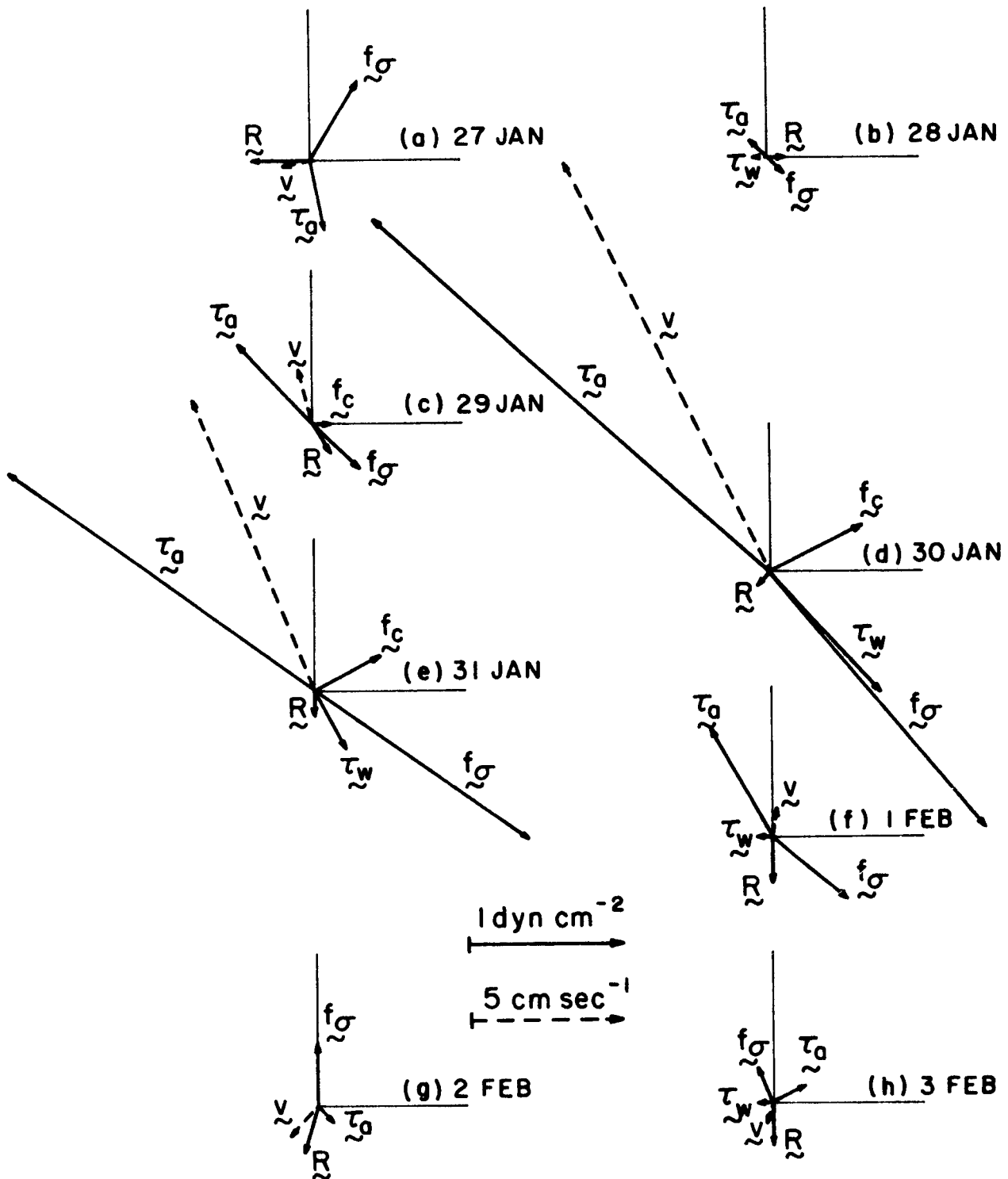


Figure 28. Force Balance at Node Nearest Blue Fox for Each Day. Scale vectors show magnitude of forces (per unit area) and velocity (dashed). Air stress τ_a , water stress τ_w , ice stress divergence f_σ , Coriolis force f_c and ice velocity v are each shown. If any vector is missing, then it is zero on that day. Cartesian axes are aligned with all other axes in this report.

ANNUAL REPORT

Contract #03-5-022-56

Research Unit 99

Task Order #6

Reporting Period: 4/1/76-3/31/77

Number of Pages: 11

THE ENVIRONMENTAL GEOLOGY AND GEOMORPHOLOGY OF THE
GULF OF ALASKA COASTAL PLAIN AND THE COASTAL ZONE OF
KOTZEBUE SOUND

Dr. P. Jan Cannon
Principal Investigator
Department of Solid Earth Science
University of Alaska

March 31, 1977

ANNUAL REPORT FOR YEAR ENDING March 31, 1977

Project Title: The Environmental Geology and Geomorphology of the Gulf of Alaska Coastal Plain and the Coastal Zone of Kotzebue Sound

Contract Number: 03-5022-56

Task Order Number: 6

Principal Investigator: Dr. P. Jan Cannon

I. Task Objectives of Kotzebue Sound Project:

- A. To produce three maps, with explanations, which will display certain baseline data necessary for an environmental assessment of the regions. The maps will be constructed from various types of remote sensing data.
 - 1. Environmental geologic map of the entire forelands from Cape Prince of Wales to Cape Lisburne which will include the lowlands of the Kobuk Delta, the Noatak Delta, and the Kotzebue Moraine.
 - 2. A coastal landforms map of the region identifying and describing important geomorphic features.
 - 3. A map which indicates potential tectonic and geomorphic hazards.
- B. To produce a report on the unique geologic setting of the Kobuk Delta indicating the possible effects (beneficial and adverse) of petroleum related development in the area.
- C. Direct the acquisition of remote sensing data of the area for Cannon, Hayes and other investigators.
- D. Construct a mosaic of the area of sequential LANDSAT data for Cannon, Hayes, and other investigators.
- E. Construct an annotated mosaic of the area from SLAR imagery.

II. Introduction:

Environmental geologic data must be displayed in spatial format if a realistic evaluation is to be made of an area. If changes are induced, natural environments respond in all dimensions. Therefore, components of natural environments must be displayed in a spatial framework which portrays

their degree of physical association. This makes it necessary to display environmental information on maps, because point values cannot convey a complete indication of the degree of interface between components. This is important if predictive model studies are to be made of the area. Sequential information is needed if rates and magnitudes of change are to be included in an environmental evaluation. This demand of sequential observations makes it necessary that the most neoterial data be obtained of the area of investigation.

A geomorphic history is based on the construction of a chronology of geomorphic events. Spatial information and sequential observations of large portions of the coastal zone is necessary in order to construct a chronology. Landforms are the products of the manner in which the energy of geomorphic agents (such as wind, water, and ice) is expended upon terrestrial materials. Since geomorphic agents interact to various degrees at or near the earth's surface, a variety of landforms can be generated in almost any locality. Landforms are, therefore, a record of the geomorphic agents which have dominated or are presently dominating the patterns of energy interchange at some point on the earth.

The assemblage of landforms and the geomorphic processes which are effected, as a result of the creation of the assemblage, form that which is termed "the environment" of a particular area on the earth's surface. The identification of a landform or of an assemblage of landforms provides information about the environment which can be used to evaluate the natural history of the environment and to appraise the impact of induced changes.

III. Current State of Knowledge:

The Chukchi Sea Coastal Forelands from Cape Prince of Wales to Cape Lisburne have been studied by several people during the last thirty years. However, most of these investigations were related to sea level fluctuations and the archeological importance of the Bering Land Bridge. There are two outstanding collections of data about the area: 1) Wilimovsky, N. J., and Wolfe, J. N., 1966, eds., Environment of the Cape Thompson region, Alaska: U.S. Atomic Energy Commission; 2) Hopkins, D. M., 1967, ed., The Bering Land Bridge: Stanford University Press. Both of these books contain abundant point data about the region. The Chukchi Sea Forelands are quite deserving of intense study because they exhibit a complex history of sea level fluctuations. This history is unique because both tectonic and eustatic changes in sea level are recorded. The record exists because the geomorphic processes which usually destroy the indicative features in a short time are retarded by the effects of the arctic winter.

IV. Study Area:

The Chukchi Sea Forelands consist of geomorphic features that show regular deposition is occurring in some areas, while intense erosion is occurring in other areas. A nearly complete range of depositional or erosional features appears to exist between the extremes.

The forelands are divided into four geomorphic divisions for this investigation. The four divisions are: 1) Lisburne Headlands, 2) Kivalina Coastal Complex, 3) Kotzebue Sound, and 4) Shishmaref Barrier Island-Beach Systems.

The northern most division is the Lisburne Headlands which extend south from Cape Lisburne to Kilikralik Point. Erosion is so intense in this division that it is dangerous to work in the area because landslides (rockfalls) can be observed daily.

The Kivalina Coastal Complex includes the stretch of coast from Kilikralik Point southeastward to Cape Krusenstern. The major geomorphic features of this division are Point Hope, Cape Thompson, Kivalina Lagoon, and Cape Krusenstern.

The Kotzebue Sound division includes several major geomorphic features which border the Sound. Starting at Cape Krusenstern and going clockwise around the Sound, the major geomorphic features are Sheshalik Spit, Noatak Delta, Baldwin Peninsula, Hotham Inlet, Kobuk Delta, Eschscholtz Bay, Goodhope Bay, and Cape Espenberg. This range of features indicates that the geomorphic history of Kotzebue Sound is quite complex. Kotzebue Sound itself is a shallow, sediment-filled embayment. The major portion of its sediments come from the Kobuk and Noatak Rivers. Minor contributions of sediments come from the Selawik and Buckland Rivers.

The southernmost division is the Shishmaref Barrier Island-Beach System. This division extends southwestward from Cape Espenberg to Cape Prince of Wales. The major geomorphic features are the large lagoons and inlets, and the sheltering chain of barrier islands. Abandoned beach ridges and the volcanic maars of the Devil Mountain area are minor, but nonetheless important geomorphic features.

V. Sources, Methods and Rationale of Data Collection:

The following lists the data sources and the methods planned to produce the products:

1. Evaluate existing literature and correspond with on-going projects in the area.
2. Search for and interpret any existing raw data on erosion and deposition.
3. Comparison of sequential mapping of coastal areas.
4. Photogeologic interpretations of low-altitude aerial photography.
5. Comparison of sequential LANDSAT imagery.
6. Geomorphic interpretation of radar imagery.
7. Low altitude aerial reconnaissance, this is very important part of ground truth measurements and map unit verification.

8. Identification of major shoreline processes.
9. Evaluation of historical records.
10. Identification of the materials which comprise the shoreline features.
11. Field observations and measurements of shoreline changes from previous and current studies.
12. Interpretation of the shoreline morphostratigraphy.
13. Compilation of a landforms map of the region.
14. Compilation of an environmental geologic hazards map of the region.
15. Compilation of a shoreline stability map.
16. Construction of an environmental energy flow model for the region.
17. Analysis of the future effects of natural processes and man-induced effects.

The preceding statements are an outline of an approach to meet the scientific objectives and establish information which is to be displayed or discussed in the products. The initial step is to make a temporary identification of the existing landforms. The second step therefore is to verify the landform identification. The landform verification is approached by utilizing the principles of the concept of multiple working hypotheses. In some cases the landform verification will necessitate ground reconnaissance. The verification of other landforms may call for a regional look at the geomorphic system. Often in geomorphology the answers are found outside of the area of specific interest. A delta quite often reflects factors that exist in the watershed of the streams at points somewhat removed from the delta itself. Therefore just looking at the delta itself will never answer all the questions. Directions of sampling, evaluation, and interpretation continually change as information is collected and exchanged.

VI. Results:

- A. Low-altitude, color IR photography was acquired of the area by NOS. This is excellent photography and should provide a tremendous amount of useful information to P.I.'s other than Cannon and Hayes. The archaeologists, biologists, and oceanographers in the OCS program can view this photography at the Geophysical Institute, University of Alaska, Fairbanks.

- B. Five overlapping strips of radar imagery were acquired of the Kobuk Delta. Single strips of radar imagery were also acquired of the coastline from Cape Prince of Wales to Cape Lisburne.
- C. Because of the range in types of landforms and intensity of geomorphic processes in the area of investigation, the study area was divided into four main geomorphic divisions (see section IV. Study Area).
- D. Wave action in the larger lagoons is intense enough to generate longshore currents within the lagoons. The longshore currents have sufficient energy to transport materials and are therefore reshaping shorelines inside the lagoon.
- E. Ice effects appear to be minor along the shorelines.
- F. Lakes appear to form as a function of time in prograding shorelines. The suspected process is dewatering and subsequent compaction of unconsolidated materials.
- G. Prior to the 3 meter rise in sea level some 4,000 years ago, the Noatak and Kobuk Rivers had built a delta between Sheshalik Spit and Baldwin Peninsula. The drowned distributary channels of this delta apparently influence the present flow of water from Hotham Inlet and the Noatak River into Kotzebue Sound.

VII. Discussion:

The need for neoteric data of the coastal zone was satisfied with the acquisition of radar imagery and low-altitude, color and color IR aerial photography of the area. LANDSAT imagery of the area was acquired covering the time span of 1972 through 1975. There exists LANDSAT imagery of both break-up and freeze-up seasons.

In order to facilitate discussion and mapping, the coastal zone is divided into four geomorphic divisions. Figure 1 shows the two northern divisions, the Lisburne Headlands and the Kivalina Coastal Complex. The Lisburne Headlands is the smallest of the four divisions. However, within this division the most intense erosion is occurring.

The Kivalina Coastal Complex exhibits a large range of features and processes. Materials are eroded from the Cape Thompson area and distributed in both directions along the coast from the Cape. As the result of "Project Chariot", Cape Thompson and the Kivalina Coastal Complex have been documented in great detail (Wilimovsky and Wolfe, 1966). Since most of the field work for "Project Chariot" was done seventeen years ago, it is being used as a reference to geomorphic changes for this investigation. Raised shorelines in this division attest to a long history of shoreline changes (Hopkins, 1967). Throughout this division the barrier islands in front of the narrow lagoons all show features caused by washover during storms. Both fan deltas and washover rills occur on the lagoon side of the

barrier islands. The washover materials (mainly gravels) are pocked with numerous depressions, five to thirty centimeters deep and twenty to one hundred and forty centimeters across. These features are microkettles formed by the melting of ice under the washover materials. The ice is from chunks tossed up by storms and from the formation of the kaimoo. Kaimoo is the name given by the Eskimo to the ice and gravel rampart formed at the onset of winter on the surface of the beaches. The kaimoo has a significant effect on coastal processes because its formation marks the end of effective wave action on the upper part of the beach.

Point Hope is presently being built out on the south side by sediments from Cape Thompson. The north side of Point Hope is, at present, only being maintained with sediments carried off of the apex of the point and with minor sediments from the Kukpuk River. The effects of recent undercutting and erosion are exhibited along most of the north side of the point. The unconsolidated materials of Point Hope apparently rest on a broad wave-cut bench of bedrock.

In the southeastern part of this division are various geomorphic features which indicate that the Noatak River at one time emptied into the Chukchi Sea, at the present site of Killikmak Creek, twenty-five kilometers north of Cape Krusenstern. Tectonic uplift blocked the flow of the Noatak River and created a large lake in the depression where the village of Noatak is located. The lake was breached to the south and the present outlet of the Noatak River was established. The dates of these events are not yet clear to this investigator. However, the abandoned shorelines of the lake might provide artifacts which would help date the events.

After the establishment of the Noatak River outlet into Kotzebue Sound (the third geomorphic division), the Noatak and Kobuk Rivers jointly built a large delta between the Baldwin Peninsula and Sheshalik Spit (Figure 2). About 4,000 years ago sea level rose nearly three meters and the delta was submerged. The outline of the delta can be clearly seen on the bathymetric charts of the sound. The flow of water from the Noatak and Kobuk Rivers is presently still influenced by the distributary channels of that submerged delta. This can be seen on the LANDSAT imagery in Figure 3.

The last rise in sea level drowned the lower Kobuk River valley and created Hotham Inlet and the large lakes that branch off it. Sequential data indicates that the large lakes are increasing in area, probably due to the melting of permafrost by the incursion of sea water.

The fourth geomorphic division, the Shishmaref Barrier Island-Beach System (Figure 4) differs from the other geomorphic divisions in several aspects. One outstanding aspect is that the beach materials are mainly sand, whereas on the other beaches, gravel predominates. Geomorphic features indicate major transport of materials towards the ENE and storm waves have built large washover fan deltas into the lagoons.

References

- Hopkins, D. M., ed., 1967, *The Bering Land Bridge*: Stanford University Press.
- Wilimovsky, N. J., and Wolfe, J. N., eds., 1966, *Environment of the Cape Thompson region, Alaska*: U.S. Atomic Energy Commission.

VIII. Conclusions:

Due to the retarding effect of the Arctic climate some geomorphic features (such as old shorelines and deltas) have been uniquely preserved. The delineation of past shorelines and deltas will perhaps indicate potential archaeological sites.

The coastal zone exhibits a large range of geomorphic features and within the coastal zone the interaction of major geomorphic processes is complex. Due to this complexity, consideration of environmental problems and potential developments within the coastal zone will have to be done on a location by location basis. Environmental assessments must be made by geomorphic divisions with special attention being given to specific features within the divisions.

IX. Need for Further Study:

- A. The formation of lakes as a function of time in beach materials.
- B. The compaction or consolidation of sediments in the region.
- C. The relative chronology of major geomorphic events.
- D. The draining of lakes in some specific areas.
- E. The potential effects of wave action in large lagoons.
- F. The stability of the large deltaic features.
- G. The natural future evolution of the region.

X. Summary of 4th Quarter Operations:

- A. Began preparation of first draft of maps.
- B. Continued interpretative analysis of remote sensing data.
- C. Participated in OCS Beaufort/Chukchi Sea synthesis meeting at Barrow.
- D. Made preparations for pre-break-up and break-up ice studies.

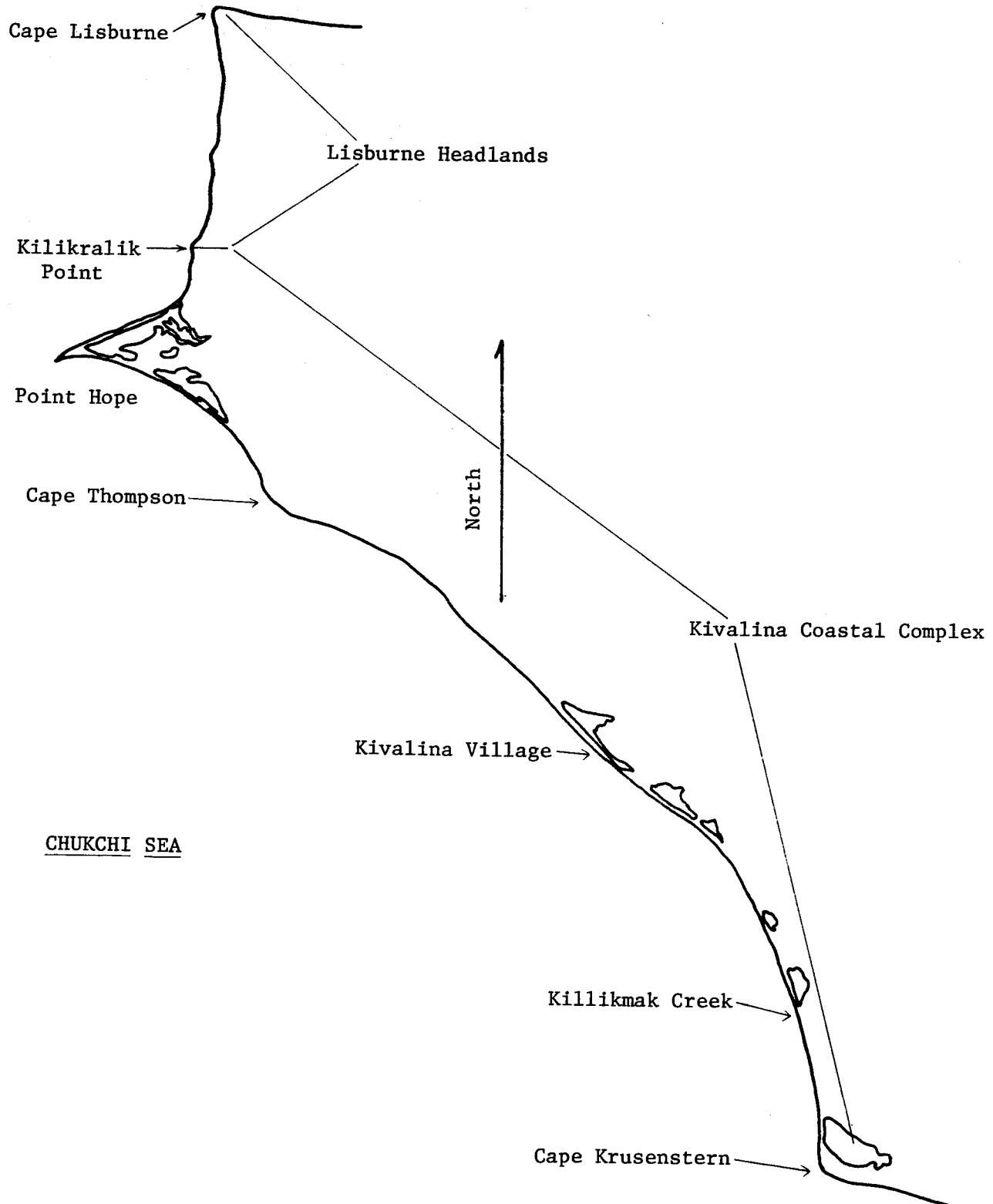
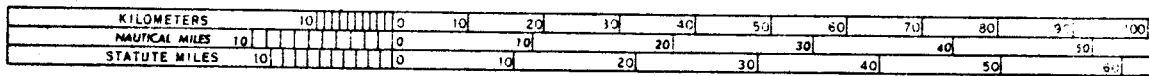
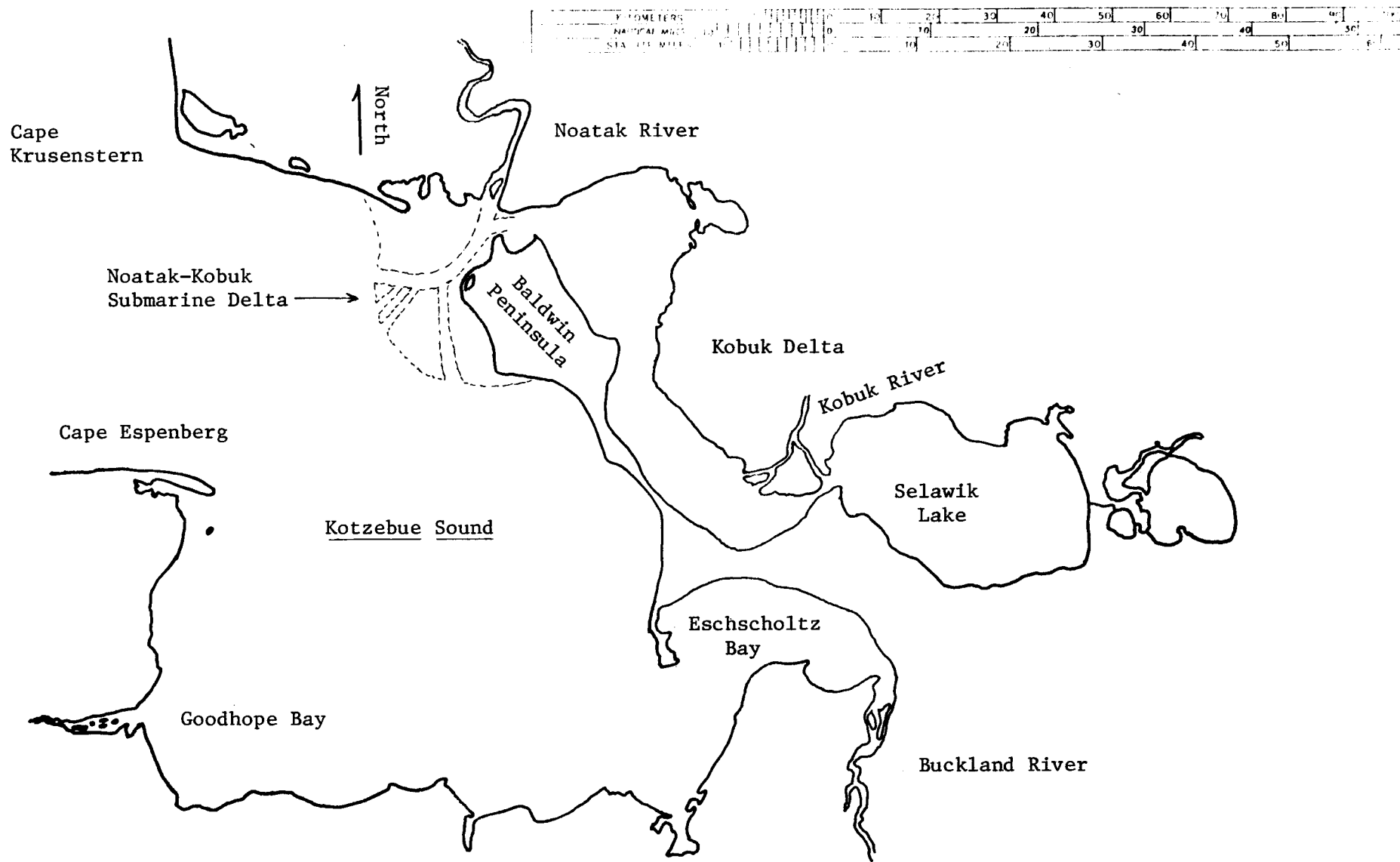


Figure 1. Major features of the two northern geomorphic divisions, the Lisburne Headlands and the Kivalina Coastal Complex.

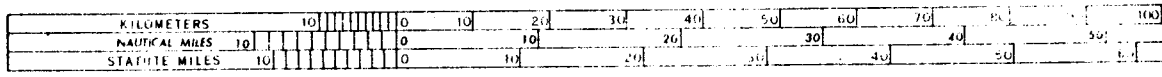


342

Figure 2. Major features of Kotzebue Sound.



Figure 3. LANDSAT image of Kotzebue Sound. Date 02JUN73, Frame number 1314-22043, Band 7, scale is same as Figure 2. Dark area extending from Noatak River past Kotzebue and into sound is open water over channel in submarine Noatak-Kobuk delta.



344

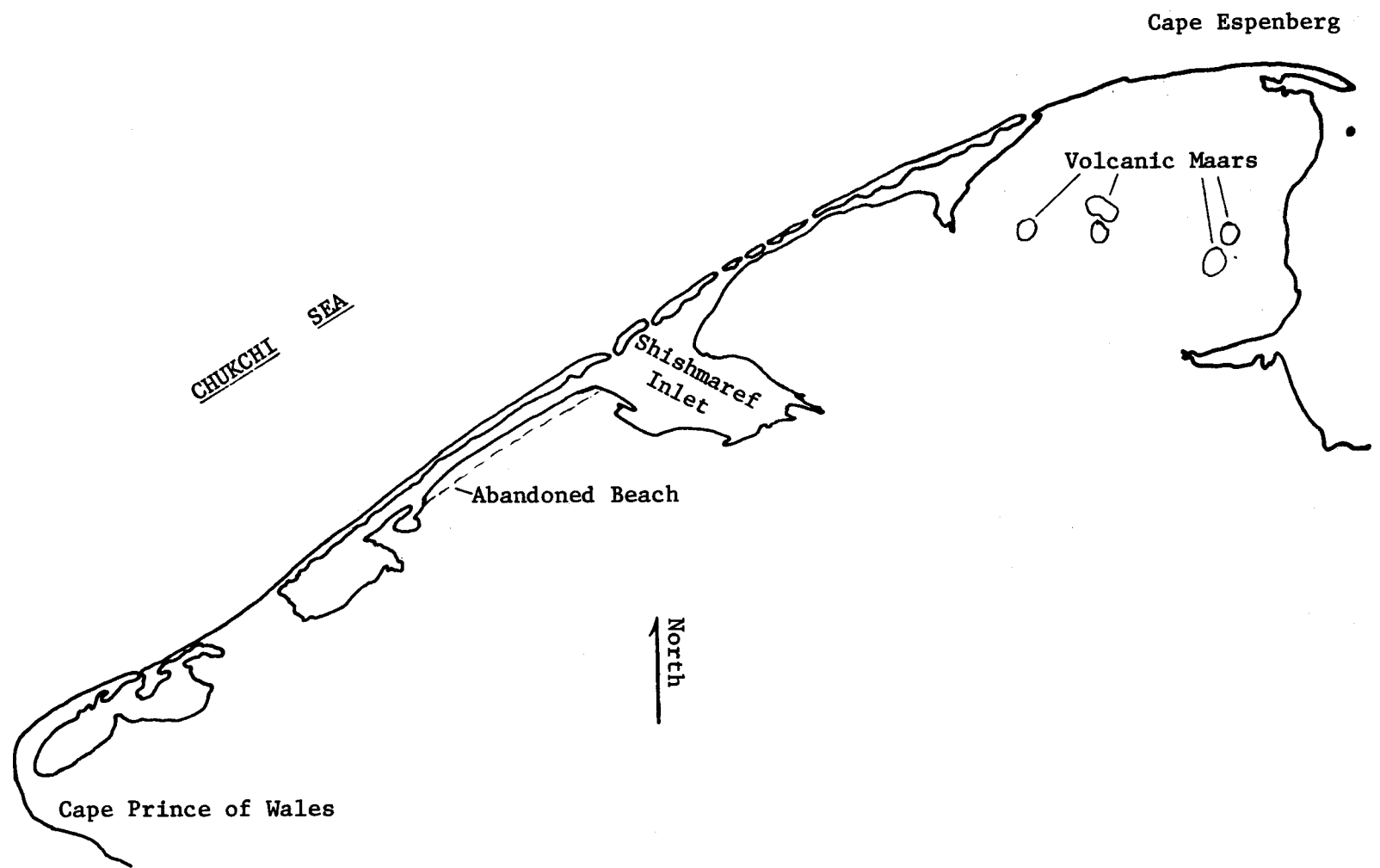


Figure 4. Major geomorphic features of Shishmaref Barrier Island-Beach System.

OCS COORDINATION OFFICE

University of Alaska

ENVIRONMENTAL DATA SUBMISSION SCHEDULE

DATE: March 31, 1977

CONTRACT NUMBER: 03-5-022-56 T/O NUMBER: 6 R.U. NUMBER: 99

PRINCIPAL INVESTIGATOR: Dr. P. Jan Cannon

No environmental data are to be taken by this task order as indicated in the Data Management Plan. A schedule of submission is therefore not applicable.

NOTE: ¹ Data Management Plan has been approved by M. Pelto; we await approval by the Contract Officer.

FINAL REPORT

THE ENVIRONMENTAL GEOLOGY AND GEOMORPHOLOGY
OF THE GULF OF ALASKA COASTAL PLAIN

Dr. P. Jan Cannon
Assistant Professor of Geology
Division of Geoscience
University of Alaska
Fairbanks, Alaska 99701

TABLE OF CONTENTS

I. Task Objectives 1

II. Introduction. 2

III. General Description of Area 2

IV. Introduction to Radar Imagery 5

V. Application of Radar Imagery to Environmental Geologic
Mapping of Coastal Zones.11

VI. Mapping the Gulf of Alaska Coastal Plain with
Radar Imagery14

VII. Conclusions23

References Cited.27

LIST OF TABLES

Table 1 Commonly used radar bands 6
Table 2 Some advantages of radar imagery. 7
Table 3 Acquisition conditions for remote sensing data. 10
Table 4 Comparison of radar wavelengths and the information
pertinent to coastal studies which is displayed
on radar imagery. 13
Table 5 Explanation of map units. 28

LIST OF MAPS

Map 1 Major landforms of the Gulf of Alaska coastal plain. . . 30
Map 2 Environmental geologic hazards of the Gulf of
Alaska coastal plain 31
Map 3 Major lineaments of the Gulf of Alaska coastal plain . . 32
Map 4 Shoreline stability of the Gulf of Alaska
coastal plain. 33
Map 5 Major beach materials of the Gulf of Alaska
coastal plain. 34

LIST OF FIGURES

Figure 1 Index map. 4
Figure 2 Diagram of antenna-look-direction. 8
Figure 3 K-band, real aperture, radar imagery of Sabine Pass. . .15

Figure 4	Radar imagery of the Yakataga District.	16
Figure 5	Mosaic of radar imagery of Icy Bay and the Western section of the Malaspina District	17
Figure 6	Mosaic of radar imagery of the Eastern section of the Malaspina District	18
Figure 7	Mosaic of radar imagery of the major portion of the Yakutat District	19
Figure 8	Radar imagery of part of the Yakutat District, showing Dry Bay	20
Figure 9	Radar imagery of the Yakutat District	21

FINAL REPORT
FOR
GULF OF ALASKA

December 30, 1976

Project Title: The Environmental Geology and Geomorphology of
the Gulf of Alaska Coastal Plain

Contract Number: 03-5-022-56

Task Order Number: 6

Principal Investigator: Dr. P. Jan Cannon

I. Task Objectives

- A. To produce three maps of the coastal plain section of the Gulf of Alaska
- B. To produce a report on the application of radar imagery to the environmental geologic mapping of coastal zones
- C. To construct an annotated mosaic of the area from radar imagery
- D. To indicate the effects (beneficial and adverse) that oil and gas development might have in relation to the geologic setting.

II. Introduction

This report presents information which can be used in an environmental assessment of the coastal plain of the Gulf of Alaska. It also contains an evaluation of radar imagery as a major information source for environmental geological mapping.

This report contains five maps which display certain baseline data necessary for an environmental assessment of the coastal plain. During the planning stages of this project, it was thought that the data could be displayed on three maps. However, the number of maps had to be increased to five in order to adequately present the information concerning the environment.

It was necessary to increase the number of task objectives in order to improve the communication of information. Also, the presentation and discussion of task objectives have been arranged within this report in a manner which will increase the utilization of the information.

III. General Description of Area

The coastal plain of the Gulf of Alaska is a narrow strip of land (1 to 40 km wide) which extends some 600 km from Icy Point to the western margin of the Copper River Delta. The upper or inland margin is bordered with the high mountains of the Chugach, St. Elias, and Fairweather Ranges, which extend in elevation from 3,650 to 5,800 meters. The area is usually overcast and cold. Obtaining aerial photographs of this area is almost impossible. Due to the geographic location of the Gulf of Alaska on the Earth and the fact that two ranges of the highest mountains on the North

American continent lie just to the north of the Gulf of Alaska, the area has a climate that is unusually warm for its latitude. However, this relative warmth is offset by the situation that the same factors that make temperatures warmer also help produce high amounts of precipitation (average 302 cm per year), almost continual overcast conditions, and an impact zone for some of the worst storms created on the entire planet.

The coastal plain has been described as having a diversified topography carved in Tertiary rocks. The assemblage of landforms in the area is indeed quite diverse which is unlike most coastal plains on this planet. However, this diversity is valuable in constructing a chronology of the geomorphic events which have occurred in the area. The coastal plain is crossed in several places by fiords and active glaciers. The assemblage of landforms includes: morainal belts, dead ice moraines, thermokarst pits, outwash plains, meltwater streams, marine terraces, abandoned beach ridges, large tidal flats in shallow bays, and the associated longshore features of bars, spits, and backwater lagoons. The materials of the coastal plain consist of till, gravels, sand, mud, ice, and various mixtures of these materials.

The portion of the coastal plain which will be the most involved with petroleum development is a section 255 km long, from Dry Bay westward to Cape Yakataga. This section, therefore, was the subject of this intense environmental geologic investigation as a part of the overall environmental assessment. The area can be divided into three physiographic zones separated by large fiords: the Yakutat District, the Malaspina District, and the Yakataga District (Fig. 1).

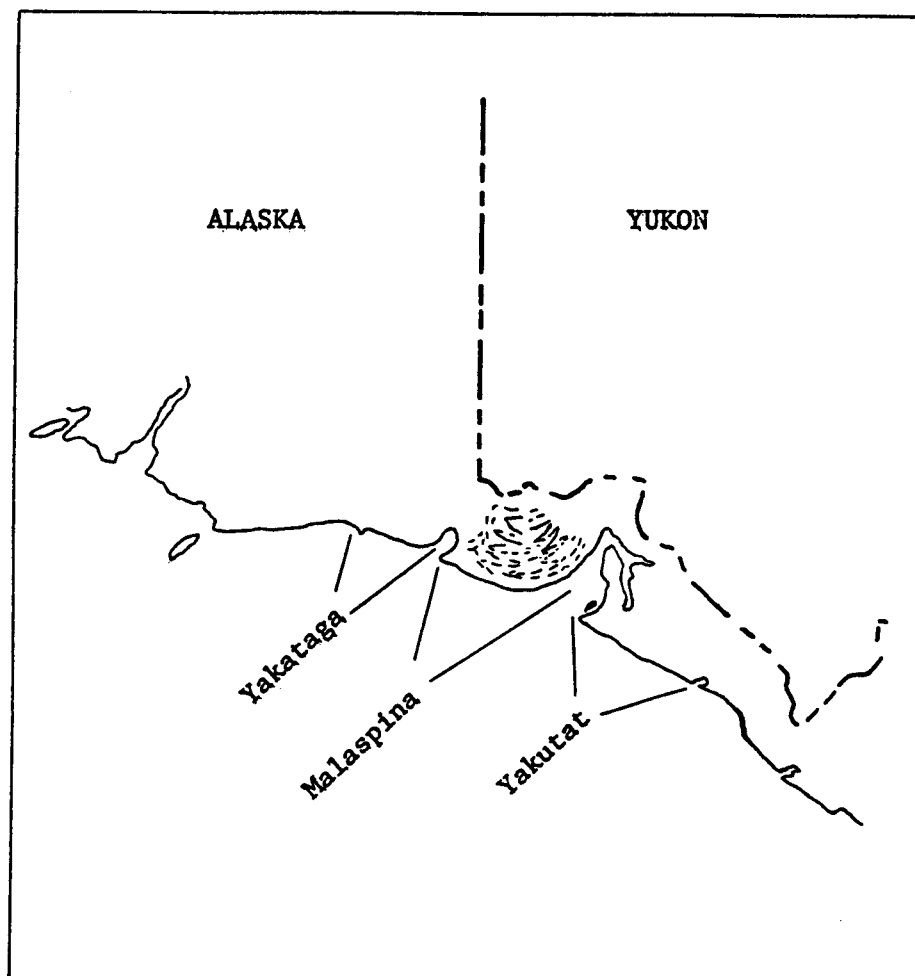


Figure 1. Index map showing the location of the Yakataga, Malaspina and Yakutat Districts. The three physiographic districts are separated by large fiords. The Yakataga District is a narrow strip of coastal plain between Icy Bay and Cape Yakataga. The Malaspina District is between Icy Bay and Yakutat Bay and consists of the Malaspina Glacier and the Malaspina Forelands. The Yakutat District is comprised of the coastal plain deposits that extend from Dry Bay and the Alsek River northwestward to Yakutat Bay.

IV. Introduction to Radar Imagery

Radar is an acronym devised from radio detection and ranging. It is an active system which means that it generates the energy that is ultimately recorded. Taking normal photographs in the dark with a flash bulb is an example of an active system. Of all the operating imaging sensors, radar operates at the longest wavelengths and the lowest frequencies. The wavelengths most commonly used for imaging radar systems are between 0.86 cm and 3.3 cm (Table 1). The radar frequencies range from 36.0 Gigahertz (GHz) to around 10.0 GHz. One Hertz is equal to one cycle per second and one GHz is equal to 10^9 cps. The present day radar systems are only a single wavelength of great spectral purity which means the systems are monochromatic.

Radar imagery is a spatial display of the relative differences in returns of radar energy from surface features. It should be kept in mind that although the radar imagery gives the appearance of a black-and-white photograph with low illumination, it is not a photograph, but an electronically constructed image of the various ways in which surface features reflect the radar energy. Some of the advantages of radar imagery are listed in Table 2.

Since radar imagery is acquired by an active system, the direction of illumination (called the look direction) can be oriented in a manner which provides the most useful results (Fig. 2). The altitude of imagery acquisition can be changed by altering the height of the aircraft, carrying the radar system, above the surface of the terrain. Also, the depression angle (the angle between a horizontal plane and the path of

TABLE 1
COMMONLY USED RADAR BANDS

<u>Bands</u>	<u>Frequency</u>	<u>Wavelengths</u>
P	300 MHz	1 meter
UHF	300 MHz-1 GHZ	1 meter - 30 cm
L	1-2 GHz	30-15 cm
S	2-4 GHz	15-7.5 cm
C	4-8 GHz	7.5-3.75 cm
X	8-12.5 GHz	3.75-2.4 cm
K _μ	12.5-18 GHz	2.4-1.67 cm
K	18-26.5 GHz	1.67-1.13 cm
K _α	26.5-40 GHz	1.13-0.75 cm
M _μ	40 GHz	0.75 cm

One Gigahertz (GHz) is equal to 10^9 cycles per second and one Megahertz (MHz) is equal to 10^6 cps. The wavelengths most commonly used for imaging radar systems are between 0.86 and 3.3 cm.

TABLE 2

SOME ADVANTAGES OF RADAR IMAGERY

1. Technique is independent of weather, time of day and time of year.
2. Landform recognition and identification is more rapid on radar imagery than on photographs or other types of imagery.
3. Provides immediate reconnaissance and interpretation.
4. Affords much greater areal coverage than cameras, like the aerial metric cameras, carried at the same altitude; provides a different perspective.
5. Does not produce the foreshortening or convergence effect seen in oblique aerial photographs.
6. Saves time and money in some cases due to the increased areal coverage per flight-line mile.
7. Commonly shows more stream detail than a topographic map at the same scale (this depends upon the system used).
8. Can provide quantitative geomorphic data.
9. By use of a synthetic aperture antenna system, radar resolution is (theoretically) rendered independent of height of the aircraft above the terrain.
10. Data can be stored on magnetic tape.

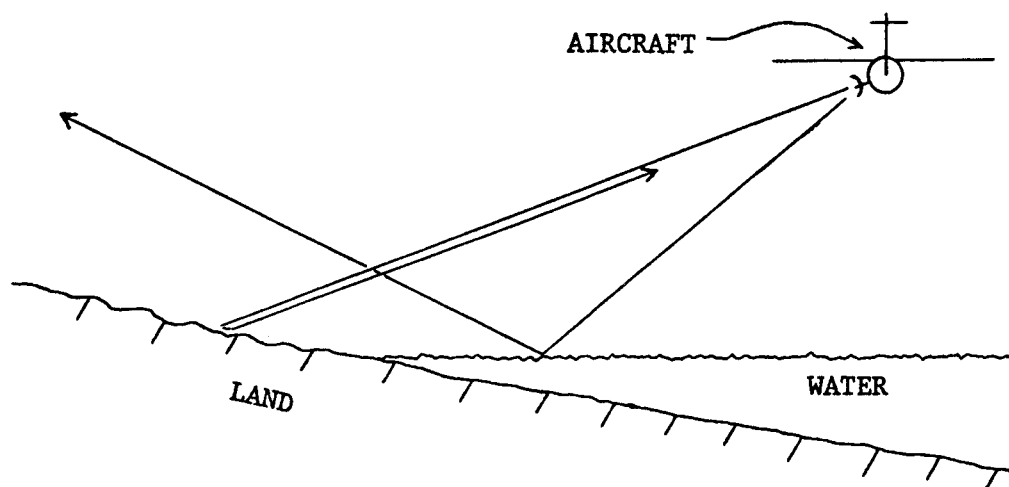


Figure 2. Diagram showing the correct antenna-look-direction for coastal studies. The antenna look-direction should be towards the coast. This means that the aircraft should be flying over the water. Having the look-direction towards the coast will enhance the minor relief features of the coastal plain and beach and will lessen the possible obscuration of important coastal features by shadow-effects from high relief features near the upper margin of the coastal plain.

the returning beam of radar energy which is to be recorded) can be altered to provide an increase or decrease in the shadow-effect, whichever is desired. The shadow-effect on features of relief is due to the side-looking nature (oblique illumination) of the radar imaging systems. For simplicity, side-looking airborne radar (SLAR) imagery is referred to as just "radar imagery" throughout this report.

Radar imagery can be obtained by two different antenna systems referred to as real and synthetic aperture systems. Real aperture (sometimes called brute force) refers to radar systems using the physical size of the antenna to determine the region of ground that is discriminated by the beamwidth. Synthetic aperture radar systems use only a part of the beamwidth; the signals returned are stored, and then processed in the same way that a physically larger antenna would process them. In other words, the returned signals are electronically interpreted to the sum equivalent of the same return as would be received by a physically larger antenna. The imagery provided by the real aperture system is considered to be the optimum source of information for environmental geologic mapping and geomorphic reconnaissance because of its greater dynamic range relative to the synthetic aperture system and more useful resolution.

X-band, real aperture radar imagery was obtained of the Gulf of Alaska coastal plain at the scales of 1:500,000 and 1:250,000. The area was covered with one strip of imagery at the scale of 1:500,000, and with four overlapping strips of imagery at the scale of 1:250,000. The radar imagery was used as the most up-to-date data source and as a mapping base. Since radar imagery can be obtained nearly anytime a fully instrumented aircraft can fly (see Table 3 on acquisition conditions for remote

TABLE 3

ACQUISITION CONDITIONS FOR REMOTE SENSING DATA

<u>Remote Sensing Data Types</u>	<u>Day Clear Sky</u>	<u>Day Overcast*</u>	<u>Night Clear Sky</u>	<u>Night Overcast*</u>
Black and white photography - Visible range	Yes	No	No	No
Color Photography - Visible range	Yes	No	No	No
Infrared Photography - Black and white	Yes	No	No	No
Infrared Photography - False color	Yes	No	No	No
Multiband Photography	Yes	No	No	No
Radar Imagery	Yes	Yes	Yes	Yes
Thermal Infrared Imagery	Yes	No	Yes	No
Satellite Photography	Yes	No	No	No
Satellite Imagery	Yes	No	Yes	No

*Clouds between sensor and target

sensing data), radar imagery was used as the principle data source.

V. Application of Radar Imagery to Environmental Geologic Mapping of Coastal Zones

Since the acquisition of radar imagery is so flexible, it is important that the methods and parameters involved in acquiring radar imagery of coasts be accurately expressed and followed. The antenna look-direction should be towards the coast (Fig. 2). This means that the aircraft should be flying over the water. Having the look-direction towards the coast will enhance the minor relief features of the coastal plain and beach and will lessen the possible obscuration of important coastal features by shadow-effects from high relief features near the upper margin of the coastal plain.

The acquisition altitude for the radar imagery can be very important. Vegetation discrimination is important for most coastal investigations and the best information about vegetation is displayed on radar imagery which is acquired at altitudes below 3,000 meters above the terrain. Discrimination between beach materials of various coarse sizes is also possible at these low altitudes with radar imagery obtained in the K-band region of the wavelengths (Cannon, 1974a).

Coastal areas which are of extreme environmental importance, in relation to petroleum exploration and development, are usually broad flat plains. Because these coastal plains have such low relief features it is often difficult to identify the important landforms. The low relief landforms of coastal plains, having relief differences of less than three meters, can be enhanced on radar imagery acquired with small depression

angles. The small depression angles increase the radar shadow-effect on low relief features, which helps in the identification of minor landforms.

The single most important factor in the amount of information displayed on radar imagery of a planetary surface is the physical interaction of the propagated radar energy with surface features. In other words, the physical size and geometry of surface features in relation to the wavelength of the radar energy determine the major differences in reflected radar energy which are indicated on radar imagery. The shorter the wavelength the greater the amount of information that can be obtained and displayed on the radar imagery. A comparison of the size of wavelength with the amount of information displayed on the resulting radar imagery of the most used radar systems is shown in Table 4. The type and amount of information needed in an investigation, therefore, prescribes the wavelength region to be utilized in obtaining radar imagery of any area.

The information in Table 4 is based on the optimum data types. The K- and X-band imagery is real aperture imagery and the L-band imagery is from a synthetic aperture system. For all geologic investigations real aperture imagery is superior to synthetic aperture imagery (Cannon, 1975).

Coastal plains in temperate or tropical regions especially lend themselves to the applications of radar imagery. These types of coasts are usually cloudy and the ability of radar imagery to record information through a cloud cover means that data can be collected most anytime.

The most important environmental information along these types of coasts is related to water bodies and vegetation differences. Therefore, the ability of the shorter wavelength radar system to discriminate between vegetation types and clearly delineate surface water features makes it a

TABLE 4

COMPARISON OF RADAR WAVELENGTHS AND THE INFORMATION PERTINENT
TO COASTAL STUDIES WHICH IS DISPLAYED ON RADAR IMAGERY

<u>Information Sources</u>	<u>K-Band*</u>	<u>X-Band*</u>	<u>L-Band+</u>
Beach Materials	good	inadequate	inadequate
Landforms	good	good	inadequate
Land-Water Contact	good	good	marginal
Minor-Vegetation	good	marginal	inadequate
Major-Vegetation	good	good	inadequate
Ice Surface Features	good	good	marginal
Ice Structure	good	good	good
Cultural Features	good	good	inadequate

*K- and X-band data from real aperture imagery
+L-band data from synthetic aperture imagery

Note: For a visual comparison of real aperture imagery with synthetic aperture imagery, see Cannon, 1974, pp. 764-766 (from Annual Report for Year Ending March 31, 1976).

very valuable technique. The units on an environmental geologic map are the components of natural systems and man-made features. K-band, real aperture, radar imagery of the coastal plain of Texas and Louisiana (Fig. 3) is a good example of the vegetation discrimination abilities of radar imagery (Cannon, 1974b). All land-water contacts, the coastline as an example, appear extremely sharp on radar imagery due to the strong contrast in reflective properties of the land and water.

VI. Mapping the Gulf of Alaska Coastal Plain With Radar Imagery

X-band, real aperture, radar imagery was obtained of the Gulf of Alaska Coastal Plain at the scales of 1:250,000 and 1:500,000. The area was covered with four overlapping strips of imagery at the scale of 1:250,000 (see Figs. 4, 5, 6, 7, and 8) and with one strip of imagery at the scale of 1:500,000 (see Fig. 9). The radar imagery was used as the most up-to-date data source and as a mapping base. The foremost factor influencing the choice of radar imagery as the major data source was the demand for neoteric data.

Two maps were made of the area showing data taken directly from the radar imagery. One is Map 1 which shows the major landforms of the area. The other is Map 3 which is a map of the major lineaments which cross the area. The information from Map 1 and Map 3 was combined to produce Map 2. Map 2 indicates the natural environmental geologic hazards of the Gulf of Alaska coastal plain.

The shoreline shown on the radar imagery and the shoreline shown in 1951 aerial photography of the area were compared to produce Map 4.



Figure 3. K-band, real aperture, radar imagery of the Sabine Pass area of Texas and Louisiana. This is a good example of the vegetation discrimination abilities of radar imagery (Cannon, 1974b). All land-water contacts, the coastline as an example, appear extremely sharp on radar imagery due to the strong contrast in reflective properties of the land and water. The most important environmental information along these types of coasts is related to water bodies and vegetation differences. Therefore, the ability of the shorter wavelength radar system to discriminate between vegetation types and clearly delineate surface water features makes it a very valuable technique. The units on an environmental geologic map are the components of natural systems and man-made features.

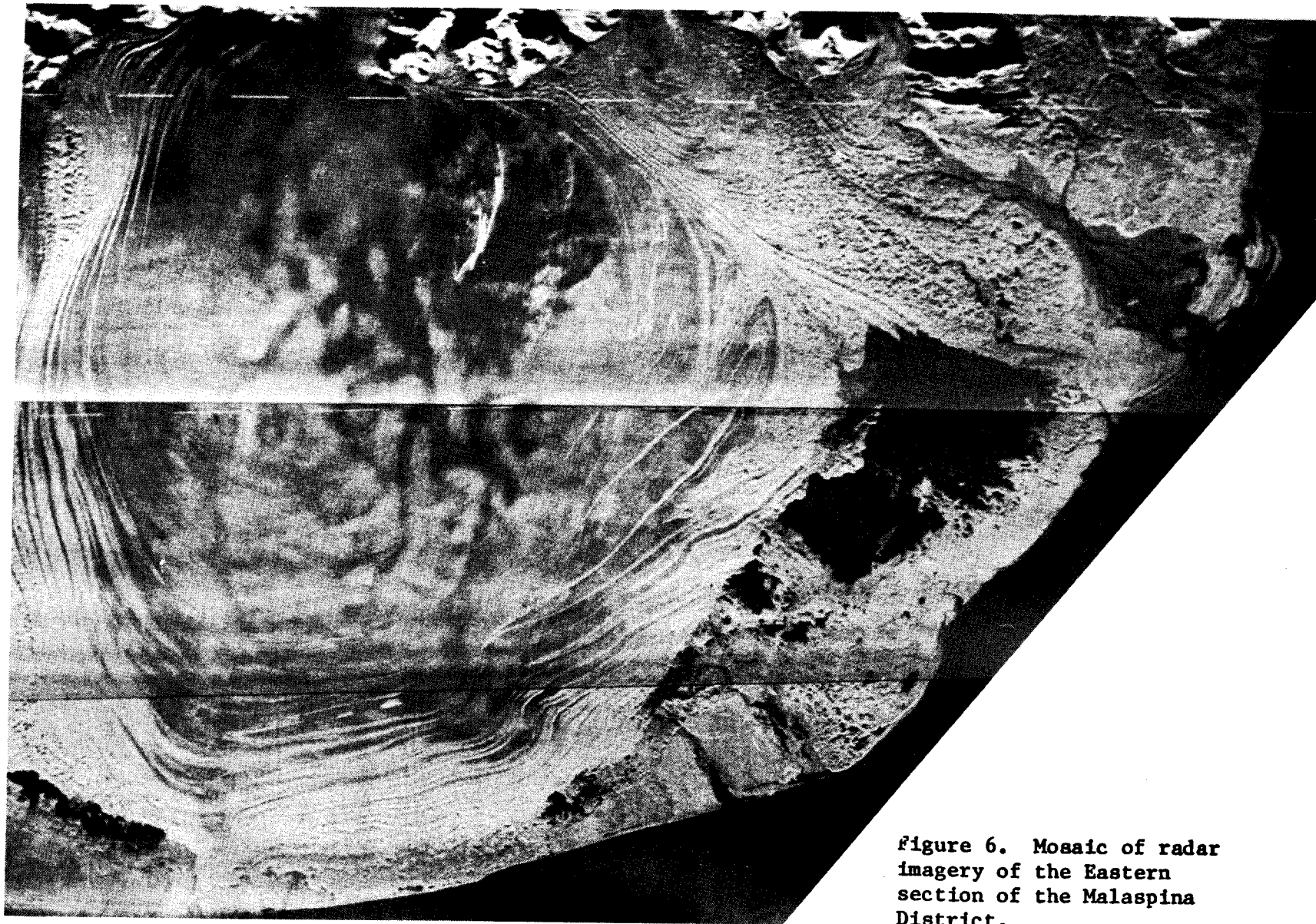


Figure 6. Mosaic of radar imagery of the Eastern section of the Malaspina District.

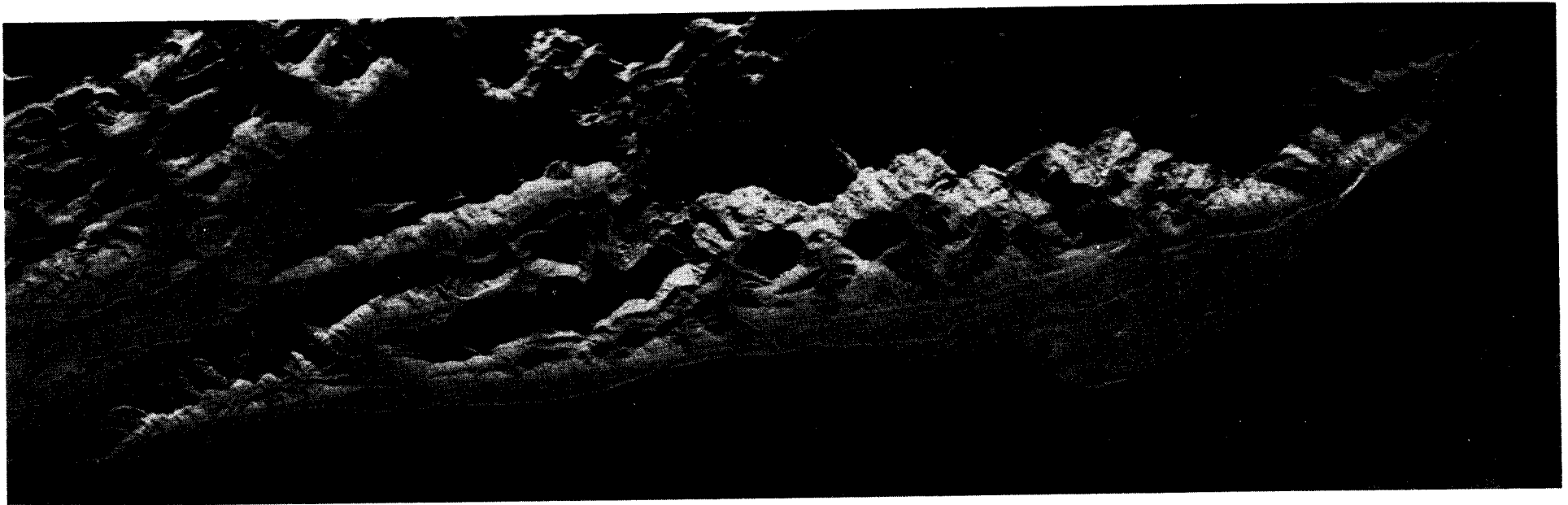
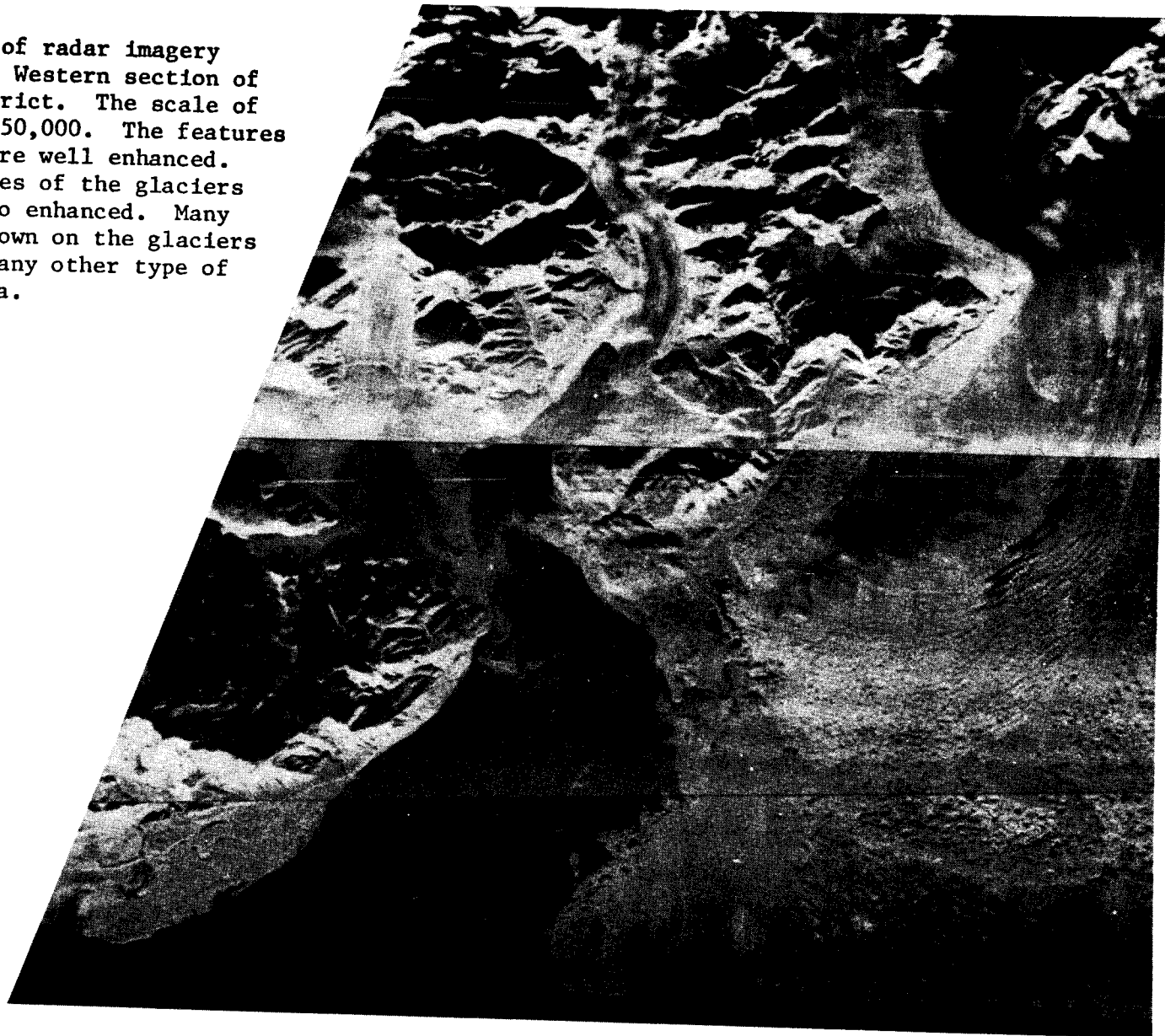


Figure 4. Radar imagery of the Yakataga District. This X-band, real aperture, radar imagery was acquired at a scale of 1:250,000. The data shown on Map 1 and Map 3 were taken from this imagery.

Figure 5. Mosaic of radar imagery of Icy Bay and the Western section of the Malaspina District. The scale of the imagery is 1:250,000. The features of the forelands are well enhanced. The various features of the glaciers themselves are also enhanced. Many of the features shown on the glaciers cannot be seen on any other type of remote sensing data.



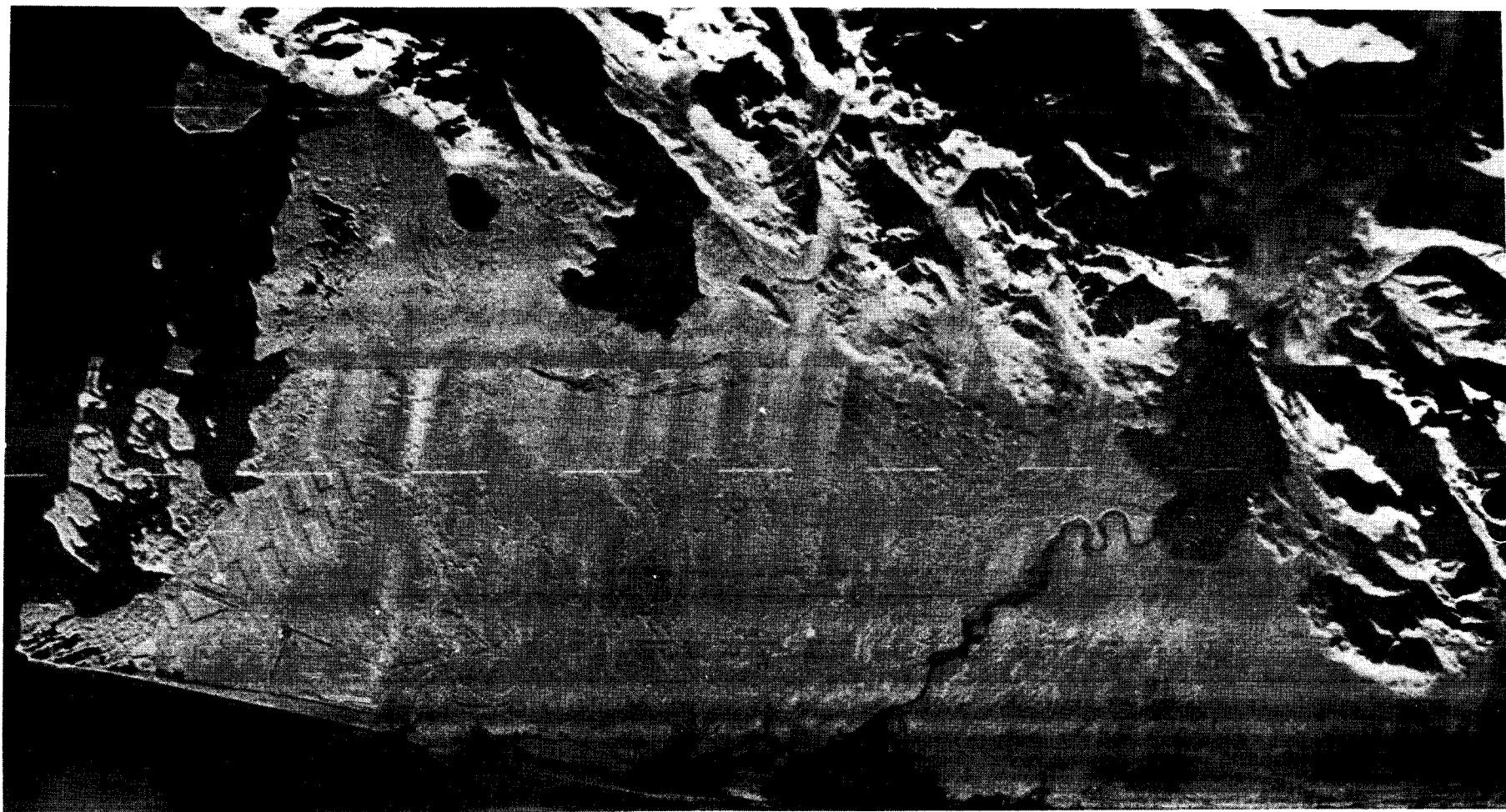


Figure 7. Mosaic of radar imagery of the major portion of the Yakutat District.

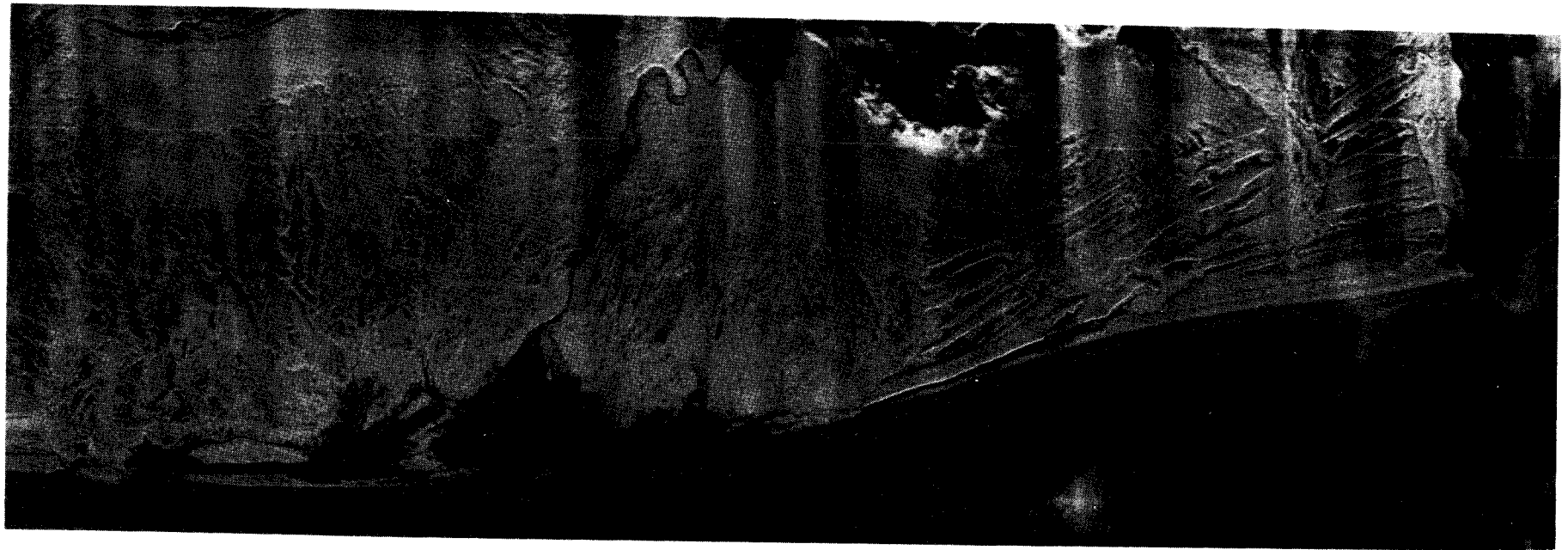


Figure 8. Radar imagery of part of the Yakutat District, showing Dry Bay. This radar imagery was taken during a storm, through a solid cloud cover and a heavy rain. Note the beach ridges next to Dry Bay which are cut by the outburst flood features that radiate out from Harlequin Lake. This imagery was taken at a scale of 1:250,000.



Figure 9. Radar imagery of the Yakutat District taken at the scale of 1:500,000. Compare this imagery with Map 1, Map 2, and Map 3.

Map 4 indicates the stability of the shoreline. Information obtained from low altitude aerial reconnaissance was added to the data to produce the indications of the direction of dominant longshore drift also shown on Map 4.

Map 5 shows the major beach materials along the Gulf of Alaska coastal plain. The information used to make this map was obtained from field work and low altitude aerial reconnaissance. If K-band, real aperture, radar imagery had been obtained instead of the X-band imagery, the beach materials could have been resolved from the radar imagery.

Map 1 exhibits 14 different units which are explained in Table 5. The map unit called Outburst Flood Deposits was the most unexpected feature mapped. This is an area radial to Harlequin Lake which has been crossed by an outburst flood of enormous extent, apparently within the last three or four hundred years. The freshness of the flood features and age of the vegetation indicates this time frame. The units of Map 1 can be located easily on the radar imagery of Figures 4 through 9.

Map 2 has five units which are explained on the map. The map unit which indicates areas where large rip currents are generated during storms was determined by observations made from radar imagery taken during storms and from low altitude aerial reconnaissance flights flown during storms. Map 2 should be the most useful of the five maps because it indicates the most severe hazards that should be considered in the development of the area. Map 2 should be used with Map 1 and Map 3 in order to fully understand the hazards indicated on Map 2.

Map 3 was an unexpected result of this investigation. Several large lineaments were detected on the radar imagery (see Figs. 7 and 9), which

extend completely across the coastal plain of the Yakutat District.

The ability of radar imagery to enhance such lineaments is well documented (Rowan and Cannon, 1970; Cannon, 1974b). Each lineament shown on Map 3 was verified on a summer scene of LANDSAT imagery. Lineaments detected on the radar imagery but not found on LANDSAT imagery were not placed on Map 3 except for those lineaments which cross major ice masses (discussed later). The detection of lineaments on LANDSAT imagery cannot be taken lightly. A chapter by J. Everett and D. S. Simonett (in Lintz and Simonett, 1976) clearly points this out. The number of lineaments detected and their validity (Lintz and Simonett, 1976, p. 101) is causing the re-evaluation of many geologic settings.

These lineaments which cross the coastal plain could well be related to active faults. There are active faults in the area which have been offset vertically as much as 2.5 meters within the last 80 years and the activity of these faults has been well documented (Tarr and Martin, 1912).

An account of continuous and severe tectonic activity in the nearby Lituya Bay area over a period of 125 years (Miller, 1960) provides conclusive evidence as to the structural instability of the region.

Similar lineaments were mapped in the Malaspina and Yakataga Districts. The outstanding result of this mapping was the location of the lineaments which cross the Malaspina ice mass. The radar imagery used to locate the lineaments across the ice mass is shown in Figures 5 and 6. It appears that vertical tectonic movement along the lineaments is reflected in the overlying ice mass. This is of environmental importance because vertical movement of the ice mass influences the rate of ablation. The detection and location of the lineaments across the Malaspina ice mass is unique and can be done only by using the radar imagery.

VII. Conclusions

Landforms are the products of the manner in which the energy of geomorphic agents (such as wind, water, and ice) is expended upon terrestrial materials. Since geomorphic agents interact to various degrees at or near Earth's surface, a variety of landforms can be generated in almost any locality. Landforms are, therefore, a record of the geomorphic agents which have dominated or are presently dominating the patterns of energy interchange at some point on the Earth.

The assemblage of landforms and the geomorphic processes which are effected as a result of the creation of the assemblage forms that which is termed the environment of a particular area on the Earth's surface. The identification of a landform or of an assemblage of landforms provides information about the environment which can be used to evaluate the natural history of the environment and to appraise the impact of induced changes.

The natural environments of Alaska contain or cover natural resources of food, wildlife and energy. The natural environments of Alaska are currently of economic importance from all aspects. Therefore, landforms which are studied in order to evaluate the natural environments and to appraise the impact of changes in the environment are termed "critical landforms". This is done so as to emphasize their relationship to situations currently of economic importance.

Environmental geologic data must be displayed in spatial format if a realistic evaluation is to be made of an area. If changes are induced, natural environments respond in all dimensions. Therefore, components of natural environments must be displayed in a spatial framework which portrays their degree of physical association. This makes it necessary to display environmental information on maps, because point values cannot convey a complete indication of the degree of interface between components.

Sequential information is needed if rates and magnitudes of change are to be included in an environmental evaluation. This demand of sequential observations makes it necessary that the most neoteric data be obtained of the area of investigation. In Alaska there are three major

problems in obtaining sequential and neoterical data; inclement weather, winter darkness and inaccessible terrain. Therefore, the choice of a data source was partly influenced by the information listed in Table 3 on acquisition conditions.

Radar imagery is an adequate tool to use in the environmental evaluations of diverse types of coasts. There are three important factors to keep in mind when acquiring radar imagery of coasts. One, the look-direction should be towards the landward side of the coast away from the water. Two, the altitude of acquisition should be low in order to maximize the return of radar energy. Three, the depression angles should be small so that the important low relief features of coasts can be enhanced. The amount of information displayed on radar imagery is related to the wavelength of the radar energy used. Usually the greatest amount of information can be obtained with the shorter wavelengths. In mapping large regions, radar imagery would be less expensive than photographic coverage of the same area, and it would take less time to map from radar imagery than it would from low- or intermediate-altitude aerial photographs. Aerial photographs must be viewed stereoscopically in order to observe what can be seen with the unaided eye on radar imagery, hence the difference in map compilation time.

X-band, real aperture radar imagery of the Gulf of Alaska coastal plain is adequate both as a mapping base and as a source of important environmental geologic data. It is essential to an environmental assessment of an area that information be as current as possible. In some areas the most current data can be acquired only with the use of radar imagery. The radar imagery of the Gulf of Alaska coastal plain indicates

that severe environmental geologic hazards, such as earthquakes, surface movements along active faults, and outburst floods, have occurred recently and will continue to occur with a relatively high frequency.

Analysis of the geomorphic features of the coastal plain indicates that the seaward portion of the Yakutat District is comprised of sediments from the Alsek River. The continued existence of the area depends upon a continual supply of sediments from the Alsek River.

Natural processes are modifying parts of the coastal plain at a relatively rapid rate. These processes include the formation of large lakes by glacial ablation and the erosion of headlands due to changes in the sediment supply from glaciers. It is necessary to emphasize that the changes are natural and not the result of man's activities. In an area like the Gulf of Alaska, radar imagery is the only tool which can be used to adequately monitor the results of natural processes.

Radar imagery is being used successfully to map landforms in Alaska. It provides necessary neoteric data in spite of adverse weather conditions and the darkness of the Arctic winter. Radar imagery can provide information about glacial ice masses that cannot be obtained by any other remote sensing technique at present. It has been employed as a reconnaissance tool for some time, now radar imagery is being used as a mapping tool.

References Cited

Cannon, P. J., 1974a, Rock type discrimination using radar imagery: in Remote Sensing of Earth Resources, v. III, F. Shahroskhi, editor, p. 339-352.

_____, 1974b, The application of radar imagery to environmental geologic mapping: in Approaches to Environmental Geology, Report of Investigations No. 81, Bureau of Economic Geology, The Univ. of Texas at Austin, p. 224-236.

_____, 1975, The application of radar imagery to specific problems of Interior Alaska: in NASA Earth Resources Survey Symposium, June 1975, Proceedings, v. 1-B, p. 761-768.

Miller, D. J., 1960, Giant waves in Lituya Bay Alaska: U.S. Geol. Survey Prof. Paper 354-C, p. 51-86.

Tarr, R. S., and Martin, Lawrence, 1912, Earthquakes at Yakutat Bay, Alaska, in September, 1899, with a preface by G. K. Gilbert: U.S. Geol. Survey Prof. Paper 64, pt. 1, p. 1-144.

The following were added:

Lintz, Joseph, and Simonett, D.S., eds., 1976, Remote sensing of environment: Addison-Wesley Pub. Co., Reading, MA., 694 pp.

Rowan, L. C., and Cannon, P. J., 1970, Remote sensing investigations near Mill Creek, Oklahoma: Okla. Geol. Notes, v. 30, no. 6, 127-135.

TABLE 5

EXPLANATION OF MAP UNITS

(These units are shown on Map 1, Major Landforms of the Gulf of Alaska Coastal Plain)

Mo Moraines of Old Glaciers

Abandoned moraines of retreated glaciers which contain little or no ice. These areas support good stands of native timber and contain numerous lakes.

OF Outburst Flood Deposits

An area radial to Harlequin Lake which was crossed by an outburst flood of enormous extent, apparently within the last three or four hundred years. This could have been caused by a surge of the Yakutat Glacier and there are no indications that it could not happen again.

Owd Outwash, well drained

Areas of higher, better drained, outwash on the Yakutat Foreland. These areas contain no ice and support good stands of native timber. The outwash is from retreated glaciers. These areas are the most stable and the most desirable of the region.

Opd Outwash, poorly drained

Extensive swampy, areas on the Yakutat Foreland which were formed of outwash from retreated glaciers.

A Alluvial materials

Areas where materials are in active transport by high runoff from streams. These areas are the most frequently flooded during storms.

OA Outwash and Alluvial materials

Areas where meltwater is or has created broad flats. These areas are also reworked by streams discharge but are not flooded with the frequent storms like the areas indicated as Alluvial materials.

Mp Moraines of Present Glaciers

Moraines marginal to the Malaspina ice mass which contains large amounts of ice. The ice is melting rapidly and new lakes are continually being formed. This terrain is chaotic and unstable.

HBl High Beach series, oldest

The oldest, highest, and most discontinuous series of abandoned beaches on the Yakutat and Yakataga Forelands. The well drained soils support good stands of native timber.

TABLE 5 (Cont'd)

HB2 High Beach series, intermediate

The discontinuous series of abandoned beaches on the Yakutat and Yakataga Forelands which physically lies between the uppermost and the lowest high beach series. This is a very distinctive series of beaches exhibited on the SLAR. The well drained soils support good stands of native timber.

HB3 High Beach series, youngest

The lowest and most continuous deposits of the High Beach series. The upper limit is marked by the gold bearing black sands of the Yakutat Foreland. In most areas this series of abandoned beach lines support good stands of native timber.

LB Lower Beach

The most unstable beach materials, which are in active transit along the shore. The materials are directly derived from the discharge of streams and outwash. These areas suffer minor changes daily and major changes during storms.

TF Tidal Flat, extensive

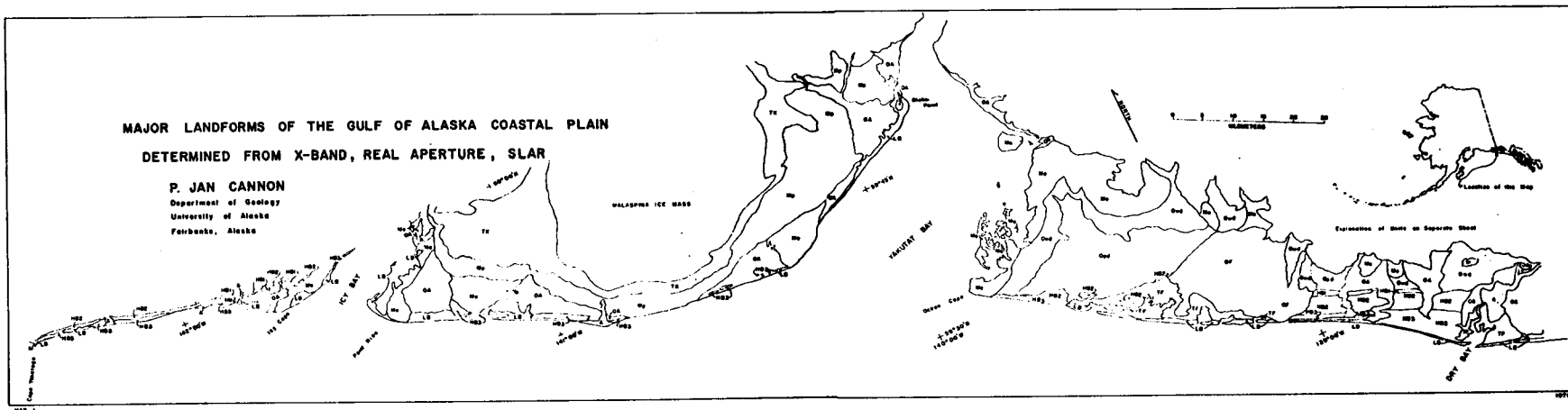
Extensive, low beach, materials on the Yakutat Foreland which are inundated with sea water during high flood tides and storms.

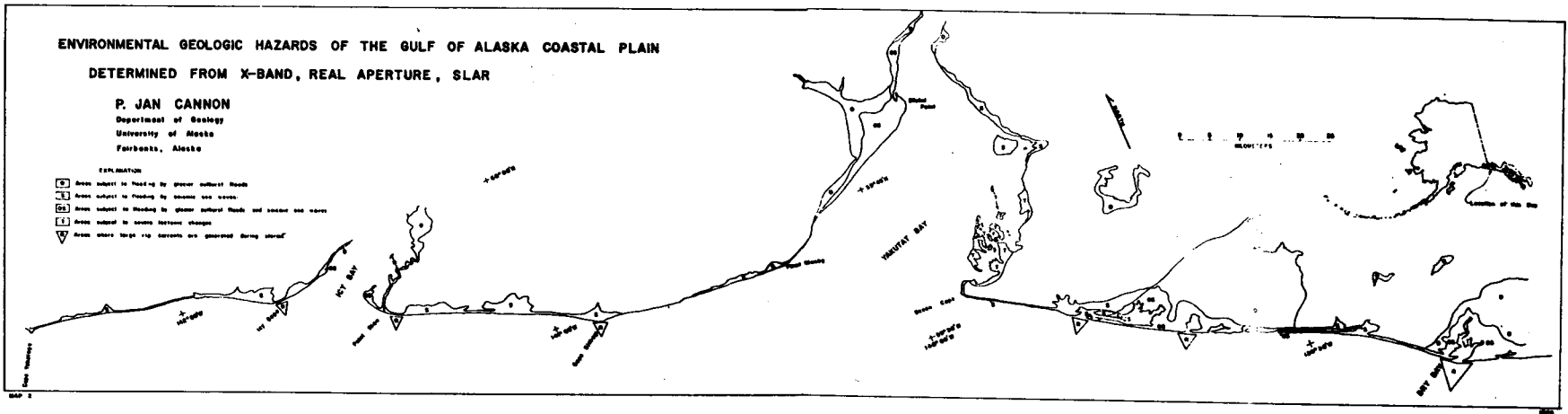
br Bedrock

Indicates some of the more important bedrock exposures in the area.

TK Thermokarst Terrain

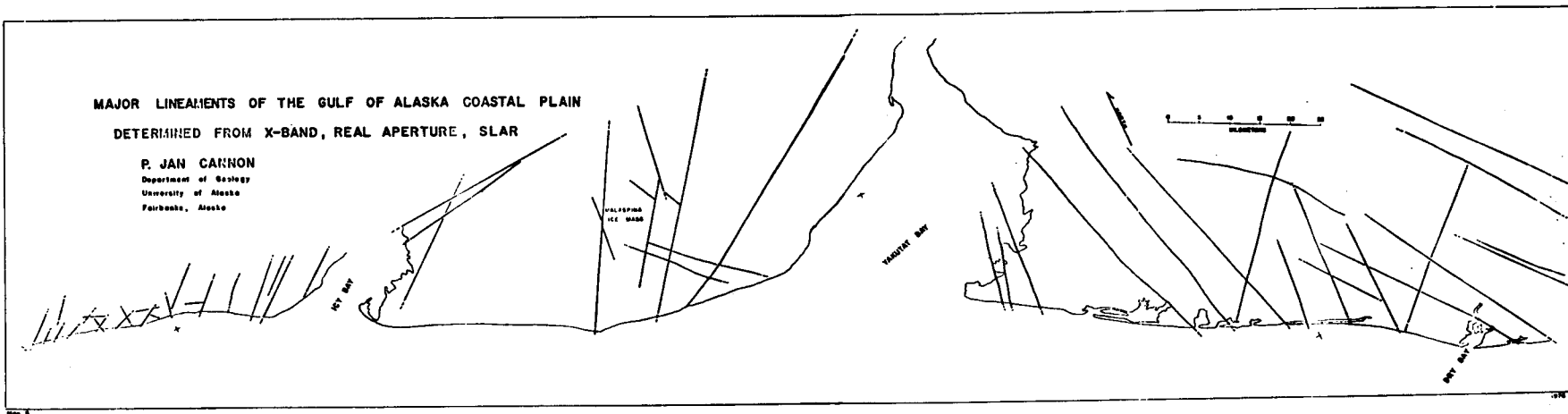
Area on the margin of the Malaspina Ice Mass where the most active melting is occurring. The area is pitted with collapse features.

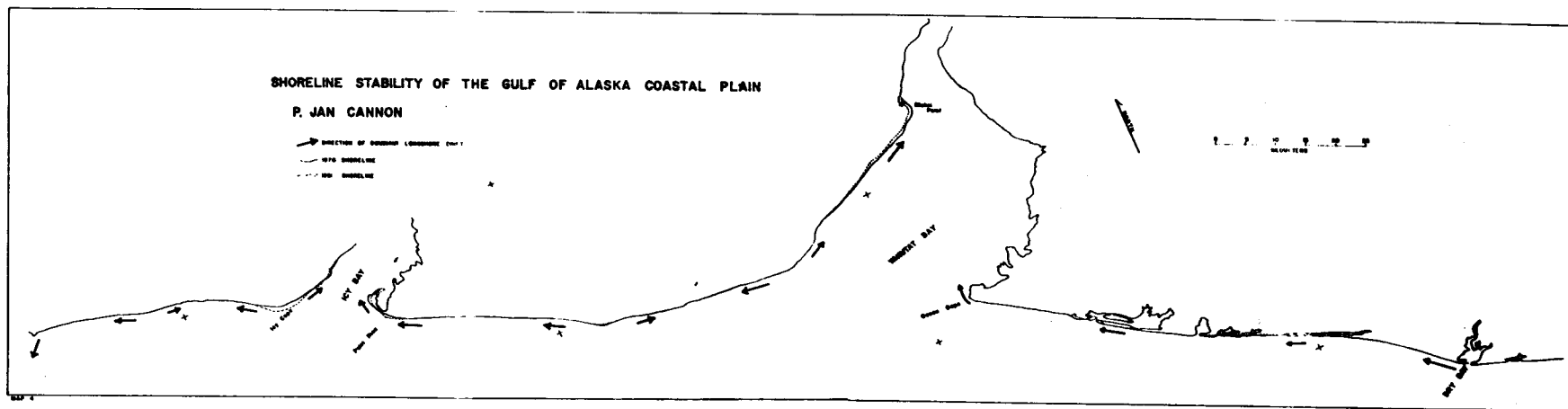


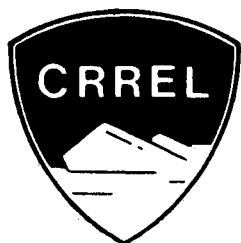


MAJOR LINEAMENTS OF THE GULF OF ALASKA COASTAL PLAIN
DETERMINED FROM X-BAND, REAL APERTURE, SLAR

P. JAN CANNON
Department of Geology
University of Alaska
Fairbanks, Alaska







Contract no. - 01-50-22-2313
Research Unit no. - RU105
Reporting period - 1 April 1976 -
31 March 1977
Number of pages - 10

ANNUAL REPORT

DELINEATION AND ENGINEERING CHARACTERISTICS OF
PERMAFROST BENEATH THE BEAUFORT SEA

Principal Investigator:
P. V. Sellmann

Associate Investigators:
S. Blouin
J. Brown
E. Chamberlain
I. Iskandar
H. Ueda

1 April 1977

CORPS OF ENGINEERS, U.S. ARMY
COLD REGIONS RESEARCH AND ENGINEERING LABORATORY
HANOVER, NEW HAMPSHIRE

TABLE OF CONTENTS

	<u>Page No.</u>
I. Summary	1
II. Introduction	1
III. Current state of knowledge	2
IV. Study area	2
V. Sources, methods and rationale	4
VI. Results	5
VII. Discussion	5
VIII. Conclusions	8
IX. Needs for further study	8
X. Summary of 4th quarter operations	8

I. SUMMARY

The overall objectives of the CRREL participation in the subsea permafrost program are to quantify the engineering characteristics of permafrost beneath the Beaufort Sea and to determine their relationship to temperature, sediment type, ice content and chemical composition. These data, in conjunction with those obtained from other Beaufort Sea geological projects, are being used to ascertain the distribution of subsea permafrost. The CRREL spring 1976 drilling and in situ probing investigations provided numerous samples, data, and subsequent interpretations and have furthered our understanding of subsea permafrost.

Permafrost was present in the four holes drilled at Prudhoe Bay. Ice-bonded permafrost was absent in the upper 30 meters of sediment up to 17 kilometers from shore. Based on negative temperature gradients and pore water chemistry, ice-bonded permafrost should be encountered at 30- and 43-meter depths at sites PB-2 and PB-3, respectively. It appears that the depth to the ice-bonded permafrost decreases with increasing distance from shore and depth of water.* Highly over-consolidated marine clays were encountered seaward of Reindeer Island. The overconsolidation probably resulted from the freeze-thaw history. The presence of these stiff, marine clay deposits is an important consideration for siting structures associated with offshore developments.

Adequate delineation of the engineering properties of subsea permafrost is necessary in order to evaluate the hazards in and constraints of oil and gas developments in the Beaufort Sea.

II. INTRODUCTION

CRREL's involvement in the BLM-OCS subsea permafrost program was designed to provide the near-surface samples and data necessary to characterize engineering properties of subsea permafrost. We are working closely with the USGS and University of Alaska OCS projects and the ongoing ONR project of Lewellen which was previously based at Barrow. Our efforts involve rotary drilling and drive sampling and shallow probing using the spring ice cover as a stable platform. The two-year investigation is limited to the Prudhoe Bay area; however, the combined results of our studies and others can be cautiously extrapolated to other areas along the U. S. Beaufort Sea coast.

* in the cross-section defined by our borehole

Specific objectives can be listed as follows:

(1) Drill the subsea permafrost at Prudhoe Bay, obtain undisturbed samples, conduct engineering tests on the samples, and provide access holes for temperature logging.

(2) Evaluate probe methods for rapid acquisition of subsea engineering and thermal data.

(3) Determine the chemical composition of the interstitial pore water.

Data collected and their interpretation will provide the information necessary to evaluate the subsea permafrost hazards which may exist during petroleum exploration and development. Identification of these potential hazards will lead to the development of appropriate constraints or guidelines and will provide the background data for industry-sponsored, site-specific investigations.

III. CURRENT STATE OF KNOWLEDGE

The data from several drilling programs supported by NOAA and industry at Prudhoe Bay and the Navy (ONR) program at Barrow indicate that permafrost is present to depths in excess of 80 meters. One additional industry hole on Reindeer Island in Prudhoe Bay suggests bonded permafrost existed in two zones from 0 to 20 m and from 90 to 125 m, although this hole was never thermally logged. The studies conducted by Osterkamp and Harrison (1976)* in Prudhoe Bay established the depth of bonded permafrost along a single line in upwards of 2 meters of water. Lewellen's drilling program at Barrow indicates that bonded permafrost is very near the surface in the zone along the coast where sea ice freezes to the seabed. Thermal data indicate that subsea permafrost is present at least 17 km offshore at Prudhoe and 11 km offshore at Barrow.

Considerable subsea permafrost is indicated by the Canadian government and industry studies from the Mackenzie River region. Drilling and thermal data there have confirmed the widespread presence of subsea permafrost. The top of the bonded permafrost was mapped based on industry seismic investigations.

Other OCS subsea permafrost projects cover the current state of knowledge in more detail.

IV. STUDY AREA

The 1976 drill sites were jointly selected by USGS and CRREL personnel to provide a range of thermal and depositional settings. Two sites were situated within Prudhoe Bay and one site was located north of the barrier islands. These sites were accurately positioned in the field by USGS personnel using a Del Norte ranging system which, based on electronic triangulation, can locate stations with 1 meter (3 ft) accuracy.

* Osterkamp, T. E. and W. D. Harrison, 1976. Subsea permafrost at Prudhoe Bay, Drilling Report. Geophysical Institute Report UAG-R-245, University of Alaska

Detailed information for each site is:

Site	General location	Lat/Long	Water depth (m)	Hole depth from drill collar (m)
PB-1	Approximately 2 miles north of old ARCO dock in center of Prudhoe Bay	70°20.9'N 148°19.3'W	2.7	33.8
PB-2	Approximately 2 miles north of Reindeer Island	70°30.7'N 148°18.1'W	11.6	42.8
PB-3	Approximately 3 miles northeast of the new ARCO dock	70°25.9'N 148°26.6'W	5.9	51.5

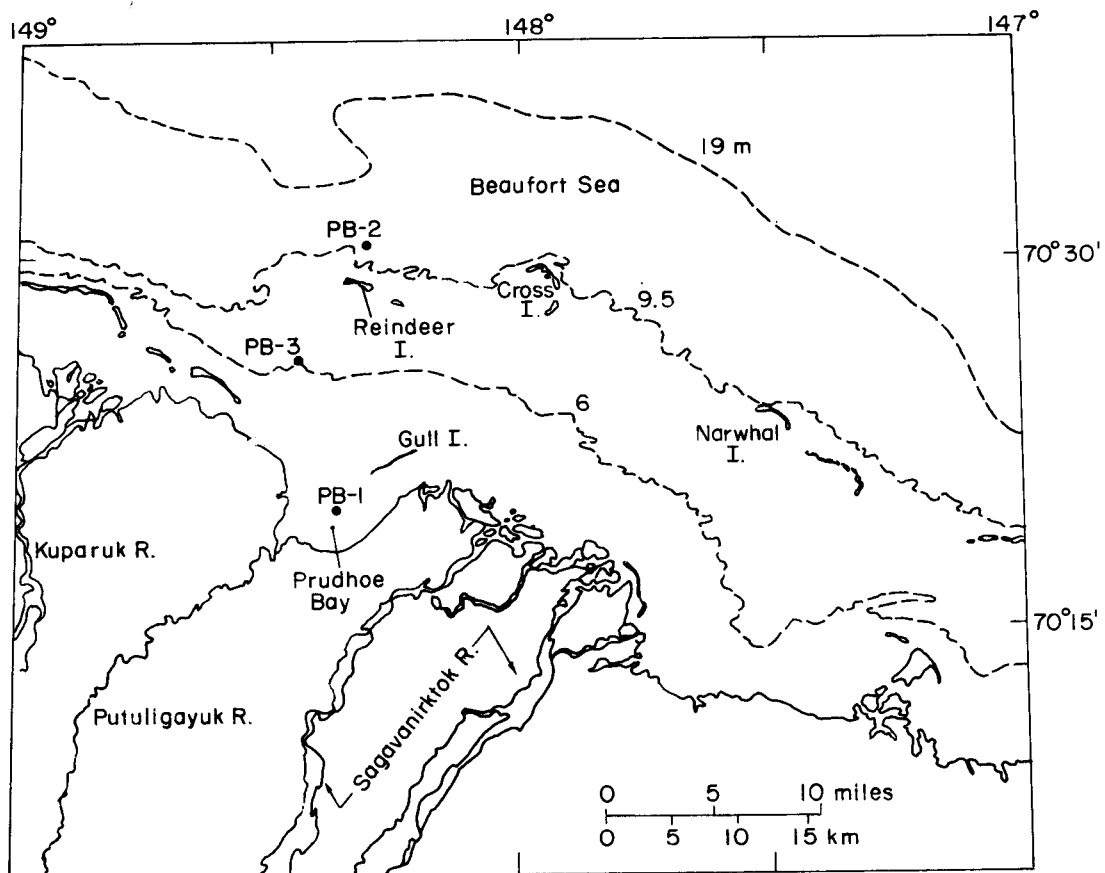


Figure 1. Location map for CRREL 1976 drill sites

V. SOURCES, METHODS AND RATIONALE OF DATA COLLECTION

CRREL Special Report 76-12, entitled "Operational Report, 1976, USACRREL-USGS Subsea Permafrost Program, Beaufort Sea, Alaska," by P. V. Sellmann, R. I. Lewellen, H. T. Ueda, E. Chamberlain, and S. E. Blouin presents details of the 1976 sample acquisition and operations. Briefly, an Acker drill and a Bean horizontal Triplex pump were employed for the drilling. Most samples were obtained by drive sampling thereby reducing the potential for chemical contamination. Rotary sampling techniques were used in coarse-grained materials.

The holes were logged at the time of drilling to provide a complete description of the materials encountered. These logs were based on 1) cores, 2) wash samples, and 3) drillers' observations of penetration characteristics. Preliminary logs of these holes were prepared by the USGS and are reported elsewhere (Sellmann et al. 1976).

Subsampling of the core was also completed in the field. Cores were split for detailed examination of engineering properties, chemical analysis, dating and paleontology. The cores were subsequently boxed and transported to one of two locations, CRREL, Hanover, or the USGS, Menlo Park.

On completion of a hole, a 5cm plastic (PVC) casing was installed for thermal logging purposes. Temperature measurements were made at these sites by the USGS personnel using a thermistor probe. Temperature profiles were obtained after the installation of the PVC casing and on several occasions after the initial logging. Sites were revisited as late as early June in an attempt to establish equilibrium profiles for each hole. Results of this study are covered in USGS reports.

Both dynamic and static penetrometer tests in the sediments were conducted using the sea ice as a platform. For the dynamic tests, a standard 64-kg hammer dropped 0.76 m was used to drive the probe string, which was made up of EW drill rod surrounded by EX casing. The probe consisted of a 60° hardened steel cone attached to the drill rod and a 150-mm-long sleeve welded to the base of the casing. The cone and sleeve both had a diameter of 57 mm. The point and sleeve could be driven simultaneously or separately by temporarily adding 0.3-m sections of casing or rod at the top of the probe string as desired. The static penetrometer used the same probe string and was pushed by a hydraulic cylinder mounted atop a quadropod anchored to the sea ice. The temperature profile was determined by filling the bore of the rod with a non-freezing fluid and inserting a thermistor temperature probe. Normally, the temperature in the drill rod fluid was allowed to stabilize 12 hours before readings were taken.

In the laboratory, undrained, unconsolidated triaxial compression tests were conducted at confining pressures estimated to be equivalent to the in situ overburden pressures on samples prepared from core specimens obtained from the three drill sites. The samples were 50 mm in diameter and 115 mm in length. The samples were tested unfrozen, the test temperatures being maintained at $0^{\circ}\text{C} \pm 1^{\circ}\text{C}$ (chemical analysis of the pore water revealed that the freezing point was -1.8°C or lower). The tests were conducted at a constant rate of strain of approximately 0.045/min.

Interstitial water was extracted from thawed PB-1 and PB-3 samples by centrifugation at 3000 rpm for 30 minutes using special filtering centrifuge tubes commercially available from Millipore Corporation made of plastic and Teflon to assure that the samples were kept free of metal contamination. Interstitial water was extracted from PB-2 samples by shaking the sample with 20 ml of deionized water for one hour, then centrifuging as above, because of low water contents.

Immediately after extraction, interstitial water was analyzed for carbonate, bicarbonate, and pH. The total soluble salts (expressed as specific conductance) were determined by electrical conductivity measurements. A Model A Beckman pH meter was utilized for pH measurements. Carbonate and HCO_3 were determined by titration in the presence of phenolphthalein and M.O. indicators. A 303 Perkin-Elmer Atomic Absorption spectrophotometer was used for analyses of sodium, potassium, calcium, and magnesium. Calcium and magnesium were determined in the presence of 0.1% lanthanum. Chloride was determined by titration with AgNO_3 and sulfate was determined according to Hach Chemical methods.

VI, VII. RESULTS AND DISCUSSION

The main results of the 1976 field project have been summarized in two papers intended for presentation at the Third International Conference on Permafrost in Edmonton, Alberta, Canada, July 1978. These papers are:

- (1) Engineering properties of subsea permafrost in the Prudhoe Bay region of the Beaufort Sea -- E. J. Chamberlain, P. V. Sellmann, S. E. Blouin, D. M. Hopkins, and R. I. Lewellen.
- (2) Chemistry of interstitial water from subsea permafrost, Prudhoe Bay, Alaska -- I. K. Iskandar, T. E. Osterkamp, and W. D. Harrison.

In addition, a more detailed report on the engineering properties has been prepared for CRREL publication. A bibliography of Soviet subsea permafrost and related investigations was prepared. This bibliographic effort has been transferred to Dr. Vigdorichik at INSTAAR, University of Colorado.

The following highlights the results of our investigations to date, but intentionally leaves out extensive reference to the data. Preprints of the above reports are available upon request.

The field logs all show a fine-grained surface section of marine sediments (fine sand, silt and clay) 4.5 to 8.8 m thick. These appear to overlie beach sediments (well-rounded gravel, coarse sand and some mud). The lower part of the marine mud sequence at site PB-2 contains abundant small pebbles and granules. The fine-grained marine materials are soft and weak at sites PB-1 and PB-3 while at site PB-2 they appear to be very stiff and overconsolidated. The marine sequence is underlain by poorly sorted angular gravel lacking any organic remains and appears to be approximately 18 m thick at sites PB-1 and PB-3 and less than 5 m thick at PB-2. All boreholes terminate in what appears to be an alluvial section of well-sorted sand, pebbly sand and gravel containing lenses of detrital wood and plant fragments. The index properties reveal

that, with few exceptions, the fine-grained silts and clays at sites PB-1 and PB-3 have the high moisture contents commonly encountered in marine environments, while the clays at site PB-2 have lower water contents in the range of their plastic limits.

As no ice-bonded samples were recovered, it was initially concluded that ice-bonded permafrost lay at some unknown distance beneath the bottom of the drill holes. However, because of the extremely difficult driving conditions at the termination depths at PB-2 and PB-3, it was suspected that ice-bonded permafrost might have been encountered. From our chemistry data, it is estimated that the freezing point of the interstitial water at sites PB-2 and PB-3 was approximately -1.8°C . Extrapolating the straight line segments of the USGS temperature profiles downward to intercept the -1.8°C isotherm resulted in estimated depths to ice-bonded permafrost for sites PB-2 and PB-3 of 29.9 and 43.3 m respectively. These depths correlate extremely well with the 29.5- and 44.2-m depths at which drilling and sampling was terminated because of collapsed casing or very high penetration resistances. Since site PB-2 is farther from shore and in deeper water than site PB-3, it appears that the depth to ice-bonded permafrost decreases with increasing distance from shore and water depth.

Field Tests: At site PB-1, the static penetration resistances were very low (< 2 megapascals) throughout the fine-grained section. Upon entering the coarser-grained sands and gravels, the static penetration resistance rapidly increased to 24 megapascals, where measurements were terminated. Because of equipment difficulties, dynamic penetration data were obtained only in the fine-grained section. The range of penetration resistances was between 12 and 24 blows per meter.

At site PB-2, a few static penetration results were obtained, but they are of questionable quality because of rod buckling problems in the deep water. The dynamic cone capacity rises sharply in the upper 1.4 m of silty sand to nearly 200 blows/m and falls abruptly to 50 to 100 blows/m in the clays beneath.

The cone penetration data at site PB-3 show the best correlation. Both the static and dynamic cone penetration data show an increase of penetration resistance through the upper meter of loose silty sand, a relatively constant penetration resistance through the next meter of more compact silt, and a decrease in the next 0.5 m of softer silts to a relatively low penetration resistance in the next $2\frac{1}{2}$ m of very soft silt. At a penetration depth of approximately 5 m a very stiff layer of sand was encountered and the penetration resistance increased rapidly with increasing penetration depth.

The greatest penetration depth was achieved at an auxiliary site (PB-4). Using the dynamic cone penetrometer, approximately 11 m of penetration was achieved, the penetration resistance being approximately 100 blows/m below a depth of 2 m with an increase to near 250 blows/m near 10 m of penetration. The static cone penetration resistance increased to 8 MPa at the 2-m penetration depth and remained constant to 5 m depth.

Laboratory Strength Tests: For site PB-1, sediments are weak to a depth of 5 m or more, the maximum shear strength being 45 kilopascals, while at a depth near the boundary of the fine-grained marine sediments and the coarser-grained glacial outwash material the shear strength increases to 134 kilopascals.

At site PB-2, there is a gradual but significant increase of shear strength with depth. In the overlying sandy material, the shear strength is approximately 84 kilopascals. Near the top of the stiff marine clay section, the strength is only a slightly greater 92 kilopascals but it increases to 225 kilopascals near the bottom.

At site PB-3, the shear strength decreases with depth in the marine section as softer and finer-grained materials are encountered. In the upper half of this section, the strength is as high as 107 kilopascals, while near the bottom it is approximately 28 kilopascals.

Because the clay samples taken from site PB-2 appeared to be overconsolidated, laboratory consolidation tests were conducted on two selected samples, one obtained from core PB-2-05 and the other from PB-2-07. These tests revealed overconsolidation stresses of 3800 and 3600 kilopascals, respectively. The resulting overconsolidation ratios (the ratio of the overconsolidation pressure to the in situ stress) were 99 and 53.

Chemistry: Hole PB-1 is located in the center of a small closed basin where there was 0.72 m of water under 1.90 m of sea ice. The conductivity of the water under the ice was 93 mmhos/cm, which indicates that the water was not subject to circulation or mixing with sea water. The conductivity of the interstitial water varied from 61 to 72 mmhos/cm. Conductivity values of interstitial water from PB-3 sediments were essentially constant with depth and ranged from 43 to 51 mmhos/cm. The conductivity of overlying sea water was about 53 mmhos/cm. With the exception of the top sample from PB-2, the conductivity of the interstitial water from the PB-2 sediments was similar to that of the sediments from PB-3. Sea water from PB-2 showed slightly lower conductivity values than sea water from PB-3 (49-50 mmhos/cm).

Analysis of interstitial water for selected ions indicated that chloride ranged from 20 to 30 parts per thousand (ppt) in PB-1 and from 12 to 19 ppt in PB-3. Sulfate ranged from 2 to 11 ppt in all the samples. Bicarbonates were very low as expected (<0.5 ppt). Calcium and magnesium ranged from 0.2 to 0.8 ppt and from 0.3 to 0.9 ppt, respectively. In general, potassium in interstitial water was higher than that in sea water samples.

The top 4 meters of the sediments near shore (PB-1 and PB-3) contain much higher CaCO₃ than the sediment further offshore (PB-2). Values of CaCO₃ in the former ranged from 15.5 to 21.3% in PB-1 and from 13.9 to 27.5% in PB-3. This could best be explained by ion exchange reaction in the sediment-brine systems. At high concentration of NaCl, Na displaces Ca and Mg from the exchange sites, then precipitates CaCO₃ and MgCO₃ as the concentration in the interstitial water exceeds the solubility product. In contrast, organic carbon was very low (<3%) and was slightly higher in PB-2 than in PB-3.

VIII. CONCLUSIONS

1. Temperatures below 0°C were present at all sites studied during the spring of 1976.
2. Ice-bonded permafrost did not occur within the upper 30 m of subsea sediments in a region extending from 1 to 17 km distance offshore.
3. Negative gradients in thermal data and analysis of pore water chemistry suggest that ice is present at 29.9- and 43.3-m depths at sites PB-2 and PB-3 respectively. Because site PB-2 is in the deepest water and is farthest from shore, it appears that the depth to ice-bonded permafrost may be decreasing with increasing distance from shore, at least in the cross-section defined by our boreholes.
4. Shallow, highly overconsolidated marine clays occur seaward of Reindeer Island, while softer marine muds occur inside the barrier island along our study line. The dense marine clays probably have been overconsolidated by freezing and thawing.
5. In situ cone penetration resistance data can be obtained using the sea ice as a platform. This information can be used to delineate the occurrence of soft and stiff marine materials as well as dense sands and gravels and provide rapid access for thermal data.
6. Salinity and ionic composition of interstitial water from Prudhoe Bay subsea permafrost vary from site to site. Conductivity of the interstitial water ranged between 43 and 72 mmhos/cm, but is relatively uniform in each section.

IX. NEEDS FOR FURTHER STUDY

The 1976 and 1977 subsea permafrost drilling and probing project was confined to the Prudhoe Bay area. The results from Prudhoe and the previous studies at Barrow provide only two points for the entire U. S. Beaufort Sea. A third area to the west of the Colville River delta should also be drilled in order to provide desired ground truth for regional maps and models. Data from additional offshore environments including areas of major fresh water discharges, areas of rapid coastal erosion and offshore deposition, and deeper shelf waters should also be investigated for subsea permafrost. It is also desirable to have at least one hole that penetrates the bonded permafrost in deep water (20 to 30 meters deep).

Complementary to the drilling approach are the analyses of the existing first-return seismic data obtained by industry. We have begun to explore the availability and costs of these data. Assuming they are available, funds will be required to process and interpret them.

X. SUMMARY OF 4TH QUARTER OPERATIONS

A. Field Activities

1. Field trip schedule: During January and February, activities consisted of attendance at two workshops: the National Academy of Sciences Committee

on Permafrost Workshop in Hanover, NH, and the OCSEAP's Workshop at Barrow, Alaska. The Committee on Permafrost meeting 6 and 7 January 1977 devoted one-half day to reviewing the status of subsea permafrost. Prior to the meeting, all CRREL project personnel met for two days with other subsea permafrost investigators including Osterkamp, Lachenbruch and Hopkins. The discussions summarized plans for 1977 and provided an opportunity to explore means by which industry-obtained geophysical data could be employed for the OCS investigations. Sellmann followed up with a visit to the Geological Survey of Canada in Ottawa to further explore the requirements for processing the near-surface offshore seismic data.

The Barrow Workshop, summarized elsewhere, led to the development of a general but speculative map of subsea permafrost distribution for the U. S. Beaufort Sea. On the return from Barrow, a short visit was made to Prudhoe Bay by Sellmann and Osterkamp to arrange for spring logistics and to further assess the ice thickness. On 3 March, ice thicknesses ranged between 45 and 48 in. Before committing the spring drilling project to the field, Dr. Nevel of CRREL was asked to evaluate the minimum sea ice thickness required for the various drilling and probing operations. It was ascertained that ice thicknesses of 34 in. would provide adequate strength for the rotary drilling and camp operations.

The 1977 field party departed Hanover for Prudhoe Bay on 21 and 22 March 1977. The first week at Prudhoe Bay was spent mobilizing the equipment, some of which had been shipped by truck from Hanover, NH to Prudhoe Bay in February. The drilling party was on the ice and ready to drill on 30 March 1977.

2. Scientific Party as of 1 April 1977 at Prudhoe Bay consisted of the following:

Scott Blouin	CRREL	Probe investigations
Edwin Chamberlain	CRREL	Engineering tests and core logging
Allan Delaney	CRREL	Drilling support
Donald Garfield	CRREL	Probe investigations
David Hopkins	USGS	Geology
Robert Lewellen	Arctic Research	Drilling and thermal investigations
Paul Sellmann	CRREL	Drilling and geology
Herbert Ueda	CRREL	Drilling support

3. Methods - Field sampling and laboratory analyses.

The 1977 program will be based on equipment and methods described in the 1976 operational report (Sellmann et al. 1976). Heavier casing and a pneumatic casing hammer are being employed. A State of Alaska Miscellaneous Land Use Permit was arranged for by the OCSEAP Fairbanks Office.

4. Sample locations -- Spring 1977 sites will be reported upon in the next quarterly report.

5. Data collected or analyzed -- No new field data were collected during the quarter.

6. Milestone charts -- All activities are on schedule.

B. Problems encountered/recommended changes

In general, planning and implementation of the field program have progressed reasonably well. Project personnel have had to devote considerable time to logistics as well as in responding to OCS requests and meetings. Although these are necessary to fulfill the overall objectives of the program, they detract from completion of the technical aspects of the scientific project.

C. Estimate of funds obligated.

As of 31 March 1977, a total of \$93,500 of the total \$225,000 FY77 funding had been obligated.

OFFSHORE PERMAFROST STUDIES, BEAUFORT SEA

D. M. Hopkins and others
U.S. Geol
345 Midd
Menlo Pa

*Environ
Assess. of
outer
Cont.
Shelf*

This study is designed to obtain data on the distribution of offshore permafrost, based on thermally instrumented boreholes. Three boreholes were drilled during the summer of 1976 and three additional boreholes will be placed during spring, 1977.

ge of offshore permafrost in the Prudhoe Bay area. Three additional boreholes

The 1976 boreholes, combined with data obtained by the University of Alaska in 1975 and a single borehole placed on Reindeer Island by Humble Oil Company some years earlier, show that the subsea sediments are below 0°C throughout the Beaufort Sea shelf at least as far as 13 km offshore and suggest that sub-zero temperatures are found to the edge of the shelf. In shallow water areas where winter ice rests on the bottom, the subsea sediments are ice-bonded beginning at a depth of a few meters and extending to depths of several hundred meters. Further offshore, the subsea sediments are soaked with liquid brine to depths of 50 m or more, but relict ice-bonded permafrost is commonly present at greater depths on those parts of the shelf that lie landward of the 20-m isobath.

The report presents detailed data on paleomagnetic character and fossil content of the sediments and an extensive discussion of the thermal data.

INTRODUCTION

Research during the last decade (Hunter, Judge, and others, 1976; Lewellen, 1976; and Osterkamp and Harrison, 1976) has shown that, contrary to earlier inferences permafrost extends far offshore on the continental shelf of the Beaufort Sea. Both ice-bonded permafrost and permafrost consisting of brine-soaked sediments at a temperature below 0°C were shown to be present. However, very little was known about the distribution, thickness, state, and temperature of offshore subsea permafrost.

The temperature and state of subsea sediments affects their bearing strength, stability, and excavation characteristics. Geothermal temperature is also a factor in the distribution of potential blow-out situations involving clathrates; and ice-bonded permafrost acting as an aquaclude is a factor in the distribution of potential blow-out situations involving artesian water. Thus, knowledge of offshore permafrost is essential if disasters are to be avoided during the exploration and development of petroleum on the outer continental shelf of the Beaufort Sea.

Our study undertakes to obtain direct knowledge of offshore permafrost based on thermally instrumented boreholes in the Prudhoe Bay area, and on the study of cores and cuttings from those boreholes. The study is a joint effort of the Geological Survey and R. E. Lewellen of Arctic Research Inc. (R.U. 204) and the Cold Regions Research and Engineering Laboratories (CRREL) (R.U. 105). It is closely coordinated with permafrost-probe and modeling studies at the University of Alaska, Fairbanks (R.U. 253, 255, and 256), seismic refraction studies at the University of Alaska, Anchorage (R.U. 271), and a study oriented toward development of a predictive model for distribution of offshore permafrost at the Institute of Arctic and Alpine Research (INSTAAR), University of Colorado (no Research Unit number assigned). Our study not only provides site-specific information on the permafrost situation in the Prudhoe Bay area (an area expected to see very early offshore exploration) but also provides essential data needed for the development of more general predictive models of offshore permafrost in the Beaufort and Chukchi Seas.

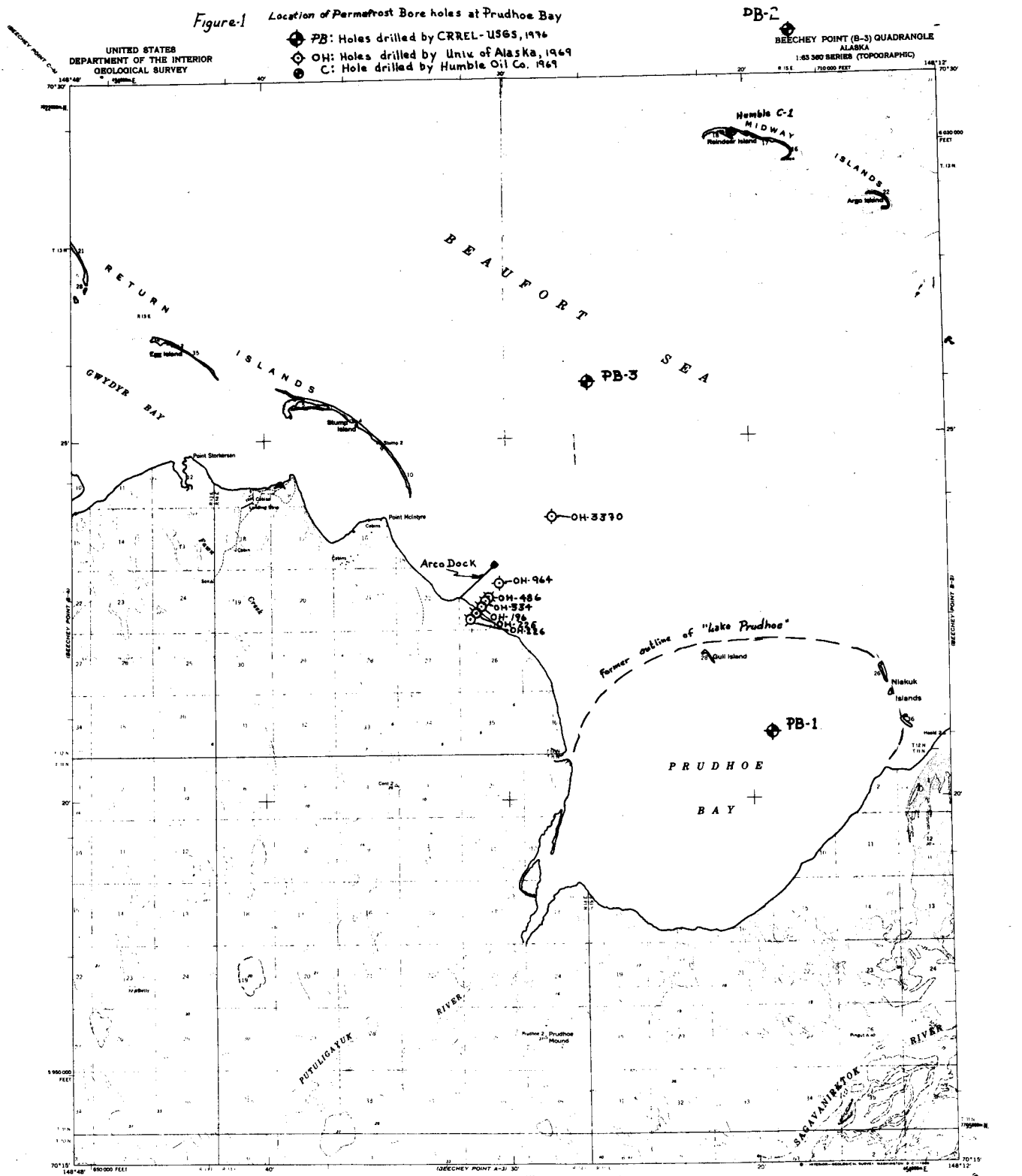
DATA GATHERING

Four boreholes were placed through the shorefast ice in the Prudhoe Bay area during spring, 1976. The first two, PB-1 and PB-1A, were placed near the center of Prudhoe Bay; a third, PB-2, was placed about 3 km seaward from Reindeer Island, and a fourth, PB-3, was placed in Stefansson Sound about midway between Reindeer Island and the ARCO dock on the mainland shore (fig. 1). PB-2 and PB-3 were placed so that they would lie along a line defined by boreholes previously placed nearer shore and onshore by T. Osterkamp and W. Harrison and by an engineering-test borehole placed on Reindeer Island by Humble Oil Company (fig. 2).

An important objective was to obtain intact core material for use in engineering tests, extraction of interstitial water, and recovery of stratigraphic, geochronological, and paleo-environmental information. Cores were attempted at intervals ranging 0.5 to 6 m and samples of cuttings ("wash samples") were collected in the intervals that were not cored (figs. 3-6). The cores were divided in the field and splits apportioned to CRREL and USGS. All wash samples were retained by the Geological Survey. Engineering tests, granulometric analyses, and analyses of interstitial water were conducted at CRREL and are reported in the 1977 Annual Report for R.U. 104. The Geological Survey samples were used for stratigraphic, paleontological, geochronological, and paleoecological studies.

Cores and wash samples retained by the Geological Survey were used for recovery of information about the age, environment, and climatic or thermal history of the Beaufort Sea shelf--information needed for thermal modeling and development of predictive models of the distribution of offshore permafrost. All of the cores of fine-grained material were radiographed in order to identify character of stratification, distribution of fossil mollusks and ice-rafted pebbles, and evidence of ice-gouging of the sea bottom in ancient times (Appendix I). Pebbles were then washed and identified from cores through the marine mud and clay section of borehole PB-2. Oriented samples were collected from marine mud and clay in cores from PB-2; from these cores, the paleomagnetic

Figure 1 Location of Permafrost Bore holes at Prudhoe Bay



UNITED STATES
DEPARTMENT OF THE INTERIOR
GEOLOGICAL SURVEY

◆ PB: Holes drilled by CRREL-USGS, 1976
○ OH: Holes drilled by Univ of Alaska, 1969
◻ C: Hole drilled by Humble Oil Co. 1969

DB-2
BEECHY POINT (B-3) QUADRANGLE
ALASKA
1:63 500 SERIES (TOPOGRAPHIC)
1:63 500 FEET

Mapped by the Army Map Service
Edited and published by the Geological Survey
Control by USGS and USACE
Topography by photogrammetric methods from aerial photographs
taken 1955, last annotated 1955. Map not held checked
Selected hydrographic data compiled from USCGS
Chart 5472 (1955). This information is not intended
for navigational purposes.
Universal Transverse Mercator projection. 1927 North American datum
10,000 foot grid based on Alaska coordinate system, zone 6
zone 4, shown in blue.
Land lines represent unsurveyed and unmarked locations
provided by the Bureau of Land Management
Form U-3, United Mercator
Lake elevations are uncharted

APPROXIMATE MEAN
DECLINATION 1955

SCALE 1:63 500

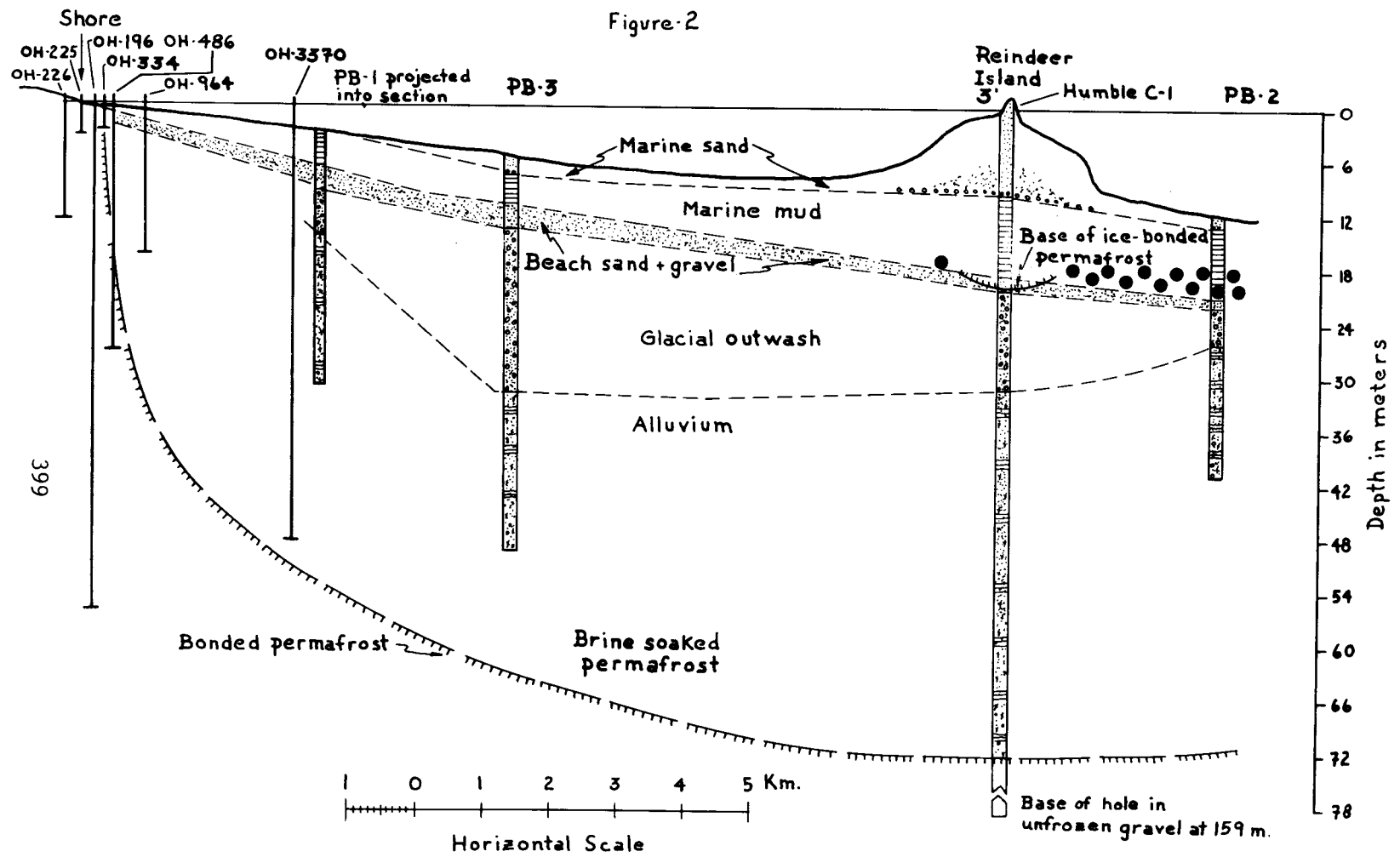
CONTOUR INTERVAL 50 FEET
DASHED LINES REPRESENT 25-FOOT CONTOURS
CONTAIN IS MEAN SEA LEVEL
DEPTH CURVES AND SOUNDINGS IN FEET DATUM IS MEAN LOW WATER
ROCKING SOUNDINGS ARE THE APPROXIMATE LINE OF MEAN LOW WATER
THE MEAN RANGE OF TIDE IS APPROXIMATELY 13.5 FEET

FOR SALE BY U. S. GEOLOGICAL SURVEY
FAIRBANKS, ALASKA 99701, DENVER, COLORADO 80225, OR WASHINGTON, D.C. 20242
A POLAR EDITION TOPOGRAPHIC MAP AND SERIES IS AVAILABLE ON REQUEST



BEECHY POINT (B-3), ALASKA
N7015-W14812/15 A 36
1955

Figure-2



orientation of the magnetic field at the time of sedimentation was determined (Appendix II).

Material suitable for radiocarbon-dating proved to be scarce. Wood in sufficient quantity for a radiocarbon date was obtained at a single level near the base of the marine mud section in borehole PB-1. A sample probably large enough for radiocarbon-dating (Appendix III) has been accumulated by hand-picking detrital organic fragments dispersed in sand and gravel deep in borehole PB-3, and marine clay near the top of borehole PB-2 contains considerable fine organic material, possibly enough to permit a radiocarbon data on a bulk sediment sample, but neither of these samples has been analyzed at the time of writing.

Geochronological studies based on racemization ratios for amino acids in mollusks shells are underway. Analyses of ancient samples from the Beaufort Sea and Chukchi Sea region have shown that the method is useful as a correlation tool. Now, we are attempting to develop a quantitative geochronology calibrated by amino-acid racemization ratios in radiocarbon-dated Holocene shells from the Beaufort Sea region and to apply this calibration to racemization ratios to be determined on mollusk shells from PB-2 and PB-3.

Paleontological studies include identification of foraminifera (Appendix IV) and mollusks (Appendix V) from the marine mud and clay in all four boreholes and identification of pollen in the marine section of PB-2 (Appendix VI). Ostracodes have been washed from cores and cuttings of the marine section in all five holes, but the faunas have not yet been identified.

Drillers' notes on 1976 operations are given as Appendix VII. Transient temperatures were logged daily as each hole progressed in an effort to anticipate the level at which bonded permafrost would be reached. Upon completion of boreholes PB-1, -2, and -3, plastic pipe was installed and filled with non-freezing fluid before casing was withdrawn. The borehole sites were then visited at 7- to 14-day intervals as long as ice conditions permitted, providing data from which equilibrium geothermal profiles could be calculated for each hole. Geothermal data and interpretations are given in Appendix VIII.

RESULTS

The major geothermal conclusions of the study thus far are summarized in Appendix VII, Geothermal studies.

Each of the boreholes has provided an insight into aspects of the history of the Beaufort Sea shelf and yielded data that can be generalized far beyond the Prudhoe Bay area. A discussion of the significance of boreholes PB-1 and PB-2 is still in progress, having been delayed due to the requirement that I prepare the earth-science synthesis for the Beaufort Sea shelf. However, the discussion of the significance of borehole PB-2 has been completed and is included below as an example of the sorts of information yielded by the borehole program.

Three major group of sediments can be recognized in the USGS-CRREL and University of Alaska boreholes; these units were also encountered in the upper part of the much deeper Humble Oil Company borehole on Reindeer Island (fig. 2). They include, from top to bottom, a surficial sequence of marine mud, clay, sand, and beach gravel which accumulated since the last rise in sea level; an underlying sequence of angular, sterile sand and gravel interpreted as glacial outwash deposited by the Sagavanirktok River during the last major glaciation in the Brooks Range; and finer pebbly sand, well-sorted sand, and gravel believed to represent ancient alluvium of the Sagavanirktok River because it contains scattered lenses of detrital plant material.

Holocene marine sediments

Upon entering the sea bottom, most and probably all of the offshore boreholes in the Prudhoe Bay area enter marine mud 5 to 10 m and then pass abruptly into beach sediments (well-rounded gravel and coarse sand) 1 or 2 m thick. The marine mud consistently contains scattered small, well-rounded pebbles; petrologic study indicates that these pebbles have been brought to the site by longshore drift or have been lifted from nearby beaches and ice-rafted short distances offshore. Paleomagnetic studies (Appendix II) indicate that the sediments accumulated since the last reversal of the earth's magnetic field and at a time when the field intensity differed little from that of the present. The mollusk and foraminifer faunas (Appendices IV and V) are similar to modern faunas and differ from one another only in ways that indicate changes in water depth and salinity; they indicate that water temperatures have not changed significantly during the time since deposition of the beach sediments and marine mud began. Pollen spectra (Appendix VI) indicate that the vegetation and climate onshore also has not changed greatly since accumulation of the marine section began.

These observations support the inference, based on the known sea-level history of the Chukchi and Bering Seas (fig. 7) that the marine section in offshore boreholes accumulated within the last 10,000 years. Thus, the entire continental shelf seaward as far as PB-2 first became submerged less than 10,000 years ago.

Small differences in the lithology and fossil content of the marine section from one borehole to another reflect differences in the recent history of the land or seascape at the different sites. These differences have had considerable impact upon the recent thermal history of the different sites and therefore are worth discussing in detail.

Borehole PB-2.--Borehole PB-2, 3 km seaward from Reindeer Island (fig. 3) represents an exploration of the history of the open shelf. This borehole contains a record of recent westward and shoreward migration of the Midway Island barrier chain, and it also contains a record of remarkably active ice-rafting of beach materials during the early part of the Holocene transgression of the shoreline.

Borehole PB-2 passed through pebbly sand 1.3 m thick, then through stiff, overconsolidated clay 3.8 m thick, and finally through over consolidated pebbly mud 3.9 m thick before entering the basal 1.2-m thick layer of beach gravel (fig. 8). The base of the marine section lies about 22 m below present sea level. If we assume that this beach gravel formed at a time when sea level lay 22 m below its present position, then comparison with the Bering-Chukchi sea-level curve (fig. 8) would suggest that site PB-2 was first inundated shortly before 10,000 years ago. However, consideration of the age and present position of the lowest marine beds in borehole PB-1, discussed later, suggests that the sea bottom may subside 8 m or more after initial inundation, due to thermokarst collapse. If this is correct, then the beach gravel at the base of the marine section in borehole PB-2 may once have lain as much as 8 m above its present position, and the time of first inundation may have been more nearly 9,000 years ago.

Two distinctive pebble suites are displayed in Borehole PB-2. One suite, dominated by limestone and black chert, is derived from the nearby Brooks Range and comprises the mainland beaches in the Prudhoe Bay-Gwydyr Bay area as well as the Return Island barrier chain (fig. 1). The other suite, characterized by dolomite, red granite, and white orthoquartzite, is derived ultimately by iceberg rafting from northern Canada; this suite is found in Pleistocene gravel on Flaxman Island and it comprises the gravel of the Midway Island barrier chain (Rodeick, 1975).

The basal pebbly mud in PB-2 is texturally similar to glaciomarine sediments and at first was assumed to have been deposited by icebergs derived from the Laurentide continental glacier when rising sea level set it afloat in the Amundson Gulf, ten or twelve thousand years ago. However, petrological examination by Craig Rodeick (personal commun., 12/24/76) shows that the pebbles are very well rounded and represent the local limestone-black chert suite that forms the present mainland beaches. Evidently the pebbles were lifted by shore ice and rafted a short distance offshore from a then-nearby mainland beach. The exceptional abundance of coarse material in the basal pebbly mud remains unexplained; however, pebbles of the limestone-black chert are also scattered, although very sparsely, through all except the uppermost 60 cm of the overlying marine clay.

Pebbles in the surficial pebbly sand are quite different. They consist largely of dolomite, orthoquartzite, and red granite similar to the gravel of nearby Reindeer Island. A few dolomite and red granite pebbles were also recovered from the uppermost 60 cm of the overconsolidated marine clay. These lowest pebbles of red granite and dolomite probably record the time when the Midway Island barrier chain migrated near enough to become a source of ice-rafted material at site PB-2, and the surficial pebbly fine sand probably accumulated shortly after, when the barrier chain lay so near that storm surges occasionally carried coarse material from the island to the nearby sea bed.

The surficial pebbly fine sand may, in fact, represent the eroded stump of present-day Reindeer Island. Historical records reviewed by Lewellen (1970), Wiseman and others (1973), and Barnes and others (1977) show that during the

last few decades various Beaufort Sea barrier islands have been migrating at rates ranging from 6 to 32 m, and two different islands have been migrating landward at rates of about 3 m per year. The overconsolidation of marine clay and pebbly mud at site PB-2 seems to indicate that the sediments have gone through a cycle of freezing and subsequent thawing (Annual Report, R.U. 104). This cycle of freezing and thawing would be most easily explained if one assumed that the site had lain beneath a migrating barrier island for a century or two. Reindeer Island may have migrated the 3 km from site PB-2 to its present position within the last thousand years.

The faunal and plant material from the marine section of PB-2 (fig. 5) presents several anomalies that may eventually contribute to a better understanding of the environmental history. For example, ostracodes are much rarer in the marine pebbly mud than in any other marine sediment in the Prudhoe Bay area. The foraminifer fauna records a steady deepening of the water during the accumulation of the pebbly mud, the existence of relatively deep water during the accumulation of the lower half of the overconsolidated marine clay, and then a shallowing, perhaps due to rapid sedimentation, during the accumulation of the upper part of the marine clay and the surficial pebbly fine sand (Appendix V). One sample, MF-3632, collected about a meter below the top of the marine clay, contains foraminifer tests in ten times the abundance found at any other level; the sample also yields an exceptional abundance of terrigenous debris, including wood chips, fruiting-bodies of the fresh-water alga, Chara, and seeds of the fresh-water aquatic monocot, Potamogeton.

To summarize: Site PB-2 was inundated by rapidly rising sea level, possibly as early as 10,000 years ago, but more likely about 9,000 years ago. After the beach had migrated further shoreward, large quantities of beach pebbles were ice-rafted a short distance offshore at a time when the water was deepening rapidly, probably due to a combination of thermokarst collapse and rapidly rising sea level. Salinities and water temperatures differed little from those of the present time, but some fact, possibly turbidity kept the ostracode population very low. World-wide sea level stabilized about 4,000 years ago, and this probably occurred during the interval when the marine clay was accumulating. Meanwhile, a barrier chain was building westward, possibly from gravel sources in the Flaxman Island area. Quickening sedimentation, indicated by faunal evidence of shallowing water, may have resulted from the shallowing effect of the approaching barrier chain. The continuing approach of the Midway Islands is recorded first by the appearance of ice-rafted pebbles of the dolomite suite and then by the deposition of the dolomite-rich pebbly fine sand. Finally, it seems that Reindeer Island must have migrated directly over site PB-2, resulting in the freezing and subsequent thawing, dewatering, and densification of the marine sediments at site PB-2. The passage of Reindeer Island over site PB-2 probably took place about a thousand years ago.

X. Summary of Fourth Quarter Operations

A. Ship and laboratory activities

1. No cruises

2. D. M. Hopkins, Roger Hartz, R. E. Nelson, Peggy Smith

3. Laboratory activities: Compiled maps of direction of coastal drift for Beaufort and Chukchi Seas.

Hand-picked samples for radiocarbon dates and ran date listed in Annual Report.

Identified mollusks and submitted mollusks for Amino-Acid racemization studies.

B. Problems: About half of quarter devoted to synthesis meeting and to preparation of synthesis report for Earth Science studies in Chukchi Sea. This left inadequate time for preparation of Annual Report.

C. Estimate of funds expended: \$50,000

REFERENCES CITED

- Barnes, P. W., Reimnitz, Erk, Smith, G., and Melchior, J., 1977, Bathymetric and shoreline changes, northwestern Prudhoe Bay, Alaska: U.S. Geol. Survey Open-file Rept. 77-161, 10 p.
- Hunter, J. A. M., Judge, A. S., MacAulay, H. A., and others, 1976, Permafrost and frozen sub-seabottom materials in the southern Beaufort Sea: Canada Dept. Environment, Beaufort Sea Tech. Rept. 22, 174 p.
- Lewellen, R. E., 1970, Permafrost erosion along the Beaufort Sea coast: Published by the author, Littleton, CO, 25 p.
- _____, 1976, Subsea permafrost research techniques: Louisiana State Univ., Symposium on Research Techniques in Coastal Environments, preprint, 20 p.
- Osterkamp, T. E., and Harrison, W. D., 1976, Sub-sea permafrost at Prudhoe Bay, Alaska; drilling report: Univ. Alaska Geophys. Inst. Sea Grant Rept. 76-5, 69 p.
- Rodeick, C. A., 1975, The origin, distribution, and distributional history of gravel deposits on the Beaufort Sea continental shelf, Alaska: California State Univ., San Jose, M.S. thesis, 87 p.
- Wiseman, W. J., Jr., Coleman, J. M., Gregory, J., and others, 1973, Alaska Arctic coastal processes and morphology: Louisiana State Univ. Coastal Studies Inst. Tech. Rept. 149, 171 p.

FIGURE CAPTIONS

- Figure 1. Map showing locations of drill holes.
- Figure 2. Cross-section through a series of boreholes extending from the ARCO dock on the mainland coast northeastward through Reindeer Island (fig. 1).
- Figure 3. Simplified graphic log showing sampled intervals, borehole PB-1.
- Figure 4. Simplified graphic log showing sampled intervals, borehole PB-1A
- Figure 5. Simplified graphic log showing sampled intervals, borehole PB-2
- Figure 6. Simplified graphic log showing sampled intervals, borehole PB-3
- Figure 7. Sea-level history in the Bering and Chukchi Seas.
- Figure 8. Lithology and faunal content, borehole PB-3.

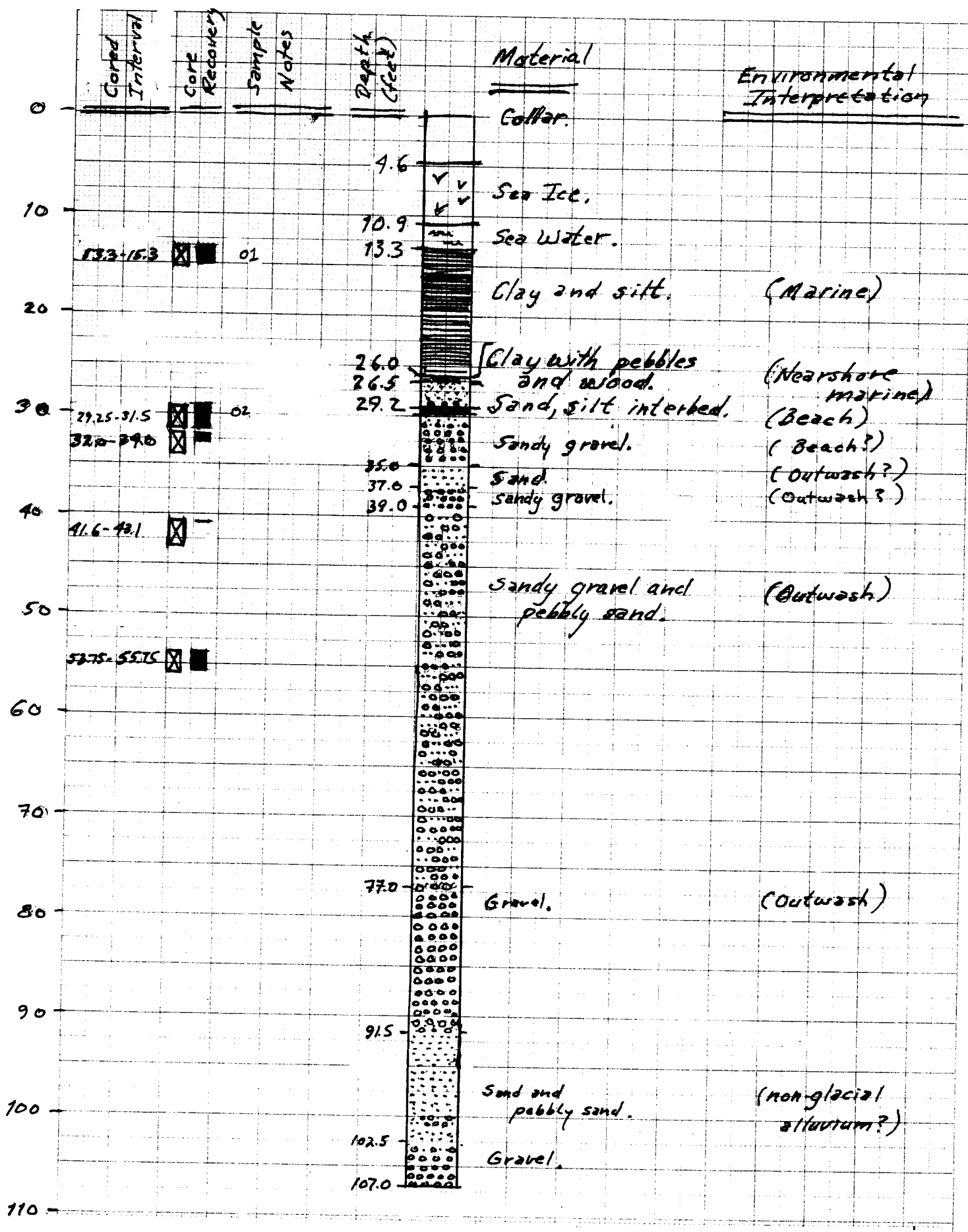


Figure 3. Borehole PB-1 (Latitude $70^{\circ}20.9'N$, Longitude $148^{\circ}19.3'W$.)

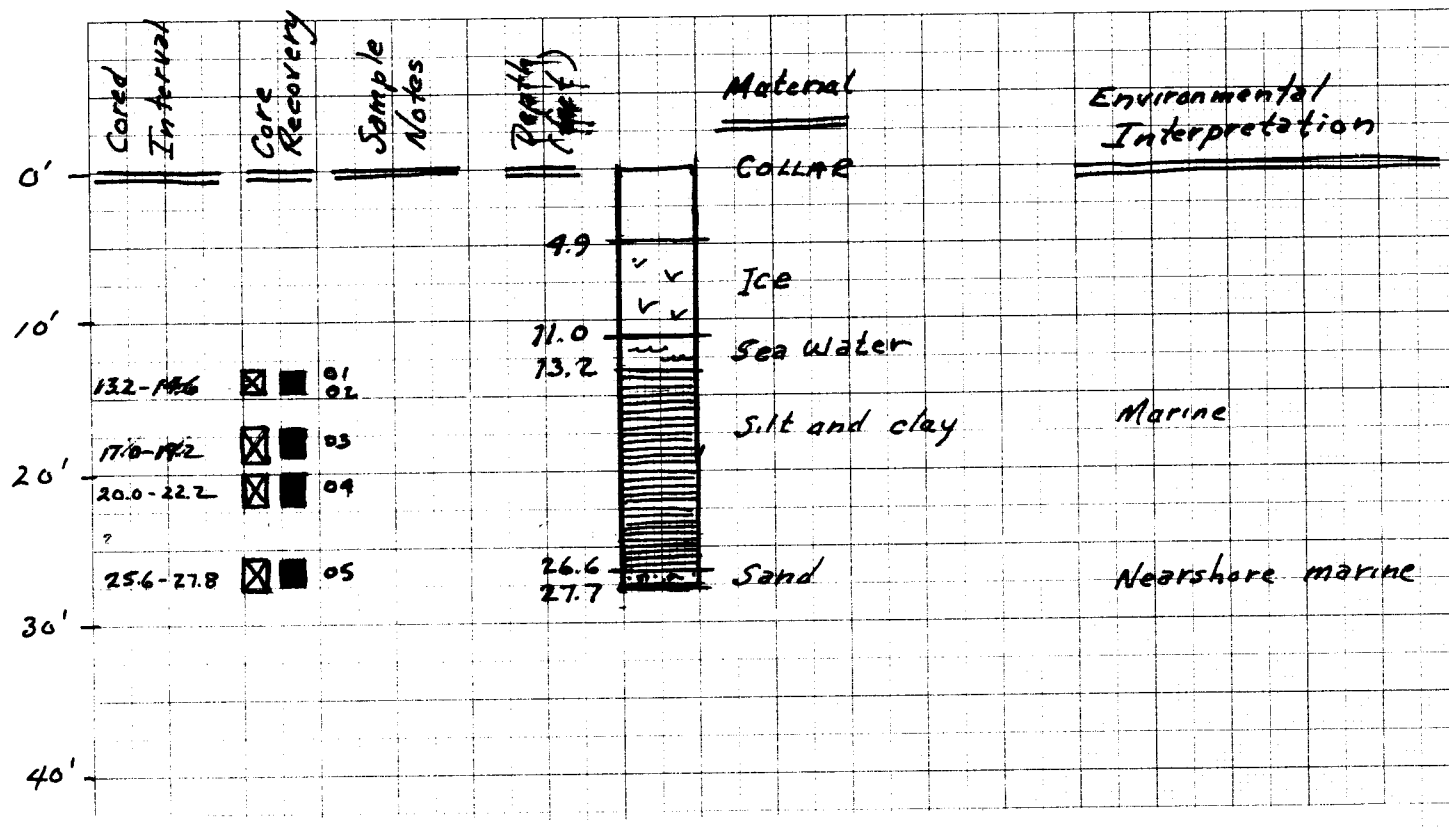


Figure 4. Borehole PB-1A (Latitude 70°20.9'N, Longitude 148°19.3'W.)

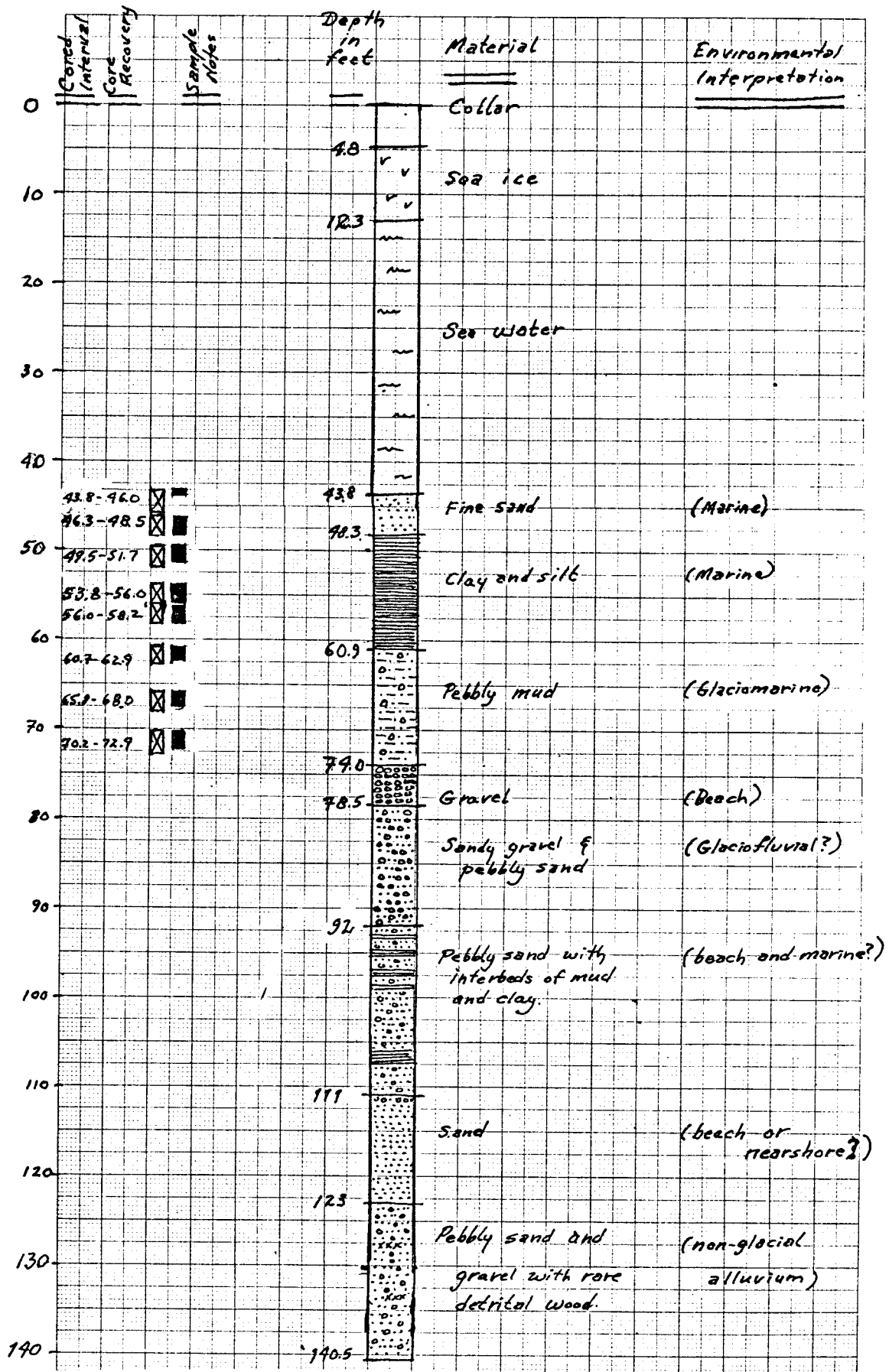


Figure 5. Borehole PB-2 (Latitude 70°30.6'N, Longitude 148°18.0'W.)

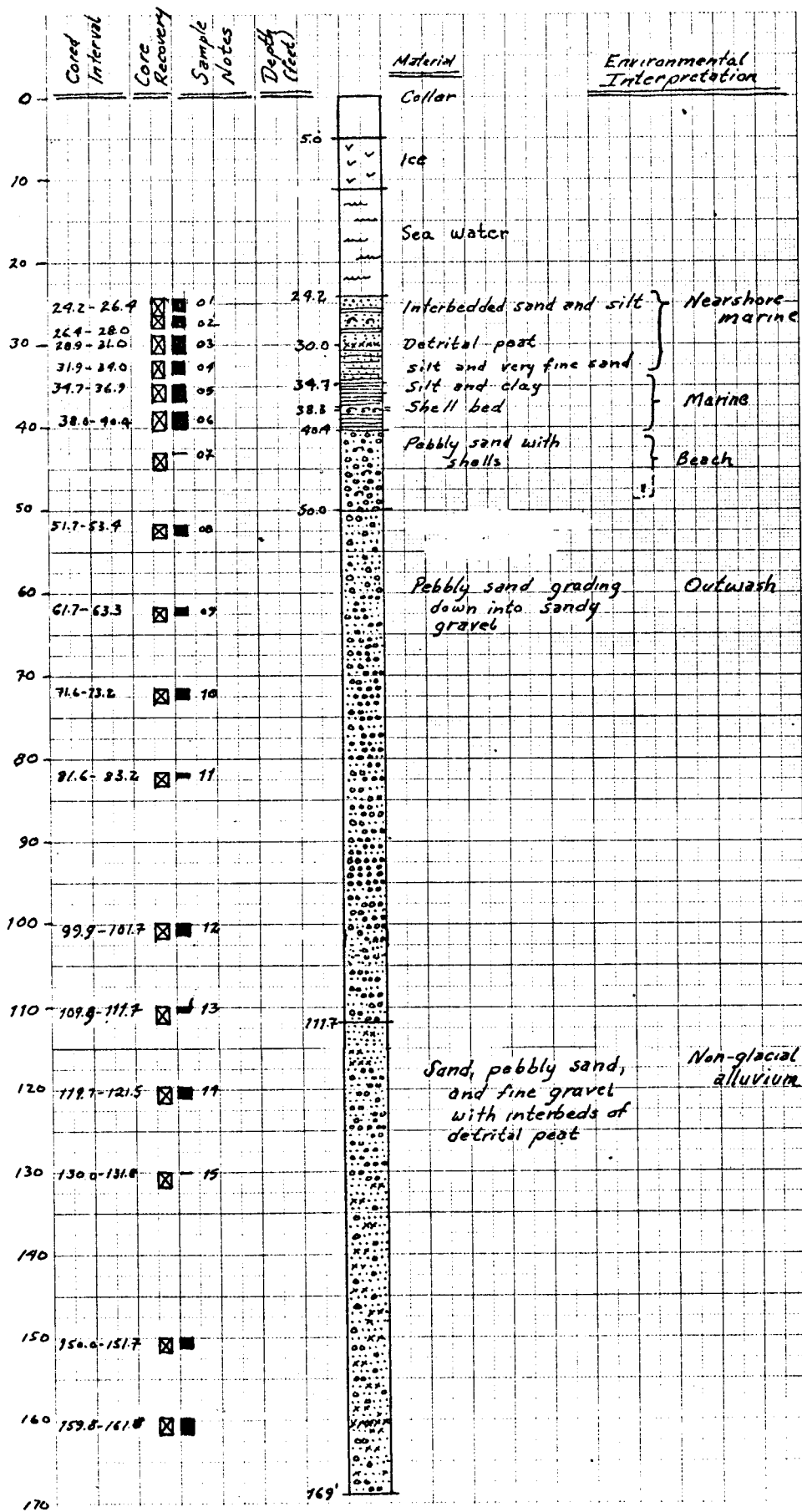


Figure 6. Borehole PB-3 (Latitude 70°25.8'N, Longitude 148°26.6'W.)

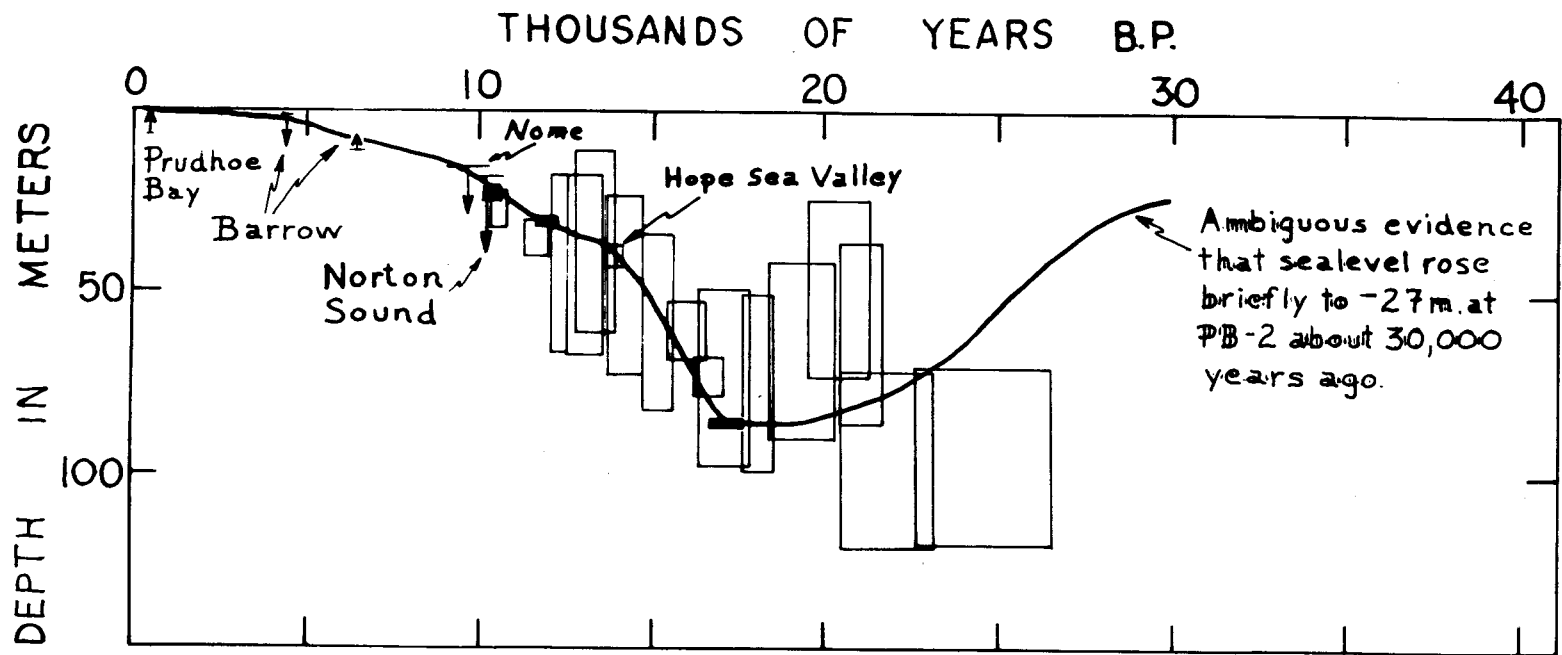
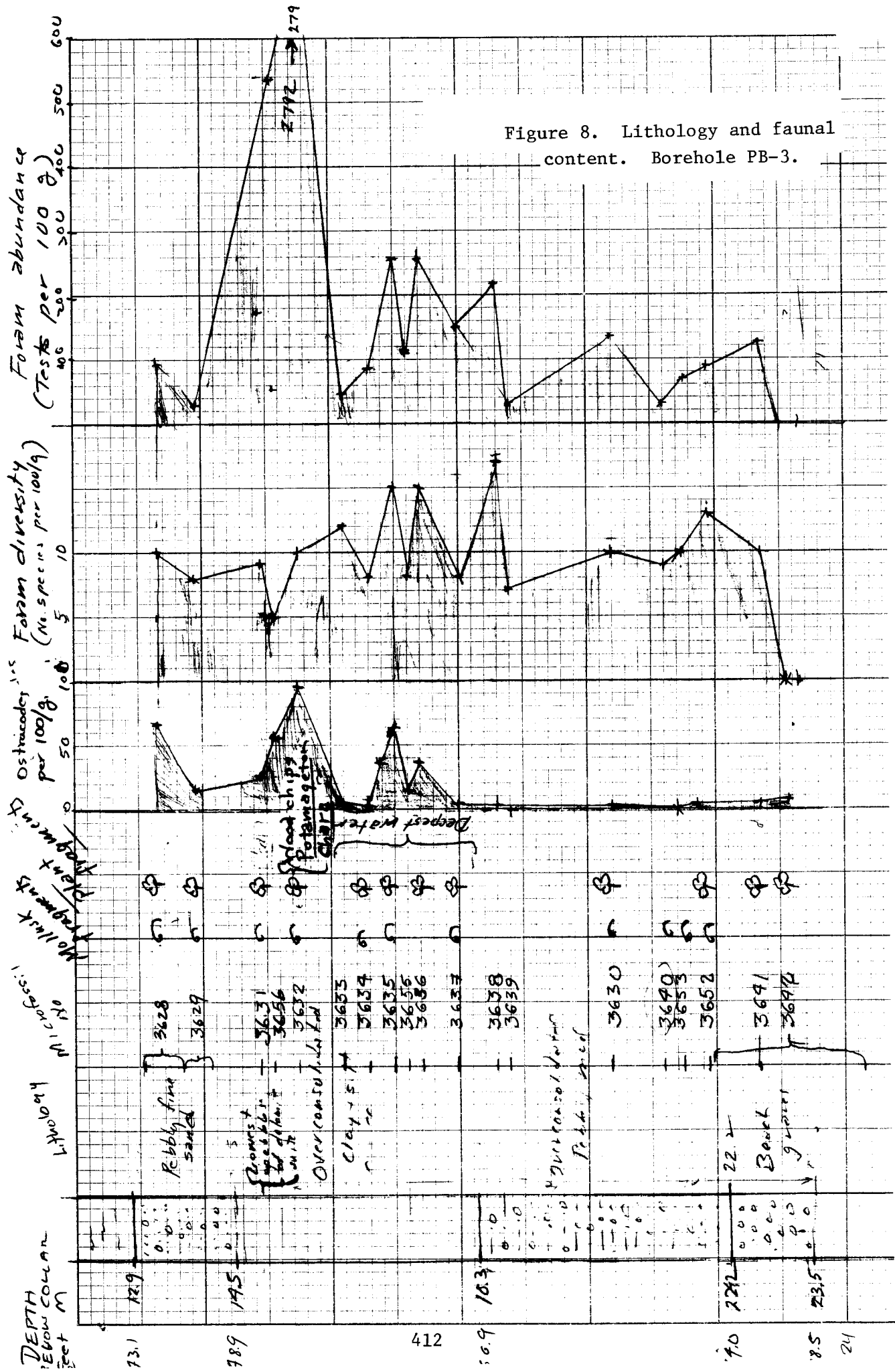


Figure 7. Sea level history in the Bering and Chukchi Seas.

Figure 8. Lithology and faunal content. Borehole PB-3.



CORE RADIOGRAPHY

P. W. Barnes
U.S. Geological Survey
345 Middlefield Road
Menlo Park, California 94025

Radiographs were taken of 29 core segments from 1976 drill holes PB 1, 1A, 2 and 3 to ascertain the character of sedimentary structures at these sites. The small cross sectional area of the cores (5 cm) precludes observations of large features, however there is considerable vertical variation in the fine structure and stratigraphy as outlined below.

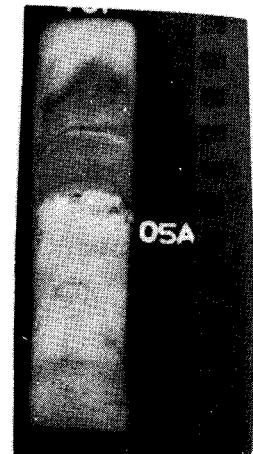
Drill Hole PB-1A

Radiographs of cores from the upper 3 meters show fine, horizontally laminated silts and clays with rare pebbles and shell fragments. The lamina are typically 2-20 m thick with poorly defined boundaries. Several fine sand layers, without internal structures, occur in the upper 25 cm (Core segments 1 thru 4B).

At about 4 m below the sea bed (Core 5A) the indistinct lamination ends at a pebble-rich sand unit without structure. This unit inversely grades to sand at the bottom of the hole (Core 5B, 4.4 m). This boundary is apparently the same boundary noted at 26-27 feet in the drill logs.

Drill Hole PB-2

In the upper 1.5 m (Cores 1 & 2) poorly stratified sands are interbedded with muds. Mud lumps and rare pebbles are present along with a few shell fragments. The sands do not show any internal structures, but this could be related to coring and handling problems.



From 2 to 3 meters (Cores 3 & 4) the sands grade downward from sandy muds to muds. Weak, indistinct layering is indicated in the upper part (Core 3) while the lower section is completely structureless mud.

Cores from 5 to 8 meters (6,7 & 8) are characterized by pebbly muds with no layering or distinct structures. These cores are strikingly similar to the homogeneous pebbly muds box-cored on the central shelf in the zone of most intense ice gouging.

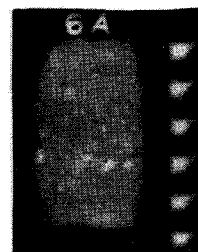
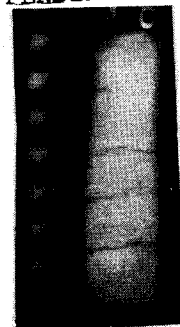
Drill Hole PB-3

Cores from the upper 5 meters (1 through 6) are composed of interbedded sands and silts with increasing amounts of silts and clays at the bottom of the section. The sands in these cores occasionally show indications of cross-bedding. Structures at the top of Cores 3 and 4 suggest disruption and possible contamination from drilling or handling. The layering in this part of the hole is sharply delineated in contrast to the vague bedding seen in either PB-1 or PB-2.

No structures were seen in the gravels which occur in cores below 5 m.

The upper few meters of each drill site have different structural characteristics which suggest that each represents deposition in a different environment. From our cursory examination of vibrocores I feel that these upper sections represent the modern depositional facies at the drill sites; bay, lagoonal, and open shelf, and thus represent the thickness of post-transgressional Holocene deposits. Based on the radiographs, the thickness of Holocene sediments at these

three sites can be roughed out as follows:	PB-1	4 m	Holocene	thickness
	PB-2	9 m	"	"
	PB-3	5 m	"	"



PALEOMAGNETISM OF MARINE SECTION
OF BOREHOLE PB-2

Jack Hillhouse
U.S. Geological Survey
345 Middlefield Road
Menlo Park, CA 94025

Twenty-six specimens from the upper third of core PB-2 were submitted for paleomagnetic analysis. After the natural remanent magnetizations (NRM) of these samples were measured, they were partially demagnetized in a 150 oersted alternating field and remeasured. This treatment removed any spurious magnetizations which the core might have acquired during drilling and storage. The magnetic signal carried by the sediment is quite strong; the NRM's averaged 1×10^{-5} emu/cm³ and typically the intensity decreased by a factor of 10 during the A.F. treatment. At the drill site the expected magnetic inclination is 80.0° assuming that the field is due to a geocentric dipole aligned with the geographic poles. As shown on the attached sheet, the cleaned inclinations determined from core PB2 all have normal polarity and are clustered around 80°. One sample, PB2-M8A, has a very low inclination (42.8°); however, M8B from the same horizon has a normal inclination, indicating that part of the core was disturbed during drilling. These sediments were deposited during a normal polarity epoch, most likely during the Brunhes epoch (0-0.7 m.y. ago). Variations in the inclination record are within the limits of normal secular variation exhibited by the geomagnetic field.

Sample No.	Approx. depth in feet	Inclination before A.F. Cleaning	Inclination after A.F. Cleaning	Intensity (emu/cm ³) after A.F. Cleaning
PB2-M18B	15.0	79.3	80.3	1.71 E-5
PB2-M18A		78.5	78.6	1.90 E-5
PB2-17B	15.3	85.8	82.6	2.69 E-5
PB2-M17A		83.0	82.7	3.08 E-5
PB2-M16	16.3	73.6	73.9	2.96 E-6
PB-M15	16.5	73.8	72.7	2.52 E-6
PB2-M14	16.6	79.5	80.1	1.42 E-6
PB2-M13	16.8	82.6	83.0	1.81 E-6
PB2-M12	17.0	81.0	79.1	1.50 E-6
PB2-M11	17.1	77.5	75.3	1.08 E-6
PB2-M10	17.2	87.8	87.8	8.01 E-6
PB2-M9	17.4	57.7	57.8	1.14 E-5
PB2-M8B	18.3	77.1	84.1	5.18 E-6
PB2-M8A		64.3	42.8	7.56 E-6
PB2-M7B	18.6	76.8	87.2	2.26 E-6
PB2-M7A		68.6	65.6	3.29 E-6
PB2-M6B	19.8	79.6	77.1	6.21 E-6
PB2-M6A		73.8	72.3	5.06 E-6
PB2-M5B	20.1	76.3	76.8	6.36 E-6
PB2-M5A		66.6	70.9	8.18 E-6
PB2-M4B	21.1	74.9	78.3	6.25 E-6
PB2-M4A		64.6	70.1	3.74 E-6
PB2-M3B	21.3	79.8	75.6	3.72 E-6
PB2-M3A		77.9	83.4	3.37 E-6
PB2-M2	21.7	61.5	65.8	2.90 E-6
PB2-M1	21.9	78.0	82.0	9.04 E-6

RADIOCARBON DATING

LAB. NO.	AGE	BOREHOLE	DEPTH BELOW SEA LEVEL (m)	MATERIAL	SIGNIFICANCE
USGS-132	490 ₊₉₀	PB-1	6.5	Large twig	Collected near base of marine section and provides an approximate age for flooding of Prudhoe Bay
_____	_____	PB-2	14.8-15.5	Dispersed fine organic matter	Collected near top of marine section below first appearance of gravel related to Reindeer Is. Dates migration of Reindeer Is.
_____	_____	PB-3	41.4-42.6	Dispersed detrital fragments in sand and gravel	Collected in and provides age estimate for alluvium below outwash
AU-115	22,300 _{+1,200}	OH3370	13.7	Wood	Collected near top of nonglacial alluvium

FORAMINERAL FAUNAS, PRUDHOE BAY BOREHOLES

Kristin McDougall
U.S. Geological Survey
345 Middlefield Road
Menlo Park, CA 94025

Twenty-three samples from the Offshore Borehole PB-1 drilled in April, 1976, as part of a joint project by CRREL, USGS, and R. E. Lewellen, to explore the thickness and state of permafrost beneath the Beaufort Sea were examined for microfossils. This hole was drilled on shore-fast ice about 4.5 feet thick through water 13 feet deep on the continental shelf in the middle of Prudhoe Bay. The results are as follows:

Mf 3603 (field no. Pb1-WS 17-18)*
Mf 3604 (field no. Pb1-WS 18-19)*
Mf 3605 (field no. Pb1-WS 19-19.5)*
Mf 3606 (field no. Pb1-WS 19.5-20)*
Mf 3607 (field no. Pb1-WS 20-20.5)*
Mf 3608 (field no. Pb1-WS 20.5-21)*
Mf 3609 (field no. Pb1-WS 21-21.5)*
Mf 3610 (field no. Pb1-WS 21.5-22)*
Mf 3611 (field no. Pb1-WS 23-25)*
Mf 3612 (field no. Pb1-WS 25-27)*
Mf 3613 (field no. Pb1-GS 1a)*
Mf 3614 (field no. Pb1-GS 2) Barren
Mf 3615 (field no. Pb1-GS)*
Mf 3616 (field no. Pb1-GS 4)*
Mf 3617 (field no. Pb1-GS 5) Barren
Mf 3618 (field no. Pb1-GS 6) Barren
Mf 3619 (field no. Pb1-GS 7b)*
Mf 3620 (field no. Pb1-GS 11) Barren
Mf 3621 (field no. Pb1-WS 37-39) Barren
Mf 3622 (field no. Pb1-WS 92-92.5) Barren
Mf 3623 (field no. Pb1-WS 94.7-100) Barren
Mf 3624 (field no. Pb1-WS 100-101) Barren
Mf 3625 (field no. Pb1-WS 101-102) Barren

*see attached checklist for faunal list

Twenty-eight samples from the Offshore Borehole Pb2, drilled in April, 1976, as part of a joint project by CRREL, USGS, and R. E. Lewellen to explore thickness and state of permafrost beneath the Beaufort Sea were examined for microfossils. This hole was drilled on shore-fast ice about 6 feet thick, through water 39 feet deep on the continental shelf about 1.5 miles north of Reindeer Island in Prudhoe Bay area.

Mf 3628 (field no. Pb2-WS 43.8-45.8)*
Mf 3629 (field no. Pb2-WS 45.8-47.0)*
Mf 3656 (field no. Pb2 GS 3)*
Mf 3631 (field no. Pb2 Clay bit 49.7)*
Mf 3632 (field no. Pb2-GS 03e)*
Mf 3633 (field no. Pb2-GS 04b)*
Mf 3634 (field no. Pb2-GS 04e)*
Mf 3635 (field no. Pb2-GS 05b)*
Mf 3655 (field no. Pb2-GS 05c)*
Mf 3636 (field no. Pb2-GS 05e)*
Mf 3637 (field no. Pb2-Clay bit 60)*
Mf 3638 (field no. Pb2-GS 06x)*
Mf 3639 (field no. Pb2-Clay bit 65.8)*
Mf 3630 (field no. Pb2-Clay bit 68)*
Mf 3640 (field no. Pb2-Clay bit 70.75)*
Mf 3653 (field no. Pb2-08A)*
Mf 3652 (field no. Pb2-08E)*
Mf 3641 (field no. Pb2-bit 72.9)*
Mf 3642 (field no. Pb2-WS 73-81)*
Mf 3643 (field no. Pb2-WS 88-92) Barren
Mf 3644 (field no. Pb2-WS 92-101)*
Mf 3645 (field no. Pb2-WS 101-111) Barren
Mf 3646 (field no. Pb2-WS 111-112) Barren
Mf 3647 (field no. Pb2-WS 123-126) Barren
Mf 3648 (field no. Pb2-WS 127-129) Barren
Mf 3649 (field no. Pb2-WS 129-131) Barren
Mf 3650 (field no. Pb2-WS 131-133) Barren
Mf 3651 (field no. Pb2-WS 133-135) Barren

*See attached checklist for faunal list

Microfossil samples were split to 100-gram standard sizes, and all foraminifera in each sample were counted. Abundance of each species is expressed as a percentage of the total number of foraminifera present in the individual sample.

Fourteen samples from the Offshore Borehole Pb-3 drilled in April, 1976, as part of a joint project by CRREL, USGS, and R. E. Lewellen to explore thickness and state of permafrost beneath the Beaufort Sea were examined for microfossils. This hole was drilled on shore-fast ice about 5.5 feet thick through water 24 feet deep in protected waters about halfway between the end of the ARCO Causeway and dock and Reindeer Island. Samples are located on the attached log.

Mf 3658 (field no. Pb3-GS 01b)*
Mf 3659 (field no. Pb3-GS 02x)*
Mf 3669 (field no. Pb3-GS B2b)*
Mf 3660 (field no. Pb3-GS 03x)*
Mf 3661 (field no. Pb3-GS 04x)*
Mf 3662 (field no. Pb3-GS 05x)*
Mf 3670 (field no. Pb3-05B 38-40.4)*
Mf 3663 (field no. Pb3 GS 06x)*
Mf 3671 (field no. Pb3-06A 38-40.4)*
Mf 3664 (field no. Pb3-WS 40-40.9)*
Mf 3665 (field no. Pb3-WS 39.9-43.0)*
Mf 3666 (field no. Pb3-WS 43-44) Barren
Mf 3667 (field no. Pb3-WS 44-46)*
Mf 3668 (field no. Pb3-WS 46-52)*

*See attached checklist for faunal list

Comments: It appears that samples Mf 3603-3611, Borehole 1, represent a very recent fauna probably indicative of the current conditions. This fauna began in Mf 3610 and Mf 3611, and increased in diversity and size as conditions became more stable and the water depth increased.

Sample Mf 3612 crosses a lithology boundary and is assumed to contain faunas representing both environments of deposition. Mf 3613 may suffer from the same problem although the log indicates it was taken within the "clay with pebbles" interval. If so, this interval was probably deposited under marine conditions not unlike those immediately above (Mf 3610).

Although predominantly barren, samples Mf 3614-3619, do indicate a marine environment (foraminifers in Mf 3616 and megafossil fragments in Mf 3616 and Mf 3619). This poor faunal assemblage may be due to a beach environment or shallow water depths with rapid sedimentation.

All older samples in this Borehole were barren of organic remains.

The recent fauna in Borehole 3 seems to be represented by samples Mf 3658 and possibly Mf 3659. Sample Mf 3664 contains a fauna indicative of the greatest water depths in this Borehole. Samples above this indicate shallowing.

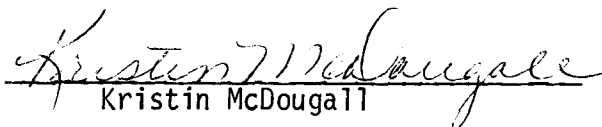
No microfauna is present within the pebbly sand interval (40.4-50.0), samples Mf 3666-3668. There are, however, megafossil fragments suggesting that this interval was probably a beach or shallow marine.

In Borehole 2 the living and/or recent faunas appear to be represented by samples Mf 3628 and 3629. Samples Mf 3631 and 3632 may also represent this recent fauna. This interval represented by Mf 3628, 3629, 3631, and 3632 could be correlated with Borehole 1, samples Mf 3603-3610 as the faunal trend is similar although representing a deeper facies and Borehole 3, sample Mf 3658.

Beginning with Mf 3633 there is a noticeable change in the fauna. Many species which have been found in the Arctic Sea at depths of 60 feet or greater appear. These "deeper water" species increase in abundance (downward in the hole) until Mf 3636 or 3637 or the base of the clay and silt sequence at 60.9. A corresponding trend was seen in Borehole 3 from Mf 3660 to 3664.

Samples Mf 3638-3641 contain a fauna similar to the subrecent fauna of this Borehole (Mf 3631-3632). This interval may have shallowed considerably and still maintained a connection with the Arctic Sea and the "deeper water" species.

All older samples, Mf 3642-Mf 3651, were barren of microfossils; and only Mf 3642 and Mf 3644 contained any organic material.


Kristin McDougall

BORE HOLE 2	Mf 3628	Mf 3629	Mf 3656	Mf 3631	Mf 3632	Mf 3633	Mf 3634	Mf 3635	Mf 3655	Mf 3636	Mf 3637	Mf 3638	Mf 3639	Mf 3630	Mf 3640	Mf 3653	Mf 3652	Mf 3641	Mf 3642	Mf 3643	Mf 3644	Mf 3645	Mf 3646	Mf 3647	Mf 3648	Mf 3649	Mf 3650	Mf 3651
<i>Bathysiphon</i> sp.					1											1	2											
<i>Succella frigida</i> (Cushman)			7	7	4	2		1	3	4	6		3	4		3												
<i>Sulonina exilis</i> Brady							1	5		7		4					1	8										
<i>Cassidulina islandica</i> Nørvang							5	19	17	20	5	27	3			9	2											
<i>Cassidulina norcrossi</i> Cushman		4				7	13	4	6	7	42	12	22	10	20	14	21	21										
<i>Cyclogyra involvens</i> (Reuss)	1					9					6	9					1											
<i>Dentalina frobisherensis</i> Loeblich & Tappan															7	3												
<i>Dentalina gracilis</i> d'Orbigny				1	2				7			1	7	2			2	2										
<i>Eiphioidella groenlandica</i> (Cushman)	20	26	4											1														
<i>Eiphiidium bartletti</i> Cushman	3	12										4																
<i>Eiphiidium clavatum</i> Cushman	5	8	53	50	49	59	53	44	40	10	12	7	29	14	36	29	52											
<i>Eiphiidium incertum</i> (Williamson)	6	35	5	2	2				2					4	7		3	2										
<i>Eiphiidium</i> sp.	4														3													
<i>Eoepionidella strombodes</i> Tappan				1																								
<i>Esosyrinx curta</i> (Cushman & Ozawa)									3																			
<i>Fissurina marginata</i> (Montagu)						1	7		3	4																		
<i>Fissurina orbignyana</i> Sequenza									7																			
<i>Glanulina laevigata</i> d'Orbigny						1	3	9																				
<i>Guttulina lacrea</i> (Walker & Jacob)	1	4	3	3	2			9	7	6	1		3	7	1	1	3											
<i>Guttulina problema</i> d'Orbigny								3																				
<i>Lagera gracillima</i> (Sequenza)					2	7							1				8											
<i>Marginulina alabra</i> d'Orbigny																	3											
<i>Oolina lineata</i> (Williamson)					2	7						1																
<i>Parajissurina himatiostoma</i> Loeblich & Tappan							7																					
<i>Protelphidium orbiculare</i> (Brady)	49	91	32	36	18	15	11	27	22	41	40	55	45	34	29	30	14											
<i>Pseudopolymorphina artica</i> MacBeth & Schmidt													4				8											
<i>Pseudopolymorphina</i> cf. <i>P. norvangliae</i> (Cushman)					.03	2																						
<i>Pseudopolymorphina</i> sp. A	5	8	2	4	2	5	4					4		3		1												
<i>Pseudopolymorphina suboblonga</i> Cushman & Ozawa	2			3													1											
<i>Pyralina</i> sp.								3																				
<i>Quinqueloculina arctica</i> (Cushman)								9	5																			
<i>Quinqueloculina seminulum</i> (Linné)	3		2	2								4	3		3	1	2											
<i>Quinqueloculina subrotunda</i> (Montagu)				1					3	8																		
<i>Silicosigmoxina groenlandica</i> (Cushman)				2																								
<i>Tritoculina trihedra</i> Loeblich & Tappan							1	3	4			1		1		3												
Megafossils	X	X	X	X	X	X	X	X	X	X	X	X	X	X	X	X	X	X	X	X	X	X	X	X	X	X	X	
Plant				X	X	X	X	X	X	X	X	X	X	X	X	X	X	X	X	X	X	X	X	X	X	X	X	
Ostracodes #	67	15	53	26	97	7	1	61	12	37	1	1	0	1	0	5	5	7										
Total %	98	101	91	102	96	99	100	91	99	92	98	100	101	98	98	98	92	0	0	0	0	0	0	0	0	0	0	
Total #	92	26	39	175	45	86	259	109	258	147	219	31	139	29	69	90	122	0	0	0	0	0	0	0	0	0		
Chara				1																								

BORE HOLE 3	Mf 3658	Mf 3659	Mf 3669	Mf 3660	Mf 3661	Mf 3662	Mf 3670	Mf 3663	Mf 3671	Mf 3664	Mf 3665	Mf 3666	Mf 3667	Mf 3668						
<i>Buccella frigida</i> (Cushman)	9	1	2	1	7	.7		2												
<i>Cyclogyra involvens</i> (Reuss)	2	2	3						.1											
<i>Ventalina ittai</i> Loeblich & Tappan	.08																			
<i>Elphidiella groenlandica</i> (Cushman)	2	13	2	2	3	56	1	40	12	100										
<i>Elphidium bartletti</i> Cushman	1	13		7	5	20		44	21											
<i>Elphidium clavatum</i> Cushman	23	3	10		8	13			17											
<i>Elphidium frigidum</i> Cushman	13	9	12	8	2		3	.7	20											
<i>Elphidium incertum</i> (Williamson)	14	2		18	10		54	.7	4											
<i>Fissurina marginata</i> (Montagu)			2																	
<i>Glandulina laevigata</i> d'Orbigny							3													
<i>Guttulina lactea</i> (Walker & Jacob)	.08								.1											
<i>Lagena gracillima</i> (Sequenza)									.1											
<i>Oolina melo</i> d'Orbigny	.08																			
<i>Protelphidium orbiculare</i> (Brady)	34	47	39	47	54	6	30	5	19											
<i>Pseudopolymorphina</i> sp. A	5	9	5	15	8	3	6	7	4											
<i>Pseudopolymorphina suboblonga</i> Cushman & Ozawa		1																		
<i>Pyrgo williamsoni</i> (Silvestri)						.7														
<i>Quinqueloculina artica</i> Cushman			3																	
<i>Quinqueloculina seminulum</i> (Linné)	2	1	20		2				2											
<i>Quinqueloculina subrotunda</i> (Montagu)			3	1																
<i>Reophax</i> cf. <i>R. scorpiurus</i> Montfort								.7												
<i>Scutuloris tegminis</i> Loeblich & Tappan	.08																			
<i>Trochammina nana</i> (Brady)	2						1													
Chara	X	X	X	X	X				1											
Mega	X	X	X	X	X	X		X	X	X	X		X	X						
Plant							X													
Ostracod	127	28	64	62	74	80	80	98	620	4	0	0	0	0						
Percent	100	101	101	99	99	100	98	100	99.3	0	0	0	0	0						
Total #	126	101	63	99	286	151	69	129	136	2	0	0	0	0						
					8															

MARINE MOLLUSKS, PRUDHOE BAY BOREHOLES

Identifications by Louis Marinovich and W. O. Addicott
 U.S. Geological Survey
 Menlo Park, CA 94025

BOREHOLE NUMBER	SAMPLE	DEPTH IN METERS	IDENTIFICATION	
PB-2	Core 02	13.9-14.6	<u>Astarte</u> sp.	
PB-2	Core 03A	14.7-15.5	<u>Astarte?</u> sp. (fragments) <u>Yoldiella?</u> sp. (fragments)	
PB-3	Core 01b	7.3-7.9	<u>Astarte</u> sp. (fragments) Taxodont bivalve (fragment) Gastropod (fragment)	
PB-3	Core 02b 02y	7.9-8.4	<u>Astarte</u> sp. (fragment) Gastropod (fragment)	
PB-3	Core 03a 03b 03x 03y		8.7-9.3	<u>Portlandia</u> sp. cf. <u>P. arctica</u> (Gray) (1) <u>Yoldiella?</u> sp. (1 valve) <u>Astarte</u> sp. (fragments) Tellinid bivalves
PB-3	Core 05b 05x	9.6-10.2		<u>Nucula</u> sp. (juvenile) <u>Nuculana?</u> sp. (1 fragment and 1 very small juvenile) <u>Astarte</u> sp. (1 valve, fragments)
PB-3	Core 06a 06x			11.4-12.1
PB-3	Bit sample	40.9' 12.3		
PB-3	W.S. 39'-43'	11.7-12.9	<u>Astarte</u> sp. cf. <u>A. brouweri</u> (Meek)	

Notes: (1) Portlandia arctica usually confined to depths of 5-10 m.

(2) Macoma balthica generally confined to very shallow, brackish water.

PRELIMINARY
REPORT ON POLLEN FROM BOREHOLE PB-2

R. E. Nelson
U.S. Geological Survey
Seattle, WA 98195

Borehole PB-2, drilled at Prudhoe Bay in 1976, was sampled at eighteen (18) levels between core depths of 48.3 and 74.0 feet (14.6-22.4 meters). These samples were taken in the pebbly mud and clay/silt horizons immediately below the fine sand at the top of the core. The samples, originally taken for paleomagnetic analysis, were forwarded to me for palynological study following magnetic investigation.

The volume of each sample was approximately 5 ml. One sample from each sample horizon was processed for pollen analysis; at horizons where replicate paleomagnetic samples were taken (for example, samples M-3a and M-3b), only samples suffixed "a" were processed.

Pollen was extracted with standard techniques, utilizing 5% KOH, 10% HCl, 48% HF, floatation in aqueous zinc chloride solution at specific gravity 1.7, and acetolysis. Identifications were made utilizing keys in Faegri and Iversen (1975), Kapp (1969), and McAndrews et al. (1973), as well as descriptive information from Erdtman (1966). Reference pollen slides were drawn from the collection of the Quaternary Palynology and Paleoecology Laboratory of the University of Washington, as well as from my own collection.

Preparations from each horizon have been scanned and preliminary counts made from five samples: PB-2-M-1, M-5a, M-9, M-13a, and M-18a. Table I summarizes the core depths and sediment types represented by each of these samples. The sediment-water interface in the core occurred at a depth of 43.8 feet (13.3 meters).

RESULTS

Pollen present in virtually all samples is sparse and in varying states

TABLE 1

Table of core depths for paleomagnetic samples analyzed for pollen content.

Sample number	Depth in Core	Lithology
PB-2-M-18a	49.5-51.7 feet (15.0-15.6 m)	clay and silt (upper)
M-13a	53.8-56.0 feet (16.3-16.9 m)	clay and silt (middle)
M- 9	56.0-58.2 feet (16.9-17.6 m)	clay and silt (lower)
M- 5a	65.8-68.0 feet (19.9-20.6 m)	pebbly mud (middle)
M- 1	70.2-72.9 feet (21.2-22.1 m)	pebbly mud (lower)

of preservation. Table II summarizes the pollen content of the five horizons thus far counted. An entire prepared microscope slide was counted for each of samples M-1, M-13a and M-18a, whereas two such slides were counted for samples M-5a and M-9. In all cases, however, the total number of pollen grains counted is less than the preferred minimum of 300. Additional slides are being prepared from sample residues and supplemental counts from these samples, as well as several others, should be completed shortly. The pollen data here presented should therefore be considered as preliminary, although they may indeed be indicative of what may be expected once final counts have been completed.

Redeposited pollen is definitely present in the core. A single grain of Aquilapollenites sp. was found in sample M-5a, and scanning a slide from sample M-3a revealed a grain of Sequoia-type. Aquilapollenites is a taxon largely limited to Cretaceous strata, though occurrences in the Oligocene of Alaska and western Siberia have been reported (Tschudy and Leopold, 1970). While it is possible that the grain of Sequoia may have been transported, by air or marine currents, from either Japan or California (the nearest stands of Taxodiaceous trees that could produce such pollen), it seems much more likely that it has been reworked from local strata of Miocene or older age. This interpretation is also supported by the virtual absence of pine in the samples, which would be a much more likely candidate for effective long-distance transport.

The regional vegetation suggested by all five pollen spectra is essentially the same as the present vegetation of the Prudhoe Bay area. The dominant vegetation type implied by the spectra is a low, wet sedge tundra with perhaps localized drier sites. Birch (probably dwarf birch, Betula nana) is not far distant, although alder is definitely not present nearby. A relatively low local pollen production rate is implied by the presence of low, but significant, amounts of spruce (Picea) pollen; spruce has probably not ranged north of the Brooks Range

TABLE II

POLLEN TAXA PERCENTAGES EXPRESSED AS A PERCENT OF TOTAL POLLEN, EXCLUSIVE OF SPORES

(+ indicates taxon present, but less than 2% of total pollen; - indicates taxon not present)

Taxon	Sample				
	M-1	M-5a	M-9	M-13a	M-18a
<u>Pinus</u> (pine)	-	-*	-	-	-
<u>Picea</u> (spruce)	4.0	4.5	+	2.8	3.7
<u>Alnus</u> (alder)	7.2	8.0	4.2	4.9	4.6
<u>Betula</u> (birch)	16.8	15.5	13.2	15.5	17.0
Graminae (grasses)	10.4	18.0	12.7	12.7	11.5
Cyperaceae (sedges)	46.4	40.5	52.1	47.2	45.0
cf. <u>Typha latifolia</u> (cattail)	+ ^o	-	-	-	-
cf. <u>Sparganium</u> (bur reed)	+ [@]	-	-	-	-
Juncaceae (rushes)	-	+	-	-	-
Liliaceae (lilies)					
cf. <u>Tofieldia</u> (False asphodel)	-	+	+	+	+
cf. <u>Polygonatum</u>	-	+	+	-	-
other Liliaceae	-	2.5	+	+	+
<u>Salix</u> (willows)	-	+	-	+	+
Polygonaceae (buckwheat family)	-	-	-	-	+
Caryophyllaceae (pink family)	+	-	+	+	+
Nymphaeaceae (water lilies), cf. <u>Nuphar</u>	+*	-	-	-	-
Ranunculaceae (buttercups)	-	-	-	-	+
Cruciferae (mustard family)	4.0	+	+	2.8	+
Crassulaceae, cf. <u>Sedum</u> (stonecrop)	-	-	-	-	+
<u>Saxifraga nivalis</u> type (saxifrage)	-	3.0	+	2.1	+
Rosaceae (rose family)	-	-	-	-	+
cf. <u>Acer</u> (maple)	-	-	-	-	+*
Umbelliferae (parsley family)	-	+	-	+	+
Ericaceae (heath family)	+	+	+	+	+
Plumbaginaceae, cf. <u>Armeria</u> (thrift)	+	-	+	-	-
Scrophularaceae (figwort family)	-	+	-	-	-
Compositae (composites), high-spine	+	-	-	+	+
Unknown	4.0	2.5	2.8	+	+
Total pollen counted	125	200	71	142	218

The following are expressed as a percent of total pollen number:

Trilete spores:					
<u>Sphagnum</u> (sphagnum)	17.6	13.0	8.5	4.9	8.3
<u>Lycopodium</u> (club moss)	2.4	5.0	4.2	2.8	2.8
<u>Botrychium</u> (moonwort)	4.8	5.0	-	+	4.1
other trilete spores	+	2.0	14.1	+	7.3
Monolete spores	+	2.0	4.2	2.1	2.8
Reworked grains#	+	5.5	23.9	8.4	11.5

Footnotes:

*single grain, worn and abraded, and probably reworked.

^o 3/4 tetrad, probably reworked.

[@] single grain, may be fourth grain of Typha tetrad.

heavily-stained, exotic types; frequently flattened and typically primitive trilete spores. Includes single grain of Aquilapollenites sp. in sample M-5a, discussed in text.

in postglacial time, and the spruce pollen present is most probably derived from sources at least 200 km distant.

The spectra from Borehole PB-2 are similar to a modern spectrum from East Oumalik Lake, which lies between the Ikpikpuk and Oumalik Rivers in the western coastal plain, as reported by Livingstone (1955), with the following logical exceptions: Alnus (alder) and grass pollen are higher, and sedge pollen correspondingly lower, at Oumalik lake than in the spectra from PB-2. This is readily understandable in view of the fact that East Oumalik Lake is a considerable distance inland from the coast, and consequently closer to the foothills where grass and alder are more important components of the vegetation.

Surprisingly, however, the closest analogy to the PB-2 spectra (in the major elements) I have found is a modern pollen sample washed from living Sphagnum by Colinvaux (1964) at Imuruk Lake, on Seward Peninsula. This spectrum consists of approximately 5% spruce, 3% alder, 13% birch, 9% grass, and 38% sedge. A critically important difference, however, is that Colinvaux also reported about 19% heaths (Ericaceae) in his sample, whereas Ericaceae never account for as much as 2% of the Prudhoe Bay spectra, although they are represented in each sample examined thus far. It should be noted also that this particular sample from Imuruk Lake was singularly anomalous among the five that Colinvaux reported.

Unfortunately, I have been unable to locate a published modern spectrum or spectra from the Prudhoe Bay region, which would obviously provide the most logical and definitive comparison for the fossil spectra from PB-2.

In summary, pollen spectra from five levels of the PB-2 core, between core depths of 49.5 and 72.9 feet (15.0 and 22.1 meters), are consistent in suggesting a regional vegetation comparable to that of the present. A postglacial age is thus suggested for all portions of the core represented by strata from which the pollen/paleomagnetic samples were drawn.

References

- Colinvaux, P. A., 1964: The environment of the Bering Land Bridge. Ecological monographs, vol. 34, no. 3, p. 297-329
- Erdtman, G., 1966: Pollen morphology and plant taxonomy: Angiosperms. New York: Hafner Publishing Co., 553 p.
- Fægri, K., and Iversen, J., 1975: Textbook of pollen analysis (3rd edition). New York: Hafner Press, 295 p.
- Kapp, R. O., 1969: Pollen and spores. Dubuque, Iowa: Wm. C. Brown Co., Publishers, 249 p.
- Livingstone, D. A., 1955: Some pollen profiles from Arctic Alaska. Ecology, vol. 36, no. 4, p. 587-600.
- McAndrews, J. H., A. A. Berti and G. Morris, 1973: Key to the Quaternary pollen and spores of the Great Lakes Region. Life sciences misc. publication, Royal Ontario Museum, Toronto. 61 p.
- Tschudy, B. D., and E. B. Leopold, 1970: Aquilapollenites (Rouse) Funkhouser - Selected Rocky Mountain taxa and their stratigraphic ranges, p. 113-167 in Symposium on palynology of the late Cretaceous and early Tertiary: Geological Society of America special paper 127.

DRILLER'S FIELD NOTES
SUBSEA PERMAFROST PROGRAM

Prudhoe Bay, Alaska
March to May, 1976
Outer Continental Shelf Program

Robert Lewellen
Arctic Research
P.O. Box 2435
Littleton, Colorado 80161

31 March

Arrived Prudhoe and started rigging up.

1 April

Still rigging up and moved sleds onto the sea ice.

P B - 12 April

Rigging operations continuing. Took 2 bottom samples with the modified stream sampler at Bore Hole PB-1. Drove Shelby tube from floor to 70 cm (2.3 ft). No recovery since sampler coned and pushed through the sediments.

3 April

About noon set up for wireline unit. Defective controls caused wireline barrel to drop out of control. Trouble shooting at 3:00 PM. The wireline hoist is defective. By 11:00 PM had set 6.1 m (20 ft) of NX casing to 6.7 m (22 ft) below collar (top of clamp sitting on tee). Collar to sediment inside casing is 4.9 m (16 ft). Collar to top of casing is 0.5 m (1.5 ft). The collar is 20 cm (8 in) above the table.

4 April

Air temperature is -22° Celsius at 9:00 AM. It is 3.4 m (11 ft) from the collar to the sea water level inside the casing. It is 1.4 m (4.5 ft) from the top of drill tee to ice surface. It is 1.6 m (5.2 ft) from top of drill tee to the sea level water surface. At noon jet augered 4.9 to 5.2 m (16 to 17 ft). Casing shoe is at 6.7 m (22 ft) below the collar. Continued with jet auger and encountered sticky black silts and clays from 4.9 to 6.7 m (16 to 22 ft). Down at 2:00 PM with brake slave cylinder failure. Lost Shelby core from 6.7 to 7.4 m

(22 to 24.3 ft) interval. Next wash out to 7.6 m (25 ft) and go in hole with smaller diameter DDC sampler. Tried to auger with jet auger from 7.5 to 8.2 m (24.5 to 27 ft) but lost circulation and hole collapsed. Will set casing to 8.2 m (27 ft). Casing drove easily with rotation and 63.5 kg (140 lb) hammer. After driving the sediments, filled casing to 7 m (23 ft) below the collar; that is 1.2 m (4 ft) of material ran back up inside the casing. At 9:00 PM tried DDC double-wall core barrel and the clay bit. Hole taped 8.7 m (28.5 ft) after 1.5 m (5 ft) core run from 8.1 to 9.6 m (26.5 to 31.5 ft). Inner barrel was about half full of material with black fine grain material above sands and gravels (a contact).

5 April

Pulled off 1.5 m (5 ft) piece of casing, added a 3.1 m (10 ft) piece and set to 9.1 m (30 ft) by 11:00 AM. Drove Lynac (6.4 cm [2.5 in] diameter sampler) from 9.8 to 10.4 m (32 to 34 ft) and recorded blow counts. Relatively clean gravels with some up to 2 cm (0.75 in) size. Next drove to 12.8 m (42 ft) with casing. Hit larger gravels at 11.6 m (38 ft). Went to 12.8 m (42 ft) with Walmac bit but hole taped only 12 m (39.5 ft) after bit run. Encountering sands which ran in the casing. After extended time in reducing pump output and slow extraction of rod, the hole taped 12.7 m (41.6 ft). Went in with Lynac but sample washed out. Need to drill air hole in hoisting plug. After Lynac run, hole taped only 12.1 m (39.8 ft). Lynac could use a better valve. Gravel and/or sands under valve could let rod water wash out the sample. The Lynac was run 12.6 to 13.1 m (41.5 to 43 ft). The 12.1 m (39.8 ft) depth measured above indicates collapse and some sand running in. Blow counts were made on the Lynac (63.5 kg [140 lb] hammer) for three 15.2 cm (6 in) drives.

6 April

Picked up six 36.3 kg (80 lb) sacks of salt gel from a Prudhoe Bay operator. Chamberlain's testing tripod collapsed and broke the Perkins generator fuel line.

7 April

Drove casing down to 15.8 (52 ft). Down to 15.5 m (51 ft) inside and cleaning casing at 1:00 PM. Will attempt to core with DDC double wall barrel. After cleanout, hole taped 15.5 m (50.7 ft). Cored interval 15.5 to 17 m (50.7 to 55.7 ft). Drove casing to 18.9 m (62 ft) but hole taped 17.3 m (56.7 ft) after drive.

8 April

Drill water temperature is about -1 to -1.5° Celsius. Cleaned out casing from 17.3 to 18.9 m (56.7 to 62 ft). Lost circulation at shoe at 18.9 m (62 ft). Hole taped 18.7 m (61.4 ft). Water level in borehole changed from 1.92 m at 11:30 AM to 1.83 m at 12:15 PM. Hole taped 18.7 m (61.3 ft) at 12:15 PM. So about 5 cm of sand ran in with the changing water level. Will attempt to drive sample with Long year split tube sampler. Drove 18.7 to 19.2 m (61.3 to 63.1 ft) for seven blows per the first 15.2 cm (6 in), 23 blows for the second 15.2 cm and 22 blows for the third 15.2 cm using a 63.5 kg (140 lb) hammer. Core recovery 18.7 to 19.2 m (61.3 to 63.1 ft) was essentially nil, with less than 2 cm in the sampler. Drill water temperature is still -1 to -1.5° Celsius. Set casing to 21.9 m (72 ft). Hole taped 20.5 m (67.2 ft) after driving to 21.9 m (72 ft) depth. At the tee sea water viscosity was 1 liter at 35 seconds with a temperature of -1° Celsius. Cleaned hole and it taped 21.6 m (71 ft). Will run in with DDC double-wall core barrel and clay bit. Taped 21.9 m (71.8 ft) after losing reaming shell and clay bit; will have to fish. Ford engine on the drill has rust, antifreeze and other debris in tank and lines. Fuel barrels were not

cleaned properly and the crew has been pumping off the bottom of the barrels. Hand pump intake needs modification. Stopped to clean tank and fuel lines.

9 April

Fishing job today for reaming shell and bit. Fished with right hand NW rod spear. Water level in casing at 8:30 AM is 4.92 m. Easily retrieved shell and bit with first fishing attempt. Larger gravels were encountered which caused the shell to jam and break off in the casing shoe. It was very difficult to pull rod and spear with junk out of hole since rocks jammed between casing and rod. Had to utilize casing clamps and cribbing between clamp and sled under-carriage. Went in with Walmac bit and drilled 60 cm (2 ft) past shoe but lost circulation. Gravel was sampled from the water courses of the Walmac bit. Attempted to wash down casing and used hammer but formation easily took water at 3.5 kg/cm^2 (50 psi). Driving to 25 m (82 ft) and very difficult. Taped 23.4 m (76.8 ft) inside casing after drive to 25 m (82 ft) depth. Drilled ahead of shoe to 27.7 m (92 ft). Hole collapsed back and sands moved up into the casing at 24.8 m (81.5 ft). Drove casing ahead to 28 m (92). Stopped at 10:00 PM.

10 April

Going in hole to clean out to 28 m (92 ft). Had to rotate from 26.5 to 28 m (87.1 to 92 ft). Drilled 18 cm (7 in) out of the shoe to 28.2 m (92.6 ft). Will go in hole with Lynac sampler. Before running sampler, the hole was taped 27.4 m (90 ft). So 60 cm (2 ft) of fine sand ran back up into the casing after 18 cm (7 in) of hole collapsed. When cleaning out, encountered some gravels in the shoe and fine sand below at 25 m (82 ft). Sands continued to slowly move into the bore with a rate of 23 cm (9 in) in 5 minutes to a depth of 27.2 m (89.3 ft). Water level in casing at 3.35 m at 11:55 AM. Collar to sands and bore was 26.8 m (87.9 ft) at 11:00 AM and 26.6 m (87.3 ft) at 11:20 AM. Sands

moved up bore 20 cm (8 in) in 20 minutes. The NX flush joint casing moves about 2 mm per blow in the fine sands at this depth using a 136 kg (300 lb) hammer. Hole tapes 28.8 m (94.6 ft) after driving to 31.1 m (102 ft) with casing. Fine sands drive very hard but drill easily with the Walmac bit. Some gravels encountered at 30.5 m (100 ft) depth. Cleaned out casing to 31.1 m (102 ft). Went in with Lynac sampler and drove 30.9 to 31.5 m (101.3 to 103.2 ft). No recovery with latex cover in basket; the end of the brass liner and core catcher bent up into the tube. Blow count with the 63.5 kg (140 lb) hammer on NW rod was as follows: The first 15.2 cm (6 in) - 41 blows, the second 15.2 cm - 40 blows, third 15.2 cm - 45 blows, and the fourth drive of only 10.2 cm (4 in) was 33 blows. Casing shoe is at 31.1 m (102 ft) and hole tapes 30.7 m (100.6 ft). Drove casing to 32.6 m (107 ft) depth. Taped 32 m (105 ft) to sediments in casing. Attempted to drill beyond 32.6 m (107 ft) depth but lost circulation. Shut down at 10:00 PM.

11 April

Have 50 cm (1.7 ft) to clean out of casing but only cleaned out to 40 cm (1.2 ft). Left 15 cm (6 in) of cuttings on the bottom of the hole. Will attempt to use double-wall barrel and core from 32.5 to 33.9 m (106.5 to 111.1 ft). Twisted off rod above the double-wall core barrel. Break occurred in rod metal only but half way along the tool joint, which is made up into the end of the rod. On attempting to core just out of the casing shoe, flowing sands moved into the annulus and increased the torque. Also it was discovered that some of the coring bits were slightly over gage. Taped 29 m (95 ft) from collar to the junk in the hole. Could pull casing and save the core barrel but due to time schedule it was decided to leave the junk in the hole and cut the casing off. Made two cuts with DDC casing cutter, one at 28.9 m (94.9 ft) and one at 8 cm above the first cut. Came out with cutter, put on 136 kg (300 lb) hammer.

Jarred back 9 cm (3.5 in) and 2.7 m (8.8 ft) slug of sand ran into and up the casing. Installed 25.8 m (84.7 ft) of 3.2 cm (1.25 in) diameter PVC for thermal measurements. Pulled 22.9 m (75 ft) of casing to discover that the cutter had merely unthreaded the first casing joint above the intended cutting location.

12 April

Hole measured 24.2 m (79.5 ft) from sea ice surface to the bottom of the PVC or 25.7 m (84.4 ft) from the collar. This is the end of Borehole PB-1.

P B - 1 A

12 April

Pulled drill sled ahead about 7.6 m (25 ft) north of PB-1 in order to obtain detailed cores of fine grain materials which overlie the sands and gravels. This second site will be designated PB-1A. Ice thickness is 1.89 m (6.2 ft), 4.1 m (13.3 ft) from the collar to bay floor and 1.5 m (4.8 ft) from collar to the ice surface. Ice surface to sea level is 20 cm (7.9 in). Living quarters are being moved to the vicinity of Reindeer Island. Shop and drill Panitchek sleds remain behind. Will use DDC Washington sampler. It is 5.2 m (17 ft) from the collar to casing shoe and 4.4 m (14.6 ft) from the collar to sediment in the hole. Drove DDC Washington sampler with 63.5 kg (140 lb) hammer and obtained excellent 66 cm (2.2 ft) core. Added 0.9 m (3 ft) of casing and drove to 6.1 m (20 ft) depth. Hole taped 5.5 m (18 ft) after drive. Cleaned hole to 6.1 m (20 ft) with jet auger. Obtained another excellent 66 cm (2.2 ft) core. Drove casing to 7 m (23 ft) depth and cleaned out 70 cm (2.3 ft) of material to 7 m. Obtained another good core and drove casing to 7.9 m (26 ft) depth. Cleaned out to 7.8 m (25.6 ft) then took another good core at 7.8 to 8.5 m (25.6 to 27.8 ft) interval. Pulled casing, drained water lines, tank and pump. It was after

midnight when work was completed.

P B - 2

The drill and shop sleds were moved to PB-2 site on the sea side of Reindeer Island.

14 April

Started working about 8:00 AM. It is 1.2 m (3.8 ft) from the table to the sea ice surface and 12 cm from the ice surface to the water level. The ice is 1.76 m (5.8 ft) in thickness, 13 m (42.7 ft) from table to sea floor, and 11.7 m (38.4 ft) sea level to sea floor and 11.8 m (38.8 ft) sea ice surface to sea floor. The collar is 30 cm (1 ft) above the table and 1.5 m (4.8 ft) above the ice surface. It is 13.3 m (43.7 ft) from collar to the sea floor. The DDC Washington sampler was driven 70 cm (2.2 ft) into the sea floor. Obtained good core of clean fine sands on top of dirty fine sands. After sampling the sea floor, casing was set. Casing was set to 14.3 m (47 ft) below the collar. Tungsten carbide DDC casing bit, not the drive shoe is being used. Casing was initially pushed into the floor with the quill pistons. However, it was necessary to put 63.5 kg (140 lb) hammer on for the last 30 cm (1 ft). There was 80 cm (2.6 ft) of material inside the casing after setting shoe at 14.3 m (47 ft) depth. Ran jet auger in tightly packed, dirty, fine sands. Sampled from 14 to 14.7 m (46 to 48.2 ft). Shoe is at 14.3 m (47 ft). It is very difficult to drive and the casing was accidentally pulled back 18 cm (7 in) when the sampler was being extracted. Rotated and flushed NX casing from 14.3 to 15.2 m (47 to 50 ft) depth with 280 to 420 kg/cm² (4,000 to 6,000 psi) on pistons. After rotating casing, 1.9 m (6.2 ft) of material ran into the casing. Wash samples were collected as casing was cleaned out. Samples were from 13.4 to 14.9 m (43.8 to 48.8 ft) and from 14.9

to 15.2 m (48.8 to 49.8 ft). A significant contact appeared at 14.8 m (48.7 ft). Hole taped 15.1m(49.7 ft) after jet auger used. Obtained another good core from 15.1 to 15.8 m (49.7 to 51.8 ft). Stopped drilling and sampling at 8:00 PM.

15 April

To work by 8:00 AM. Rotation and flushing of NX casing is not a good procedure for sealing and seating casing in this type of material. Drove casing 15.2 to 16.2 m (50 to 53 ft) with the 136 kg (300 lb) hammer and the hole taped (50.9 ft) after the drive. Went into casing with Walmac bit to clean to 16.2 m (53 ft). Delayed by frozen water lines. Taped 16.4 m (53.8 ft) after drilling materials out of casing. Went in with DDC Washington sampler and sampled 16.4 to 17.1 m (53.8 to 56 ft) interval. Recovered 57 cm (1.9 ft) of 66 cm (2.2 ft) drive sample. Core was stiff, fine grain material. Drove 90 cm (3 ft) more of casing to 17.1 m (56 ft) depth. Bore hole taped 16.9 m (55.3 ft) after drive to 17.1 m (56 ft). Cleaned out 23 cm (9 in) of sticky clays and silts. Obtained sample of material off Walmac bit. The fine materials are very cohesive, sticky, and armor the rod and bit shoulders. Hole taped 17.1 m (56 ft) after clean out. The casing is well seated into the fine material. Water level inside the casing is below sea level and did not rise or fluctuate from 1:55 PM to 3:00 PM. Went in hole with DDC Washington sampler and obtained another good core from the 17.1 to 17.7 m (56 to 58.2 ft) interval. Recovery was 30 cm (1 ft) out of 66 cm (2.2 ft). Will now attempt to drill ahead to 18.3 m (60 ft) depth or 1.2 m (4 ft) below the shoe and drive sample again. Drilling below the shoe was with a DDC cross clay bit. Fine grain materials being drilled are brownish gray in color. Drilled to 18.6 m (61 ft) depth. Material from the 17.7 to 18.6 m (58 to 61 ft) interval was sampled off the clay bit. Hole taped

18.5 m (60.75 ft) after bringing out the clay bit. DDC Washington sampler used and excellent drive samples obtained from the 18.5 to 19.2 m (60.75 to 62.9 ft) interval. Hole taped 19.2 m (62.9 ft) after sampler extracted. Recovery was 51 cm (1.7 ft) out of 66 cm (2.2 ft). It is easy to pump the mud pit volume out into the formation below the shoe even though the soils are fine-grained and dirty. Circulating fluid viscosity was 37 seconds per 1000 cc with a temperature of -1.5° Celsius. Reamed-out sampled interval and drilled ahead to 20.1 m (65.8 ft). Sampled the material which was caught on bit shoulder. Sample was from 19.2 to 20.1 m (63 to 65.8 ft) interval. Drive sampled again with the DDC Washington sampler in the 20.1 to 20.7 m (65.8 to 68 ft) interval. Formation slowly produced drilling fluids back to the pit. Recovered 51 cm (1.7 ft) of 66 cm (2.2 ft) in this interval. Hole taped 20.7 m (68 ft) after core run. Water level in the casing was 3.45 m at 9:30 PM. At 11:30 PM the water in the casing was up to the tee and slowly flowing into the pit.

16 April

At 8:00 AM the casing water level was still up to the tee. Had to drill ice out of the casing and remove ice which had frozen back in the annulus between the ice auger hole and the outside of the casing. It is difficult to chisel or remove this ice due to the small working area. The casing hole in the clamp table was cut larger in error and this error causes the casing to move too far off the borehole center line. Freeze back between the casing and the sea ice cover invariably freezes in the misalignment. Shoe is still at 17.1 m (56 ft) depth. Cleaned out to 21.6 m (70.75 ft). Pump was developing 5.3 to 10.6 kg/cm² (75 to 150 psi) as it drilled the fine-grain materials. The pressure develops partly from the intermittent plugging of bit water courses. Caught a wash

sample of cuttings from 20.7 to 21.6 m (68 to 70.75 ft). A sample was dug off of the bit and represented a part of the 20.1 to 21.6 m (65.8 to 70.75 ft) interval. Recovered 52 cm (1.7 ft) out of 66 cm (2.2 ft) with DDC Washington sampler from 21.6 to 22.2 m (70.75 to 72.9 ft). Hit a very pronounced clay, sandy gravel contact at 22.6 m (74 ft) below the collar while drilling ahead to 24.7 m (81 ft). Some circulation loss with encounter of the sandy gravels. Coarse-grained materials diminished from 23.9 to 24.4 m (78.5 to 80 ft) and grain size increased after 24.4 m (80 ft). Stopped drilling ahead at 24.7 m (81 ft). Hole taped 22.5 m (73.75 ft) after coming out with the bit. Sandy gravels collapsed into the bore. Hammered casing back in order to remove three 0.9 m (3 ft) and one 1.5 m (5 ft) pieces of casing. Changed chuck jaws to NX and will attempt to drill casing to 31.1 m (102 ft) below the collar. Contact at 22.6 m (74 ft) below the collar was reconfirmed as casing drilled and flushed in. Circulating with sea water taken from directly under the ice. No return visible since it is discharged onto the sea floor. Drilled casing to 24.4 m (80 ft) and attempted to pull back 3.1 m (10 ft) to add another piece of casing. However the hole collapsed to 22.4 m (73.5 ft) depth as expected. We were able to get 27.4 m (90 ft) of casing drilled down to table height. The side friction is so great that the casing torsion backlashes the gears. Very difficult to rotate casing under these conditions. It could not be confirmed since there was no return to the pit (just to the sea floor), but the sea water being pumped into the casing was probably, for the most part, going into the sandy fine-grained interval from 22.6 to 27.4 m (74 to 90 ft). It is doubtful that any of the pumped sea water penetrated the over-lying fine grain section or that there was a return in the annulus between the hole wall and the casing. The great friction on the rotating casing was obviously developed in the sticky clay section.

17 April

Air temperature is -24° Celsius and winds calm at 8:00 AM. Equipment down for one hour to bleed brake hydraulic system. Last night 27.4 m (90 ft) of casing was left at the table elevation. At 9:00 AM the last joint is 10 cm (4 in) above the table due to tidal action. The inside of the casing taped 26.5 m (86.8 ft) from the joint to sediments. One meter (3.2 ft) of material occupies the lower end of the casing. No doubt this slug of material was important in reducing any possible circulation up the annulus in the fine-grained section. Attempted to put on 3.1 m (10 ft) piece of casing and drive to 30.5 m (100 ft), but considerable hammer energy is absorbed into springy reaction. Casing can be turned easily with a 36 inch pipe wrench. Put quill over casing and could rotate with 21 kg/cm^2 (300 psi) on the pump, but could not wash out the casing. Rigged back to drill out casing with NW rod and Walmac bit. Casing bit is 28 m (92 ft) below the collar. Collar sediments inside the casing tapes 26.7 m (87.7 ft). Drilling and washing out casing from 26.7 to 28 m (87.7 to 92 ft). Caught wash sample from 26.8 to 28 m (88 to 92 ft). Considerable gravel encountered just below shoe. However circulation is holding. Hit black clay silts at 28.4 m (93 ft) below the collar. Still in black fine-grained material at 30.8 m (101 ft). Circulation good. Appears to grade downward from clay to sands after a capping layer of gravels. Taped 28.2 m (92.5 ft) after tripping out of hole from 30.8 m (101 ft). Hole collapsed back to casing bit depth. No circulation losses from 28 to 30.8 m (92 to 101 ft) and the cuttings from this interval were sampled. Some fine sands flowing very slowly into the casing at 2:10 PM. Will attempt to set another 3.1 m (10 ft) of casing to 31.1 m (102 ft). Did not reach 31.1 m (102 ft) depth. Left 15 cm (6 in) of casing protruding above the table. Hole taped 27.4 m (89.75 ft). Circulated sea water directly over top of casing while drilling out the casing. Drilling to 30.8 m (101 ft). Foot clamp failed and

dropped rod when adding another piece to go to 33.8 m (111 ft). Made easy fishing job. Cuttings being collected from 30.8 to 33.8 m (101 to 111 ft). Fine to medium sands with occasional gravels. Lost circulation at 33.2 m (109 ft). Drilled to 33.8 m (111 ft) with some return. Another 3.1 m (10 ft) will be attempted. Tidal movement interfering with rod clamp operation. Slip joint device not being used on the casing since casing extends above the table. Could not drill ahead another 3.1 m (10 ft). Attempted to drill ahead only 1.5 m (5 ft) for sample run but could not hold circulation. Added another 3.1 m (10 ft) joint of casing and drove to 33.5 m (110 ft) by 9:00 PM. Taped 32.3 m (106 ft) from collar to sediment in casing. Stopped at 9:30 PM.

18 April

Commenced work at 7:00 AM. Rigged up a 6.1 m (20 ft) kelly. Had been using 4.6 m (15 ft) kelly. Casing bit is at 33.5 m (110 ft). Attempting to drill to 35.4 m (116 ft) depth. Cuttings sampled from 32.3 to 33.8 m (106 to 111 ft) interval. At 35.4 m (116 ft) pulled up and added rod to go to 38.4 m (126 ft) depth. Circulation improves at 37.5 m (123 ft). Wash samples were caught, mostly sands from 35.4 to 38.4 m (116 to 126 ft). Tripped out to add more casing after bit reached 38.4 m (126 ft). From table elevation the hole taped 33.4 m (109.7 ft) after coming out with the Walmac bit. Top of casing string is 18 cm (7 in) below the table. Drove 36.6 m (120 ft) of casing. Stopped driving with the casing 8 cm (3 in) above the table. After driving, the sediments in the bore were 35.3 m (115.8 ft) below the table or 35.7 m (117 ft) below the collar elevation. Reached 38.4 m (126 ft) depth for the second time with the Walmac bit. Good circulation while drilling to 38.4 to 41.4 m (126 to 136 ft). Cuttings sampled from the entire interval. Rough drilling, bit bouncing over gravels and carrying 281 kg/cm² (4000 psi) pressure on the bit to reduce vibration. Tripped out and drove casing to 39.6 m (130 ft). Getting difficult to drive. Casing penetration

rate with 136 kg (300 lb) hammer was ten blows per 2.5 cm (inch) and now reaches 75 blows per 2.5 cm (inch). After driving 39.6 m (130 ft) of casing the sediment level was 38 m (124.5 ft) below the end of the casing string. The casing joint was left 36 cm (14 in) above the table due to the difficult driving conditions. Drilled to 41.4 m (136 ft). Added 1.2 m (4 ft) of casing and attempted to put casing bit at 41.4 m (136 ft) below the collar. The point reached lacked 30 cm (1 ft) of getting the casing down. Stopped working at 10:30 PM.

19 April

Casing bit is at 41.2 m (135.2 ft) below the table elevation. Will attempt clean out and drill to 41.4 m (136 ft). Cleaned out casing again and will try to drive a sample. Drove 40.9 m (134.2 ft) casing string to 24 cm (9.5 in) below the table. Very difficult driving conditions. After drive, the hole taped 41 m (134.5 ft) which means a 46 cm (1.5 ft) plug of material is in the lower end of the casing. Drilled out the plug and attempted to drive sample with Longyear split tube sampler. Could not even drive sampler at this depth with a 136 kg (300 lb) hammer. Jars are required. Upon removal the sampler contained a few pebbles. Attempted to use gel mud but do not have provisions for de-sanding. Drilled 41.4 to 42.7 m (136 to 140 ft) with mud before having to drop the mud and return to sea water. Mud was mixed too fast and in too large a quantity to handle easily.

20 April

Hole now taped 42.2 m (138 ft) below the collar. Installed PVC tubing and pulled the NX casing. Rigged down and moved sleds to Reindeer Island for the night.

P B - 321 April

Moved off of the island to bore hole location PB-3 at 3:30 PM. Ice thickness is 1.87 m (6.1 ft). It is 11 cm (4.3 in) from the ice surface to sea level surface and the ice surface is 5.8 m (19.2 ft) above the sea floor. Paul Sellmann drilled from 6:00 PM until quitting time. Lewellen left Prudhoe at 9:00 PM and was in Anchorage at 11:30 PM.

22 April

Lewellen left Anchorage at 7:15 PM and arrived Prudhoe at 9:00 PM.

23 April

The first Rolligon unit blew an engine, however Lewellen made the trip from ARCO dock to drill camp from 12:30 PM til 1:45 PM. Upon arrival there were two 3.1 m (10 ft), one 1.5 m (5 ft), five 0.9 m (3 ft), and one 0.6 m (2 ft) pieces of casing in the hole after fine-grained bottom soils were sampled. The 12.8 m (42 ft) string of casing had the shoe located 13.1 m (43 ft) below the table elevation. Pulled back casing strings to remove small lengths after detailed sampling in the fine-grained section by Sellmann. Reset 12.2 m (40 ft) of casing to 12.8 m (42 ft) below the collar. Sample cuttings from interval 13.1 to 13.4 m (43 to 44 ft) and 13.4 to 14 m (44 to 46 ft) circulated a total of 35 minutes with the pump. Sands ran back in the casing as another piece of drill stem was added to the drill string. Sands collapsed in the borehole and ran 1.2 m (4 ft) up into the casing. Started drilling to 15.2 m (50 ft) and with circulation problems, the sands are moving in fast enough to increase torque due to friction in the rod-casing annulus. Circulated 25 minutes getting to the 15.2 m (50 ft) depth. Tripped out with the Walmac bit and hole collapsed with the sands coming 0.6 m (2 ft) up into the casing. Drove 3.1 m (10 ft) piece of casing. The shoe

is now at 15.8 m (52 ft). After driving to 15.8 m the sediment level in casing was at 13.7 m (45 ft) below the collar. Drilled to 15.8 m (52 ft) and circulated for 10 minutes. Hole taped 15.8 m (51.7 ft) after tripping out with the bit. Drove Lynac sampler 15.8 to 16.3 m (51.7 to 53.4 ft). Blow count for last 15 cm (6 in) of drive was 41. Sands ran again and hole taped 14.6 m (48 ft) after sampler extracted. Sample recovery was 38 cm (15 in) out of 53 cm (21 in) drive with 10 to 15 cm (4 to 6 in) of disturbed material on top of the core. Stopped work at 9:00 PM.

24 April

Started to work at 7:30 AM. Started drilling toward 18.9 m (62 ft) depth but only reached about 18.4 m (60.5 ft) when sand ran in, lost circulation and plugged annulus. Drill stem stuck, but worked it loose. Circulated a total of 40 minutes while drilling to 18.9 m (62 ft) and getting the stem free. Tripped out, hole collapsed and ran 1.2 m (4 ft) up into the casing. Drove casing to 18.9 m (62 ft) below the collar and sediment level was 17.1 m (56 ft) below the collar after the drive. Cleaned out 17.1 to 18.9 m (56 to 62 ft) and circulated 10 minutes total time. Hole taped 18.8 m (61.7 ft). Ran Lynac sampler in hole and drove from 18.8 to 19.3 m (61.7 to 63.3 ft). Blow counts were as follows: 95 blows for the first 15 cm (6 in), 118 blows for the second 15 cm, 50 blows for the next 15 cm. Hole taped 18.8 m (61.5 ft) after sampler tripped out. Recovered 24 cm (9.5 in) out of 51 cm (20 in) drive. Appears to be 10 to 15 cm (4 to 6 in) of debris on top of the sample. Attempted to drill ahead and lost some circulation at 18.9 m (62 ft). All circulation was lost at 19.7 m (64.5 ft). However, continued to drill ahead to 21 m (69 ft). Sand started plugging annulus. Tripped out with Walmac bit and rigged up to drive casing to 22 m (72 ft). Started driving and pull-piece of the 136 kg (300 lb) hammer guide broke in the threads.

Guide replaced with spare. Casing advanced to 22 m (72 ft) by 5:00 PM. Hole taped 20 m (65.7 ft) to sediments after driving to 22 m. Circulated a total of about 15 minutes to clean out from 20 to 22 m (65.7 to 72 ft). After cleaning, the hole taped 21.8 m (71.6 ft). Lynac sampler run into the hole. Recovered 33 cm (13 in) out of 51 cm (20 in) for the interval 21.8 to 22.3 m (71.6 to 73.2 ft). Blow counts were recorded as follows: 130 blows for the first 15 cm (6 in), 172 blows for the second 15 cm, and 67 blows for the third 15 cm. Hole taped 21.8 m (71.7 ft) after sampler pulled out. Stopped work at 9:00 PM.

25 April

Started work at 9:00 AM. Sediments in the bore are at 21.6 m (70.7 ft) depth. About 30 cm (1 ft) of material moved in after taping the previous night. Drilled from 21.6 to 24.7 m (70.7 to 81 ft) and lost all fluid return at 22.7 m (74.5 ft). Circulated and pumped into the bore a total of 20 minutes. Drove casing to 25 m (82 ft) and hole taped 23.6 m (77.6 ft) after the drive. Drilled out to 25 m (82 ft) and hole taped 24.9 m (81.6 ft) after bit tripped out. Lynac put in the hole for drive from 24.9 to 25.4 m (81.6 to 83.3 ft). Blow count was as follows: 88 blows for the first 15 cm (6 in), 38 blows for the second 15 cm, and 27 blows for the third 15 cm. Recovered 15 cm (6 in) of 53 cm (21 in) drive. Went back in with bit and lost circulation just out of the shoe at 25 m (82 ft). No return but drilled to 27.7 m (91 ft) and circulated a total of 20 minutes. Tripped out and hole had collapsed and sands run to 23.5 m (77 ft) depth. Another 3 m piece of casing driven and attempted to drive to 28 m (92 ft) depth. Took 3 hours to drive the 3 m of casing. Extremely difficult driving. After the drive, the sediments were at 25.4 m (83.5 ft) below the collar. Top of casing string is 30.5 cm (1 ft) above the table. Will drill ahead to the shoe. Drilled out from 25.4 to 27.9 m (83.5 to 91.5 ft) then lost most of the circulation at 27.9 m

(91.5 ft). Circulation returned from 28 to 28.6 m (92 to 94 ft) and then lost again at 28.6 m (94 ft). Circulated a total of 35 minutes and drilled to 29.3 m (96 ft). Hole taped 27.4 m (90 ft) after drilling to 29.3 m (96 ft). Added 1.5 m (5 ft) piece of casing and drove until joint was 21 cm (8 in) above the table. Water level in casing at 1.98 m (6.5 ft) below the joint. Stopped working at 9:30 PM. Tide rising and moved casing joint to 13 cm (5 in) above table at 11:30 PM.

26 April

At 9:45 AM tide had risen, placing casing joint to 6 cm (2.5 in) above the table. Water level inside the casing was at 1.18 m (3.9 ft) below the joint. At 11:00 AM we have driven another 1.5 m (5 ft) of casing. Very slow driving in sands and 2.5 cm (1 in) gravels. Casing joint left at 18 cm (7 in) above table and hole tapes 28 m (92 ft) from casing joint to sediments inside the casing. Cleaned out casing catching bulk sediment samples from 28 to 29 m (92 to 95 ft). There is 29 m (95 ft) of casing set. Circulated 20 minutes with up to 21 kg/cm² (300 psi) pump pressure. Broke the hammer guide in the 7.6 cm (3 in) National pipe thread on the NX sub. Drilled ahead to 30.5 m (100 ft) and repaired hammer assembly. Took off 1.5 m piece of casing, added a 3.1 m piece and drove it down to where joint was just above the table. The hole taped 29.4 m (96.3 ft) after the drive. Cuttings sampled in the 29.9 to 30.5 m (98 to 100 ft) interval as the casing was drilled out. Hole taped 30.4 m (99.9 ft) before sampler was put in the hole. Drove Lynac from 30.4 to 31 m (99.9 to 101.7 ft) and recovered 51 cm (20 in) out of 56 cm (22 in). The blow counts were as follows: 193 blows for the first 15 cm (6 in), 121 blows for the second 15 cm, 68 blows for the third 15 cm, and 56 blows for the last 10 cm (4 in). Drilled 30.8 to 32 m (101 to 105 ft) and no return to the surface. Pump operated for about 15 minutes. Added

1.5 m piece of casing and drove to where the joint was 28 cm (11 in) above the table. Hole taped 30.9 m (101.5 ft) after the drive. Cleaned out and sampled cuttings from 30.8 to 32 m (101 to 105 ft). Drilled ahead of shoe to 33.5 m (110 ft). Lost circulation just out of the shoe but it returned enough to sample cuttings from 32.6 to 32.9 m (107 to 108 ft). Circulated for about 20 minutes. Removed 1.5 m piece of casing, added a 3.1 m piece. We stopped work at 9:30 PM.

27 April

Started working at 7:30 AM. Drive 1.5 m which placed shoe at 33.6 m (110.2 ft) below the collar. Hole taped at 32.6 m (107 ft) after drive. Cleaned out casing from 32.6 to 33.5 m (107 to 110 ft). A wash sample of the cuttings was taken. Circulated about 15 minutes. Hole taped 33.3 m (109.3 ft) after clean out. The Lynac will be run next. The blow counts are as follows: 85 blows for the first 15 cm (6 in), 35 blows for the second 15 cm, 31 blows for the third 15 cm, 25 blows for the last 7.6 cm (3 in). Recovered 17.8 cm (7 in) of 53 cm (21 in) drive. Blow count indicates resistance has dropped in this section. Attempted to drive 1.5 m more of casing without drilling ahead. Had some success in the softer section of the formation. Broke hammer guide again. Shoe was driven to 35.1 m (115.2 ft). Hole taped 34.3 m (112.5 ft) after the drive. Cleaned out the casing and caught wash samples from 34.3 to 34.7 m (112.5 to 114 ft) and from 34.7 to 35.4 m (114 to 116 ft). Attempted to drill ahead of the shoe. Got some return and drilled to 36.6 m (120 ft). Pump circulated sea water for about 25 minutes. Took off 1.5 m piece of casing. Added 3 m piece and drive another 1.5 m in the interval just drilled. Casing shoe now 36.6 m (120.2 ft) below the collar. There were sands with some gravel in the 35 to 36.6 m (115 to 120 ft) interval. Using the 136 kg (300 lb) casing hammer on a 91 cm (36 in) fall, it takes 1200 blows to drive the casing 1.5 m (5 ft). Hole taped 34.8 m (114.3 ft) after driving to 36.6 m (120.2 ft). Drilled out the casing. Collected the wash samples from 34.8 to 36.6 m (114 to 120 ft) and circulated a total of 20 minutes. Hole

taped 36.4 m (119.6 ft) and Lynac sampler placed in the hole. Blow counts were as follows: 130 blows for the first 15 cm (6 in), 70 blows for the second 15 cm, 77 blows for the third 15 cm, 37 blows for the last 8 cm (3 in). The sampler was driven from 36.5 to 37 m (119.7 to 121.5 ft) and recovered 36 cm (14 in) out of 53 cm (21 in). Attempted to drill ahead of shoe from 36.6 to 38.1 m (120.2 to 125 ft). Lost circulation at 36.9 m (121 ft). Hit 15 cm layer of gravels at 37.6 to 37.8 m (123.5 to 124 ft) and hit gravel again at 38.1 m (125 ft). Circulated a total of 20 minutes. Added 1.5 m (5 ft) piece of casing and drove shoe to 38.2 m (125.2 ft). Stopped work at 9:00 PM. Tide had casing joint at 20 cm (7.75 in) above the table at 11:07 PM.

28 April

To work by 8:00 AM. At 8:15 AM the falling tide had the casing joint 33 cm (13 in) above the table. The water level inside the casing was near the present tide level. As the tide falls a progression of ice forms downward inside the casing. Drilled out 36.9 to 38.1 m (121 to 125 ft) and ahead to 39.6 m (130 ft). Circulation beyond the shoe at 38.2 to 39.6 m (125.2 to 130 ft) lasted only 10 minutes. Took off 1.5 m (5 ft) piece of casing. Added a 3.1 m (10 ft) piece and easily drove to 39.7 m (130.2 ft). Circulated at 37.8 m (124 ft) depth at 11:20 AM. Cleaned out and pump off by 11:40 AM. Circulated in the last 60 cm (2 ft) of hole only 3 minutes. Circulating water temperatures were measured by Vaughn Marshall. Attempted to drive Lynac sampler to 39.6 m (130 ft) but flowing sands filled casing back to 36.8 m (120.7 ft). Sampler was driven in the 36.8 to 37.5 m (120.7 to 122.9 ft) interval of sand which had run into the casing. Caught some fine sands in the Lynac tube. Water level in casing was 5.8 m at 1:25 PM and was 5.3 m at 1:45 PM. This is a rise of 50 cm (19.7 in) in 20 minutes. Drove 1.5 m (5 ft) piece of casing down. The shoe is at 41.2 m (135.2 ft) and after

the drive, water level was 6.85 m (22.5 ft) at 2:25 PM. Taped 35.1 m (115.1 ft) after driving which indicated more sands moved into the casing. The casing joint is 18 cm (7 in) above the table and 1.5 m (4.8 ft) above sea level. Cleaned out to 41.1 m (135 ft). Circulation on at 3:55 PM. Considerable organic debris being washed out of the casing. The bit was at 37.5 (123 ft) inside the casing when the organic debris was encountered. Circulation off at 4:15 PM as another rod is being added. Circulated 10 minutes as the casing was drilled out from 37.5 to 40.5 m (123 to 133 ft). Added another 3.1 m (10 ft) piece of rod in order to drill out from 40.5 to 43.6 m (133 to 143 ft). Lost circulation at 42.1 m (138 ft) and almost stuck the rod as sands ran up into the annulus. Pulled rod back to shoe and slowly reduced pump volume. Circulated a total of 40 minutes. Took off 1.5 m (5 ft) piece of casing, added a 3.1 m (10 ft) piece and drove 1.5 m (5 ft) to put the shoe at 42.7 m (140.2 ft). Hole taped 40.9 m (134.1 ft) after drive. Cleaning out casing and pump on at 7:30 PM. Attempted to drill to 43.3 m (142 ft) or about 61 cm (2 ft) beyond the shoe. Reached 43.3 m (142 ft) depth and circulation time beyond the casing shoe was 5 minutes. Drove 1.5 m (5 ft) of casing to 44.3 m (145.2 ft) depth. Hole taped 43.1 m (141.3 ft) after the drive. Stopped work at 9:45 PM. At 9:15 PM the casing joint was 25 cm (10 in) above the table. At 11:05 PM it was 19 cm (7.5 in) above the table due to the rise in tide. Water level inside the casing changed from 2.49 m to 2.46 m (3 cm or 1.2 in) in the same time interval.

29 April

To work by 8:00 AM. Tide had placed the table 22 cm (8.75 in) below the casing joint and the water level in the casing was 2.05 m (6.7 ft) from the casing joint. Cleaned out casing from 43 to 44.3 m (141 to 145.2 ft). The mud pump is on at 10:00 AM. It takes about 1 minute of circulation to get a return from 42.7 m

(140 ft). Drilled ahead of shoe and circulation was good from 44.2 to 45.4 m (145 to 149 ft) but weakened at 45.4 m (149 ft). Drilled to 45.6 m (149.5 ft). Pump off at 10:45 AM. Took off 1.5 m (5 ft) piece of casing and added a 3.1 m (10 ft) piece. Now have 45.7 m (150 ft) of casing in the hole. Drove casing down by 12:30 PM. It was 42.9 m (140.7 ft) to the sediment level inside the casing after the drive. The pump is on at 12:55 PM for clean out and wash samples for the 43 to 45.7 m (141 to 150 ft) interval. Circulation off at 12:20 PM. Hole taped 45.6 m (149.6 ft) after the clean out. Lynac sampler run into the hole for sampling interval of 45.7 to 46.2 m (150 to 151.7 ft). Recovered 41 cm (16 in) out of 53 cm (21 in). The blow counts were as follows: 181 blows for the first 15 cm (6 in), 62 blows for the second 15 cm, 61 blows for the third 15 cm, and 38 blows for the last 7.6 cm (3 in) of the drive. The high blow counts for the first 15 cm reflects the sediment compaction at the shoe due to driving. By 5:00 PM the tide was falling which necessitated driving the casing down about 38.1 cm (15 in). After short drive the sands ran into the casing and up to the 41.2 m (135 ft) level. Cleaned out to 45.7 m (150 ft). Pump on at 5:50 PM and off at 6:15 PM. Tide is still falling. Put on 1.5 m (5 ft) piece of casing and drove to 47.2 m (155 ft) without drilling ahead. Now have 47.2 m (155 ft) of casing in the hole. At 9:00 PM the tide level was noted at 26 cm (10.25 in) from table up to the casing joint. Quit at 9:30 PM.

30 April

At 8:30 AM the tide level put the casing joint 29 cm (11.5 in) above the table. Cleaned out casing from 43.6 to 47.2 m (143 to 155 ft). End of casing shoe is at 47.3 m (155.2 ft). Pump in second gear but losing most of the circulation. Circulated in the casing from 9:45 AM to 9:50 AM. From 9:50 AM to 10:15 AM the circulation was returning from below the shoe as the bit drilled ahead to the

48.5 m (159 ft) depth. Took off 1.5 m (5 ft) piece of casing. Put on the 3.1 m (10 ft) piece and drove to 48.8 m (160 ft). Broke another sub while driving. After driving 3.1 m (10 ft) piece for 1.5 m (5 ft) the hole measured 46.5 m (152.5 ft) deep. Cleaned out from 46.6 to 48.8 m (153 to 160 ft). Drilled gravels inside casing from 48.2 to 48.5 m (158 to 159 ft). These gravels were left behind after winnowing out the fine sediments while previously drilling outside the casing from 47.2 to 48.5 m (155 to 159 ft). Lyncac sampler driven from 48.7 to 49.3 m (159.8 to 161.6 ft) with 100% recovery. Blow counts are as follows: 154 blows for the first 15 cm (6 in), 133 blows for the second 15 cm, 117 blows for the third 15 cm, 81 blows for the last 7.6 cm of the drive. Temperature measurements were attempted from the void left by the sampler at 48.7 to 49.3 m (159.8 to 161.6 ft). Cleaning out the casing from 48 m (157.5 ft) and attempting to drill ahead to 50.3 m (165 ft). Sediments darkened in color from 49.1 to 49.4 m (161 to 162 ft). Pump on and circulating at 6:10 PM. Pump off at 6:30 PM. Circulation was good at 49.4 m (162 ft) with woody debris returning with the cuttings. Lost circulation at 49.7 m (163 ft) but drilled to 50 m (164 ft) before coming out of the hole. Drove another 1.5 m (5 ft) piece of casing putting the shoe at 50.4 m (165.2 ft). Broke another pull piece while driving. Quit at 9:00 PM. Tide level at 11:30 PM had casing joint 17 cm (6.75 in) above the table.

1 May

Tide level at 8:30 AM had the casing joint 27 cm (10.5 in) above the table. Casing shoe at 50.4 m (165.2 ft). Cleaned out from 47.2 m (155 ft) and drilled ahead to 51.8 m (170 ft). Circulation on at 9:25 AM with good return at 51.5 m (169 ft) with 8.8 kg/cm^2 (125 psi). Circulated about 15 minutes beyond the shoe and pump off again at 10:25 AM. Removed 1.5 m (5 ft) piece of casing and started

driving a 3.1 m (10 ft) piece at 11:00 AM. After the drive the shoe will be at 51.9 m (170.2 ft). Started clean out at noon at 49.1 m (161 ft). Metal cuttings returning from 49.1 to 49.4 m (161 to 162 ft) with some obvious lost circulation indicating casing failure. Circulated about 1 hour after pulling back rod and bit to 48.8 m (160 ft). Decided to cut off casing at 47.7 m (156.4 ft) after taping to obstruction at 48.2 m (158.2 ft). PVC casing run in the hole and steel casing being pulled at 8:00 PM. Finished pulling casing at 1:00 AM on the second of May. Pulled 47.2 m (155 ft) of casing out. Casing cutter worked perfectly. Last few casing joints were badly belled. The casing threads failed due to the hard driving conditions.

2 May

Finished pulling casing at 1:00 AM and quit at that time. Took bottom samples and then began to break up the drilling camp. Shop and drill sleds departed for Gull Island at 2:00 PM. Started checking Sagavanirktok River route for pulling sleds back to the V.E. Construction camp.

3 May

Kodiak Oilfield Haulers picked up the Nabors sled, two Wanigans, generator and fuel at the old Prudhoe dock. Winds and blowing snow with large drifts delayed move of the two Panitchek sleds. However, sleds, D-6 tractor, and Bombadier tractor with trailer, reached the Sagavanirktok River bridge by midnight. Worked 6:00 AM on 3 May to 4:00 AM on 4 May. Quit when all the equipment was safely parked at the V.E. Construction camp.

4 May

Quit at 4:00 AM and back to work at 1:30 PM cleaning up the gear.

5-7 May

Prepared equipment for storage until the next drilling season.

SUB-SEA TEMPERATURES AND A SIMPLE TENTATIVE MODEL
FOR OFFSHORE PERMAFROST AT PRUDHOE BAY, ALASKA

by

Arthur H. Lachenbruch and B. Vaughn Marshall
U.S. Geological Survey, Menlo Park, California 94025

Contents

	<u>page</u>
Introduction	1
Temperature observations	2
A simple "target" model for Prudhoe Bay permafrost	6
Initial conditions and thermal properties.	10
Conditions at the boundaries of ice-bonded permafrost.	13
The upper boundary, X	13
The lower boundary, X'	15
Thermal conditions within permafrost and the evaluation of equations 13 and 16	17
Conditions controlled primarily at the upper surface X.	17
Melting from the lower surface X'	24
Temperature profiles.	30
Summary and discussion	32
Appendix	39
References	52

INTRODUCTION

In this report, we present temperatures measured in three holes drilled into the sea bed in the Prudhoe Bay region and a tentative interpretation of them in terms of the gross thermal regime and shore-line history of the area. The new holes (PB-1, PB-2, and PB-3, Figure 1) were drilled in spring, 1976 (see Sellmann, 1976) as part of a cooperative study of off-shore permafrost by the USGS, CRREL, and the University of Alaska, funded in part by the NOAA-BLM Outer Continental Shelf Environmental Assessment Program. We have included in the interpretation, results from two of the holes (#190 and #3370, Figure 1) drilled earlier by the University of Alaska (Osterkamp and Harrison, 1976).

The reader not interested in analytical details may wish to examine Figures 1, 2, and 3, and then skip to the concluding section "Summary and Discussion," page 32.

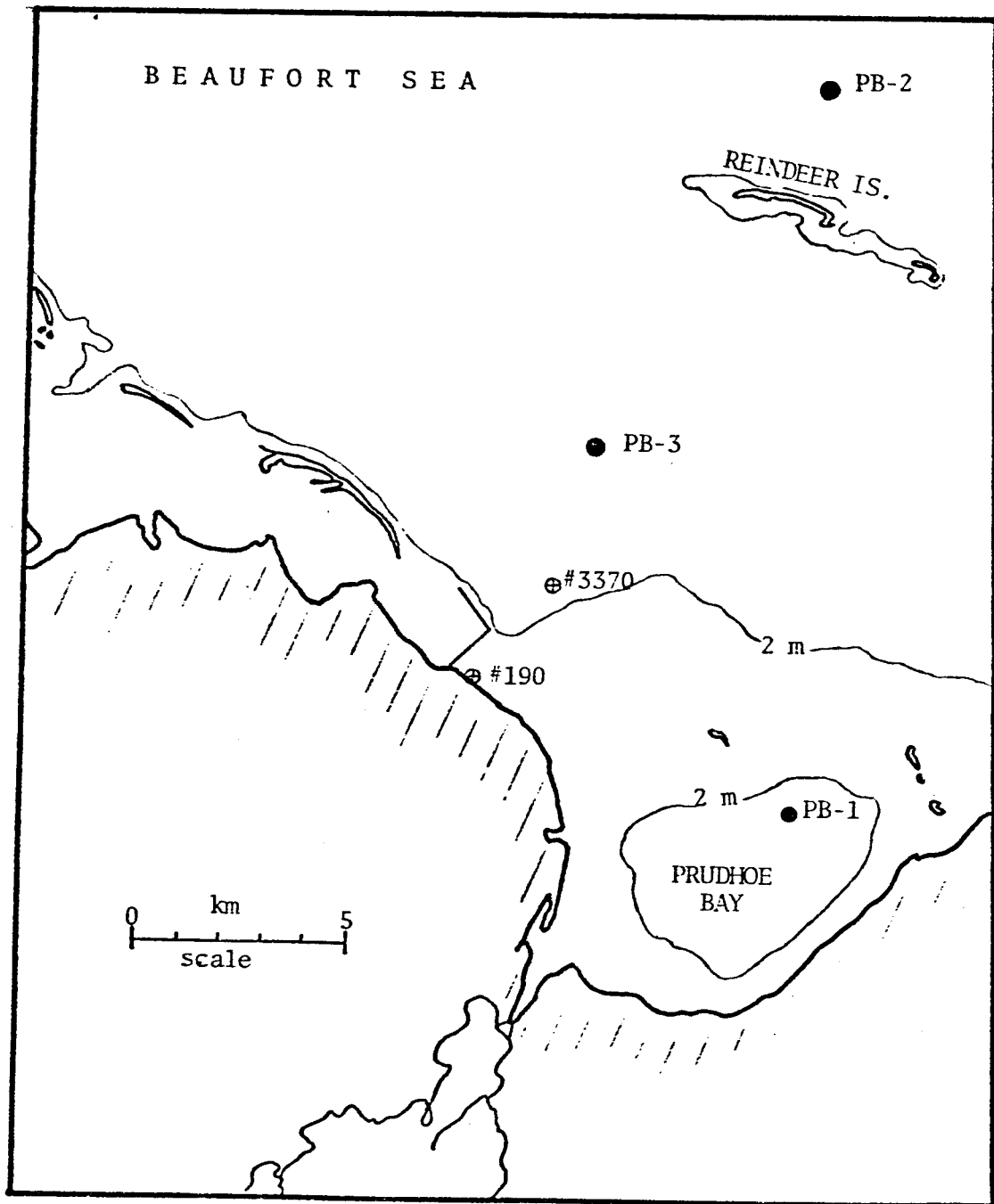


Figure 1. Map showing hole locations.

TEMPERATURE OBSERVATIONS

Temperature measurements were made by logging from the surface with the "portable mode" of instrumentation described by Sass and others (1971). Equilibrium observations were made to millidegree precision at discrete depth increments of about 1 meter. The time constant for the temperature transducer is only a few seconds, and the measurement accuracy of the system is probably a few hundredths of a centigrade degree. The observational data are presented in tabular form in the Appendix. Pre-drilling temperatures estimated for selected depths by the method of Lachenbruch and Brewer (1957) are shown with temperatures from the two University of Alaska holes in Figure 2. More refined estimates of the equilibrium temperature will be undertaken at a later date, but the results shown are adequate for the present purpose.

The line of holes drilled by the University of Alaska extends 3.37 km outward from the shoreline to a point where about 0.8 m of sea water occurs under the 2 m of ice that forms seasonally (see inset, Figure 2). Holes PB-3 and PB-2 extend that line seaward. PB-3 is 6.62 km from the shore where the combined water and ice depth is 5.8 m, and PB-2 is 17.0 km from shore beneath 11.6 m of water and ice. Conditions at PB-2 are complicated by proximity to Reindeer Island, a barrier island whose position is probably changing with time (see e.g., Hopkins and others, 1977). Hole PB-1 lies within Prudhoe Bay proper, about 3 km from the shoreline; 0.7 m of sea water underlies the 2 meters of seasonal

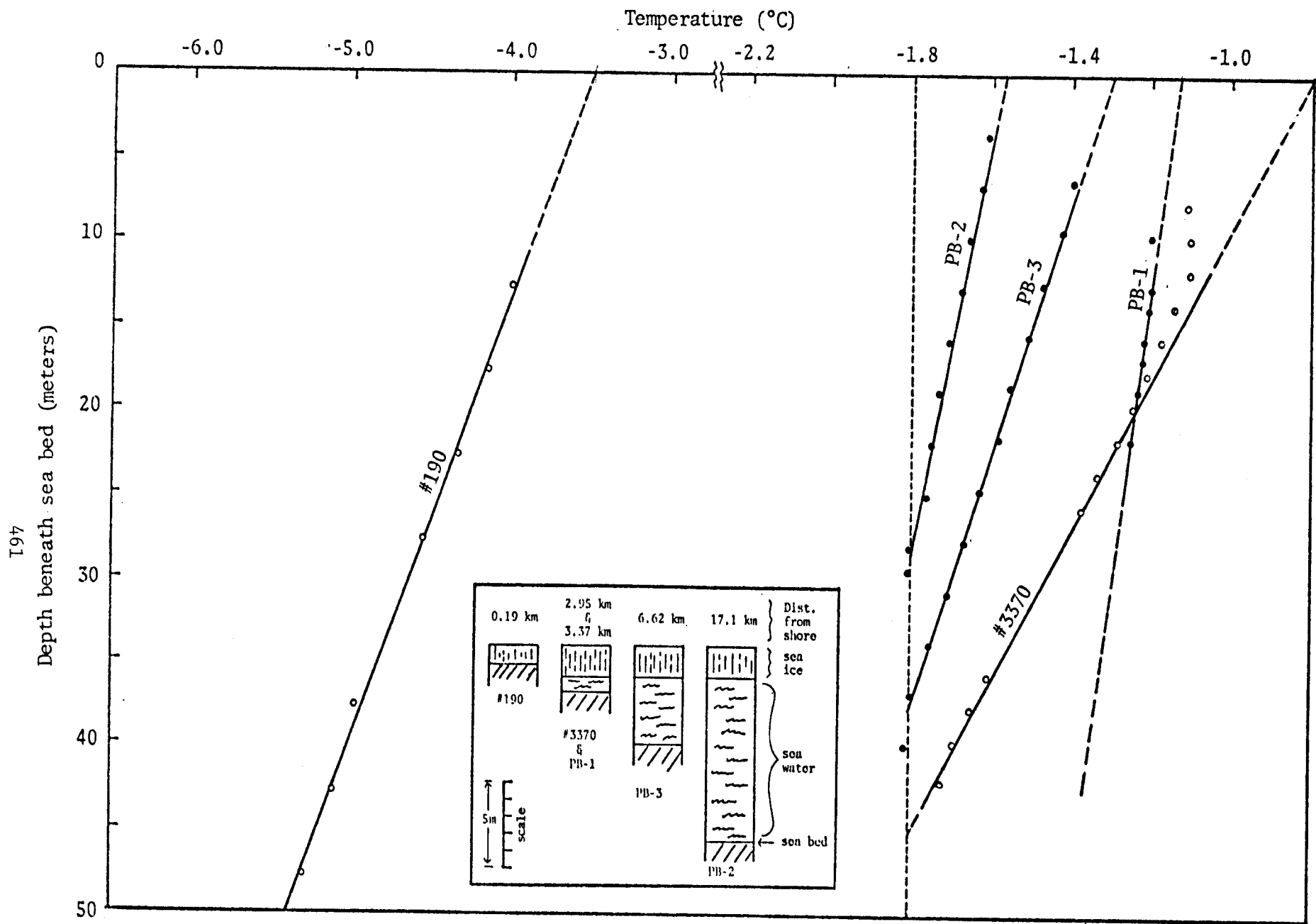


Figure 2. Estimated pre-drilling temperatures beneath sea bed for five holes in Prudhoe Bay area. (Open circles from Osterkamp and Harrison, 1976.) Inset shows distance from present shoreline and depth of sea water and seasonal ice. (Note change in temperature scale at -3.0 °C.)

ice there. Table 1 lists other information about these three holes and two of the holes (#190 and #3370) drilled by the University of Alaska and discussed by Osterkamp and Harrison (1976).

Insofar as is known, no frozen material was penetrated by holes PB-1, PB-2, and PB-3 or by hole #3370 (Osterkamp and Harrison, 1976). This is consistent with the general linearity of temperature profiles in the lower parts of these holes (Figure 2) which implies steady-state conduction in homogeneous materials with no phase changes in progress. (However, the uncertain bottom-most points on profiles PB-2 and PB-3 (Figure 2) suggest a sharp decrease in gradient; they may represent a transition at the bottom of each hole to thermal conditions in ice-bonded permafrost.) Hole 190 evidently penetrates relatively homogeneous ice-bonded material (Osterkamp and Harrison, 1976). Holes PB-3, PB-2, and 3370 were all terminated because of drilling difficulties at or near the depth of the -1.8°C isotherm (Figure 2). As -1.8°C is the approximate freezing temperature of normal sea water, this observation suggests that the reason the drilling became difficult at these depths was because ice-bonded permafrost was encountered there, and that the thawed sediments penetrated were saturated with normal sea water.

This important observation provides evidence for the temperature, θ_f , of the top boundary of ice-bonded permafrost at these localities. This boundary temperature is determined by the freezing temperature (and consequently the salinity) of interstitial water in the sediments

TABLE 1. Data for 5 offshore boreholes, Prudhoe Bay

(1)	(2)	(3)	(4)	(5)	(6)	(7)	(8)	Deposition D			(12)	(13)	(14)	(15)	(16)
								(9)	(10)	(11)					
Hole	Distance from shore (m)	Ice + water (m)	θ_o (°C)	θ_f (°C)	ϵ (°C)	X (m)	$\frac{L}{2K_s} \frac{X^2}{\epsilon}$ (yrs)	Marine (m)	$\frac{1}{2} X$ (m)	Total D (m)	$\frac{D}{X}$ (%)	$\frac{Q_f(t)}{LX}$ (%)	Total correction factor	t (yrs)	B-X' (m)
190	190	1.1	-3.5	?											
PB-1	2,950	2.7	-1.13	(-1.8?)	.67	(80?)	(11,030)	3.2	1.9	5.1	-(6%)		1.24	(145)	~ 0
3370	3,370	2.8	-0.8	-1.8	1.0	.45	2,340	3.2	1.5	4.7	-10%	54%	1.44	3,370	19 m
PB-3	6,620	5.8	-1.3	-1.8	0.5	37.5	3,250	4.8	2.4	7.2	-19%	63%	1.44	4,660	29 m
PB-2	17,100	11.6	-1.57	-1.8	0.23	28	3,940	9.1	1.5	10.6	-38%	80%	1.43	5,610	37 m

- 1) Columns 4-7 are inferences from observations.
- 2) Columns 8 and 12-14 refer to equation 13.
- 3) Columns 9, 10, 11 are estimates by David Hopkins.
- 4) Column 13 determined from equation 31.
- 5) Column 14 is the "correction" for column 8, see equation 13.
- 6) Column 15, effective time since inundation, determined from equation 35b for hole 190 and from equation 13 for others.
- 7) Column 16 determined from equations 44a and 48; for Prudhoe Bay B = 600 km.

contacting the ice-bonded interface. In principle, θ_f can lie anywhere between 0°C and the eutectic temperature for sea water (about -23°C). Harrison and Osterkamp (1976) have emphasized that the actual value of θ_f depends upon processes by which salt might be concentrated or trapped in the sea bed (e.g., by exclusion from freezing sea ice) and transported downward through the thawed sediments. They have shown that if the salt were transferred exclusively by diffusion, salinity would decrease sharply from the sea bed to the ice-bonded interface. If the salinity at the sea bottom were close to that of normal sea water (as it probably is in general when the water depth is substantially greater than ice thickness) the salinity gradient in the thawed layer would result in relatively fresh interstitial water at depth and higher values of θ_f than inferred above. The rate of degradation of ice-bonded permafrost, and in fact whether or not degradation occurs, is very sensitive to small changes in θ_f relative to the mean annual sea bed temperature, θ_o .

The best estimate of the mean annual sea bed temperature θ_o is obtained by upward extrapolation of the linear portion of the curves shown in Figure 2. The values so obtained are listed in Table 1, column 4. The values of θ_o for the four sites where the water depth is at least 3 m or so, vary from -0.8°C closest to shore to -1.57°C at the site farthest from shore. If θ_f were not less than θ_o , there would be no progressive thawing from one year to the next and the ice-bonded permafrost would persist close to the sea bed. As Osterkamp and Harrison (1976) have pointed out, this is evidently the case at hole #190 which

is typical of the near-shore region in which ice freezes to the sea bed annually. Here conductive cooling in the winter reduces the mean annual temperature, θ_o , to about -3.5°C which is probably less than the freezing temperature of interstitial water, except possibly for effects of seasonal salt concentrations. Thus within the near-shore band of grounded sea ice, it is likely that $\theta_f > \theta_o$, and ice-bonded permafrost can persist close to the sea bed. It is important to emphasize that were it not for effective salt transport through surficial sediments at the other sites, this condition ($\theta_f > \theta_o$) could obtain also in the deeper water. As Osterkamp (1975) and Harrison and Osterkamp (1976) have stressed, the parameters controlling this salt transport process must be understood before we can predict whether or not ice-bonded permafrost is likely to occur close to the sea bed. If the salt is transported primarily by movement of interstitial water, it will be important also to confirm that the heat transport is primarily conductive as is generally assumed.

A SIMPLE "TARGET" MODEL FOR PRUDHOE BAY PERMAFROST

Recognizing the hazards of premature generalization, we feel that at this time it is useful to construct a highly idealized preliminary model of the gross features of Prudhoe Bay permafrost. Although it will certainly be wrong in detail, it should serve to focus attention on the sensitive parameters and provide some guiding context for future work. It is a target model in the sense that it gives us something to "shoot" at. With this introduction we shall not further belabor the presentation with cautious qualifying remarks. A more rigorous synthesis will be presented with onshore data from the region after the completion of the 1977 fieldwork. For the most part, the following discussion is based upon well known results from heat-conduction theory and concepts that have been stated or implied in work published over the last 25 years (Terzaghi, 1952; Lachenbruch, 1957; Carslaw and Jaeger, 1959, chapter XI; Lachenbruch and others, 1962, 1966; Mackay, 1972; Gold and Lachenbruch, 1973; Sharbatyan and Shumskiy, 1974; Osterkamp, 1975; Hunter and others, 1976; Osterkamp and Harrison, 1976; Harrison and others, 1977).

The model is represented schematically in Figure 3. At the time of submergence the temperature is given by the curve $t=0$; thereafter the sea bottom is maintained at temperature θ_o , and the melting (and freezing) temperature of interstitial ice is maintained at θ_f at the upper surface and θ_f' at the lower surface of the ice-bonded permafrost. We shall assume that θ_o and θ_f have remained constant at their presently observed values since some effective date of submergence $t=0$. This, of course,

467

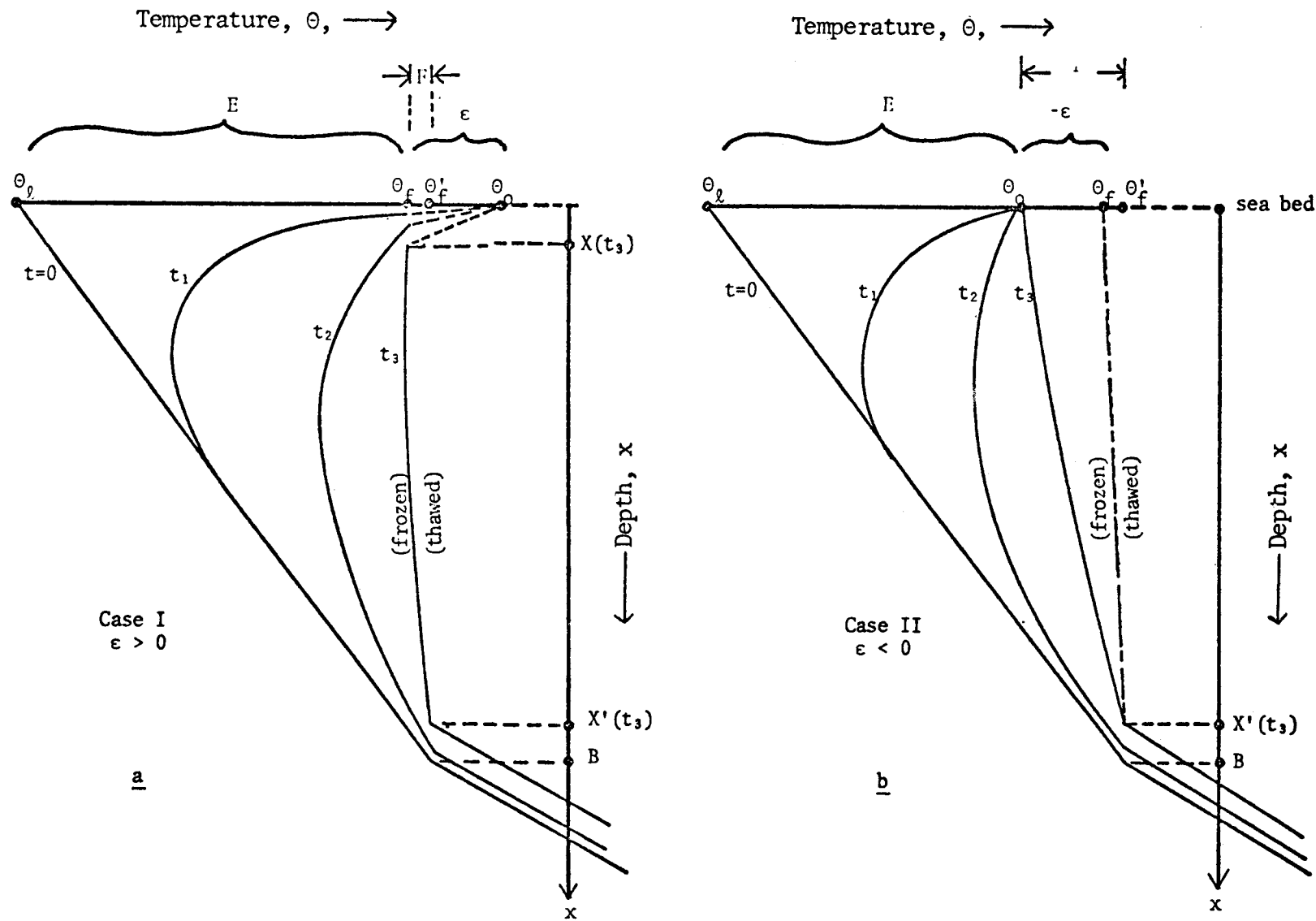


Figure 3. Schematic representation of sub-sea temperatures at successive times $t=0, t_1, t_2, t_3$, following submergence of a region underlain by ice-rich permafrost. a. Mean sea-bed temperature, θ_0 , greater than melting temperature, θ_f , at top, $X(t)$, of permafrost. b. Mean sea-bed temperature, θ_0 , less than melting temperature, θ_f , at top of permafrost.

cannot be true, but the assumption is justified by the resulting simplicity of the analysis and by our present ignorance of the time-dependence of these quantities. Figure 3a represents the case $\theta_o > \theta_f$ which results in a thawed layer at the sea bed (e.g., at holes 3374, PB-1, PB-2, and PB-3) and Figure 3b represents $\theta_o < \theta_f$ where there is only superficial thawing, resulting largely from seasonal effects (e.g., hole #190). The model is one-dimensional, i.e., we neglect horizontal transfer of heat, treating the submergence as if it were a sudden climatic change. For slow transgression and at points close to the shoreline, this assumption must be examined carefully. We assume further that essentially all of the latent heat is released over a very small temperature interval, effectively at θ_f near the top of the ice-bonded permafrost, and at θ'_f near the bottom of permafrost. We assume also that prior to submergence, a thermal steady state had been established on land, the geothermal flux, q^* , is constant and the thermal properties of the frozen (subscript "f") and thawed (subscript "t") materials are each uniform. The moisture content is assumed to be uniform also. These latter assumptions are reasonably consistent with subsurface observations on land near Prudhoe Bay.

Definitions of quantities in the analysis are as follows:

- B initial depth of permafrost (on land).
- θ_o long-term mean annual temperature at land surface (prior to submergence)
- θ_f freezing (and melting) temperature at top of ice-bonded permafrost

- θ'_f freezing (and melting) temperature at bottom of ice-bonded permafrost
- θ_o long-term mean annual temperature of sea bed at site of interest
- $\epsilon = \theta_o - \theta_f$
- $E = \theta_f - \theta_l$ or $\theta_o - \theta_l$ whichever is less
- $F = \theta'_f - \theta_f$ or $\theta'_f - \theta_o$ whichever is greater (it can be negative)
- K_f thermal conductivity of ice-bonded permafrost
- K_t thermal conductivity of thawed sediments
- α_f thermal diffusivity of ice-bonded permafrost
- ρc volumetric heat capacity of ice-bonded permafrost
- q^* steady upward geothermal flux (negative)
 $= K_f (\theta_l - \theta'_f)/B$
- X depth beneath sea bed
- $\chi = x - X$
- $X(t)$ Depth beneath sea bed to top of ice-bonded permafrost at time t
- $X'(t)$ Depth beneath sea bed to bottom of ice-bonded permafrost at time t
- $\beta = X' - X$
- L latent heat of freezing per unit volume of sediment
- q_t heat flux downward into upper surface, X , of ice-bonded permafrost (positive)
 $\approx K_s \frac{\epsilon}{X}$

q_f heat flux downward from upper surface, X , of ice-bonded permafrost

q'_f heat flux upward from lower surface, X' , of ice-bonded permafrost

q'_t heat flux upward into lower surface, X' , of ice-bonded permafrost

$$Q_f = \int_0^t q_f dt$$

$$Q'_f = \int_0^t q'_f dt$$

Q_s, Q'_s the quasi steady-state parts of Q_f and Q'_f , respectively

Q, Q' the transient parts of Q_f and Q'_f , respectively

To obtain representative numerical results for the model of Figure 3, we shall estimate the parameters for the initial condition ($t=0$) and the thermal properties from observations on shore. Then with the values of X , θ_f and θ_0 inferred from the measurements previously discussed (Table 1), we shall obtain relations for the duration of submergence t , and the vertical distribution of temperature and permafrost. The principal difficulty stems from the requirement to determine rate of movement of the upper and lower boundaries of the ice-bonded permafrost.

INITIAL CONDITIONS AND THERMAL PROPERTIES

Temperature measurements through permafrost at onshore installations near Prudhoe Bay suggest the following generalized values for the initial temperature distribution (see Figure 4 of Gold and Lachenbruch, 1973).

$$B \approx 600 \text{ m} \quad (1a)$$

$$\theta'_f \approx -1^\circ\text{C} \quad (1b)$$

$$\theta_l \approx -11^\circ\text{C} \quad (1c)$$

$$\frac{G_t}{G_f} \approx 1.8 \quad (1d)$$

Where G_t and G_f represent the thermal gradients immediately below and above the base of permafrost ($x=B$) respectively. We believe that this gradient discontinuity corresponds to a discontinuity in conductivity under steady thermal conditions. Hence

$$q'_f = q'_t$$

and consequently

$$\frac{K_f}{K_t} = \frac{G_t}{G_f} \quad (2)$$

For gas-free aggregates it is convenient to represent the thermal conductivity as the geometric mean value of the conductivities of the constituents (Sass and others, 1971). Thus if ϕ is the volume percent of water

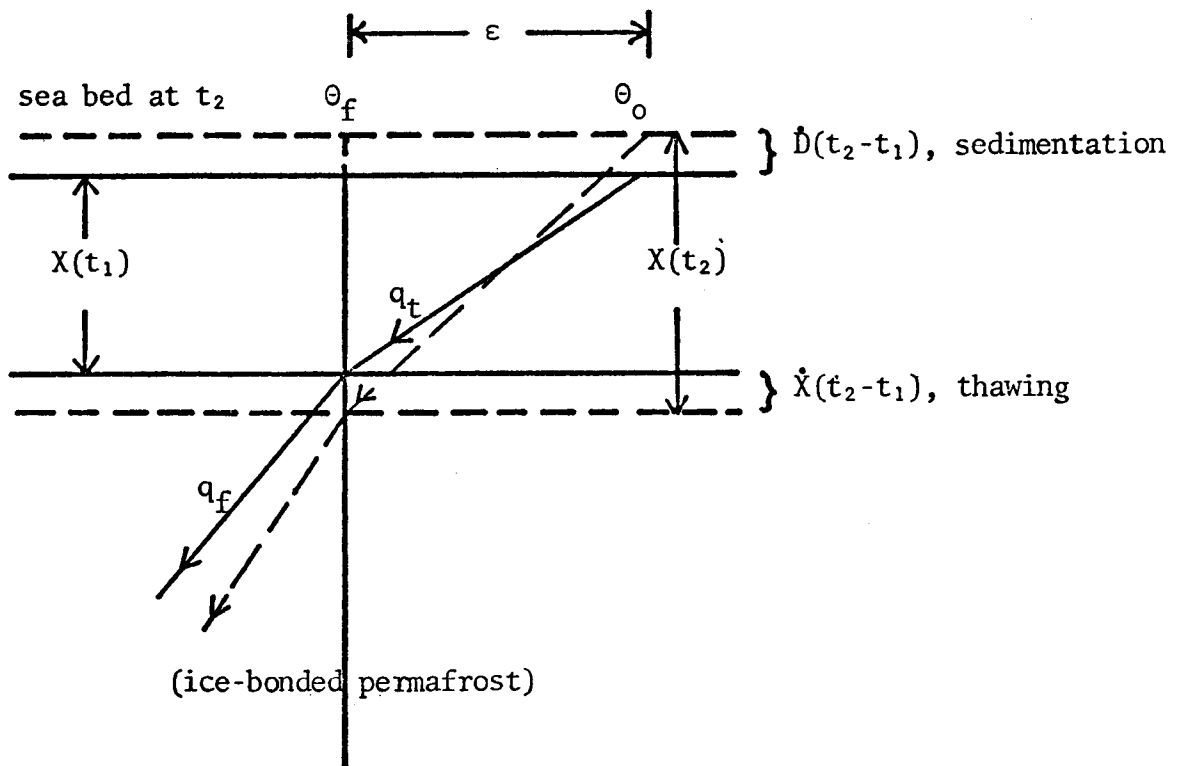


Figure 4. Simplified conditions in thawed layer to depth X beneath the sea bed at two successive times t_1 (solid lines) and t_2 (dashed lines) for case $\varepsilon > 0$. θ_o and θ_f assumed constant and quasi-steady conduction is assumed above X . Arrows on temperature curves represent heat fluxes q_t and q_f associated with gradients above and below X , respectively.

or ice we have

$$K_t \approx K_w^\phi K_s^{1-\phi} \quad (3a)$$

$$K_f \approx K_i^\phi K_s^{1-\phi} \quad (3b)$$

where

$$K_w \approx 1.3 \text{ cal/cm sec } ^\circ\text{C} \quad (4a)$$

$$K_i \approx 5.4 \text{ cal/cm sec } ^\circ\text{C} \quad (4b)$$

are respectively the conductivities of water and ice, and K_s is the mean conductivity of the remaining solids.

Combining 1d, 2, 3, and 4 yields

$$\phi \sim 40\% \quad (5)$$

which is consistent with observations made near the sea bottom (Osterkamp and Harrison, 1976).

For siliceous sediments of the type common in the Prudhoe Bay area, we have found that K_s is typically about 10 cal/cm sec $^\circ\text{C}$. Using this value with (4) and (5) in equations 3 yields

$$K_t \sim 4.4 \text{ cal/cm sec } ^\circ\text{C} \quad (6a)$$

$$K_f \sim 7.8 \text{ cal/cm sec } ^\circ\text{C} \quad (6b)$$

Taking the volumetric heat capacity (ρc) as $0.5 \text{ cal/cm}^3 \text{ }^\circ\text{C}$ for solids and $1.0 \text{ cal/cm}^3 \text{ }^\circ\text{C}$ for water we obtain for the thermal diffusivity.

$$\alpha_t \sim 0.0063 \text{ cm}^2/\text{sec} \quad (7a)$$

$$\alpha_f \sim 0.016 \text{ cm}^2/\text{sec} \quad (7b)$$

The latent heat of freezing for water is about 80 cal/cm^3 ; and for sediments with $\phi \sim 40\%$, it is

$$L = 32 \text{ cal/cm}^3 \quad (8)$$

The steady geothermal flux q^* is obtained by combining 1a, b, c and 6b.

$$\begin{aligned} q^* &= K_f \frac{\theta_l - \theta'_f}{B} \\ &= -1.3 \times 10^{-6} \text{ cal/cm}^2\text{sec} \\ &= -41 \text{ cal/cm}^2\text{yr} \quad (9) \end{aligned}$$

We are using the convention that heat flux is negative for a positive temperature gradient; i.e., upflux is negative, downflux is positive.

CONDITIONS AT THE BOUNDARIES OF ICE-BONDED PERMAFROST

The upper boundary, X. If the mean sea bottom temperature θ_0 is greater than the freezing temperature θ_f , then $\epsilon > 0$ and thawing will proceed downward from the sea bed. Simultaneously, deposition of sediments will result in thickening of the thawed layer by the amount $D(t)$ (see Figure 4). Therefore the heat balance at $x=X$ is given by

$$\frac{dX}{dt} = \frac{q_t}{L} - \frac{q_f}{L} + \frac{dD}{dt} \quad (10)$$

For the large moisture contents under consideration and relatively small sedimentation rates, X will change slowly, and temperatures within the thawed layer can be considered in a quasi-steady state. We introduce $Q_f(t)$, the total amount of sensible heat supplied to the ice-bonded permafrost through its upper surface

$$Q_f(t) = \int_0^t q_f dt \quad (11)$$

and (10) can be written

$$\frac{dX}{dt} = \frac{K_s}{L} \frac{\epsilon}{X} - \frac{1}{L} \dot{Q}_f + \dot{D} \quad (12)$$

where the dot denotes differentiation with respect to time.

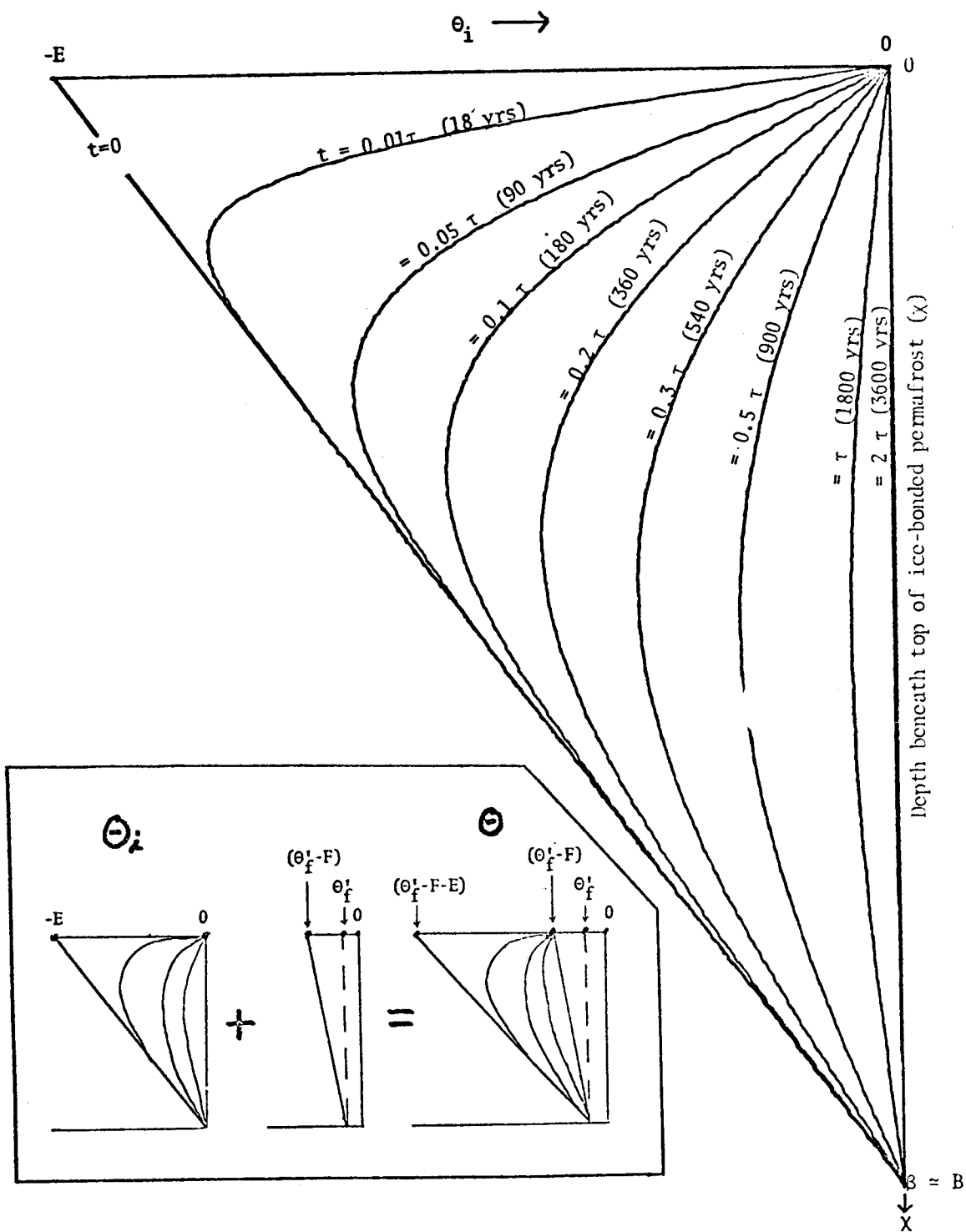


Figure 5. Transient temperature function θ_i describing depletion of the cold reserve of ice-rich permafrost. Numbers on curves are times since inundation in dimensionless units (τ) and years for conditions at Prudhoe Bay. Inset shows scheme of temperature superposition.

Equation 12 can be integrated simply if Q_f and D vary either as $t^{1/2}$ or t . The first case leads to

$$t = \frac{L}{2K_s} \frac{X^2}{\epsilon} \left[1 - \frac{D}{X} + \frac{Q_f}{L} \frac{1}{X} \right] \quad (13)$$

and the second case yields

$$t = \frac{1}{p} \left[X - \frac{K_t \epsilon}{Lp} \ln \left(1 + \frac{pL}{K_t \epsilon} X \right) \right] \quad (14a)$$

$$\text{where } p = \dot{D} + \frac{\dot{Q}_f}{L}, \text{ a constant} \quad (14b)$$

In this report, we shall consider only the first case, equation 13, which gives the time t since submergence for a case in which both the sensible heat absorbed by permafrost and the sedimentation rate are very large initially and then diminish progressively. Qualitatively, this is correct for the heat; the behavior of sedimentation rate is unknown but at least (13) provides a first-order account of it. The factor preceding the bracket in (13) is the well known approximation that neglects sedimentation, and the more important effect of sensible heat absorbed by permafrost.

For the case $\epsilon < 0$, there is, of course, no progressive thawing of the upper ice-bonded surface and $X \approx 0$.

The lower boundary, X' . The position of the lower boundary of ice-bonded permafrost, X' is determined by

$$L \frac{dX'}{dt} = q'_t - q'_f \quad (15a)$$

As the moisture content is large, X' will move slowly and we assume a quasi-steady state below the base of permafrost (i.e., in $x > X'$) and replace q'_t by q^* , the steady geothermal flux. Equation 15 can then be written

$$L \frac{dX'}{dt} = q^* - q'_f \quad (15b)$$

which yields on integration

$$B - X'(t) = - \left[\frac{q^*}{L} t - Q'_f(t) \right] \quad (16)$$

This is an expression for the thinning of ice-bonded permafrost from below after passage of time t since submergence. Unlike conditions at the upper surface, this thawing occurs irrespective of the sign of ϵ .

Our strategy is now as follows: In the next section we shall obtain expressions for Q_f and Q'_f . We can then apply our observations of X , ϵ , and D to estimate (from 13) the time of submergence t at any site. Introducing t and q^* in (16) will yield the position of the bottom of permafrost. Knowing the history of the positions of the phase boundaries

and the initial temperature distribution, we can then estimate the temperature distribution beneath any point on the sea bed.

THERMAL CONDITIONS WITHIN PERMAFROST
AND THE EVALUATION OF EQUATIONS 13 AND 16

Conditions controlled primarily at the upper surface X. The rate at which heat enters the top ($x=X$) of ice-bonded permafrost consists of two parts; a quasi-steady part, \dot{Q}_s , resulting from the constant difference in temperature between its top X and bottom X' , and a transient part, \dot{Q} , resulting from the depletion of its initial cold reserve (i.e., the heat needed to raise the temperature to melting). Hence

$$q_f = \dot{Q}_s + \dot{Q} \quad (17)$$

and (see Figures 3a, b)

$$\dot{Q}_s = -K_f \frac{F}{X' - X} \quad (18)$$

$$\text{where } F = \theta_f' - \theta_f \quad \epsilon > 0$$

$$= \theta_f' - \theta_o \quad \epsilon < 0$$

The transient part contributes heavily for early times (see e.g., curves t_1 , Figure 3), but it becomes negligible (e.g., curves t_3 , Figure 3) for later times. It will be shown (a posteriori) that for the ice-rich conditions at Prudhoe Bay, the transient decays before appreciable

permafrost thinning takes place. Hence, we can approximate the transient behavior by the temperature in a slab of constant thickness B with an initial linear temperature distribution, and with upper and lower surfaces maintained at constant temperature for $t > 0$.

For the sake of generality, we introduce the notation

$$\beta = X'(t) - X(t) \quad (19a)$$

$$\chi = x - X(t) \quad (19b)$$

but we shall ignore for the moment the time-dependence of X and X' , and in the numerical calculations we shall generally approximate β by B , showing eventually that the approximation is probably of little consequence for the cases of interest.

We can write

$$\dot{Q} = K_f \left. \frac{\partial \theta_i}{\partial \chi} \right|_{\chi=0} \quad (20)$$

where $\theta_i(t, \chi; \beta)$ is the solution to

$$\frac{\partial^2 \theta_i}{\partial \chi^2} = \frac{1}{\alpha_f} \frac{\partial \theta_i}{\partial t}, \quad 0 < \chi < \beta \quad (21)$$

with the conditions

$$\theta_i = -E(1 - \frac{\chi}{\beta}) \quad , \quad t = 0 \quad (22)$$

$$\theta_i = 0, \quad \chi=0 \text{ and } \chi=\beta \quad , \quad t > 0 \quad (23)$$

Here $E = \theta_f - \theta_l$ for case $\epsilon > 0$ (24)

$$E = \theta_o - \theta_l \text{ for case } \epsilon < 0 \quad (25)$$

The solution (modified from Carslaw and Jaeger, 1959, p. 313, equation 10) is

$$\theta_i(t, \chi; \beta) = \frac{2E}{\pi} \sum_{n=1}^{\infty} \frac{(-1)^n}{n} e^{\frac{-n^2\pi^2}{4} \frac{t}{\tau}} \sin[n\pi(1 - \frac{\chi}{\beta})] \quad (26)$$

where the time constant τ is given by

$$\tau = \frac{\beta^2}{4\alpha_f} \quad (27a)$$

$$\approx 1800 \text{ yrs for Prudhoe Bay} \quad (27b)$$

where (27b) is obtained from (1a) and (7b), assuming $\beta \approx B$. Results from (26) are shown graphically in Figure 5. It is seen that the decay of θ_i is almost complete (i.e., the sensible heat storage is negligible) for $t > \tau$. Hence it is necessary only that our approximation $\beta \approx B$ be valid for $t < \tau$.

Evaluating the derivative of (26) at $\chi=0$ yields an approximation to \dot{Q} .

$$\dot{Q} \approx 2K_f \frac{E}{\beta} \sum_{n=1}^{\infty} e^{-\frac{n^2\pi^2}{4} \frac{t}{\tau}} \quad (28)$$

Integration of (28) yields $Q(t)$, the total transient contribution after time t

$$\begin{aligned} Q(t) &\equiv \int_0^t \dot{Q} dt \\ &= \frac{4}{3} K_f \frac{E}{\beta} \tau \left[1 - \frac{6}{\pi^2} \sum_{n=1}^{\infty} \frac{1}{n^2} e^{-\frac{n^2\pi^2}{4} \frac{t}{\tau}} \right] \end{aligned} \quad (29a)$$

$$= \frac{4}{3} K_f \frac{E}{\beta} \tau [1 - .05] \quad , \quad t = \tau \quad (29b)$$

$$\approx \frac{4}{3} K_f \frac{E}{\beta} \tau \quad , \quad t > \tau \quad (29c)$$

Integration of (17) yields

$$\begin{aligned} Q_f(t) &\equiv \int_0^t q_f dt \\ &= Q(t) + \int_0^t \dot{Q}_s dt \\ &\approx \frac{K_f}{B} \left[\frac{4}{3} (E) \tau - (\theta'_f - \theta_f) t \right] \quad , \quad \epsilon > 0 \quad , \quad t > \tau \end{aligned} \quad (30)$$

Substituting the foregoing numerical values including $\theta_f = -1.8^\circ\text{C}$, $\theta'_f = -1^\circ\text{C}$ in (30), we obtain the following dimensional relation for Prudhoe Bay

$$\frac{Q_f}{L} \text{ (meters)} \approx 28 - 0.1 \times t \text{ (centuries)} \quad t > \tau \quad (31)$$

Introducing (31) in equation 13 along with observed values of marine sedimentation D and the other parameters, we obtain an estimate of the time since submergence (column 15, Table 1). The 28 meters contributed by the transient term in (30) is substantial, and the sensible heat it represents cannot be neglected. (The heat absorbed through the upper surface by the warming permafrost is equivalent to that required to melt 28 m of ice-bonded permafrost.) The second term in (31) represents the quasi-steady effect and it is sensitive to the choice of θ_f and θ'_f , the latter in particular is rather arbitrary. In Table 1, column 8, the simpler approximation neglecting sedimentation and sensible heat is compared with the adjusted values, Table 1, column 15, given by equation 13, still a crude approximation. In general, the combined effect of sedimentation and heat storage increases the estimate of t by about 45%.

It is seen from Table 1, column 7, that (excluding PB-1, to be discussed) the greatest thawing from the surface, $X - D$, is about 40 m. It occurs at hole 3370 where the time t (column 15) is substantially greater than τ . But 40 m is only 7% B , and at $t=\tau$, $X - D$ would be

appreciably less. Therefore thawing from the top of ice-bonded permafrost does not seriously jeopardize our approximation

$$\beta(\tau) \approx B$$

More general conditions for the validity of the approximation will be considered elsewhere.

Returning now to the case $\epsilon < 0$ we should like to determine the temperature gradient $\frac{\partial\theta}{\partial x}|_0$ near the sea bed in ice-bonded permafrost as a function of time to compare with the observed value at hole #190. From (17), (18), and (28) it is given approximately by

$$\begin{aligned} -\frac{\partial\theta}{\partial x}|_0 &= \frac{q_f}{K_f} \\ &\approx \frac{1}{B} \{ \theta'_f - \theta_o + 2(\theta_o - \theta_l) \sum_{n=1}^{\infty} e^{\frac{-n^2\pi^2}{4} \frac{t}{\tau}} \} \end{aligned} \quad (32)$$

or

$$2 \sum_{n=1}^{\infty} e^{\frac{-n^2\pi^2}{4} \frac{t}{\tau}} \approx \frac{1}{\theta_o - \theta_l} \{ -B \frac{\partial\theta}{\partial x}|_0 - (\theta'_f - \theta_o) \} \quad (33)$$

From Figure 2, we obtain $\frac{\partial\theta}{\partial x}|_0 \approx -38^\circ\text{C}/\text{km}$, and $\theta_o = -3.5^\circ\text{C}$ for hole 190.

Introducing the other parameters in (33) yields

$$B \frac{\partial \theta}{\partial x} \Big|_0 = -22.8^\circ\text{C}$$

$$\theta'_f - \theta_o = 2.5^\circ\text{C}$$

$$\theta_o - \theta_\ell = 7.5^\circ\text{C}$$

and (33) yields

$$2 \sum_{n=1}^{\infty} e^{\frac{-n^2\pi^2}{4} \frac{t}{\tau}} = 2.70 \quad (34)$$

This relation is satisfied by

$$\frac{t}{\tau} \approx .08 \quad (35a)$$

$$t \approx 145 \text{ yrs} \quad (35b)$$

This value is consistent with an estimate by Harrison (oral communication) made with another method (it will be discussed further below).

Melting from the lower surface X'. Following the procedure used for the upper surface, we break q'_f into its transient and steady parts.

$$q'_f = \dot{Q}'_s + \dot{Q}' \quad (36)$$

where

$$\dot{Q}'_s = \dot{Q}'_s = -K_f \frac{F}{X' - X} \quad (37)$$

We shall also use the notation

$$\begin{aligned} Q'_f &= \int_0^t q'_f \\ &= Q'_s + Q' \end{aligned} \quad (38)$$

The heat balance at the lower surface X' of ice-rich bonded permafrost is given by (15b), integration of which yields

$$-L \int_B^{X'} dX' \approx \int_0^t [q'_f - q^*] dt \quad (39)$$

$$B - X' \approx \frac{1}{L} \left\{ Q'(t) - \int_0^t K_f \frac{F}{B} dt - q^* t \right\} \quad (40)$$

It has been shown that $Q'(t)$ will not increase significantly after t exceeds τ , i.e., by time τ the sensible cold reserve has been depleted. The total amount of heat input from top and bottom required to achieve this depleted condition is

$$Q_f(\tau) - Q'_f(\tau) \approx \frac{1}{2} \rho c B E \quad (41a)$$

$$\approx 2 K_f \frac{E}{B} \tau \quad (41b)$$

where (41b) follows from (27a)

Substituting (29c) yields

$$-Q'_f(\tau) \approx \frac{2}{3} K_f \frac{E}{B} \tau \quad (42)$$

Comparing (41b) and (42) we see that one-third of the sensible heat required to warm the permafrost enters through to bottom surface.

Integrating (40) and using (42) we obtain for $t = \tau$

$$B - X'(\tau) \approx \frac{1}{L} \left\{ -\frac{2}{3} K_f \frac{E}{B} \tau - K_f \frac{F}{B} \tau - q^* \tau \right\}$$

but $q^* = -K_f \frac{E+F}{B}$

and hence

$$B - X'(\tau) \approx \frac{1}{3L} K_f \frac{E}{B} \tau \quad (43)$$

From (43) we can calculate the thinning of permafrost from the bottom during the first 1800 yrs ($t=\tau$) after submergence for the four offshore sites where $E \approx 9.2^\circ\text{C}$ and for hole 190 where $E \approx 7.5^\circ$

$$B - X'(\tau) = 7 \text{ m} , \quad t = 1800 \text{ yrs}, \quad E = 9.2^\circ\text{C} \quad (44a)$$

$$= 5.7 \text{ m} , \quad E = 7.5^\circ\text{C} \quad (44b)$$

As this is only about 1% of B, thinning from the bottom will not jeopardize our approximation

$$\beta(\tau) \approx B$$

For larger values of time ($t > \tau$), the first term in the braces, equation 40, is constant. Using (43), the subsequent thawing can be expressed

$$B - X'(t) \approx \frac{K_f E}{3LB} \tau - \frac{1}{L} \{q^*(t-\tau) - \int_{\tau}^t K_f \frac{F}{\beta} dt\} \quad (45a)$$

$$\approx \frac{K_f E}{3LB} \tau + \frac{1}{L} \{K_f \frac{E+F}{B} (t-\tau) - \int_{\tau}^t K_f \frac{F}{\beta} dt\} , \quad t > \tau \quad (45b)$$

Thus if F is small relative to E as is generally true in the case $\epsilon > 0$, the constant degradation for $t > \tau$ caused by the geothermal flux will adequately describe all but the final stages of permafrost melting ($\beta \ll B$).

We can describe the melting of the bottom of permafrost for $t > \tau$, taking account of the time-dependence of β in (45). For the small values of ϵ and large values of L of interest, it is seen from (13) and (16) that most of the permafrost thinning will take place from below for larger values of time. Retaining only X' in the denominator of the right side of (37) and observing that $\dot{Q}' \approx 0$ for $t > \tau$ we obtain

$$q'_f \approx -K_f \frac{F}{X'} \quad , \quad t > \tau \quad (46)$$

The heat balance (15b) can then be written

$$L \frac{dX'}{dt} = -|q^*| + K_f \frac{F}{X'} \quad , \quad t > \tau \quad (47)$$

As q^* is negative by our convention, we insert the absolute value to clarify the physical meaning of (47). It follows that

$$\int_{\tau}^t dt = \int_{X'(\tau)}^{X'(t)} \frac{X'}{\frac{K_f F}{L} - \frac{|q^*|}{L} X} dX'$$

or

$$t - \tau = \frac{L}{|q^*|} [X'(\tau) - X'(t)] \left\{ 1 + \frac{H}{X'(\tau) - X'(t)} \ln \left[\frac{X'(\tau) - H}{X'(t) - H} \right] \right\} \quad (48a)$$

$$\approx \frac{L}{|q^*|} [X'(\tau) - X'(t)] \quad , \quad H \approx 0 \quad (48b)$$

$$\frac{L}{|q^*|} \approx 0.78 \text{ centuries/meter, Prudhoe Bay} \quad (48c)$$

where (48c) follows from (8) and (9). In (48) H is a characteristic length defined by

$$H = \frac{FK_f}{|q^*|} \quad (49a)$$

$$= \frac{F}{E+F} B \quad (49b)$$

$$= \frac{\theta'_f - \theta_f}{\theta'_f - \theta_l} B \quad \text{for } \epsilon > 0 \quad (49c)$$

$$= \frac{\theta'_f - \theta_o}{\theta'_f - \theta_l} B \quad \text{for } \epsilon < 0 \quad (49d)$$

Equation 48a gives the time past $t=\tau$ required for the bottom of permafrost to rise to $X'(t)$ (from $X'(\tau)$ given by equation 43). The factor preceding the braces is the simple thawing by geothermal flux (48b). If the melting temperature is the same at the top and bottom of permafrost,

then $F=0$, and the quantity in braces is unity; the ice-bonded permafrost will eventually all disappear, degrading at a near-constant rate (48b and c). If $F > 0$ the degradation will proceed at a diminishing rate and a steady state will occur when $X'/B \approx F/(E+F)$. If $F < 0$, the second term in braces becomes negative and the quasi-steady flux across the ice-bonded permafrost accelerates thawing. (The final stages may, of course, be complicated by variations of Θ'_f , and for $\epsilon > 0$, by behavior of the upper surface.)

For the four offshore holes where $F = 0.8^\circ$, $E = 9.2^\circ$, the expression in braces can generally be neglected, and thawing can be computed at the rate L/q^* (or 1.28 m/century, see equation 48c) for times of interest at Prudhoe Bay. For example, for X' to reduce to 500 m from 593 m, neglecting the braces gives $(t-\tau) \approx 7,250$ yrs and including them gives 8,030 yrs. The total time, obtained by adding τ (during which time the first 7 m thawed), is 9,050 yrs neglecting braces or 9,830 accounting for them. If the model is approximately correct, it is likely that ice-bonded permafrost extends to depths on the order of 500 m beneath the observation sites at Prudhoe Bay today.

Temperature profiles. A summary expression for the approximate temperature $\theta(x,t)$ above, in, and beneath ice-rich bonded permafrost according to the present model is

$$\text{Case I} \quad \varepsilon \equiv \theta_o - \theta_f > 0$$

$$\theta \approx \theta_o - \frac{\varepsilon}{X} x, \quad 0 < x < X \quad (50a)$$

$$\approx \theta_f + \theta_i(t, X; \beta) + \frac{F}{\beta} (x - X(t)), \quad X < x < X' \quad (50b)$$

$$\approx \theta_f' - \frac{q^*}{K_t} (x - X'), \quad x > X' \quad (50c)$$

$$\text{Case II} \quad \varepsilon \equiv \theta_o - \theta_f < 0$$

$$\theta \approx \theta_o + \theta_i(t, X; \beta) + \frac{F}{\beta} x, \quad 0 < x < X' \quad (51a)$$

$$\approx \theta_f' - \frac{q^*}{K_t} (x - X'), \quad x > X' \quad (51b)$$

The quantities X and X' are functions of t given by equations 13 and 16, respectively, and $\theta_i(t, X; \beta)$ is given by equation 26. For approximations under ice-rich conditions and small ε such as those at Prudhoe Bay we can generally replace β by B in θ_i without serious error. For $t < \tau \approx 1800$ yrs at Prudhoe Bay, the temperature profiles will resemble curves t_1 or t_2 of Figure 3a for case I, and Figure 3b for case

II. For $t > \tau$, θ_i is small and the profiles will resemble curves t_3 of Figure 3a for case I, and Figure 3b for case II. Parameters for the profiles beneath each study site can be obtained from Table 1 and relations in the text. Numerical details of the results should not be taken too seriously, however, until more data are acquired to confirm the assumptions or refine the analysis.

SUMMARY AND DISCUSSION

We have presented a highly simplified analysis of thermal conditions near the shore at Prudhoe Bay. Although it cannot be "right" in detail, the exercise exposes some logical implications of the fragmentary observations presently available, it indicates the sensitivity of these implications to several of the parameters upon which the solution depends, and it serves to focus attention on the types of observations needed for a more confident analysis. The principal assumptions are:

- 1) Thawed sediments at the sea bed are saturated with normal sea water
- 2) Salinity of the ice-bonded permafrost is negligible
- 3) Prior to the last inundation, the thermal regime was in a steady state and similar to the regime observed beneath the adjacent land today
- 4) The sediments are generally siliceous and have a large porosity
- 5) The thermal conductivity of the ice-bonded and thawed material are each relatively uniform
- 6) The mean sea-bottom temperature inferred from present-day observations at each site is the value that has obtained since inundation
- 7) Horizontal heat transport is negligible relative to vertical transport.

A rather indirect justification for the first assumption has been presented in the section "Temperature Measurements"; it can easily be

confirmed by deeper drilling. Some justification for assumptions 2, 4, and 5 is provided by limited information on materials and temperatures from boreholes on and off shore. The validity of assumption 3 depends upon interpretations of shoreline chronology; the assumption is probably consistent with existing evidence at the sites under study (see Hopkins and others, 1977). Assumption 6 is arbitrary and justified largely by its simplicity and our present lack of information; more rational refinements are possible but probably unwarranted at this stage. The seventh assumption will generally be violated at sites near shore.

The analysis yields the following results:

1) It underscores the importance of distinguishing between two cases:

a) $\epsilon > 0$, and

b) $\epsilon < 0$

where $\epsilon = \theta_o - \theta_f$ and θ_o is the mean sea bed temperature and θ_f is the temperature of the upper boundary of ice-bonded permafrost (see Figure 3). In the first case ($\epsilon > 0$), permafrost thaws downward progressively from the sea bed and eventually disappears. In the second case ($\epsilon < 0$), permafrost persists near the sea bed, even in the steady state. The second case is expected in a near-shore band where sea-ice freezes to the bottom seasonally, but it is also possible at offshore locations. θ_o depends on the seasonal regime of the sea water and θ_f depends upon salt transport mechanisms in the sea bed; small changes in the relative values of θ_o and θ_f can change the sign of ϵ and convert one regime to

the other. Several aspects of this problem have been discussed in detail by Harrison and Osterkamp (1976) and Osterkamp (1975).

2) When the cold permafrost is inundated by the sea, it absorbs heat from the relatively warm sea bed above and from geothermal flux rising from below. After an initial period, the duration of which is easily calculated, temperatures in the ice-bonded permafrost become nearly uniform at the value determined by the melting temperatures of its upper and lower surfaces. For conditions at Prudhoe Bay the time required to reach this near-isothermal condition is about 1800 years; for submergence times less than this, appreciable negative thermal gradients are expected beneath the top of ice-bonded permafrost.

3) A substantial amount of the heat conducted downward through the sea bed is consumed in warming the permafrost to its melting temperature (not melting it) in the initial phases. For conditions at Prudhoe Bay, the total amount of this heat is equivalent to that required to melt 28 m of ice-bonded permafrost. This heat requirement, neglected in simpler models, can have a substantial effect on the estimate of time of inundation calculated from the observed depth of thawing at the sea bed. For the present data it increases the time by 50%-80% (Table 1, column 13).

4) One-third of the heat required to deplete the initial sub-freezing cold reserve of permafrost is supplied by geothermal flux entering through the lower boundary. Thus, for conditions at Prudhoe Bay the lower surface of permafrost rises only about 7 m during the

first 1800 years, and thereafter it rises at the near-constant rate of about $1 \frac{1}{4}$ m/century.

5) The rate of thawing of the upper surface of ice-bonded permafrost diminishes progressively with time because the thickness of the insulating thawed layer increases. According to the model, the present rate of thawing of the upper surface of ice-bonded permafrost is about 1 cm/yr at #3370, $\frac{1}{2}$ cm/yr at PB-3, and $\frac{1}{3}$ cm/yr at PB-2. Hence at present, permafrost is degrading faster at its lower surface ($1 \frac{1}{4}$ cm/yr, see 4) above) than at its upper surface at all sites, and the disparity will increase with time. According to our interpretation of the thermal data, the thawed layer at the sea bed is thinnest at PB-2 (column 7, Table 1), the site that is farthest from shore, and hence the one that has been submerged the longest. The analysis resolves this paradox because the sea bed at PB-2 is colder and it thaws more slowly, as indicated by the rates just cited (see also Table 1, columns 4 and 6). These conclusions are sensitive to assumptions 6 and 7 which could be seriously violated at PB-2, for example, by migration of Reindeer Island. Uncertainties of this sort can easily be resolved with additional drilling for thermal observations.

6) The rate of sedimentation plays an important role in the heat transfer between the sea bottom and the upper surface of ice-bonded permafrost. The thickness of the thawed layer that insulates permafrost is the combined effect of thawing and sedimentation. Failure to account

for sedimentation can lead to substantial errors in attempts to estimate the period of inundation from observations of temperature and thickness of the thawed layer beneath the sea bed. A very crude mathematical account of sedimentation leads to adjustments of the inundation time by as much as 40% at the Prudhoe Bay sites; more realistic accounts will probably have larger effects.

With all of its shortcomings, the analytical model was applied formally to observations at holes #190, #3370, PB-3, and PB-2. The calculated effective time of inundation is shown in Figure 6 as a function of distance from the present shoreline (see also Table 1, column 15). Taken at face value, the results suggest a period of rapid transgression (at the rate of 10 m/yr) terminating some 4000 years ago at a point presently perhaps 4 or 5 km from shore. Thereafter, they suggest a slow transgression at the rate of 1 m/yr up to the present shoreline position. The latter rate is consistent with geomorphic estimates of thermal erosion of the present shoreline (see Hopkins and others, 1977); the former would suggest a rapid rise of sea level in the past. However, these numerical results should not be taken too seriously; it is easy to think of uncertainties in the assumption that could change the results substantially. It is probably fortuitous that the rate of transgression, 10 m/yr, from PB-2 to PB-3 (Figure 6) is the same as the value determined by Hopkins (written communication) from sea level curves; a completely independent source of information. The absolute values of his times of inundation are, however, generally larger than

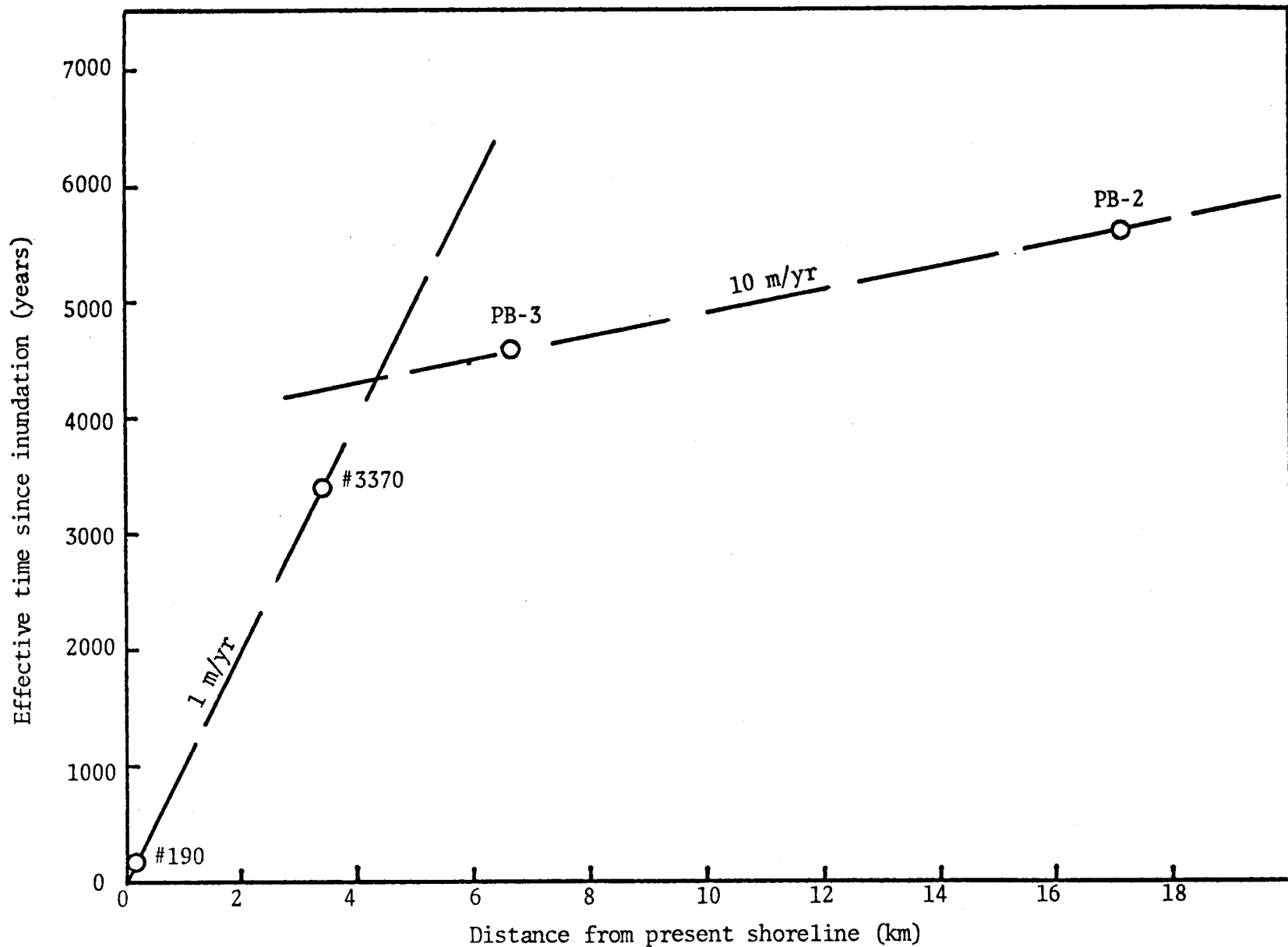


Figure 6. Effective time since inundation, t , determined from formal application of equation 13 for the three offshore holes and equation 35b for #190. Slopes of dashed lines suggest rate of shoreline transgression.

ours by a factor of about 2, and consequently his estimate of the transgression rate for the most recent phase is about half of ours (about 1/2 m/yr). (One other curious, and perhaps no less fortuitous result of our calculation is that hole 3370 which is 3370 m from shore has a calculated inundation time of 3370 years.)

As the three offshore holes all have inundation times substantially greater than the 1800 years required to deplete the cold reserve, the analysis indicates that the temperature profiles beneath these holes are described by the curve labeled t_3 in Figure 3a. That is the ice-bonded permafrost is nearly isothermal and near its melting temperature. The temperature and depth parameters (θ_o , θ_f , X , X') for the curves at each site are given in Table 1. Note that the base of permafrost has risen only a few tens of meters (column 16). Thus the model suggests that near isothermal ice-rich permafrost (at temperatures close to melting) extends to depths of 500 m or so beneath the four offshore holes.

Temperatures beneath hole 190 would follow a curve like t_1 , Figure 3b. According to the model, the actual position of the transient part of this curve is about midway between curves labeled $\tau = 0.05$ and $\tau = 0.1$, Figure 5. The curve parameters θ_o , θ_f , X and X' are given in Table 1; θ_ℓ and θ_f^1 can reasonably be assumed to be -11°C and -1°C , respectively. For a refined analysis at this site, departures from assumption 7 should be examined.

The hole PB-1 lies within Prudhoe Bay proper, a bathymetric basin (see Figure 1). PB-1 and hole 3370 are both about 3 km from shore, and

their sea-bed temperatures measured to depths of 20+ m are comparable (Figure 2). However, the thermal gradient is anomalously low at PB-1. A formal extrapolation to the -1.8° isotherm yields a thaw depth of 80+ m, and a formal calculation of the duration of submergence yields 13000+ years for PB-1 (Table 1). There are two simple ways of explaining this anomaly:

1) The sediments beneath PB-1 contain water of low salinity and consequently the top of ice-bonded permafrost lies well above the -1.8°C isotherm, i.e., Θ_f is relatively high.

2) The sediments at PB-1 were "pre-heated" beneath a large thaw lake whose shoreline eventually was breached by the sea to form Prudhoe Bay proper. Mean annual bottom temperatures of large thaw lakes on the coastal plain generally vary from about 0°C to about $+1.5^{\circ}\text{C}$ depending upon whether or not they are brackish; where the lakes are less than 2 m deep their temperatures can be lower (Lachenbruch and others, 1962). Thus the negative temperature gradient at PB-1 tends to support the first explanation although it does not preclude the second. A recent radiocarbon date suggests that marine conditions commenced at PB-1 only 600 years ago (David Hopkins, written communication). As this allows little time for thawing, it supports the ancestral lake explanation. The problem can be resolved by drilling to 100 m in Prudhoe Bay; the resolution bears upon the question of whether or not ice-rich permafrost exists beneath Prudhoe Bay proper.

A P P E N D I X

Temperature Measurements in Holes PB-1, PB-2, and PB-3

Hole PB-1

Date: April 12, 1976

Depth of ice and water: 2.68 m

Depth (m) (below sea bed)	Temperature (°C)
5.85	-1.249
6.46	-0.972
7.99	-0.965
9.51	-0.967
11.03	-0.973
12.56	-0.993
14.08	-0.998
15.61	-1.014
17.13	-0.977
18.65	-1.026
20.18	-1.062
21.58	-1.065

Hole PB-1

Date: April 14, 1976

Depth of ice and water: 2.68 m

Depth (m) (below sea bed)	Temperature (°C)
5.24	-1.272
5.85	-1.089
6.46	-1.076
7.07	-1.070
7.68	-1.067
8.29	-1.066
8.90	-1.070
9.51	-1.073
10.12	-1.077
10.73	-1.081
11.34	-1.089
11.95	-1.098
12.56	-1.105
13.17	-1.108
13.78	-1.107
14.39	-1.107
15.00	-1.111
15.61	-1.112
16.22	-1.107
16.82	-1.096
17.43	-1.092
18.04	-1.105
18.65	-1.125
19.26	-1.145
20.18	-1.166
21.58	-1.357

Hole PB-1

Date: April 23, 1976

Depth of ice and water: 2.68 m

Depth (m) (below sea bed)	Temperature (°C)
5.24	-1.326
5.85	-1.151
6.46	-1.135
7.07	-1.129
7.68	-1.126
8.29	-1.124
8.90	-1.125
9.51	-1.124
10.12	-1.121
10.73	-1.125
11.34	-1.127
11.95	-1.127
12.56	-1.133
13.17	-1.136
13.78	-1.140
14.39	-1.140
15.00	-1.141
15.61	-1.143
16.22	-1.146
16.82	-1.160
17.43	-1.168
18.04	-1.172
18.65	-1.179
19.26	-1.181
19.87	-1.177
20.48	-1.186
21.09	-1.209
21.64	-1.215

Hole PB-1

Date: May 3, 1976

Depth of ice and water: 2.68 m

Depth (m) (below sea bed)	Temperature (°C)
5.85	-1.184
6.46	-1.162
7.07	-1.152
7.68	-1.141
8.29	-1.144
8.90	-1.142
9.51	-1.145
10.12	-1.145
10.73	-1.149
11.34	-1.153
11.95	-1.157
12.55	-1.162
13.17	-1.166
13.78	-1.170
14.39	-1.172
15.00	-1.177
15.61	-1.180
16.22	-1.181
16.82	-1.184
17.43	-1.190
18.04	-1.193
18.65	-1.199
19.26	-1.202
19.87	-1.206
20.48	-1.213
21.09	-1.218
21.55	-1.225

Hole PB-1

Date: June 8, 1976

Depth of ice and water: 2.68 m

Depth (m) (below sea bed)	Temperature (°C)
6.10	-1.301
6.71	-1.236
7.32	-1.216
7.92	-1.202
8.53	-1.193
9.14	-1.186
9.75	-1.182
10.36	-1.180
10.97	-1.180
12.19	-1.182
13.72	-1.188
15.24	-1.197
16.76	-1.206
18.29	-1.216
19.81	-1.227
21.34	-1.239
21.55	-1.243

Hole PB-2

Date: April 21, 1976

Depth of ice and water: 11.65 m

Depth (m) (below sea bed)	Temperature (°C)	Depth (m) (below sea bed)	Temperature (°C)
0.55	-1.559	15.79	-1.626
1.16	-1.512	16.40	-1.628
1.77	-1.492	17.01	-1.631
2.38	-1.479	17.62	-1.631
2.99	-1.466	18.23	-1.631
3.60	-1.458	18.84	-1.628
4.21	-1.452	19.45	-1.625
4.82	-1.452	20.06	-1.619
5.43	-1.453	20.67	-1.606
6.04	-1.455	21.28	-1.591
6.64	-1.458	21.88	-1.580
7.25	-1.463	22.49	-1.576
7.86	-1.466	23.10	-1.584
8.47	-1.475	23.71	-1.603
9.08	-1.485	24.32	-1.652
9.69	-1.532	24.93	-1.671
10.30	-1.587	25.54	-1.684
10.91	-1.607	26.15	-1.701
11.52	-1.608	26.76	-1.711
12.13	-1.603	27.37	-1.720
12.74	-1.610	27.98	-1.727
13.35	-1.614	28.59	-1.743
13.96	-1.616	29.20	-1.755
14.57	-1.614	29.38	-1.751
15.18	-1.616		

Hole PB-2

Date: April 26, 1976

Depth of ice and water: 11.65 m

Depth (m) (below sea bed)	Temperature (°C)	Depth (m) (below sea bed)	Temperature (°C)
0.24	-1.679	14.57	-1.642
0.55	-1.660	15.18	-1.654
0.85	-1.658	15.79	-1.664
1.16	-1.616	16.40	-1.667
1.77	-1.588	17.01	-1.667
2.38	-1.581	17.62	-1.668
2.99	-1.551	18.23	-1.668
3.60	-1.528	18.84	-1.671
4.21	-1.515	19.45	-1.665
4.81	-1.510	20.05	-1.687
5.42	-1.514	20.66	-1.689
6.03	-1.521	21.27	-1.686
6.64	-1.532	21.88	-1.683
7.25	-1.545	22.49	-1.684
7.86	-1.561	23.10	-1.690
8.47	-1.576	23.71	-1.696
9.08	-1.599	24.32	-1.686
9.69	-1.614	24.93	-1.685
10.30	-1.623	25.54	-1.717
10.91	-1.633	26.15	-1.751
11.52	-1.639	26.76	-1.767
12.13	-1.633	27.37	-1.774
12.74	-1.638	27.98	-1.780
13.35	-1.638	28.59	-1.787
13.96	-1.643	29.20	-1.795
		29.23	-1.794

Hole PB-2

Date: May 6, 1976

Depth of ice and water: 11.65 m

 Depth (m)
 (below sea bed)

Temperature (°C)

 Depth (m)
 (below sea bed)

Temperature (°C)

0.24	-1.688
0.55	-1.683
0.85	-1.674
1.16	-1.665
1.46	-1.651
1.77	-1.641
2.07	-1.630
2.38	-1.616
2.68	-1.605
2.99	-1.589
3.29	-1.576
3.60	-1.567
3.90	-1.560
4.21	-1.557
4.51	-1.554
4.81	-1.553
5.12	-1.554
5.42	-1.555
5.73	-1.558
6.03	-1.362
6.34	-1.566
6.64	-1.571
6.95	-1.575
7.25	-1.579
7.86	-1.592
8.47	-1.606
9.08	-1.621
9.69	-1.633
10.30	-1.639
10.91	-1.644

11.52	-1.648
12.13	-1.648
12.74	-1.652
13.35	-1.656
13.96	-1.659
14.57	-1.665
15.18	-1.673
15.79	-1.680
16.40	-1.686
17.01	-1.690
17.62	-1.692
18.23	-1.695
18.84	-1.698
19.45	-1.697
20.05	-1.707
20.66	-1.715
21.27	-1.720
21.88	-1.723
22.49	-1.725
23.10	-1.727
23.71	-1.725
24.32	-1.711
24.93	-1.705
25.54	-1.735
26.15	-1.761
26.76	-1.776
27.37	-1.784
27.98	-1.791
28.59	-1.797
29.20	-1.802
29.23	-1.802

Hole PB-2

Date: June 8, 1976

Depth of ice and water: 11.65 m

Depth (m) (below sea bed)	Temperature (°C)	Depth (m) (below sea bed)	Temperature (°C)
0.15	-1.659	14.78	-1.689
0.76	-1.648	15.39	-1.697
1.37	-1.630	16.00	-1.705
1.98	-1.615	16.61	-1.711
2.59	-1.607	17.22	-1.714
3.20	-1.599	17.83	-1.717
3.81	-1.597	18.44	-1.722
4.42	-1.597	19.05	-1.726
5.02	-1.599	19.66	-1.732
5.64	-1.604	20.27	-1.736
6.25	-1.609	20.88	-1.738
6.86	-1.618	21.49	-1.738
7.48	-1.627	22.10	-1.736
8.08	-1.636	22.71	-1.732
8.69	-1.644	23.32	-1.735
9.30	-1.648	23.93	-1.741
9.91	-1.652	24.54	-1.758
10.51	-1.656	25.15	-1.770
11.12	-1.660	25.75	-1.780
11.73	-1.664	26.36	-1.789
12.34	-1.668	26.97	-1.795
12.95	-1.671	27.58	-1.800
13.56	-1.675	28.10	-1.805
14.17	-1.682		

Hole PB-3

Date: May 1, 1976

Depth of ice and water: 5.84 m

Depth (m) (below sea bed)	Temperature (°C)	Depth (m) (below sea bed)	Temperature (°C)
0.25	-1.502	20.98	-1.454
0.86	-1.401	21.59	-1.458
1.47	-1.345	22.20	-1.465
2.08	-1.314	22.81	-1.473
2.69	-1.295	23.42	-1.487
3.30	-1.285	24.03	-1.510
3.91	-1.282	24.64	-1.528
4.52	-1.280	25.25	-1.538
5.13	-1.278	25.86	-1.541
5.74	-1.273	26.46	-1.545
6.35	-1.273	27.07	-1.549
6.96	-1.276	27.68	-1.549
7.57	-1.287	28.29	-1.545
8.18	-1.299	28.90	-1.543
8.79	-1.312	29.51	-1.547
9.40	-1.327	30.12	-1.558
10.00	-1.342	30.73	-1.571
10.62	-1.350	31.34	-1.580
11.22	-1.358	31.95	-1.592
11.83	-1.366	32.56	-1.592
12.44	-1.373	33.17	-1.576
13.05	-1.384	33.78	-1.570
13.66	-1.395	34.39	-1.585
14.27	-1.401	35.00	-1.603
14.88	-1.404	35.61	-1.601
15.49	-1.405	36.22	-1.590
16.10	-1.410	36.83	-1.575
16.71	-1.402	37.44	-1.574
17.32	-1.407	38.05	-1.579
17.93	-1.432	38.66	-1.592
18.54	-1.452	39.27	-1.588
19.15	-1.450	39.87	-1.483
19.76	-1.449	40.15	-1.374
20.37	-1.451		

Hole PB-3

Date: May 3, 1976

Depth of ice and water: 5.84 m

Depth (m) (below sea bed)	Temperature (°C)	Depth (m) (below sea bed)	Temperature (°C)
0.25	-1.613	20.98	-1.503
0.86	-1.491	21.59	-1.506
1.47	-1.437	22.20	-1.511
2.08	-1.442	22.81	-1.518
2.69	-1.406	23.42	-1.527
3.30	-1.375	24.03	-1.547
3.91	-1.355	24.64	-1.573
4.52	-1.341	25.25	-1.583
5.13	-1.338	25.86	-1.590
5.74	-1.337	26.46	-1.597
6.35	-1.336	27.07	-1.601
6.96	-1.337	27.68	-1.602
7.57	-1.339	28.29	-1.601
8.18	-1.345	28.90	-1.597
8.79	-1.357	29.51	-1.605
9.40	-1.365	30.12	-1.623
10.01	-1.375	30.73	-1.642
10.62	-1.383	31.34	-1.652
11.22	-1.391	31.95	-1.654
11.83	-1.399	32.56	-1.652
12.44	-1.408	33.17	-1.654
13.05	-1.418	33.78	-1.657
13.66	-1.432	34.39	-1.663
14.27	-1.441	35.00	-1.677
14.88	-1.447	35.61	-1.686
15.49	-1.450	36.22	-1.690
16.10	-1.454	36.83	-1.686
16.71	-1.453	37.44	-1.684
17.32	-1.449	38.05	-1.705
17.93	-1.470	38.66	-1.709
18.54	-1.497	39.27	-1.692
19.15	-1.502	39.88	-1.654
19.76	-1.500	40.18	-1.620
20.37	-1.500	40.39	-1.599

Hole PB-3

Date: May 6, 1976

Depth of ice and water: 5.84 m

Depth (m) (below sea bed)	Temperature (°C)	Depth (m) (below sea bed)	Temperature (°C)
0.25	-1.639	19.76	-1.528
0.56	-1.598	20.37	-1.530
0.86	-1.534	20.98	-1.534
1.17	-1.474	21.59	-1.539
1.47	-1.471	22.20	-1.544
1.78	-1.473	22.81	-1.550
2.08	-1.470	23.42	-1.560
2.69	-1.443	24.03	-1.583
3.30	-1.420	24.64	-1.597
3.91	-1.404	25.25	-1.608
4.52	-1.386	25.86	-1.618
5.13	-1.366	26.46	-1.625
5.74	-1.360	27.07	-1.629
6.35	-1.360	27.68	-1.631
6.96	-1.361	28.29	-1.633
7.57	-1.364	28.90	-1.635
8.18	-1.372	29.51	-1.643
8.79	-1.380	30.12	-1.658
9.40	-1.389	30.73	-1.673
10.01	-1.398	31.34	-1.681
10.62	-1.406	31.95	-1.686
11.22	-1.415	32.56	-1.690
11.83	-1.424	33.17	-1.697
12.44	-1.434	33.78	-1.705
13.05	-1.445	34.39	-1.715
13.66	-1.456	35.00	-1.726
14.27	-1.464	35.61	-1.734
14.88	-1.469	36.22	-1.739
15.49	-1.474	36.83	-1.743
16.10	-1.478	37.44	-1.746
16.71	-1.479	38.05	-1.752
17.32	-1.484	38.66	-1.753
17.93	-1.502	39.27	-1.747
18.54	-1.521	39.88	-1.740
19.15	-1.526	40.18	-1.734
		40.36	-1.863

References

Carslaw, H. S., and J. C. Jaeger, 1959, Conduction of Heat in Solids: Oxford Univ. Press, London, 386 p.

Gold, L. W., and A. H. Lachenbruch, 1973, Thermal conditions in permafrost--A review of North American literature, in Permafrost--The North American Contribution to the Second International Conference: Natl. Acad. Sci., p. 3-23.

Harrison, W. D., P. D. Miller, and T. E. Osterkamp, 1977, Permafrost beneath the Chukchi Sea - Preliminary report: Alaska Univ. Geophys. Inst. Quart. Rept. (Oct. 31 - Dec. 31, 1976).

Harrison, W. D., and T. E. Osterkamp, 1976, A coupled heat and salt transport model for sub-sea permafrost: Alaska Univ. Geophys. Inst. Rept. UAG R-247, 21 p.

Hopkins, D. M., P. W. Barnes, N. Biswas, J. Cannon, E. Chamberlain, J. Dygas, W. Harrison, A. S. Naidu, D. Nummedal, J. Rogers, P. Sellmann, M. Vigdorichik, W. Wiseman, and T. Osterkamp, 1977, Earth science studies, in Synthesis of scientific studies of the Beaufort Sea: Natl. Atmospheric and Oceanic Administration, in press.

Hunter, J. A. M., A. S. Judge, H. A. MacAulay, R. L. Good, R. M Gagne, and R. A. Burns, 1976, The occurrence of permafrost and frozen sub-seabottom materials in the southern Beaufort Sea, in Beaufort Sea Tech. Rept. #22: Victoria, B.C., Dept. Environment, 174 p.

Lachenbruch, A. H., 1957, Thermal effects of the ocean on permafrost: Geol. Soc. America Bull., v. 68, p. 1515-1530.

Lachenbruch, A. H., and M. C. Brewer, 1959, Dissipation of the temperature effect of drilling a well in Arctic Alaska: U.S. Geol. Survey Bull. 1083-C, p. 73-109.

Lachenbruch, A. H., M. C. Brewer, G. W. Greene, and B. V. Marshall, 1962, Temperatures in permafrost, in Temperature--Its measurement and control in science and industry: Reinhold Publ. Corp., New York, v. 3, p. 791-803.

Lachenbruch, A. H., G. W. Greene, and B. V. Marshall, 1966, Permafrost and the geothermal regimes, in Environment of the Cape Thompson Region, Alaska: USAEC Div. Tech. Inf., p. 149-165.

Mackay, J. R., 1972, Offshore permafrost and ground ice, southern Beaufort Sea, Canada: Canadian Jour. Earth Sci., v. 9, p. 1550-1561.

Osterkamp, T. E., 1975, A conceptual model of offshore permafrost: Alaska Univ. Geophys. Inst. Rept. UAG R-234.

Osterkamp, T. E., and W. D. Harrison, 1976, Subsea permafrost at Prudhoe Bay, Alaska--Drilling report: Alaska Univ. Geophys. Inst. Rept. UAG R-245.

Sass, J. H., A. H. Lachenbruch, and R. J. Munroe, 1971, Thermal conductivity of rocks from measurements on fragments and its application to heat-flow determinations: Jour. Geophys. Research, v. 76, p. 3391-3401.

Sass, J. H., A. H. Lachenbruch, R. J. Munroe, G. W. Greene, and T. H. Moses, Jr., 1971, Heat flow in the western United States: Jour. Geophys. Research, v. 76, p. 6376-6413.

Sharbatyan, A. A., and P. A. Shumskiy, 1974, Extreme estimations in geothermy and geocryology: U.S. Army Corps Engineers Cold Regions Research and Eng. Lab. Rept. TL 465 [Draft Translation 465].

Terzaghi, K., 1952, Permafrost: Boston Soc. Civil Engineers Jour., v. 39, p. 1-50.

